Springer Proceedings in Complexity

Douw G. Steyn
Nadine Chaumerliac *Editors*

Air Pollution Modeling and its Application XXIV

Springer

Springer Proceedings in Complexity

Springer Complexity

Springer Complexity is an interdisciplinary program publishing the best research and academic-level teaching on both fundamental and applied aspects of complex systems—cutting across all traditional disciplines of the natural and life sciences, engineering, economics, medicine, neuroscience, social and computer science.

Complex Systems are systems that comprise many interacting parts with the ability to generate a new quality of macroscopic collective behavior the manifestations of which are the spontaneous formation of distinctive temporal, spatial or functional structures. Models of such systems can be successfully mapped onto quite diverse "real-life" situations like the climate, the coherent emission of light from lasers, chemical reaction-diffusion systems, biological cellular networks, the dynamics of stock markets and of the internet, earthquake statistics and prediction, freeway traffic, the human brain, or the formation of opinions in social systems, to name just some of the popular applications.

Although their scope and methodologies overlap somewhat, one can distinguish the following main concepts and tools: self-organization, nonlinear dynamics, synergetics, turbulence, dynamical systems, catastrophes, instabilities, stochastic processes, chaos, graphs and networks, cellular automata, adaptive systems, genetic algorithms and computational intelligence.

The three major book publication platforms of the Springer Complexity program are the monograph series "Understanding Complex Systems" focusing on the various applications of complexity, the "Springer Series in Synergetics", which is devoted to the quantitative theoretical and methodological foundations, and the "SpringerBriefs in Complexity" which are concise and topical working reports, case-studies, surveys, essays and lecture notes of relevance to the field. In addition to the books in these two core series, the program also incorporates individual titles ranging from textbooks to major reference works.

More information about this series at http://www.springer.com/series/11637

Douw G. Steyn · Nadine Chaumerliac
Editors

Air Pollution Modeling and its Application XXIV

Springer

Editors
Douw G. Steyn
Earth, Ocean and Atmospheric Sciences
The University of British Columbia
Vancouver, BC
Canada

Nadine Chaumerliac
LaMP CNRS
Université Blaise Pascal
Aubière
France

ISSN 2213-8684 ISSN 2213-8692 (electronic)
Springer Proceedings in Complexity
ISBN 978-3-319-24476-1 ISBN 978-3-319-24478-5 (eBook)
DOI 10.1007/978-3-319-24478-5

Library of Congress Control Number: 2015957097

Printed on acid-free paper

This Springer imprint is published by SpringerNature
The registered company is Springer International Publishing AG Switzerland

Preface

In 1969, the North Atlantic Treaty Organization (NATO) established the Committee on Challenges of Modern Society (CCMS). From its inception, the committee supported studies of air pollution as one of its priorities. An important NATO/CCMS activity relating to air pollution was the periodic organization of a conference series called *International Technical Meeting on Air Pollution Modelling and its Application* (ITM). This activity continued until 2013, under the successor of NATO/CCMS, the NATO Committee on Science for Peace and Security (NATO/SPS). NATO Pilot Countries organizing these meetings have been: The United States of America; Federal Republic of Germany; Belgium; The Netherlands; Denmark; Portugal and Canada. In 2013 the ITM continued its meeting series independently of NATO/SPS.

This volume contains the abstracts of papers and posters presented at the 34th ITM, held in Montpellier, France, from 4 to 8 May 2015. The 34th ITM was organized by LaMP/OPGC, CNRS (Host Country) and The University of British Columbia (Pilot Country). Key topics presented at this ITM were: local and urban scale modelling; regional and intercontinental modelling; data assimilation and air quality forecasting; model assessment and verification; aerosols in the atmosphere; interactions between climate change and air quality; air quality and human health.

The ITM was attended by 114 participants representing 20 countries. Invited papers were presented by Patrick Armand, France (Emergency modelling), Heinke Schluenzen, Germany (Model evaluation), Peter Builtjes, The Netherlands (Developments in Integrated Modelling) and Mian Chin, USA (Modelling atmospheric aerosols).

On behalf of the ITM Scientific Committee and as organizers and editors, we would like to thank all the participants who contributed to the success of the meeting. We especially recognize the organizational and support efforts of the chairpersons and rapporteurs. Finally, special thanks to the sponsoring institutions: LaMP/OPGC,

CNRS/INSU, CEA, CNES, ADEME, INERIS, the city of Montpellier, Environment Canada and The University of British Columbia (Canada).

The next meeting will be held in September 2016 in Chania, Crete, Greece.

Douw G. Steyn
Scientific Committee Chair

Nadine Chaumerliac
Local Conference Organizer

Organizing Committee

Members of the Scientific Committee for the 34th International Technical Meeting (ITM) on Air Pollution Modelling and Its Application

Clemens Mensink	Belgium
Ekaterina Batchvarova	Bulgaria
Douw Steyn	Canada
Wanmin Gong	Canada
Sven-Erik Gryning	Denmark
Nadine Chaumerliac	France
Heinke Schlunzen	Germany
George Kallos	Greece
Silvia Trini Castelli	Italy
Hilde Fagerli	Norway
Ana Isabel Miranda	Portugal
Oriol Jorba	Spain
Renske Timmermans	The Netherlands
Selahattin Incecik	Turkey
Tony Dore	UK
Rohit Mathur	USA
Werner Klug	Germany (honorary life member)
Han van Dop	The Netherlands (honorary life member)
Frank Schiermeier	USA (honorary life member)

History of International Technical Meeting on Air Pollution Modelling and Its Application

Pilot Studies

1969–1974	Air Pollution Pilot Study (*Pilot Country: USA*)
1975–1979	Air Pollution Assessment Methodology and Modelling (*Pilot Country: Germany*)
1980–1944	Air Pollution Control strategies and Impact Modelling (*Pilot Country: Germany*)

Pilot Follow-Up Meetings

Pilot Country—USA (*R.A. McCormick, L.E. Niemeyer*)		
February 1971	Eindhoven, The Netherlands	First Conference on Low Pollution Power Systems Development
July 1971	Paris, France	Second Meeting of the Expert Panel on Air Pollution Modelling

NATO/CCMS International Technical Meetings (ITM) on Air Pollution Modelling and Its Application

Subsequent meetings were supported by the NATO Committee for Challenges to Modern Society and were designated NATO/CCMS International Technical Meetings (ITM) on Air Pollution Modelling and its Application.

October 1972	Paris, France 3rd TM
May 1973	Oberursel, Federal Republic of Germany 4th ITM
June 1974	Roskilde, Denmark 5th ITM
Pilot Country—Germany (*Erich Weber*)	
September 1975	Frankfurt, Federal Republic of Germany 6th ITM
September 1976	Airlie House, USA 7th ITM
September 1977	Louvain-la-Neuve, Belgium 8th ITM
August 1978	Toronto, Canada 9th ITM
October 1979	Rome, Italy 10th ITM
Pilot Country—Belgium (*C. De Wispelaere*)	
November 1980	Amsterdam, The Netherlands 11th ITM
September 1981	Menlo Park, California, USA 12th ITM
September 1982	Ile des Embiez, France 13th ITM
September 1983	Copenhagen, Denmark 14th ITM
April 1985	St. Louis, Missouri, USA 15th ITM
Pilot Country—The Netherlands (*H. van Dop*)	
April 1987	Lindau, Federal Republic of Germany 16th ITM
September 1988	Cambridge, United Kingdom 17th ITM
May 1990	Vancouver, BC, Canada 18th ITM
September 1991	Ierapetra, Greece 19th ITM
Pilot Country—Denmark (*Sven-Erik Gryning*)	
November 1993	Valencia, Spain 20th ITM
November 1995	Baltimore, Maryland, USA 21st ITM
May 1997	Clermont-Ferrand, France 22nd ITM
September 1998	Varna, Bulgaria 23rd ITM
May 2000	Boulder, Colorado, USA 24th ITM
Pilot Country—Portugal (*Carlos Borrego*)	
September 2001	Louvain-la-Neuve, Belgium 25th ITM
May 2003	Istanbul, Turkey 26th ITM
October 2004	Banff, Canada 27th ITM
May 2006	Leipzig, Germany 28th ITM

NATO/CCMS International Technical Meetings (ITM) on Air Pollution Modelling and Its Application

In 2007 the NATO Committee for Challenges to Modern Society was disbanded and replaced by the NATO Committee on Science for Peace and Security (NATO/SPS), which continued its support for the ITM.

September 2007	Aveiro, Portugal 29th ITM
Pilot Country—Canada (*Douw Steyn*)	
May 2009	San Francisco, California, USA 30th ITM
September 2010	Torino, Italy 31st ITM
May 2012	Utrecht, The Netherlands 32nd ITM

International Technical Meetings (ITM) on Air Pollution Modelling and Its Application

In 2012 the NATO Committee on Science for Peace and Security refocused its mandate, and the ITM became independent of NATO/SPS support.

September 2013	Miami, USA 33rd ITM
May 2015	Montpellier, France 34th ITM

List of Participants

Belgium

Delcloo Andy
Andy.Delcloo@oma.be
Ringlaan 3
B-1180 Ukkel

Lefebvre Wouter
wouter.lefebvre@vito.be
Boeretang 200
2400 Mol

Lenartz Fabian
f.lenartz@issep.be
Rue du Chéra 200
4000 Liège

Mensink Clemens
clemens.mensink@vito.be
Boeretang 200
2400 Mol

Canada

Falsafi Pedram
p.falsafi@gmail.com
Riverside Place Apts.
K1G 3T6
OTTAWA

Gong Wanmin
wanmin.gong@ec.gc.ca
4905 Dufferin Street
M3H 5T4
Toronto

Hakami Amir
amir_hakami@carleton.ca 1125
Colonel By Drive
K1S 5B6
Ottawa

Makar Paul
paul.makar@ec.gc.ca
4905 Dufferin Street
M3H 5T4 Toronto

Moisseeva Nadya
nmoisseeva@eos.ubc.ca
411-2925 Glen Dr
V3B7H9
Coquitlam

Moran Mike
Mike.Moran@ec.gc.ca
Environment Canada
M3H 5T4 Toronto

Pappin Amanda
amandapappin@cmail.carleton.ca
1125 Colonel By Drive
K1S 5B6 Ottawa

Seagram Annie
afseagram14@yahoo.ca
2020–2207 Main Mall
V6T 1Z4 Vancouver, BC

Steyn Douw
dsteyn@eos.ubc.ca
EOS
V6T 1Z4 Vancouver, BC

Weinstein Benjamin
bweinste@eos.ubc.ca
P.O. Box 4717
V0J2N0 Smithers

China

Chen Jianmin
jmchen@fudan.edu.cn
Department of Environmental Science and Engineering
Fudan University
Shanghai 200433

Croatia

Gasparac Goran
ggasparac@gekom.hr
Geophysical and Ecological Modeling Ltd.
Zagreb

Denmark

Brandt Jorgen
jbr@envs.au.dk
Frederiksborgvej 399
DK-4000 Roskilde

Geels Camilla
cag@envs.au.dk
Margrethehaabsvej 115
DK-4000 Roskilde

Estonia

Reis Ketlin
ketlin.reis@hotmail.com
Kastani 9-12
50409 Tartu
Finland

Jalkanen Jukka-Pekka
jukka-pekka.jalkanen@fmi.fi
Erik Palmen's Square 1
00101 Helsinki

Karppinen Ari
ari.karppinen@fmi.fi
Erik Palmenin Aukio 1
FI-00101 HELSINKI

Kukkonen Jaakko
jaakko.kukkonen@fmi.fi
Erik Palmenin Aukio 1
FI-00101 Helsinki

Prank Marje
marje.prank@fmi.fi
Erik Palmenin Aukio 1
FI-00560 Helsinki

Soares Joana
joana.soares@fmi.fi
Erik Palminen Aukio 1
FI-00560 Helsinki

Sofiev Mikhail
mikhail.sofiev@fmi.fi
Erik Palmenin Aukio 1
FI-00560 Helsinki

Vira Julius
julius.vira@fmi.fi
P.O. Box 503
FI-00101 Helsinki

France

Abdallah Charbel
abdallac@cerea.enpc.fr
9 Av. Blaise Pascal
77420 Champs sur Marne

Armand Patrick
patrick.armand@cea.fr
DIF/DASE/SRCE—Batiment G
91297 Arpajon

Arteta Joaquim
joaquim.arteta@meteo.fr
42 av G. Coriolis
31057 Toulouse

Beekmann Matthias
matthias.beekmann@lisa.u-pec.fr
Université Paris Est Créteil
94140 Créteil

Carissimo Bertrand
carissim@cerea.enpc.fr
6 Quai Watier
78400 Chatou

Chaumerliac Nadine
N.Chaumerliac@opgc.univ-bpclermont.fr
LaMP CNRS, Université Blaise Pascal
63171 Aubière Cedex

Cholakian Arineh
arineh.cholakian@lisa.u-pec.fr
39 rue d'estienne d'orves
92130 Issy les moulineaux

Chrit Mounir
mounir.chrit@enpc.fr
23, Rue Bruant
75013 Paris

Deguillaume Laurent
L.Deguillaume@opgc.univ-bpclermont.fr
24 avenue des Landais BP80026
63171 Aubière Cedex

Foret Gilles
Gilles.Foret@lisa.u-pec.fr
61 avenue du Général de Gaulle
94010 Créteil

Flossmann Andrea
A.Flossmann@opgc.univ-bpclermont.fr
LaMP/UBP
63171 Aubière Cedex

Joly Mathieu
mathieu.joly@meteo.fr
29 rue d'Andorre
31120 Pinsaguel

Lacressoniere Gwendoline
gwendoline.lacressonniere@lisa.u-pec.fr
61 avenue du Général de Gaulle
94010 Créteil

Leriche Maud
maud.leriche@aero.obs-mip.fr
Laboratoire d'Aérologie UMR5560 CNRS
31400 Toulouse

Nabat Pierre
pierre.nabat@meteo.fr
CNRM-GAME – Météo-France, UMR3589
42 avenue Gaspard Coriolis
31400 Toulouse, France

Perroux Hélène
H.Perroux@opgc.univ-bpclermont.fr
24 avenue des Landais BP80026
63171 Aubière Cedex

Planche Celine
c.planche@opgc.univ-bpclermont.fr
24 avenue des landais
63171 Aubière Cedex

Ribeiro Mickael
M.Ribeiro@opgc.univ-bpclermont.fr
LAMP Université Blaise Pascal
63171 Aubière Cedex

Russias Marie
M.Russias@opgc.cnrs.fr
OPGC
63171 Aubière Cedex

Vadot Françoise
F.Vadot@opgc.univ-bpclermont.fr
LaMP
63171 Aubière Cedex

Wei Xiao
xiao.wei@edf.fr
6 quai Watier
78401 Chatou

Zhu Shupeng
zhus@cerea.enpc.fr
6-8 Avenue Blaise Pascal
77420 Champs sur Marne

Germany

Backes Anna M.
Anna.Backes@hzg.de
Helmholtz-Zentrum Geesthacht
Institute of Coastal Research
Max-Planck-Strasse 1
21502 Geesthacht

Banzhaf Sabine
sabine.banzhaf@met.fu-berlin.de
Dieffenbachstr. 11
10967 Berlin

Bieser Johannes
johannes.bieser@hzg.de
Max-Planck-Str. 1
21502 Geesthacht

Fallmann Joachim
joachim.fallmann@kit.edu
Kreuzeckbahnstr. 19
82467 Garmisch-Partenkirchen

Forkel Renate
renate.forkel@kit.edu
Kreuzeckbahnstr. 19
82467 Garmisch-Partenkirchen

Mues Andrea
andrea.mues@iass-potsdam.de
Berliner Strasse 130
14467 Potsdam

Neumann Daniel
daniel.neumann@hzg.de
Max-Planck-Str. 1
21502 Geesthacht

Remig Moritz
moritz.remig@iass-potsdam.de
Berliner Strasse 130
14467 Potsdam

Schluenzen K. Heinke
heinke.schluenzen@uni-hamburg.de
Am Pellerbruch 3a
21271 Hanstedt

Wolke Ralf
wolke@tropos.de
TROPOS
04318 Leipzig

Greece

Kallos George
kallos@mg.uoa.gr
University of Athens, School of Physics
15784 Athens

Kioutsioukis Ioannis
kioutio@upatras.gr
DG-Joint Research Center/IES
TP441, JRC
21027, Ispra

Ireland

Donnelly Aoife
DONNELAO@tcd.ie
Civil Engineering
Dublin

Naughton Owen
naughto@tcd.ie
Civil Engineering
Dublin

Israel

Kishcha Pavel
pavel@cyclone.tau.ac.il
Ramat Aviv
69978 Tel Aviv

Manor Alon
alonmanor@gmail.com
DAVID ELAZAR 4
54032 GIVAT SHMUEL

Italy

Bonafe Giovanni
midable@gmail.com
viale Silvani, 6
40122 Bologna

D'Isidoro Massimo
m.disidoro@gmail.com
Via Martiri di Monte Sole 4
40129 Bologna

Galmarini Stefano
stefano.galmarini@gmail.com
tp 100 21027
Ispra

Piersanti Antonio
piersanti@enea.it
Via Martiri di Monte Sole 4
40129 Bologna

Righini Gaia
gaia.righini@enea.it
Via Martiri di Monte Sole 4
40129 Bologna

Solazzo Efisio
efisio.solazzo@jrc.ec.europa.eu
via sagittario
21021 Angera

Trini Castelli Silvia
s.trinicastelli@isac.cnr.it
CNR-ISAC
I-10133 Torino

Japan

Kawashima Shigeto
sig@kais.kyoto-u.ac.jp
Saiin Hidericho112-611
615-0065 Kyoto

Poland

Blaszcak Barbara
barbara.blaszczak@ipis.zabrze.pl
Institute of Environmental Engineering
Polish Academy of Sciences
34 M. Skłodowska-Curie St.
41-819 Zabrze

Mathews Barbara
barbara.mathews@ipis.zabrze.pl
LENARTOWICZA 28
41-800 Zabrze

Walaszek Kinga
kinga.walaszek@uni.wroc.pl
Kosiby 8
51-621 Wroclaw

Portugal

Miranda Ana Isabel
miranda@ua.pt
Department of Environment and Planning
3810-193 Aveiro

Spain

Baldasano Jose M.
jose.baldasano@bsc.es
Jordi Girona 29
08034 Barcelona

Jorba Oriol
oriol.jorba@bsc.es
Calle Jordi Girona, 31
08034 Barcelona

Ratola Neto
nrneto@um.es
Universidade de Murcia
Departamento de Fisica
30100 Murcia

Rivas Lara Ioar
irivas.creal@gmail.com
Doctor Aiguader, 88
08003 Barcelona

Switzerland

Aksoyoglu Sebnem
sebnem.aksoyoglu@psi.ch
Paul Scherrer Institute
5232 PSI Villigen

Ciarelli Giancarlo
giancarlo.ciarelli@psi.ch
Hohtalstrasse 15A
5408 Ennetbaden

Taiwan, ROC

Tsai Jiun-Horng
jhtsai@mail.ncku.edu.tw
Dept. Environ. Eng. National
Cheng Kung University
701 Tainan

The Netherlands

Builtjes Peter
peter.builtjes@tno.nl
P.O. Box 80015
3584 CB Utrecht

Timmermans Renske
renske.timmermans@tno.nl
P.O. Box 80015
3508 TA Utrecht

Van der Swaluw Eric
Eric.van.der.Swaluw@rivm.nl
P.O. Box 1
3720 BA Bilthoven

Turkey

Incecik Selahattin
incecik@itu.edu.tr
Istanbul Technical University
34469 Istanbul

UK

Neal Lucy
lucy.neal@metoffice.gov.uk
Met Office
EX1 3PB Exeter

Dore Anthony
todo@ceh.ac.uk
Centre for Ecology and Hydrology
EH26 OQB Midlothian

Medeiros Joana
j.s.medeiros2@herts.ac.uk
23 Bradshaws
AL10 9QS Hatfield

Ots Riinu
R.Ots@ed.ac.uk
4/5 Grange Loan EH9 2NR
Edinburgh

Sutton Paul
paul.sutton@rwe.com
RWE Generation UK
SN5 6PB Swindon

Werner Malgorzata
malgorzata.werner@uni.wroc.pl
29 The Cross
WR1 3PZ Worcester

USA

Alessandrini Stefano
alessand@ucar.edu
3450 Mitchell Lane
80301 Boulder

Arunachalam Saravanan
sarav@unc.edu
100 Europa Drive, Suite 490
27517 Chapel Hill

Astitha Marina
astitha@engr.uconn.edu
261 Glenbrook Rd
06269 Storrs-Mansfield

Boone Scott
stboone@live.unc.edu
100 Goldston Ave
27510 Carrboro

Chin Mian
mian.chin@nasa.gov
8800 Greenbelt Rd.
20771 Greenbelt, Maryland

Cox Jacqueline
jackie.cox@coe.gatech.edu
225 North Avenue
30332 Atlanta

Garcia Valerie
garcia.val@epa.gov
65 Sunny Glen Lane
23927 Clarksville

Hanna Steven
hannaconsult@roadrunner.com
7 Crescent Ave.
Kennebunkport ME 04046-7235

Henneman Lucas
lhenneman@gmail.com
1234 Francis Street
30318 Atlanta

Hogrefe Christian
hogrefe.christian@epa.gov
109 T.W. Alexander Dr
27711 RTP, NC

Isakov Vlad
Isakov.Vlad@epa.gov
109 TW Alexander Drive
27711 RTP, NC

Ivey Cesunica
sunni.ivey@gmail.com
6203 Morgan Place Court NE
30324 Atlanta

Lee Pius
pius.c.lee@gmail.com
5830 University Research Court
20740 college park

Napelenok Sergey
napelenok.sergey@epa.gov
109 T.W. Alexander
27111 Research Triangle Park

Odman Mehmet
odman@gatech.edu
311 Ferst Drive
30332-0512 Atlanta, GA

Pleim Jonathan
Pleim.jon@Epa.gov
109 T.W. Alexander Drive
27709 RTP, NC

Porter Paul
porter@if.uidaho.edu
1776 Science Center Drive, Suite 306
Idaho Falls, ID 83402

Ran Limei
lran@unc.edu
100 Europa Dr., Suite
490 27517 Chapel Hill

Rao S.T.
strao@ncsu.edu
2316 Heartley Drive
27615-1114 Raleigh

Stajner Ivanka
ivanka.stajner@noaa.gov
1325 East West Hwy
20910-3283 Silver Spring

Wong David
Wong.david-C@Epa.gov
109 T.W. Alexander Drive
27709 RTP, NC

Contents

Part VII Model Assessment and Verification

Contributors

Mia Aarnio Finnish Meteorological Institute, Helsinki, Finland

Jan Aben RIVM, Bilthoven, BA, The Netherlands

Paul Agnew Met Office, FitzRoy Road, Exeter, UK

Bruce Ainslie Environment Canada, Vancouver, Canada; Air Quality Research Unit, Meteorological Service of Canada, Environment Canada, Vancouver, BC, Canada

A. Akingunola Air Quality Research Division, Environment Canada, Toronto, ON, Canada

Sebnem Aksoyoglu Laboratory of Atmospheric Chemistry, Paul Scherrer Institute (PSI), Villigen, Switzerland

A. Alastuey Institute for Environmental Assessment and Water Research (IDÆA-CSIC), Barcelona, Spain

M. Àlvarez-Pedrerol Centre for Research in Environmental Epidemiology (CREAL), Barcelona, Spain

Pinhas Alpert Department of Geosciences, Tel-Aviv University, Tel-Aviv, Israel

Mikael Skou Andersen Department of Environmental Science, Aarhus University, Roskilde, Denmark

Camilla Andersson Swedish Meteorological and Hydrological Institute, Norrkoping, Sweden; Department of Environmental Science, Aarhus University, Roskilde, Denmark

Spyros Andronopoulos National Centre for Scientific Research "Demokritos", Aghia Paraskevi, Greece

Federico Angelini ENEA UTAPRAD-DIM, Frascati, Italy

Helen ApSimon Imperial College, London, UK

Wyat Appel Atmospheric Modeling and Analysis Division, U.S. EPA, Research Triangle Park, Durham, NC, USA

Patrick Armand CEA, DAM, DIF, Arpajon, France

Joaquim Arteta CNRM-GAME/Météo-France, Toulouse, France

Saravanan Arunachalam Institute for the Environment, University of North Carolina, Chapel Hill, NC, USA

Marina Astitha Department of Civil and Environmental Engineering, University of Connecticut, Storrs, CT, USA

Robert Atlas Atlantic Oceanographic and Meteorological Laboratory, NOAA, Miami, FL, USA

J.-L. Attié Centre National de Recherches Météorologiques (CNRM), Météo-France-CNRS, University of Toulouse, Toulouse, France; Laboratoire D'Aérologie, CNRS-Univ, Toulouse, France

Armin Aulinger Helmholtz-Zentrum Geesthacht, Institute of Coastal Research, Geesthacht, Germany

Anna M. Backes Helmholtz-Zentrum Geesthacht, Institute of Coastal Research, Geesthacht, Germany

A. Baklanov World Meteorological Organization, Geneva, Switzerland; Danish Meteorological Institute, Copenhagen, Danmark

J.M. Baldasano Earth Sciences Department, Barcelona Supercomputing Center—Centro Nacional de Supercomputación (BSC-CNS), Barcelona, Spain; Environmental Modelling Laboratory, Technical University of Catalonia, Barcelona, Spain

Urs Baltensperger Laboratory of Atmospheric Chemistry, Paul Scherrer Institute (PSI), Villigen, Switzerland

A. Balzarini Ricerca sul Sistema Energetico (RSE SpA), Milan, Italy

Larry Band Institute for the Environment, University of North Carolina at Chapel Hill, Chapel Hill, USA

Sabine Banzhaf Institute of Meteorology, Freie Universität Berlin, Berlin, Germany

Christelle Barbet Laboratoire de Météorologie Physique (LaMP), CNRS, Université Clermont Auvergne, Université Blaise Pascal, Aubière Cedex, France

Nikolaos Bartsotas Atmospheric Modeling and Weather Forecasting Group, School of Physics, University of Athens, Athens, Greece

Timothy Barzyk Human Exposure and Atmospheric Sciences Division, National Exposure Research Laboratory, Office of Research and Development, U.S. EPA, Research Triangle Park, Durham, NC, USA

Sara Basart Earth Sciences Department, Barcelona Supercomputing Center—Centro Nacional de Supercomputación (BSC-CNS), Barcelona, Spain

Kathrin Baumann-Stanzer Central Institute for Meteorology and Geodynamics, Vienna, Austria

Stephen R. Beagley Air Quality Research Division, Environment Canada, Toronto, ON, Canada; National Prediction Operations, Meteorological Service of Canada, Environment Canada, Montreal, Canada

Matthias Beekmann LISA/IPSL, Laboratoire Interuniversitaire des Systèmes Atmosphériques, UMR CNRS 7583, Université Paris Est Créteil (UPEC) et Université Paris Diderot (UPD), Créteil, Paris, France

Roberto Bellasio Enviroware Srl, Concorezzo, Italy

Pascal Bellavance Transportation Division, Environment Stewardship Branch, Environment Canada, Gatineau, Canada

Eva Berbekar Budapest University of Technology and Economics, Budapest, Hungary

Alexandre Berger Laboratoire d'Aérologie (LA), CNRS, Université de Toulouse, Université Paul Sabatier, Toulouse, France

Luc Bertand Institut Scientifique de Service Public, Liège, Belgium

Huisheng Bian Atmospheric Chemistry and Dynamics Laboratory, NASA Goddard Space Flight Center, Greenbelt, MD, USA; University of Maryland Baltimore County, Baltimore, MD, USA

Roberto Bianconi Enviroware Srl, Concorezzo, Italy

Arastoo Pour Biazar Department of Atmospheric Science, University Alabama, Huntsville, AL, USA

Johannes Bieser Helmholtz-Zentrum Geesthacht, Institute of Coastal Research, Geesthacht, Germany; Deutsches Zentrum für Luft- und Raumfahrt, Institute of Atmospheric Physics, Weßling, Germany

Frank Binkowski Institute for the Environment, University of North Carolina at Chapel Hill, Chapel Hill, USA

Karsten Bolding Department of Bioscience, Aarhus University, Aarhus, Denmark

Giovanni Bonafè ARPA, Regional Agency for Environmental Protection in the Emilia-Romagna, Bologna, Italy

Paolo Bonasoni CNR-ISAC, Bologna, Italy

Scott Boone University of North Carolina, Chapel Hill, NC, USA

Agnes Borbon Laboratoire Interuniversitaire des Systèmes Atmosphériques (LISA), Créteil, France

Carlos Borrego CESAM & Department of Environmental and Planning, University of Aveiro, Aveiro, Portugal

L. Bouso Centre for Research in Environmental Epidemiology (CREAL), Barcelona, Spain

Christine Braban Centre for Ecology & Hydrology, Edinburgh, UK

Jørgen Brandt Department of Environmental Science, Aarhus University, Aarhus, Denmark

Olivier Brasseur Brussels Environment, Brussels, Belgium

M. Bressi LSCE, Laboratoire des Sciences du Climat et de l'Environnement, CNRS-CEA-UVSQ, Gif-sur-Yvette, France

J. Brook Air Quality Research Division, Environment Canada, Toronto, ON, Canada

David Brown ANL, Argonne, IL, USA

D. Brunner Laboratory for Air Pollution/Environmental Technology, Empa, Swiss Federal Laboratories for Materials Science and Technology, Dübendorf, Switzerland

P. Builtjes Department of Climate, Air and Sustainability, TNO, Utrecht, The Netherlands; Free University Berlin (FUB), Berlin, Germany

Jakob Bønløkke Section of Environment, Occupation, and Health, Department of Public Health, Aarhus University, Aarhus C, Denmark

Barbara Błaszczak Institute of Environmental Engineering, Polish Academy of Sciences, Zabrze, Poland

Marek Błaś Institute of Geography and Regional Development, Wroclaw University, Wroclaw, Poland

Chenxia Cai California Air Resources Board, Sacramento, CA, USA

Bertrand Carissimo Research and Teaching Center in Atmospheric Environment (CEREA), EDF R&D, Chatou, France

Gregory Carmichael Department of Chemical and Biochemical Engineering, University of Iowa, Iowa City, IA, USA

D. Carrer Centre National de Recherches Météorologiques (CNRM), Météo-France-CNRS, Toulouse, France

Kenneth S. Carslaw School of Earth and Environment, ICAS, University of Leeds, Leeds, UK

X. Ceamanos Centre National de Recherches Météorologiques (CNRM), Météo-France-CNRS, Toulouse, France

J.-P. Chaboureau Laboratoire D'Aérologie, CNRS-Univ, Toulouse, France

Howard Chang Emory University, Atlanta, GA, USA

Joseph Chang HSSAI, Falls Church, VA, USA

Michael E. Chang Brook Byers Institute for Sustainable Systems, Georgia Institute of Technology, Atlanta, GA, USA

Nadine Chaumerliac Laboratoire de Météorologie Physique (LaMP), CNRS, Université Clermont Auvergne, Université Blaise Pascal, Aubière Cedex, France

Jack Chen National Prediction Operations, Meteorological Service of Canada, Environment Canada, Montreal, Canada; Marine and Ice Service, Meteorological Service of Canada, Environment Canada, Ottawa, Canada

Weiwei Chen Air Resources Laboratory (ARL), NOAA, College Park, MD, USA; Northeast Institute of Geography and Agroecology, Chinese Academy of Sciences, Changchun, China

P. Cheung Air Quality Research Division, Environment Canada, Toronto, ON, Canada

I. Chiapello Laboratoire D'Optique Atmosphérique (LOA), USTL-CNRS, Villeneuve D'Ascq, France

Irene Chiesa University of Bologna UNIBO, Bologna, Italy

Mian Chin Atmospheric Chemistry and Dynamics Laboratory, NASA Goddard Space Flight Center, Greenbelt, MD, USA

Arineh Cholakian Laboratoire Interuniversitaire des Systèmes Atmosphériques (LISA), Créteil, France

Jesper Heile Christensen Swedish Meteorological and Hydrological Institute, Norrköping, Sweden; Department of Environmental Science, Aarhus University, Roskilde, Denmark

S. Chung Boston University School of Public Health, Boston, MA, USA

Luisella Ciancarella Laboratory for Atmospheric Pollution, ENEA—Bologna Research Center, Bologna, Italy

Giancarlo Ciarelli Laboratory of Atmospheric Chemistry, Paul Scherrer Institute (PSI), Villigen, Switzerland

A. Colette INERIS, Verneuil-en-Halatte, France

Aurélie Colomb Laboratoire de Météorologie Physique (LaMP), CNRS, Université Clermont Auvergne, Université Blaise Pascal, Aubière Cedex, France

Kristina Conrady Meteorological Institute, CEN, University of Hamburg, Hamburg, Germany; Department of Earth Sciences, Uppsala University, Uppsala, Sweden

Ellen Cooter Office of Research and Development, U.S. Environmental Protection Agency, RTP, Durham, NC, USA

Sophie Cousineau National Prediction Operations, Meteorological Service of Canada, Environment Canada, Montreal, Canada

Giuseppe Cremona Laboratory for Atmospheric Pollution, ENEA—Bologna Research Center, Bologna, Italy

Paolo Cristofanelli CNR-ISAC, Bologna, Italy

James Crooks Office of Research and Development, U.S. Environmental Protection Agency, RTP, Durham, NC, USA

R.L. Curier Department of Climate, Air and Sustainability, TNO, Utrecht, The Netherlands

Arlindo M. da Silva Global Modeling and Assimilation Office, NASA/GSFC, Greenbelt, MD, USA

A. Darlington Air Quality Research Division, Environment Canada, Toronto, ON, Canada

Sushil K. Dash Indian Institute of Technology Delhi, New Delhi, India

M. de Castro Centre for Research in Environmental Epidemiology (CREAL), Barcelona, Spain

Koen De Ridder VITO, Flemish Institute for Technological Research, Urban Climate Team, Mol, Belgium

Francesco De Simone CNR—Istituto Inquinamento Atmosferico, U.O.S. di Rende, UNICAL-Polifunzionale, Rende, Italy

R. De Troch Royal Meteorological Institute of Belgium, Brussels, Belgium; Department of Physics and Astronomy, Ghent University, Ghent, Belgium

Wilco de Vries RIVM, Bilthoven, BA, The Netherlands

Stefano Decesari CNR-ISAC, Bologna, Italy

A. Deckmyn Royal Meteorological Institute of Belgium, Brussels, Belgium

Priscilla Declerck Brussels Environment, Brussels, Belgium

Laurent Deguillaume Laboratoire de Météorologie Physique (LaMP), CNRS, Université Clermont Auvergne, Université Blaise Pascal, Aubière Cedex, France

H. Delbarre Laboratoire de Physico-Chimie de L'Atmosphère (LPCA), Univ. Du Littoral Côte D'Opale-CNRS, Dunkirk, France

A.W. Delcloo Royal Meteorological Institute of Belgium, Brussels, Belgium

Bruce R. Denby Norwegian Institute for Air Research, Kjeller, Norway

F. Deutsch VITO Flemish Institute for Technological Research, Mol, Belgium

C. Di Biagio LISA,UPEC-UDDP7-CNRS, IPSL, Créteil, France

Luca Di Liberto ISAC-CNR, Rome, Italy

Phil Dickerson Environmental Protection Agency (EPA), Washington, USA

Thomas Diehl Atmospheric Chemistry and Dynamics Laboratory, NASA Goddard Space Flight Center, Greenbelt, MD, USA; Joint Research Center, Ispra, Italy

Davide Dionisi ISAC-CNR, Rome, Italy

D. Donaire Centre for Research in Environmental Epidemiology (CREAL), Barcelona, Spain

Anthony J. Dore Centre for Ecology and Hydrology, Edinburgh, UK

John Douros Aristotle University of Thessaloniki, Thessaloniki, Greece

Roland Draxler National Oceanic and Atmospheric Administration (NOAA), Washington, USA

Christophe Duchenne CEA, DAM, DIF, Arpajon, France

François Dulac Laboratoire des Sciences du Climat et de l'environnement, LSCE, CEA-CNRS-UVSQ, Gif-sur-Yvette, France

Eric Dupont Research and Teaching Center in Atmospheric Environment (CEREA), EDF R&D, Chatou, France

Laura Duque CESAM & Department of Environmental and Planning, University of Aveiro, Aveiro, Portugal

Pierre Durand Laboratoire d'Aérologie, LA, Toulouse, France

D. Edwards National Center for Atmospheric Research (NCAR), Boulder, USA

George Efthimiou University of Western Macedonia, Kozani, Greece; National Centre for Scientific Research "Demokritos", Aghia Paraskevi, Greece

L. El Amraoui Centre National de Recherches Météorologiques (CNRM), Météo-France-CNRS, Toulouse, France

Stefan Emeis Institute for Meteorology and Climate Research (IMK-IFU) of the Karlsruhe Institute of Technology (KIT), Garmisch-Partenkirchen, Germany

M. Engardt SMHI, Norrköpping, Sweden

J. Escobar LA, UMR 5560 CNRS/Université Paul Sabatier Toulouse 3, Toulouse, France

H. Eskes Royal Netherlands Meteorological Institute (KNMI), AE De Bilt, The Netherlands

Hans Estrup Department of Bioscience, Aarhus University, Aarhus, Denmark

Joachim Fallmann Institute for Meteorology and Climate Research (IMK-IFU) of the Karlsruhe Institute of Technology (KIT), Garmisch-Partenkirchen, Germany

Pedram Falsafi Department of Civil and Environmental Engineering, Carleton University, Ottawa, Canada

Joana Ferreira CESAM & Department of Environmental and Planning, University of Aveiro, Aveiro, Portugal

Paul R. Field School of Earth and Environment, ICAS, University of Leeds, Leeds, UK; Met Office, Exeter, UK

Frans Fierens IRCEL/CELINE, Brussels, Belgium

Johannes Flemming European Centre for Medium-Range Weather Forecasts, Reading, UK

Andrea I. Flossmann Laboratoire de Météorologie Physique, Université Clermont Auvergne, Université Blaise Pascal, Clermont-Ferrand, France; CNRS, INSU, UMR 6016, LaMP, Aubière, France

G. Foret Laboratoire Interuniversitaire des Systèmes Atmosphériques (LISA), Université Paris Est et 7, CNRS, Créteil, France

Renate Forkel Institute for Meteorology and Climate Research (IMK-IFU) of the Karlsruhe Institute of Technology (KIT), Garmisch-Partenkirchen, Germany

Paola Formenti Laboratoire Interuniversitaire des Systèmes Atmosphériques (LISA), Créteil, France

Shannon Fox DHS S&T CSAC, Aberdeen Proving Ground, Aberdeen, MD, USA

Evelyn Freney Laboratoire de Météorologie Physique (LaMP), CNRS, Université Clermont Auvergne, Université Blaise Pascal, Aubière Cedex, France

Vladimir Fuka Faculty of Mathematics and Physics, Department of Meteorology and Environment Protection, Charles University, Prague, Czech Republic

Stefano Galmarini European Commission, Joint Research Centre, Institute for Environment and Sustainability, Air and Climate Unit, Ispra, Italy

Boris R. Galvis Environmental Engineering Department, Universidad de La Salle, Bogotá, Colombia

Chuen-Meei Gan Atmospheric Modeling and Analysis Division, National Exposure Research Laboratory, U.S. Environmental Protection Agency, RTP, Durham, NC, USA

Fernando Garcia-Menendez Center for Global Change Science, Massachusetts Institute of Technology, Boston, MA, USA

Valerie Garcia Office of Research and Development, U.S. Environmental Protection Agency, RTP, Durham, NC, USA

Claudio Gariazzo INAIL Research Center, Monteporzio Catone, Italy

M. Gauss EMEP MSC-W, Norwegian Meteorological Institute, Oslo, Norway

D. Gazen LA, UMR 5560 CNRS/Université Paul Sabatier Toulouse 3, Toulouse, France

Goran Gašparac Geophysical and Ecological Modeling Ltd., Zagreb, Croatia

Camilla Geels Department of Environmental Science, Aarhus University, Aarhus, Denmark; Swedish Meteorological and Hydrological Institute, Norrköping, Sweden

Christian Gencarelli CNR—Istituto Inquinamento Atmosferico, U.O.S. di Rende, UNICAL-Polifunzionale, Rende, Italy

V. Ghersi AIRPARIF, Agence de surveillance de la qualité de l'air, Paris, France

Stefania Gilardoni CNR-ISAC, Bologna, Italy

Eric Gilbert Research and Teaching Center in Atmospheric Environment (CEREA), EDF R&D, Chatou, France

Robert Gilliam Atmospheric Modeling and Analysis Division, U.S. EPA, Research Triangle Park, Durham, NC, USA

O. Giot Royal Meteorological Institute of Belgium, Brussels, Belgium; Plant and Vegetation Ecology (PLECO), University of Antwerp, Antwerp, Belgium

Gian Paolo Gobbi CNR-ISAC, Roma Tor Vergata, Roma, Italy

Wanmin Gong Air Quality Research Division, Environment Canada, Toronto, ON, Canada

S. Gravel Air Quality Research Division, Environment Canada, Toronto, ON, Canada

Chris Green AMEC, London, UK

Branko Grisogono Department of Geophysics, Faculty of Science, University of Zagreb, Zagreb, Croatia

Valerie Gros Laboratoire des Sciences du Climat et de l'environnement, LSCE, CEA-CNRS-UVSQ, Gif-sur-Yvette, France

Jonathan Guth Météo-France CNRM-GAME, Toulouse, France

Steen Gyldenkærne Department of Environmental Science, Aarhus University, Aarhus, Denmark

Edith Gégo Porter-Gego, Idaho Falls, ID, USA

Amir Hakami Department of Civil and Environmental Engineering, Carleton University, Ottawa, ON, Canada

Jane Hall Centre for Ecology & Hydrology, Bangor, UK

R. Hamdi Royal Meteorological Institute of Belgium, Brussels, Belgium

Eric Hamonou Laboratoire des Sciences du Climat et de l'environnement, LSCE, CEA-CNRS-UVSQ, Gif-sur-Yvette, France

Steven Hanna Hanna Consultants, Kennebunkport, ME, USA

Kaj M. Hansen Department of Environmental Science, Aarhus University, Aarhus, Denmark

Berit Hasler Department of Environmental Science, Aarhus University, Aarhus, Denmark

K. Hayden Air Quality Research Division, Environment Canada, Toronto, ON, Canada

Brandon Hayes ORISE, Oakridge National Laboratory, Oak Ridge, TN, USA

John Hearn Lee University, Cleveland, TN, USA

Ian M. Hedgecock CNR—Istituto Inquinamento Atmosferico, U.O.S. di Rende, UNICAL-Polifunzionale, Rende, Italy

Antti Hellsten Finnish Meteorological Institute, Helsinki, Finland

Carlijn Hendriks Department Climate, Air Quality and Sustainability, TNO, Utrecht, TA, The Netherlands

Lucas R.F. Henneman Georgia Institute of Technology, Atlanta, GA, USA

Hartmut Herrmann Leibniz Institute for Tropospheric Research (TROPOS), Leipzig, Germany

Ole Hertel Department of Environmental Science, Aarhus University, Roskilde, Denmark

Bruce Hicks MetCorps, Norris, TN, USA

Brian Hinckley ORISE, Oakridge National Laboratory, Oak Ridge, TN, USA

M. Hirtl Zentralanstalt für Meteorologie und Geodynamik, ZAMG, Vienna, Austria

Christian Hogrefe Atmospheric Modeling and Analysis Division, National Exposure Research Laboratory, U.S. Environmental Protection Agency, RTP, Durham, NC, USA

Heather A. Holmes Department of Physics, University of Nevada Reno, Reno, NV, USA

L. Honzak University Ljubljana, SPACE-SI, Ljubljana, Slovenia

Hans Hooyberghs VITO, Flemish Institute for Technological Research, Urban Climate Team, Mol, Belgium

Yongtao Hu School of Civil and Environmental Engineering, Georgia Institute of Technology, Atlanta, GA, USA

Otto Hänninen Department of Health Protection, National Institute for Health and Welfare, Kuopio, Finland

Ulas Im Department of Environmental Science, Aarhus University, Roskilde, Denmark

Vlad Isakov Atmospheric Modeling and Analysis Division, National Exposure Research Laboratory, U.S. Environmental Protection Agency, RTP, Durham, NC, USA

Cesunica E. Ivey School of Civil and Environmental Engineering, Georgia Institute of Technology, Atlanta, GA, USA

Peter Jackson Environmental Science and Engineering Program, University of Northern British Columbia, Prince George, BC, Canada

J.-P. Jalkanen Finnish Meteorological Institute, Helsinki, Finland

Corinne Jambert Laboratoire d'Aérologie, LA, Toulouse, France

Stijn Janssen VITO, Mol, Belgium

Steen Solvang Jensen Department of Environmental Science, Aarhus University, Roskilde, Denmark

Amela Jeričević Croatian Civil Aviation Agency, Zagreb, Croatia

Kaat Jespers VITO, Mol, Belgium

Pedro Jiménez-Guerrero Department of Physics, Regional Campus of International Excellence "Campus Mare Nostrum", University of Murcia, Murcia, Spain

Mathieu Joly CNRM-GAME/Météo-France, Toulouse, France

Sander Jonkers TNO, Netherlands Organization for Applied Research, Utrecht, The Netherlands

O. Jorba Earth Sciences Department, Barcelona Supercomputing Center, Barcelona, Spain

Béatrice Josse CNRM-GAME/Météo-France, Toulouse, France

M. Jozwicka Department of Climate, Air and Sustainability, TNO, Utrecht, The Netherlands

Katarzyna Juda-Rezler Faculty of Environmental Engineering, Warsaw University of Technology, Warsaw, Poland

W. Junkermann Karlsruhe Institute of Technology (KIT), IMK-IFU, Garmisch-Partenkirchen, Germany

Klara Jurcakova Institute of Thermomechanics AS CR, Prague, Czech Republic

Marko Kaasik Institute of Physics, University of Tartu, Tartu, Estonia

George Kallos Atmospheric Modeling and Weather Forecasting Group, University of Athens, School of Physics, Athens, Greece

Daiwen Kang Computer Sciences Corporation, RTP, Durham, NC, USA

Leena Kangas Finnish Meteorological Institute, Helsinki, Finland

Matthias Karl Norwegian Institute for Air Research, Kjeller, Norway

Ari Karppinen Finnish Meteorological Institute, Helsinki, Finland

Mari Kauhaniemi Finnish Meteorological Institute, Helsinki, Finland

Shigeto Kawashima Kyoto University, Kyoto, Japan

Jean-Pierre Kervern Université de Grenoble, Grenoble, France

Matthias Ketzel Department of Environmental Science, Aarhus University, Roskilde, Denmark

Menno P. Keuken TNO, Netherlands Organization for Applied Research, Utrecht, The Netherlands

Kiki CNRM-GAME/Météo-France, Toulouse, France

Hyun-Cheol Kim NOAA Air Resources Laboratory, College Park, MD, USA; Cooperative Institute for Climate and Satellites, University of Maryland, College Park, MD, USA

Ioannis Kioutsioukis European Commission, Joint Research Centre, Institute for Environment and Sustainability, Air and Climate Unit, Ispra, Italy; Laboratory of Atmospheric Physics, Physics Department, University of Patras, Rio, Greece

Pavel Kishcha Department of Geosciences, Tel-Aviv University, Tel-Aviv, Israel

Krzysztof Klejnowski Institute of Environmental Engineering, Polish Academy of Sciences, Zabrze, Poland

Satoshi Kobayashi Kyoto University, Kyoto, Japan

T. Koskentalo Helsinki Region Environmental Services Authority, Helsinki, Finland

A. Kousa University of Hertfordshire, Hatfield, UK

R. Kouznetsov Finnish Meteorological Institute, Helsinki, Finland

Ewa Krajny Monitoring and Modeling of Air Pollution Department, Institute of Meteorology and Water Management–National Research Institute, Katowice, Poland

Richard Kranenburg Department Climate, Air Quality and Sustainability, TNO, Utrecht, TA, The Netherlands

Maciej Kryza Department of Climatology and Atmosphere Protection, Institute of Geography and Regional Development, University of Wroclaw, Wroclaw, Poland

Tom Kucsera Atmospheric Chemistry and Dynamics Laboratory, NASA Goddard Space Flight Center, Greenbelt, MD, USA; Universities Space Research Association, Columbia, MD, USA

Jaakko Kukkonen Finnish Meteorological Institute, Helsinki, Finland

Jonilda Kushta Atmospheric Modeling and Weather Forecasting Group, University of Athens, School of Physics, Athens, Greece

G. Lacressonnière Laboratoire Interuniversitaire des Systèmes Atmosphériques (LISA), Université Paris Est et 7, CNRS, Créteil, France

Joakim Lagner Department of Environmental Science, Aarhus University, Roskilde, Denmark

W. Lahoz Norwegian Institute for Air Research (NILU), Kjeller, Norway

Tony C. Landi CNR-ISAC, Bologna, Italy

Anne Sofie Lansø Department of Environmental Science, Aarhus University, Aarhus, Denmark

A. Lauer Institute for Advanced Sustainability Studies, Potsdam, Germany; Deutsches Zentrum für Luft- und Raumfahrt (DLR), Institut für Physik der Atmosphäre, Oberpfaffenhofen, Germany

B. Laurent LISA,UPEC-UDDP7-CNRS, IPSL, Créteil, France

Dirk Lauwaet VITO, Flemish Institute for Technological Research, Urban Climate Team, Mol, Belgium

David Lavoué Georgia Institute of Technology, Atlanta, GA, USA

Pius Lee NOAA Air Resources Laboratory, College Park, MD, USA

Wouter Lefebvre VITO, Flemish Institute for Technological Research, Urban Climate Team, Mol, Belgium

Bernd Leitl Meteorological Institute, University of Hamburg, Hamburg, Germany

Fabian Lenartz Institut Scientifique de Service Public, Liège, Belgium

Maud Leriche Laboratoire d'Aérologie (LA), CNRS, Université de Toulouse, Université Paul Sabatier, Toulouse, France

Jonathan Levy Boston University School of Public Health, Boston, MA, USA; University of North Carolina, Chapel Hill, NC, USA

S.-M. Li Air Quality Research Division, Environment Canada, Toronto, ON, Canada

Ewa Liana Institute of Meteorology and Water Management National Research Institute, Wroclaw, Poland

J. Liggio Air Quality Research Division, Environment Canada, Toronto, ON, Canada

Cong Liu Georgia Institute of Technology, Atlanta, GA, USA

Diogo Lopes CESAM & Department of Environmental and Planning, University of Aveiro, Aveiro, Portugal

Myriam Lopes CESAM & Department of Environmental and Planning, University of Aveiro, Aveiro, Portugal

Sarah Lu Atmospheric Sciences Research Center, State University of New York, Albany, NY, USA

Deborah Luecken Atmospheric Modeling and Analysis Division, National Exposure Research Laboratory, U.S. Environmental Protection Agency, RTP, Durham, NC, USA

Huiying Luo Department of Civil & Environmental Engineering, University of Connecticut, Storrs-Mansfield, CT, USA

Lynn Lyons Transportation Division, Environment Stewardship Branch, Environment Canada, Gatineau, Canada

J.-F. Léon Laboratoire D'Aérologie, CNRS-Univ, Toulouse, France

Susanne Lützenkirchen City of Oslo—Agency for Urban Environment, Oslo, Norway

Bino Maiheu VITO, Flemish Institute for Technological Research, Urban Climate Team, Mol, Belgium

P.A. Makar Air Quality Research Division, Environment Canada, Toronto, ON, Canada

Marc Mallet Laboratoire d'Aérologie, CNRS-Université Paul Sabatier, Toulouse, France

Astrid Manders Department Climate, Air Quality and Sustainability, TNO, Netherlands Organization for Applied Research, Utrecht, The Netherlands

Graham W. Mann School of Earth and Environment, ICAS, University of Leeds, Leeds, UK; National Centre for Atmospheric Sciences, School of Earth and Environment, University of Leeds, Leeds, UK

Nicolas Marchand Laboratoire Chimie Environnement, LCE, Marseille, France

Virginie Marecal CNRM-GAME/Météo-France, Toulouse, France

C. Mari LA, UMR 5560 CNRS/Université Paul Sabatier Toulouse 3, Toulouse, France

John H. Marsham School of Earth and Environment, ICAS, University of Leeds, Leeds, UK

G. Marson Air Quality Research Division, Environment Canada, Toronto, ON, Canada

V. Marécal CNRM-GAME, Météo France/CNRS, Toulouse, France

Barbara Mathews Institute of Environmental Engineering, Polish Academy of Sciences, Zabrze, Poland

Rohit Mathur Atmospheric Modeling and Analysis Division, National Exposure Research Laboratory, U.S. Environmental Protection Agency, RTP, Durham, NC, USA

L. Matilainen Helsinki Region Environmental Services Authority, Helsinki, Finland

Volker Matthias Helmholtz-Zentrum Geesthacht, Institute of Coastal Research, Geesthacht, Germany

Jeffery McQueen National Oceanic and Atmospheric Administration (NOAA), Washington, USA

Frédérik Meleux INERIS, Paris, France

C. Mensink VITO Flemish Institute for Technological Research, Mol, Belgium

L. Menut Laboratoire de Météorologie Dynamique, IPSL, CNRS/INSU, Ecole Polytechnique, Ecole Normale Supérieure, Palaiseau, France

Matteo Michelotti ARPA, Bologna, Italy

Martine Michou CNRM-GAME/Météo-France, Toulouse, France

Wojciech Mill Institute of Environmental Protection–National Research Institute, Warsaw, Poland

C. Maya Milliez Univ. Paris Est Electricite de France, Chatou Cedex, France

Enrico Minguzzi ARPA Emilia-Romagna, Bologna, Italy

Ana Isabel Miranda CESAM & Department of Environmental and Planning, University of Aveiro, Aveiro, Portugal

Nadya Moisseeva The University of British Columbia, Vancouver, Canada

Michael D. Moran Air Quality Research Division, Environment Canada, Toronto, ON, Canada

Antonella Morgillo ARPA Emilia-Romagna, Bologna, Italy

Heather Morrison Air Quality Research Division, Environment Canada, Toronto, ON, Canada

Nicolas Moussiopoulos Aristotle University of Thessaloniki, Thessaloniki, Greece

A. Mues Institute for Advanced Sustainability Studies, Potsdam, Germany

James A. Mulholland School of Civil and Environmental Engineering, Georgia Institute of Technology, Atlanta, GA, USA

Rodrigo Munoz-Alpizar National Prediction Operations, Meteorological Service of Canada, Environment Canada, Montreal, Canada

Mark S. Murphy Innovate!, Inc., Alexandria, VA, USA; Atmospheric Modeling and Analysis Division, National Exposure Research Laboratory, US Environmental Protection Agency, Research Triangle Park, NC, USA

Luc Musson-Genon Research and Teaching Center in Atmospheric Environment (CEREA), EDF R&D, Chatou, France

Aarne Männik Institute of Physics, University of Tartu, Tartu, Estonia

Pierre Nabat Centre National de Recherches Météorologiques (CNRM), Météo-France-CNRS, Toulouse, France

Sergey L. Napelenok Atmospheric Modeling and Analysis Division, National Exposure Research Laboratory, U.S. Environmental Protection Agency, RTP, Durham, NC, USA

Lucy Sarah Neal Met Office, FitzRoy Road, Exeter, UK

Daniel Neumann Helmholtz-Zentrum Geesthacht, Institute of Coastal Research, Geesthacht, Germany

Claus Nielsen University of Oslo, Oslo, Norway

Ole -Kenneth Nielsen Department of Environmental Science, Aarhus University, Roskilde, Denmark

M. Nieuwenhuijsen Centre for Research in Environmental Epidemiology (CREAL), Barcelona, Spain

A. Nyiri EMEP MSC-W, Norwegian Meteorological Institute, Oslo, Norway

Tavs Nyord Department of Engineering, Aarhus University, Aarhus, Denmark

M. Talat Odman School of Civil and Environmental Engineering, Georgia Institute of Technology, Atlanta, GA, USA

Hanna Ojrzyńska Department of Climatology and Atmosphere Protection, University of Wroclaw, Wroclaw, Poland

Mohammad Omary University of North Carolina at Chapel Hill, Chapel Hill, NC, USA

Riinu Ots Institute of Physics, University of Tartu, Tartu, Estonia

Tim Oxley Imperial College, London, UK

B. Pabla Air Quality Research Division, Environment Canada, Toronto, ON, Canada

Jorge E. Pachón Environmental Engineering Department, Universidad de La Salle, Bogotá, Colombia

Lucia Paci University of Bologna, Bologna, Italy

Li Pan Air Resources Laboratory (ARL), NOAA, College Park, MD, USA; Cooperative Institutes for Satellite and Climate, University of Maryland, College Park, MD, USA

M. Pandolfi Institute for Environmental Assessment and Water Research (IDÆA-CSIC), Barcelona, Spain

Amanda J. Pappin Department of Civil and Environmental Engineering, Carleton University, Ottawa, ON, Canada

Platon Patlakas Atmospheric Modeling and Weather Forecasting Group, University of Athens, School of Physics, Athens, Greece

Luc Patryl CEA, DAM, DIF, Arpajon, France

Tomasz Pecka Institute of Environmental Protection–National Research Institute, Warsaw, Poland

J. Pelon Laboratoire Atmosphères, Milieux, Observations Spatiales (LATMOS), CNRS-UPMC-UVSQ, Paris, France

Stefani Penn Boston University School of Public Health, Boston, MA, USA

Herve Petetin LISA/IPSL, Laboratoire Interuniversitaire des Systèmes Atmosphériques, UMR CNRS 7583, Université Paris Est Créteil (UPEC) et Université Paris Diderot (UPD), Paris, France; CNRS and Université Paul Sabatier, Laboratoire d'Aérologie, Toulouse, France

J.-E. Petit LSCE, Laboratoire des Sciences du Climat et de l'Environnement, CNRS-CEA-UVSQ, Gif-sur-Yvette, France

Anton Petrov National Institute of Meteorology and Hydrology-Bulgarian Academy of Sciences, Sofia, Bulgaria

Tuukka Petäjä University of Helsinki, Helsinki, Finland

V.-H. Peuch ECMWF, Shinfield Park, Reading, Berkshire, UK

Brad Pierce National Environmental Satellite and Information Service (NESDIS), Madison, WI, USA

Antonio Piersanti Laboratory for Atmospheric Pollution, ENEA—Bologna Research Center, Bologna, Italy

Céline Planche Laboratoire de Météorologie Physique, Université Blaise Pascal, OPGC/CNRS UMR 6016, Clermont-Ferrand, France; School of Earth and Environment, ICAS, University of Leeds, Leeds, UK

Jonathan Pleim Atmospheric Modeling and Analysis Division, National Exposure Research Laboratory, US Environmental Protection Agency, Research Triangle Park, NC, USA

Marlene Schmidt Plejdrup Department of Environmental Science, Aarhus University, Roskilde, Denmark

Matthieu Plu CNRM-GAME/Météo-France, Toulouse, France

Aditya A. Pophale School of Civil and Environmental Engineering, Georgia Institute of Technology, Atlanta, GA, USA

P. Steven Porter Porter-Gego, Idaho Falls, ID, USA

George Pouliot Atmospheric Modeling and Analysis Division, National Exposure Research Laboratory, U.S. Environmental Protection Agency, RTP, Durham, NC, USA

Marje Prank Finnish Meteorological Institute, Helsinki, Finland

André S.H. Prévôt Laboratory of Atmospheric Chemistry, Paul Scherrer Institute (PSI), Villigen, Switzerland

Christopher Purr Meteorological Institute, CEN, University of Hamburg, Hamburg, Germany

J.L. Pérez Technical University of Madrid (UPM), ESMG, Madrid, Spain

María P. Pérez Environmental Engineering Department, Universidad de La Salle, Bogotá, Colombia

Jumaan Al Qahtani Saudi Aramco Oil Company, Dhahran, Saudi Arabia

Markus Quante Helmholtz-Zentrum Geesthacht, Institute of Coastal Research, Geesthacht, Germany

X. Querol Institute for Environmental Assessment and Water Research (IDÆA-CSIC), Barcelona, Spain

Aniko Rakai Budapest University of Technology and Economics, Budapest, Hungary

Limei Ran Institute for the Environment, University of North Carolina, Chapel Hill, NC, USA

S.T. Rao Department of Marine, Earth & Atmospheric Sciences, North Carolina State University, Raleigh, NC, USA

T. Rasila Finnish Meteorological Institute, Helsinki, Finland

Nuno Ratola Department of Physics, Regional Campus of International Excellence "Campus Mare Nostrum", University of Murcia, Murcia, Spain; LEPABE, Faculty of Engineering, University of Porto, Porto, Portugal

F. Ravetta Laboratoire Atmosphères, Milieux, Observations Spatiales (LATMOS), CNRS-UPMC-UVSQ, Paris, France

Ketlin Reis Institute of Physics, University of Tartu, Tartu, Estonia

Stefan Reis Centre for Ecology & Hydrology, Edinburgh, UK

Magdalena Reizer Faculty of Environmental Engineering, Warsaw University of Technology, Warsaw, Poland

Helder Relvas CESAM & Department of Environmental and Planning, University of Aveiro, Aveiro, Portugal

J.-B. Renard Laboratoire de Physique et Chimie de L'Environnement et de L'Espace (LPC2E), CNRS-Univ, Orléans, France

Nele Renders VITO, Mol, Belgium

Isabella Ricciardelli ARPA Emilia-Romagna, Bologna, Italy

Gaia Righini Laboratory for Atmospheric Pollution, ENEA—Bologna Research Center, Bologna, Italy

K. Riikonen Finnish Meteorological Institute, Helsinki, Finland

Matteo Rinaldi CNR-ISAC, Bologna, Italy

I. Rivas Institute for Environmental Assessment and Water Research (IDÆA-CSIC), Barcelona, Spain; Centre for Research in Environmental Epidemiology (CREAL), Barcelona, Spain

Chul-Un Ro Air Quality Research Division, Environment Canada, Toronto, ON, Canada

G. Roberts Centre National de Recherches Météorologiques (CNRM), Météo-France-CNRS, Toulouse, France

Shawn Roselle Atmospheric Modeling and Analysis Division, National Exposure Research Laboratory, U.S. Environmental Protection Agency, RTP, Durham, NC, USA

A. Rosso AIRPARIF, Agence de surveillance de la qualité de l'air, Paris, France

J.-L. Roujean Centre National de Recherches Météorologiques (CNRM), Météo-France-CNRS, Toulouse, France

M. Rupakheti Institute for Advanced Sustainability Studies, Potsdam, Germany; Himalayan Sustainability Institute, Kathmandu, Nepal

Armistead G. Russell School of Civil and Environmental Engineering, Georgia Institute of Technology, Atlanta, GA, USA

Constanza Saavedra Environmental Engineering Department, Universidad de La Salle, Bogotá, Colombia

Rushabh D. Sakhpara School of Civil and Environmental Engineering, Georgia Institute of Technology, Atlanta, GA, USA

Zissis Samaras Aristotle University of Thessaloniki, Thessaloniki, Greece

R. San José Technical University of Madrid (UPM), ESMG, Madrid, Spain

O. Sanchez AIRPARIF, Agence de surveillance de la qualité de l'air, Paris, France

R. Sarda-Estève LSCE, Laboratoire des Sciences du Climat et de l'Environnement, CNRS-CEA-UVSQ, Gif-sur-Yvette, France

Karine N. Sartelet CEREA, Joint Laboratory Ecole Des Ponts ParisTech - EDF R&D, Université Paris-Est, Champs-sur-Marne, France

Mourad Sassi National Prediction Operations, Meteorological Service of Canada, Environment Canada, Montreal, Canada

Ferd Sauter RIVM, Bilthoven, BA, The Netherlands

Sébastien Sauvage Sciences de l'Atmosphère et Génie de l'Environnement, Douai, France

Martijn Schaap Department Climate, Air Quality and Sustainability, TNO, Utrecht, TA, The Netherlands

K. Schepanski Leibniz Institute for Tropospheric Research, Leipzig, Germany

K. Heinke Schlünzen Meteorological Institute, CEN, University of Hamburg, Hamburg, Germany

W. Schröder Leibniz-Institute for Tropospheric Research (TROPOS), Leipzig, Germany

Roland Schrödner Leibniz Institute for Tropospheric Research (TROPOS), Leipzig, Germany

Per E. Schwarze Department of Air Pollution and Noise, Norwegian Institute of Public Health, Oslo, Norway

J. Sciare LSCE, Laboratoire des Sciences du Climat et de l'Environnement, CNRS-CEA-UVSQ, Gif-sur-Yvette, France

Annie F. Seagram Air Quality Research Unit, Meteorological Service of Canada, Environment Canada, Vancouver, BC, Canada

Karine Sellegri Laboratoire de Météorologie Physique (LaMP), CNRS, Université Clermont Auvergne, Université Blaise Pascal, Aubière Cedex, Clermont-Ferrand, France

Florence Sevault CNRM-GAME—Météo-France, UMR3589, Toulouse, France

B. Sic Centre National de Recherches Météorologiques (CNRM), Météo-France-CNRS, Toulouse, France

M. Sicard Remote Sensing Laboratory (RSLab)/IEEC-CRAE, Univ. Politècnica de Catalunya, Barcelona, Spain

Torben Sigsgaard Section of Environment, Occupation, and Health, Department of Public Health, Aarhus University, Aarhus C, Denmark

Pilvi Siljamo Finnish Meteorological Institute, Helsinki, Finland

Carlos Silveira CESAM & Department of Environmental and Planning, University of Aveiro, Aveiro, Portugal

Mahendra P. Singh Ansal Institute of Technology and Management, Lucknow, India

Vikas Singh National Atmospheric Research Laboratory, Tirupathi, India; Centre for Atmospheric and Instrumentation Research (CAIR), University of Hertfordshire, Hatfield, UK

Guillaume Siour Laboratoire Interuniversitaire des Systèmes Atmosphériques (LISA), Université Paris Est et 7, CNRS, Créteil, France

Carsten Ambelas Skjøth National Pollen and Aerobiology Research Unit, Institute of Science and the Environment, University of Worcester, Worcester, UK

Michelle Snyder Institute for the Environment, University of North Carolina, Chapel Hill, NC, USA

J. Soares Finnish Meteorological Institute, Helsinki, Finland

S. Sobolowski UNI Research, The Bjerknes Centre for Climate Research, Bergen, Norway

Mikhail Sofiev Finnish Meteorological Institute, Helsinki, Finland

Michael Sohn LBNL, Berkeley, CA, USA

Ranjeet S. Sokhi Centre for Atmospheric and Instrumentation Research (CAIR), University of Hertfordshire, Hatfield, UK

E. Solazzo European Commission—DG Joint Research Centre, Institute for Environment and Sustainability, Ispra, Italy

F. Solmon Earth System Physics, Int. Centre for Theoretical Physics (ICTP), UNESCO-IAEA, Trieste, Italy

Samuel Somot CNRM-GAME—Météo-France, UMR3589, Toulouse, France

Thomas Spicer University of Arkansas, Fayetteville, AR, USA

R. Staebler Air Quality Research Division, Environment Canada, Toronto, ON, Canada

Ivanka Stajner National Oceanic and Atmospheric Administration (NOAA), Washington, USA

Boris Starobinets Department of Geosciences, Tel-Aviv University, Tel-Aviv, Israel

Douw Steyn Department of Earth, Ocean and Atmospheric Sciences, The University of British Columbia, Vancouver, BC, Canada

Michele Stortini ARPA-SIMC, Bologna, Italy

C. Stroud Air Quality Research Division, Environment Canada, Toronto, ON, Canada

Marzenna Strońska Institute of Meteorology and Water Management National Research Institute, Wroclaw, Poland

J. Sunyer Centre for Research in Environmental Epidemiology (CREAL), Barcelona, Spain

John Paul Sutton RWE Generation UK, Windmill Hill Business Park, Swindon, UK

Mark Sutton Centre for Ecology & Hydrology, Edinburgh, UK

Mariusz Szymanowski Institute of Geography and Regional Development, Wroclaw University, Wroclaw, Poland

Elisa Sá CESAM & Department of Environmental and Planning, University of Aveiro, Aveiro, Portugal

Yann Tambouret Boston University Research Computing Services, Boston, MA, USA

Keita Tanaka Kyoto University, Kyoto, Japan

Sim Tang Centre for Ecology & Hydrology, Edinburgh, UK

Youhua Tang Air Resources Laboratory (ARL), NOAA, College Park, MD, USA; Cooperative Institutes for Satellite and Climate, University of Maryland, College Park, MD, USA

Richard Tavares Laboratory of Hydrodynamics, Energetics and Atmospheric Environment and Institute for Research on Urban Sciences and Techniques, Nantes, France

P. Termonia Royal Meteorological Institute of Belgium, Brussels, Belgium; Department of Physics and Astronomy, Ghent University, Ghent, Belgium

Hans Thodsen Department of Bioscience, Aarhus University, Aarhus, Denmark

Marie Tilbee Met Office, FitzRoy Road, Exeter, UK

Andreas Tilgner Leibniz Institute for Tropospheric Research (TROPOS), Leipzig, Germany

Karen Timmermann Department of Bioscience, Aarhus University, Aarhus, Denmark

R. Timmermans Department of Climate, Air and Sustainability, TNO, Utrecht, The Netherlands

Gianni Tinarelli ARIANET Srl, Milan, Italy

Velle Toll Institute of Physics, University of Tartu, Tartu, Estonia

Fausto Tomei ARPA, Bologna, Italy

Rodica Tomozeiu ARPA, Bologna, Italy

Daniel Tong Air Resources Laboratory (ARL), NOAA, College Park, MD, USA; Cooperative Institutes for Satellite and Climate, University of Maryland, College Park, MD, USA; Center for Spatial Information Science and Systems, George Mason University, Fairfax, VA, USA

Ennio Tosi University of Bologna UNIBO, Bologna, Italy

Oleg Travnikov Meteorological Synthesizing Center-East of EMEP, 8/5, Moscow, Russia

Silvia Trini Castelli Institute of Atmospheric Sciences and Climate, National Research Council, Turin, Italy

S. Trivikrama Rao North Carolina State University, Raleigh, NC, USA

Carlo Trivisano University of Bologna, Bologna, Italy

Dennis Trolle Department of Bioscience, Aarhus University, Aarhus, Denmark

Ioannis Tsagatakis Ricardo-AEA, London, UK

G. Tsegas Laboratory of Heat Transfer and Environmental Engineering, Aristotle University, Thessaloniki, Greece

Svetlana Tsyro EMEP MSC-W, Norwegian Meteorological Institute, Oslo, Norway

P. Tulet LACY, UMR 8105 CNRS/Université La Réunion/Météo-France, Réunion, France

Enrico Turrini Department of Mechanical and Industrial Engineering, University of Brescia, Brescia, Italy

Rafał Ulańczyk Institute of Environmental Protection–National Research Institute, Warsaw, Poland

Sikchya Upadhayay National Oceanic and Atmospheric Administration (NOAA), Washington, USA; Syneren Technologies Corporation, Arlington, USA

Line Vancraeynest VMM, Flemish Environment Report (MIRA), Aalst, Belgium

Addo van Pul RIVM, Bilthoven, BA, The Netherlands

H. Denier van der Gon Department of Climate, Air and Sustainability, TNO, Netherlands Organization for Applied Research, Utrecht, The Netherlands

Eric van der Swaluw RIVM, Bilthoven, BA, The Netherlands

K. Vandermeiren CODA-CERVA Veterinary and Agrochemical Research Centre, Tervuren, Belgium

Charlotte Vanpoucke IRCEL-CELINE, Brussels, Belgium

R. Vautard Laboratoire des Sciences du Climat et de l'Environnement, LSCE, CEA-CNRS-UVSQ, Gif-sur-Yvette, France

Guus Velders RIVM, Bilthoven, BA, The Netherlands

Akula Venkatram Department of Mechanical Engineering, University of California, Riverside, CA, USA

Jordy Vercauteren VMM, Antwerp, Belgium

Robert Vet Air Quality Research Division, Environment Canada, Toronto, ON, Canada

P. Viaene VITO Flemish Institute for Technological Research, Mol, Belgium

M. Viana Institute for Environmental Assessment and Water Research (IDÆA-CSIC), Barcelona, Spain

Massimo Vieno Centre for Ecology & Hydrology, Edinburgh, UK

Giulia Villani ARPA, Bologna, Italy

J. Vincent LISA,UPEC-UDDP7-CNRS, IPSL, Créteil, France

Roxanne Vingarzan Air Quality Research Unit, Meteorological Service of Canada, Environment Canada, Vancouver, BC, Canada

Julius Vira Finnish Meteorological Institute, Helsinki, Finland

Lina Vitali Laboratory for Atmospheric Pollution, ENEA—Bologna Research Center, Bologna, Italy

Marialuisa Volta Department of Mechanical and Industrial Engineering, University of Brescia, Brescia, Italy

Stijn Vranckx VITO, Mol, Belgium

Tim Wade Office of Research and Development, U.S. Environmental Protection Agency, RTP, Durham, NC, USA

Jun Wang NOAA/NCEP/EMC, College Park, MD, USA

L. Watson CNRM-GAME, Météo France/CNRS, Toulouse, France

Kinga Wałaszek Department of Climatology and Atmosphere Protection, University of Wroclaw, Wroclaw, Poland

Xiao Wei Research and Teaching Center in Atmospheric Environment (CEREA), EDF R&D, Chatou, France

A. Weigelt Helmholtz-Zentrum Geesthacht, Institute of Coastal Research, Geesthacht, Germany

Benjamin Weinstein Department of Earth, Ocean and Atmospheric Sciences, The University of British Columbia, Vancouver, BC, Canada

J. Werhahn Institute for Meteorology and Climate Research (IMK-IFU), Karlsruhe Institute of Technology (KIT), Garmisch-Partenkirchen, Germany

Małgorzata Werner Department of Climatology and Atmosphere Protection, University of Wroclaw, Wroclaw, Poland; National Pollen and Aerobiology Research Unit, University of Worcester, Worcester, UK

Mark Whitmire Noblis, Falls Church, VA, USA

Roy Wichink Kruit Department Climate, Air Quality and Sustainability, TNO, Utrecht, TA, The Netherlands; RIVM, Bilthoven, MA, The Netherlands

W. Wobrock Laboratoire de Météorologie Physique, Université Clermont Auvergne, Université Blaise Pascal, Clermont-Ferrand, France; CNRS, INSU, UMR 6016, LaMP, Aubière, France

Ralf Wolke Leibniz Institute for Tropospheric Research (TROPOS), Leipzig, Germany

David Wong Atmospheric Modeling and Analysis Division, National Exposure Research Laboratory, U.S. Environmental Protection Agency, RTP, Durham, NC, USA

May Woo Boston University School of Public Health, Boston, MA, USA

Matthew Woody University of North Carolina at Chapel Hill, Chapel Hill, NC, USA

Jia Xing Atmospheric Modeling and Analysis Division, National Exposure Research Laboratory, U.S. Environmental Protection Agency, RTP, Durham, NC, USA

Xiangnan Xing ORISE, Oakridge National Laboratory, Oak Ridge, TN, USA

Tetsuji Yamada YSA, Santa Fe, NM, USA

Jaemo Yang Department of Civil & Environmental Engineering, University of Connecticut, Storrs-Mansfield, CT, USA

R. Žabkar University Ljubljana, SPACE-SI, Ljubljana, Slovenia

Marianne Zandersen Department of Environmental Science, Aarhus University, Aarhus, Denmark

Junhua Zhang Air Quality Research Division, Environment Canada, Toronto, ON, Canada

Q. Zheng Air Quality Research Division, Environment Canada, Toronto, ON, Canada

Jialei Zhu Nanjing University, Nanjing, China

Shupeng Zhu CEREA, Joint Laboratory Ecole Des Ponts ParisTech - EDF R&D, Université Paris-Est, Champs-sur-Marne, France

Part I
Aerosols in the Atmosphere

Chapter 1
Aerosols in the Atmosphere: Sources, Transport, and Multi-decadal Trends

Mian Chin, Thomas Diehl, Huisheng Bian and Tom Kucsera

Abstract We present our recent studies with global modeling and analysis of atmospheric aerosols. We have used the Goddard Chemistry Aerosol Radiation and Transport (GOCART) model and satellite and in situ data to investigate (1) long-term variations of aerosols over polluted and dust source regions and downwind ocean areas in the past three decades and the cause of the changes and (2) anthropogenic and volcanic contributions to the sulfate aerosol in the upper troposphere/lower stratosphere.

1.1 Introduction

Aerosols are liquid or solid particles suspended in the air with typical diameters ranging from a few nanometers (10^{-9} m) to a few tens of micrometers (10^{-6} m). Source of aerosols includes desert and soil dust, wildfire smoke, sea salt particles produced mainly by breaking bubbles in the ocean spray, volcanic eruption, and anthropogenic activities. Major aerosol species in the troposphere are dust, sea salt, black carbon (BC), organic carbon (OC) or sometime called particulate organic matter (POM), sulfate, and nitrate. A large fraction of aerosols is natural in origin, including desert dust, wildfire smoke, sea salt, and volcanic aerosols, whereas

M. Chin (✉) · T. Diehl · H. Bian · T. Kucsera
Atmospheric Chemistry and Dynamics Laboratory, NASA Goddard Space Flight Center, Greenbelt, MD, USA
e-mail: mian.chin@nasa.gov

T. Diehl
Joint Research Center, Ispra, Italy

H. Bian
University of Maryland Baltimore County, Baltimore, MD, USA

T. Kucsera
Universities Space Research Association, Columbia, MD, USA

D.G. Steyn and N. Chaumerliac (eds.), *Air Pollution Modeling and its Application XXIV*, Springer Proceedings in Complexity,
DOI 10.1007/978-3-319-24478-5_1

others are from human activities, such as fossil fuel combustions from industries and energy use, agriculture land cleaning, and transportation.

Aerosols are removed from the atmosphere by wet and dry depositions that establish average tropospheric aerosol lifetimes at about a few days. Despite their relatively short lifetimes, aerosols originating from one region can travel long distances to affect the environment of downwind regions. This transport demonstrates the hemispheric to global scope of aerosol influences.

Aerosols exert a variety of impacts on the environment. Aerosol particles (aka particulate matter or PM) have long been recognized to affect human health and visibility. Aerosols also have climate effects by interactions with solar and terrestrial radiation and with cloud and precipitation. The net cooling effects caused by aerosols is believed to mask the warming effects caused by greenhouse gases. However, the challenging of quantifying the aerosol climate effects arises from the immerse diversity of aerosols (not only in particle sizes, composition, and origin, but also in the highly variable spatial and temporal distributions), the multifaceted atmospheric processes of aerosol formation and removal, and the complex physical, chemical, and optical properties of aerosol particles. One consequence of this heterogeneity is that the aerosol impacts must be understood and quantified on a regional rather than just a global-average basis.

Anthropogenic activities have caused considerable changes in aerosol composition and loading. Historical emission inventories have estimated that trends in anthropogenic emission are closely tied to economic growth, population density, and technological development, which may explain the regional aerosol variability shown in the long-term observation records. For example, aerosol optical depth (AOD) trends from the satellite and surface-based observations suggest that in the past three decades, the amount of anthropogenic aerosol has de-creased over North America and Europe due to enforced emission control policy, but has increased over East and South Asia due to the fast economic development. This increase of Asian pollution in the past decade was suggested to be responsible to cause the observed increasing trends of aerosol extinction in the stratosphere via the efficient Asian monsoon convective transport; however, the quantification is difficult because of the frequent injection of volcanic clouds to the upper troposphere and lower stratosphere (UTLS) that could overwhelm the signal of Asian pollution in the stratosphere.

Global chemistry transport models are essential tools to integrate our current knowledge of emissions and atmospheric processes of aerosols, analyze remote sensing and in situ observations, and assess the impact in the past, present, and future climate scenarios. We present here our recent studies using the Goddard Chemistry Aerosol Radiation and Transport (GOCART) model and observations on (1) multi-decadal variations of aerosol concentrations and AOD over different regions and (2) anthropogenic and volcanic contributions to the stratospheric aerosols. We will first introduce the GOCART model simulations of atmospheric aerosols and describe the observation datasets, then present the results and analysis, followed by conclusions.

1.2 GOCART Model Simulation of Aerosols in the Atmosphere

The GOCART model is a chemistry transport model driven by the assimilated meteorological fields from the NASA Modern Era Reanalysis for Research and Applications (MERRA). The horizontal resolution of model simulation in this work is at 1.25° longitude by 1° latitude (or 2.5° by 2° for the 30-year simulation) and 72 vertical levels from the surface to 0.01 hPa. Aerosol simulations in GOCART include sulfate, dust, BC, OC, and sea-salt, and the sulfate precursor gas species of SO_2 and dimethyl sulfide (DMS). The "building blocks" of the model include emissions from anthropogenic and natural sources, advection, shallow and deep convections, dry deposition, wet scavenging, and chemical transformation. Aerosol particle sizes are parameterized as a function of relative humidity. Aerosol optical properties, such as extinction, absorption, backscattering, are calculated from the refractive indices and size distributions, both depending on the type of aerosols and wavelengths.

Emissions of SO_2, BC, and OC from fossil fuel and biofuel combustions and biomass burning are taken from the existing emission inventories (A2-ACCMIP, Diehl et al. 2012 or more recent HTAP emission, http://htap.org). Volcanic SO_2 emissions are taken from a recent compilation that includes emission amounts and plume heights based on the volcanic activity database from the Smithsonian Institution's Global Volcanism Program, the satellite observations of SO_2 from the Total Ozone Mapping Spectrometer (TOMS) and the Ozone Monitoring Instrument (OMI), and ancillary information from other observations reported in the literature (Diehl et al. 2012). Dust emissions are calculated as a function of surface topography, surface bareness, 10-m wind speed, and ground wetness (Ginoux et al. 2001). Sea salt and DMS emissions from the ocean are calculated as a function of 10-m wind speed (also the sea water concentration of DMS for calculating DMS emissions). Biogenic source of OC is parameterized as a fraction of monoterpene emission. More detailed description of GOCART model can be found in our previous publications (Chin et al. 2002, 2009, 2014 and references therein.).

1.3 Observations

Aerosol data products from remote sensing and in situ measurements, together with associated time periods and measured quantities used in this study are listed in Table 1.1. They include AOD from satellite observations by AVHRR, TOMS, SeaWiFS, MISR, MODIS, UTLS aerosol extinction profile from SCHIAMACHY and CALIOP, column SO_2 from OMI, and surface concentration from the IMPROVE, EMEP, and University of Miami networks and in the Arctic. All data used in this study are monthly averages.

Table 1.1 Observation data used in this study

Dataset	Location	Period
Satellite AOD		
AVHRR-CDR	Global, ocean	1981–2009
AVHRR-GACP	Global, ocean	1981–2005
TOMS	Global, land + ocean	1980–1992, 1996–2001
SeaWiFS	Global, land + ocean	1997–2009
MISR	Global, land + ocean	2000–2009
MODIS-Terra	Global, land + ocean	2000–2009
MODIS-Aqua	Global, land + ocean	2002–2009
Satellite SO_2 and UTLS aerosol extinction profile		
OMI SO_2	Global	2004–2009
SCHIAMACHY ext.	UTLS	2002–2009
CALIOP ext.	UTLS	2006–2009
Surface aerosol species concentrations		
IMPROVE	U.S.	1988–2007
EMEP	Europe	1980–2008
Arctic	Arctic	1980–2009
Univ. Miami	Islands or coast	1980–2009

1.4 Multi-decadal Aerosol Variations Over Land and Ocean Regions

We divide the globe into 15 land, 12 ocean, and 2 polar regions in our analysis, although in this talk we focus mostly on the NH major pollution source regions, namely USA, Europe, East Asia, and South Asia, the major dust regions of Sahara and Sahel, and their immediate downwind oceanic regions. Note that East Asia and South Asia also contain considerable dust source areas. To investigate the regional trends, we first compare the AOD time series from satellite retrievals and model simulations over these regions (unfortunately the reliable satellite retrievals over land are only available after 1998). The most pronounced feature during the 30-year time period is the worldwide influence of large volcanic eruptions of El Chichón in 1982 and Pinatubo in 1991; sulfate aerosols formed from these big volcanic eruptions can last for several years. For the periods lacking major volcanic influence (i.e., in the mid- to late 1980s and in the 2000s), there is a decreasing AOD trend over the pollution source regions of USA and Europe, and the model shows that such a decrease is mostly driven by the decline of aerosol from combustion AOD, in line with the fossil fuel/biofuel emission reduction trends in these regions. The reduction over Europe is particularly remarkable with the total and combustion AOD in the late 2000s are only about half and one-third of their corresponding values in the early 1980s from. In contrast, over East and South Asia the

combustion AOD has increased significantly by 40 and 120 %, respectively, for the same period of time. However, the overall increase of total AOD is less than 20 % in East and South Asia because of the relatively large amount of dust aerosols in these regions that either have negligible trend (in East Asia) or a decreasing trend (in South Asia) to mask the increasing trend of anthropogenic AOD. The decrease of aerosols over the US and Europe is further corroborated by the long-term surface concentrations measurements from the IMPROVE and EMEP networks.

Over the dust source regions, the model shows a general decreasing trend of dust AOD in Sahara and Sahel since the mid-1980s, but an upward trend in Middle East in the 2000s. There results are consistent with the satellite observations that are mostly available since 2000. Although there are noticeable differences in satellite data over the ocean, one consistent and persistent feature is the decrease of AOD over the tropical North Atlantic in the past three decades. This weakening of dust transport from North Africa to the North Atlantic is also evident in the long-term surface dust concentration record at Barbados where the dust is predominantly from North Africa via trans-Atlantic transport. The decrease of dust over North Africa and tropical North Atlantic can be attributed to the weakening of surface winds over North Africa that has suppressed the dust emission, and the increase of precipitation over the ocean that has made scavenging of dust more efficient. Such meteorological condition shifts are closely connected to the warming of the sea surface in the past three decades.

Despite significant changes of aerosol levels over many regions, model-calculated global average AOD show little trends over the 30 years, because a global averaged number conceals not only the opposing regional changes but also the large spatial inhomogeneity of aerosols. Therefore, assessing aerosol impacts should be done on regional-scale analysis.

1.5 Anthropogenic and Volcanic Contributions to the Decadal Stratospheric Aerosol Change

The fast economic growth in South and East Asia in recent decades has led to an accelerated increase of pollutant emissions. During the summer monsoon season, deep convection can transport pollutants from the boundary layer to the UTLS, evidently shown in the satellite observations of enhanced CO and aerosol in the UTLS region, which led to an hypothesis that the Asian pollution may have caused the increase of stratospheric aerosol levels (Hofmann et al. 2009). On the other hand, volcanic eruptions can inject SO_2 directly into the upper troposphere and stratosphere to produce sulfate aerosols at high altitudes where residence time is much longer, making a disproportionately larger contribution than anthropogenic sources to the aerosol loading in the UTLS compared to their respective emission strengths. To assess the relative contributions of anthropogenic versus volcanic sources to the UTLS aerosols in the last decade, we have performed three model

experiments: (a) base simulation with all emissions, (b) simulation without anthropogenic emissions, and (c) simulation without volcanic emissions. The difference between (a) and (b) is the anthropogenic contribution and between (a) and (c) is the volcanic contribution to the total aerosol loading.

Our base simulations of SO_2 from anthropogenic and volcanic sources are compared with satellite observations from the OMI instrument on the Aura satellite, and UTLS aerosol extinction profiles with the SCHIAMACHY instrument on the European ENVISAT satellite and CALIOP on CALIPSO satellite. The model captures the volcanic events that had large impact on stratospheric aerosol detected by satellite, although discrepancy exists on the absolute magnitude. With the tagged simulations isolating the volcanic and anthropogenic contributions, it is clear that the stratospheric aerosol is overwhelmingly volcanic origin in the past decade (2000–2009). Although the ratio of volcanic/anthropogenic SO_2 emission is only 1:4 on decadal average, the ratio of corresponding stratospheric sulfate amounts is disproportionally 2:1, due to the high altitude injections of volcanic emissions. On the other hand, Asian anthropogenic aerosol does seem to show an increasing trend, in the UTLS region, but its influence is mostly confined in the upper troposphere with well-organized seasonal variations. The model suggests that the volcanic sources could be more responsible than the anthropogenic sources for the apparent increasing trend of stratospheric aerosol in the past decade at certain locations.

1.6 Conclusions

We have presented our recent studies on the decadal to multi-decadal aerosol variations in different regions of the world, estimated the anthropogenic and natural source contributions to these changes, and assess the impact of long-range transport of aerosol from the polluted source regions to the receptor regions. We have found:

Over land regions dominated by pollution aerosols, the 30-year AOD and surface concentration trends are generally consistent with the direction of the regional pollutant emission changes, with aerosol decreasing in USA and Europe but increasing in South Asia and East Asia. Over the Arctic, the model and long-term surface measurements show a significant decrease of sulfate concentrations since the early 1990s, aligned with the decreasing trends over Europe.

There is a general decreasing trend of dust over North Africa and downwind regions in the tropical North Atlantic in the past 30 years, which is driven by the reduction of dust emission in North Africa and an increase of precipitation over the North Atlantic, both likely the results of a North Atlantic Ocean warming trend that has lead to the changes in atmospheric circulation and precipitation.

Despite the significant changes over many regions, model-calculated global averaged AOD values show little trends over land and ocean on a global, annual scale, because increases and decreases in different land regions tend to cancel each other in the global average and little changes occur over large open ocean areas. A globally averaged number conceals not only opposing regional changes but also

the large spatial inhomogeneity of aerosols. This highlights the need for regional-scale analyses, as global average values are not sufficient for assessing aerosol trends and impacts.

Both satellite data and model have shown that even without major explosive volcanic eruptions, volcanic emissions frequently perturb the stratospheric "background" aerosols, making it difficult to define non-volcanic background aerosol values in the stratosphere. Overall, volcanic aerosol is twice as much as the anthropogenic aerosol in the stratosphere in the past decade, which could be more responsible for the decadal increase trend of stratospheric aerosols observed in certain locations.

Acknowledgments We gratefully acknowledge the satellite groups (AVHRR, TOMS, SeaWiFS, MISR, MODIS, CALIOP, SCHIMACHY, OMI) and observation networks (IMPORVE, EMEP, University of Miami) for the aerosol data used in this work, and support by NASA MAP, Aura, and ACMAP programs.

Question and Answer

Questioner: Ivanka Stajner

Question: In the comparison for early years AVHRR and TOMS data are used giving different trends over oceans. Are these data of trend-quality? What are the particular retrieval data sets? Can different sensitivity of AVHRR and TOMS to aerosol composition explain different trends?

Answer: These earlier datasets were not designed for detecting aerosols, therefore the retrieval ability and data quality of the aerosol products suffer by several limitations of the instruments. For example, AVHRR does not provide the aerosol retrieval over land and TOMS has to exclude large amount of data that are affected by the clouds. Nonetheless, the AVHRR Climate Data Record dataset we used in this study has been created for the purpose of assessing aerosol trends, albeit only over oceans. TOMS data, on the other hand, are used mainly for features, not for quantitative assessment. The positive oceanic aerosol trends from TOMS is within the uncertainty range of the TOMS data, particularly over the low AOD areas, so it should not be referred as "trends". Over high AOD regions such as high dust and pollution areas, trends from TOMS are consistent with the expected AOD changes.

Questioner: S.T. Rao

Question: From your analysis, what can you say about the aerosol impact on climate from volcanoes versus anthropogenic forcings given different residence times of aerosols from these two sources? How do you attribute aerosols from anthropogenic or volcanic sources?

Answer: Volcanic effects are mostly in the free troposphere and lower stratosphere because of the emission injection heights, in contrast with the near-surface anthropogenic emissions. However, volcanic aerosol have longer lifetime than

anthropogenic aerosol, mainly because they are located far above the surface thus not subject to efficient dry and wet removals. Globally, volcanic forcing is much smaller than the anthropogenic forcing, but in the UTLS it can be the dominant aerosol component. We use the model to separate volcanic and anthropogenic aerosols by "tagging" the emission sources.

Questioner: Jose M. Maldasano

Question: In the results presented with respect to the Middle East area, it has indicated that the AOD had increase in the past ten to fifteen years due to mineral dust, when in that area in recent years has been the Iraq and Syria wars, and also a strong urban and industrial development in all gulf countries, has an explanation for this? Was threshold value has been used to discriminate the AOD due to mineral dust?

Answer: The Middle East AOD increase in the past decade has been observed by satellite data. The Angstrom exponent from the ground-based AERONET observations over the Middle East shows that such an increase is mainly due to the coarse-mode dust aerosols, indicated by the decreasing of the Angstrom exponent in the past decade. Our model simulation supports such findings with our tagged source simulations that show the AOD increase over the Middle East is mainly due to the increase of dust rather than anthropogenic aerosols.

References

Chin M, Ginoux P, Kinne S, Torres O, Holben BN, Duncan BN, Martin RV, Logan JA, Higurashi A, Nakajima T (2002) Tropospheric aerosol optical thickness from the GOCART model and comparisons with satellite and sunphotometer measurements. J Atmos Sci 59:461–483

Chin M, Diehl T, Dubovik O, Eck TF, Holben BN, Sinyuk A, Streets DG (2009) Light absorption by pollution, dust and biomass burning aerosols: a global model study and evaluation with AERONET data. Ann Geophys 27:3439–3464

Chin M, Diehl T, Tan Q et al (2014) Multi-decadal aerosol variations from 1980 to 2009: a perspective from observations and a global model. Atmos Chem Phys 14:3657–3690

Dieh T, Heil A, Chin M, Pan X, Streets DG, Schultz M, Kinne S (2012) Anthropogenic, biomass burning, and volcanic emissions of black carbon, organic carbon, and SO_2 from 1980 to 2010 for hindcast model experiments. Atmos Chem Phys Discuss 12:24895–24954

Ginoux P, Chin M, Tegen I, Prospero J, Holben B, Dubovik O, Lin S-J (2001) Sources and global distributions of dust aerosols simulated with the GOCART model. J Geophys Res 106:20255–20273

Hofmann D, Barnes J, O'Neill M, Trudeau M, Neely R (2009) Increase in background stratospheric aerosol observed with lidar at Mauna Loa Observatory and Boulder, Colorado. Geophys Res Lett 36:L15808. doi:10.1029/2009GL039008

Chapter 2
Modelling Organic Aerosol in Europe: Application of the CAMx Model with a Volatility Basis Set Within the Eurodelta III Exercise

Giancarlo Ciarelli, Sebnem Aksoyoglu, André S.H. Prévôt and Urs Baltensperger

Abstract In the framework of EURODELTAIII model inter-comparison exercise (Bessagnet et al. 2014), we performed preliminary tests with a volatility basis set (VBS) scheme in the CAMx model to predict the fine organic aerosol concentrations in Europe during one of the EMEP measurement campaigns (February–March 2009). In addition to the traditional (no VBS) approach for organic aerosol modelling, two different assumptions regarding the volatility distribution of primary organic particles were simulated and results compared against aerosol mass spectrometer (AMS) measurements. For the period studied in this work, using the volatility proposed by Robinson et al. (2007) decreased OA concentrations while volatility distribution according to Tsimpidi et al. (2010), Shrivastava et al. (2011) improved the results by about 27 %.

2.1 Introduction

Traditional Chemical Transport Models (CTMs) treat POA as non-volatile. (Aksoyoglu et al. 2011). Various recent studies however, have revealed the semi-volatile nature of POA, through its dynamic equilibrium of organic aerosol with its gasphase, and the importance of semi-volatile (SVOC) and intermediate volatility (IVOC) organic compounds as SOA precursors (Robinson et al. 2007; Donahue et al. 2006). In order to describe the absorptive partitioning and ongoing oxidation of the atmospheric material, a volatility basis set (VBS) where organic species are organized into surrogates according to their volatility was developed and started to be used in models (Donahue et al. 2011, 2012). In this study, we

G. Ciarelli · S. Aksoyoglu (✉) · A.S.H. Prévôt · U. Baltensperger
Laboratory of Atmospheric Chemistry, Paul Scherrer Institute (PSI), 5232 Villigen, Switzerland
e-mail: sebnem.aksoyoglu@psi.ch

D.G. Steyn and N. Chaumerliac (eds.), *Air Pollution Modeling and its Application XXIV*, Springer Proceedings in Complexity,
DOI 10.1007/978-3-319-24478-5_2

applied the CAMx model with VBS approach (Koo et al. 2014) to an EMEP measurement campaign period in Europe to investigate effects of two different VBS parameterization on modeled OA concentrations.

2.2 Simulation Setup

Simulations with CAMx-VBS (version CAMx5.41_VBS) (from Environ) were performed for the period between 25.02.2009 and 26.03.2009. The model domain consists of one grid covering Europe with a horizontal resolution of 0.25° × 0.25°. The latitude and longitude grid extended from 25.125°W to 45.125°E and 29.875° N to 70.125°N resulting in 281 by 161 grid cells with a total number of 33 sigma-layers. Meteorological fields required by CAMx are calculated from ECMWF data (http://www.ecmwf.int/), using the IFS dataset provided by the EURODELTAIII community at 0.2° resolution. Annual total gridded anthropogenic emissions were prepared and provided by INERIS (Institut National de l'Environnement Industriel et des Risques) within the EURODELTAIII model intercomparison exercise at 0.25° × 0.25° resolution and combined with biogenic emissions calculated using the Model of Emissions of Gases and Aerosols from Nature, MEGANv2.1.

2.3 Organic Aerosol Chemistry in CAMx-VBS

Wood burning and hydrocarbon-like emissions were allocated in two different primary sets consisting of five volatility bins ranging from 10^{-1} to 10^{3} μg m^{-3} in saturation concentrations (C*). Two other sets are used in the model to allocate secondary organic aerosol (SOA) from anthropogenic (ASOA) (e.g. xylene and toluene) and biogenic (e.g. isoprene, monoterpenes) precursors (BSOA). These sets also allocate oxidation products from POA vapours, i.e. oxidized primary organic aerosol (OPOA). The 2D volatility space retrieved by Donahue et al. (2011, 2012) was used to distribute the organic molecular structures for each of the bins and sets. Oxidation processes are modelled by shifting C* by a factor of 10 in the next lower volatility bin, increasing the oxidation state and reducing the carbon number to account for fragmentation. OH reaction rates are assumed to be 4×10^{-11} cm^3 $molecule^{-1}$ s^{-1} for the reaction of POA vapors with OH and 2×10^{-11} cm^3 $molecule^{-1}$ s^{-1} for aging of anthropogenic secondary organic aerosol (ASOA). Aging of BSOA and wood burning vapours are currently under investigation.

Two sensitivity tests were performed in order to constrain the amount of semi-volatile oganic compounds SVOCs: for the first one, POA emissions were distributed following the volatility distribution proposed by Robinson et al. (2007) (scenario S2), whereas in the second test the volatility distribution estimated from ambient measurement data in Mexico City was used (scenario S3) (Tsimpidi et al.

2010; Shrivastava et al. 2011). Intermediate volatile organic compounds (IVOCs) were assumed to be 1.5 × POA for both cases. The sensitivity tests were compared to a base case scenario where no VBS scheme was considered (S1 scenario). Thus, a total of 3 different scenarios were evaluated.

2.4 Results

Model results were evaluated against data from HR-ToF-AMS of non-refractory submicron particulate matter and positive matrix factorization analysis (PMF) at 10 sites in Europe during the EUCAARI intensive measurement campaign (Crippa et al. 2014). The scatter plots in Figs. 2.1 and 2.2 show comparison of daily average organic aerosol (OA) concentrations during February–March 2009. When the semi-volatile dynamics of primary organic aerosol is not taken into account (scenario S1), the model under-predicts OA concentrations by about −71 % (MFB) with an observed and modelled average concentrations of 3.05 μg m^{-3} and 1.19 μg m^{-3} respectively (Fig. 2.1). In the S2 scenario POA emissions are allowed to evaporate following the volatility distribution proposed by Robinson et al. (2007) and to undergo chemical oxidation. In this case modelled OA concentration decreases by about 44 % with respect to S1, predicting an average OA concentration of 0.67 μg m^{-3} (Fig. 2.2). On the other hand, the S3 scenario based on ambient measurement data, improved OA model performance reducing the mean

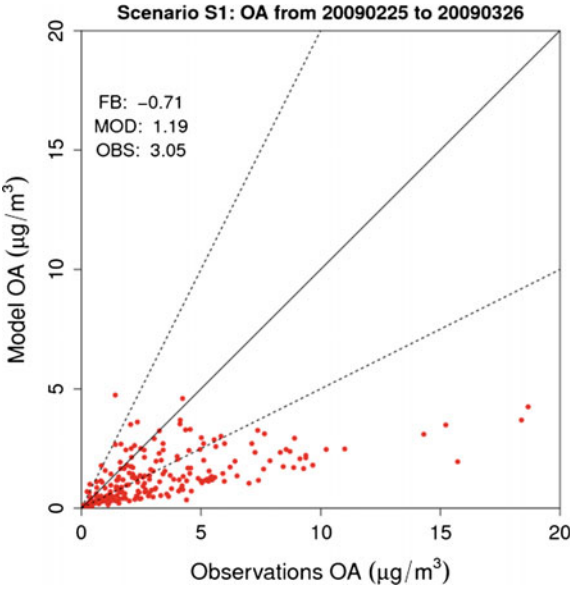

Fig. 2.1 Modelled organic aerosol (OA) daily average for S1 scenario versus measurements during the 2009 EUCAARI measurement campaign (Crippa et al. 2014). *Solid lines* indicate the 1:1 line. *Dotted lines* are the 1:2 and 2:1

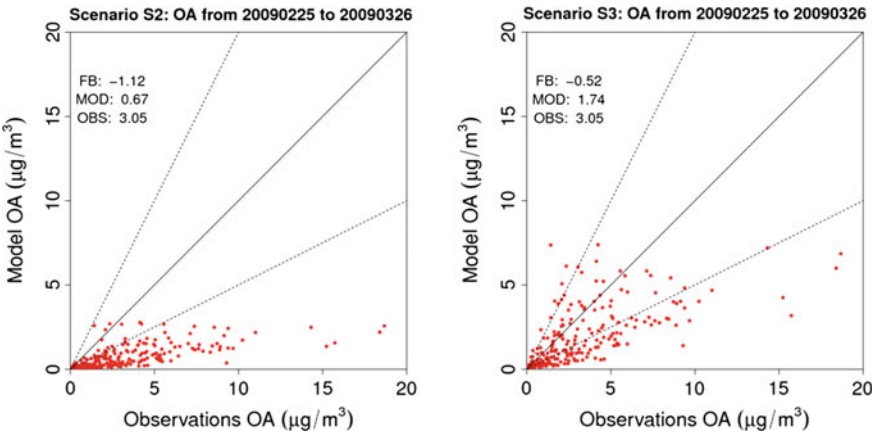

Fig. 2.2 Modelled organic aerosol (OA) daily average for S2 and S3 scenarios versus measurements during the 2009 EUCAARI measurement campaign (Crippa et al. 2014). *Solid lines* indicate the 1:1 line. *Dotted lines* are the 1:2 and 2:1

fractional bias by about 27 % respect to S1. Predicted OA concentrations were found to be 1.74 µg m^{-3} on average (Fig. 2.2).

2.5 Conclusions

Three different parameterizations for treating organic aerosol in the CAMx model were evaluated. Including evaporation and oxidation processes of primary organic particles with the volatility distribution proposed by Robinson et al. (2007), lowered the modelled OA mass with respect to the non-volatile scenario (S1). On the other hand, volatility distribution based on ambient measurements, scenario S3, (Tsimpidi et al. 2010; Shrivastava et al. 2011) brought model and observations in a better agreement by reducing the negative bias for OA by about 27 %. However, for this study, the assumed amount of SVOCs is poorly constrained and, in the absence of specific emissions data, it represents often a crude method for taking into account semi-volatile material. Uncertanties also remain in terms of amount of IVOC constrained and aging processes parameterization. Further sensitivity tests are planned to investigate their effect on the modelled organic aerosol.

Acknowledgments This work was financially supported by the Swiss Federal Office for the Environment (FOEN). We are grateful to ENVIRON for providing us with the CAMx VBS and the EURODELTA community for proving model input data.

Questioner: P. Builtjes

Question: You compared the results of non-VBS against VBS-aging for station in Europe. Did you see any differences in improvement between rural and urban-type stations?
Answer: There is one site classified as urban and with elevated organic concentration which is the site of Barcelona. For this site total OA concentrations increase is in general higher than the increase at rural sites. Effects of further aging of BSOA and wood burning vapours are currently under investigation.

References

Aksoyoglu S, Keller J, Barmpadimos I, Oderbolz D, Lanz VA, Prévôt ASH, Baltensperger U (2011) Aerosol modelling in Europe with a focus on Switzerland during summer and winter episodes. Atmos Chem Phys 11:7355–7373

Bessagnet B, Colette A, Meleux F, Rouïl L, Ung A, Favez O, Cuvelier C, Thunis P, Tsyro S, Stern R, Manders A, Kranenburg R, Aulinger A, Bieser J, Mircea M, Briganti G, Cappelletti A, Calori G, Finardi S, Silibello C, Ciarelli G, Aksoyoglu S, Prévôt A, Pay M-T, Baldasano JM, García Vivanco M, Garrido JL, Palomino I, Martín F, Pirovano G, Roberts P, Gonzalez L, White L, Menut L, Dupont J-C, Carnevale C, Pederzoli A (2014) The EURODELTA III exercise "Model evaluation with observations issued from the 2009 EMEP intensive period and standard measurements in Feb/Mar 2009". MSC-W Technical Report

Crippa M, Canonaco F, Lanz VA, Äijälä M, Allan JD, Carbone S, Capes G, Ceburnis D, Dall'Osto M, Day DA, DeCarlo PF, Ehn M, Eriksson A, Freney E, Hildebrandt Ruiz L, Hillamo R, Jimenez JL, Junninen H, Kiendler-Scharr A, Kortelainen A-M, Kulmala M, Laaksonen A, Mensah AA, Mohr C, Nemitz E, O'Dowd C, Ovadnevaite J, Pandis SN, Petäjä T, Poulain L, Saarikoski S, Sellegri K, Swietlicki E, Tiitta P, Worsnop DR, Baltensperger U, Prévôt ASH (2014) Organic aerosol components derived from 25 AMS data sets across Europe using a consistent ME-2 based source apportionment approach. Atmos Chem Phys 14:6159–6176

Donahue NM, Robinson AL, Stanier CO, Pandis SN (2006) Coupled partitioning, dilution, and chemical aging of semivolatile organics. Environ Sci Technol 40:2635–2643

Donahue NM, Epstein SA, Pandis SN, Robinson AL (2011) A two-dimensional volatility basis set: 1. organic-aerosol mixing thermodynamics. Atmos Chem Phys 11:3303–3318

Donahue NM, Kroll JH, Pandis SN, Robinson AL (2012) A two-dimensional volatility basis set e part 2: diagnostics of organic-aerosol evolution. Atmos Chem Phys 12:615–634

Koo B, Knipping E, Yarwood G (2014) 1.5-Dimensional volatility basis set approach for modeling organic aerosol in CAMx and CMAQ. Atmos Environ 95:158–164

Robinson AL, Donahue NM, Shrivastava MK, Weitkamp EA, Sage AM, Grieshop AP, Lane TE, Pierce JR, Pandis SN (2007) Rethinking organic aerosol: semivolatile emissions and photochemical aging. Science 315:1259–1262

Shrivastava M, Fast J, Easter R, Gustafson WI Jr, Zaveri RA, Jimenez JL, Saide P, Hodzic A (2011) Modeling organic aerosols in a megacity: comparison of simple and complex representations of the volatility basis set approach. Atmos Chem Phys 11:6639–6662

Tsimpidi AP, Karydis VA, Zavala M, Lei W, Molina L, Ulbrich IM, Jimenez JL, Pandis SN (2010) Evaluation of the volatility basis-set approach for the simulation of organic aerosol formation in the Mexico City metropolitan area. Atmos Chem Phys 10:525–546

Chapter 3
The Role of Aerosols in Low and Upper Atmospheric Layers Condensation

George Kallos, Jonilda Kushta, Nikolaos Bartsotas, Platon Patlakas, Marina Astitha and Jumaan Al Qahtani

Abstract Airborne particles of anthropogenic and/or natural origin have certain direct and indirect effects in the atmosphere. Radiative transfer is the category of processes related to aerosols and clouds (direct effects). Indirect effects are always associated with condensates at various atmospheric layers. Condensation within the tropospheric layers is mainly related to aerosol physical and chemical properties, thermodynamical and dynamical processes. As it was found in various studies, there is a strong relationship between aerosols and extreme weather events such as deep convection and extreme rainfall. Low-level condensation is associated with low-cloud formation and fog. In this presentation we will discuss the condensation processes within the lower and upper troposphere and how they are affected by the various types of aerosols. New model development related to nucleation processes and condensation at different levels is discussed. The model used for development and application is the fully-coupled atmospheric modeling system RAMS/ICLAMS. Model simulations have been performed for selected cases related to (i) extreme precipitation events and (ii) low-level condensation and fog formation in the Euro-Mediterranean and Arabian Peninsula. The sensitivity tests showed that the explicit activation of aerosols as CCN and IN causes changes in the precipitation distribution as well as in its spatiotemporal patterns. Fog formation near the coastline and low-cloud formation mechanisms are controlled by the thermal cooling and moisture evaporation by the surface. The accurate simulation of the microphysical processes involved in formation and dissipation of fog depends on several variables.

G. Kallos (✉) · J. Kushta · N. Bartsotas · P. Patlakas
Atmospheric Modeling and Weather Forecasting Group, University of Athens, School of Physics, University Campus, Bldg PHYS-V, 15784 Athens, Greece
e-mail: kallos@mg.uoa.gr

M. Astitha
Department of Civil and Environmental Engineering, University of Connecticut, Storrs, CT, USA

J.A. Qahtani
Saudi Aramco Oil Company, Dhahran, Saudi Arabia

D.G. Steyn and N. Chaumerliac (eds.), *Air Pollution Modeling and its Application XXIV*, Springer Proceedings in Complexity,
DOI 10.1007/978-3-319-24478-5_3

3.1 Introduction

Severe precipitation and fog can affect many human activities. The explicit representation of the condensation mechanisms is important for the accurate simulation of the precipitation distribution, as well as the onset and severity of fog. Apart from configuration factors, mainly vertical resolution, another parameter that plays a significant role in model performance is the inclusion of the contribution of airborne particles in the microphysical processes. In order to assess such interactions, the integrated coupled atmospheric and chemical model RAMS/ICLAMS has been used. The model includes online natural and anthropogenic aerosols cycles, photochemistry and chemical mechanisms. The feedback of aerosols on radiation is assessed through the use of size and humidity dependents optical properties based on OPAC database (Hess et al. 1998). Mineral dust, sea salt and several anthropogenic aerosols can also act as condensation nuclei (Solomos et al. 2011; Kushta et al. 2014). The model is used for different test periods over Europe and Arabian Peninsula (AP) in order to assess condensation mechanisms in proximity to and away from dust sources. The European case under study is the 2003 storm in Fella, which is considered a signature heavy precipitation event, mainly due to the enormous rainfall rates that exceeded 400 mm within a mere 12 h. This specific storm took place in August 29th, 2003 and is attributed to a return period of more than 500-years. The reason for the study of this case was the presence of small but crucial concentrations of in-cloud dust during the event. Dust particles, even in small number concentrations, can affect ice nucleation processes. The AP cases refer to a number of low visibility and fog presence over the East Coast of the Saudi Arabia (SA) which is a frequent phenomenon all year round, with dust and sea salt being a contributor in several cases. Fog is defined as low level (near surface) condensation. Dust contributes to fog mainly through morning radiative cooling and delay in vertical dispersal. The contribution of sea salt is noticed when frontal activity is present bringing both sea salt particles and water vapor inland. The sensitivity cases over AP analyze the role of several configuration and parameterization factors and secondly the contribution of aerosols.

3.2 Sensitivity Tests

(a) Fella heavy rain storm—August 29th, 2003
The case under study is the 2003 heavy precipitation event during the summer month of August, over Fella. The rainfall rates exceeded the enormous value of 400 mm within a mere 12 h as depicted in Fig. 3.1.

The main factors behind this high rainfall magnitude, as other cases in the region, remained the orographic enhancement of precipitation and the deep convection processes. However, it was noticed that during the day of the event mineral dust from Saharan desert was present in the atmosphere. Dust particles

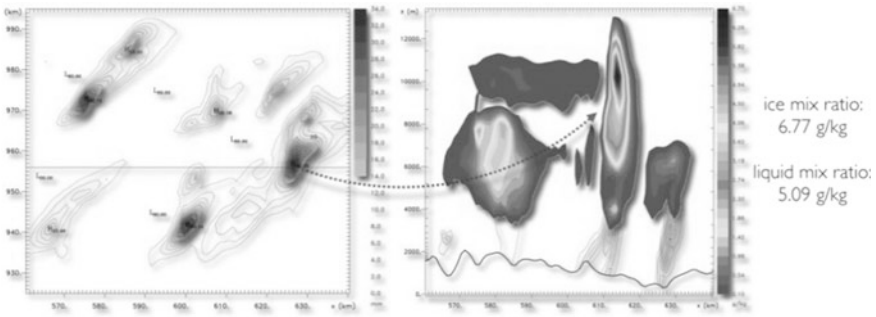

Fig. 3.1 1 h Accumulated precipitation (*left plot*) and liquid (*contour*) and ice (*color*) mixing ratio (*right plot*) over Fella on August 29th, 2003 at 11:00 UTC

are rather hydrophobic (they have a hygroscopicity of $\sim$65 %) but when caught upon updrafts that exceed 20 m/s like the ones in the present case, they can travel from near-ground altitudes all the way to the tropopause. In such low temperatures, they become hydrophilic. Subsequently, they trigger ice nucleation and lead to high precipitation amounts. This stood as an excellent case to perform some sensitivity tests with the new ice nuclei scheme (Barahona/Nenes (2009) vs Standard Meyers (1997)), the results of which underline the role of ice processes in heavy precipitation events in mountainous areas. Indeed, the dominant contribution of dust particles was noticed through their activation as ice nuclei rather than cloud condensation nuclei as seen in Fig. 3.2.

(b) Fog formation over East Coast of Arabian Peninsula
Fog is usually categorized as radiation, advection or frontal fog depending on the dominant formation mechanisms (radiative cooling, vertical mixing or addition of water vapour due to frontal activity respectively). The accuracy of a model in simulating fog events depend on the quality and resolution of the initialization data and vertical resolution of the lower boundary layer. These

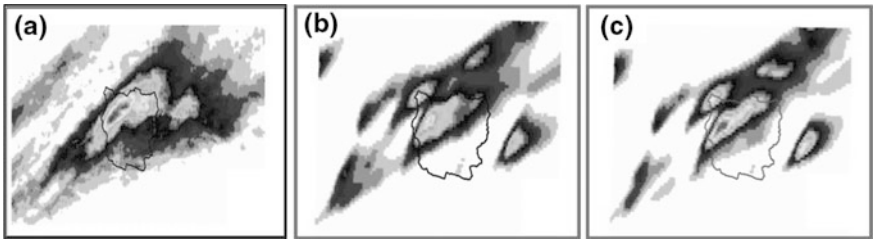

Fig. 3.2 12H accumulated precipitation from **a** radar observations, **b** model results from simulation with CCN activation and **c** model results from the simulation with CCN and IN activation

requirements result from the quasi-microscale nature of fog formation processes. Therefore, we first examined the governing factors that influence fog formation:

- Initial and boundary conditions: The quality of the data that are used to force the simulation is very important for the proper representation of the local scale meteorological conditions and soil data. The initialization of the model has been performed with the use of NCEP data (0.50^{o}) and LAPS (Local Analysis and Prediction System) which includes local observations at a higher resolution (0.15^{o}).
- Horizontal and vertical resolution: Fog formation is mainly a boundary layer process. During night hours and stable conditions that favour the formation of fog, the depth of the boundary layer can be as low as 100–200 m. In order to resolve these processes an adequate number of model layers are required inside the boundary layer. We have used two runs with two grids each (Grid1/Grid2), with spatial resolution of 24 km/6 km in the first case and 8 km/2 km respectively. For the vertical resolution we have tried 100 and 50 m resolution bringing the model's first free level at 48 and 23 m respectively.
- Cloud droplet formation: A different approach for the nucleation of small embryo droplets near the surface needs to be considered, taking also into account the aerosol concentrations near the area that may serve as CCN and play an important role on the amount of formatted fog droplets and their optical properties.

The initialization of the model from LAPS, that has a higher resolution output and assimilated local observational data, showed a better comparison with reported low visibility in the area (Fig. 3.3). This may be attributed to a better representation of the wind field in this case of low level condensation during January 6th, 2011. Wind speed is an important factor in fog formation and dissipation processes with winds greater than 2 m s^{-1} usually inducing vertical mixing of drier air and

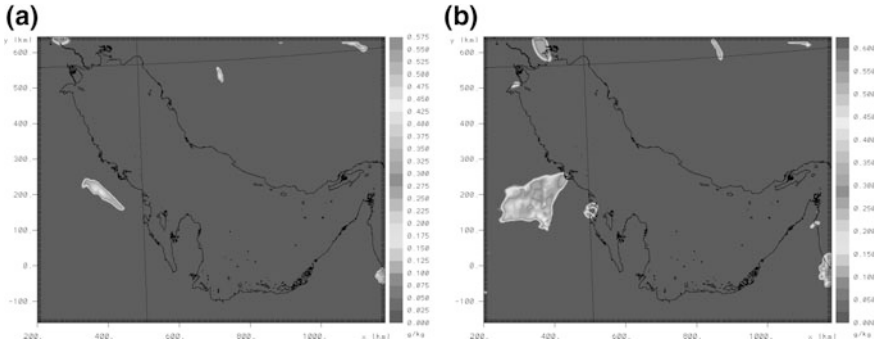

Fig. 3.3 Cloud mixing ratio (g/kg) on January 6th, 2011 at 04:00 UTC initialization data from **a** NCEP and **b** LAPS

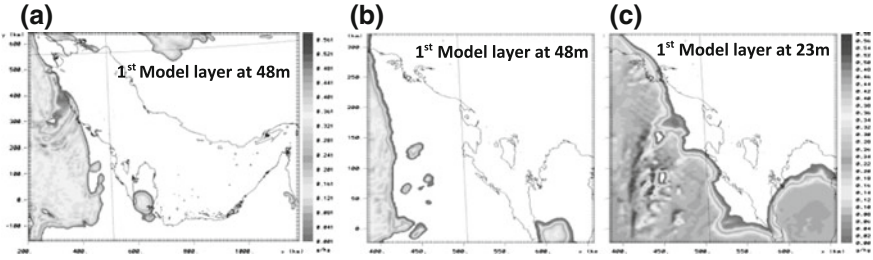

Fig. 3.4 Cloud mixing ratio (g/kg) on December 21, 2012 at 04:00 UTC with **a** grid spacing 24 × 24 km and 6 × 6 km ($\mathbf{Z_1 = 48\ m}$), **b** grid spacing 8 × 8 km and 2 × 2 km ($\mathbf{Z_1 = 48\ m}$) and **c** grid spacing 8 × 8 km and 2 × 2 km with $\mathbf{Z_1 = 23\ m}$

therefore fog dispersal. On the other hand, as seen in Fig. 3.4, the vertical resolution is the factor that mostly influences model results, rather than horizontal resolution. In a case of heavy fog due to low level clouds on December 21st, 2012, the use of the 23 m first free level significantly enhanced condensation near surface leading to fog formation and low visibility as reported by METAR stations present in the area.

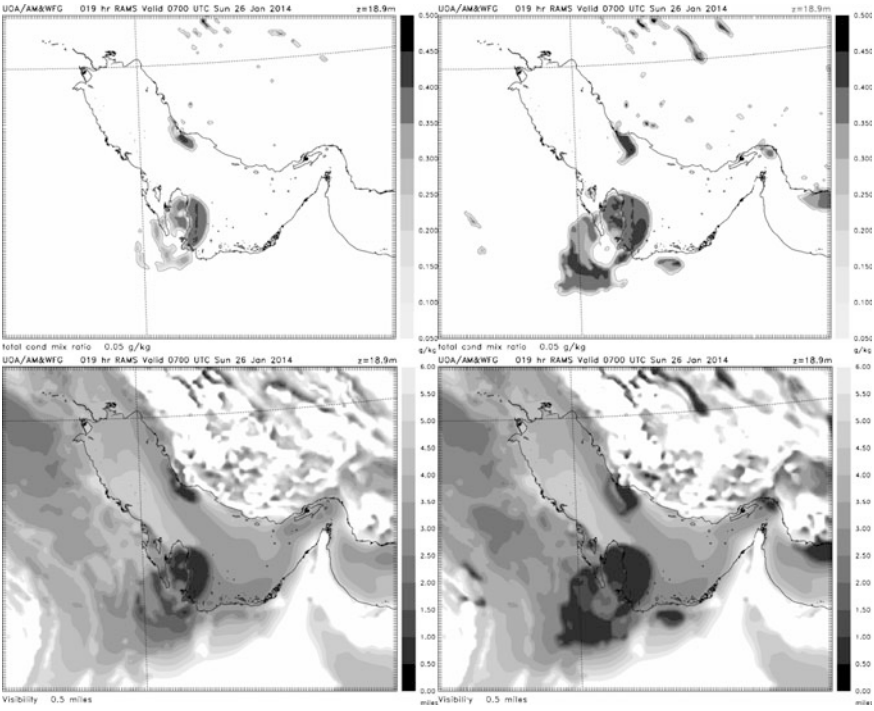

Fig. 3.5 Total condensates (*top plots*) and visibility in miles (*bottom plots*) on 26 January 2014, at 07:00 UTC from the clean case (*left*) and polluted case (*right*)

Another case of heavy fog over the area of interest, where we tested the new nucleation scheme, took place over Al Ahsa and Dammam stations in SA during morning hours (January 26th, 2014). We additionally calculated visibility based on the concentrations of condensates (liquid and ice phase) and aerosols, as well as relative humidity values. Two runs were performed: Clean (CL) and Polluted (PL). In the clean case the aerosol pollutants present in the atmosphere were not taken into consideration in the microphysical processes while in the polluted case these aerosols can be activated as CCN. In both cases the parameters included in the calculation of visibility were the same. As seen in Fig. 3.5, both runs capture the presence of fog over the area but in the PL case the situation is more severe with enhanced and persistent condensation and visibility values falling below one mile. In the CL case the visibility improves during the morning hours indicating a more rapid dispersion of the heavy fog (less condensates).

3.3 Conclusions

Severe precipitation events and fog formation are phenomena that can be affected by the aerosols present in the atmosphere. Small concentrations of airborne particles can modify the spatiotemporal distribution of precipitation, as well as the onset and duration of fog, due to their interference with the condensation processes by providing available CCN and IN. Models used to simulate such phenomena must yield accurate representation of wind and surface parameters with proper configuration, as well as explicit calculation of particle nuclei.

References

Barahona D, Nenes A (2009) Parameterizing the competition between homogeneous and heterogeneous freezing in ice cloud formation - polydisperse ice nuclei. Atmos Chem Phys 9:5933–5948

Hess M, Koepke P, Schult I (1998) Optical properties of aerosols and clouds: the software package OPAC. Bull Am Meteorol Soc 79:831–844

Kushta J, Kallos G, Astitha M, Solomos S, Spyrou C, Mitsakou C, Lelieveld J (2014) Impact of natural aerosols on atmospheric radiation and consequent feedbacks with the meteorological and photochemical state of the atmosphere. J Geophys Res. doi:10.1002/2013JD020714

Meyers MP, Walko RL, Harrington JY, Cotton WR (1997) New RAMS cloud microphysics parameterization. part II: the two moment scheme. Atmos Res 45:3–39. doi:10.1016/S0169-8095(97)00018-5

Solomos S, Kallos G, Kushta J, Astitha M, Tremback C, Nenes A, Levin Z (2011) An integrated modeling study on the effects of mineral dust and sea salt particles on clouds and precipitation. Atmos Chem Phys 11:873–892. doi:10.5194/acp11-873-2011

Chapter 4
A Multi-model Case Study on Aerosol Feedbacks in Online Coupled Chemistry-Meteorology Models Within the COST Action ES1004 EuMetChem

R. Forkel, D. Brunner, A. Baklanov, A. Balzarini, M. Hirtl, L. Honzak, P. Jiménez-Guerrero, O. Jorba, J.L. Pérez, R. San José, W. Schröder, G. Tsegas, J. Werhahn, R. Wolke and R. Žabkar

Abstract The importance of different processes and feedbacks in online coupled chemistry-meteorology models for air quality simulations and weather prediction was investigated in COST Action ES1004 (EuMetChem). Case studies for Europe were performed with different models as a coordinated exercise for two episodes in

R. Forkel (✉) · J. Werhahn
Institute for Meteorology and Climate Research (IMK-IFU),
Karlsruhe Institute of Technology (KIT), Kreuzeckbahnstr 19,
82467 Garmisch-Partenkirchen, Germany
e-mail: renate.forkel@kit.edu

D. Brunner
Laboratory for Air Pollution/Environmental Technology, Empa,
Swiss Federal Laboratories for Materials Science and Technology,
8600 Dübendorf, Switzerland

A. Baklanov
World Meteorological Organization, Geneva, Switzerland

A. Baklanov
Danish Meteorological Institute, Copenhagen, Danmark

A. Balzarini
Ricerca sul Sistema Energetico (RSE SpA), Milan, Italy

M. Hirtl
Zentralanstalt für Meteorologie und Geodynamik, ZAMG, Vienna, Austria

L. Honzak · R. Žabkar
University Ljubljana, SPACE-SI, Ljubljana, Slovenia

P. Jiménez-Guerrero
University Murcia, MAR-UMU, Murcia, Spain

O. Jorba
Earth Sciences Department, Barcelona Supercomputing Center, Barcelona, Spain

D.G. Steyn and N. Chaumerliac (eds.), *Air Pollution Modeling and its Application XXIV*, Springer Proceedings in Complexity,
DOI 10.1007/978-3-319-24478-5_4

2010 in order to analyse the aerosol direct and indirect radiative effect and the response of different models to aerosol-radiation interactions.

4.1 Introduction

Aerosols are known to have an impact on weather and climate directly via radiation and via their impact on cloud formation. Fully coupled "online" meteorology-chemistry models, which became during the last years increasingly popular for air quality simulations, provide the possibility to account for feedback mechanisms between simulated aerosol concentrations and meteorological variables. With the increasing number and diversity of this type of models, the question is arising how different models respond to simulated feedback effects.

In order to analyse the response of different models to the aerosol direct and indirect aerosol radiative effect, case studies for Europe were performed with different models in a coordinated exercise of Working Groups 2 and 4 of the COST Action ES1004 EuMetChem (http://www.eumetchem.info/).

4.2 Method

Two episodes are considered: the Russian heat wave and wildfires episode in summer 2010 (25 July–15 August 2010) and an autumn episode with enhanced cloud cover and rain and including an of Saharan dust transport to Europe (2–15 October 2010). These episodes and the areas of interest as shown in Figs. 4.1 and 4.2 had been identified during the previous AQMEII phase2 modelling inter-comparison exercise (Galmarini et al. 2015). They were selected for the current exercise on behalf of their strong potential for direct and indirect aerosol effects on meteorology (Makar et al. 2015; Forkel et al. 2015).

The models compared here are COSMO-MUSCAT (Wolke et al. 2012) and WRF-Chem (Grell et al. 2011) with different chemistry and physics options as summarized by Forkel et al. (2015). Except for a WRF-Chem simulation with

J.L. Pérez · R. San José
Technical University of Madrid (UPM), ESMG, Madrid, Spain

W. Schröder · R. Wolke
Leibniz-Institute for Tropospheric Research (TROPOS), Leipzig, Germany

G. Tsegas
Laboratory of Heat Transfer and Environmental Engineering, Aristotle University, Thessaloniki, Greece

increased resolution (denoted as case CS2) for Russia and surroundings and the COSMO-MUSCAT simulation of the fire episode, the simulations cover entire Europe. Simulations with each model are performed without and with considering the direct radiative effect of the simulated aerosol. If possible, the direct as well as the indirect aerosol effect are considered in a third simulation. The common setup for the participating models and a unified output strategy allow analysing the model output with respect to similarities and differences in the model response to the aerosol direct effect and aerosol cloud interactions.

4.3 Results and Discussion

For the simulations including the direct aerosol effect a 10 to 100 Wm^{-2} lower average downward shortwave radiation at the ground was found than for the corresponding baseline simulations. Accordingly, an almost 1 degree lower mean temperature was found for the fire areas in Russia (Fig. 4.1). For these areas, the inclusion of aerosol radiative effects resulted in better agreement with observed temperatures. Outside the fire area and for the October episode the direct aerosol effect resulted in mean temperature decrease of less than 0.25 degrees for most of the analysed area (Fig. 4.2).

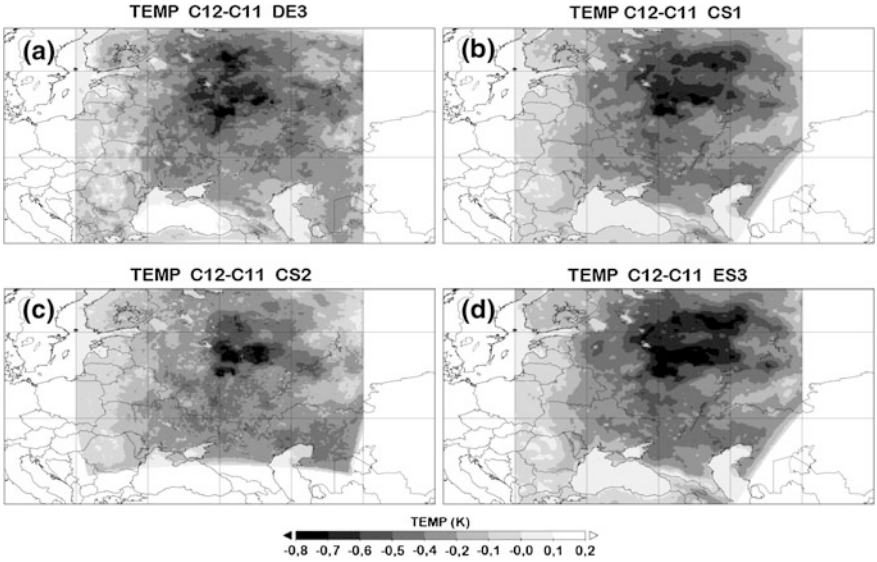

Fig. 4.1 Difference in mean temperature at 2 m from simulations with and without the direct aerosol radiative effect of the simulated aerosol for the Russian heat wave and fire episode in July/August 2010 **a** COSMO-MUSCAT; **b** WRF-Chem with MADE/SORGAM chemistry and Morrison microphysics; **c** same as **b** but with 9.9 instead of 23 km grid width; **d** WRF-Chem with CBMZ/MOSAIC chemistry and Morrison microphysics

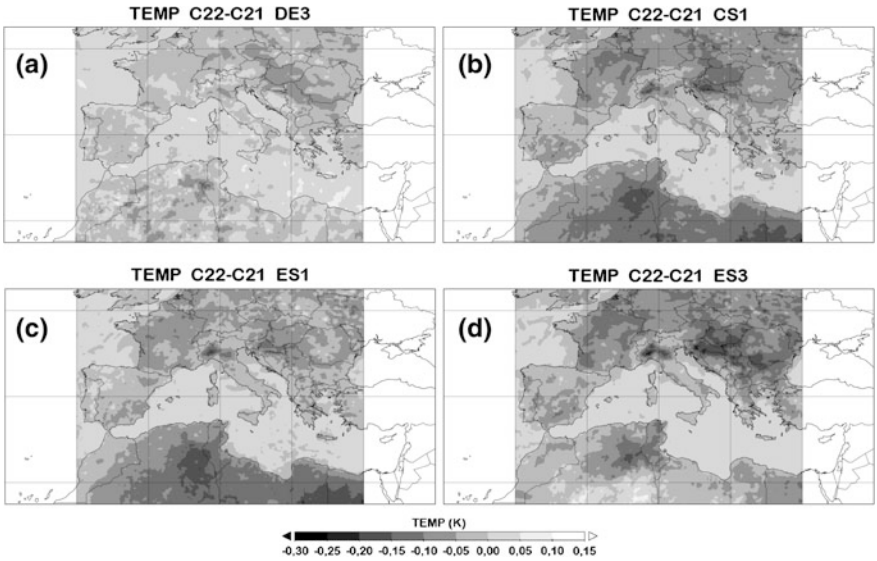

Fig. 4.2 As Fig. 4.1, but for the October 1010 episode. Please note the different temperature scales in Figs. 4.1 and 4.2 and that **c** shows results for case ES1 (WRF-Chem with MADE/SORGAM chemistry and Lin microphysics) instead of CS2

The results also indicate that, except for extreme aerosol hotspots, the variability of the response to aerosol meteorology interactions between the models or model configurations can be of the same magnitude as the simulated aerosol effects. The variation in model response is still more pronounced for cloudy areas when both the direct and the indirect effect are considered (not shown).

Part of these differences due to aerosol radiative effects can also be attributed to different base case configurations of the different models, like the assumed aerosol climatologies if no radiative effects of simulated aerosols are considered. Another reason for inter-model differences can be attributed to different ways how aerosol radiative properties are calculated. Differences due to the indirect effect also depend on the assumptions on cloud condensation nuclei formation if no simulated aerosol concentrations are considered for aerosol cloud interactions.

4.4 Concluding Remarks

It cannot be generalized whether the inclusion of aerosol radiative effects and aerosol cloud interactions based on simulated aerosol concentrations does improve the simulation results. The inter-model variation of the response of different online coupled models suggests that further work comparing the methodologies and parameterizations used to represent the direct and indirect aerosol effect in these models is still necessary.

Acknowledgments We gratefully acknowledge the support of the German Federal Ministry of Education and Research (BMBF), REKLIM, the Spanish Ministry of Economy and Competitiveness, the Ministry of Higher Education, Science, Sport and Culture. We acknowledge the contribution of TNO (anthropogenic emissions database); ECMWF/MACC project & Meteo-France/CNRM-GAME (chemical boundary conditions), the Finnish Meteorological Institute FMI (fire emissions), the AQMEII initiative, the Centro de Supercomputacion y Visualizacion de Madrid (CESVIMA), and the Spanish Supercomputing Network (BSC).

Questions and Answers

Questioner: Steven Hanna

Question: You presented many results comparing models with each other and with observations. Can you comment on whether the differences were significant, using standard statistical tests?

Answer: Looking at physical plausibility the decrease in downward solar radiation and daytime temperature due to the direct aerosol effect is robust for all model configurations. The same holds for WRF-Chem for the pronounced decrease in cloud water content and increase in solar radiation for cloudy conditions in the case of very low aerosol concentrations.

The differences in solar radiation and temperature between the simulations including the direct and indirect effect and the baseline case were tested for statistical significance using the Student's t-test at different levels of significance ($\alpha = 0.01$, 0.05, and 0.1). For the October episode and the area shown in Fig. 4.2 no significant differences in mean solar radiation and mean temperature between the baseline case and the simulations including the direct and indirect effect were found. Also for the fire episode differences between mean temperature and radiation from the simulations with and without the direct aerosol effect were not significant for the major part of the area shown in Fig. 4.1. Only for the region with high fire emissions, the differences in mean solar radiation and temperature were found to be significant during the second half of the fire episode—however only for $\alpha = 0.1$.

References

Forkel R, Balzarini A, Baró R, Bianconi R, Curci G, Jiménez-Guerrero P, Hirtl M, Honzak L, Lorenz C, Im U, Pérez JL, Pirovano G, San José R, Tuccella P, Werhahn J, Žabkar R (2015) Analysis of the WRF-Chem contributions to AQMEII phase2 with respect to aerosol radiative feedbacks on meteorology and pollutant distributions. Atmos Environ 115:630–645. doi:10.1016/j.atmosenv.2014.10.056

Galmarini S et al (2015) Preface. Atmos Environ 115:340–344. doi:10.1016/j.atmosenv.2015.06.009

Grell G, Freitas SR, Stuefer M, Fast J (2011) Inclusion of biomass burning in WRF-Chem: impact of wildfires on weather forecasts. Atmos Chem Phys 11:5289–5303. doi:10.5194/acp-11-5289-2011

Makar PA, Gong W, Milbrandt J, Hogrefe C, Zhang Y, Curci G, Žabkar R, Im U, Balzarini A, Baró R, Bianconi R, Cheung P, Forkel R, Gravel S, Hirtl M, Honzak L, Hou A, Jiménez-Guerrero P, Langer M, Moran M.D, Pabla B, Pérez JL, Pirovano G, San José R, Tuccella P, Werhahn J, Zhang J, Galmarini S (2015) Feedbacks between air pollution and weather, Part 1: effects on weather. Atmos Environ 115:442–469. doi:10.1016/j.atmosenv.2014.12.003

Wolke R, Schröder W, Schrödner R, Renner E (2012) Influence of grid resolution and meteorological forcing on simulated European air quality: a sensitivity study with the modeling system COSMO-MUSCAT. Atmos Environ. doi:10.1016/j.atmosenv.2012.02.085

Chapter 5
Influence of Ammonia Emissions on Aerosol Formation in Northern and Central Europe

Anna M. Backes, Armin Aulinger, Johannes Bieser, Volker Matthias and Markus Quante

Abstract High concentrations of particles pose a threat to human health and the environment. In this study the influence of ammonia (NH_3) emissions on aerosol concentration in central Europe is investigated. Depending on crop growth, temperature and local legislation individual temporal profiles for fertilizer and manure application are calculated for each model grid cell of the SMOKE-EU emission model. The emission data was used as input for the CMAQ chemical transport model. Comparisons to EMEP observations indicate that the new ammonia emission module leads to a better agreement of modeled and observed concentrations. The model was used then to assess the influence of emission changes. It was found that a reduction of ammonia emissions by 50 % lead to a 24 % reduction of total $PM_{2.5}$ concentrations in the model domain during winter, mainly driven by reduced formation of ammonium nitrate.

5.1 Introduction

The emission of reactive nitrogen into the atmosphere causes numerous problems of global significance, such as air pollution, eutrophication and soil acidification. The share of NH_3 emissions in European air pollution is constantly increasing, as there has been little progress in controlling agricultural ammonia emissions. Diverse studies suggested that a temporal component based on meteorological variables should be considered when applying ammonia emissions in a chemistry transport model (CTM) due to their high temporal variability (Skjøth et al. 2004;

A.M. Backes (✉) · A. Aulinger · J. Bieser · V. Matthias · M. Quante (✉)
Helmholtz-Zentrum Geesthacht, Institute of Coastal Research, Max-Planck-Strasse 1, 21502 Geesthacht, Germany
e-mail: Anna.Backes@hzg.de
e-mail:

J. Bieser
DLR—Deutsches Luft und Raumfahrtzentrum, Institut für Physik der Atmosphäre, Münchener Straße 20, 82234 Weßling, Germany

D.G. Steyn and N. Chaumerliac (eds.), *Air Pollution Modeling and its Application XXIV*, Springer Proceedings in Complexity,
DOI 10.1007/978-3-319-24478-5_5

Gyldenkærne et al. 2005; Denier van der Gon 2011). The approach was particularly designed to fit the needs of scenario studies for investigating the influence of different ammonia abatement strategies on the formation of particles. The setup of the study utilizes three scenarios varying in intensity and release time of NH_3 emissions which have been modelled with the CTM CMAQ: a political, a technical and a behavioural scenario.

5.2 Temporal Emission Profiles

The annual NH_3 emissions have been temporally distributed across the year on the basis of the meteorological variables wind speed and surface temperature, resulting in individual ammonia emission data for every grid cell and every hour. Parts of the newly developed parameterization are a modified version of the dynamical ammonia emission parameterization by Skjøth et al. (2004) and Gyldenkærne et al. (2005). To improve the reliability of the approach, modifications were made in various parts. They were applied especially in the animal husbandry related sector by creating a more detailed set of subsectors and a more detailed geographical distribution of the emissions (Fig. 5.1).

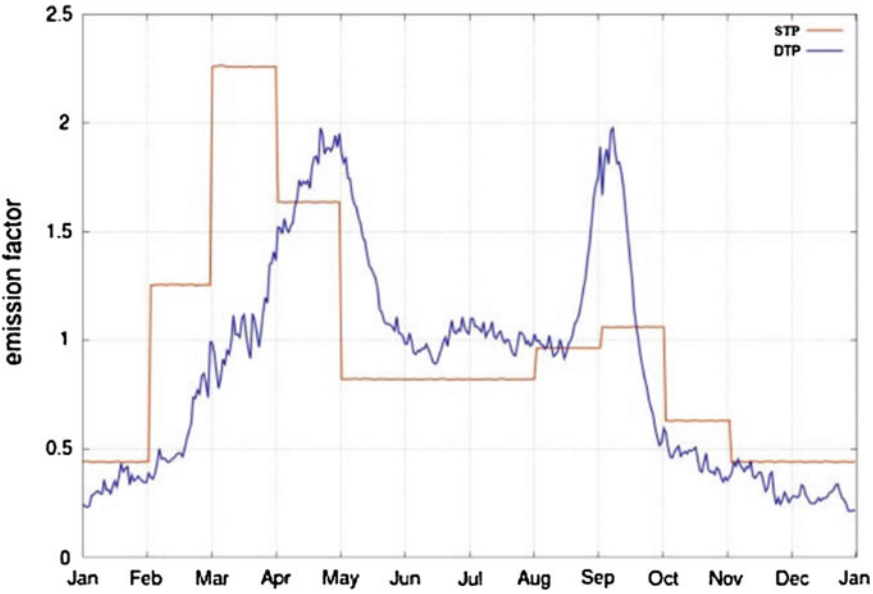

Fig. 5.1 Annual variation of the daily NH_3 emission. An emission factor of one represents the annual average. The static Standard Temporal Profile (STP) represents the temporal variability as used in the LOTOS—EUROS model (Schaap et al. 2005). The Dynamical Temporal Profile (DTP) represents the daily mean over all grid cells of the central European domain except for those containing exclusively water

5.3 Model Set-up and Evaluation

The emissions for the reference year 2008 were processed by the SMOKE-EU model suitable for the CTM CMAQ. The modelling domain was set up with a grid cell size of 24 × 24 km^2 and 30 vertical layers. The Carbon Bond 5 (CB 05) photochemical mechanism was used, TM5 global chemistry transport model system delivered the boundary conditions and the meteorological fields were derived from COSMO-CLM 4.8. The correlation of measured and modelled NH_3 concentration has improved significantly for 12 out of 16 European EMEP measurement stations. An improvement of the Normalized Mean Error (NME) and the Normalized Mean Bias (NMB) could be seen for the species NH_4^+ and NO_3^-.

5.4 NH_3 Emission Scenarios

Three scenarios were investigated:

The political scenario (NEC 2020) based on the National Emission Ceilings coming into force 2020 (Amann et al. 2011). The technical scenario (MTFR) represents the maximum technical feasible reduction (Amann et al. 2011). The behavioural scenario (RCAP) is based on a reduced consumption of animal products. It assumes a European society whose diet is based on the recommendation of the Harvard medical school (Willett and Skerrett 2005). To calculate the decrease in NH_3 the actual consumption per country were compared with the consumption in case of the recommended diet. The percentage of reduction per species and country could was applied on the gridded livestock inventories of the Food and Agriculture Organization (FAO) (FAO 2007).

5.5 Results and Discussion

A constant decrease of ammonia emissions can be recognized in every scenario as well as in the reference case from spring to winter, intermitted by an autumn peak of emissions. Strongest concentration reductions are found for the RCAP scenario in summer (−46 %), autumn (−46 %) and winter (−59 %), whereas the weaker spring concentrations decline (−23 %) is still a stronger decrease than any achieved in the other scenarios. The RCAP scenario concentrations of NO_3^- in comparison to the reference case is highest in autumn (−50 %) and winter (−48 %). The RCAP scenario shows a severe decrease in the $PM_{2.5}$ concentrations, mainly noticeable in winter (−24 %) and autumn (−22 %) (Fig. 5.2).

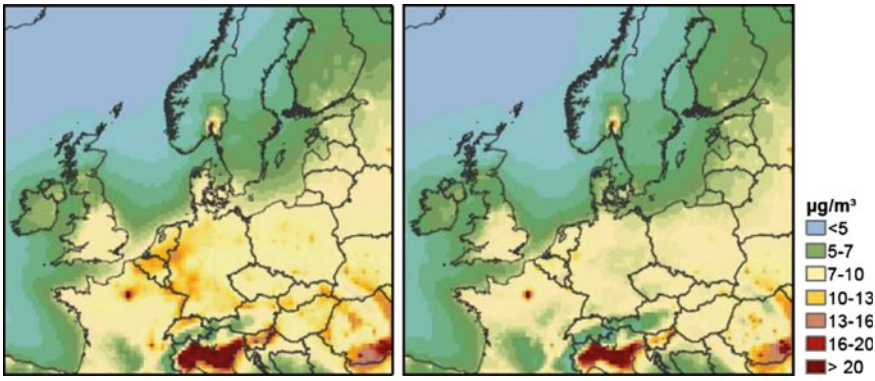

Fig. 5.2 Winter $PM_{2.5}$ concentrations for the reference scenario (*left*) and the RCAP scenario (*right*)

5.6 Conclusion

The implementation of dynamical temporal profiles for NH_3 emissions has improved the correlation between modelled and observed NH_3 concentrations significantly for most EMEP measurement stations. Moreover, it has led to an improvement of the NME and NMB of NH_3, NH_4^+ and NO_3^-. The model results concerning particulate SO_4^{2-} have not been influenced as there were no regions with an NH_3 limitation in the formation of secondary sulphate particles.

It was found that the time of the year when NH_3 emissions are reduced is an important factor for the formation of secondary inorganic particles. A shift of NH_3 emissions from winter to spring resulted in a strong decline of winter $PM_{2.5}$ concentrations. This can be explained by higher NO_X emissions and the shallow boundary layer during winter time. A reduction of fertilizer related NH_3 emissions during spring and summer, which is in line with current European legislation (NEC2020), had only a small impact on $PM_{2.5}$ concentrations. The RCAP scenario ($\sim$50 % NH_3 emission reduction with a strong focus on winter emissions) led to an annual reduction of total N deposited of up to 50 % for grid cells located in areas with intensive livestock farming and a reduction in total $PM_{2.5}$ concentration of about 25 %. This was mainly driven by a reduction in the formation of ammoniumnitrate. The main conclusion of this study, is the remarkable potential for air quality that a reduction of NH_3 emission in the cold season bears during which the potential of reduction within the sector animal farming and husbandry is highest.

Questions and Answers

Questioner Name: Anthony Dore

Q: Your model has a different temporal ammonia emission profile for each grid square. How well can you capture different regional farming practices and national legislation on the timing of application of fertilizer and manure?

A: Regional farming practices are only taken into account through the crop growth model and its dependency on the meteorological conditions. The results of the model study show that the application of manure and fertilizer takes place earlier in the year if the regional climate is warmer, which is e.g. visible if comparing southern France and Denmark. Additionally the first and last day of fertilizer application and manure application per country if mentioned in the legislation have been adopted to capture the legislations. In countries with a federal system the closed periods, adopted from a study of the European commission on the variation of manure N efficiency throughout Europe (EC 2009), differ from region to region. The closed periods used in this study represent a simplified version of reality as they don't differentiate between regional legislations (EC 2009).

Questioner Name: Wouter Lefebvre
Q: Can you specify the decrease in meat consumption in the RCAP scenario?
A: To calculate the decrease in NH_3 arising from the consumption change, the actual consumption of ruminant, pork and poultry meat (including eggs) per country has been compared with the consumption in case of a healthy diet. The data of meat consumption per capita has been adopted from the statistic division of the food and agriculture organization (FAOSTAT 2014) for all countries of the European Union. The per capita consumption of ruminant meat consists of food commodities of cattle, sheep and goat meat in 2008. The difference of the actual consumed amount and the recommended amount has been calculated for the three categories, so that the percentage of reduction per species and country could be applied on the gridded livestock inventories of the Food and Agriculture Organization (FAO) (FAO 2007).

E.g. for Poland the percentage of ruminants per grid cell has been decreased by 25 % the percentage of pork by 93 % and the percentage of poultry by 43 %. For the Netherlands the decrease in ruminants is higher (79 %), while pork decreases by 89 % and poultry by 60 % per grid cell. Other sectors as manure application have not been affected by this decrease in animal density. As the recommendation assumes no change in the intake of milk products, only cattle and no change in the amount of dairy cows has been considered in the calculations. A change in the export of animal products has not been considered either, assuming that other regions in the world with an increasing consumption will be able to meet their own market demands in the future (FAOSTAT 2014; FAO 2007).

Questioner Name: Sebnem Aksoyoglu
Q: We did a similar study using the TNO emission inventory. The modelled and measured NH_3 temporal profile were different. Measurements had higher peaks in summer than in spring. Did you have a similar case in your domain?

A: Our emission model is based on a statistical approach. Thus, we cannot reproduce single emission peaks. However, the main fertilization peak which is assumed at the beginning of Mach in the 'standard temporal profiles' occurs much later in our emission model. For the central European domain shown in this work it is, on average, at the beginning of May (Fig. 5.1). In colder regions it can be as late as June.

Questioner Name: Limei Ran
Q: How many crops are modeled in the crop growth model?
A: The crop growth parameters used are based on the four crop types: spring, barley, winter wheat, sugar beets, and grass crops.
Q: What is the main cause of the peak in NH_3 emission in the fall?
A: The main cause for the peak in NH_3 emissions in the fall is the dumping of surplus manure on fields due. This effect is assumed to be a reaction on a European law forcing the farmers to have enough capacity of manure storage in relation to the amounts of animals for the whole winter.

Questioner Name: P.J.H. Builtjes
Q: How big is the largest difference between the EDGAR and the EMEP files?
A: Total European ammonia emissions are quite similar in both emission inventories. However, EDGAR has a better spatial resolution and distinguishes between emissions from agricultural activity and animal husbandry. On the other hand, we found a few unexplained features in the EDGAR inventory. For example, there were extremely high emissions from agriculture in Luxembourg which we deemed unrealistically high. Thus, we used the national totals from EMEP to adjust the EDGAR inventory.

References

Amann M, Bertok I, Borken-Kleefeld J, Heyes C, Cofala J, Höglund-isaksson L, Klimont Z, Rafaj P, Schöpp W, Wagner F (2011) Cost-effective emission reductions to improve air quality in Europe in 2020. In: NEC scenario analysis report Nr. 8. (8)

Denier van der Gon HD, Hendriks C, Kuenen J, Segers A, Visschedijk A (2011) TNO Report. Description of current temporal emission patterns and sensitivity of predicted AQ for temporal emission patterns. EU FP7 MACC deliverable report D_D-EMIS_1.3

EC (2009) Study on variation of manure N efficiency throughout Europe, Annex1. http://ec.europa.eu/environment/water/water-nitrates/pdf/Annex_1_Man_N_Effic.pdf

FAO (2007). Gridded livestock of the world 2007. G.R.W.Wint and T.P.Robinson. http://www.fao.org/Ag/againfo/resources/en/glw/home.html. Accessed 11 Nov 2014

FAOSTAT (2014) Food Supply—Livestock and Fish Primary Equivalent. http://faostat3.fao.org/download/D/FS/E. Accessed 10 Nov 2014)

Gyldenkærne S, Skjøth CA, Hertel O, Ellermann T (2005) A dynamical ammonia emission parameterization for use in air pollution models. J Geophys Res. doi:10.1029/2004JD005459

Schaap M, Roemer M, Sauter F, Boersen G, Timmermans R (2005) LOTOS-EUROS: Documentation. http://www.lotos-euros.nl/doc/LOTOS-EUROS-v11-documentation.pdf (17.11.2014)

Skjøth CA, Hertel O, Gyldenkærne S, Ellermann T (2004) Implementing a dynamical ammonia emission parameterization in the large-scale air pollution model ACDEP. J Geophys Res 109 (D6):D06306. doi:10.1029/2003JD003895

Willett WC, Skerrett PJ (2005) Eat drink and be healthy: the Harvard Medical School guide to healthy eating. Free Press, New York

Chapter 6
Modeling Formation of SOA from Cloud Chemistry with the Meso-NH Model: Sensitivity Studies of Cloud Events Formed at the Puy de Dôme Station

A. Berger, M. Leriche, L. Deguillaume, C. Mari, P. Tulet, D. Gazen and J. Escobar

Abstract The majority of the organic fraction of aerosols is suspected to be of secondary origin. However, the sources, chemical composition and formation mechanisms of secondary organic aerosols (SOA) remain one of the least understood processes relevant to the atmosphere. Laboratory experiments, in situ measurements and numerical simulations recently highlighted the formation of SOA through aqueous chemistry in humid aerosol particles and in cloud droplets. However, there is still a need to evaluate the relative relevance of SOA formation through aqueous chemistry in comparison to classical gas to particles conversion pathways. Cloud resolving model (CRM) allows simulating the complex aerosols-cloud-chemistry interactions. Meso-NH (Mesoscale Non-Hydrostatic atmospheric model) CRM model includes a cloud chemistry module and an aerosol module, which allows representing the formation of SOA due to aqueous phase reactivity. The model is applied on a cloud event observed at the puy de Dôme Mountain. Comparing simulations with or without the cloud chemistry module activated assesses the contribution of the cloud chemistry in the SOA formation. Results show a significant contribution of aqueous phase reactivity in the formation of SOA downstream the Mountain.

A. Berger · M. Leriche (✉) · C. Mari · D. Gazen · J. Escobar
LA, UMR 5560 CNRS/Université Paul Sabatier Toulouse 3, Toulouse, France
e-mail: maud.leriche@aero.obs-mip.fr

L. Deguillaume
LaMP, UMR 6016 CNRS/Université Blaise Pascal Clermont-Ferrand II, Aubière, France

P. Tulet
LACY, UMR 8105 CNRS/Université La Réunion/Météo-France, Réunion, France

D.G. Steyn and N. Chaumerliac (eds.), *Air Pollution Modeling and its Application XXIV*, Springer Proceedings in Complexity,
DOI 10.1007/978-3-319-24478-5_6

6.1 Introduction

The role of aerosol particles and their interactions with clouds in the climate change is still subject to large uncertainties (IPCC 2013). Among aerosol particles the organic particles, and in particular the secondary ones, are still badly quantified. As numerous studied showed the potential role of aqueous phase reactivity as a source of SOA, the relevance of this source is still subject to controversy. CRM model allows simulating the complex interactions between dynamics, chemistry, aerosol particles and clouds and is an ideal tool to study the formation of SOA from aqueous phase reactivity in clouds. In this study, the Meso-NH CRM model is applied on a cloud event observed at the puy de Dôme Mountain in July 2011 in order to assess the formation of SOA from cloud chemistry.

6.2 Simulation Set-up

The Meso-NH model (Lafore et al. 1998) simulates small scales (LES type) to synoptic scale and can be run in a two-way nested mode involving up to 8 nesting stages. The model includes parameterizations for gaseous chemistry (Tulet et al. 2003), aerosol particles including microphysics and chemistry (Organic Inorganic Log-normal Aerosol Model including SOA (ORILAM-SOA), Tulet et al. 2006) and cloud chemistry (Leriche et al. 2013). Recently a parameterization of aerosol activation in cloud droplets ABRK (Abdul-Razzak et al. 2004) has been included in the model (Berger 2014). This parameterization allows computing the cloud condensation nuclei (CCN) spectra as a function of the physico-chemical properties of aerosol particles coming from the aerosol module ORILAM-SOA. In addition, the gaseous chemical mechanism including the formation of SOA precursors has been supplemented with an aqueous mechanism including the aqueous formation of SOA precursors from isoprene chemistry (Berger 2014).

During summer 2011, an intensive field campaign took place at the puy de Dôme station. From this campaign, measurements are available for the number concentration and chemical composition of fine particles, for the mixing ratio of some volatile organic compounds (including isoprene and mono-terpenes) and for the chemical composition of the cloud water and the liquid water content (LWC) if a cloud was present. Routine measurements are available for meteorological parameters (temperature, humidity, wind) and for trace gases (O_3, NO_x, SO_2).

To study the formation of SOA from cloud chemistry, an orographic cloud is an ideal event: stable cloud for several hours located on the summit of the mountain allowing designing a 2D scenario. During the campaign, only one event is typically an orographic cloud: it is the event observed the 6th of July 2011, which occurred from 6:00 local time (LT) to 11:00 LT. The direction of the 2D domain is deduced from the main wind direction (West-Southwest, maritime air mass). Initial meteorological conditions come from a radio-sounding extracted from the ECMWF

(European Center for Medium-range Weather Forecasts) re-analysis and located upstream the puy de Dôme Mountain. For trace gases initialization, measurements sampled at 6:00 LT are used and are supplemented by data from literature. The log-normal distributions of the Aitken and accumulation modes are initialized based upon the Scanning Mobility Particle-Sizer Spectrometer (SMPS) measurements at 6:00 LT. The chemical composition of aerosols for Aitken and accumulation modes is initialized using observed chemical composition of fine particles. For organic part, only the primary organic aerosol (POA) is initialized.

6.3 Results

First, the microphysical characteristics of the simulated cloud obtained with the ABRK parameterization and with the classical Twomey approach TWO (Cohard et al. 1998) are compared. For both cases, the simulated cloud is similar with a maximum LWC around 0.7 g m^{-3} and a droplet diameter in the range 2–14 μm at 10:00 LT. However, because in the TWO parameterization the number concentration of cloud droplets are not directly related to the aerosol number concentration, a difference is observed for the cloud droplet number concentration with a range 100–180 cm^{-3} for ABRK and 200–340 cm^{-3} for TWO at 10:00 LT. The total activated CCN mass concentration is in the range 10–17 μg m^{-3} at 10:00 LT.

To illustrate the aqueous phase chemical production of organic acids leading to the formation of SOA, the relative difference between a simulation considering aqueous chemistry and a simulation without aqueous chemistry is computed as:

$$Diff(\%) = \frac{\left(r_g + r_w\right)^{aq} - \left(r_g\right)^{no\_aq}}{\left(r_g\right)^{no\_aq}} \times 100$$

r_g and r_w are the mixing ratio of the chemical species in gaseous phase and aqueous phase, respectively. The superscript "aq" and "no_aq" refer to the simulation with aqueous chemistry and without aqueous chemistry, respectively.

In ORILAM-SOA, the SOA6 class is formed from the oxalic acid and the pyruvic acid. Whereas these organic acids are a very slow production in gaseous phase, their aqueous phase production is very fast from the oxidation products of isoprene and monoterpenes. Figure 6.1 shows a strong production of these acids inside the cloud. Downstream of the mountain, when cloud droplets evaporate, oxalic and pyruvic acids are released in the gas phase where they partition with the aerosol particles forming SOA6. The same effect is simulated for sulfuric acid, which is produced in cloud droplets by the oxidation of sulfur dioxide.

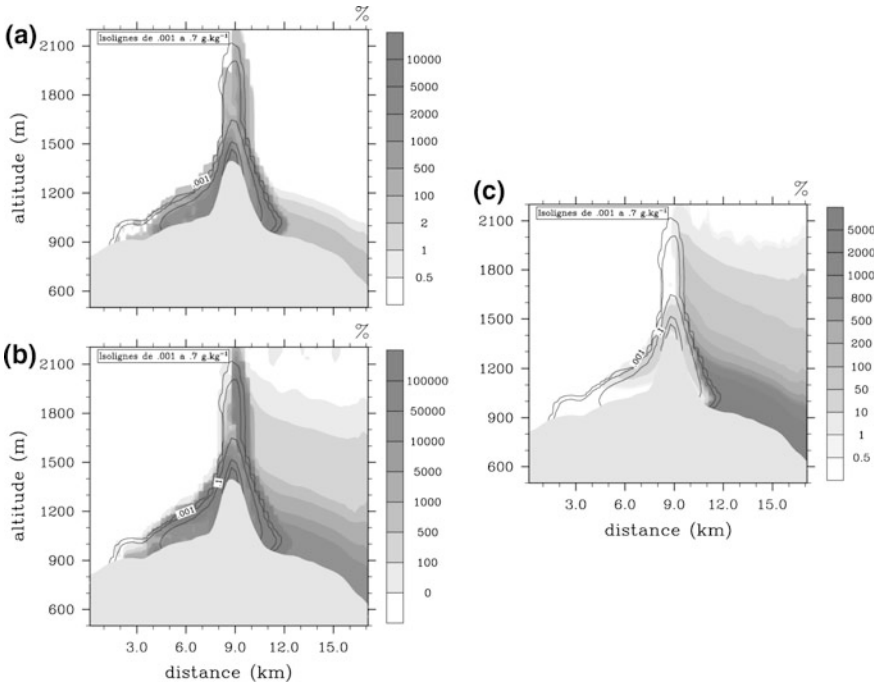

Fig. 6.1 Relative difference (%) as defined in equation below for oxalic acid (**a**), pyruvic acid (**b**) and SOA6 (**c**) at 10:00 LT. The *grey* isolines are the LWC in g kg^{-1}

6.4 Conclusion

A 2D simulation of an orographic cloud observed at the puy de Dôme station is performed with the CRM Meso-NH including aqueous chemistry in cloud, an aerosol module and a parameterization of the cloud droplets nucleation from aerosol particles. This study highlights the formation of SOA from the production of organic acids inside cloud droplets by aqueous phase reactivity.

Acknowledgments The authors are very grateful to the Agence Nationale de la Recherche (ANR) for its financial support through the CUMULUS project (ANR-10-BLAN-0617). Computer resources were provided by CINES (Centre Informatique National de l'Enseignement Supérieur). We acknowledge everyone at the GAW puy de Dôme station. We also would like to thank the Meso-NH team for its technical assistance.

References

Abdul-Razzak H, Ghan SJ (2004) Parameterization of the influence of organic surfactants on aerosol activation. J Geophys Res 109:D03205. doi:10.1029/2003JD004043

Berger A (2014) Modélisation multi-échelles de la composition chimique des aérosols: impacts des processus physico-chimiques des nuages sur la formation des aérosols organiques secondaires. Ph.D. thesis, Paul Sabatier University, Toulouse, France

Cohard JM, Pinty JP, Bedos C (1998) Extending twomey's analytical estimate of nucleated cloud droplet concentrations from CCN spectra. J Atmos Sci V 55:3348–3357

IPCC (2013) Climate change, 2013: the physical science basis. In: Stocker TF, Qin D, Plattner GK et al. (eds) Contribution of Working Group I to the Fifth Assessment Report of the Intergovernmental Panel on Climate Change. Cambridge University Press, Cambridge, United Kingdom, New York, NY, USA, p 1535

Lafore JP, Stein J, Asencio N et al (1998) The meso-NH atmospheric simulation system, part I, Adiabatic formulation and control simulations. Ann Geophys V 16:90–109

Leriche M, Pinty JP, Mari C, Gazen D (2013) A cloud chemistry module for the 3-D cloud-resolving mesoscale model Meso-NH with application to idealized cases. Geosci Model Dev V 6:1275–1298. doi:10.5194/gmd-6-1275-2013

Tulet P, Crassier V, Solmon F, Guedalia D, Rosset R (2003) Description of the Mesoscale Nonhydrostatic Chemistry model and application to a transboundary pollution episode between northern France and southern England. J Geophys Res 108. doi:10.1029/2000JD000301

Tulet P, Grini A, Griffin R, Petitcol S (2006) ORILAM-SOA: a computationally efficient model for predicting secondary organic aerosols in 3D atmospheric models. J Geophys Res 111:D23208. doi:10.1029/2006JD007152

Chapter 7
Modelling of Externally-Mixed Particles in the Atmosphere

Shupeng Zhu and Karine N. Sartelet

Abstract This study presents the development of a new 3D size-composition resolved aerosol model (SCRAM). It solves the aerosol dynamic evolution for external mixtures taking into account the processes of coagulation, condensation/evaporation and nucleation. Both the size of particles and the mass fraction of each chemical compound are discretised. For a given particle size, particles of different chemical compositions may co-exist. Chemical components can be grouped into aggregates to reduce computational cost. SCRAM is coupled to the air quality model Polair3d/Polyphemus, and its performance to model air quality over Greater Paris is evaluated, as well as the consequences of the internally mixed assumption on aerosol distribution, composition and optical properties.

7.1 Introduction

Atmospheric particles significantly impact climate as well as human health. Thus, it is important to accurately simulate and forecast their concentrations. Most commonly used air quality models assume that particles are internally mixed (i.e., particles of a same diameter have the same chemical composition), largely for computational reasons. However, this assumption is disproved by measurements, especially close to sources (Mallet et al. 2004). In fact, the mixing state of particles is important for aerosol source identification, radiative effects, cloud droplet activation, and particle composition. The Size-Composition Resolved Aerosol Model (SCRAM) solves the aerosol dynamic evolution for external mixtures taking into account the processes of coagulation, condensation/evaporation (C/E) and

S. Zhu (✉) · K.N. Sartelet
CEREA, Joint Laboratory Ecole Des Ponts ParisTech - EDF R&D, Université Paris-Est, 77455 Champs-sur-Marne, France
e-mail: zhus@cerea.enpc.fr

K.N. Sartelet
e-mail: sartelet@cerea.enpc.fr

D.G. Steyn and N. Chaumerliac (eds.), *Air Pollution Modeling and its Application XXIV*, Springer Proceedings in Complexity,
DOI 10.1007/978-3-319-24478-5_7

nucleation. SCRAM is coupled to the air quality model Polair3d/Polyphemus, and simulations over greater Paris are performed to evaluate the mixing state of particles.

7.2 Model Description

In SCRAM, for a given particle size, particles of different chemical compositions may co-exist. Both the size of particles and the mass fraction of chemical compounds are discretised. For each size section, particles may have different compositions depending on the mass fraction of chemical compounds. Three aerosol dynamic processes are taken into account: coagulation, C/E, and nucleation. The parametrisation of Vehkamäki et al. (2002) for the homogeneous binary nucleation of sulphate and water is used for nucleation. For coagulation, the collision of particles caused by Brownian motion is simulated (Dergaoui et al. 2013). C/E is modelled using a bulk equilibrium approach for organics, while a fully dynamic approach or a hybrid approach may also be used for inorganics. In this paper, after C/E, the moving-center algorithm is used for mass-number redistribution among fixed size sections. For more details about the discretization methods, the mathematical derivation and model validations, please refer to Zhu et al. (2015). The SCRAM model was integrated into the Polair3D air quality model of the Polyphemus air quality platform for 3D simulations over the Paris area. The Carbon Bond model CB05 (Sarwar et al. 2008) is used for gas-phase chemistry, ISORROPIA (Nenes et al. 1998) for the formation of inorganic aerosols and the H^2O model for SOA formation (Couvidat et al. 2012).

7.3 Simulation over Paris Area

The simulation set-up is the same as described by Couvidat et al. (2013). The size distribution is discretized into 5 sections between 0.01 and 10 μm. The mass fractions of 5 groups of chemical compounds (inorganics, dust, black carbon (BC), hydrophilic and hydrophobic organics) are discretized into 3 mass-fraction sections ([0.0,0.2], [0.2,0.8], [0.8,1.0]), leading to 20 compositions for each size section. The particles that are dominated by one chemical group (mass fraction within [0.8,1.0]) are considered “unmixed”. Simulations are performed for 7 days, starting 28 June 2009. Two simulations are compared: the first simulation assumes particles are internally mixed; the other one assumes particles are externally mixed. In both case, C/E is computed dynamically for inorganics and nucleation is not taken into account. After comparing the time evolution of $PM_{2.5}$ between the two simulation results and observational data, it is found that the influence of the mixing-state assumption on $PM_{2.5}$ concentration is not significant. However, the chemical compositions are different. For inorganic species, external mixing leads to higher

NO_3 concentration in average over the domain (1.05 μg m^{-3} internal vs. 1.45 μg mm^{-3} external), but lower NH_4 concentration (1.39 μg m^{-3} internal vs. 1.27 μg m^{-3} external).

Figure 7.1a shows the spatial distribution of the unmixed BC percentage over Paris region during the morning rush at 5:00 UTC on 29 June obtained from the external mixing simulation. Regions with heavy traffic have higher unmixed BC percentages. The time evolution of the total BC mass and the unmixed BC percentage at an urban site Gennevillers is plotted in Fig. 7.1b, where an correlated trend between these two curves is observed. These results indicate that the BC mixing state is highly related to local emissions in urban areas, as it takes time for the newly emitted unmixed particles to mix with background concentrations. Besides, the BC mixing results from a rural site Fontainebleau shows that BC particles are generally more mixed compared to the urban site Gennevillers, and more BC particles are found to be mixed with organic compounds at the rural site.

The influence of the mixing state on particle optical properties is also investigated. AOD values are computed from the concentrations outputs of the externally and internally mixed simulations. In the algorithm computing the AOD, BC is assumed to be either core or well mixed. In average over the domain, AOD values computed from outputs of the internally and externally mixed simulations are more different (10 %) than those computed from outputs of the same simulation but with different assumptions in the AOD algorithm (BC core vs well mixed) (5 %). This indicates that the external mixing assumption may provide more detailed AOD information than the traditional BC core mixing assumption. The contribution of each particle population to the total AOD is also investigated. Particles dominated by inorganics and hydrophobic organics are found to be the largest contributors to the AOD values.

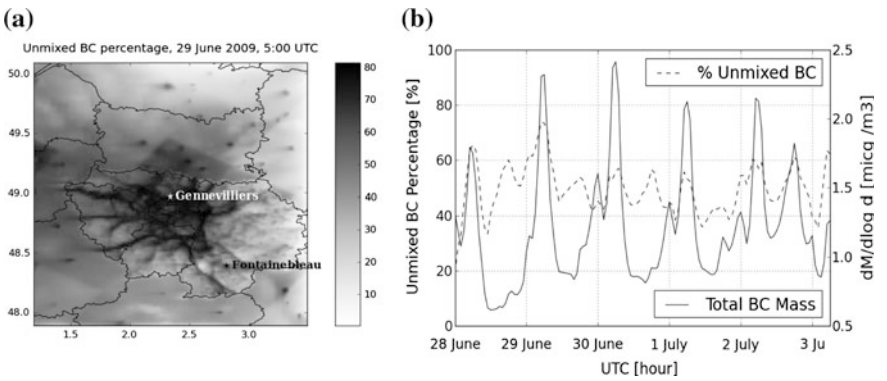

Fig. 7.1 Spatial distribution of BC mixing state over Paris region and time evolution of total BC mass and mixing percentage at Gennevilliers (which location is indicated in sub-figure (a)). **a** Unmixed BC distribution **b** Time evolution of BC mass and mixing state

7.4 Conclusions

The ability of SCRAM to investigate the particle mixing state is evaluated through a 3D simulation over the Greater Paris region. Valuable information about the mixing state is obtained through the comparisons between internal and external simulations. Although the total $PM_{2.5}$ concentrations are little impacted by the mixing state, it influences the $PM_{2.5}$ composition, e.g., the relative importance of NH_4 and NO_3 concentrations in $PM_{2.5}$. The unmixed BC percentage is found to increase during morning rush hours. Beside, particle optical properties are also studied, with large differences between AOD computed from the externally and internally mixed simulations in Paris reaching locally percentages as high as 80 %.

Questions and Answers

QUESTIONER: Mounir Chrit
QUESTION: Can you explain why external mixing leads to higher nitrate concentration, but lower ammonium concentration?

ANSWER: This is caused by the heterogeneous ammonium abundance compared to the sulphate fraction within each particle type in case of external mixing. Some particles are in an ammonia rich environment, leading to the condensation of more nitrate, while others are in an ammonia poor environment, leading to the condensation of less ammonia. One example is presented in Fig. 7.2.

QUESTIONER: Pius Lee
QUESTION: Would your internal/external mixing study depends on chemical environments e.g., NH3 rich etc. Would your study be extended to seasonal influence, such as ambient temperature, activity coefficient etc.?

ANSWER: Yes, it does. Under the same chemical environment, external and internal mixing may result to different PM distribution. The current simulation is conducted in summer conditions, and we would like to study the seasonal influence by doing a simulation in a winter period in the future.

QUESTIONER: Paul Makar
QUESTION: What was the relative computational requirements of your internally mixed vs externally mixed version of your model?

ANSWER: With the current particle type discretization, the additional computational cost of external mixing is about 10 times that of internal mixing.

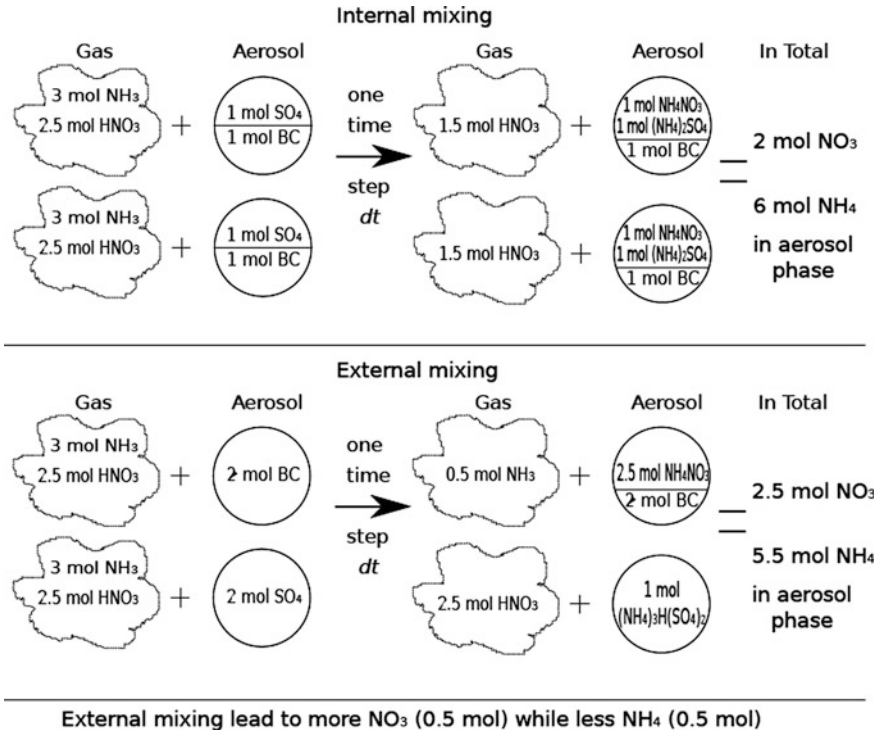

Fig. 7.2 Inorganic aerosol formation under different mixing assumptions

References

Couvidat F, Debry É, Sartelet K, Seigneur C (2012) A hydrophilic/hydrophobic organic (H_2O) aerosol model: development, evaluation and sensitivity analysis. J Geophys Res: Atmos (1984–2012), 117(D10)

Couvidat F, Kim Y, Sartelet K, Seigneur C, Marchand N, Sciare J (2013) Modeling secondary organic aerosol in an urban area: application to paris, france. Atmos Chem Phys 13(2):983–996

Dergaoui H, Sartelet KN, Debry É, Seigneur C (2013) Modeling coagulation of externally mixed particles: sectional approach for both size and chemical composition. J Aerosol Sci 58(0):17–32. ISSN 0021-8502

Mallet M, Roger J, Despiau S, Putaud J, Dubovik O (2004) A study of the mixing state of black carbon in urban zone. J Geophys Res: Atmos (1984–2012), 109(D4)

Nenes A, Pandis SN, Pilinis C (1998) Isorropia: a new thermodynamic equilibrium model for multiphase multicomponent inorganic aerosols. Aquat Geochem 4(1):123–152

Sarwar G, Luecken D, Yarwood G, Whitten GZ, Carter WP (2008) Impact of an updated carbon bond mechanism on predictions from the cmaq modeling system: Preliminary assessment. J Appl Meteorol Climatol 47(1):3–14

Vehkamäki H, Kulmala M, Napari I, Lehtinen KE, Timmreck C, Noppel M, Laaksonen A (2002) An improved parameterization for sulfuric acid–water nucleation rates for tropospheric and stratospheric conditions. J Geophys Res: Atmos (1984–2012), 107(D22):AAC-3

Zhu S, Sartelet KN, Seigneur C (2015) A size-composition resolved aerosol model for simulating the dynamics of externally mixed particles: Scram (v 1.0). Geosci Model Dev 8(6):1595–1612

Chapter 8
Regional Modeling of Aerosol Chemical Composition at the Puy de Dôme (France)

Christelle Barbet, Laurent Deguillaume, Nadine Chaumerliac, Maud Leriche, Alexandre Berger, Evelyn Freney, Aurélie Colomb, Karine Sellegri, Luc Patryl and Patrick Armand

Abstract Organic aerosols (OA) represent a large fraction (from 20 to 90 %) of the submicron particulate mass and it is mainly composed of secondary organic aerosols (SOA). Despite the ubiquity of OA in the atmosphere, there are still large uncertainties in understanding the formation pathways of SOA. Consequently, OA sources and physico-chemical transformations during their transport are poorly represented in chemistry-transport models and large gaps still remain between simulated and measured OA concentrations. The ability of the WRF-CHEM model to reproduce the organic aerosol mass concentration originated from anthropogenic or/and biogenic emissions is evaluated. From this perspective, simulations for two contrasted air masses are performed with WFR-Chem using the Volatility Basis Set (VBS) approach dedicated to the formation of SOA. Simulations results are compared to aerosol measurements performed at the puy de Dôme station with a compact Time-of-Flight Aerosol Mass Spectrometer for two episodes in autumn 2008 and in summer 2010. Moreover, measurements of both anthropogenic and biogenic VOCs are used to access the capacity of the WRF-Chem model to correctly simulate the concentrations levels of the gas precursors of the SOA.

C. Barbet · L. Deguillaume · N. Chaumerliac (✉) · E. Freney · A. Colomb · K. Sellegri
Laboratoire de Météorologie Physique (LaMP), CNRS, Université Clermont Auvergne, Université Blaise Pascal, 4 av. Blaise Pascal TSA, 60026 CS 60026 63178 Aubière Cedex, France
e-mail: n.chaumerliac@opgc.univ-bpclermont.fr

M. Leriche · A. Berger
Laboratoire d'Aérologie (LA), CNRS, Université de Toulouse, Université Paul Sabatier, 4 av. Edouard Belin, 31400 Toulouse, France

L. Patryl · P. Armand
CEA, DAM, DIF, F-91297 Arpajon, France

D.G. Steyn and N. Chaumerliac (eds.), *Air Pollution Modeling and its Application XXIV*, Springer Proceedings in Complexity,
DOI 10.1007/978-3-319-24478-5_8

8.1 Introduction

In the atmosphere, aerosol particles play a key role on both climate change and human health due to their effect on air quality. These particles are made of a complex mixture of both organic and inorganic species emitted by several sources. Although the sources and the production mechanisms for inorganic species are now quite well understood, the characterization of the organic fraction is much more difficult to achieve. Chemistry-transport models developed to better understand the organic aerosol formation processes underestimate the organic aerosol concentrations both at regional and global scales and especially during summertime periods (Knote et al. 2011).

Remaining sources of uncertainties concern emissions but also dry deposition of SOA gas precursors together with parameters controlling the SOA formation (yields, oxidation rates of OCVs) used in the VBS approach.

8.2 Model Description

The model used in this study is the version 3.4.1 of the WRF-Chem model (Grell et al. 2005). The RACM chemical mechanism (Stockwell et al. 1997) is used with 84 species and 252 reactions among which the oxidation of VOCs from both anthropogenic and biogenic sources. This mechanism is coupled with the aerosol module MADE (Ackermann et al. 1998) for the inorganic fraction of aerosols and, since recently, with the VBS (Ahmadov et al. 2012) parameterization for the SOA formation. The aerosol species treated are the inorganic ions (NH_4^+, NO_3^-, SO_4^{2-}, Cl^-), elemental carbon (EC), organic matter (primary and secondary OA), water, sea salt, and mineral dust.

Alkanes, alkenes, toluene, xylene, and cresol emitted by anthropogenic activities and isoprene, monoterpenes, and sesquiterpenes from biogenic sources are all oxidized by the hydroxyl radical $HO^{\cdot}$, O_3 or nitrate radicals $NO_3^{\cdot}$ in the gas-phase mechanism. Once these species are oxidized, the VBS parameterization is used to partition the organic matter produced between gas and aerosol phases according to their volatility. The VBS parameterization includes a four-bin volatility basis set with saturation concentrations (C^*) ranging from 1 to 1000 μg m^{-3} at 298 K and separated by one order of magnitude. The SOA yields are different for two regimes (high- and low-NO_x conditions) and the organic condensable vapours (OCVs), i.e. first generation VOCs oxidation products that condense on particles, may undergo a chemical aging by oxidizing with the $HO^{\cdot}$ radicals.

Anthropogenic emissions are taken from the MACCity inventory (Lamarque et al. 2010). Data are available with a spatial resolution of 0.5° per 0.5° and with a monthly temporal resolution from 1990 to 2010. Biogenic emissions are calculated online using MEGAN (Guenther et al. 2006). MEGAN quantifies the net biogenic

isoprene emissions, estimates VOCs, nitrogen oxides emissions. Biomass burning emissions are derived from the Fire Inventory from NCAR version 1.0 (FINNv1) with a daily temporal resolution and a spatial resolution close to 1 km.

8.3 Simulating Aerosol Particles with the WRF-Chem Model

WRF-Chem model outputs are compared with in situ cToF-AMS aerosol measurements made at the puy de Dôme (PUY) station site during Autumn 2008 and Summer 2010 (Freney et al. 2011).

Figure 8.1 provides the temporal evolution of sulphate (SO_4^{2-}), nitrate (NO_3^-), ammonium (NH_4^+), chlorine (Cl^-), black carbon (BC) and organics mass concentrations measured at the PUY station and simulated by the WRF-Chem model for the summer event. The mass concentrations of inorganic species modeled are fairly close to those observed whereas the mass concentrations of organic aerosol are strongly underestimated by the model (Barbet et al. 2015).

For this particular 2010 event where unexpected high concentrations were observed (12.5 µg m^{-3}), the model globally underestimates the levels of OA concentrations. VOCs concentrations calculated in the model were much below observed ones, especially for anthropogenic VOCs such as alkanes and aromatic compounds.

Several statistical performance measures recommended by Chang and Hanna (2004) have been applied to the baseline simulation, and to a series of sensitivity tests on emissions, dry deposition factor, SOA yields and oxidation rates of OCVs, taken individually, then combined and further all integrated (Table 8.1). Conclusions of those tests (only shown for the 2010 case but also valid for 2008

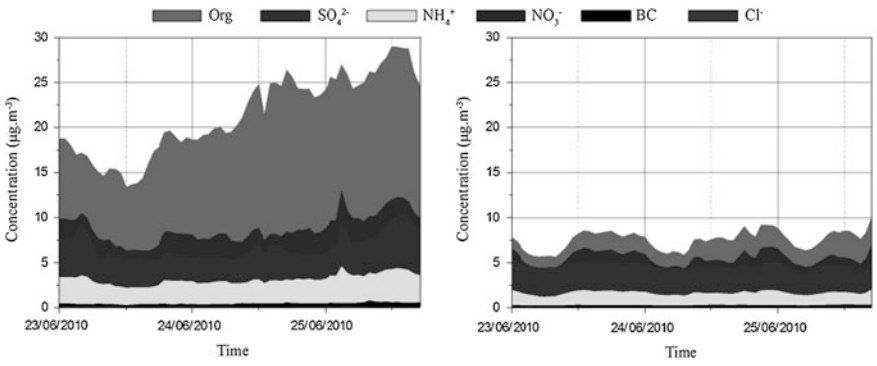

Fig. 8.1 Temporal evolution of the aerosol mass concentrations measured at the puy de Dome station (*left*) and simulated by the WRF-Chem model (*right*) for Summer 2010

Table 8.1 Statistical results compared with statistical performance measures and criteria acceptance for SOA mass concentrations for the baseline run and for sensitivity tests (individual and combined) for the summer 2010 period

Simulations	NMSE < 1.5	FB	FAC	VG	MG
		|FB| < 0.3	>0.5	<4	0.7 < MG < 1.3
Baseline	4.5	1.4	0.0	27.7	6.1
BVOC emissions x2	3.5	1.4	0.0	16.2	5.3
AVOC emissions x2	3.2	1.3	0.0	13.0	4.9
Dry deposition/2	3.8	1.4	0.0	18.7	5.5
BSOA yields × 2	2.7	1.3	0.0	9.5	4.4
ASOA yields × 2	2.2	1.2	0.0	6.0	3.8
Oxydation rate of OCVs	2.3	1.2	0.0	6.6	3.9
Dry deposition and emissions	2.3	1.2	0.0	7.1	4.0
Oxydation rate of OCVs and SOA yields	*0.2*	0.4	*1.0*	*1.2*	*1.4*
All effects	*0.1*	*0.2*	*1.0*	*1.1*	*1.2*

Italic values indicate good model performance

situation) are that uncertainties on SOA formation and aging processes explained the major part of the discrepancies observed between modeled and measured SOA mass concentrations.

References

Ackermann IJ, Hass H, Memmesheimer M, Ebel A, Binkowski FS, Shankar U (1998) Modal aerosol dynamics model for Europe: development and first applications. Atmos Environ 32:2981–2999. doi:10.1016/S1352-2310(98)00006-5

Ahmadov R, McKeen SA, Robinson AL, Bahreini R, Middlebrook AM, de Gouw JA, Meagher J, Hsie E-Y, Edgerton E, Shaw S, Trainer M (2012) A volatility basis set model for summertime secondary organic aerosols over the eastern United States in 2006. J Geophys Res 117:D06301. doi:201210.1029/2011JD016831

Barbet C, Deguillaume L, Chaumerliac N, Leriche M, Freney E, Colomb A, Sellegri K, Patryl L, Armand P (2015) Evaluation of aerosol chemical composition simulations by the WRF-Chem model at the Puy de Dôme mountain (France). AAQR. doi:10.4209/aaqr.2015.05.0342

Chang JC, Hanna SR (2004) Air quality model performance evaluation. Meteorol Atmos Phys 87:167–196. doi:10.1007/s00703-003-0070-7

Freney EJ, Sellegri K, Canonaco F, Boulon J, Hervo M, Weigel R, Pichon JM, Colomb A, Prévôt ASH, Laj P (2011) Seasonal variations in aerosol particle composition at the puy de Dôme research station in France. Atmos Chem Phys 11:13047–13059. doi:10.5194/acp-11-13047-2011

Grell GA, Peckham SE, Schmitz R, McKeen SA, Frost G, Skamarock WC, Eder B (2005) Fully coupled "online" chemistry within the WRF model. Atmos Environ 39:6957–6975. doi:10.1016/j.atmosenv.2005.04.027

Guenther A, Karl T, Harley P, Wiedinmyer C, Palmer PI, Geron C (2006) Estimates of global terrestrial isoprene emissions using MEGAN (Model of Emissions of Gases and Aerosols from Nature). Atmos Chem Phys 6:3181–3210. doi:10.5194/acp-6-3181-2006

Knote C, Brunner D, Vogel H, Allan J, Asmi A, Äijälä M, Carbone S, van der Gon HD, Jimenez JL, Kiendler-Scharr A et al (2011) Towards an online-coupled chemistry-climate model: evaluation of trace gases and aerosols in COSMO-ART. Geosci Model Dev 4:1077–1102. doi:10.5194/gmd-4-1077-2011

Lamarque J-F, Bond TC, Eyring V, Granier C, Heil A, Klimont Z, Lee D, Liousse C, Mieville A, Owen B, Schultz MG et al (2010) Historical (1850–2000) gridded anthropogenic and biomass burning emissions of reactive gases and aerosols: methodology and application. Atmos Chem Phys 10:7017–7039. doi:10.5194/acp-10-7017-2010

Stockwell WR, Kirchner F, Kuhn M, Seefeld S (1997) A new mechanism for regional atmospheric chemistry modeling. J Geophys Res 102:25847–25879. doi:199710.1029/97JD00849

Chapter 9
Effect of Sea Salt Emissions on Anthropogenic Air Pollution and Nitrogen Deposition in Northwestern Europe

Daniel Neumann, Johannes Bieser, Armin Aulinger and Volker Matthias

Abstract The North Sea region is characterised by several anthropogenic activities such as shipping, agriculture, industry and tourism. These activities go along with emissions of air pollutants such as NO_X, NH_3, and SO_2 leading to the formation of HNO_3, H_2SO_4, and particulate matter. Gaseous bases and acids (mainly HNO_3, H_2SO_4 and NH_3) tend to form new particles or to condense on existing ones. Meteorological conditions and size distribution of existing particles affect partitioning of these substances between gas and particle phase and between particle modes. In the marine troposphere, sea salt particles (mainly Cl^-, Na^+ and SO_4^{2-}) account for a considerable amount of fine and coarse particles providing surface for condensation of above mentioned substances. The presence of sea salt may also affect N deposition because dry deposition velocities of gaseous substances and different particle modes vary considerably. In the presented study, the effect of sea salt emissions on atmospheric air pollution in the North Sea region was analysed by the means of the Community Multiscale Air Quality (CMAQ) Model. We simulated on a 24×24 km^2 grid including the North and Baltic Sea. It was found, that the presence of sea salt increases coarse mode NH_4^+ and NO_3^- concentrations considerably while fine mode concentrations are decreased. This leads to increased total N deposition in coastal regions. At the same time, the deposition distant to the shore on the land as well as into the ocean decreases. However, this study shows that on spatial average only about 5 % of N deposition into the North Sea is caused by sea salt particles. Locally, the effect of sea salt on N deposition is partly higher. Therefore, sea salt emissions in regional air quality models are important for pre-

D. Neumann (✉) · J. Bieser · A. Aulinger · V. Matthias
Helmholtz-Zentrum Geesthacht, Institute of Coastal Research, Max-Planck-Str. 1, 21502 Geesthacht, Germany
e-mail: daniel.neumann@hzg.de

J. Bieser
Deutsches Zentrum für Luft- und Raumfahrt, Institute of Atmospheric Physics, Münchener Straße 20, 82234 Weßling, Germany

D.G. Steyn and N. Chaumerliac (eds.), *Air Pollution Modeling and its Application XXIV*, Springer Proceedings in Complexity,
DOI 10.1007/978-3-319-24478-5_9

dicting the partitioning of anthropogenic pollutants between gas and particle phase and their deposition patterns correctly.

9.1 Introduction

In the North Sea region, considerable amounts of air pollutants, such as NO_X, NH_3, SO_2, and primary fine and coarse particles, are emitted by anthropogenic activities into the atmosphere. The named species may react to HNO_3 and H_2SO_4 and form fine particles. Fine particles ($PM_{2.5}$) may cause cardiovascular and respiratory diseases, NO_X may lead to the formation of smog, H_2SO_4 acidifies rain, and nitrogen deposition into water bodies stimulates eutrophication.

The presence of large numbers of fine and coarse particles, such as coarse sea salt particles, may affect the behavior of these pollutants in the atmosphere. Gaseous HNO_3, H_2SO_4, and NH_3 tend to condense on particles instead of forming new ones. Coarse particles depose faster than fine particles. Therefore, sea salt emissions are expected to affect the deposition of nitrogen species.

Traditionally, sea salt emissions have been parameterized based on the 10 m wind speed (Monahan and Muircheartaigh 1980; Lewis and Schwartz 2004). In recent years, new parameterizations considering more parameters were published (Martensson et al. 2003; Jaeglé et al. 2011; Ovadnevaite et al. 2014). However, there is still considerable uncertainty in parameterized sea salt emissions. In particular, sea salt emissions close to the coast, denoted as surf zone emissions, contain high uncertainty due to local varying coastal features such as shallow sand beaches and cliffs.

In the presented study, the effect of sea salt emissions on atmospheric nitrogen compounds in the North Sea region was analyzed by the means of the Community Multiscale Air Quality (CMAQ) Model.

9.2 Materials and Methods

The simulations were performed with CMAQ Version 5.0.1 with cb05tump gas phase chemistry mechanism and aero05 aerosol mechanism (see for details: www.airqualitymodeling.org/cmaqwiki). Aero05 includes the condensation of HCl, NH_3, HNO_3, and H_2SO_4 on particles, the evaporation back into the atmosphere (except of H_2SO_4), and the formation of particles. The simulations were performed on a 72×72 km^2 grid covering Europe and on a nested 24×24 km^2 grid covering the North and Baltic Seas. The time period was winter and summer 2008. However, only winter 2008 is considered here. The emission were created by SMOKE-EU (Bieser et al. 2011) except of the shipping emissions (Aulinger et al. 2015). The meteorology was calculated by COSMO-CLM (Geyer 2014).

The sea salt emissions in CMAQ are generated by the parameterization of Gong (Gong 2003; Kelly et al. 2010) in which the emissions are scaled by a wind dependent

function denoted as white cap coverage (Monahan and Muircheartaigh 1980). In addition in this study, the sea salt emissions are linearly scaled by local salinity because the parameterization was derived for a fixed salinity (35 g/kg). In a 50 m wide stripe along the coast, denoted as surf zone, the white cap coverage is set to its maximum (Kelly et al. 2010). Three sea salt emission scenarios were considered in this study: standard sea salt emissions (*base* scenario), standard sea salt emissions without special treatment of the surf zone (*noSurf*) and, no sea salt emissions (*zero*).

Simulation results are compared to measurements of the EMEP station DE0009R (Zingst). Information on the station can be obtained via the EMEP website.

9.3 Results

The time series on the left of Fig. 9.1 show modeled and measured Na^+ and $HNO_3 + NO_3^-$ concentrations at Zingst, Germany. The sum parameter is chosen because these measurements performed with 3-filter packs do not guarantee a clear distinction. Na^+ concentrations are well predicted in their temporal resolution. Peak concentrations are overestimated. Surf zone emissions do only slightly contribute to total Na^+ concentrations. In $HNO_3 + NO_3^-$, the difference between the *base* and *zero* cases is low compared to the variability between modeled and measured concentrations.

The right plot in Fig. 9.1 shows the nitrogen deposition in January and February. The plot is thought as base line for Fig. 9.2. In general, deposition is higher above the land. Nitrogen compounds are also blown onto the North Sea and depose there.

Figure 9.2 left shows the effect of decreased surf zone emissions on nitrogen deposition. Deposition decreases mainly on the land side up to 4 grid cells (≈100 km) inland. There is nearly no effect on the deposition above the North Sea. The effect of the surf zone is low compared to the total depositions shown in

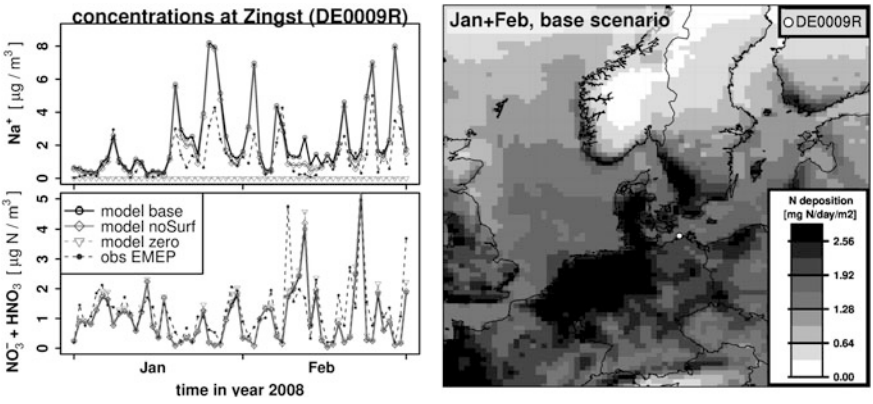

Fig. 9.1 *Left* daily average Na^+ and $HNO_3 + NO_3^-$ concentrations at the EMEP station Zingst (DE0009R). *Right* modeled nitrogen deposition (wet + dry) in January and February 2008 (NO_X HNO_3, NH_3, N_2O_5, NO_3^-, NH_4^+). Results are based on the model scenario *base*

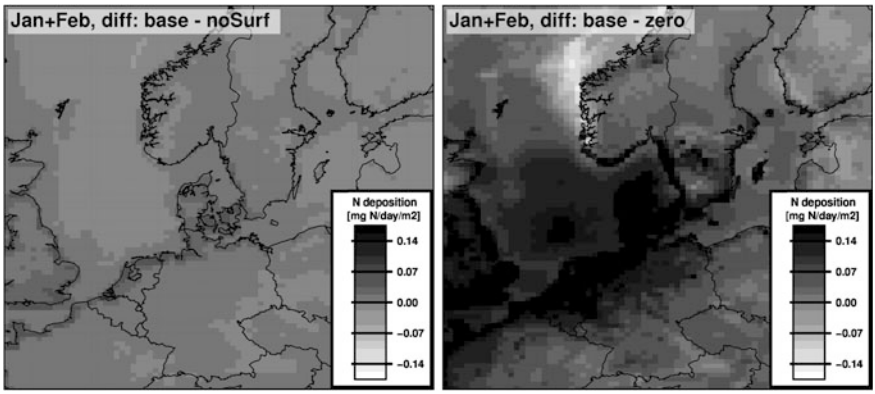

Fig. 9.2 Differences of nitrogen deposition in winter between *base* and *noSurf* scenarios (*left*), and *base* and *zero* scenarios (*right*). Nitrogen deposition is calculated as in Fig. 9.1

Fig. 9.1. Figure 9.2 right shows nitrogen deposition in the absence of sea salt emissions. The deposition into the North Sea and in coastal regions decreases considerably. On average, about 7 % of nitrogen deposition into North Sea water can be attributed to sea salt particles.

9.4 Discussion and Conclusion

It was shown that sea salt emissions affect nitrogen deposition in the North Sea region but the effect is quite low. However in some coastal regions, the affect of sea salt is relevant. Measurement data from Zingst (Fig. 9.1 left) show that variations in the sea salt emissions do not improve predicted $HNO_3 + NO_3^-$ concentration.

Solely two month (January and February) are considered in this study. Short term meteorological conditions affect the model results considerably. Especially, nitrogen deposition patterns in the central North Sea and in inland regions are affected by precipitation and wind. Therefore, longer time scales need to be considered.

As the Na^+ time series in Fig. 9.1 show, sea salt emissions are overestimated during winter. During summer (not shown), no overestimation takes place. Since average wind speed is highest during winter, we assume that overestimating arises at high wind speeds. We plan to test two more modern sea salt emission parameterizations (Martensson et al. 2003; Ovadnevaite et al. 2014) in order to reduce overestimation.

Acknowledgments We thank the EMEP network for providing EMEP measurement data. We appreciate comments of J. Kelly, U. Shankar and colleagues on the sea salt emission module of CMAQ. Finally, we wish to thank the programmers and maintainers of CMAQ, R, cdo and NCO code.

References

Aulinger A, Matthias V, Zeretzke M, Bieser J, Quante M, Backes A (2015) The impact of shipping emissions on air pollution in the greater north sea region—part 1: current emissions and concentrations. Atmos Chem Phys Discuss 15(8):11277–11323

Bieser J, Aulinger A, Matthias V, Quante M, Builtjes P (2011) SMOKE for Europe—adaptation, modification and evaluation of a comprehensive emission model for Europe. Geosci Model Dev 4(1):47–68

Geyer B (2014) High-resolution atmospheric reconstruction for Europe 1948–2012: coastDat2. Earth Syst Sci Data 6(1):147–164

Gong SL (2003) A parameterization of sea-salt aerosol source function for sub- and super-micron particles. Global Biogeochem Cycles 17(4):7

Jaeglé L, Quinn PK, Bates TS, Alexander B, Lin J-T (2011) Global distribution of sea salt aerosols: new constraints from in situ and remote sensing observations. Atmos Chem Phys 11 (7):3137–3157

Kelly JT, Bhave PV, Nolte CG, Shankar U, Foley KM (2010) Simulating emission and chemical evolution of coarse sea-salt particles in the community multiscale air quality (CMAQ) model. Geosci Model Dev 3(1):257–273

Lewis ER, Schwartz SE (2004) Sea salt aerosol production: mechanisms, methods, measurements and models—a critical review. AGU, Washington, D.C.

Martensson EM, Nilsson ED, de Leeuw G, Cohen LH, Hansson H-C (2003) Laboratory simulations and parameterization of the primary marine aerosol production. J Geophys Res Atmos 108(D9):4297–4308

Monahan EC, Muircheartaigh IO (1980) Optimal power-law description of oceanic whitecap coverage dependence on wind speed. J Phys Oceanogr 10(12):2094–2099

Ovadnevaite J, Manders A, de Leeuw G, Ceburnis D, Monahan C, Partanen A-I, Korhonen H, O'Dowd CD (2014) A sea spray aerosol flux parameterization encapsulating wave state. Atmos Chem Phys 14(4):1837–1852

Chapter 10
Spatial and Temporal Variations in Aerosol Properties in High-Resolution Convection-Permitting Simulations in an Idealized Tropical Marine Domain

Céline Planche, Graham W. Mann, Kenneth S. Carslaw, John H. Marsham and Paul R. Field

Abstract We carry out high-resolution idealized tropical simulations in a general circulation model with interactive aerosol microphysics to investigate aerosol variations relevant to operational weather forecasting and convection permitting sub-climate scales. We quantify the temporal and spatial variations in aerosol properties. The aerosol structure is driven by aerosol microphysics processes and dynamical processes which influence aerosol properties, emission and transport on scales not resolved by climate models.

10.1 Introduction

Successive IPCC climate Assessment Reports (Boucher et al. 2013; among others) have identified the indirect radiative forcing of aerosols as having a high level of uncertainty that need to be constrained for improved prediction of anthropogenic climate change. In order to assess climate model to capture this indirect aerosols forcing, the understanding of the aerosols properties and the microphysical interactions of aerosols and clouds at cloud scales is needed. Multiple modeling studies

C. Planche (✉)
Laboratoire de Météorologie Physique, Université Blaise Pascal, OPGC/CNRS UMR 6016, Clermont-Ferrand, France
e-mail: C.Planche@opgc.univ-bpclermont.fr

C. Planche · G.W. Mann · K.S. Carslaw · J.H. Marsham · P.R. Field
School of Earth and Environment, ICAS, University of Leeds, Leeds, UK

G.W. Mann
National Centre for Atmospheric Sciences, School of Earth and Environment, University of Leeds, Leeds, UK

P.R. Field
Met Office, Exeter, UK

D.G. Steyn and N. Chaumerliac (eds.), *Air Pollution Modeling and its Application XXIV*, Springer Proceedings in Complexity,
DOI 10.1007/978-3-319-24478-5_10

using aerosol module have indeed explored the main features of the aerosols distributions over regions and the globe (e.g. Sofiev et al. 2011) but only few studies have explored the aerosols properties and their cloud interactions at high resolution (e.g. Ekman et al. 2006).

The main objective of this study is to investigate the temporal and spatial variation of aerosols at convection-permitting resolution ($\sim$1 km), and assess the relevance of aerosol representation for operational weather forecasting and climate simulations. In order to well characterize the dynamical influence on cloud-relevant aerosol properties, an aerosol microphysics scheme applied at high-resolution within an idealized three-dimensional aqua-planet tropical case is used.

10.2 Model Description

The UK Chemical and Aerosol (UKCA) sub-model of the Met Office Unified Model (MetUM) is used, including the GLOMAP-mode aerosol microphysics scheme (Mann et al. 2010) which calculates the evolution of 4 aerosol components (SU, SS, BC, POM) in 5 size modes (Table 10.1). The dust aerosols are transported separately in the existing 6-bin MetUM scheme (Woodward 2001). The aerosol processes are simulated in a size-resolved manner following the original GLOMAP-bin approach (Spracklen et al. 2008).

Anthropogenic emissions of SO_2 and BC/OC are taken from the relevant grid-cell from the IPCC AR5 global emission data (Lamarque et al. 2010), with monoterpene and biomass BC/OC emissions from the GEIA and GFEDv2 databases respectively. The model also includes interactive emissions of DMS and sea-spray and an online tropospheric chemistry scheme, enabling the role of dynamical variations in aerosol sources to also be assessed.

The aerosol features are analyzed in a high-resolution idealized tropical simulation using the UKCA aerosol scheme incorporated in the MetUM which provides

Table 10.1 Standard aerosol configuration for GLOMAP-mode

Index	Name	Size range	Composition	Soluble	σ_g
1	nucsol	D < 10 nm	SU, POM	Yes	1.59
2	Aitsol	10 nm < D < 100 μm	SU, BC, POM	Yes	1.59
3	accsol	100 nm < D < 1 μm	SU, BC, POM, SS	Yes	1.59
4	coasol	D < 1 μm	SU, BC, POM, SS	Yes	2.00
5	Aitins	10 nm < D < 100 nm	BC, POM	No	1.59

The size distribution is described by lognormal modes with varying geometric mean diameter D and fixed geometric standard deviation σ_g. Particle number and mass are transferred between modes when D exceeds the upper limit for the mode. Names are given in function of the aerosols mode ('*nuc*', '*Ait*', '*acc*' and '*coa*' are for '*nucleation*', '*Aitken*', '*accumulation*' and '*coarse*') and their solubility properties ('*sol*' and '*ins*' mean the aerosols are '*soluble'* or '*insoluble'*). The aerosols can be composed of sulphate (SU), primary organic matter (POM), black carbon (BC), or sea-salt (SS)

the dynamical and the thermodynamical frameworks with a 1.5 km horizontal resolution. The simulation timestep is 30 s and the UKCA scheme is called every 10 timesteps, i.e. every 5 min. This model configuration permits the formation of a deep convective cloud which becomes precipitating after 4 h of simulation.

10.3 Aerosol Properties at Sub-climate Scales

The UKCA model outputs for this aqua-planet idealized case, where the sea-salt aerosols are dominant, are statistically studied in order to figure out aerosols trends at sub-climate scales. Figure 10.1 shows the temporal evolution of the mean and the associated standard deviation of the aerosol radius and concentration for the sea-salt accsol and coasol modes at the surface.

Until 8 h of integration (i.e. during the spin-up time), the concentration and radius fields have a large deviation for both modes due to the extreme variability of the dynamical properties. The mean radius and concentration of the aerosols from the coarse mode are then decreasing (Figs. 10.1b, d). The sedimentation of the largest aerosol particles induces this decrease in the mean aerosol size as well as in the concentration. For the accsol mode, the size of the aerosols remains quite the

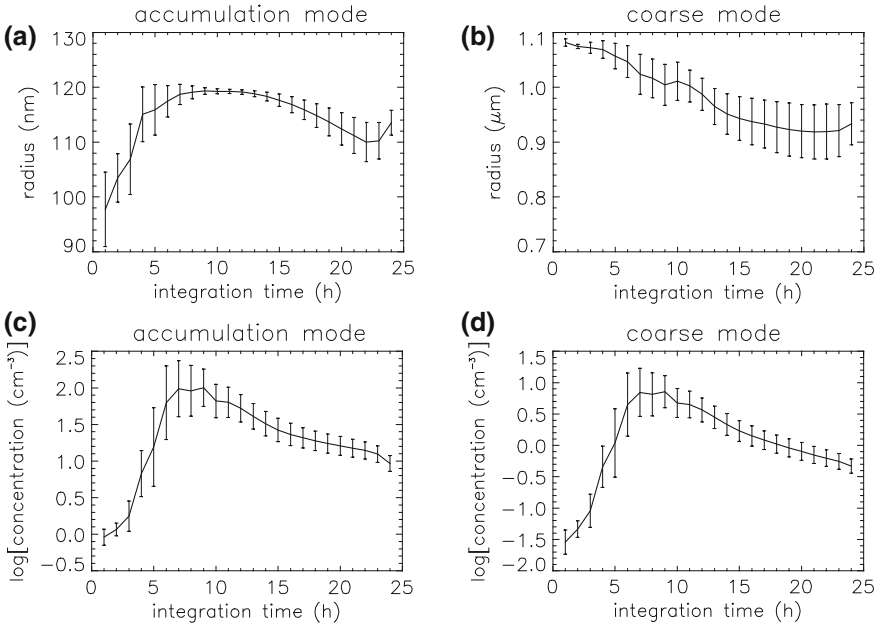

Fig. 10.1 Time series of the mean ± one standard deviation of the geometric radius (**a**, **b**) and the logarithm of the concentration (**c**, **d**) of the surface aerosols from the accumulation (**a**, **c**) and coarse (**b**, **d**) soluble modes

same between 9 and 14 h of simulation, decreases till 21 h and then rises until the end of the integration while the concentration is decreasing all along the simulation (except during the spin-up time). The aerosol emissions are strongly dependent of the horizontal wind speeds which are high between 9 and 14 h of simulations. The aerosol emissions seem to follow a mode with a geometric mean radius closed to 120 nm and with a small fixed geometric standard deviation. Between 15 and 21 h, as for the coarsol mode, the sedimentation is important reducing the mean radius and the concentration of the aerosols. Moreover, the impaction scavenging can also impacts the aerosol concentration since the precipitation rate is important during this period. After 21 h of simulations, the aerosol coagulation and condensation processes seem to be dominated since the concentration decreases while the mean size increases.

This analysis shows the extreme variability of the aerosol properties on high-scales which is not resolved by climate models generally used for estimate the aerosol indirect impact.

References

Boucher O, Randall D, Artaxo P, Bretherton C, Feingold G, Forster P, Kerminen V-M, Kondo Y, Liao H, Lohmann U, Rasch P, Satheesh SK, Sherwood S, Stevens B, Zhang XY (2013) Clouds and aerosols. In: Stocker TF, Qin D, Plattner G-K, Tignor M, Allen SK, Boschung J, Nauels A, Xia Y, Bex V, Midgley PM (eds) Climate change 2013: the physical basis. Contribution of working group I to the fifth assessment report of the intergovernmental panel on climate change. Cambridge University Press, Cambridge

Ekman A, Wang C, Ström J, Krejci R (2006) Explicit simulation of aerosol physics in a cloud-resolving model: aerosol transport and processing in free troposphere. J Atmos Sci 63:682–695

Lamarque J-F, Bond TC, Eyring V, Granier C, Heil A, Klimont Z, Lee D, Liousse C, Mieville A, Owen B, Schultz MG, Shindell D, Smith SJ, Stehfest E, Van Aardenne J, Cooper OR, Kainuma M, Mahowald N, McConnell JR, Naik V, Riahi K, van Vuuren DP (2010) Historical (1850–2000) gridded anthropogenic and biomass burning emissions of reactive gases and aerosols: methodology and application. Atmos Chem Phys 10:7017–7039. doi:10.5194/acp-10-7017-2010

Mann GW, Carslaw KS, Spracklen DV, Ridley DA, Manktelow PT, Chipperfield MP, Pickering SJ, Johnson CE (2010) Description and evaluation of GLOMAP-mode: a modal global aerosol microphysics model for the UKCA composition-climate model. Geosci Model Dev 3:519–551

Sofiev M, Soares J, Prank M, de Leeuw G, Kukkonen J (2011) A regional-to-global model of emission and transport of sea salt particles in atmosphere. J Geophys Res 116:D21302

Spracklen DV, Carslaw KS, Kulmala M, Chipperfield MP, Mann GW (2008) Contribution of particle formation to global cloud condensation nuclei concentrations. Geophys Res Lett 35: L06808

Woodward S (2001) Modeling the atmospheric life cycle and radiative impact of mineral dust in the Hadley Centre climate model. J Geophys Res 106(D16):18115–18166

Chapter 11
Analysis of National Verses Long-Range Transport Contribution to Organic and Inorganic Aerosol Load in Selected Location in Poland

Barbara Błaszczak, Magdalena Reizer, Katarzyna Juda-Rezler, Ewa Krajny, Barbara Mathews and Krzysztof Klejnowski

Abstract The paper investigates $PM_{2.5}$ levels and composition in 3 different locations in Poland for cold and warm period of 2013. The highest share of SOC and POC in $PM_{2.5}$ was found in heating season, which was probably due to an increase in the activity of local emission sources of PM, especially biomass burning and fossil fuel combustion in residential sector, while SIA contribution in $PM_{2.5}$ mass was relatively constant during heating and non-heating period at all 3 sites. During non-heating season air mass back trajectories were grouped into 5 clusters representing mostly westerly flows (50–72 %). During heating season the trajectories were grouped into 6 clusters coming mostly from eastern directions (54–64 %).

11.1 Introduction

Fine particulate matter ($PM_{2.5}$) is composed mainly of carbon compounds and water-soluble ions (e.g. Rogula-Kozłowska et al. 2014). At the time of entry into force air quality standards for $PM_{2.5}$ there have been a need to consider the contribution of secondary aerosols, resulting from chemical and photochemical

B. Błaszczak (✉) · B. Mathews · K. Klejnowski
Institute of Environmental Engineering, Polish Academy of Sciences,
34 M. Skłodowska-Curie St, 41-819 Zabrze, Poland
e-mail: barbara.blaszczak@ipis.zabrze.pl

M. Reizer · K. Juda-Rezler
Faculty of Environmental Engineering, Warsaw University of Technology,
20 Nowowiejska St, 00-653 Warsaw, Poland

E. Krajny
Monitoring and Modeling of Air Pollution Department, Institute of Meteorology and Water Management–National Research Institute, 10 Bratków St,
40-045 Katowice, Poland

D.G. Steyn and N. Chaumerliac (eds.), *Air Pollution Modeling and its Application XXIV*, Springer Proceedings in Complexity,
DOI 10.1007/978-3-319-24478-5_11

transformations, their role in global climate change and impacts on the living standards of the population. The secondary component greatly affect the concentration and chemical composition of fine PM and includes secondary inorganic aerosol (SIA) and secondary organic aerosol (SOA).

11.2 Sampling Location and Methodology

During heating (H) and non-heating (NH) period in 2013, diurnal samples of $PM_{2.5}$ were taken, with the use of low-volume samplers, at three air quality monitoring stations in Poland: Szczecin (urban background, UB), Trzebinia (UB) and Zloty Potok (regional background, RB) (Fig. 11.1).

Sunset Laboratory carbon analyzer and a Herisau Metrohm AG ion chromatograph were used to determine the contents of carbon (organic—OC, and elemental—EC) and water-soluble ions, respectively. SIA was the sum of the concentrations of $PM_{2.5}$-bound non sea salt sulphate, nss-SO_4^{2-}, (Sillanpää 2006), NO_3^- and NH_4^+. Secondary and primary organic carbon (respectively SOC and POC) levels were estimated following the methodology of Castro et al. (1999):

$$\mathrm{SOC} = \mathrm{OC} - (\mathrm{OC/EC})_{\mathrm{pri}} \cdot \mathrm{EC} \tag{11.1}$$

$$\mathrm{POC} = \mathrm{OC} - \mathrm{SOC} \tag{11.2}$$

where $(OC/EC)_{pri}$ is the ratio of primary OC to EC. To estimate $(OC/EC)_{pri}$ a least-squares regression was performed for the 10 % samples with the lowest OC/EC ratio (Strader et al. 1999).

The Hybrid Single-Particle Lagrangian Integrated Trajectory (HYSPLIT) model was used to calculate 3-day backward trajectories of air masses arriving to each location at 10 m above ground level. A non-hierarchical k-means cluster analysis was further applied to group the modelled trajectories into clusters.

City	Coordinates	Measurement period
1 – Szczecin	14°39'48" E 53°22'51" N	H: Jan-Mar 2013 (n = 83) NH: May-Jul 2013 (n = 78)
2 – Trzebinia	19°28'41" E 50°09'23" N	H: Feb-Mar 2013 (n = 55) NH: May-Jul 2013(n = 90)
3 – Zloty Potok	19°27'29" E 50°42'38" N	H: Jan-Mar 2013 (n = 89) NH: Apr 20-Jul 2013(n = 86)

Fig. 11.1 Location of measurement sites

11.3 $PM_{2.5}$ Chemical Compositions—Percentage of Organic and Inorganic Aerosol Load

The levels of $PM_{2.5}$ as well as carbon and ionic constituents revealed spatial and seasonal variations, Table 11.1. Elevated concentrations of $PM_{2.5}$, OC and EC were found during heating period due to higher anthropogenic emission and unfavorable atmospheric conditions. Levels of above mentioned compounds were comparable for Trzebinia and Zloty Potok sites from Southern Poland and higher than in Szczecin in Northern-Western part of the country.

Water-soluble inorganic species in general follow a mass abundance pattern: $SO_4^{2-} > NO_3^- > NH_4^+$, Table 11.1. Higher concentrations of inorganic ions were observed during heating period at all sites.

Generally, a higher share of SOC and POC was found in heating season, which was probably due to an increase in the activity of local emission sources of PM, especially biomass burning and fossil fuel combustion in domestic furnaces and in small local heating plants.

The share of SIA was, in general, higher than SOC contribution, especially in $PM_{2.5}$ samples from Szczecin. Inorganic ions contents showed spatial variation with the highest levels recorded in Trzebinia, located in highly urbanized and industrialized Silesia region, and the lowest observed at RB site in Zloty Potok.

The obtained results revealed that SIA contribution in $PM_{2.5}$ mass was relatively constant during heating and non-heating period at all 3 sites, however contribution of individual inorganic ions to $PM_{2.5}$ mass showed different seasonal variations, which agreed well with literature data (e.g. Rogula-Kozłowska et al. 2014).

Table 11.1 Concentrations of $PM_{2.5}$ and its selected compounds (average ± standard deviation; $\mu g/m^3$)

Component	Szczecin		Trzebinia		Złoty Potok	
	Heating	Non-heating	Heating	Non-heating	Heating	Non-heating
$PM_{2.5}$	23.0±16.6	8.5±3.2	38.9±16.8	16.6±5.1	33.3±19.4	16.3±4.9
OC	8.0±6.6	2.7±1.0	15.6±6.5	4.5±1.4	12.5±7.8	4.5±1.2
EC	1.6±1.0	0.7±0.3	4.0±4.0	1.2±0.4	2.2±1.3	0.8±0.3
OC/EC	4.7±1.2	4.4±1.4	4.9±1.3	4.1±1.3	5.8±1.1	5.9±1.2
SOC	4.4±4.7	1.2±0.7	13.0±6.4	3.7±1.3	4.8±3.6	1.7±0.8
POC	3.6±2.2	1.5±0.7	2.6±2.7	0.8±0.3	7.8±4.8	2.8±0.9
nss-SO_4^{2-}	2.4±2.2	1.5±0.6	4.6±3.1	3.4±1.4	2.7±1.2	1.8±0.6
NO_3^-	3.0±2.3	0.8±0.8	3.2±1.6	0.8±0.3	2.0±1.1	0.7±0.4
NH_4^+	1.8±1.7	0.5±0.3	2.9±1.7	1.0±0.5	1.1±0.7	0.3±0.2
SIA	7.2±6.0	2.8±1.4	10.8±5.9	5.1±1.8	5.8±2.9	2.7±0.9

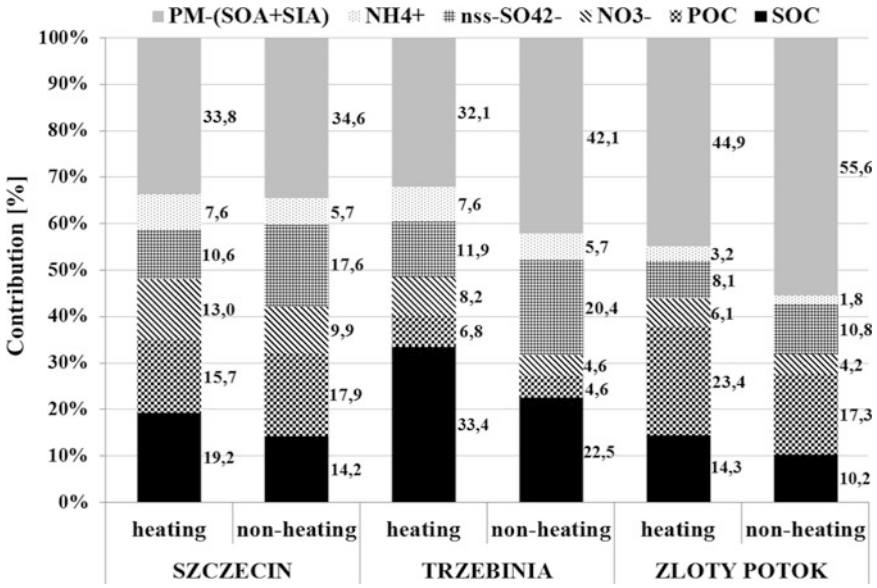

Fig. 11.2 The seasonal percentages of the main groups of the chemical components in $PM_{2.5}$ at three sampling sites in Poland

The share of nss-SO_4^{2-} was higher in summer (enhanced photochemistry), opposite to NO_3^- and NH_4^+ with higher contribution to $PM_{2.5}$ mass registered during heating season (owing to the thermal instability of the ammonium nitrate) (Fig. 11.2).

11.4 Air Mass Back Trajectories

Figure 11.3 shows 5 final cluster centers for non-heating season and 6 cluster centers for heating season in all investigated locations. For non-heating season cluster centers represent mostly westerly flows, accounted for almost 65, 50 and 72 % of the trajectories, respectively for Szczecin, Trzebinia and Zloty Potok. In contrary, for heating season cluster centers represent mostly easterly flows, accounted for almost 64, 57 and 54 % of the trajectories, respectively for Szczecin, Trzebinia and Zloty Potok. During both analyzed periods, slow trajectories representing 16–28 % of the data indicate national and/or regional transport of air pollution.

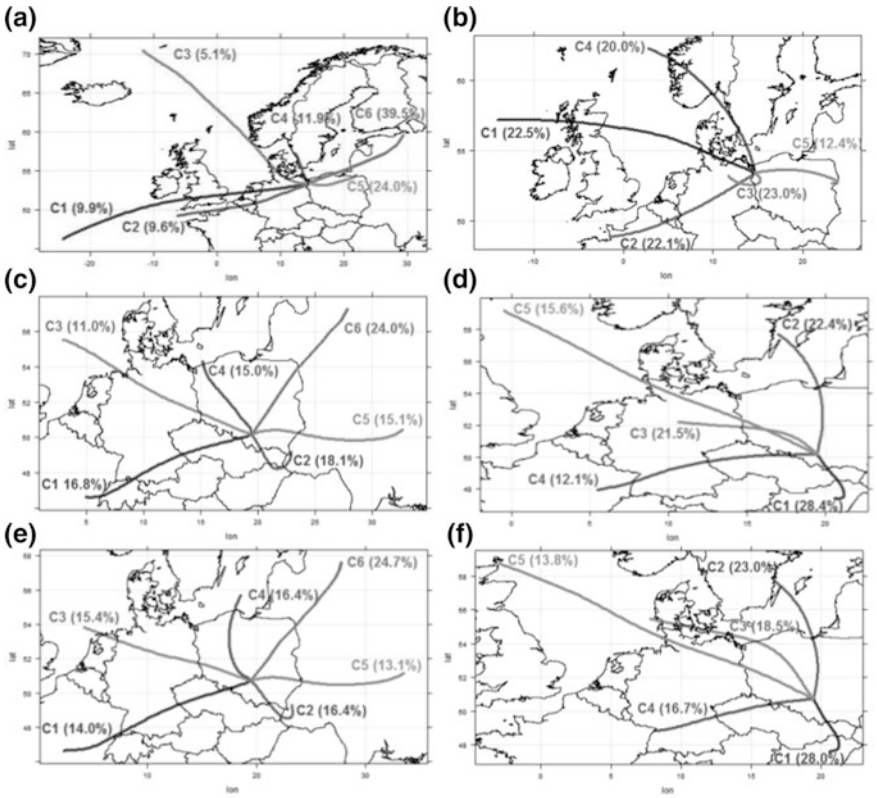

Fig. 11.3 The air mass back trajectory cluster centers for Szczecin (*A, B*), Trzebinia (*C, D*) and Zloty Potok (*E, F*) in Poland, calculated for heating (*left column*) and non-heating (*right column*) periods of 2013. The percentage of trajectories occurring in each cluster is shown in parentheses

Acknowledgments This work was supported by the Polish National Science Centre partly under PRELUDIUM funding scheme 2nd edition, Project no. UMO-2011/03/N/ST10/05542 and partly under OPUS funding scheme 2nd edition, Project no. UMO-2011/03/B/ST10/04624. The authors also gratefully acknowledge the NOAA Air Resources Laboratory (ARL) for the provision of the HYSPLIT transport and dispersion model (http://www.arl.noaa.gov/ready.php).

References

Castro LM, Pio CA, Harrison RM et al (1999) Carbonaceous aerosol in urban and rural European atmospheres: estimation of secondary organic carbon concentrations. Atmos Environ 33:2771–2781

Rogula-Kozłowska W, Klejnowski K, Rogula-Kopiec P et al (2014) Spatial and seasonal variability of the mass concentration and chemical composition of $PM_{2.5}$ in Poland. Air Qual Atmos Health 7:41–58

Sillanpää M, Hillamo R, Saarikoski S et al (2006) Chemical composition and mass closure of particulate matter at six urban sites in Europe. Atmos Environ 40:212–223
Strader R, Lurmann F, Pandis SN (1999) Evaluation of secondary organic aerosol formation in winter. Atmos Environ 33:4849–4863

Part II
Focus on Mediterranean Aerosols

Chapter 12
Impact of Aerosols in Regional Climate Projections Over the Mediterranean Area

Pierre Nabat, Kiki, Samuel Somot, Marc Mallet and Martine Michou

Abstract The Mediterranean region is characterized by the accumulation of aerosols from numerous and various sources, which have very important effects on its climate. Therefore, the evolution of aerosols in future is expected to influence climate projections over this region which is already seen as a climate change "hotspot". In this study realized in the framework of the ChArMEx and HyMeX programmes of the MISTRALS initiative, we consider a regional climate modelling approach, using the ALADIN-climate model which includes an interactive aerosol scheme, in order to better understand the future evolution of aerosols and their impact on future climate. Simulations have been carried out over past (1971–2000) and future (2071–2100) periods. The evolution of aerosols is driven both by changes in anthropogenic emissions, and the changes in climate variables, such as surface wind, that drive natural emissions such as dust uplift. Both a decrease in sulfate aerosols coming from Europe and an increase of dust emissions in northern Africa are expected by the end of the 21st Century. The decrease in sulfate concentrations could contribute to about 10 % of the expected warming over Europe.

12.1 Motivations

Atmospheric aerosols significantly influence climate through their impact on radiative budget and clouds (Kaufman et al. 2002). In the Mediterranean region, various and numerous aerosols are observed, because of the presence of different sources around this region: industrial and urban aerosols from Europe and North African towns, biomass burning from Eastern Europe, dust aerosols from Africa,

P. Nabat (✉) · Kiki · S. Somot · M. Michou
CNRM-GAME – Météo-France, UMR3589, 42 Avenue Gaspard Coriolis, Toulouse, France
e-mail: pierre.nabat@meteo.fr

M. Mallet
Laboratoire D'Aérologie, CNRS-Université Paul Sabatier, Toulouse, France

D.G. Steyn and N. Chaumerliac (eds.), *Air Pollution Modeling and its Application XXIV*, Springer Proceedings in Complexity,
DOI 10.1007/978-3-319-24478-5_12

and marine particles from the sea. These aerosols show a strong spatio-temporal variability and a resulting large variety in aerosol optical properties over this basin (Lelieveld et al. 2002; Basart et al. 2009). Through their interactions with solar and thermal radiation, they have very important effects on its climate (e.g. Spyrou et al. 2013; Nabat et al. 2015a). Due to their high spatio-temporal variability, studies at the regional scale are therefore necessary to better understand the role of aerosols in regional climate system (Giorgi et al. 2002).

Besides, the evolution of aerosols in future is expected to influence climatic projections over the Mediterranean which is already seen as a climate change "hotspot" (Giorgi 2006). Over the past three decades, sulfur emissions have considerably been reduced in Europe because of new air pollution legislation and economic crises in the 1980s, leading to a decrease of sulfate aerosol concentration over the Euro-Mediterranean region since 1980. As a matter of fact, Nabat et al. (2014) have shown that this aerosol decrease was the main cause for the brightening effect observed in this region during the same period, and has also significantly contributed to the surface warming of the last three decades. This result confirms the important role of aerosols in climate trends, and raises a similar question for regional climate in the 21st Century.

In the present work realized in the framework of the ChArMEx and HyMeX programmes of the MISTRALS initiative, we consider a regional climate modelling approach in order to better understand the future evolution of aerosols and their impact on future climate.

12.2 Methodology

We use here the regional climate model ALADIN-Climate in the version 5.3 described in Nabat et al. (2015b), with a 50 km horizontal resolution. This model includes an interactive aerosol scheme for the main species present in this region (desert dust, sea-salt, sulfate and carbonaceous particles), which has been evaluated in previous studies at the global (Michou et al. 2015) and regional (Nabat et al. 2015b) scales. Dust and sea-salt emissions are calculated on-line in the model, depending on atmospheric dynamics (surface wind) and soil characteristics. Anthropogenic emissions (for sulfate, black carbon and organic carbon aerosols) are based on inventories, coming from the ACCMIP initiative (Lamarque et al. 2010).

Simulations have been carried out over two thirty-year periods covering the historical (1971–2000) and future climate (2071–2100). Both simulations are driven by the CNRM-CM5 model (Voldoire et al. 2012) as lateral boundary forcing. The future simulation follows the RCP8.5 (Representative Concentration Pathway) scenario.

12.3 Results

The evolution of aerosols is driven both by changes in anthropogenic emissions included in the different RCP (Representative Concentration Pathway) scenarios considered in our study, and the changes in climate variables (surface wind, humidity, temperature, …). We present here the evolution of the different aerosol types, as well as their consequences on regional climate.

Figure 12.1 presents the mean aerosol optical depth (AOD) of the historical simulation for the five aerosol types. The spatial structure of AOD is dominated by a maximum in northern Africa due to dust aerosols, and a second maximum in Europe due to sulfate aerosols. These patterns are close to previous estimations of AOD over the Euro-Mediterranean region (Nabat et al. 2013).

Compared to the historical simulation, the future simulation shows important differences in AOD, as presented in Fig. 12.2. On the one hand, anthropogenic species, and notably sulfate aerosols, have considerably been reduced. This decrease logically follows the decrease in sulfur emissions, which is expected and represented in the ACCMIP inventories. On the other hand, ALADIN-Climate simulates a slight increase in dust AOD in the southern part of the domain. This increase is due to an increase of dust emission, because of increasing surface wind These changes in the aerosol content have also been compared to the previous global simulations carried out in the ACCMIP initiative (Lamarque et al. 2013).

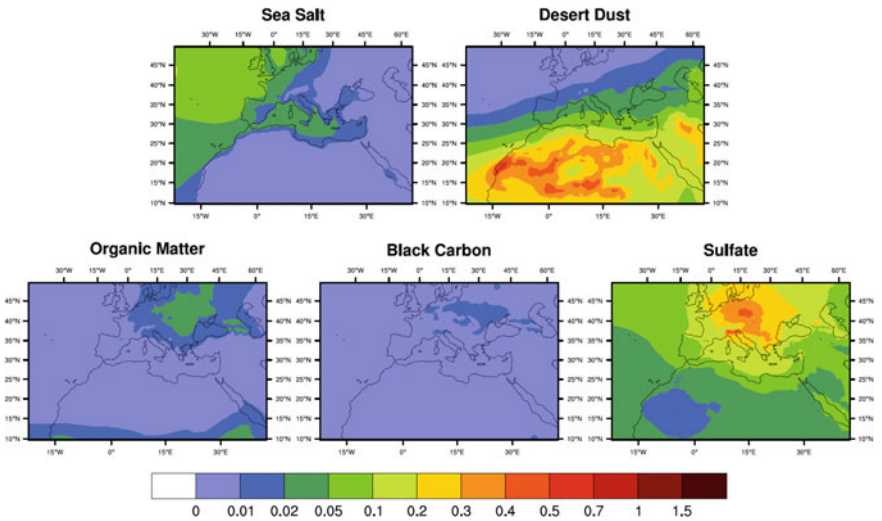

Fig. 12.1 Mean aerosol optical depth at 550 nm for the historical simulation (1971–2000) for the five aerosol types

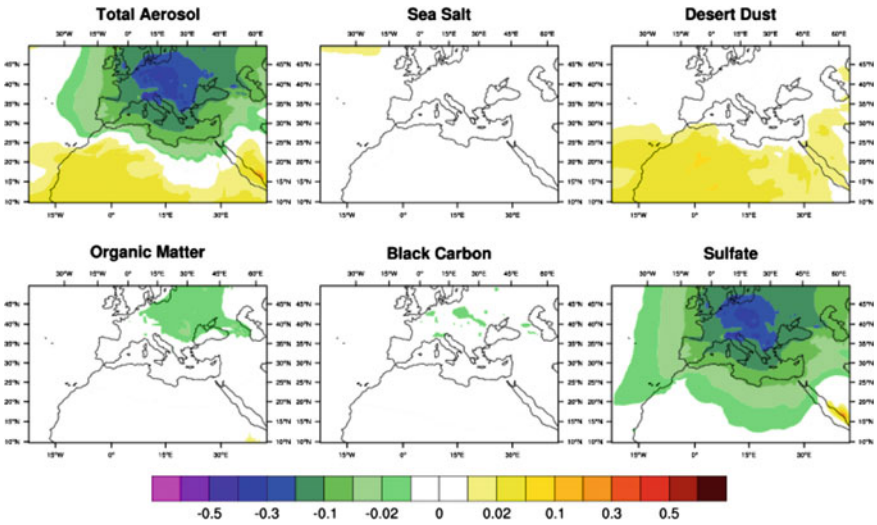

Fig. 12.2 Mean difference in aerosol optical depth at 550 nm between the future (2071–2100) and historical (1971–2000) simulations for the total and the five aerosol types

As a consequence, this decrease in AOD has an impact on radiative budget and regional climate. The decrease of AOD in Europe up to 0.4 caused by the sulfate reduction has led to the increase of incident surface radiation from 10 to 30 Wm^{-2}. In northern Africa, where the increase of AOD is about 0.1, surface radiation has decreased in the future simulation, up to -20 Wm^{-2}. The Mediterranean Sea has an increase in surface radiation up to 10 Wm^{-2} caused by the negative AOD anomaly of 0.05–0.2 combined to the decrease in cloud cover.

A comparison with a sensitivity simulation where historic anthropogenic emissions have been implemented in the future climate, surface radiation is shown to be almost constant in Europe, showing the prevailing rôle of sulfate aerosols in driving the evolution of surface radiation. On the contrary, the decrease over northern Africa is also observed in this simulation, as the increase in dust concentrations is due to an increase in surface wind.

With regards to surface temperature, the effects of the evolution of aerosols in Europe can be also deduced from this sensibility simulation with constant historic anthropogenic emissions in future. The difference between these two future simulations reveals that climate in Europe is on average +0.3 °C higher when anthropogenic emissions do not decrease. This is due to the direct effect of aerosols that is kept at a high level in the sensitivity simulation. Therefore, the sulfate decrease in Europe is responsible for 10 % of the warming in this region.

12.4 Conclusion

The present work is the first study using regional climate simulations with interactive aerosols to analyse the future evolution of aerosols and their effects on regional climate over the Mediterranean. The main result is a decrease of sulfate aerosols due to a decrease in anthropogenic emissions over Europe, leading to an increase of surface radiation and a contribution to regional warming of 10 % by the end of the 21st century. It is also worth mentioning that dust aerosol loads have been found to increase in future climate over northern Africa, because of changes in surface wind. This analysis is still ongoing to better identify climate processes linked to aerosols in future regional climate.

References

Basart S, Pérez C, Cuevas E, Baldasano JM, et Gobbi GP (2009) Aerosol characterization in Northern Africa, Northeastern Atlantic, Mediterranean Basin and Middle East from directsun AERONET observations. Atmos Chem Phys 9:8265–8282

Giorgi F, Bi X, et Qian Y (2002) Direct radiative forcing and regional climatic effects of anthropogenic aerosols over East Asia: a regional coupled climate-chemistry/aerosol model study. J Geophys Res 107:D20. doi:10.1029/2001JD001066

Giorgi F (2006) Climate change hot-spots. Geophys Res Lett 33:L08707. doi:10.1029/2006GL025734

Kaufman YJ, Tanré D, et Boucher O (2002) A satellite view of aerosols in the climate system. Nature 419:215–223

Lelieveld J, Berresheim H, Borrmann S, Crutzen PJ, Dentener FJ, Fischer H, Feichter J, Flatau PJ, Heland J, Holzinger R, Korrmann R, Lawrence MG, Levin Z, Markowicz KM, Mihalopoulos N, Minikin A, Ramanathan V, de Reus M, Roelofs GJ, Scheeren HA, Sciare J, Schlager H, Schultz M, Siegmund P, Steil B, Stephanou EG, Stier P, Traub M, Warneke C, Williams J, et Ziereis H (2002) Global air pollution crossroads over the Mediterranean. Science 298:794–799. doi:10.1126/science.1075457

Lamarque J-F, Bond TC, Eyring V, Granier C, Heil A, Klimont Z, Lee D, Liousse C, Mieville A, Owen B, Schultz MG, Shindell D, Smith SJ, Stehfest E, Van Aardenne J, Cooper OR, Kainuma M, Mahowald N, McConnell JR, Naik V, Riahi K, et van Vuuren DP (2010) Historical (1850–2000) gridded anthropogenic and biomass burning emissions of reactive gases and aerosols: methodology and application. Atmos Chem Phys 10:7017–7039. doi:10.5194/acp-10-7017-2010

Lamarque J-F, Shindell DT, Josse B, Young PJ, Cionni I, Eyring V, Bergmann D, Cameron-Smith P, Collins WJ, Doherty R, Dalsoren S, Faluvegi G, Folberth G, Ghan SJ, Horowitz LW, Lee YH, MacKenzie IA, Nagashima T, Naik V, Plummer D, Righi M, Rumbold ST, Schulz M, Skeie RB, Stevenson DS, Strode S, Sudo K, Szopa S, Voulgarakis A, et Zeng G (2013) The Atmospheric Chemistry and Climate Model Intercomparison Project (ACCMIP): overview and description of models, simulations and climate diagnostics. Geosci Model Dev 6:179–206. doi:10.5194/gmd-6-179-2013

Michou M, Nabat P, Saint-Martin D (2015) Development and basic evaluation of a prognostic aerosol scheme (v1) in the CNRM climate model CNRM-CM6. Geosci Model Dev 8:501–531. doi:10.5194/gmd-8-501-2015

Nabat P, Somot S, Mallet M, Chiapello I, Morcrette J-J, Solmon F, Szopa S, Dulac F, Collins W, Ghan S, Horowitz LW, Lamarque JF, Lee YH, Naik V, Nagashima T, Shindell D, Skeie R (2013) A 4-D climatology (1979–2009) of the monthly tropospheric aerosol optical depth distribution over the Mediterranean region from a comparative evaluation and blending of remote sensing and model products. Atmos Meas Tech 6:1287–1314. doi:10.5194/amt-6-1287-2013

Nabat P, Somot S, Mallet M, Sanchez-Lorenzo A, Wild M (2014) Contribution of anthropogenic sulfate aerosols to the changing Euro-Mediterranean climate since 1980. Geophys Res Lett 41:5605–5611. doi:10.1002/2014GL060798

Nabat P, Somot S, Mallet M, Sevault F, Chiacchio M, Wild M (2015a) Direct and semi-direct aerosol radiative effect on the mediterranean climate variability using a coupled regional climate system model climate dynamics 44:1127–1155. doi:10.1007/s00382-014-2205-6

Nabat P, Somot S, Mallet M, Michou M, Sevault F, Driouech F, Meloni D, Di Biagio C, Formenti P, Di Sarra A, Sicard M, Léon J-F, Bouin M-N (2015b) Dust aerosol radiative effects during summer 2012 simulated with a coupled regional aerosol-atmosphere-ocean model over the Mediterranean region. Atmos Chem Phys 15:3303-3326. doi:10.5194/acp-15-3303-2015

Spyrou C, Kallos G, Mitsakou C, Athanasiadis P, Kalogeri C, et Iacono M (2013) Modeling the radiative effects of desert dust on weather and regional climate. Atmos Chem Phys 13:5489–5504. doi:10.5194/acp-13-5489-2013

Voldoire A, Sanchez-Gomez E, y Mélia DS, Decharme B, Cassou C, Sénési S, Valcke S, Beau I, Alias A, Chevallier M, Déqué M, Deshayes J, Douville H, Fernandez E, Madec G, Maisonnave E, Moine MP, Planton S, Saint-Martin D, Szopa S, Tyteca S, Alkama R, Belamari S, Braun A, Coquart L, Chauvin F (2012) The CNRM-CM5.1 global climate model: description and basic evaluation. Clim Dyn 40. doi:10.1007/s00382-011-1259-y

Chapter 13
Extensive Comparison Between a Set of European Dust Regional Models and Observations in the Western Mediterranean for the Summer 2012 Pre-ChArMEx/TRAQA Campaign

Sara Basart, F. Dulac, J.M. Baldasano, P. Nabat, M. Mallet, F. Solmon, B. Laurent, J. Vincent, L. Menut, L. El Amraoui, B. Sic, J.-P. Chaboureau, J.-F. Léon, K. Schepanski, J.-B. Renard, F. Ravetta, J. Pelon, C. Di Biagio, P. Formenti, I. Chiapello, J.-L. Roujean, X. Ceamanos, D. Carrer, M. Sicard, H. Delbarre, G. Roberts, W. Junkermann and J.-L. Attié

Abstract The present analysis focuses on the model capability to properly simulate long-range Saharan dust transport for summer 2012 in the Western Mediterranean. The present contribution shows an intercomparison of a set of 9 European regional dust model simulations. An exhaustive comparison of model outputs against other

S. Basart (✉) · J.M. Baldasano
Earth Sciences Department, Barcelona Supercomputing Center—Centro Nacional de Supercomputación (BSC-CNS), Barcelona, Spain

F. Dulac
Laboratoire Des Sciences Du Climat et de L'Environnement (LSCE), CEA-CNRS-USVQ, Gif-Sur-Yvette, France

J.M. Baldasano
Environmental Modelling Laboratory, Technical University of Catalonia, Barcelona, Spain

P. Nabat · L. El Amraoui · B. Sic · J.-L. Roujean · X. Ceamanos · D. Carrer · G. Roberts · J.-L. Attié
Centre National de Recherches Météorologiques (CNRM), Météo-France-CNRS, Toulouse, France

M. Mallet · J.-P. Chaboureau · J.-F. Léon · J.-L. Attié
Laboratoire D'Aérologie, CNRS-Univ, Paul Sabatier, OMP, Toulouse, France

F. Solmon
Earth System Physics, Int. Centre for Theoretical Physics (ICTP), UNESCO-IAEA, Trieste, Italy

B. Laurent · J. Vincent · C. Di Biagio · P. Formenti
LISA,UPEC-UDDP7-CNRS, IPSL, Créteil, France

D.G. Steyn and N. Chaumerliac (eds.), *Air Pollution Modeling and its Application XXIV*, Springer Proceedings in Complexity,
DOI 10.1007/978-3-319-24478-5_13

models and observations can reveal weaknesses of individual models, provide an assessment of uncertainties in simulating the dust cycle and give additional information on sources for potential model improvement. The model outputs are compared against a variety of both ground-based and airborne in situ and remote sensing measurements performed during the pre-ChArMEx/TRAQA field campaign. For this kind of study, multiple and different observations are combined to deliver a detailed idea of the structure and evolution of the dust cloud and the state of the atmosphere at the different stages of the event.

13.1 Introduction

Surrounded by mountains and several continents and affected by different types of pollution, the Mediterranean Sea is a natural laboratory for studying the variability of the chemical composition in the lower atmospheric layers and the interaction between pollutants from distant regions. The Chemistry-Aerosol Mediterranean Experiment (ChArMEx, http://charmex.lsce.ipsl.fr) is a French initiative which set up an international coordinated experimental and modelling effort based on the most updated tools, for an assessment of the present and future state of the atmospheric environment in the Mediterranean Basin, and of its impact on the regional

L. Menut
Laboratoire de Météorologie Dynamique, IPSL, CNRS/INSU, Ecole Polytechnique, Ecole Normale Supérieure, Université Paris 6, Ecole Nationale Des Ponts et Chaussées, Palaiseau, France

K. Schepanski
Leibniz Institute for Tropospheric Research, Leipzig, Germany

J.-B. Renard
Laboratoire de Physique et Chimie de L'Environnement et de L'Espace (LPC2E), CNRS-Univ, Orléans, France

F. Ravetta · J. Pelon
Laboratoire Atmosphères, Milieux, Observations Spatiales (LATMOS), CNRS-UPMC-UVSQ, Paris, France

I. Chiapello
Laboratoire D'Optique Atmosphérique (LOA), USTL-CNRS, Villeneuve D'Ascq, France

M. Sicard
Remote Sensing Laboratory (RSLab)/IEEC-CRAE, Univ. Politècnica de Catalunya, Barcelona, Spain

H. Delbarre
Laboratoire de Physico-Chimie de L'Atmosphère (LPCA), Univ. Du Littoral Côte D'Opale-CNRS, Dunkirk, France

W. Junkermann
Karlsruhe Institute of Technology (KIT), IMK-IFU, Garmisch-Partenkirchen, Germany

climate, air quality, and marine biogeochemistry. The target is short-lived particulate and gaseous tropospheric trace species which are the cause of poor air quality events, have two-way interactions with climate, and impact the marine biogeochemistry, in a context of strong regional anthropogenic and climatic pressures.

Atmospheric aerosols in the north-western Mediterranean region are mainly composed by sea salt, anthropogenic pollution (from industrialized high populated coastal cities) and Saharan dust aerosols. The present study focuses on the analysis of the model capability to properly simulate long-range Saharan dust transport during summer 2012 in the Western Mediterranean. Moreover, the use of ensemble forecasts to improve event predictability is analysed.

13.2 Methods

The present study uses 9 regional dust models that are run at different centres in Europe which are presented in Table 13.1. All models produced 24 h forecasts beginning at 0UTC (except RegCM and Aladin-CCM, which are not forced by meteorological fields every 24 h) in order to investigate their performance and ability to predict the dust outbreaks over the Mediterranean from 1st June to 31st August 2012. Various model output fields at 3-hourly resolution were processed for comparative purposes. The research teams at the modelling centres configured their

Table 13.1 Summary of the main features of the 9 regional models included in the present contribution

Dust model	Institution	Meteo driver initial fields	Spatial resolution	Radiative feedbacks
ALADIN-Dust	CNRM-GAME	ARPEGE ARPEGE	24 km × 24 km 70 layers	No
ALADIN-CCM	CNRM-GAME	ERA-Interim/ERA-Interim	50 km × 50 km 31 layers	Yes
BSC-DREAM8b v2	BSC-CNS	ETA NCEP-FNL	0.33° × 0.33° 24 Eta-layers	Yes
CHIMERE	LISA, LMD and INERIS	ECMWF ERA-Interim	0.25° × 0.25° 15 σ-layers	No
COSMO-MUSCAT	TROPOS	COSMO GME	0.25° × 0.25° 40 σ-layers	Yes
MESO-NH	Laboratorie d'Aerologie	ECMWF ERA-Interim	15 km × 15 km 15 σ-layers	Yes
MOCAGE	CNRM-GAME, Meteo-France and CNRS	ARPEGE ERA-Interim	0.2° × 0.2° 47 σ-layers	No
NMMB/BSC-Dust	BSC-CNS	NMMB NCEP-FNL	0.25° × 0.25° 40 σ-layers	No
RegCM	Laboratorie d'Aerologie	ECMWF ERA-Interim	25 km × 25 km 23 layers	Yes

own model experiments. Therefore, the horizontal and vertical resolution, domain size, driving boundary conditions, dust field initial conditions, land surface conditions, dust emission and deposition parameterizations as well as dust physical and optical properties vary between the models. Some of these features are summarised in Table 13.1.

The numerical weather prediction and European air quality communities have for some time been exploring the potential of multi-model ensembles to enhance understanding of forecast uncertainty. Similarly, a multi-model median product is also generated from the set of different predictions of the dust models interpolated to a common grid mesh.

The model outputs are compared against a variety of both ground-based and airborne in situ and remote sensing measurements performed during the pre-ChArMEx/TRAQA field campaign (Attié et al. 2014). The model outputs are also compared with satellite aerosol products, which provide a description of the spatial aerosol distribution over the basin. These observational datasets provide a complete set of exceptional quantitative constraints for model simulations of this period.

13.3 Results and Discussions

The aerosol optical depth (AOD) model intercomparison for summer 2012 (1st June–31st August) shows that the intensity and the spread of the Saharan dust intrusion over Europe reproduced by the models present large differences. Not only do dust emission schemes rely on various assumptions, but also their implementation within a regional model presents challenges. Significant biases are found between different regional models even when they have the same dust emission scheme implemented. Following (Basart et al. 2009), the dust AOD comparison against 4 AERONET sun photometers (Barcelona, Palma de Mallorca, Avignon and Lampedusa) shows that the set of models are able to reproduce the seasonal AOD variability with correlations >0.6 except for the climate model RegCM (not shown here). In this respect, the multi-model median product shows the best results (with correlation >0.8).

On late June 2012, a strong dust outbreak (with origin over Algeria) was observed over the Western Mediterranean coinciding within the intensive ChArMEx/TRAQA experimental campaign (Dulac et al. 2013; see Fig. 13.1). High aerosol concentrations were observed between 1 and 5 km by CALIPSO and LOAC flights from Martigues (France) meanwhile desert dust was predicted in altitudes <5 km (above sea level, a.s.l; see Fig. 13.1) with maximum dust concentrations at $\sim$3.5 km (not shown here). Aerosols at high altitudes (between 3 and 7 km a.s.l.) were not predicted by the dust models. Observations and air-mass backward trajectories confirmed that these upper aerosols were associated to forest fires with origin in the south-eastern Iberian Peninsula as confirmed by.

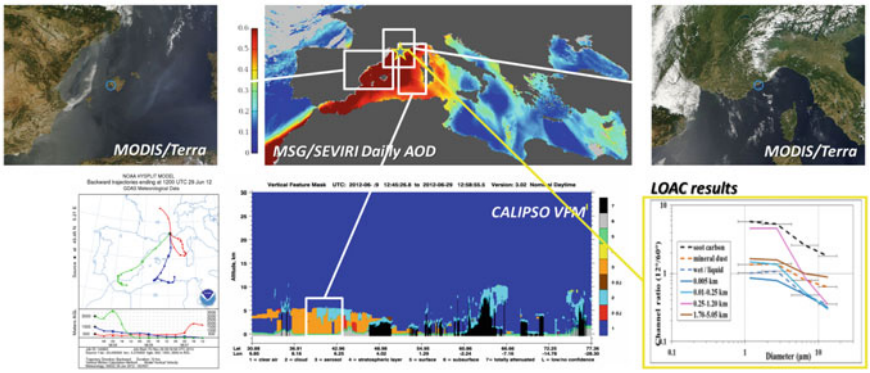

Fig. 13.1 Satellite and ground-based observations as well as backtrajectories at Martingues (at arrivals at 500, 1500 and 3000 m a.s.l.) collected during 29th June 2012

These preliminary results demonstrate that the dust models are useful to complement dust-related observations over the total aerosol load, understand the dust processes and predict the impact of dust. Moreover, it is shown the potential use of multi-model ensembles to enhance understanding of forecast uncertainty.

Acknowledgments The authors want to acknowledge the OMP/SEDOO for the ChArMEx data portal and to CNES for balloon operations and funding. The other main sponsors of the campaign were ADEME and INSU under the umbrella of the programmes PRIMEQUAL and MISTRALS. LOAC was developed with funding from ANR.

References

Attié JL, Ravetta F, Durand P, El Amraoui L, Di Biaggio C, Dulac F, Sicard M, Renard J-B, Fleury L, Bourdon A, Verdier N (2014) Transport of pollution and air quality experiment over the Mediterranean basin (TRAQA/ChArMEx campaign). In: EGU general assembly conference abstracts, vol 16. p 12125

Basart S, Pérez García-Pando C, Cuevas E, Baldasano Recio JM, Gobbi P (2009) Aerosol characterization in Northern Africa, Northeastern Atlantic, Mediterranean basin and Middle East from direct-sun AERONET observations

Dulac F, Nicolas JB, Sciare J, Mallet M, Léon JF, Pont V, … Ravetta F (2013) The summer 2012 Saharan dust season in the western Mediterranean with focus on the intense event of late June during the Pre-ChArMEx campaign. In: EGU general assembly conference abstracts, vol 15, p 12108

Chapter 14
A Modelling Perspective of the Summer 2013 and 2014 ChArMEx/SAFMED Chemistry Intensive Campaigns: Origin of Photo-Oxidant and Aerosol Formation over the Western Mediterranean

Arineh Cholakian, Matthias Beekmann, Guillaume Siour, Hervé Petetin, Agnes Borbon, Paola Formenti, Evelyne Freney, Valerie Gros, Corinne Jambert, Jean-Pierre Kervern, Nicolas Marchand, Sébastien Sauvage, Jean Sciare, Pierre Durand, Karine Sellegri, Eric Hamonou and François Dulac

Abstract During summers 2013 and 2014, two three weeks intensive campaign took place over the western Mediterranean basin in order to investigate photo-oxidant and aerosol sources over the region. Within the frame of the MISTRALS/ChArMEx (Chemistry-Aerosol Mediterranean Experiment) program and the ANR/SAFMED (Secondary Aerosol Formation in the MEDiterranean) project, this campaign included an extensive experimental set-up based on ground-based, balloon-borne,

A. Cholakian (✉) · M. Beekmann · G. Siour · H. Petetin · A. Borbon · P. Formenti
Laboratoire Interuniversitaire des Systèmes Atmosphériques (LISA),
Université Paris Est et 7, CNRS, Créteil, France
e-mail: arineh.cholakian@lisa.u-pec.fr

M. Beekmann
e-mail: matthias.beekmann@lisa.u-pec.fr

C. Jambert · P. Durand
Laboratoire d'Aérologie, LA, Toulouse, France

E. Freney · K. Sellegri
Laboratoire de Météorologie Physique, LaMP, Clermont-Ferrand, France

V. Gros · J. Sciare · E. Hamonou · F. Dulac
Laboratoire des Sciences du Climat et de l'environnement, LSCE,
CEA-CNRS-UVSQ, Gif-sur-Yvette, France

J.-P. Kervern
Université de Grenoble, Grenoble, France

N. Marchand
Laboratoire Chimie Environnement, LCE, Marseille, France

S. Sauvage
Sciences de l'Atmosphère et Génie de l'Environnement, Douai, France

D.G. Steyn and N. Chaumerliac (eds.), *Air Pollution Modeling and its Application XXIV*, Springer Proceedings in Complexity,
DOI 10.1007/978-3-319-24478-5_14

aircraft and satellite measurements. In this paper, a modeling perspective of the campaign is given, based on simulations with the regional chemistry-transport model, CHIMERE, in a configuration shaped for the Mediterranean region. Major sources of photo-oxidants, and aerosols are addressed: long range transport from continental Europe, pollution build-up from shipping emissions, marine emissions, organic aerosol formation from biogenic and anthropogenic VOC emissions, dust emissions.

14.1 Introduction

The Mediterranean basin receives a vast amount of emissions from different sources, both anthropogenic and biogenic. This region experiences high gaseous pollution levels originating from Europe (Millan et al. 1997), especially during summer-time when the photochemical activity is at its maximum. Another source of pollutants in this region is the high amounts of emissions resulting from shipping activities (Marmer et al. 2009). Furthermore, the basin is impacted by natural emissions such as biogenic continental emissions and also oceanic natural emissions. Dust particles are also known to be transported from northern Africa to this region. The complexity resulting from the multitude of sources mentioned above dictates the need to modify existing models to correspond better to the specific conditions seen in this region. The SAFMED project provides an excellent opportunity to test and improve the existing models. The sensitivity of pollutants concentrations to specific sources will also be evaluated.

14.2 Model Set-up

The model used to accomplish this task is the CHIMERE off-line chemistry-transport model (Menut et al. 2013). Two nested domains were used for the simulations presented in this article. The outside domain was chosen to cover the whole Europe as well as the northern Africa to take into account the transport of continental emissions and dust emissions respectively. The nested domain covers the western Mediterranean basin where ground-based (Cape Corse, Mallorca), aircraft and balloon-borne measurements were performed during SAFMED (July–August 2013). Certain external forcings, summarized below, need to be provided for CHIMERE.

- Meteorological parameters are taken from NCEP and processed by WRF.
- HTAP is used as the anthropogenic emissions inventory, as it includes also emissions in North Africa (Janssens-Maenhout et al. 2012).
- Boundary conditions are taken from LMDz_INCA3 (Hauglustaine et al. 2004).

- Biogenic emissions of certain species are taken from MEGAN.
- Oceanic emissions of dimethyl sulfide were also added to improve the results (Lana et al. 2011).

For the moment, standard CHIMERE aerosol scheme (Bessagnet et al. 2009) is used to simulate aerosols. In the future, the Volatility Basis Set scheme (Donahue et al. 2011) will be used to improve the simulation of secondary organic aerosols.

14.3 Results and Discussion

There is a general good agreement between the simulated meteorological parameters and observed data (correlation of 0.7 and bias of +2 °C for temperature). When comparing gaseous species, an important overestimation is observed for NOx (sum of NO and NO_2). This fact led us to perform sensitivity studies on the shipping emissions which will be discussed later. Concerning particulate matter, an extensive amount of work remains to be done to improve the simulation of particles in CHIMERE for the Mediterranean basin. Figure 14.1 presents the simulated contribution of different aerosols in PM1 (particles with a diameter less than 1 µm)

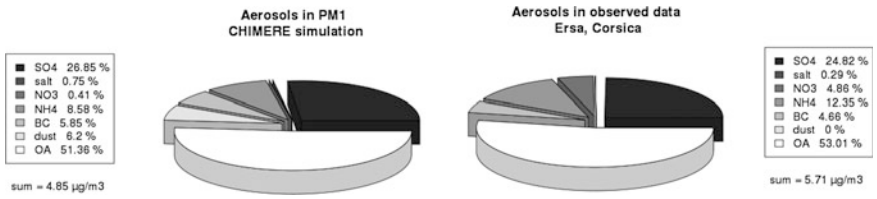

Fig. 14.1 Simulated contribution of aerosols (*left*), measured contribution of aerosols (*right*)

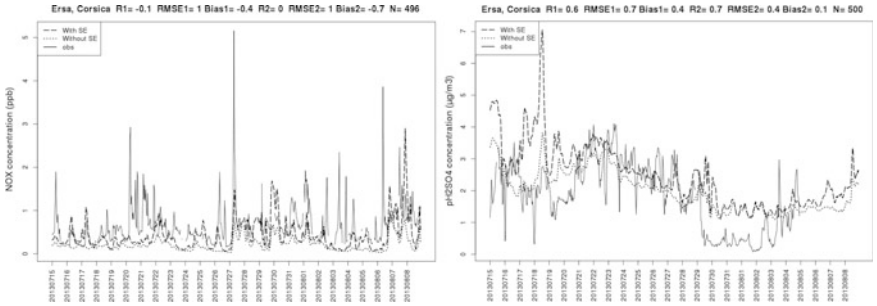

Fig. 14.2 Concentration of NOx and sulfate particles compared for reference simulations, sensitivity study and observations. *SE* shipping emissions, *obs* observations

on the site of Ersa, Corsica, compared with measured values. The overestimation of sulfates, underestimation of nitrates and organic matter and general overestimation of PM1 is evident in this figure.

As mentioned above, the overestimation of NOx in the simulations, combined with overestimation of sulfate particles in the Corsica region, led us to believe there could be an overestimation in the shipping emission inventory used in the simulations. As a means to test this hypothesis, a sensitivity study was performed by removing all shipping emissions from emission database used in CHIMERE. In Fig. 14.2, reference simulations (simulations containing shipping emissions as input), the sensitivity study and also measurements are compared. The NOx are directly emitted by ships. In addition, SO_2 shipping emissions can act as a precursor for production of sulfate particles. The overestimation of these two species in the reference simulations may be explained, among other reasons, by the overestimation of shipping emissions in this region. To better present the effects of these emissions, 2D maps of the reference simulations and the sensitivity study are shown in Fig. 14.3. The species presented are PM2.5 (particles with a diameter smaller

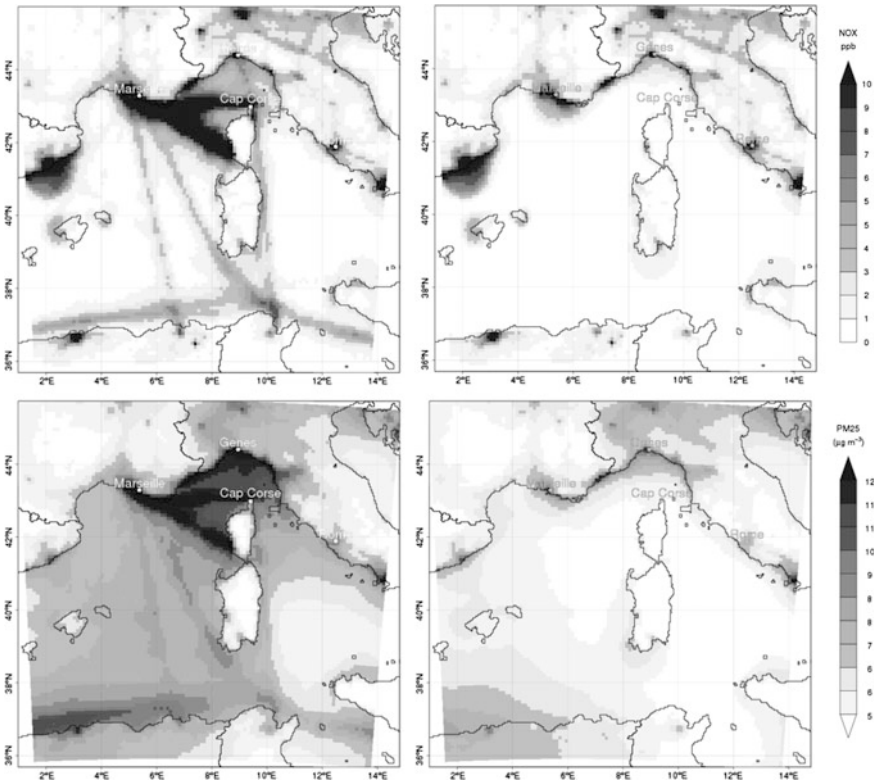

Fig. 14.3 2D field images of NOx and PM2.5 for simulations with shipping emissions (*left*) and without shipping emissions (*right*)

than 2.5 μm) and NOx. The difference shown in these images emphasizes the importance of shipping emissions in simulations of the Mediterranean region. However, the first comparison with measurements indicates that shipping emissions are probably overestimated. In future work, several emission inventories will be compared with respect to measurements in order to select the most realistic one, and then, to evaluate the contribution of shipping emissions to pollutant levels in the western Mediterranean basin.

Questions and Answers

Questioner: J. P. Jalkanen.

Question: Why did you not include the option of revising the ship emission inventories?

Answer: We did include the revision of shipping emission inventories; we ran two different series of simulations using HTAP-V2 shipping emissions and also MACC-III shipping emissions. This is still a work in progress, so we presented the inventories that we have revised until now.

Questioner: J. P. Jalkanen.
Question: What year did you use for ship emission inventories?
Answer: We used HTAP-V2 and MACC-III emissions both for 2010.

Questioner: P.A. Makar.
Question: Did you treat the ship emissions as area sources or like large point sources?

Answer: The anthropic emissions inventory that we use treats shipping emissions as area sources; just as it does for other types of emissions.

References

Bessagnet B, Menut L, Curcu G et al (2009) Regional modeling of carbonaceous aerosols over Europe-focus on secondary organic aerosols. Atmos Chem 61:175–202. doi:10.1007/s10874-009-9129-2

Donahue NM, Epstein SA, Pandis SN, Robinson AL (2011) A two-dimensional volatility basis set. Atmos Chem Phys 11:3303–3318. doi:10.5194/acp-11-3303-2011

Hauglustaine DA, Hourdin F, Jourdain L, Filiberti M-A et al (2004) Interactive chemistry in the Laboratoire de Meteorologie Dynamique general circulation model: description and background tropospheric chemistry evaluation. J Geophys Res. doi:10.1029/2003JD003957

Janssens-Maenhout G, Dentener F, van Aardenne J et al (2012) EDGAR-HTAP: a harmonized gridded air pollution emission dataset based on national inventories. JRC Sci Tech Rep. doi:10.2788/14102

Lana A, Bell TG, Simo R et al (2011) An updated climatology of surface dimethyl sulfide concentrations and emission fluxes in the global ocean. Glob Biogeochem Cycles. doi:10.1029/2010GB003850

Marmer E, Dentener F, Aardenne JV et al (2009) What can we learn about ship emission inventories from measurements of air pollutants over the Mediterranean sea? Atmos Chem Phys 9:6815–6831

Menut L, Bessagnet B, Khvorostyanov D et al (2013) CHIMERE 2013: a model for regional atmospheric composition modeling. Geosci Model Dev 6:981–1028. doi:10.5196/gmd-6-981-2013

Millan MM, Salvador R, Mantilla E (1997) Photooxidant dynamics in the Mediterranean basin in summer: results from European research projects. Geophys Res 102:8811–8823

Chapter 15
Aerosol Variability and Weather Regimes over the Mediterranean Region

Pierre Nabat, Samuel Somot, Marc Mallet, Florence Sevault and Martine Michou

Abstract The Mediterranean region is characterized by the accumulation of aerosols from numerous and various sources, which show a strong spatio–temporal variability and a resulting large variety in aerosol optical properties over this basin. This study realized in the framework of the ChArMEx initiative aims at explaining this aerosol variability and the relationship between aerosol loads and weather conditions. From a regional simulation carried out with the ALADIN-climate model including an interactive aerosol scheme for the main species present in this region (desert dust, sea-salt, sulfates and carbonaceous particles), we have identified typical synoptic conditions that favour high aerosol loads over the Mediterranean, or on the contrary that are opposed to these high aerosol loads. These weather regimes are based on a statistical method of automated classification. This method enables to characterize the effects of aerosols on climate for each weather regime, and the links between aerosol variability and climate oscillations such as the North-Atlantic Oscillation (NAO).

15.1 Motivations

Atmospheric aerosols significantly influence climate through their impact on radiative budget and clouds (Kaufman et al. 2002). In the Mediterranean region, various and numerous aerosols are observed, because of the presence of different sources around this region: industrial and urban aerosols from Europe and North African towns, biomass burning, from Eastern Europe, dust aerosols from Africa, and marine particles from the sea. These aerosols show a strong spatio–temporal

P. Nabat (✉) · S. Somot · F. Sevault · M. Michou
CNRM-GAME—Météo-France, UMR3589, 42 Avenue Gaspard Coriolis, Toulouse, France
e-mail: pierre.nabat@meteo.fr

M. Mallet
Laboratoire d'Aérologie, CNRS-Université Paul Sabatier, Toulouse, France

D.G. Steyn and N. Chaumerliac (eds.), *Air Pollution Modeling and its Application XXIV*, Springer Proceedings in Complexity,
DOI 10.1007/978-3-319-24478-5_15

variability and a resulting large variety in aerosol optical properties over this basin (Lelieveld et al. 2002; Basart et al. 2009), with ensuing impacts on regional climate (e.g. Spyrou et al. 2013; Nabat et al. 2015a). Maximal aerosol loads are observed in spring and summer, namely in the dry season favouring a longer residence time for atmospheric aerosols. Besides, dust outbreaks characterized by large plumes of Saharan desert dust particles, are more frequent in this season. Such high aerosol loads influence both meteorology and climate, because of the induced perturbations of temperature and humidity profiles, static stability and atmospheric dynamics (Pérez et al. 2006). A better understanding of this aerosol variability could therefore help numerical weather forecast and climate prediction.

This study realized in the framework of the ChArMEx initiative aims at explaining this aerosol variability and the relationship between aerosol loads and weather conditions, through analyses of regional climate coupled simulations.

15.2 Methodology

We use here the regional climate system model CNRM-RCSM5 in the version described in Nabat et al. (2015b) with a 50 km horizontal resolution. This model system includes a coupling between the different components of the regional climate system, namely the atmosphere (with ALADIN-Climate), the ocean (with NEMOMED8), the land surface (with ISBA) as well as an interactive aerosol scheme for the main species present in this region (desert dust, sea-salt, sulfate and carbonaceous particles). This aerosol scheme has been evaluated in previous studies at the global (Michou et al. 2015) and regional (Nabat et al. 2015b) scales. Dust and sea-salt emissions are calculated on-line in the model, depending on atmospheric dynamics (surface wind) and soil characteristics. Anthropogenic emissions (for sulfate, black carbon and organic carbon aerosols) are based on inventories, coming from the ACCMIP initiative (Lamarque et al. 2010).

A multi-annual simulation has been carried out over the 1979–2013 period, driven by the ERA-Interim reanalysis (Dee et al. 2011) as lateral boundary forcing.

15.3 Results

The atmospheric aerosol content depends highly on meteorological conditions, given for example the impact of surface wind and soil humidity on dust emission, that of atmospheric circulation on aerosol transport and that of precipitation on aerosol deposition. As a matter of fact, we have tried to identify more precisely the links between aerosols, clouds, and atmospheric circulation.

First of all, the analysis of the multi-annual simulation reveals that on average aerosol optical depth (AOD) is lower during days with low cloud cover, and reciprocally for days with high cloud cover. Figure 15.1 presents the AOD average

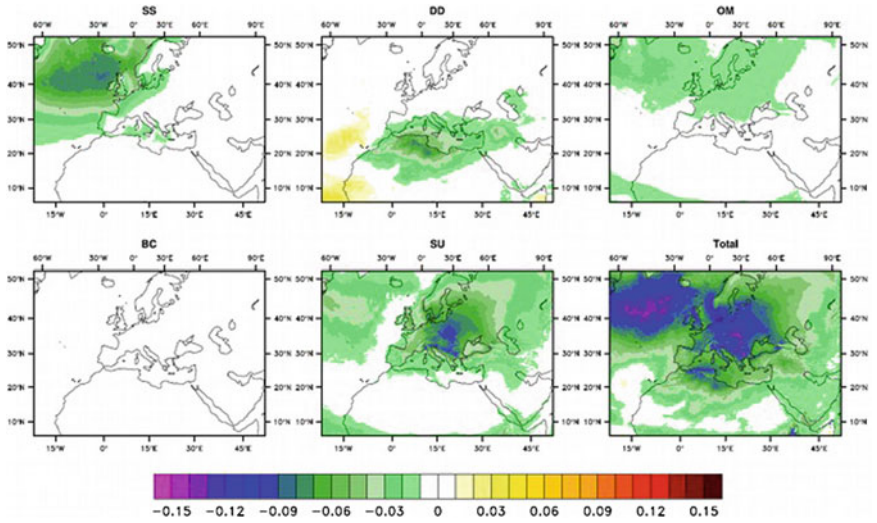

Fig. 15.1 AOD average difference for total and each aerosol type (*SS* sea-salt, *DD* desert dust, *OM* organic matter, *BC* black carbon and *SU* sulfate) between the set of days when cloud cover is lower than 10 % and the set of all the days

difference between the set of days when cloud cover is low (under 10 %) and the set of all the days. The decrease of AOD during days with low cloud cover is due to sea salt aerosols over the Atlantic ocean, dust aerosols over the Mediterranean region, and sulfate aerosols in Europe.

More generally, as mentioned in previous studies (Moulin et al. 1997; Ginoux et al. 2004), climate oscillations such as the North-Atlantic Oscillation (NAO) impact the atmospheric aerosol content. In our simulation, a high correlation has notably been found between the NAO index and dust AOD in northern Africa and in the Mediterranean region, especially in winter. A positive phase of the NAO index is associated with high dust loads over northern Africa and the Atlantic Ocean, and low dust loads over the Eastern Mediterranean, and reciprocally for the negative phase.

In the present work, the analysis is going further through a characterization of the aerosol variability in function of weather regimes. These weather regimes are based on a statistical method of automated classification (Vautard 1990), which has been applied to the ERA-Interim data set. Four weather regimes have been identified: Atlantic ridge, NAO+, NAO− and blocking. This method enables us to characterize the effects of aerosols on climate for each weather regime, and the links between aerosol variability and atmospheric dynamics.

Figure 15.2 presents the anomalies of each weather regime in terms of sea level pressure, AOD and cloud cover. Typical synoptic conditions are found to favour high aerosol loads (for example, NAO + in northern Europe and in northern Africa, blocking over the Southern Mediterranean), while others are on the contrary opposed to high aerosol loads (for example Atlantic ridge over the Atlantic ocean,

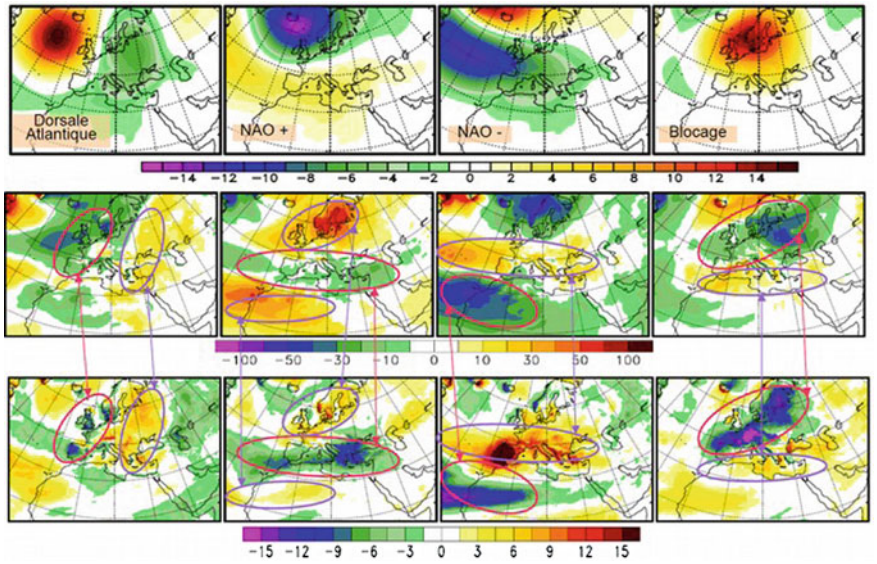

Fig. 15.2 Anomalies for each winter weather regime (Atlantic Ridge/NAO+/NAO-/Blocking) in terms of sea level pressure (*top*, hPa), AOD (*middle*) and cloud cover (*bottom*, %)

NAO− in northern Africa). In almost all cases, cloud cover anomalies share the same sign as AOD anomalies.

This analysis thus highlights similarities between aerosol and cloud variations, which could be all the more important to understand as the direct aerosol radiative effect is generally weaker under cloudy conditions. Climate models using only monthly AOD fields instead of prognostic aerosol variables could thus overestimate the effect of aerosols during cloudless days.

References

Basart S, Pérez C, Cuevas E, Baldasano JM, Gobbi GP (2009) Aerosol characterization in Northern Africa, Northeastern Atlantic, Mediterranean Basin and Middle East from directsun AERONET observations. Atmos Chem Phys 9:8265–8282

Dee DP, Uppala SM, Simmons AJ, Berrisford P, Poli P, Kobayashi S, Andrae U, Balmaseda MA, Balsamo G, Bauer P, Bechtold P, Beljaars ACM, van de Berg L, Bidlot J, Bormann N, Delsol C, Dragani R, Fuentes M, Geer AJ, Haimbergere L, Healy SB, Hersbach H, Holm EV, Isaksen L, Kallberg P, Köhler M, Matricardi M, McNally AP, Monge-Sanzf BM, Morcrette JJ, Park BK, Peubey C, de Rosnaya P, Tavolato C, Thépaut JN, Vitart F (2011) The ERA-Interim reanalysis: configuration and performance of the data assimilation system. Q J R Meteorol Soc 137:553–597. doi:10.1002/qj.828

Ginoux P, Prospero JM, Torres O, Chin M (2004) Long-term simulation of global dust distribution with the GOCART model: correlation with North Atlantic oscillation. Model Wind Eros Aeol Process 19:113–128. doi:10.1016/S1364-8152(03)00114-2

Kaufman YJ, Tanré D, Boucher O (2002) A satellite view of aerosols in the climate system. Nature 419:215–223

Lelieveld J, Berresheim H, Borrmann S, Crutzen PJ, Dentener FJ, Fischer H, Feichter J, Flatau PJ, Heland J, Holzinger R, Korrmann R, Lawrence MG, Levin Z, Markowicz KM, Mihalopoulos N, Minikin A, Ramanathan V, de Reus M, Roelofs GJ, Scheeren HA, Sciare J, Schlager H, Schultz M, Siegmund P, Steil B, Stephanou EG, Stier P, Traub M, Warneke C, Williams J, Ziereis H (2002) Global air pollution crossroads over the Mediterranean. Science 298(794–799):2002. doi:10.1126/science.1075457

Lamarque J-F, Bond TC, Eyring V, Granier C, Heil A, Klimont Z, Lee D, Liousse C, Mieville A, Owen B, Schultz MG, Shindell D, Smith SJ, Stehfest E, Van Aardenne J, Cooper OR, Kainuma M, Mahowald N, McConnell JR, Naik V, Riahi K, van Vuuren DP (2010) Historical (1850–2000) gridded anthropogenic and biomass burning emissions of reactive gases and aerosols: methodology and application. Atmos Chem Phys 10:7017–7039. doi:10.5194/acp-10-7017-2010

Michou M, Nabat P, Saint-Martin D (2015) Development and basic evaluation of a prognostic aerosol scheme (v1) in the CNRM climate model CNRM-CM6. Geosci Model Dev 8:501–531. doi:10.5194/gmd-8-501-2015

Moulin C, Lambert CE, Dulac F, Dayan U (1997) Control of atmospheric export of dust from North Africa by the North Atlantic oscillation. Nature 387:691–694

Nabat P, Somot S, Mallet M, Sevault F, Chiacchio M, Wild M (2015a) Direct and semi-direct aerosol radiative effect on the Mediterranean climate variability using a coupled regional climate system model. Cli Dyn 44:1127–1155. doi:10.1007/s00382-014-2205-6

Nabat P, Somot S, Mallet M, Michou M, Sevault F, Driouech F, Meloni D, di Sarra A, Di Biagio C, Formenti P, Sicard M, Léon J-F, Bouin M-N (2015b) Dust aerosol radiative effects during summer 2012 simulated with a coupled regional aerosol-atmosphere-ocean model over the Mediterranean region. Atmos Chem Phys 15:3303–3326. doi:10.5194/acp-15-3303-2015

Pérez C, Nickovic S, Baldasano JM, Sicard M, Rocadenbosch F, Cachorro VE (2006) A long Saharan dust event over the western Mediterranean: Lidar, Sun photometer observations, and regional dust modeling. J Geophys Res 111:D15214. doi:10.1029/2005JD006579

Spyrou C, Kallos G, Mitsakou C, Athanasiadis P, Kalogeri C, Iacono M (2013) Modeling the radiative effects of desert dust on weather and regional climate. Atmos Chem Phys 13:5489–5504. doi:10.5194/acp-13-5489-2013

Vautard R (1990) Multiple weather regimes over the North Atlantic: analysis of precursors and successors. Mon Weather Rev 118:2056–2081. doi:10.1175/1520-0493(1990)118<2056:MWROTN>2.0.CO;2

Part III
Air Quality Effects on Human Health, Ecosystems and Economy

Chapter 16
Assessment of Population Exposure to Particulate Matter for London and Helsinki

J. Kukkonen, V. Singh, R.S. Sokhi, J. Soares, A. Kousa, L. Matilainen, L. Kangas, M. Kauhaniemi, K. Riikonen, J.-P. Jalkanen, T. Rasila, O. Hänninen, T. Koskentalo, M. Aarnio, C. Hendriks and A. Karppinen

Abstract Most epidemiological studies have been conducted based on relations between pollution concentrations measured at fixed ambient air quality monitoring sites, or modelled values using land-use regression models, and various health indicators. However, such simplistic modelling ignores several crucial factors, such as, (i) the activity patterns of individuals, i.e. people's day-to-day movements, and (ii) the differences between indoor and outdoor air. We have developed a mathematical model for the determination of human exposure to ambient air pollution in an urban area, called EXPAND (EXposure model for Particulate matter And Nitrogen oxiDes). The model combines (i) predicted concentrations, and (ii) information on people's activities and location of the population, to evaluate the spatial and temporal variation of average exposure of the urban population to ambient air pollution in different microenvironments. In particular, the model takes into account the movements of the population and the infiltration from outdoor to indoor air. We

J. Kukkonen (✉) · J. Soares · L. Kangas · M. Kauhaniemi · K. Riikonen · J.-P. Jalkanen · T. Rasila · M. Aarnio · A. Karppinen
Finnish Meteorological Institute, Helsinki, Finland
e-mail: jaakko.kukkonen@fmi.fi

V. Singh
National Atmospheric Research Laboratory, Tirupathi, India

R.S. Sokhi · A. Kousa
University of Hertfordshire, Hatfield, UK

L. Matilainen · T. Koskentalo
Helsinki Region Environmental Services Authority, Helsinki, Finland

O. Hänninen
National Institute for Health and Welfare, Helsinki, Finland

C. Hendriks
TNO, Utrecht, The Netherlands

D.G. Steyn and N. Chaumerliac (eds.), *Air Pollution Modeling and its Application XXIV*, Springer Proceedings in Complexity,
DOI 10.1007/978-3-319-24478-5_16

present fine-resolution numerical results on annual spatial concentration, time activity and population exposures to $PM_{2.5}$ in London and in the Helsinki Metropolitan Area, for 2008 and 2009. We have shown that the effect of neglecting the movements of the population, which is the currently commonly applied procedure, can result in an underprediction of exposure by several tens of per cent.

16.1 Introduction

Exposure models vary from simple relations of the health aspects with the outdoor air concentrations up to comprehensive deterministic exposure models (e.g. Ashmore and Dimitripoulou 2009; Soares et al. 2014). The aims of this paper are (i) to illustrate the benefits of using more detailed exposure modelling that allows for the movements of the populations, and (ii) to present selected illustrative numerical results for human exposure to fine particulate matter ($PM_{2.5}$) in London and in the Helsinki Metropolitan Area for 2008.

16.2 Methods

The traffic flows, emissions and atmospheric dispersion in London were evaluated using the OSCAR modelling system (Sokhi et al. 2008). In case of Helsinki Metropolitan Area (HMA), the transportation planning model EMME2, national emission models and the roadside dispersion model CAR-FMI were applied. In addition, the population exposure model EXPAND (Soares et al. 2014) was applied for HMA. For London, the exposures in various micro-environments were evaluated using a similar, although relatively slightly simpler population exposure model.

We addressed results computed for 2008 and 2009. In case of London, all local sources and the regional background (RBG) were included. In case of HMA, the computations included the RBG, the vehicular emissions, shipping, and major stationary sources. For a more detailed description of the emission and dispersion computations in London, the reader is referred to Singh et al. (2013), and in case of Helsinki, to Soares et al. (2014).

16.3 Results

The diurnal variation of population activities in various microenvironments in London and the Helsinki Metropolitan Area is presented in Fig. 16.1. For HMA, children that are younger than or equal to 10 years have been excluded from the

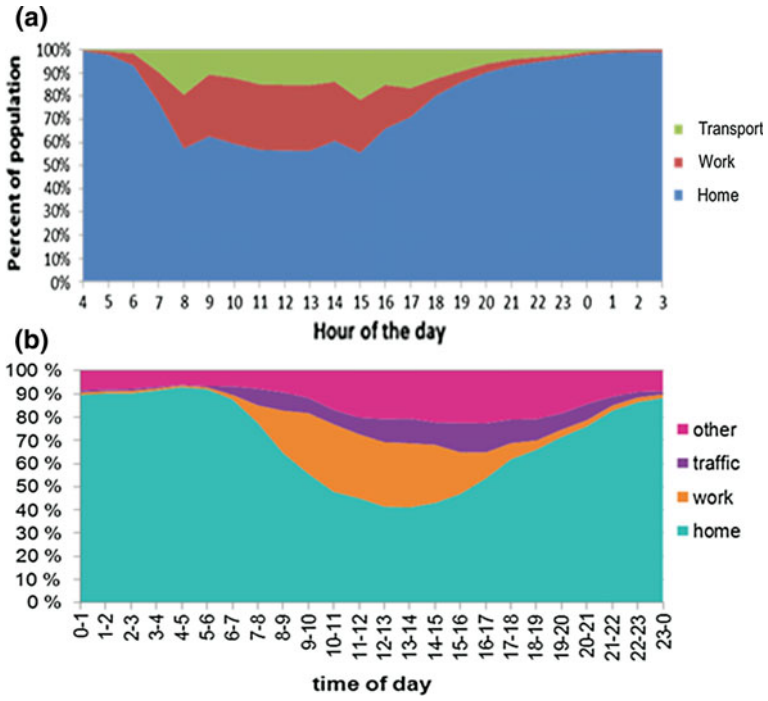

Fig. 16.1 a–b. The percentage of population in various micro-environments against the hour of the day, in London (*upper panel*) and in Helsinki Metropolitan Area (*lower panel*) in 2008

data of this figure; however, they are included in the subsequent exposure computations. In the data presented in Fig. 16.4, we have combined indoor and outdoor time activity in each microenvironment.

On average, people spent most of their time in the home environment in both cities. As expected, people also spent a substantial fraction of their time in traffic and in other activities (these include shopping and various recreational activities).

Example results of the population exposures to $PM_{2.5}$ in London and HMA have been presented in Figs. 16.2 and 16.3. In London, most of the total exposure occurred at home and workplace environments (86 %), and a smaller fraction (14 %) in traffic. In HMA, the exposure at home is responsible for most of the exposure, 60 %, whereas the work and other activities exposures are responsible for most of the rest of the exposure, i.e. 19 and 17 %, respectively.

We have presented the spatial distributions of the predicted annual average population exposures in the Helsinki Metropolitan Area in 2008 in Fig. 16.3a–b, for the total exposure and separately for homes. These distributions exhibit characteristics of both the corresponding spatial concentration distributions and time activities. For total exposure, there are elevated values in the Helsinki city centre, along major roads and streets, and in the vicinity of urban district centres. The high

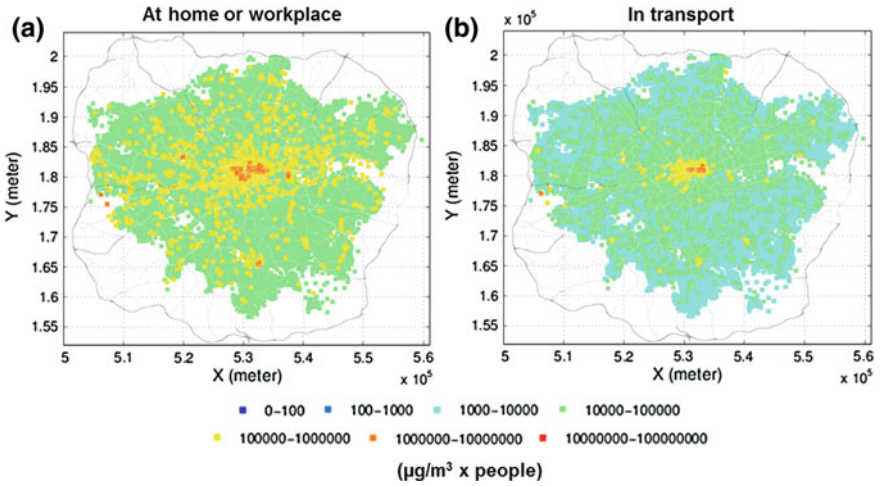

Fig. 16.2 a–b. The population exposure to $PM_{2.5}$ in London in 2008, presented separately for home and workplace environments, and for transport. The unit of exposure is $\mu g/m^3$ × the number of persons

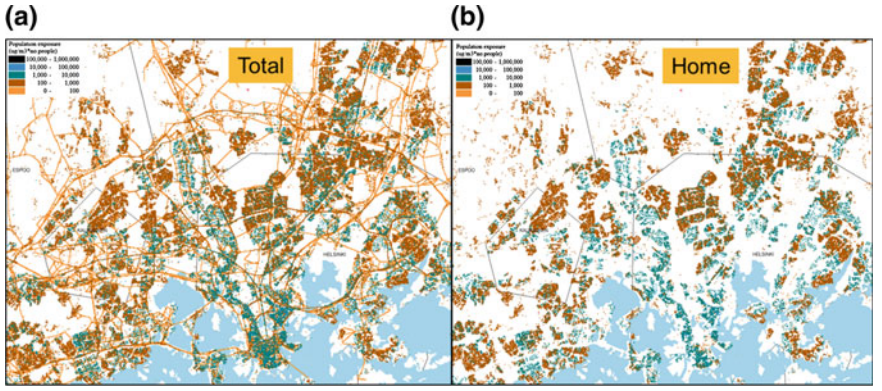

Fig. 16.3 a–b. The population exposure to $PM_{2.5}$ in Helsinki Metropolitan Area in 2008, presented separately for total exposure (all micro-environments combined) and for home environments. The unit of exposure is $\mu g/m^3$ x the number of persons

home and work exposures in the centre of Helsinki were caused both by the relatively high concentrations and the highest population and workplace densities in the area. The exposure at homes is more evenly dispersed throughout the region, as a substantial fraction of residences are located in suburban areas.

16.4 Conclusions

Exposures were substantially higher in central parts of both cities and in the vicinity of urban district centres, compared with the suburban areas. Most of the total exposure occurred at home and workplace environments in both cities. In London, this fraction was 86 %. In Helsinki Metropolitan Area (HMA), the shares of total exposure were: 60 % at home, 17 % at work, 4 % in traffic and 19 % in other micro-environments.

In both cities, people in transportation were exposed to substantially higher $PM_{2.5}$ concentrations, compared with work or home environments. In London, 73 % of exposure was caused by regional concentrations, 19 % by the urban non-road transport sources and 8 % was caused by road transport emissions. In HMA, 86 % of the exposure was caused by long range transported concentrations, 12 % from local vehicular emissions and 2 % from shipping.

In London for $PM_{2.5}$, the current method predicted approximately one fourth (26 %) higher total population exposure, compared with using population-weighted concentrations at residential locations. For pollutants that are more dominated by local urban sources (such as, e.g., PM_{10}, particulate number concentrations or NO_2), this error in using only residential exposure would be expected to be substantially higher, compared with the corresponding error in case of $PM_{2.5}$. We conclude that the inaccuracies of exposure assessments that have been made only based on residential exposures (or on population-weighted concentrations) can be substantial. Appropriate exposure assessments that allow for the actual locations and movements of the populations should therefore be taken into account in exposure assessments.

The presented models and results can be used in urban and traffic planning. The use of such models also facilitates the evaluation of health effects in terms of micro-environments, source categories, and age or any other groups of the population. The use of such models also makes it possible to include more realistic treatments of the outdoor-indoor infiltration of pollutants in various micro-environments. The models are applicable in other urban areas worldwide, provided that the appropriate time-activity surveys will be available.

Acknowledgments This work was funded by EU Seventh Framework Programme—(ENV.2009.1.2.2.1) project TRANSPHORM.

Questions and Answers

QUESTIONER: H. Schluenzen
QUESTION: How are indoor emissions considered? Are they included and what do we know?

ANSWER: This study addressed only the influence of outdoor air pollution on the population exposure. We took into account exposures caused by (i) pollution in

outdoor air and (ii) outdoor air pollution that has been infiltrated to indoor air. A natural follow-up of this study would be to take into account also indoor air pollution sources.

In general, indoor air quality is determined by infiltration, ventilation and indoor pollution sources. Clearly, indoor air sources can in some cases have a substantial effect on the population exposure to air pollutants. A few examples of indoor pollution sources are smoking, heating and cooking. For instance, the influences of active or passive smoking in indoor environments is commonly larger than those caused by outdoor air pollution.

QUESTIONER: A. Hakami

QUESTION: If inaccuracies resulting from outdoor-indoor infiltration and population movements are already included in epidemiological estimates, then will this higher level of detail improve health impact assessments?

ANSWER: The problem is that the factors that you mentioned are commonly not included. Most of the epidemiological studies have been conducted based on pollution concentrations measured at fixed ambient air quality monitoring sites, or modelled values using land-use regression models. Such methods do not in any way allow for the infiltration of pollution indoors and population movements.

Since the urban population spends typically 80–95 % of their time indoors, the exposure to particles is commonly dominated by exposure in indoor environments. However, many previous approaches have ignored the differences between indoor and outdoor air.

In this study, we have allowed in a more realistic manner for the movements of people and outdoor-indoor infiltration. We have also shown that including these effects has a substantial effect on the evaluated health outcomes: these can change the predicted population exposure by tens of per cent or more.

QUESTIONER: D. Wong

QUESTION: How long is your study, i.e., how many years of data are included? Did you include data on man-made or natural barriers in your study? I have done CDF work that shows that obstacles have a significant effect on concentrations.

ANSWER: The computations that I presented were done for hourly averaged data within 1 year. It would of course be possible to repeat the computations for some other years. Clearly, the exposure of the whole urban population for different years can be totally different for specific hourly and daily values, but annually averaged values change slowly from year to year.

The dispersion modelling and the spatial averaging do not allow either for the dispersion in street canyons or the very fine-scale concentration distributions above the roads and streets. In some previous studies, we have also conducted both street canyon modelling, using the OSPM model, and CFD modelling for specific locations in Helsinki. You are correct of course that by using such methods the fine scale (meters or tens of meters) concentration distributions could be modelled more

accurately. However, for practical reasons it was not possible in this study to use street canyon or CFD models for the tens or hundreds or street canyons in these cities.

References

Ashmore MR, Dimitripoulou C (2009) Personal exposure of children to air pollution. Atmos Environ 43:128–141. doi:10.1016/j.atmosenv.2008.09.024

Kousa A, Kukkonen J, Karppinen A, Aarnio P, Koskentalo T (2002) A model for evaluating the population exposure to ambient air pollution in an urban area. Atmos Environ 36:2109–2119. doi:10.1016/S1352-2310(02)00228-5

Singh V, Sokhi R, Kukkonen J (2013) PM2.5 concentrations in London for 2008—A modeling analysis of contributions from road traffic. J Air Waste Manag accepted, http://dx.doi.org/10.1080/10962247.2013.848244

Soares J, Kousa A, Kukkonen J, Matilainen L, Kangas L, Kauhaniemi M, Riikonen K, Jalkanen J-P, Rasila T, Hänninen O, Koskentalo T, Aarnio M, Hendriks C, Karppinen A (2014) Refinement of a model for evaluating the population exposure in an urban area. Geosci Model Dev 7:1855–1872. doi:10.5194/gmd-7-1855-2014. www.geosci-model-dev.net/7/1855/2014/

Sokhi RS, Mao H, Srimath TGS, Fan S, Kitwiroon N, Luhana L, Kukkonen J, Mervi Haakana K, van den Hout D, Boulter P, McCrae IS, Larssen S, Gjerstad KI, Jose RS, Bartzis J, Neofytou P, van den Breemer P, Neville S, Kousa A, Cortes BM, Karppinen A, Myrtveit I (2008) An integrated multi-model approach for air quality assessment: development and evaluation of the OSCAR Air Quality Assessment System. Environ Model Softw 23:268–281

Chapter 17
Calculation of Source-Receptor Matrices for Use in an Integrated Assessment Model and Assessment of Impacts on Natural Ecosystems

Anthony Dore, Stefan Reis, Tim Oxley, Helen ApSimon, Jane Hall, Massimo Vieno, Maciej Kryza, Chris Green, Ioannis Tsagatakis, Sim Tang, Christine Braban and Mark Sutton

Abstract A computationally efficient atmospheric chemical transport model (FRAME) was used to generate source-receptor concentration and deposition data from a variety of spatially distributed and point sources of nitrogen and sulphur emissions. The model was evaluated by comparison with measurements of nitrogen compounds in the gaseous, particulate and aqueous phase and found to be fit for purpose as a policy tool for assessing the effects of future emissions controls. A scenario for the year 2030 predicted that 64 % of the area of natural ecosystems in the UK would be subject to deposition of nitrogen exceeding critical loads.

A. Dore (✉) · S. Reis · M. Vieno · S. Tang · C. Braban · M. Sutton
Centre for Ecology & Hydrology, Edinburgh, UK
e-mail: todo@ceh.ac.uk

T. Oxley · H. ApSimon
Imperial College, London, UK

J. Hall
Centre for Ecology & Hydrology, Bangor, UK

M. Kryza
Wrocław University, Wrocław, Poland

C. Green
AMEC, London, UK

I. Tsagatakis
Ricardo-AEA, London, UK

D.G. Steyn and N. Chaumerliac (eds.), *Air Pollution Modeling and its Application XXIV*, Springer Proceedings in Complexity,
DOI 10.1007/978-3-319-24478-5_17

17.1 Introduction and Model Description

Deposition of nitrogen occurs both as oxidized nitrogen (emitted primarily as NO_x from combustion processes) and reduced nitrogen (emitted mostly as NH_3 from agricultural sources). This leads to the eutrophication of terrestrial and fresh water ecosystems promoting excessive plant growth and causing a reduction in water quality. Field experiments have correlated nitrogen deposition to a loss of bioviersity in a wide range of ecosystems. Nitrogen deposition has been identified as a global environmental concern.

Atmospheric chemical transport models can be used to assess changes in nitrogen deposition based on future predictions of atmospheric emissions and thus provide the basis for the quantification of changes in impacts. Source-receptor matrices link the emissions of pollutants from specific sources to air concentrations and deposition of pollutants. They are indispensable input data for integrated assessment models (IAMs, Oxley et al. 2013) to evaluate measures to abate pollutant emissions. IAMs are widely used to generate scenarios and to identify optimised strategies for improved air quality and reduced pollutant deposition.

FRAME (Fine Resolution Multi-pollutant Atmospheric Exchange) is a Lagrangian model using straight line trajectories (Dore et al. 2012) with a 1° angular resolution which runs at either a 1 km or a 5 km horizontal resolution over the British Isles and 50 km resolution over Europe with a fine vertical grid spacing (1 m at the surface). Area emissions are injected into sector dependent levels and point source emissions are treated with a plume rise routine. Vertical diffusion in the air column is calculated using K-theory eddy diffusivity. Wet deposition is calculated using a 'constant drizzle' approximation driven by an annual rainfall map. Five land classes are considered and a vegetation specific canopy resistance parameterisation is employed to calculate dry deposition of SO_2, NO_2 and NH_3. The model chemistry includes gas phase and aqueous phase reactions of oxidised sulphur and oxidised nitrogen as well as aerosol formation. To generate source-receptor data for the integrated assessment model, 619 simulations were undertaken. These involved 25 % reductions in emissions from individual targeted spatially distributed and point sources from five regions of the United Kingdom (England, Scotland, Wales, Northern Ireland and London). Data from the EMEP Eulerian model (Simpson et al. 2012) was used to calculate the contribution to concentration and deposition from non-UK European sources.

17.2 Results

The FRAME model was found to give a good representation of aerosol and gas concentrations of nitrogen compounds as well as wet deposition when compared with measurements from the UK national monitoring networks. Table 17.1 illustrates the correlation with annually averaged measurements of gas, aerosol and

Table 17.1 Statistics for the FRAME model correlation with annual average measurements of precipitation concentration (μM l^{-1}) and air concentrations (μg m^{-3}) for the year 2012 (N: number of samples; R: Pearson correlation coefficient, NMB: Normalised Mean Bias; FAC2: 'Factor Of 2' percentage of modelled points less than twice and greater than half the measured value)

	N	R	NMB	FAC2
NH_4^+ in precipitation	38	0.94	−0.07	92
NO_3^- in precipitation	38	0.92	−0.01	92
NH_3 gas	88	0.72	0.17	80
NO_2 gas	26	0.98	−0.30	96
NH_4^+ particulate	30	0.94	−0.19	82
NO_3^- particulate	30	0.95	−0.09	86

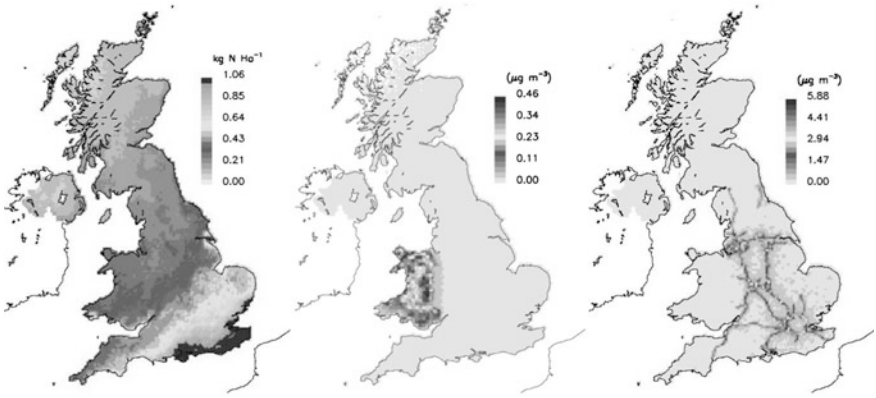

Fig. 17.1 Examples of source-receptor data for the year 2025: Dry deposition of NO_y from international shipping (*left*); NH_3 concentrations from poultry in Wales (*centre*); NO_x concentrations from heavy goods vehicles in England (*right*)

precipitation concentration for the year 2012. The model generally satisfied the criteria for 'fitness for purpose' of: $-0.2 < NMB < 0.2$ and $FAC2 > 50$.

Examples of a selection of source-receptor data generated with the FRAME model using projected emissions estimates for the year 2025 are illustrated in Fig. 17.1. These comprise: dry deposition of NO_y from international shipping, NH_3 concentrations from poultry in Wales and NO_x concentrations from heavy goods vehicles in England. Such sets of deposition and concentration data are correlated to emissions for specified sources and can be re-combined in an integrated modelling framework using projected emissions reductions based on targeted technical measures. This leads to estimates of different future nitrogen deposition scenarios depending on the adoption of control measures based on their implementation costs.

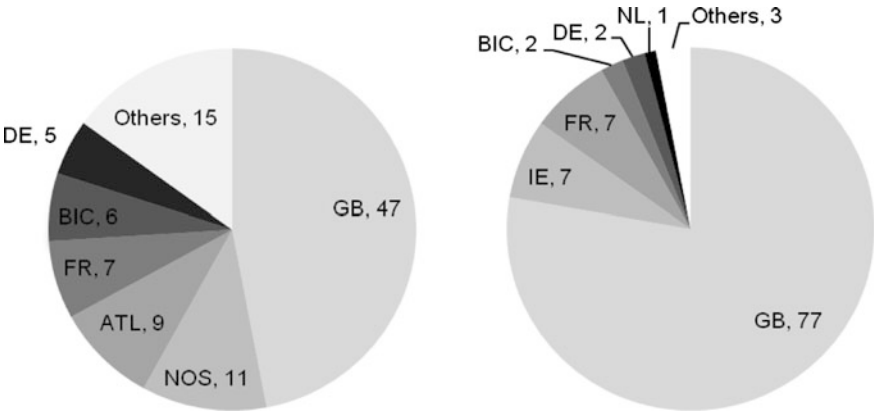

Fig. 17.2 Contribution to NO_x deposition (*left*) and NH_x deposition (*right*) in the UK from different European countries (including international shipping: NOS North Sea, ATL Atlantic) calculated with the EMEP model for 2012

The computationally efficient FRAME model (with a run time of 15 min on a single 16 core node) is effective at performing multiple simulations. However the EMEP Eulerian model (Simpson et al. 2012) is better suited for estimating the trans-boundary component of nitrogen deposition originating from emissions sources in other European countries. The contribution to oxidised and reduced nitrogen deposition in the UK from European countries as well as international shipping calculated with EMEP is illustrated in Fig. 17.2. It is evident that NH_x deposition is predominantly from domestic sources (due to efficient dry deposition of locally emitted ammonia). The picture for NO_x deposition is however more complex with long range transport of nitrate aerosol originating from international shipping and other European countries contributing more than half of the deposition.

Using existing legislation for the introduction of technical measures to reduce emissions of NO_x and NH_3, a scenario for the year 2030 was defined. The exceedance of critical loads for nutrient nitrogen deposition was calculated for the future scenario and compared to the baseline year 2010 (Table 17.2). These results show that nitrogen deposition will continue to pose a risk to natural ecosystems over the next two decades. Further control of emissions of both ammonia (primarily from the UK) and of oxides of nitrogen from European sources and international shipping will be necessary in order to reduce the threat to biodiversity from eutrophication.

Table 17.2 Exceedance of critical loads for the years 2010 and 2030 for different ecosystems in the UK based on emissions projections using existing policy

Broad habitat	Habitat area (km^2)	Percentage area exceeded	
		2010	2030
Acid grassland	15,235	64.4	58.9
Calcareous grassland	3,578	94.4	95.8
Dwarf shrub heath	24,826	47.6	43.1
Bog	5,526	47.2	44.7
Montane	3,129	86.0	79.0
Coniferous woodland (managed)	8,383	91.5	90.0
Broadleaved woodland (managed)	7,482	97.6	97.3
Fagus woodland (unmanaged)	719	100.0	100.0
Acidophilous oak (unmanaged)	1,434	96.4	93.8
Scots Pine (unmanaged)	204	48.5	39.8
Other unmanaged woodland	1,761	95.5	95.3
Dune grassland	323	46.2	46.3
Saltmarsh	427	0.9	2.1
All habitats	73,027	67.5	64.2

17.3 Conclusion

The use of source-receptor relationships from an atmospheric chemical transport model allows the rapid re-construction of future scenarios for concentration and deposition of pollutants based on implementation of technical measures to reduce atmospheric emissions. The focus of this work is on the deposition of nitrogen. Large areas of natural ecosystems in the UK were calculated to be subject to nitrogen deposition in exceedance of critical loads for the year 2030. This indicates that future UK and European policy will need to be applied to control nitrogen emissions in order to protect natural ecosystems.

Acknowledgments This study was supported by the UK Department for the Environment, Food and Rural Affairs and the Natural Environment Research Council

Questions

Wouter Lefebvre: Do you take into account compensation points and $v_d = f(C_{NH3})$ relationships?

Answer: As the model runs in a fast 'annual average' mode, it is not suitable for inclusion of canopy compensation point calculations. The deposition velocity of ammonia is calculated separately to six different surface types (forest, moorland,

improved grassland, arable, urban and water) using a canopy resistance formulation with the canopy resistance based on annual average values.

Questioner: Have you tested your assumption of linearity?

Answer: The change in nitrogen deposition has been tested for different percentage reductions in emissions from a single point source. These revealed a close to linear relationship for smaller emissions changes with some divergence for large percentage emissions reductions (close to 100 %). Source receptor relationships were calculated with a 25 % reductions in emissions for each source to avoid the non-linear chemical perturbation associated with higher percentage emissions changes.

References

Dore AJ, Kryza M, Hall J, Hallsworth S, Keller V, Vieno M, Sutton MA (2012) The influence of model grid resolution on estimation of national scale nitrogen deposition and exceedance of critical loads. Biogeosciences 9:1597–1609

Oxley T, Dore AJ, Kryza M, ApSimon H (2013) Modelling future impacts of air pollution using the multi-scale UK Integrated Assessment Model (UKIAM). Environ Int 61:17–35

Simpson D, Benedictow A, Berge H, Bergstrom R, Emberson LD, Fagerli H, Hayman GD, Gauss M, Jonson JE, Jenkin ME, Nyíri, Richter AC, Semeena VS, Tsyro S, Tuovinen J-P, Valdebenito Á, Wind P (2012) The EMEP MSC-W chemical transport model—technical description. Atmos Chem Phys 12:7825–7865

Chapter 18
Using a Coupled Modelling System to Examine the Impacts of Increased Corn Production on Groundwater Quality and Human Health

Valerie Garcia, Ellen Cooter, James Crooks, Brandon Hayes, Brian Hinckley, Mark Murphy, Tim Wade and Xiangnan Xing

Abstract Attributing nitrogen (N) in the environment to emissions from agricultural management practices is difficult because of the complex and inter-related chemical and biological reactions associated with N and its cascading effects across land, air and water. Such analyses are critical, however, in understanding the benefits and disbenefits associated with environmental management options. Coupled physical models present new opportunities to understand relationships among environmental variables across multiple sources, pathways and scenarios. Because they trace the environmental fate of pollutant concentrations found in the environment through first-principle physical and chemical processes, they shed new light on these complex interactions and how they will respond under various management scenarios. In this study, we use a coupled modeling system to holistically assess the impacts of increased corn production on groundwater and air quality. In particular, we show how the models provide new information on the drivers for contamination in groundwater and air, and then relate pollutant concentration changes attributed to potential changes in corn production between 2002 and 2022 to health and cost outcomes.

V. Garcia (✉) · E. Cooter · J. Crooks · T. Wade
Office of Research and Development, U.S. Environmental Protection Agency, RTP, 109 TW Alexander Drive, Durham 27711, NC, USA
e-mail: garcia.val@epa.gov

B. Hayes · B. Hinckley · X. Xing
ORISE, Oakridge National Laboratory, Oak Ridge, TN, USA

M. Murphy
Innovate!, Inc., Alexandria, VA, USA

D.G. Steyn and N. Chaumerliac (eds.), *Air Pollution Modeling and its Application XXIV*, Springer Proceedings in Complexity,
DOI 10.1007/978-3-319-24478-5_18

18.1 Introduction

Human-induced N is emitted into the atmosphere predominantly from burning fossil fuel. Nitrogen interacts in the atmosphere to form ozone and particulate matter, increasing human health risks of pulmonary and cardio-vascular disease and death. Atmospheric N deposited to the earth's surface, and N placed on crops as part of agricultural management practices produces excess N in the soil, and also interacts with N in the atmosphere at soil and plant surfaces. Excess N leaches into sources of drinking water, increasing human health risks of 'blue baby syndrome', hypertension, and some cancers and birth defects. Thus, understanding complex multi-media, multi-pollutant environmental problems requires a holistic approach to comprehensively investigate the benefits and disbenefits of mitigating actions (VanGrinsven et al. 2013).

18.2 Approach

In this study, we applied a coupled air quality modelling system that was then partially coupled to an agricultural management model (Cooter et al. 2012; Fig. 18.1) to examine the impact of N inputs from corn production on ecosystem and human health. The coupled system accounts for N deposited or emitted to and from the land surface, providing a unique opportunity to examine the effect of management practices (e.g., type of fertilization, tilling, irrigation) on groundwater and air quality. We performed extensive multi-variate regression modelling to investigate the rich dataset of model variables for associations between agricultural

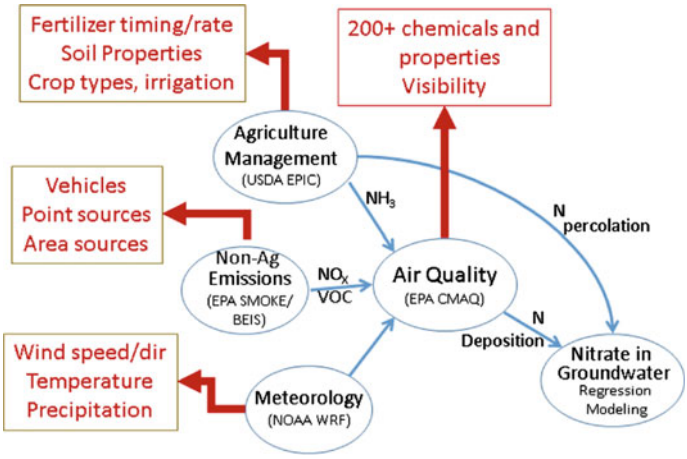

Fig. 18.1 Coupled models used in study and examples of available variables from each model

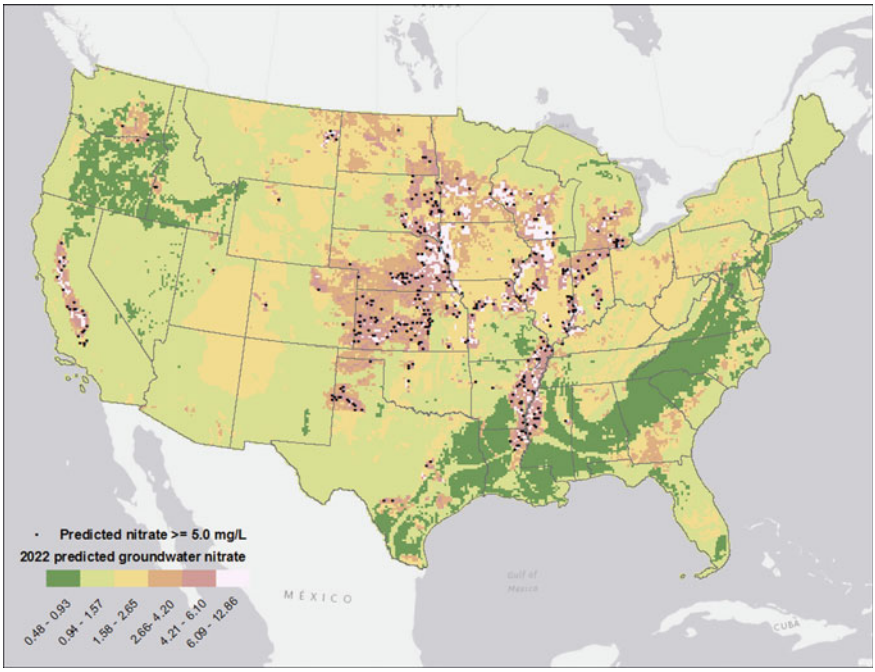

Fig. 18.2 Predicted groundwater nitrate in 2022. Circles represent those grid cells that increased to >5 mg/L as compared to 2002 due to increased corn production

management practices and nitrogen contamination in groundwater and the atmosphere.

We then applied the regression model to predict and contrast pollution levels between two corn production scenarios (Fig. 18.2). Finally, we applied published health impact functions (e.g., spina bifida, cardio-vascular mortality rates) and economic impact functions (e.g., loss of work/school days, decontamination of wells) to comprehensively investigate the impacts of N pollution from increased corn production.

18.3 Results and Discussion

Changes in atmospheric ozone and particulate matter concentrations between the two corn production scenarios were minor in comparison to other emission control actions such as the Clean Air Interstate Rule and Tier III Motor Vehicle and Emission and Fuel Standards. In examining the emissions attributable to increased

corn production only, we found that increased NOx occurred in less populated areas in California and the Midwest. NOx increases in urban areas result in lower ozone concentrations due to titration. Because these ozone decreases occur in highly populated areas, they resulted in an overall decrease in health incidences and a decrease in related costs. Regression modeling revealed that aquifer type, percent land use, total deposition, number of animal feeding operations, N fertilizer and soil properties were all important predictors of N in groundwater. Of particular note, no association was seen with total N fertilizer placed on all crops, but a very strong association ($P < 0.0001$) was seen when the variable is refined to represent fertilizer placed on irrigated (as opposed to rain-fed) crops, specifically grain corn (as opposed to other crops, including corn grain silage). This strong association may be due to several factors, such as the prevalence of unconsolidated aquifers in drier areas of the nation, and vertical leaching from irrigated watering techniques, quantities and timing. To calculate health impacts, we have identified a health impact function for excess spina bifida cases resulting from exposure to drinking water with >5 mg/L groundwater nitrate. In these preliminary results, nitrate in groundwater was predicted to increase 5 mg/L in 4 % of groundwater locations, resulting in a slight risk increase of spina bifida birth defects.

18.4 Summary

This study demonstrates the value of using a coupled modeling system to investigate the response of perturbations to complex environmental processes such as the effect of agricultural management practices on N as it moves through the environment. For example, past studies have revealed associations between nitrate groundwater contamination and N loadings. The coupled modeling system allowed us to refine the N loading variable to reveal an important driver to groundwater contamination associated with N fertilizer placed on irrigated grain corn. This new knowledge was used to assess vulnerability to excess spina bifida cases using a preliminary future corn production scenario.

Acknowledgments and Disclaimer Although this work has been reviewed and approved for publication by the U.S. Environmental Protection Agency, it does not necessarily reflect the views and policies of the agency.

Questioner

No questions were asked of speaker.

References

VanGrinsven HJ, Holland M, Jacobsen BH, Klimont Z, Sutton MA, Willems WJ (2013) Costs and benefits of nitrogen for Europe and implications for mitigation. Environ Sci Technol 47:3571–3579

Cooter EJ, Bash JO, Benson V, Ran L (2012) Linking agricultural crop management and air quality models for regional to national-scale nitrogen assessments. Biogeosciences 9:6095–6127

Chapter 19
Future Air Quality Related Health Effects in Europe and the Nordic Region—Sensitivity to Changes in Climate, Anthropogenic Emissions, Demography and Building Stock

Camilla Geels, Camilla Andersson, Otto Hänninen, Anne Sofie Lansø, Carsten Ambelas Skjøth, Per E. Schwarze and Jørgen Brandt

Abstract Future changes in population exposures to ambient air pollution are inherently linked with long-term trends in outdoor air quality, but also with changes in the building stock. Moreover, the burden of disease is further driven by the ageing of the European populations. This study aims to assess the impact of changes in climate, emissions, building stocks and population on air pollution related human health impacts across Europe in the future. Therefore an integrated assessment model combining atmospheric models and health impacts have been

C. Geels (✉) · A.S. Lansø · J. Brandt
Department of Environmental Science, Aarhus University, Aarhus, Denmark
e-mail: cag@envs.au.dk

A.S. Lansø
e-mail: asla@envs.au.dk

J. Brandt
e-mail: jbr@envs.au.dk

C. Andersson
Swedish Meteorological and Hydrological Institute, Norrkoping, Sweden
e-mail: Camilla.andersson@smhi.se

O. Hänninen
Department of Health Protection, National Institute for Health and Welfare, Kuopio, Finland
e-mail: Otto.hanninen@thl.fi

C.A. Skjøth
Institute of Science and the Environment, University of Worcester, Worcester, UK
e-mail: c.skjoth@worc.ac.uk

P.E. Schwarze
Department of Air Pollution and Noise, Norwegian Institute of Public Health, Oslo, Norway
e-mail: Per.schwarze@fhi.no

D.G. Steyn and N. Chaumerliac (eds.), *Air Pollution Modeling and its Application XXIV*, Springer Proceedings in Complexity,
DOI 10.1007/978-3-319-24478-5_19

setup for projections of the future developments in air pollution related premature mortality. The focus is here on the regional scale impacts of exposure to surface ozone (O_3), Secondary Inorganic Aerosols (SIA) and primary particulate matter (PPM).

19.1 Introduction and Study Setup

Air pollution is the most important environmental factor associated with health impacts (WHO 2014). In the future potential changes in both climate and anthropogenic and natural emissions will alter the surface concentration of O_3 and particulate matter (Colette et al. 2013, Langner et al. 2012) and thereby the air pollution levels humans are exposed to. Both O_3 and PM are linked to negative health impact and premature mortality (WHO 2013). As these health effects are age-dependent, the general trend in Europe towards an aging society can also modify premature mortality. Within the European Union (EU) energy savings and hence a more energy efficient building stock have been high on the agenda for many years. Such changes will be important for the infiltration rate of outdoor pollution into the houses and hence for the general exposure of the population. In the current study we have used an integrated assessment system in order to investigate future air pollution related health effects, and how sensitive the estimates are to a number of the parameters mentioned above. An overview of the system based on the integrated model system EVA (Brandt et al. 2013) and the involved models and driving input data is given in Fig. 19.1. Simulations are made for the three decades: 2000–2009, 2050–2059 and 2080–2089.

Importantly, assessments for the future are associated with significant uncertainties e.g. due to the use of scenarios for the development in climate and emissions. A detailed description of the system, the uncertainties and results can be found in Geels et al. (2015). The largest limitation of the current study is the omission of Secondary Organic Aerosols (SOA) that due to the complex processes involved not was included in the used models, at the start of this study. Possible differences in toxicity of the various particles/aerosols are also not included here.

19.2 Results and Discussion

The sensitivity of the health outcome to changes in drivers is tested stepwise and for the two future periods (2050s and 2080s) relative to the present day (2000s). The resulting changes as simulated by the two different chemistry transport models (DEHM and MATCH) are shown for the Nordic region in Table 19.1. Very similar results are obtained across Europe. Climate change alone is here projected to change premature mortality by a few percent, but the result depends on the model

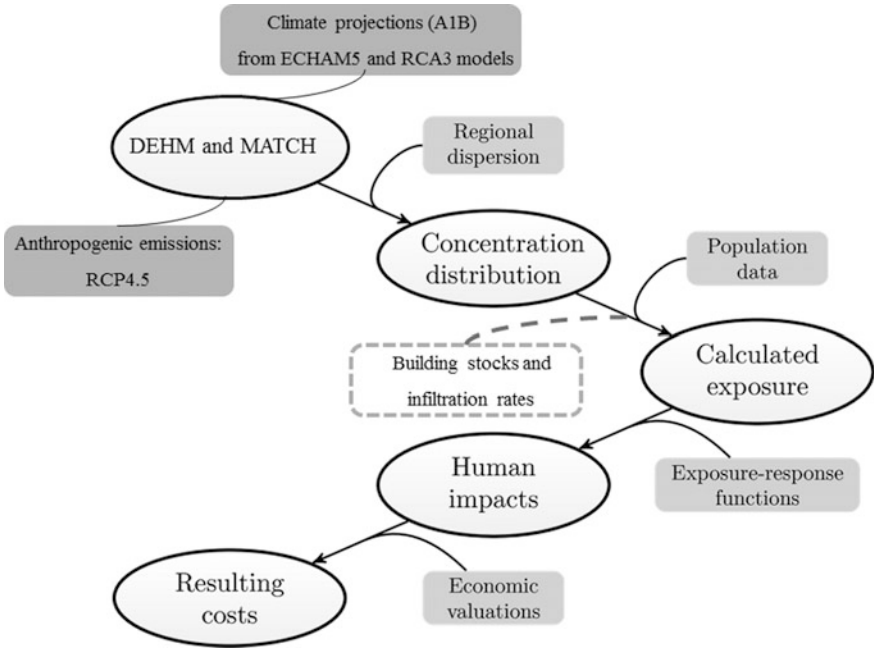

Fig. 19.1 An overview of the models and the scenarios used in the current study. The *dashed line* and the *dashed box* illustrates the new addition to the system, which is tentatively accounted for here—for the first time in relation to climate change exposure scenarios

Table 19.1 The change in chronic mortality in the Nordic region relative to the 2000s

Models	Decade	Climate change (CC) (%)	CC + emissions (%)	CC + emissions + infiltration (%)
DEHM-EVA	2050s	−2	−64	−81
	2080s	−6	−80	−92
MATCH-EVA	2050s	+2	−65	−82
	2080s	+3	−81	−92

used. A more robust result is obtained for the combined climate and emission projection, where the assessment projects a significant and large decrease of up to about 80 % in air-pollution related mortality. The projected changes in building stock and hence infiltration rates have the potential to bring down the future air pollution related health effects in the Nordic region substantially. Simulations for the European region show that changes in the demography also have a small, but significant impact on the assessment in parts of Europe. New knowledge on NH_3 emissions indicates an increase in emissions from the agricultural sector by up to ca. 40 % due to climate change (Skjøth and Geels 2013; Sutton et al. 2013).

We include a scenario using these new emissions to evaluate if increased emission of ammonia due to climate change might have an impact on the PM levels and the related health effects. A small (4 %) increase in the mortality was obtained at the European scale, but in agricultural regions (e.g. Germany and Poland) this increase was significant.

19.3 Conclusion

An integrated assessment system linking air pollution and health effects has been used to simulate future conditions. We have extended the system to describe changes in infiltration rates and the possible impacts on the exposure in the Nordic countries. Even if energy saving are highly prioritised in EU, the resulting impacts on the building stock and hence infiltration rates have not previously been included in long term projections of air pollution related premature mortality. When more data on the development in the building stock across Europe becomes available our approach can and should be elaborated. Our study also shows that using present day demography for future projections can introduce a systematic bias to the estimates. Therefore valid projections of the European demography are needed in order to limit the uncertainty. The uncertainty related to assessments like this is in general high and the projections should merely be used to illustrate a possible tendency in the future and the sensitivity to included drivers.

Acknowledgments This study was mainly funded through the Nordic Council of Ministers (the KOL-1204 project).

Questions and Answers

QUESTIONER: S. Aksoyoglu.
QUESTION: Results of the two models for PM2.5 are different. Since you don't have any SOA, the difference must be in inorganic aerosols—do you know the reason for this?

ANSWER: The two models are based on different chemical schemes and are also forced by slightly different data sets of climate data. Analysis of the different components of the total PM2.5 simulated by the models, show that the main difference is linked to the nitrate part of the secondary inorganic aerosols. The DEHM model tends to overestimate this component, which partly can be due to the lower resolution in the DEHM model.

QUESTIONER: S. Arunachacam.
QUESTION: When you increased ammonia (NH_3) emission by 35 % under future climate, did you also increase PM2.5 such as NOx and SOx too? If not, how

realistic is the assumption? Can you comment on the 35 % increase leading to only a 4 % increase in health effects?

ANSWER: New studies show that the projected temperature increase in Europe can lead to an increase of the ammonia emissions in the agricultural sector of up to 40 % towards the end of the century. So we make a special scenario run for the 2080s based on projected changes in climate and anthropogenic emissions, but where the projected NH_3 emissions have been increased by 35 %. The temperature effect on ammonia emissions is well known, but is currently not included in standard emission scenarios. More detailed emission modelling studies are necessary in order to make a more firm estimate of the NH_3 increase, but we believe that it is realistic to assume that these emissions will increase in a warmer world. Comparing the estimated number of chronic deaths in the standard simulation for 2080s with this new simulation, show that the increased ammonia emissions lead to a 4 % increase in the chronic mortality in Europe. Ammonia contributes to the formation of particles through chemical transformation into ammonium aerosols in the atmosphere. As this component form a smaller fraction of the total PM2.5 mass than e.g. nitrate, the assumed increase in the NH_3 emission only leads to a small increase in the health effects.

QUESTIONER: Lefebvre.
QUESTION: Is it correct to reduce the infiltration rates due to tightening of the building stock? Is this assuming filtering?

ANSWER: The current health impacts are estimated based on relationship between outdoor air quality and population exposures in the situations prevailing in cities that have been included in the epidemiological cohort studies. As long as this concentration-exposure (C-E) relationship remains the same, the use of the C-R relationships from these studies is appropriate directly. Then when we look at longer periods/scenarios where the time-activity, or building stock as in this case, is changing, we cannot use the same C-R values as such without introducing a bias. Therefore we aimed at creating a building tightening scenario based on the European policy objectives on energy efficiency of buildings and subsequently estimated implications on infiltration efficiency of particles. Optimally such a model needs to account for lower penetration/changes in the ventilation rates and air residence times indoors. Moreover, also the particle size distribution, if changing, would play a role.

References

Brandt J et al (2013) Contribution from the ten major emission sectors in Europe and Denmark to the health-cost externalities of air pollution using the EVA model system—an integrated modelling approach. Atmos Chem Phys 13:7725–7746

Colette A et al (2013) European atmosphere in 2050, a regional air quality and climate perspective under CMIP5 scenarios. Atmos Chem Phys 13:7451–7471

Geels C, Andersson C, Hänninen O, Lansø AS, Schwarze P, Skjøth CA, Brandt J (2015) Future premature mortality due to O_3, Secondary Inorganic Aerosols and Primary PM in Europe—Sensitivity to Changes in Climate, Anthropogenic Emissions, Population and Building stock. Int J Environ Res Public Health 12(3):2837–2869

Langner J et al (2012) A multi-model study of impacts of climate change on surface ozone in Europe. Atmos Chem Phys 12:10423–10440

Skjøth CA, Geels C (2013) The effect of climate and climate change on ammonia emissions in Europe. Atmos Chem Phys 13:117–128

Sutton MA et al (2013) Towards a climate-dependent paradigm of ammonia emission and deposition. Philos Trans R Soc B Biol Sci 368

WHO. 2013. Review of evidence on health aspects of air pollution – REVIHAAP Project. Denmark: World Health Organization

WHO (2014) 7 million premature deaths annually linked to air pollution. http://www.who.int/mediacentre/news/releases/2014/air-pollution/en/. Accessed 30 Oct 2014

Chapter 20
High-Resolution Modelling of Health Impacts and Related External Cost from Air Pollution Using the Integrated Model System EVA

Jørgen Brandt, Mikael Skou Andersen, Jakob Bønløkke, Jesper Heile Christensen, Kaj Mantzius Hansen, Ole Hertel, Ulas Im, Steen Solvang Jensen, Matthias Ketzel, Ole -Kenneth Nielsen, Marlene Schmidt Plejdrup, Torben Sigsgaard and Camilla Geels

Abstract EVA (Economic Valuation of Air pollution), a multi-scale and high-resolution integrated model system for assessing health impacts and related external costs from air pollution), has been further developed by implementing the air quality model, UBM, with a 1 km × 1 km resolution covering the whole of Denmark. The high-resolution model is coupled to the long-range chemistry-transport model DEHM (Danish Eulerian Hemispheric Model) in a configuration with four nested domains. By using this system, a high-resolution assessment of health impacts from air pollution and related external cost has been conducted for Denmark for the year 2012.

20.1 Introduction

According to WHO, air pollution is now the world's largest single environmental health risk. Around 3.7 million people died prematurely in 2012 as a result of air pollution exposure from outdoor emission sources (WHO 2014). In Europe, recent results (Brandt et al. 2013a, b) show that outdoor air pollution caused 570,000 premature deaths in 2011. The health effects are associated with $PM_{2.5}$, NO_2, CO,

J. Brandt (✉) · M.S. Andersen · J.H. Christensen · K.M. Hansen · O. Hertel · U. Im · S.S. Jensen · M. Ketzel · O.-KennethNielsen · M.S. Plejdrup · C. Geels
Department of Environmental Science, Aarhus University, Frederiksborgvej 399, 4000 Roskilde, Denmark
e-mail: jbr@envs.au.dk

J. Bønløkke · T. Sigsgaard
Section of Environment, Occupation, and Health, Department of Public Health, Aarhus University, Bartholins Allé 2, Building1260, 8000 Aarhus C, Denmark

D.G. Steyn and N. Chaumerliac (eds.), *Air Pollution Modeling and its Application XXIV*, Springer Proceedings in Complexity,
DOI 10.1007/978-3-319-24478-5_20

SO_2 and O_3. Of these, $PM_{2.5}$ and O_3 are the most extensively used in studies of economic costs, as their effects are dominant compared to the other species. Atmospheric particles are considered responsible for increased mortality and morbidity, primarily via cardiovascular and respiratory diseases. A review from Hoek et al. (2013) includes the most comprehensive analysis of cardio-respiratory impacts in long-term studies and concludes that the long-term effect for total mortality is 6.2 % per 10 $\mu g/m^3$ increase in $PM_{2.5}$.

Air pollution, in general, is a transboundary and scale dependent challenge with global, regional, national and local sources giving rise to large geographic variability and thereby large differences in the geographical distribution of human exposure to air pollution. Therefore a multi-scale model system is needed capable of describing the contribution from intercontinental, regional, national and local sources covering the area of interest at very high resolution.

20.2 Methodology and Results

A high-resolution assessment of health impacts from air pollution and related external cost has been conducted for Denmark using a further developed version of the integrated EVA model system (Brandt et al. 2013a, b). EVA is based on the impact-pathway methodology, where the site-specific emissions will result, via atmospheric transport and chemistry, in a concentration distribution, which together with detailed population data, is used to estimate the population-level exposure. Using exposure-response functions and economic valuations, the exposure is transformed into impacts on human health and related external costs.

In this study we have used a coupling of two chemistry transport models to calculate the air pollution concentration from hemispheric scale down to urban background scale. The Danish Eulerian Hemispheric Model (DEHM, Christensen 1997; Frohn et al. 2002; Brandt et al. 2012) was applied to calculate the air pollution levels from hemispheric scale with a resolution of 150 km × 150 km down to regional scale with a resolution of 5.6 km × 5.6 km using four nested domains. The Urban Background Model (UBM, Berkowicz 2000; Brandt et al. 2001, 2003) is an offline model, coupled to DEHM to further calculate the air pollution at a 1 km × 1 km resolution covering the whole of Denmark using results from DEHM as boundary conditions. Both the emission data as well as the population density has been represented in the model system with the same high resolution.

In Fig. 20.1 (left), the annual mean values of $PM_{2.5}$ for Denmark for the year 2012 are shown. $PM_{2.5}$ concentrations are the main reason for cases of mortality due to long-term exposure, which is also shown in Fig. 20.1 (right). Figure 20.1 (left) clearly shows a decreasing south-to-north gradient, caused by the dominant transport of air masses from upwind sources. The greater Copenhagen area clearly stands out in terms of number of premature deaths. In Table 20.1, the number of cases for the different health outcomes in EVA due to the total air pollution levels is given. The impact from short-term exposure of O_3 is given as “acute deaths”. The

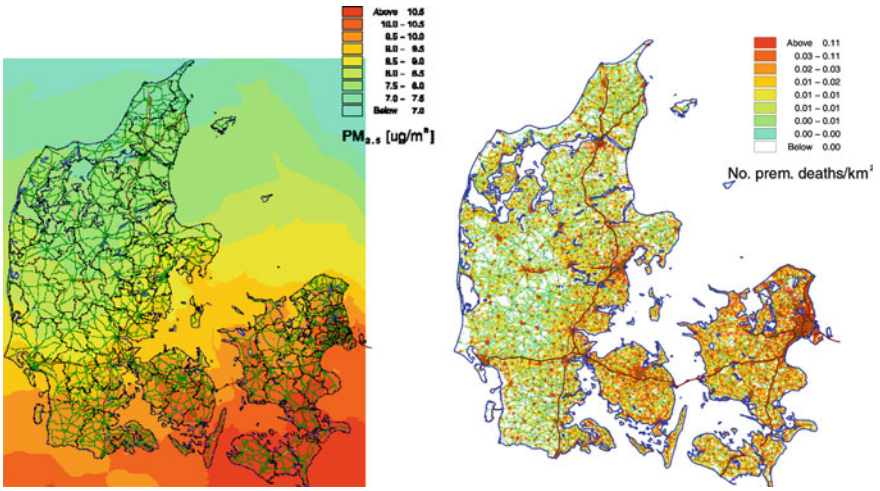

Fig. 20.1 *Left figure* annual mean concentrations of $PM_{2.5}$ in $\mu g/m^3$ for the year 2012. *Right figure* number of premature deaths due to $PM_{2.5}$ concentrations for the same year

Table 20.1 The number of cases for the different health outcomes in the EVA model system due to the total air pollution levels for the year 2012 for the whole of Denmark

Health outcome	Number of cases
Chronic bronchitis	3360
Restricted activity days	3430000
Respiratory hospital admissions	170
Cerebrovascular hospital admissions	420
Congestive heart failure	305
Lung cancer	510
Bronchodilator use children	90000
Bronchodilator use adults	657000
Cough children	311000
Cough Adults	676000
Lower Respiratory Symptoms Children	120000
Lower Respiratory Symptoms Adults	244000
Acute premature deaths	98
Chronic YOLL	35700
Total no. of premature deaths	3470
Infant mortality	4

total annual number of premature deaths due to the total air pollution levels is estimated to nearly 3500 cases. However, in these calculations, the contribution from SOA and other missing mass has been added from measurements to obtain "mass closure". This can be done, assuming that the missing mass is long-range transported and that the ratio of missing PM mass is the same over the relatively

small model domain covering Denmark. Total external costs for Denmark have been estimated to 3.7 billion euros for the year 2012.

20.3 Conclusions

A multi-scale and high-resolution integrated model system, EVA, has been developed for assessing impacts on human health from air pollution and related external costs. The model system has now been extended to very high resolution down to 1 km × 1 km covering the whole of Denmark. The system can be used to assess the contribution from different emission sectors for quantifying the effects from different measures in policy making.

Acknowledgments This project has been funded by DCE—National Centre for Environment and Energy

References

Berkowicz R (2000) A simple model for urban background pollution. Environ Monit Assess 65:259–267

Brandt J, Christensen JH, Frohn LM, Palmgren F, Berkowicz R, Zlatev Z (2001) Operational air pollution forecasts from European to local scale. Atmos Environ 35(1):S91–S98

Brandt J, Christensen JH, Frohn LM, Berkowicz R (2003) Air pollution forecasting from regional to urban street scale—implementation and validation for two cities in Denmark. Phys Chem Earth 28:335–344

Brandt J, Silver JD, Frohn LM, Geels C, Gross A, Hansen AB, Hansen KM, Hedegaard GB, Skjøth CA, Villadsen H, Zare A, Christensen JH (2012) An integrated model study for Europe and North America using the Danish Eulerian hemispheric model with focus on intercontinental transport. Atmos Environ 53:156–176

Brandt J, Silver JD, Christensen JH, Andersen MS, Bønløkke J, Sigsgaard T, Geels C, Gross A, Hansen AB, Hansen KM, Hedegaard GB, Kaas E, Frohn LM (2013a) Contribution from the ten major emission sectors in Europe to the Health-Cost Externalities of Air Pollution using the EVA Model System—an integrated modelling approach. Atmos Chem Phys 13:7725–7746

Brandt J, Silver JD, Christensen JH, Andersen MS, Bønløkke J, Sigsgaard T, Geels C, Gross A, Hansen AB, Hansen KM, Hedegaard GB, Kaas E, Frohn LM (2013b) Assessment of past, present and future health-cost externalities of air pollution in europe and the contribution from international ship traffic using the eva model system. Atmos Chem Phys 13:7747–7764

Christensen JH (1997) The Danish Eulerian Hemispheric Model—a three-dimensional air pollution model used for the Arctic. Atm Env 31:4169–4191

Frohn LM, Christensen JH, Brandt J (2002) Development of a high resolution nested air pollution model—the numerical approach. J Comput Phys 179:68–94

Hoek G, Krishnan RM, Beelen R, Peters A, Ostro B, Brunekreef B et al (2013) Long-term air pollution exposure and cardio- respiratory mortality: a review. Environ Health 12:43

WHO (2014) http://www.who.int/mediacentre/news/releases/2014/air-pollution/en/. Accessed 28 Sep 2014

Chapter 21
Health Parameters Under Climate Change Projections for Airborne Benzo[a]Pyrene

Pedro Jiménez-Guerrero and Nuno Ratola

Abstract Semi-volatile organic pollutants (SVOCs) have a recognized impact on the environment and some of them have been banned in many countries for that reason. Others are not regulated in air quality legislation, except for benzo(a)pyrene (BaP), a polyaromatic hydrocarbon resulting from natural and anthropogenic combustion processes. The EU set an annual average limit of 1 ng/m^3 in air and some health parameters can also be inferred from the correspondent ecotoxicity thresholds established for this chemical. With the help of chemistry transport models, the evolution of these parameters can be assessed under climate change scenarios, along with the BaP concentrations themselves. Hence, a scenario with MM5-CHIMERE driven by ECHAM5 SRES A2 forcing were calculated for the years 1991 to 2050, in a European domain with a spatial resolution of 25 km. An enhanced risk of lung cancer was registered throughout the covered area, deriving from a parallel increase in the BaP levels in air.

21.1 Introduction

Polycyclic aromatic hydrocarbons (PAHs) are widespread chemicals of concern due to their carcinogenicity and mutagenic properties (IARC 2010). Plus, having high lipid solubility, they are absorbed in the lung tissue, skin, breast or intestines, which raises the potential risk of affecting human health (Kim et al. 2013). With these evidences, monitoring programs and modelling strategies are needed to better evaluate their presence and fate over a large geographical area to help

P. Jiménez-Guerrero (✉) · N. Ratola
Department of Physics, Regional Campus of International Excellence "Campus Mare Nostrum", University of Murcia, Murcia, Spain
e-mail: pedro.jimenezguerrero@um.es

N. Ratola
LEPABE, Faculty of Engineering, University of Porto, Rua Dr. Roberto Frias, 4200-465 Porto, Portugal

D.G. Steyn and N. Chaumerliac (eds.), *Air Pollution Modeling and its Application XXIV*, Springer Proceedings in Complexity,
DOI 10.1007/978-3-319-24478-5_21

decision-making on their impacts in the future. PAHs are released into the environment via many natural and anthropogenic sources and can be found in either gas or particulate phase in the atmosphere (Ramírez et al. 2011). Almost entirely in particulate-bound material, benzo(a)pyrene (BaP) is the only PAH with a legal limit set by the European Union (Directive 2004/107/EC, amended by Regulation 219/2009) for air: 1 ng/m^3 as mean for a year on PM10. As we are dealing with hazardous substances, it is also important to consider health issues and some guidelines have been presented in literature to characterize their harmful potential (Butterfield and Brown 2012). The impact of climate change on air quality is a crucial topic (Jiménez-Guerrero et al. 2013) and can also play a decisive part on the expression of these parameters, yet need downscaled scenarios, with the highest spatial resolution possible. The aim of this work is thus to evaluate the impact of climate change on future levels of benzo[a]pyrene over Europe until 2050 under the A2 SRES scenario.

21.2 Experimental

The regional modelling set-up used in this study consists of a coupling between a climatic version of the MM5 model and CHIMERE chemistry transport model, on a domain covering most of Europe with a spatial resolutions of 25 km and 24 sigma levels are in the vertical, up to 100 hPa. The regional climate simulations driving the CTM were performed using the regional climate model MM5 driven by the European Centre/Hamburg 5-Run1 simulation forced by the SRES-A2 scenario, which lies towards the upper end of the IPCC emission range. Further details on the regional climate simulations and the validation of the present-day simulations can be found in Jerez et al. (2013). In the current study, simulations cover the period from 1991 to 2050. Simulations for present-day climatologies (1991–2010) have been compared to a time slice covering 2031–2050. In order to isolate the possible effects of climate change on the ground concentrations of air pollution, unchanged anthropogenic emissions derived from the European Monitoring and Evaluation Programme (EMEP) database are considered not accounting for possible changes on vegetation, land use, anthropogenic pollutant emission changes or any feedbacks from the chemical compounds to the meteorological fields, but allowing changes in natural emissions.

21.3 Results and Discussion

Results reveal that the modelled BaP concentrations for the 1991–2010 period exceed 0.1 ng m^{-3} as annual averages in some areas in Europe, namely Portugal, Spain, Netherlands, Germany or Italy, and rising above 0.5 ng m^{-3} over parts of Poland. Overall, and as expected, the highest modelled levels are found where most

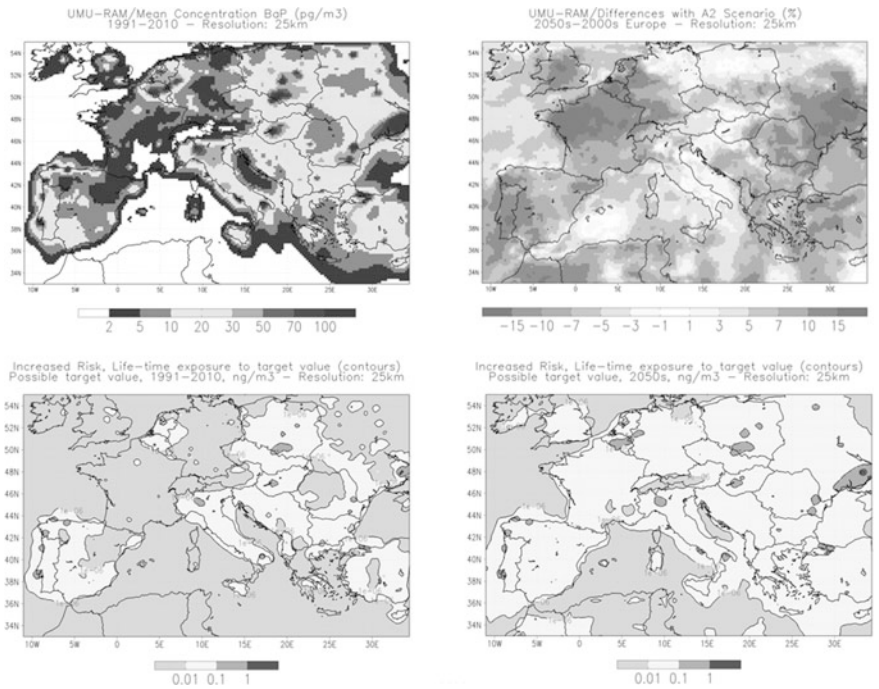

Fig. 21.1 (*Top*, *left*) Present day mean concentrations of BaP over Europe (1991–2010) (pg m^{-3}) and (*top*, *right*) percentual increase in the levels of this compound for the 2031–2050 period under the SRES A2 scenario compared to present-day levels. (*Bottom*) Exceedances of the possible target values (shaded, ng m^{-3}) and associated increased risk of lung cancer, life-time exposure to the target value (contours), as defined by the Quantitative Risk Assessment included in Butterfield and Brown (2012). (*Bottom*, *left*) Present-day conditions; (*bottom*, *right*) SRES A2 scenario

anthropogenic sources like traffic, building heating or industrial combustion occur, that is, in urban (e.g. Lisbon, Portugal) and industrial locations (Ruhr area, Germany). The concentrations obtained for the 2031–2050 period under the SRES A2 scenario show the highest increases over western France (up to 25 %), an area with a very low current BaP incidence (Fig. 21.1, top). In the areas with the highest BaP presence (for instance, eastern Europe and western Iberia), there are projections of a about 15 % increases. The general decay of precipitation modelled for future climates (e.g. Jiménez-Guerrero et al. 2013) suggest less wet deposition of BaP and the consequent increase of its air concentration. As an example of the health parameters available for BaP, we selected the increased risk of lung cancer due to industrial exposure to PAHs. The European Union calculated the increased risk for three possible target values: 0.01 ng m^{-3} with an associated increased risk of 1×10^{-6}; 0.1 ng m^{-3} (increased risk of 1×10^{-5}); and 1 ng m^{-3} (increased risk of 1×10^{-4}). Being the last value the EU limit for the annual mean concentration of BaP (1 ng m^{-3}), the upper limit of the additional life-time risk should be below 1×10^{-4} (Butterfield and Brown 2012). Considering the present-day scenario, this

target is only exceeded in Ukraine. However, as seen in Fig. 21.1 (bottom), for SRES A2-driven projections, the risks of lung cancer escalate noticeably all over Europe. Although the 1 ng m^{-3} target value is still only exceeded in Ukraine, a greatly larger area in Europe surpasses the 0.1 ng m^{-3} mark, such as over the Ruhr Valley in Germany or the Netherlands. In view if these findings it can be stated that the general increased risk of lung cancer over Europe (1×10^{-6} for the present scenario) becomes an order of magnitude higher (1×10^{-5}).

21.4 Conclusions

The regional climate modelling coupling (MM5-RCM and CHIMERE) used in simulations comprising present conditions (1991–2010) and the future SRES A2 scenario (2031–2050) show the plausible influence of climate change on the atmospheric concentrations of BaP and on the increased risk of lung cancer over Europe. For BaP incidence, the A2 scenario revealed a projection of regional increase in the levels up to 25 % in some areas and about 15 % in a vast portion of the domain. In terms of health indicators, the general increased risk of lung cancer in Europe becomes an order of magnitude higher under the A2 scenario: 1×10^{-5} versus 1×10^{-6} for the present scenario.

Acknowledgments This work was partially funded by the European Union Seventh Framework Programme-Marie Curie COFUND (FP7/2007–2013) under UMU Incoming Mobility Programme ACTion (U-IMPACT) Grant Agreement 267143. The Spanish Ministry of Economy and FEDER (project DIDIER CGL2013-48491-R) are acknowledged for their partial funded. Dr. Pedro Jiménez-Guerrero acknowledges the Ramón y Cajal programme.

Question and Answer

QUESTIONER: Jaakko Kukkonen

QUESTION: Small-scale combustion is also responsible for the emissions of BaP. These emissions will very likely increase in the future, caused by climate change reduction policies that favour the use of renewable energy. How is this projected increase of BaP emissions reflected in your results?

ANSWER: In the approach followed in this contribution, the main objective is to to isolate the possible effects of climate change on the ground concentrations of air pollution. Therefore, the hypothesis of unchanged anthropogenic emissions has been implemented in the simulations. Therefore, BaP emissions coming from anthropogenic combustion processes have been kept constant.

References

Butterfield DM, Brown RJC (2012) Polycyclic aromatic hydrocarbons in Northern Ireland. National Physical Laboratory Report AS66, Teddington, Middlesex, UK, 86 pp

IARC (2010) Monographs on the evaluation of carcinogenic risks to humans—some non-heterocyclic polycyclic aromatic hydrocarbons and some related exposures, vol. 92. Lyon-France, 858 pp

Jerez S, Jiménez-Guerrero P, Montávez JP, Trigo RM (2013) Impact of the North Atlantic Oscillation on European aerosol ground levels through local processes: a seasonal model-based assessment using fixed anthropogenic emissions. Atmos Chem Phys 13:11195–11207

Jiménez-Guerrero P, Gómez-Navarro JJ, Baró R, Lorente R, Ratola N, Montávez JP (2013) Is there a common pattern of future gas-phase air pollution in Europe under diverse climate change scenarios? Clim Change 121:661–671

Kim K-H, Jahan SA, Kabir E, Brown RJC (2013) A review of airborne polycyclic aromatic hydrocarbons (PAHs) and their human health effects. Environ Int 60:71–80

Ramírez N, Cuadras A, Rovira E, Marcé RM, Borrull F (2011) Risk assessment related to atmospheric polycyclic aromatic hydrocarbons in gas and particle phases near industrial sites. Environ Health Perspect 119:1110–1116

Chapter 22
Modeling the Air Quality and Public Health Benefits of Increased Residential Insulation in the United States

Saravanan Arunachalam, Matthew Woody, Mohammad Omary, Stefani Penn, S. Chung, May Woo, Yann Tambouret and Jonathan Levy

Abstract According to the Residential Energy Consumption Survey (RECS), homes in the United States consume approximately 10 quadrillion BTUs of energy each year, including electricity consumption for cooling, various fuels utilized for space heating, and other end uses. Electricity consumption will influence emissions from power plants, and these along with direct residential fuel combustion will also contribute to emissions of multiple key pollutants, with corresponding air quality and health impacts. We have developed models to quantify the energy savings associated with increased residential insulation and to estimate in monetary terms the environmental and public health benefits. We are considering both retrofits to existing housing and new construction, focusing on the 2012 International Energy Conservation Code (IECC), which specifies R-values and U-factors by climate zone and a number of other structural components and design specifications. We are applying EnergyPlus to a series of template files to estimate energy savings by fuel type and state, for both retrofits and new construction. To determine the emissions reductions related to reduced electricity generation, we used EPA's AVERT tool. AVERT uses the basic attributes of electricity dispatch modeling to determine the power plants most likely influenced by energy efficiency programs, and provides the direct nitrogen oxide (NOx), sulfur dioxide (SO_2), and carbon dioxide (CO_2) emissions reductions on a plant-by-plant basis. For residential combustion, we used

S. Arunachalam (✉) · M. Woody · M. Omary
University of North Carolina at Chapel Hill, Chapel Hill, NC, USA
e-mail: sarav@email.unc.edu

S. Penn · S. Chung · M. Woo · J. Levy
Boston University School of Public Health, Boston, MA, USA

Y. Tambouret
Boston University Research Computing Services, Boston, MA, USA

D.G. Steyn and N. Chaumerliac (eds.), *Air Pollution Modeling and its Application XXIV*, Springer Proceedings in Complexity,
DOI 10.1007/978-3-319-24478-5_22

EPA's AP-42 database and other resources to quantify direct emissions by fuel type (including natural gas, fuel oil, and wood). To model the health benefits of the criteria pollutant emissions, we linked the emissions reductions due to increased energy efficiency with the Community Multiscale Air Quality (CMAQ) model. We developed a series of simulations using CMAQ v4.7.1 instrumented with the Decoupled Direct Method (DDM), an advanced sensitivity analysis technique that allows us to estimate the influence of individual pollutants from individual sources or regions. We considered direct residential combustion by state, leveraging Census and housing start data to determine spatial patterns of emissions within states, and modeled individual power plants in geographic groupings using a design of experiments that allow us to estimate the impacts for all major power plants on the grid. We focused on fine particulate matter and ozone concentrations, as the key drivers of monetized health impacts. As CMAQ provides concentration estimates by grid cell, we are able to determine total public health benefits in terms of avoided mortality and morbidity as well as the distribution of those benefits for directly modeled facilities and locations. We estimate 19,000 premature deaths per year associated with EGU emissions, with more than half of the EGU-related health impacts attributable to emissions from seven states with significant coal combustion. We also estimate 10,000 premature deaths per year associated with residential combustion emissions, driven by primary $PM_{2.5}$ emissions. In general, primary $PM_{2.5}$ health damage functions are an order of magnitude larger than those of secondary $PM_{2.5}$ precursors. Our findings reinforce the significance of source-specific assessment of air quality and health impacts for developing public health policies.

22.1 Introduction

Fine particulate matter ($PM_{2.5}$) and ozone (O_3) are key pollutants that are shown to have adverse health impacts in exposed populations. Various emissions sources including electric generating units (EGUs) and residential combustion (RC) emissions (from all fuel types) spread across the U.S. are known to contribute to elevated levels of these pollutants. RC and EGU emissions are directly tied to energy demand in the U.S. and knowing their contribution to total health risk, from individual states as well as precursor emissions will provide valuable inputs for studying the nexus between energy demand, emissions, air quality and health risk. Residential combustion is mostly a ground-level source with fairly localizing impacts, whereas EGUs being elevated sources tend to have much larger footprints at downwind distances. They thus provide interesting contrasts both from a control strategy perspective and health damage function perspective. Previous studies have

quantified sector-specific contribution to total health risk in the U.S. as well as in the world. However, limited studies have attempted to quantify these health risks by region, as well as attribute the total $PM_{2.5}$ and O_3 to a specific precursor species.

22.2 Methodology

We use the Community Multiscale Air Quality (CMAQ) model (Byun and Schere, 2006) instrumented with the Decoupled Direct Method (DDM) for particulate matter (Dunker 1984; Napelenok et al. 2006) at the core of this study. Based upon previous state-specific zero-out simulations of SO_2 from EGU emissions and their spatial footprint, we developed a design of experiments such that individual states are combined in multiple groups, and CMAQ-DDM-3D simulations are used to predict $PM_{2.5}$ and O_3 contributions from each state-specific EGU and RC emissions. We modeled January and July 2005 to address seasonality, with a 2-week spin-up period for each month. We created 40 groups of states for EGU emissions, and 29 groups of states for RC emissions. For e.g., Group 19 for RC had emissions from California and Ohio. We instrumented DDM to track six precursor emissions species from a given state. These included primary $PM_{2.5}$ (PEC, POC and $PM_{2.5}$) and precursors to secondary $PM_{2.5}$ (NO_x, SO_2 and VOC). For O_3, we tracked NO_x and VOC emissions. The modeling domain is for the continental U.S. at 36-km resolution, and used meteorological inputs from the Weather Research and Forecast (WRF) model driven by Modern-Era Retrospective-Analysis for Research Applications (MERRA) and emissions inventories from the EPA's National Emissions Inventories (NEI) for 2005 processed through the SMOKE modeling system. Model output concentrations were then linked with population and mortality rate data from the Center for Disease Control and Prevention (CDC). Concentration-response functions associating concentrations with health effects were derived from the epidemiological literature to estimate premature mortality counts due to $PM_{2.5}$ and O_3 from each state for the two source sectors. Both total health risk counts, as well health risk damage functions (health risk normalized by 1,000 tons of precursor emissions) were computed in each case.

In addition, the gridded health risk numbers from simulations with multiple states were processed through an image separation algorithm to separate individual state-specific contributions. However, at the time of this submission, this work is still in progress, and only aggregate numbers from each simulation are presented.

22.3 Results

We computed $PM_{2.5}$ and O_3 formed in each state, due to each source region as defined by the 40 RC and 29 EGU groups in CMAQ-DDM simulations. Table 22.1 summarizes the precursor emissions in the U.S. from RC and EGU source sectors. As an illustration of the results, Figure22.1 shows the CMAQ-DDM predicted $PM_{2.5}$ contributions from RC emissions from Group 10 (Oregon and Washington, D.C) and Group 19 (California and Ohio) in each downwind state, broken down by each precursor species. In general, one can see the large contributions from POC emissions to total $PM_{2.5}$ from each region (Fig. 22.1).

In Fig. 22.2, we present the health damage functions (health risk normalized by 1,000 tons of precursor emissions) for each of the 6 precursor species for residential combustion emission. In general, these health damage functions are higher for primary than for secondary $PM_{2.5}$ precursor species. Table 22.2 summarizes the total U.S.-wide premature mortality due to $PM_{2.5}$ from the RC and EGU emissions, but attributed to each precursor emissions species.

Table 22.1 Summary of precursor emissions in the U.S. from RC and EGU source sectors

	CO	NO_X	VOC	NH_3	SO_2	$PM_{2.5}$
Domain total (M Tons/year)	111.9	23.1	91.9	3.8	15.1	4.4
Residential combustion (%)	2.7	1.6	0.6	0.2	1.1	9.0
EGUs (%)	0.5	16.1	0.04	0.6	68.8	11.4

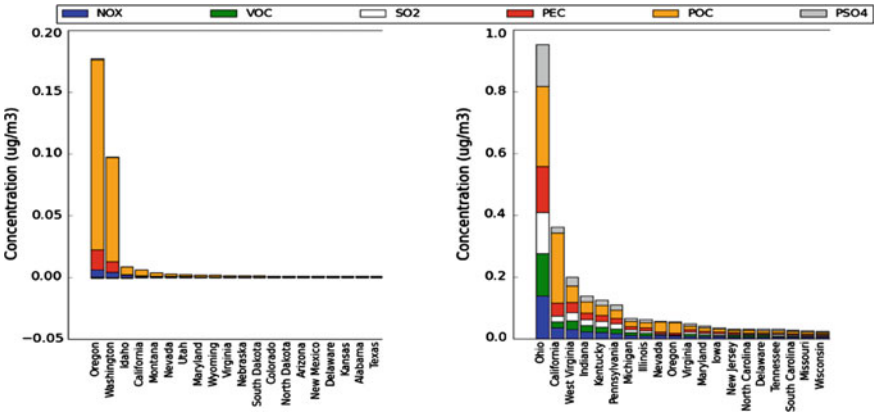

Fig. 22.1 $PM_{2.5}$ formed due to each precursor species from Group 10 (OR, DC) (*left*) and Group 19 (CA, OH) (*right*), organized by magnitudes in receptor states

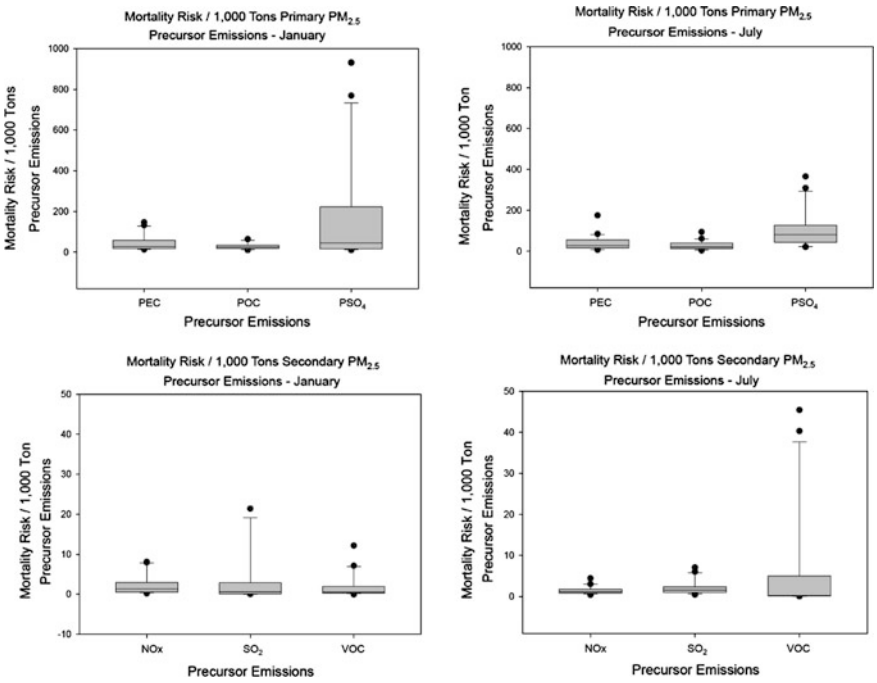

Fig. 22.2 Health damage function (health risk normalized per 1,000 tons of precursor emissions of RC)—primary (*top*) and secondary (*bottom*) during January 2005 (*left*) and July 2005 (*right*). Each dot is total risk from each CMAQ simulation (before separating the individual states)

Table 22.2 Total U.S.-wide premature mortality due to $PM_{2.5}$ from the RC and EGU emissions, attributed to each precursor emissions species

Precursor and Pollutant	RC	EGU
PEC → $PM_{2.5}$	1,200	570
POC → $PM_{2.5}$	5,500	540
PSO_4 → $PM_{2.5}$	710	2,500
NO_x → $PM_{2.5}$	910	3,600
SO_2 → $PM_{2.5}$	620	9,900
VOC → $PM_{2.5}$	700	320
NOx → O_3	−590	1,300
VOC → O_3	990	6.4
Total	10,000	19,000

22.4 Conclusions

We modeled emissions from two major source sectors related to energy consumption in the U.S.—residential combustion due to all fuel types, and electric generating units using a novel approach with CMAQ-DDM and developed air quality and health risk estimates due to $PM_{2.5}$ and O_3 on a state-specific basis, and

by precursor emissions. Results from our work show that RC emissions cause 10,000 premature mortalities, while EGU emissions cause 19,000 premature mortalities. RC-related premature mortalities are dominated by POC emissions, while those from EGUs are dominated by SO_2 emissions. The novelty of our results are in the ability to break down the health risk by source region, and specific precursor using the DDM technique, and provides valuable insights on developing energy policy for states, such as under the proposed Clean Power Plan in the U.S.

Acknowledgments This work was funded under an award from the North American Insulation Manufacturers Association to UNC and Boston University.

Questioner Name: Amir Hakami

Q: Have you looked at the assumption of the groupings specifically Kentucky and New York for non-overlapping plumes?

A: Yes, we did. While initially they looked like two states that would have non-overlapping plumes, after the modeling was completed, we found that these two plumes overlapped in their spatial footprints. We performed detailed analyses of all model outputs from the initial grouping, and if we found plume overlaps that could lead to problems in separating individual state impacts, we remodeled some of those states explicitly, and post-processed them further.

References

Dunker AM (1984) The decoupled direct method for calculating sensitivity coefficients in chemical kinetics. J Chem Phys 81:2385–2393

Napelenok S, Cohan D, Hu Y, Russell A (2006) Decoupled direct 3D sensitivity analysis for particulate matter (DDM-3D/PM). Atmos Environ 40:6112–6121

Chapter 23
Estimating the Impact of Air Pollution Controls on Ambient Concentrations

Lucas R.F. Henneman, Cong Liu, David Lavoué, Howard Chang, James A. Mulholland and Armistead G. Russell

Abstract This work describes the development and application of a statistical model that links electricity generating unit (EGU) and mobile source emissions with a city center monitoring cite. The model uses estimated emissions and measured concentrations over the period 2000–2012 in Atlanta, GA, USA to develop counterfactual time series of daily ozone concentrations. Further, the model estimates the sensitivity of observed ozone to each emissions sector. Results show that emissions control policies have had little effect on annual median ozone, have decreased 90th percentile ozone, and have increased 10th percentile ozone. Sensitivities to EGU and mobile emissions are compared and agree well with similar sensitivities calculated using a first-principles chemical transport model.

23.1 Introduction

Air pollution controls are costly, and improved public and environmental health serve as justification for these controls. There has been increased interest in investigating the accountability of these controls in terms of providing their anticipated air quality and health benefits. In this research, funded by the Health Effects Institute, we investigate the links between past regulatory actions, meteorology, ambient air pollution concentrations, and health outcomes in Atlanta, Georgia, USA.

Legal basis for quality regulations in Atlanta are grounded in the 1990 Clean Air Act Amendments. Since this time, the United States Environmental Protection Agency (US EPA) has promulgated a number of regulations aimed at reducing the number of negative health effects attributable to ambient exposure. This research focuses specifically on the impacts on ambient concentrations of air pollutants of

L.R.F. Henneman (✉) · C. Liu · D. Lavoué · J.A. Mulholland · A.G. Russell
Georgia Institute of Technology, Atlanta, GA, USA
e-mail: lhenneman@gmail.com

H. Chang
Emory University, Atlanta, GA, USA

D.G. Steyn and N. Chaumerliac (eds.), *Air Pollution Modeling and its Application XXIV*, Springer Proceedings in Complexity,
DOI 10.1007/978-3-319-24478-5_23

the following regulations: the Acid Rain Program (1995), the Tier 2 Vehicle and Gasoline Sulfur Program (2004), the Heavy-Duty Highway Rule (2007), the Clean Air Interstate Rule (2008).

This study demonstrates the formulation of statistical models to relate concentrations in Atlanta to estimated emissions after accounting for effects of meteorological fluctuations in ambient concentrations. Previous methods to estimate the sensitivities of air pollution levels have used chemical transport models (CTMs), using both brute force (e.g. Digar and Cohan 2010) and direct methods (e.g. Dunker 1981) (1,2). CTMs have the benefit of explicitly including information on atmospheric chemistry and physics, but generally take more time and computational resources to run.

Statistical models developed here are applied to estimated changes in emissions due to control actions to develop counterfactual time series of air pollution concentrations. Counterfactual concentrations allow for the quantification of the difference in air quality metrics that can be attributed to recent control actions implemented in the region. The comparison of results from statistical modeling and a regional CTM provides evidence that statistical methods are a viable method to estimate relationships between emissions sources and observations.

23.2 Method

Data used for this work is from the SouthEastern Air Research and Characterization (SEARCH) network's Jefferson Street Station located in downtown Atlanta (33.77ºN, 84.41ºW) (Atmospheric Research and Analysis 2014). Daily metrics of ozone, $PM_{2.5}$, NO_x, and various meteorological parameters were developed from hourly measurements over 13 years (2000–2012). Daily emissions of NO_x and SO_2 from 14 electricity generating units (EGUs) in Atlanta's nonattainment area were downloaded from the EPA's Air Markets Database. EPA's Mobile Vehicle Emissions Simulator (MOVES2010b) was used to estimate daily emissions of NO_x, $PM_{2.5}$, and Volatile Organic Compounds (VOCs) from mobile sources.

Nonlinear filtering and regression detrending based on a Taylor Series decomposition are used to meteorologically detrend ambient air pollution concentrations using methods similar to Kuebler et al. (2001). Each daily air pollution metric time series is detrended into 5 components: long-term (period > 365 days), seasonal (period = 365 days), weekly (period = 7 days), short-term (period < 365 days), and white noise (period = 1 day). Kolmogorov-Zurbenko (1991) filtering and regressions against meteorological variables (wind speed, temperature, relative humidity, rainfall, and solar radiation) are used to quantify fluctuations at each period, and the short-term component is removed from the ambient concentration signals, leaving fluctuations that are not associated with meteorological fluctuations (Henneman et al. 2015).

The detrended signals (C_{det}) are then used as the response in the following linear model:

$$C_{det} = \beta * \boldsymbol{E} + \epsilon \tag{23.1}$$

where $\boldsymbol{E}$ is a matrix of estimated daily emissions from EGUs and mobile sources in the Atlanta area. The models parameters β, which give the relationships between measured concentrations and emissions, are termed *sensitivities*. Sensitivities are combined with estimates of changes in emissions attributable to controls to estimate the magnitude of the observed concentration avoided (or added) by specific controls. In the case of some pollutants–particularly ozone–reduced emissions of precursors can lead to increases in ambient concentrations. This amount is then combined with observed concentrations to calculate a counterfactual time series of concentrations for each pollutant. These are used to assess the effectiveness of each regulation at reducing ambient air pollution concentrations.

The empirical sensitivities provide a point of comparison with related sensitivities calculated in regional chemical transport models. Results from the statistical modeling are compared to results from CMAQ-DDM (Community Multiscale Air Quality Model with the Decoupled Direct Method).

23.3 Results

Detrended annual average concentrations of NO_x, CO, and SO_2 each fell more than 50 % between 2000 and 2012. Total $PM_{2.5}$ concentrations fell by 47 %, and this reduction was driven in part by decreases in sulfate, organic carbon, and elemental carbon aerosols over this period. Median ozone levels, meanwhile, have changed very little across the study period. Instead, the highest ozone concentrations have decreased while the lowest concentrations have increased.

Ozone sensitivities to total NO_x emissions (Empirical S_{TOT}) included in the statistical modeling show a dependence on ozone concentration (Fig. 23.1). This corroborates findings by Liao et al. (2008), which showed that CMAQ-DDM sensitivities in Atlanta have a linear relationship with ozone concentrations (Liao et al. 2008).

Annual median counterfactual ozone does not differ much from the observed (Fig. 23.2). The spread of the annual distributions, however, increases drastically. This is expected due to the observed shrinking of the annual distributions that have been a consequence of reducing ambient concentrations of ozone precursor pollutants. In 2012, for example, changes in emissions are estimated to have reduced 90th percentile ozone from 109 ppb to 65 ppb, and 75th percentile ozone from 84 ppb to 55 ppb. 50th percentile ozone is estimated to have decreased by 4 ppb.

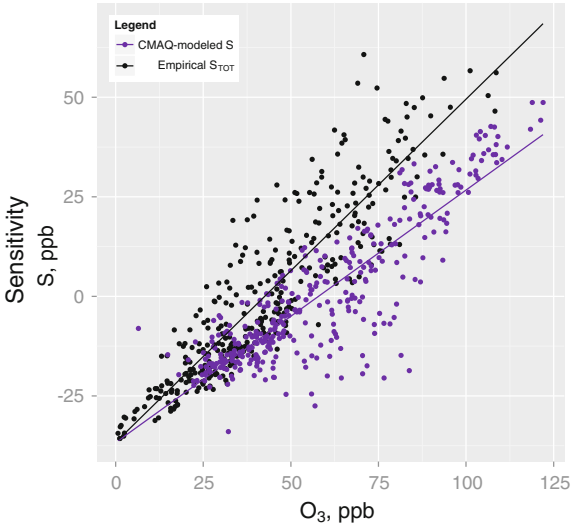

Fig. 23.1 First-order empirical sensitivities derived using statistical modeling in this study (S_{TOT}) and CMAQ modeled sensitivities to emissions from the Atlanta area in 2001

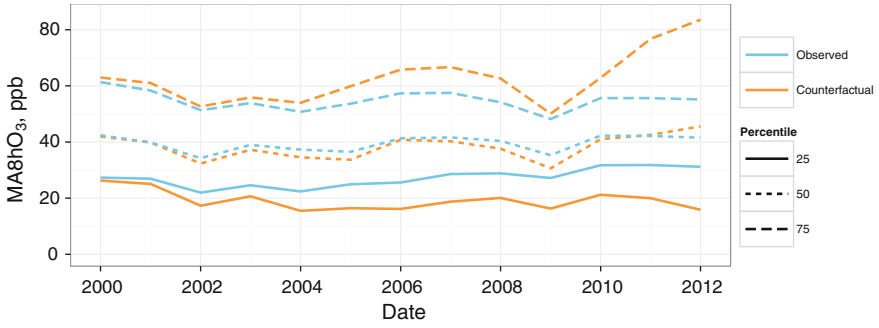

Fig. 23.2 Annual observed and counterfactual ozone percentiles

23.4 Discussion

Air pollution regulations that target ozone in the United States are written to penalize the highest ozone values. In this regard, these regulations have been successful. Even though median ozone has not changed and lowest values have increased, the highest levels have decreased substantially compared to counterfactual. This is due to the nature of the ozone response to emissions of precursors in Atlanta. On days with high ozone, a reduction in NO_x leads to a reduced ozone concentration (NO_x limited). However, on days with low ozone, a reduction in NO_x causes an increase in ozone (reduced NO_x titration).

The agreement between sensitivities estimated by the statistical modeling here and those calculated by CMAQ-DDM provide further evidence that the two approach reality. This work shows that statistical models are an alternative method to computationally intensive CTMs, and are feasible to run for long time series. The drawback of these models is that they are limited by the availability of observations of ambient concentration, meteorology, and emissions estimates. Further, similar to CTMs, they are limited by the accuracy of emissions estimates used to drive the calculations.

The daily results calculated using statistical methods based on observations provide an opportunity to assess whether changes in total exposure to ozone has an effect on negative health impacts using epidemiological analyses. This project is being performed with the aim of estimating the number of negative health effects that have been avoided due to regulatory actions implemented in Atlanta.

23.5 Key Findings

Ambient pollution trends show that concentrations of primary pollutants have decreased since 2000 after accounting for variability due to meteorological fluctuations. Long (13 year) time series of ambient concentrations are linked to estimated emissions from electricity generating units and mobile sources through statistical modeling. The parameters from the statistical modeling are the sensitivities of ambient pollution to emissions, and are compared to similar sensitivities calculated by CMAQ-DDM. Highest concentrations of ozone have decreased due to the policies, but median values have been resistant to change as low ozone values have increased.

Acknowledgments This material is based upon work supported by Health Effects Institute and the National Science Foundation Graduate Research Fellowship under Grant No. DGE-1148903.

Question and Answer

Questioner: Dr. Amir Hakami

Question: Does the error associated with the detrended values overlap the observations?

Answer: The error associated with the daily estimates of the detrended concentrations tends to be small compared to the change from the observed value. For ozone, for instance, the mean absolute daily contribution of meteorology is 8.4 ppb. The 95 % confidence interval on the mean absolute contribution is less than 3 ppb. The process of variable selection in the detrending model eliminates those covariates that might add significant error to the detrended values.

References

Atmospheric Research and Analysis (2014) http://www.atmospheric-research.com/studies/SEARCH/index.html

Digar A, Cohan DS (2010) Efficient characterization of pollutant-emission response under parametric uncertainty. Environ Sci Technol [Internet] 44(17):6724–6730. http://www.ncbi.nlm.nih.gov/pubmed/20701284. Accessed 1 Sep 2010

Dunker A (1981) Efficient calculation of sensitivity coefficients for complex atmospheric models. Atmos Environ [Internet] (1). http://www.sciencedirect.com/science/article/pii/000469818190305X. Accessed 7 May 2014

Henneman L, Holmes H, Mulholland J, Russell A (2015) Meteorological detrending of primary and secondary pollutant concentrations: methods application and evaluation using long-term (2000–2012) detailed data. Atmos Environ. http://www.sciencedirect.com/science/article/pii/S1352231015302521

Kuebler, Jerome, Hubert van den Bergh, Armistead, Russell G (2001) Long-term trends of primary and secondary pollutant concentrations in Switzerland and their response to emission controls and economic changes. Atmos Environ 35(8)(January):1351–1363. 10.1016/S1352-2310(00)00401-5 http://linkinghub.elsevier.com/retrieve/pii/S1352231000004015

Liao K-J, Tagaris E, Napelenok SL, Manomaiphiboon K, Woo J-H, Amar P et al (2008) Current and future linked responses of ozone and PM2.5 to emission controls. Environ Sci Technol [Internet] 42(13):4670–4675. http://www.ncbi.nlm.nih.gov/pubmed/18677989. Accessed 1 Jul 2008

Zurbenko IG (1991) Spectral analysis of nonstationary time series. Int Stat Rev 39:163–173

Chapter 24
Assessment of Damage to Vegetation in Belgium Based on an Ozone Flux Model Approach

P. Viaene, F. Deutsch, C. Mensink, K. Vandermeiren, Line Vancraeynest, Charlotte Vanpoucke and Frans Fierens

Abstract Elevated tropospheric ozone concentrations are not only harmful for human health, but they may also have detrimental effects on vegetation. Currently, an ozone exposure index (AOT40) and critical levels for the protection of vegetation have been agreed upon at European level based on the atmospheric ozone concentration and exposure time. Plants are however mainly affected by the ozone actually interacting with the plant tissue which could well be only a small part of the available ozone. Methods have therefore been developed for estimating ozone uptake by plants and to obtain reliable dose-response relationships based on the ozone flux. In this chapter we present a modelling procedure that integrates the DO3SE model for calculating the phytotoxic ozone dose with ECMWF meteorology and ground level ozone concentration maps to produce estimates of the ozone impact on yield and biomass accumulation of crops, forest trees and grassland. The procedure is applied to a Belgium for the year 2009 and compared with the results published for EMEP and used to quantify the impact of ozone on potato and wheat crop yields in 2009.

P. Viaene (✉) · F. Deutsch · C. Mensink
VITO Flemish Institute for Technological Research, Boeretang 200,
2400 Mol, Belgium
e-mail: peter.viaene@vito.be

C. Mensink
e-mail: Clemens.Mensink@vito.be

K. Vandermeiren
CODA-CERVA Veterinary and Agrochemical Research Centre,
Leuvensesteenweg 17, 3080 Tervuren, Belgium
e-mail: Karine.Vandermeiren@coda-cerva.be

L. Vancraeynest
VMM, Flemish Environment Report (MIRA), Dr. de Moorstraat 24-26,
9300 Aalst, Belgium
e-mail: l.vancraeynest@vmm.be

C. Vanpoucke · F. Fierens
IRCEL-CELINE, Kunstlaan Avenue des Arts 10-11, 1210 Brussels, Belgium
e-mail: fierens@irceline.be

D.G. Steyn and N. Chaumerliac (eds.), *Air Pollution Modeling and its Application XXIV*, Springer Proceedings in Complexity,
DOI 10.1007/978-3-319-24478-5_24

24.1 Introduction

Excessive tropospheric ozone concentrations are not only harmful for human health but also have detrimental effects on plants. Current practice is to assess O_3 exposure based on the AOT40 (Accumulated Ozone exposure over a Threshold of 40 ppb) which has been defined in the European Air Quality Directive 2008/50/EC, as the sum of hourly O_3 concentrations above a threshold of 40 ppb, between 8 and 20 h CET during the growing season. The European long term objective is 3000 ppb h which is considered the critical level for O_3 damage to sensitive crops and natural vegetation.

The impact of O_3 on vegetation is however primarily correlated to the amount of O_3 entering a plant, which is only partially represented by the ambient O_3 concentration. O_3 uptake is controlled by the stomatal conductance of the leaf stomata which also regulates CO_2 and H_2O exchange. The degree of opening of the leaf stomata is dependent upon environmental conditions (temperature, air and soil moisture, irradiance …) and plant-specific characteristics (number of stomata, phenology …).

To obtain better estimates of O_3 damage, in the last 10 years efforts were made to develop methods for the estimation of O_3 uptake by plants and to obtain reliable dose-response relations based on the O_3 flux. This has resulted in a new indicator for estimating the O_3 impact on yield and biomass accumulation of crops, forest trees and grassland: the Phytotoxic Ozone Dose, POD_Y (mmol O_3 m^{-2} plant leaf area), which is the sum of the hourly stomatal O_3 flux over a threshold of Y nmol O_3 m^{-2} s^{-1} accumulated during daylight hours over the growing season.

One of the models for calculating stomatal conductance that have been developed is the DO_3SE model (Deposition of O_3 and Stomatal Exchange, Emberson et al. (2000)). The DO_3SE code has been implemented in the EMEP model (Simpson et al. 2012) for integrated assessment modelling purposes. The next chapters describe the development and results of a model based on DO_3SE for the calculation of POD_Y for Belgium.

24.2 Model Development

24.2.1 Calculation Procedure

The stomatal O_3 flux through the leaf area above a threshold value Y ($F_{st,Y}$) is defined as:

$$F_{st,Y} = g_{sto} C_{z1}(O_3) - Y \tag{24.1}$$

with:

$C_{z1}(O_3)$ the hourly average O_3 concentration at the top of the canopy [nmol/m^3]

g_{sto} stomatal conductance [m/h]

Y a vegetation specific threshold flux value [nmol O_3/m^2/h]

The O_3 concentration is considered at the top of the canopy where solar irradiation is highest and the leaves also contribute most to biomass production but also to O_3 uptake. The stomatal conductance (g_{sto}) calculation is based on the DO_3SE module as implemented in EMEP and takes into consideration the effects of sunlight, vapour pressure deficit, temperature, vegetation development and soil moisture. Soil moisture is not considered in EMEP v4.4 on which our implementation is based and was therefore added as an option to test its effect on POD_Y.

POD_Y is calculated by accumulating $F_{st,Y}$ over the daylight hours and vegetation specific growing season. POD_Y values can be compared with receptor-specific critical levels in order to determine whether the limit value for a particular detrimental effect was not exceeded or may be interpreted as such as an indicator for the risk of negative effects.

By using a dose response curve the POD_Y can also be used to quantify crop yield losses. For potatoes Calvo et al. (2007), Gerosa et al. (2008), Mills et al. (2011) and Pleijel et al. (2007) propose the following dose response function to relate relative yield (RY) to POD_6:

$$RY = 1.01 - 0.013\,POD_6 \tag{24.2}$$

while for wheat the relation:

$$RY = 1.00 - 0.038\,POD_6 \tag{24.3}$$

can be found in Mills et al. (2011), Piikki et al. (2008) and Pleijel et al. (2007).

24.2.2 Model Inputs

A 4 km × 4 km resolution map of hourly O_3 concentrations was derived from hourly observed values using the RIO interpolation method (Janssen et al. 2008). O_3 concentrations were converted to canopy height as proposed in the Mapping Manual (Mills et al. 2011). The air temperature, relative humidity, cloud attenuation and soil moisture index inputs for the model were based on ECMWF IFS forecasts interpolated to the same resolution as the O_3 concentration input. The 4 soil moisture indices provided by the ECMWF IFS for the soil profile are combined into a single soil moisture stress indicator by taking into consideration a vegetation specific root distribution (Jackson et al. 1996). Using the above inputs POD_Y values can be calculated at 4 km × 4 km resolution. By combining this result with crop specific land cover information, the actual total crop loss can be estimated based on dose response functions. Land cover maps for 4 generic vegetation types (temperate crop, temperate deciduous forest, temperate coniferous forest and grass) as well as

for wheat and potatoes were derived for Belgium by combining a detailed 10 m land cover map for Flanders (Poelmans and Van Daele 2014) with respectively the CORINE 2006 land cover data (http://www.eea.europa.eu/data-and-maps/figures/corine-land-cover-2006-by-country) for the generic crops and the Walloon crop census data (SIGEC) for wheat and potatoes.

24.3 Results and Discussion

24.3.1 Validation

To validate the implementation of the POD_Y calculation for Belgium we compared the results obtained with our model for 2009 to those obtained with EMEP which can be downloaded from (http://webdab.emep.int/Unified_Model_Results/). In our calculations the effect of soil moisture was neglected as is the case in the EMEP calculations. For the generic vegetation type temperate crop the POD_3 was considered and results are shown in Fig. 24.1. As can be seen our results compare favourably to those obtained from EMEP considering the vast difference in resolution between both results. Note that in the map produced by our model results are only shown for areas where temperate crops occur. This has the advantage of highlighting only those zones where the POD_Y results are relevant for the vegetation type considered.

24.3.2 Calculation of Crop Loss

Based on the response curves for potatoes (24.2) and wheat (24.3) crop yield losses were also estimated for 2009. For Flanders, the model results indicate a decrease in

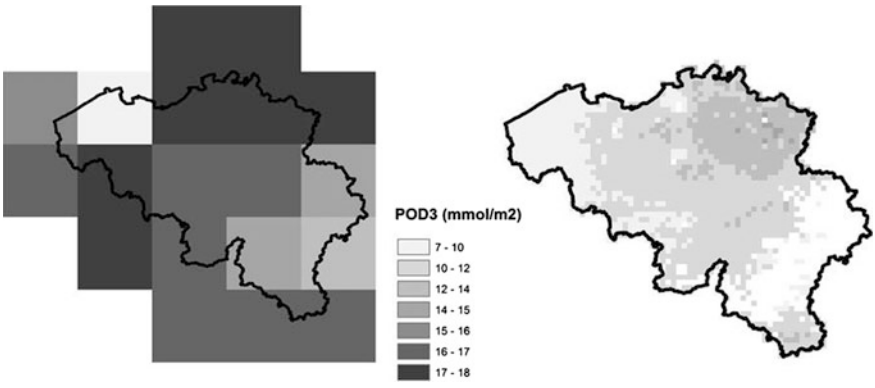

Fig. 24.1 POD_3 (mmol/m^2) for a temperate crop calculated with DO_3SE implemented in the EMEP model (*left*) and our own implementation for 2009 (*right*)

Table 24.1 Average effect of soil moisture on POD_Y in 2009

Vegetation	% reduction POD_Y
Potato	0.05 %
Temperate crop	0.05 %
Grass	5.66 %
Temperate deciduous forest	2.16 %
Temperate coniferous forest	0.65 %
Wheat	0.08 %

potato crop yield of 4.7 % on average in 2009. Average potato yield that year was 45 ton/ha which implies a loss of 2.2 ton/ha or a total loss of 97 kton which translates to 8.9 MEuro at the price paid for potatoes in 2009. In the same vein losses for wheat based on (3) using the POD_6 results amounted to 10 %. With an average yield of 9.6 ton/ha in 2009 this corresponds to a loss of 1.1 ton/ha amounting to a loss of 76 kton or 8.8 MEuro in Flanders.

24.3.3 Soil Moisture

To assess the effect of soil moisture we used the low resolution soil moisture input from the ECMWF IFS and compared these results with the results of the model run in which we neglected the soil moisture. Based on these values for 2009 a rather limited effect of soil moisture on POD_Y was found (Table 24.1). In other, drier years the effect could be larger than what was found for 2009. The bigger effect found for grass land is related to the limited rooting depth for grass compared to the other vegetation types. The rooting depth for wheat was assumed to be the same as for a generic crop. As wheat is a type of grass this could be unreasonable and imply that also for wheat a larger effect of soil moisture is to be expected. The differences in effect of soil moisture on POD_Y between the crop and the forest vegetation types is attributable to differences in the growing season and the spatial distribution of the POD_Y values between these vegetation types.

24.4 Conclusions

We have developed a model based on the DO_3SE module for calculating POD_Y values for Belgium. One of the advantages of the model is the use of observed (interpolated) ozone concentrations instead of modelled ozone concentrations, which reduces the uncertainty of the POD_Y calculations. The model is able to reproduce the results currently calculated by EMEP. Based on the model results and response curves that relate POD_Y to crop yield, crop loss can be estimated. The

effect of considering soil moisture on POD_Y was also investigated. For the year considered this effect seems rather small but this has to be corroborated for other years.

Questions and Answers

Questioner: Jon Pleim
Question: Another way to do this could be with coupled Met/AQ models that have land surface models with stomatal conductance and consistent calculations of O3 dry dep. So, O3 fluxes to vegetation are already computed accounting for soil moisture stress. Is this approach being pursued?
Answer: In this particular application we applied an existing O3flux calculation procedure, more specifically the DO3SE model as implemented in the EMEP model (Emberson et al. 2000) and as input for this model we used measured O_3 concentrations and the meteorology as calculated by the ECMWF model. Where it is true that by doing this it is quite unlikely that the vegetation exchange fluxes calculated in DO3SE and the ECMWF will be consistent we believe that the advantage of using measurements for the O_3 concentration, a very detailed O3flux calculation procedure in combination with high quality ECMWF meteorology is probably more accurate than using a code such as WRFCHEM to model meteorology and O_3 fluxes in a coupled way.
Questioner: Peter Builtjes
Question: Are you happy with the soil moisture index (SMI) of ECMWF? Especially since they are using their own land use (*Author: shouldn't this be soil types?*) categories?
Answer: Since we ingest the SMI ($= \frac{\theta-\theta_{WP}}{\theta_{FC}-\theta_{WP}}$) directly to calculate the soil moisture factor in the DO3SE we don't have to worry about the soil types that ECMWF is using. Initially we tried using the volumetric soil moisture, θ from ECMWF directly but that turned out to be the wrong way to do this precisely because of the unknown underlying soil map used by ECMWF. Off course one can also wonder how accurate the SMI calculated by ECMWF is and whether this is not more a tuning parameter in a model that is mainly used for wheather forecasting.

References

Calvo E, Martin C, Sanz M (2007) Ozone sensitivity differences in five tomato cultivars: visible injury and effects on biomass and fruits. Water Air Soil Pollut 186:167–181
Emberson LD, Ashmore MR, Cambridge HM, Simpson D, Tuovinen J-P (2000) Modelling stomatal ozone flux across Europe. Environ Pollut 109:403–413

Gerosa G, Marzuoli R, Finco A, Ebone A, Tagliaferro F (2008) Ozone effects on fruit productivity and photosynthetic response of two tomato cultivars in relation to stomatal fluxes. Ital J Agron 3:61–70

Jackson RB, Canadell J, Ehleringer JR, Mooney HA, Sala OE, Schulze ED (1996) A global analysis of root distributions for terrestrial biomes. Oecologia 108:389–411

Janssen S, Dumont G, Fierens F, Mensink C (2008) Spatial interpolation of air pollution measurements using CORINE land cover data. Atmos Environ 42:4884–4903

Mills G, Pleijel H, Büker P, Braun S, Emberson L, Harmens H, Hayes F, Simpson D, Grünhage L, Karlsson P-E, Danielsson H, Bermejo V, Gonzalez Fernandez I (2011) Manual on methodologies and criteria for modelling and mapping critical loads & levels and air pollution effects, risks and trends. Chapter 3: mapping critical levels for vegetation. UNECE

Poelmans L, Van Daele T (2014) Landgebruikskaart NARA-T 2014: studie uitgevoerd in opdracht van: INBO 2014/RMA/R/45. VITO, Mol

Simpson D, Benedictow A, Berge H, Bergström R, Emberson LD, Fagerli H, Flechard CR, Hayman GD, Gauss M, Jonson JE, Jenkin ME, Nyíri A, Richter C, Semeena VS, Tsyro S, Tuovinen J-P, Valdebenito Á, Wind P (2012) The EMEP MSC-W chemical transport model—technical description. Atmos Chem Phys 12:7825–7865

Piikki K, De Temmerman L, Ojanpera K, Danielsson H, Pleijel H (2008) The grain quality of spring wheat (Triticum aestivum L.) in relation to elevated ozone uptake and carbon dioxide exposure. Eur J Agron 28:245–254

Pleijel H, Danielsson H, Emberson L, Ashmore MR, Mills G (2007) Ozone risk assessment for agricultural crops in Europe: further development of stomatal flux and flux-response relationships for European wheat and potato. Atmos Environ 41:3022–3040

Chapter 25
Health Benefits of Emission Controls: A Multi-pollutant and Multi-health Outcome Analysis

Amanda Pappin and Amir Hakami

Abstract We create a streamlined approach for estimating the U.S. public health benefits of emission control, on a per-ton basis. We do so by incorporating epidemiological and economic valuation data into the adjoint of an atmospheric chemical transport model. We estimate benefits-per-ton of emission control for chronic mortality and acute morbidity endpoints. Our results indicate that benefits-per-ton of NO_x reduction are highly variable from source-to-source or location-to-location. We find that mortality due to long-term exposure comprises a significant portion of the total benefits of NO_x control for ozone air quality management.

25.1 Introduction

Acute and chronic exposure to ambient air pollution has been directly linked with adverse human health outcomes. Globally, exposure of populations to $PM_{2.5}$ is estimated to result in 3.5 million premature deaths/year, with another 700,000 deaths/year attributed to ozone exposure (Anenberg et al. 2010). Criteria pollutants such as $PM_{2.5}$ and ozone therefore pose substantial public health risks even at levels below current regulatory standards (U.S. EPA 2009, 2013). Managing this public health burden is a multidisciplinary undertaking informed by epidemiology, atmospheric science and engineering, economics, and policy. Among various approaches to regulating emissions, benefit-cost analysis aims to directly account for the public health and environmental impacts of emission abatement options. We create a streamlined approach for estimating the public health benefits of reducing emissions for a spectrum of health outcomes of varying severity.

A. Pappin · A. Hakami (✉)
Department of Civil and Environmental Engineering, Carleton University, Ottawa, Canada
e-mail: amir_hakami@carleton.ca

D.G. Steyn and N. Chaumerliac (eds.), *Air Pollution Modeling and its Application XXIV*, Springer Proceedings in Complexity,
DOI 10.1007/978-3-319-24478-5_25

25.2 Methodology

We use adjoint sensitivity analysis in a chemical transport model to estimate relationships between sources of emissions and public health. We use the adjoint of the Community Multiscale Air Quality model (CMAQ) with the standard 36 km U.S. EPA modeling domain spanning over the continental U.S. and southern Canada. Our simulations are conducted over May–September 2007 to capture the ozone season.

We define our adjoint cost function as the total (monetized) societal damage incurred by ozone exposure in the U.S. population. We consider respiratory mortality due to long-term ozone exposure and acute morbidity according to the U.S. EPA's Benefits Mapping and Analysis Program (BenMAP). We estimate emission control benefits for various morbidity endpoints, including respiratory emergency room visits (RERVs), respiratory hospital admissions (RHAs), and acute respiratory symptom days (ARSDs). Our definition of the adjoint cost function for acute morbidity endpoints is equivalent to that developed by Pappin and Hakami (2013a, b). For chronic endpoints, we apply a variation of that function that draws upon the long-term, average ozone concentration as a measure of exposure

$$J = V \sum_{(x,y)} M_0 P \cdot (1 - e^{-\beta C})$$

where J is the total, monetized respiratory mortality count attributable to long-term ozone exposure in the U.S. population, M_0 is the respiratory mortality rate (yr^{-1}) in a given (x,y) location, P is the population >30 years of age in a given location, β is 0.00392 ppb^{-1} for daily 1 h maximum ozone (Jerrett et al. 2009), and C is the average daily 1 h maximum concentration of ozone in a given location. The adjoint cost function is integrated over all grid-cell locations (x,y) that fall within the boundaries of the U.S. For acute morbidity endpoints, we apply βs of 0.003 ppb^{-1} for RERVs (Wilson et al. 2005) and 0.00493 ppb^{-1} for RHAs (Schwartz 1995) and baseline morbidity rates from BenMAP. For mortality and ARSDs, we apply willingness to pay valuation measures (V, above) of $7.9 million (2008 USD; U.S. EPA 2010) and $50.55 (from BenMAP), respectively. For RERVs and RHAs, we apply mean cost-of-illness valuation measures of $311.55 and $20,666, respectively, according to those used in BenMAP. Mortality and morbidity rates for 2007 from BenMAP are processed to our 36 km resolution domain.

25.3 Results and Discussion

We scale sensitivity outputs of the adjoint model to estimate the public health benefit of reducing 1 ton of NO_x emissions (referred to as benefit-per-ton or marginal benefit). Our estimates of benefit-per-ton are for NO_x emitted at the surface layer from any given model grid-cell location. We note that the benefit-per-ton

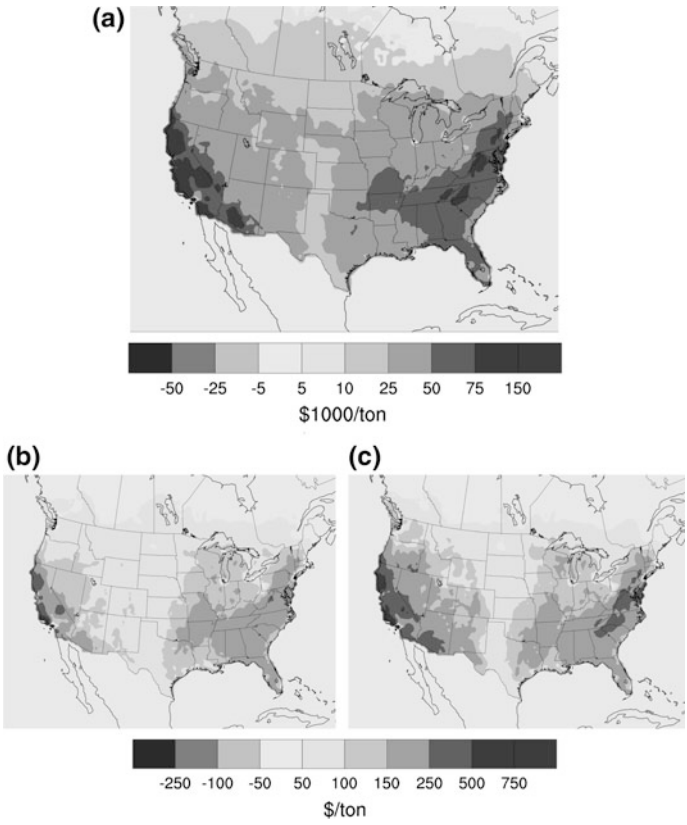

Fig. 25.1 Benefits-per-ton of NO_x control from sources across North America. Benefits in **a** are due to averted mortality associated with long-term ozone exposure in the U.S. Benefits in **b** are due to averted RHAs and RERVs in the U.S. population, and in **c** are due to averted ARSDs. Benefit-per-ton estimates are for NO_x emitted from the surface layer according to the temporal distribution of emissions over the ozone season of 2007

estimates depicted here indicate the public health benefit that would be collectively gained across the U.S., and do not reveal information about the distribution of societal benefits across different populations.

The dominant feature of Fig. 25.1 is the strong spatial component of NO_x benefits-per-ton. Benefits-per-ton show similar spatial variability among all damage endpoints, though the magnitude of estimates is substantially higher for mortality (Fig. 25.1a) than for acute morbidity endpoints (Fig. 25.1b, c). Sources located close to and upwind of major population centers generally carry large benefits-per-ton due to their ability to influence exposed populations. Benefits-per-ton based on long-term ozone exposure are significantly larger than those based on short-term exposure found in previous work (Pappin and Hakami 2013a). The largest benefits-per-ton are estimated to occur upwind of Los Angeles, California, at $340,000/ton.

Interpretation of benefits-per-ton presented here should consider the limitations and uncertainties inherent in emissions and chemical transport modeling, epidemiological findings, and in economic valuation measures. Our estimation of benefits-per-ton based on chronic ozone exposure and mortality should be interpreted as long-term benefits to the U.S. population that would not be immediately realized and would take time to develop.

Long-term mortality accounts for a substantial fraction of the total benefits of NO_x control. Inclusion of long-term risk estimates in health impact assessments such as these without consideration for acute morbidity is unlikely to vastly underestimate the overall benefits.

Questions and Answers

Questioner Name: S.T. Rao

Q: Have you looked into the costs ($/ton) associated with emission reductions needed to achieve a targeted improvement in ozone and NO_2 levels and associated health benefits?

A: While we do not have detailed information about the abatement costs for NO_x control, our findings suggest a significant discrepancy between costs and benefits, with benefits far exceeding current per-ton abatement costs. For example, the average NO_x permit price in the CAIR emissions market in 2007 was ~$900/ton. Our findings of benefits-per-ton exceeding $50,000/ton in many places indicate significant net benefits to be gained by emissions control.

Questioner Name: Renske Timmermans

Q: Are the NO_x emission reductions for specific sources? Will the effect depend on the source sectors where the emissions are reduced?

A: Our estimates of benefits-per-ton are specific to each source location (i.e., model grid cell and layer). Sector-specific information can be obtained by an emission-weighting of adjoint sensitivities. For mobile vs point sources, for example, the main difference in benefit-per-ton estimates is given by the vertical layers of emission release, which have different transport pathways and potentially different impacts on human health. For emitted species such as NO_x, we find that the strongest predictor of benefits-per-ton is location rather than emission sector or source type. For primary PM, source sector would potentially play an important role in the magnitude of benefit-per-ton estimates due to its varying chemical composition and other characteristics depending on source type.

References

Anenberg SC, Horowitz LW, Tong DQ et al (2010) An estimate of the global burden of anthropogenic ozone and fine particulate matter on premature human mortality using atmospheric modeling. Environ Health Perspect 118:1189–1195

Jerrett MJ, Burnett RT, Pope A III et al (2009) Long-term ozone exposure and mortality. N Engl J Med 360:1085–1095

U.S. Environmental Protection Agency (EPA) (2010) Guidelines for preparing economic analyses: Chap. 7—analyzing benefits, Washington, DC

Pappin AJ, Hakami A (2013a) Source attribution of health benefits from air pollution abatement in Canada and the United States: an adjoint sensitivity analysis. Environ Health Perspect 121:572–579

Pappin AJ, Hakami A (2013b) Attainment vs exposure: ozone metric responses to source-specific NOx controls using adjoint sensitivity analysis. Environ Sci Technol 47:13519–13527

Schwartz J (1995) Short term fluctuations in air pollution and hospital admissions of the elderly for respiratory disease. Thorax 50:531–538

U.S. Environmental Protection Agency (EPA) (2009) Integrated science assessment for particulate matter, Research Triangle Park, NC

U.S. Environmental Protection Agency (EPA) (2013) Integrated science assessment for ozone and related photo-chemical oxidants, Research Triangle Park, NC

Wilson AM, Wake CP, Kelly T, Salloway JC (2005) Air pollution, weather, and respiratory emergency room visits in two northern New England cities: an ecological time-series study. Environ Res 97:312–321

Chapter 26
Air Quality Modelling to Support Decision-Making: Scenario and Optimization Approaches

Helder Relvas, Ana Isabel Miranda, Enrico Turrini, Diogo Lopes, Carlos Silveira, Joana Ferreira, Myriam Lopes, Elisa Sá, Laura Duque, Carlos Borrego and Marialuisa Volta

Abstract In this work a multi-objective approach to define air quality policies is proposed based on the RIAT+ (Regional Integrated Assessment Modelling Tool) system. The solutions of the decision problem represent cost-effective policies at the sectorial level. The methodology is being applied to the Porto urban area, one of the most polluted areas in Portugal, and optimal control policies up to 2020 will be selected.

H. Relvas (✉) · A.I. Miranda · D. Lopes · C. Silveira · J. Ferreira · M. Lopes
E. Sá · L. Duque · C. Borrego
CESAM & Department of Environmental and Planning, University of Aveiro, Aveiro, Portugal
e-mail: helder.relvas@ua.pt

A.I. Miranda
e-mail: miranda@ua.pt

D. Lopes
e-mail: diogojlopes@ua.pt

C. Silveira
e-mail: carlos.silveira@ua.pt

J. Ferreira
e-mail: jferreira@ua.pt

M. Lopes
e-mail: myr@ua.pt

E. Sá
e-mail: mariaelisasa@ua.ptl

L. Duque
e-mail: laura.duque@ua.pt

C. Borrego
e-mail: cborrego@ua.pt

D.G. Steyn and N. Chaumerliac (eds.), *Air Pollution Modeling and its Application XXIV*, Springer Proceedings in Complexity,
DOI 10.1007/978-3-319-24478-5_26

26.1 Introduction

The 2008 European Air Quality Directive (AQD) (2008/50/EC) requires European Member States (EMS) to design appropriate Air Quality Plans (AQP) for zones and agglomerations where the air quality does not comply with the limit values and to assess possible emission reduction measures to improve concentration levels. The use of modelling to support environmental authorities to plan air quality control policies is now quite widespread, and in the last decade EMS have developed and applied a wide range of different methods to assess the effects of local and regional emission abatement policy options on air quality and human health (Borrego et al. 2012; Mediavilla-Sahagún and Apsimon 2003). Notwithstanding the last years air quality improvements we are still facing a continued wide-spread of exceedances, particularly regarding particulate matter (PM), nitrogen oxides and ozone (EEA European Environment Agency 2014). Integrated assessment methodologies (IAM), which include Chemical Transport Models, can contribute to a better assessment and planning by providing cost-effective emission reduction measures to improve air quality, reduce human exposure and protect human health.

Between 2001 and 2005, the AQD daily limit value for PM10 has been exceeded in three of the four agglomerations of the Northern Region of Portugal, namely in Porto Litoral. Thus, the development of an AQP to reduce PM10 levels was mandatory. It was designed based on a scenario approach and using the TAPM (The Air Pollution Model), which was applied over the study region for the reference situation, and for a reduction scenario with emissions re-estimated considering the implementation of abatement measures (Borrego et al. 2012). An optimization approach was applied to the Porto urban area aiming to go further identifying the most-efficient measures to improve the air quality through the application of the RIAT+ tool (Pisoni and Volta 2009).

26.2 Methodology

A full 3D deterministic multi-phase modelling system describing the non-linear dynamics linking precursor emissions to air pollutant concentrations cannot be embedded and run in real time within the RIAT+ optimization procedure because of its computational requirements (Carnevale et al. 2009). Thus, a series of long term simulations was performed beforehand with the TAPM model (Hurley et al. 2008).

E. Turrini · M. Volta
Department of Mechanical and Industrial Engineering, University of Brescia, Brescia, Italy
e-mail: enrico.turrini@ing.unibs.it

M. Volta
e-mail: volta@ing.unibs.it

The results of the simulations are then used to derive relations between emission sources and air quality indicators at given receptor sites (Source-Receptor (S-R)) which can then be used directly in the optimization algorithm. Artificial Neural Networks (ANN) are used in RIAT+ to derive these S-R relationships. The following input data was prepared:

I. Technical measures, their emission reduction potential and associated costs (preferably coming from an already available database, such as the GAINS database which contains a large data set collected for Portugal);
II. Emission data disaggregated (annual emissions data were obtained from the 2009 Portuguese national inventory);
III. Simulation of 10 emission reduction scenarios with the TAPM (needed for the establishment of S-R models);
IV. Population data to estimate health effects using the ExternE-Methodology.

The RIAT+ system provides the optimal levels (or necessary) of each technology application and the corresponding emission reduction, the Air Quality Index (AQI) (through S/R models) and costs (external and internal).We used the minimum set of 10 scenarios needed to train neural networks within RIAT+. Starting from the 2009 Portuguese emission inventory, which was disaggregated to a spatial grid of 2×2 km^2 resolution, three different emission levels were considered to establish these scenarios: B (base case), A (medium emission reductions) and H (high emission reductions). The B case considers the evolution of 2009 emissions taking into account the fulfillment of 2020 CLE (Current Legislation Emissions) increased by 15 % to enhance the identification bounds for ANN guarantying the correct identification of source-receptor models. The H case is associated to the maximum feasible reduction of emissions at 2020 (MFR2020), decreased by 15 %. The A level is obtained as the average between B and H levels.

26.3 Results

The TAPM model has been applied for the defined 10 scenarios and considering the 2012 meteorological year. In the context of neural networks it is impossible to know a priori which ANN structure produces the best results. Figure 26.1 shows the scatter plots obtained comparing TAPM and ANN results, for all cells of the domain.

The scatter plot shows the good performance of the ANN, with a Normalized Root Mean Square Error (RMSE) of 0.34 and a correlation coefficient of 0.95, and confirms that the ANN system has the capability to simulate the nonlinear source–receptor relationship between PM10 mean concentration and the emission of precursors. RIAT+ was then applied in the optimization mode and Fig. 26.2 indicates the costs of different efficient solutions after the optimization process.

The Pareto Curve (a curve providing the optimal solutions ranked by costs) shows that a PM10 mean concentration of 28.5 μg.m^{-3} can be reached adopting emission

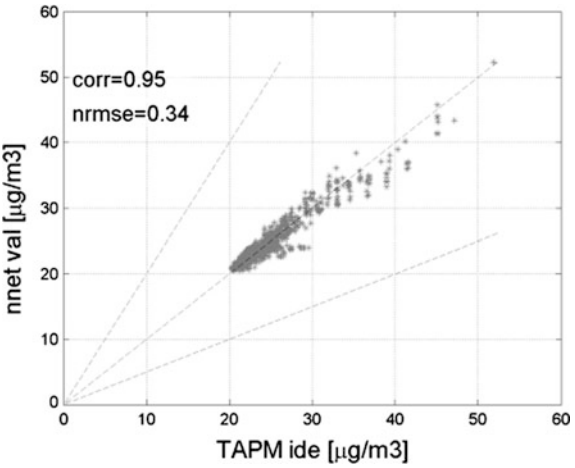

Fig. 26.1 Scatter plot between ANNs and TAPM concentration values for PM10

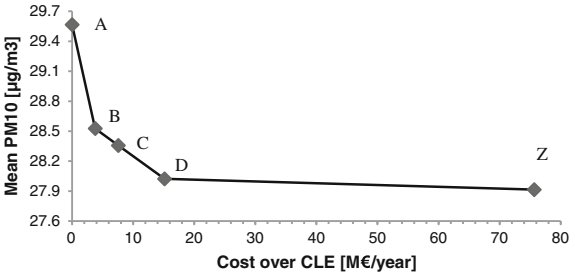

Fig. 26.2 Pareto curve for the optimization of PM10 yearly mean concentrations

reduction technologies costing around 3.8 Million € per year (point B). While points A and Z represent extreme cases, for which no actions or maximum effective reductions, respectively, are implemented, the other points of the Pareto Curve are intermediate solutions (possible combinations of reduction measures and their cost).

26.4 Conclusions

Source-Receptor robust relationships were obtained based on the TAPM yearly simulations for the set of 10 emission reduction scenarios, and the trained neural networks. The optimization allowed selecting cost-effective policies taking simultaneously into account the costs of their implementation (internal costs) and the health costs (external costs). Therefore, applying the trained system with a list of available technologies from a previous database allows identifying the sectors where to focus the mitigation activities and to estimate associated costs, but a more concrete list of measured has to be decided and discussed with stakeholders and policy makers.

Acknowledgments The authors would like to acknowledge the financial support of the Portuguese Ministry of Science, Technology and Higher Education, through the Foundation for Science and Technology (FCT), for the funding of research project MAPLIA (PTDC/AAG-MAA/4077/2012), supported in the scope of the Competitiveness Factors Thematic Operational Programme (COMPETE) of the Community Support Framework III and by the European Community Fund FEDER. This work has also been done in the scope of the research project APPRAISAL (FP7 Grant Agreement number 303895).

References

Borrego C, Sá E, Carvalho A, Sousa S, Miranda AI (2012) Plans and programmes to improve air quality over Portugal: a numerical modelling approach. Int J Environ Pollut 48(1–4):60–68

Carnevale C, Finzi G, Pisoni E, Volta M (2009) Neuro-fuzzy and neural network systems for air quality control. Atmos Environ 43:4811–4821

EEA European Environment Agency (2014) Air quality in Europe, 2014 report, EEA report No 5/2014. Copenhagen

Hurley P, Edwards M, Luhar A, (2008) TAPM V4. part 2: Summary of some verification studies. CSIRO Marine and Atmospheric Research Paper No. 26

Mediavilla-Sahagún A, Apsimon HM (2003) Urban scale integrated assessment of options to reduce PM10 in London towards attainment of air quality objectives. Atmos Environ 37(33):4651–4665 ISSN 1352-2310

Pisoni E, Volta M (2009) Modeling pareto efficient PM10 control policies in Northern Italy to reduce health effects. Atmos Environ 43:3243–3248

Chapter 27
Recent and Future Changes in Nitrogen and Sulphur Emission, Deposition and the Exceedance of Critical Loads for the Region of South-West Poland and Eastern Saxony

Maciej Kryza, Małgorzata Werner, Wojciech Mill, Tomasz Pecka, Rafał Ulańczyk, Anthony J. Dore, Marek Błaś, Mariusz Szymanowski, Ewa Liana and Marzenna Strońska

Abstract In this work we use the FRAME model to assess the changes in sulphur and nitrogen deposition for the 2000–2030 period in the Poland-Saxony transboundary area. The results show that the sulphur and oxidised nitrogen deposition was significantly decreased (by 60 and 45 % respectively). This resulted in significant reduction of the ecosystems affected by acidification. Deposition of reduced nitrogen resulting in eutrophication is currently, and forecast to remain, the main threat for the ecosystems of this area.

M. Kryza (✉) · M. Werner · M. Błaś · M. Szymanowski
Institute of Geography and Regional Development, Wroclaw University, Wroclaw, Poland
e-mail: maciej.kryza@uni.wroc.pl

M. Werner
National Pollen and Aerobiology Research Unit, University of Worcester, Worcester, UK

W. Mill · T. Pecka · R. Ulańczyk
Institute of Environmental Protection–National Research Institute, Warsaw, Poland

A.J. Dore
Centre for Ecology and Hydrology, Edinburgh, UK

E. Liana · M. Strońska
Institute of Meteorology and Water Management National Research Institute, Wroclaw, Poland

D.G. Steyn and N. Chaumerliac (eds.), *Air Pollution Modeling and its Application XXIV*, Springer Proceedings in Complexity,
DOI 10.1007/978-3-319-24478-5_27

27.1 Introduction

The transboundary area of SW Poland, Czech Republic and Saxony has a long history of ecological problems related with sulphur (S) and nitrogen (N) deposition. This was mainly due to brown coal consumption in energy production and the chemical industry located in this area. Large areas of forests were destroyed because of acid deposition of sulphur and nitrogen compounds, and the region was named the Black Triangle. After the year 1990 the emissions from coal combustion were significantly abated (Mill 2006). There were many reasons behind this, including environmental concerns, but also political and economic changes in Central Europe. The emission abatements were especially significant for S, and, to a less extent, for oxidised N (NO_x).

In this work we use the atmospheric chemistry transport model FRAME to assess the changes in S and N deposition in this area for past and future years. Information on deposition is used to calculate the exceedances of critical loads (CL) of nutrient N and CL of acidifying S and N to assess the environmental impact of deposition on ecosystems in the past, present and future.

27.2 Data and Methods

The regional atmospheric transport model FRAME provides information on the annual mean oxidised sulphur as well as oxidised and reduced nitrogen air concentrations and deposition. A detailed description of the FRAME model is given in Singles et al. (1998) and Dore et al. (2006). Details on the model configuration for Poland can be found in Kryza et al. (2011). Here, the model was applied for the transboundary area of Poland, Czech Republic and Germany on a 1 km × 1 km spatial grid. The model results were compared with wet deposition measurements available in the model domain for the year 2010. The results are summarized using the bias, fraction of two (FAC2), mean absolute error (MAE) and determination coefficient (R^2) statistics in Table 27.1.

The emission inventory is based on the official emission data available for Saxony and Brandenburg, and the emission data developed with the approach presented by Kryza et al. (2010) for the area of Poland. The emission inventory was developed at a 1 km × 1 km grid resolution for the area of Poland and Saxony for the year 2010. For the remaining areas of the study domain, we used the MACC TNO emission inventory (Kuenen et al. 2011).

Table 27.1 FRAME model performance for wet deposition in year 2010

	BIAS (kg)	MAE (kg)	FAC2 (-)	R^2 (-)
NH_x	−0.69	0.81	1.00	0.74
NO_x	−0.29	0.37	1.00	0.89
SO_x	1.10	1.15	1.00	0.87

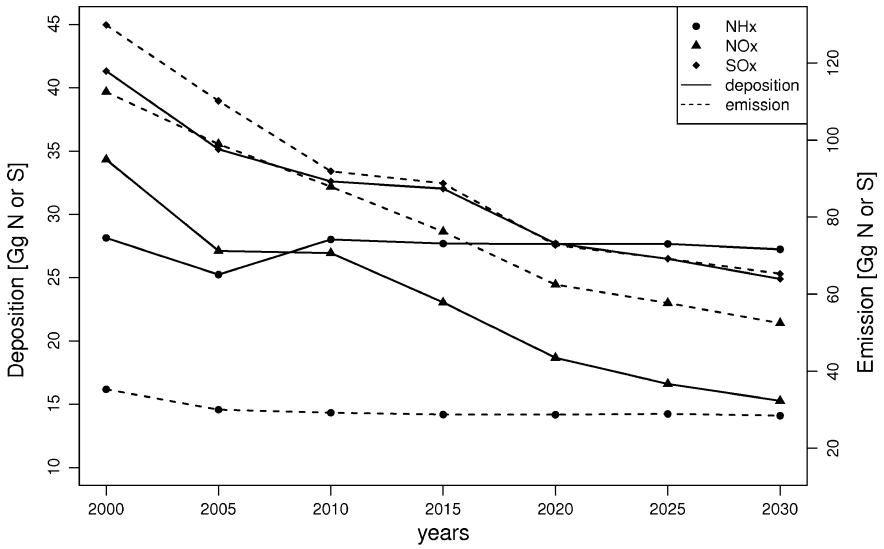

Fig. 27.1 Changes in deposition and emission of S and N compounds during the years 2000–2030

The emission inventory developed for the year 2010 was rescaled backwards and forwards in time using country and SNAP sector dependent scaling factors. For past years (2005 and 2000), we used the EMEP WebDAB database to calculate scaling factors. The scaling factors for future years (2015–2030) were developed from the GAINS PRIMES emission projection. Total emission within the study domain is summarized in Fig. 27.1.

The critical load (CL) mean the highest deposition of acidifying compounds (CL of acidity) or nutrient nitrogen (CL for eutrophication) below which no harmful effects in ecosystems occur. CLs were calculated using the Simple Mass Balance model (Nilsson and Grennfelt 1988; UBA 2004), and this approach was previously applied e.g. for Poland (Kryza et al. 2013). The exceedances of CLs describes the ecosystems at risk of acidification and/or eutrophication.

27.3 Results

Emission abatements during the years 2000–2030 have a strong impact on deposition in the study area (Fig. 27.1). The downward trend is especially strong in SO_x and NO_x, while for NH_x deposition and emission remains stable. Noticeably, the total mass of deposited N–NH_x exceed N–NO_y after year 2010. Figure 27.2 shows the spatial pattern of total (dry + wet) deposited sulphur and reduced nitrogen for years 2000 and 2030. The largest deposition is calculated for the mountainous

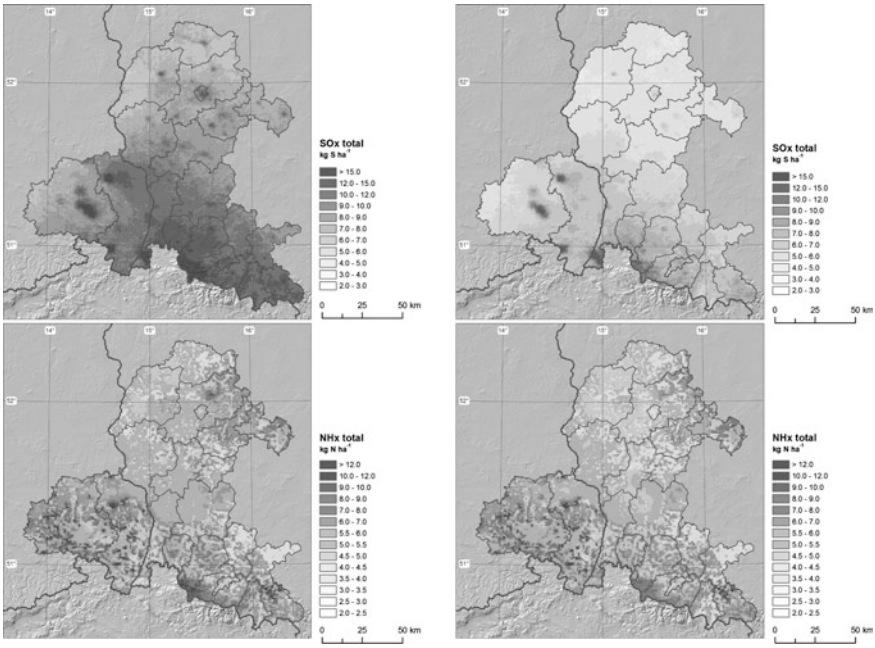

Fig. 27.2 Total deposition of SO_x (*top*) and NH_x (*bottom*) in year 2000 (*left*) and 2030 (*right*)

areas. There are very small changes in NH_x deposition if years 2000 and 2030 are compared.

There is a significant decrease in the total area with the critical loads for acidity exceeded, from 7 % in year 2000 to 0.8 % in year 2030. The total area with the critical loads for eutrophication exceeded also decrease from 72 % in year 2000 to 39 % in year 2030, but from these numbers one can see that the projected emission abatements are insufficient to fully protect all ecosystems (Fig. 27.3).

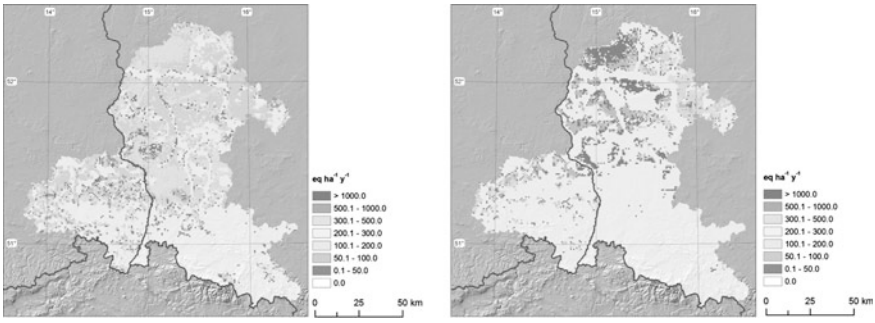

Fig. 27.3 Exceedances of the nutrient CL for the years 2000 (*left*) and 2030 (*right*)

27.4 Summary and Conclusions

The main findings from this study are:

- There are large reductions in S and oxidized N deposition (of 60 and 45 % in total mass for the study area, respectively) in the study area and this reflects the efforts related with emission abatements. This results in a decrease of the areas with exceedance of the critical loads for acidity.
- Eutrophication of natural ecosystems is a major concern for this area. The main source of N after year 2010 will be ammonium. Considering the emission scenarios until the year 2030, there will be still c.a. 40 % of the ecosystems threatened by the exceedance of the nutrient critical loads.

References

Dore AJ, Vieno M, Fournier N, Weston KJ, Sutton MA (2006) Development of a new wind-rose for the British Isles using radiosonde data, and application to an atmospheric transport model. Q J Roy Meteorol Soc. doi:10.1256/qj.05.198

Kryza M, Werner M, Blas M, Dore AJ, Sobik M (2010) The effect of emission from coal combustion in nonindustrial sources on deposition of sulfur and oxidized nitrogen in poland. J Air Waste Manag Assoc. doi:10.3155/1047-3289.60.7.856

Kryza M, Dore AJ, Blas M, Sobik M (2011) Modelling deposition and air concentration of reduced nitrogen in Poland and sensitivity to variability in annual meteorology. J Environ Manage. doi:10.1016/j.jenvman.2010.12.008

Kryza M, Mill W, Dore AJ, Werner M, Blas M (2013) Calculation of sulphur and nitrogen deposition with the frame model and assessment of the exceedance of critical loads in Poland. Ecol Chem Eng S. doi:10.2478/eces-2013-0020

Kuenen JH, Denier van der Gon A, Visschedijk van der Brugh H (2011) High resolution European emission inventory for the years 2003–2007. TNO report TNO-060-UT-2011-00588, Utrecht. https://gmes-atmosphere.eu/documents/deliverables/d-emis/

Mill W (2006) Temporal and spatial development of critical loads exceedance of acidity to Polish forest ecosystems in view of economic transformations and national environmental policy. Environ Sci Policy. doi:10.1016/j.envsci.2006.05.002

Nilsson J, Grennfelt P (1988) Critical loads for sulphur and nitrogen. Report from a workshop held at Skokloster, Sweden, 19–24 March 1988

Singles R, Sutton MA, Weston KJ (1998) A multi-layer model to describe the atmospheric transport and deposition of ammonia in Great Britain. Atmos Environ. doi:10.1016/S1352-2310(97)83467-X

UBA (2004) Manual on Methodologies and Criteria for Modelling and mapping critical Loads and Levels and Air Pollution Effects, Risks and Trends, Umweltbundesamt, Berlin

Chapter 28
Black Carbon Exposure of Schoolchildren in Barcelona

I. Rivas, L. Bouso, D. Donaire, M. Pandolfi, M. de Castro, M. Viana, M. Àlvarez-Pedrerol, M. Nieuwenhuijsen, A. Alastuey, J. Sunyer and X. Querol

Abstract Black carbon (BC; a good tracer of road traffic emissions) concentrations from personal monitoring of 46 school children showed the highest levels in comparison with the corresponding fixed stations in schools and in a reference urban background station. Commuting periods showed extreme concentration peaks and the concentration was 2.9 times higher than at home. Children spent only 5.6 % of their time on commuting but received 19.6 % of their daily dose. Moreover, they received 36.5 % of the dose at schools. Therefore, traffic density around schools and typical school commuting routes should be reduced.

28.1 Introduction

Black Carbon (BC) is a good tracer of traffic emissions and may operate as a universal carrier of many chemical components which have adverse effects on human health. Although epidemiological studies are usually based in data collected from few fixed monitoring stations, personal monitoring is the most accurate methodology to evaluate the exposure of a population (Jantunen et al. 2002). This is because it takes into account all the microenvironments in which people spend their time (Ashmore and Dimitroulopoulou 2009).

This work is within the framework of the BREATHE study and its objective is to determine the BC dose received by 46 school children and to evaluate the relationship between BC concentrations from personal monitoring and stations at schools (indoor and outdoor) and in an urban background (UB) site.

I. Rivas (✉) · M. Pandolfi · M. Viana · A. Alastuey · X. Querol
Institute for Environmental Assessment and Water Research (IDÆA-CSIC), Barcelona 08034, Spain
e-mail: irivas@creal.cat

I. Rivas · L. Bouso · D. Donaire · M. de Castro · M. Àlvarez-Pedrerol · M. Nieuwenhuijsen · J. Sunyer
Centre for Research in Environmental Epidemiology (CREAL), Barcelona 08003, Spain

D.G. Steyn and N. Chaumerliac (eds.), *Air Pollution Modeling and its Application XXIV*, Springer Proceedings in Complexity,
DOI 10.1007/978-3-319-24478-5_28

28.2 Materials and Methods

Personal measurements of BC concentrations during 48 h from 53 children (aged between 7–10 years old) were carried out from March 2012 to February 2013. Only weekdays were considered. Forty-five children were included in the study, with a minimum of 24 h of data. These children attended 25 different schools from Barcelona (NE Spain), where indoor (in a single classroom) and outdoor (in the playground) BC concentrations were also monitored. Personal and school BC concentrations were measured by means of a MicroAeth AE51 (AethLabs, USA), which is a small and light device that children can carry easily in a belt bag. Simultaneously, a Multi Angle Absorption Photometer (MAAP Thermo) was employed at a urban background (UB) station. BC concentrations were corrected by offline site-specific EC gravimetric samples.

Children also filled in a Time-Activity Diary, reporting every time they changed location and activity and the locations were classified as "classroom" if they were inside the school building, "school playground", "home", "commuting" and "other".

28.3 Results and Discussion

Similar BC concentrations were recorded in all the monitoring stations (geometric means in $ng \cdot m^{-3}$: 864 and 865 in school playgrounds and classrooms, respectively; 939 in the UB station; 1,035 from personal measurements), with the highest concentrations observed in personal monitoring, due to peak concentration events occurred during commuting (Fig. 28.1). In fact, personal BC concentrations were 20 % higher than at the school fixed stations and 10 % higher than at UB.

Road traffic rush hours coincide with children commuting to school. In fact, commuting periods were clearly evident in the personal measurements because of high BC peaks (Fig. 28.1) and were an average of 2.9 times higher than mean concentrations at home. The ratio $BC_{commuting}/BC_{home}$ ranged between 0.8 to 26.7 (median = 2.5). There is a great variability among each child's time-series. In accordance to what Dons et al. (2011) concluded, differences in BC concentrations to what children are exposed are due to differences between their time-activity pattern and the corresponding location.

For the daily dose determination, different inhalation rates (obtained from Buonanno et al. 2011, except for commuting, which was set to 0.91) were assigned to each location according to the most common activity usually carried out there.

Children spent only 5.6 % of their daily time on commuting, but they received 19.6 % of their daily dose to BC. At school, children are subjected to 36.5 % of

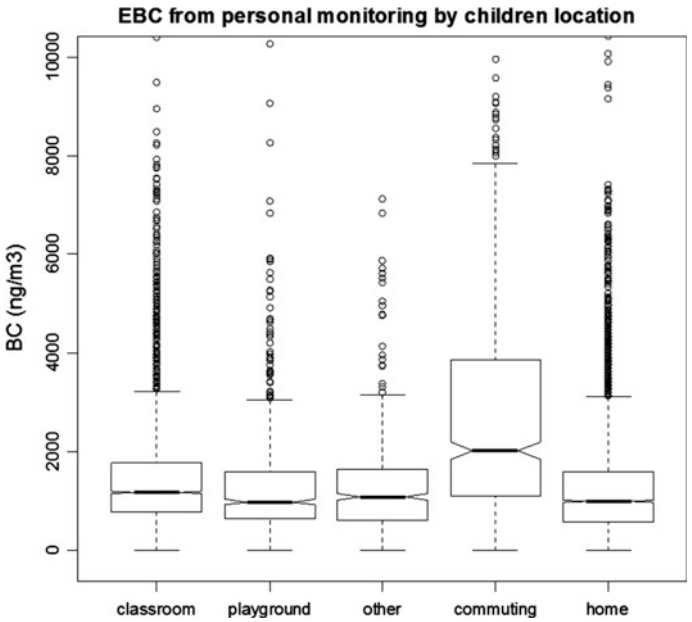

Fig. 28.1 BC concentration (ng/m^3) from personal monitoring by the corresponding microenvironment where children reported to be

their daily exposure (spending there 30.1 % of their day). Therefore, reducing traffic intensities around schools and in typical school commuting routes could be helpful to considerably diminish the dose of BC received by the attending children.

References

Ashmore MR, Dimitroulopoulou C (2009) Personal exposure of children to air pollution. Atmos Environ 43:128–141. doi:10.1016/j.atmosenv.2008.09.024

Buonanno G, Giovinco G, Morawska L, Stabile L (2011) Tracheobronchial and alveolar dose of submicrometer particles for different population age groups in Italy. Atmos Environ 45:6216–6224. doi:10.1016/j.atmosenv.2011.07.066

Dons E, Int Panis L, Van Poppel M, Theunis J, Willems H, Torfs R, Wets G (2011) Impact of time–activity patterns on personal exposure to black carbon. Atmos Environ 45:3594–3602. doi:10.1016/j.atmosenv.2011.03.064

Jantunen M, Hänninen O, Koistinen K, Hashim JH (2002) Fine PM measurements: personal and indoor air monitoring. Chemosphere 49:993–1007

Chapter 29
Developing a New Management Tool—a Holistic View on the Nitrogen Cycle

Camilla Geels, Kaj M. Hansen, Hans Estrup, Hans Thodsen, Dennis Trolle, Karsten Bolding, Berit Hasler, Marianne Zandersen, Steen Gyldenkærne, Tavs Nyord and Karen Timmermann

Abstract New agricultural technologies can reduce the emissions of ammonia associated with e.g. manure spreading. Reduced emissions to the atmosphere have the potential to limit the negative impacts of reactive nitrogen (N_r) on terrestrial ecosystems and human health. But could the new technologies transfer more N_r to the watershed instead and hence lead to increased eutrophication in the aquatic environment? In order to answer questions like this a holistic approach is necessary. Therefore a new management tools is under development at the Danish Center for Energy and Environment (DCE), Aarhus University, where models describing the fate of N_r in the relevant compartments (atmosphere, watershed and aquatic systems) are linked.

C. Geels (✉) · K.M. Hansen · B. Hasler · M. Zandersen · S. Gyldenkærne
Department of Environmental Science, Aarhus University, Aarhus, Denmark
e-mail: cag@envs.au.dk

K.M. Hansen
e-mail: kmh@envs.au.dk

B. Hasler
e-mail: bh@envs.au.dk

M. Zandersen
e-mail: mz@envs.au.dk

S. Gyldenkærne
e-mail: sgy@envs.au.dk

H. Estrup · H. Thodsen · D. Trolle · K. Bolding · K. Timmermann
Department of Bioscience, Aarhus University, Aarhus, Denmark
e-mail: hea@bios.au.dk

H. Thodsen
e-mail: hath@bios.au.dk

D. Trolle
e-mail: dtr@bios.au.dk

K. Bolding
e-mail: bolding@bios.au.dk

D.G. Steyn and N. Chaumerliac (eds.), *Air Pollution Modeling and its Application XXIV*, Springer Proceedings in Complexity,
DOI 10.1007/978-3-319-24478-5_29

29.1 Introduction

It is well known that the anthropogenic use of N_r is related to negative impacts on the environment and human health (ENA 2013). The many forms of N_r can inter-react and transform and have a cascade of effects through different compartments of the environment (Galloway et al. 2003). International and national goals for reducing the loss of N_r to the environment requires advanced management tools based on a detailed description of the different parts of the nitrogen cycle. So far the policies and management of N_r have separated the various N_r forms and compartments, but it is now acknowledged that a holistic and interdisciplinary methodology is needed (ENA 2013). A close link to economic models is also important in order to base the policy on valid estimates of the abatement costs and focus on cost-efficient reductions in the nutrient loads.

The agricultural sector is large in Denmark and research related to technology developments, emission factors and the transformation/transport in atmosphere and hydrosphere have been carried out for many years. A multi-model approach has recently been used to simulate the effects and costs of suggested N_r limiting strategies in the Baltic Sea catchment area (Wulff et al. 2014). In the new DEEMON project (Dynamic Ecological and Economic Models of Nutrients) we want to take this a step further to also include the atmospheric component of the nitrogen cycle. This is possible due to the interdisciplinary research carried out at the Centre for Energy and Environment at Aarhus University.

29.2 Setup

The overall structure of the management tool is illustrated in Fig. 29.1. The tool will be setup for the Limfjord area in the northern part of Denmark as an initial test case. The 180 km long Limfjord connects the Nord Sea and Kattegat and is located within an important agricultural region. The models describing the processes in each of the compartments will be forced by the same emission data sets and provide the necessary flow between the compartments.

New methods for application of manure on the fields have been carried out, with replicated measurements of the emission of ammonia to the atmosphere and e.g. the uptake of nutrients in the plants as well as the yield. Together with emissions factors from the literature, these data will form the basis for a number of scenarios

K. Timmermann
e-mail: kt@bios.au.dk

T. Nyord
Department of Engineering, Aarhus University, Aarhus, Denmark
e-mail: tavs.nyord@eng.au.dk

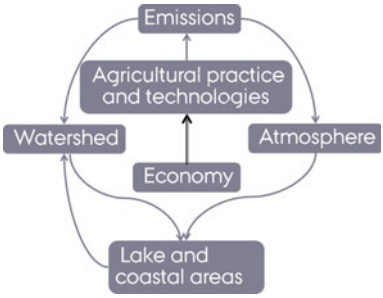

Fig. 29.1 An overview of the suggested management tool. Existing state-of-the-art models describing the N_r dynamics in each compartment will be coupled and the link to the economic model will make it possible to associate a reduction target with the most cost-effective mitigation technique

describing the emission to the atmosphere as well as the part available for sediment transport in the watershed.

The chemistry-transport model DEHM (the Danish Eulerian Hemispheric Model) simulates the processes within the atmosphere compartment (Christensen 1997; Geels et al. 2012). DEHM is setup with several nested domains, allowing for a relatively high spatial resolution over Demark (5.6 km × 5.6 km) and coverage of the international sources contribution to the N load over the region.

The watershed hydrological transport model SWAT (the Soil and Water Assessment Tool) will describe the dynamic sediment and P transport within the catchment area (as e.g. described in Lu et al. 2015). The SWAT model will provide loadings of nutrients to a marine biogeochemical model describing the processes in the marine and costal area (Timmermann et al. 2010). The input from the atmosphere into the marine compartment is provided by the DEHM model, which estimates dry and wet deposition of the various N-components. These loadings will also be used as input to the GOTM-FABM-PCLake model (Bruggeman and Bolding 2014) describing the status in a freshwater system within the region.

Finally the cost minimization model TargetEconN (Konrad et al. 2014) has been setup for the Limfjord area using the same data (soil type, land-use, crop rotation, fertilizer and manure use) as the SWAT model. By combining the minimization model with the other models in Fig. 29.1., the abatement measures to reach a specific environmental objective (e.g. a freshwater quality) at the lowest possible cost, can be identified. Due to the use of a number of data sets on land parcel level (typically a few hectares, but with large variations) it is possible to estimate the effectiveness, potential and cost of mitigation measures of each land parcel separately.

29.3 Conclusion

The overall aim of the DEEMON project is to setup a management tool linking models describing the fate of nutrients in the main compartments (atmosphere, watershed and aquatic systems) and a cost minimization model. Thereby the full effect of e.g. implementing new technologies in the agricultural sector can be evaluated. The use of the tool can also give us a better understanding of the processes driving the coupled N_r cycle and the relative importance of e.g. the atmospheric input vs the input through the catchment to marine coastal areas. In order to obtain a "good ecological status" as required in EU Directives, research based management tools like the present are important.

Acknowledgments The DEEMON project is funded by the Danish Center for Energy and Environment, Aarhus University.

References

Bruggeman J, Bolding K (2014) A general framework for aquatic biogeochemical models. Environ Model Softw 61:249–265

Christensen JH (1997) The Danish Eulerian hemispheric model—A three-dimensional air pollution model used for the Arctic. Atmos Environ 31:4169–4191

ENA (2013) The European nitrogen assessment. In: Sutton MA et al (ed) Cambridge University Press, Cambridge

Geels C, Andersen HV, Ambelas Skjøth C, Christensen JH, Ellermann T, Løfstrøm P et al (2012) Improved modelling of atmospheric ammonia over Denmark using the coupled modelling system DAMOS. Biogeosciences 9:2625–2647

Galloway JN, Aber JD, Erisman JW, Seitzinger SP, Howarth RW et al (2003) The nitrogen cascade. BioScience 53(4):341–356

Konrad M, Andersen HE, Thodsen H, Termansen M, Hasler B (2014) Cost-efficient reductions in nutrient loads; identifying optimal spatially specific policy measures. Water Resour Econ 7:39–54

Lu S, Kronvang B, Audet J, Trolle D, Andersen HE, Thodsen H et al (2015) Modelling sediment and total phosphorus export from a lowland catchment: comparing sediment routing methods. Hydrol Process 29(2):280–294

Timmermann K, Markager S, Gustafsson KE (2010) Streams or open sea? Tracing sources and effects of nutrient loadings in a shallow estuary with a 3D hydrodynamic–ecological model. J Mar Syst 82:111–121

Wulff F, Humborg C, Andersen HE, Blicher-Mathiesen G, Czajkowski M, Elofsson K et al (2014) Reduction of Baltic Sea nutrient inputs and allocation of abatement costs within the Baltic Sea catchment. Ambio 43(1):11–25

Chapter 30
Variability in Ozone Metrics with Emission Reductions and Its Application in Health Impact Assessment

Amanda J. Pappin and Amir Hakami

Abstract With advancing evidence of long-term health risks of ozone exposure, cumulative exposures are of interest for air quality regulation. The current form of the ozone air quality standard in the United States pertains to an extreme value (the design value) of the ozone distribution. Using atmospheric chemical transport modeling, we examine how well attainment metrics correlate with average exposure levels. We use forward sensitivity analysis to contrast the responses of two types of ozone metrics to widespread emission reductions. One such metric is based on extreme values of the ozone distribution used for attainment designation, while the other is the seasonal average ozone concentration indicative of long-term exposure levels. We find that in locations that have high day-to-day variability in ozone concentrations, design values are more sensitive to emission reductions and are least indicative of changing exposure levels with emission reductions.

30.1 Introduction

Evidence of increased health risks associated with short and long-term exposure to ground-level ozone has led to increasingly stringent air quality regulations in North America. Current ambient air quality standards for ozone in the United States pertain to extreme values of the ozone probability distribution. That is, attainment of standards is determined by comparing a 3-year average of the fourth-highest measured concentration each year to the level of standard (U.S. EPA 2013). While much of the improvement in air quality in past years can be attributed to an attainment-based regulatory framework, one obvious question is how well the current form of standard represents exposure levels. As elevated health risks of

A.J. Pappin (✉) · A. Hakami
Department of Civil and Environmental Engineering, Carleton University, Ottawa, ON, Canada
e-mail: amandapappin@cmail.carleton.ca

D.G. Steyn and N. Chaumerliac (eds.), *Air Pollution Modeling and its Application XXIV*, Springer Proceedings in Complexity,
DOI 10.1007/978-3-319-24478-5_30

long-term exposure to ozone become more abundant in the epidemiological literature, there may be a shift to regulate long-term exposure levels relevant to chronic health outcomes.

30.2 Methodology

We use atmospheric chemical transport modeling to characterize ozone probability distributions and how well attainment measures indicate cumulative exposure levels. We use the Community Multiscale Air Quality model (CMAQ) version 4.5.1 to estimate ozone probability distributions across Canada and the United States. We use a modeling domain extending over southern Canada and the continental United States at a 36-km grid cell resolution. Our simulations are conducted over May 1 to September 30, 2007 in order to capture the ozone season.

We estimate ozone probability distributions using simulated daily maximum 8-hr average (DM8A) ozone concentrations from CMAQ. We assume that the sample of ozone concentrations simulated over the summer of 2007 is representative of ozone concentrations over the full year used for attainment designation. We calculate probability-weighted fourth-highest concentrations or design values assuming Gaussian ozone probability distributions. Our calculation of probabilistic design values follows the method established in previous work (Pappin and Hakami 2013). We use forward brute-force sensitivity analysis to examine how various ozone metrics respond to widespread emission controls. Our emission scenarios consist of a baseline of 2007 and an abatement scenario with a 20 % reduction in anthropogenic emissions across the United States. We scale our sensitivity estimates to amount to the influence of a nation-wide 10 % reduction in emissions on mean ozone concentrations and design values (in units of ppb) in each receptor grid cell.

30.3 Results and Discussion

We characterize ozone probability distributions using the mean and standard deviation as measures of location and spread. It is noted that for each location, cumulative exposure over the ozone season is a linear function of mean ozone concentration. We therefore use mean ozone concentrations over the summer of 2007 as indicators of cumulative exposure. Ozone exposure is highly variable across Canada and the United States, with the highest concentrations in proximity to (or downwind of) major emission sources (Fig. 30.1a). Variability in day-to-day ozone concentrations is high in Fig. 30.1b when the standard deviations of local probability distributions are large (reaching up to 30 ppb). Standard deviations tend to be highest near large emission sources and coastal areas or major bodies of water

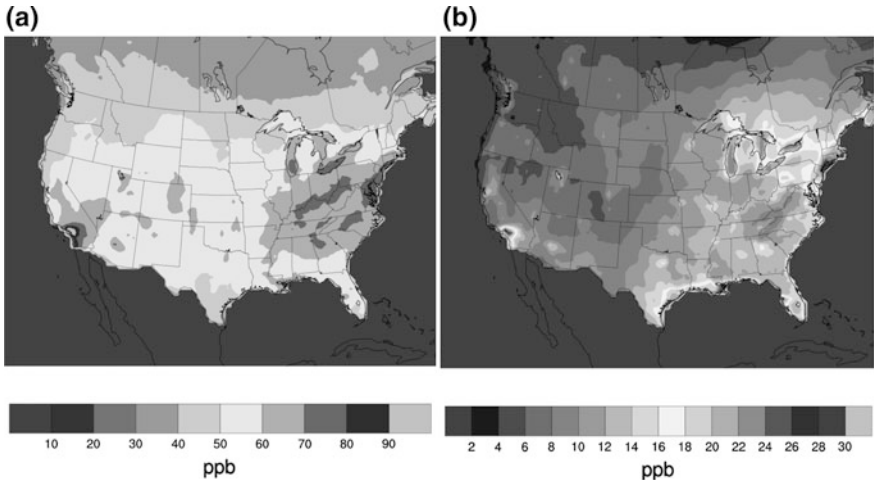

Fig. 30.1 Measures of location and spread describing local ozone probability distributions. Values in (**a**) are mean ozone concentrations, and in (**b**) are standard deviations calculated over May 1 to September 30, 2007

in California and the south and northeastern United States and around the Great Lakes region.

We estimate the sensitivity of mean ozone and design values to widespread reductions in emissions (Fig. 30.2) using forward sensitivity analysis. Our findings reveal that design values are more sensitive to emission reductions than mean ozone concentrations and vary across finer spatial scales (Fig. 30.2b). Discrepancies between sensitivities of design values and mean ozone concentrations (i.e., Fig. 30.2b minus Fig. 30.1a) in Fig. 30.2c are highest in southeastern Canada, California, and the south and northeast regions of the United States. The spatial distribution of sensitivities in Fig. 30.2c follow a similar pattern to standard deviations of local ozone probability distributions (Fig. 30.1b). This finding indicates that attainment of standards in locations with large day-to-day variability in ozone concentrations (a high standard deviation) is very sensitive to emissions. Small (or zero) values in Fig. 30.2c indicate locations where design values are a good indicator of cumulative exposure over the ozone season. In such locations, emission controls similarly act on attainment metrics and measures of ozone exposure such as mean concentration, and improvement in attainment with emission reductions approximates the level of improvement expected in exposure levels.

Our results show that regulation of ground-level ozone using extreme values of the ozone probability distribution does not necessarily yield the same information about cumulative exposure levels relevant to chronic health impacts. As epidemiological evidence advances and provides evidence for long-term health risks of ozone exposure, public health and air quality management would benefit from air quality regulations that specify cumulative exposure limits.

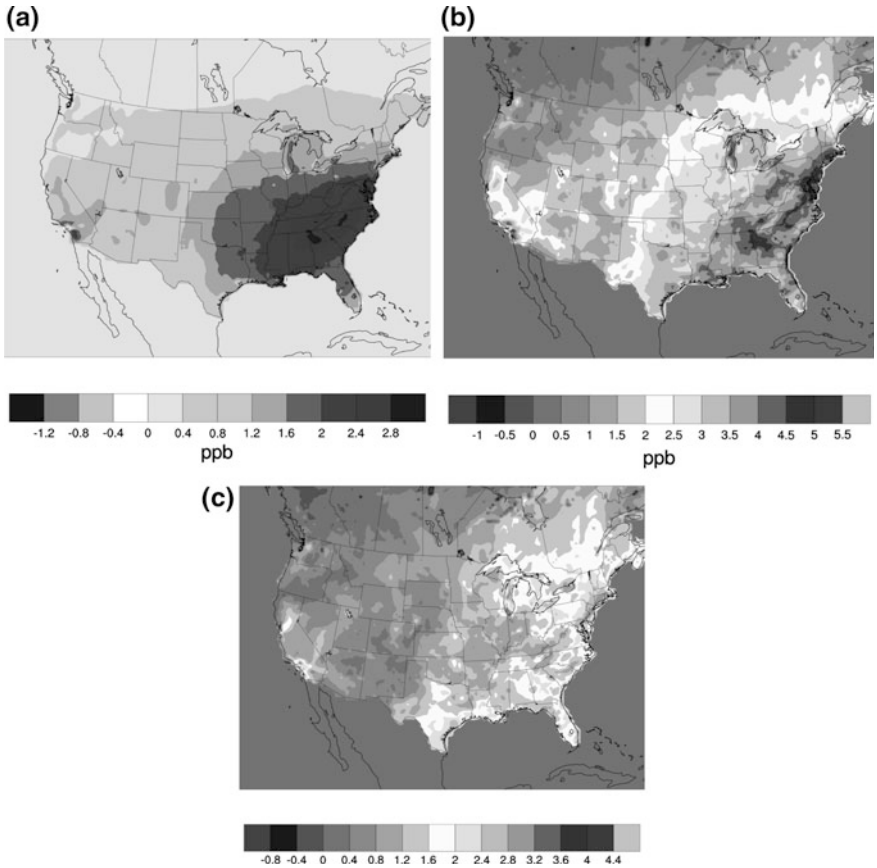

Fig. 30.2 Sensitivity of ozone metrics to a 10 % reduction in anthropogenic emissions across the United States. *Top left tile* (**a**) shows reductions in mean ozone concentrations due to widespread emission reductions. *Top right tile* (**b**) shows reductions in design values due to widespread emission reductions. *Bottom centre tile* (**c**) shows the difference between (**b**) and (**a**), or the difference between sensitivities of design values and mean ozone concentration to widespread 10 % emission reductions. Positive values in (**a**) and (**b**) indicate a reduction in ozone with emission controls

References

Pappin AJ, Hakami A (2013) Attainment vs exposure: ozone metric responses to source-specific NO_x controls using adjoint sensitivity. Environ Sci Technol 47:13519–13527

U.S. Environmental Protection Agency (EPA) (2013) Integrated science assessment for ozone and related photo-chemical oxidants. Research Triangle Park, NC

Part IV
Interactions Between Air Quality and Climate Change

Chapter 31
The Future: Earth System Modelling

P.J.H. Builtjes

Abstract Earth system modelling will be the kind of modelling that will be performed more and more. After some philosophical remarks, an overview will be given of some science questions that can only be properly treated by earth system models. The focus of these science questions will be on emissions. Concerning meteorology, the problems still existing with the atmospheric boundary layer will be presented. Data-assimilation will be addressed as an application issue, which can only be carried out more objectively with earth system models. The paper ends with ten rules for correct modelling.

31.1 Introduction

Chemical transport modelling is moving, and should be moving in the direction of earth system modelling, not only on a global, but also on a regional scale. In the context of this presentation I would like to define earth system modelling as integrated modelling in which the atmosphere, the hydrosphere, the biosphere and its crucial role by photo-synthesis, and the geosphere are taken into account, with the solar energy and the internal energy of the earth as driving forces.

Climate models including chemical transport models, so fully interactive chemistry-climate models have been extended into earth system models by including the representation of biogeochemical cycles. This means that current earth system models should contain an interactive carbon-cycle, and an interactive representation of aerosols and ozone. (Flato et al. 2013), see also the new Springer journal: Modelling Earth Systems and Environment.

P.J.H. Builtjes (✉)
Free University Berlin (FUB), Carl-Heinrich-Becker-Weg 6-10, 12165 Berlin, Germany
e-mail: peter.builtjes@tno.nl

P.J.H. Builtjes
Department of Climate, Air and Sustainability, TNO, Princetonlaan 6, 3584 CB Utrecht, The Netherlands

D.G. Steyn and N. Chaumerliac (eds.), *Air Pollution Modeling and its Application XXIV*, Springer Proceedings in Complexity,
DOI 10.1007/978-3-319-24478-5_31

The definition of earth system models that I will use here is: Interactive chemistry-climate models with representation of the biochemical cycles. Or, in ITM-wording: air pollution models with biochemical cycles, biosphere dynamics.

The biosphere dynamics/the biochemical cycle should address all biogenic and the natural/geogenic emissions. Obviously, the models should also contain all anthropogenic emissions.

Recent research indicates that the biosphere, more precisely the plants and forests, do play a much more active, and in a way intelligent role than assumed until now. The plants and forests do actively react on changes in the environment, and in response, influence their environment (Morton 2008; Benson 2012). These active interactions—as far as they are known—should be included in chemistry-climate models. Also, plants might even react on much smaller time-scales then we mostly assume. Observations show that the CO2 uptake flux of plants will react to radiation changes on the scale of minutes (Kesteren 2013).

The essential role of the plants and forests for the earth system can also be illustrated by the fact that humans do need plants and forests, but plants and forests do not need us.

The move forward from chemical transport modelling to earth system modelling will be presented first from a philosophical point of view, then focused on the science aspects and finally from the focus on application. Although I would have liked to consider the earth system as a whole including the hydrosphere and the geosphere, based on my restricted knowledge I will focus on the atmosphere.

31.2 The Philosophical Point of View

The concept that the earth can and should be seen as one interrelated "complete" system is first expressed by Schopenhauer (1844). In short: The representation is what we see, perceive, the will is the system what is behind the perceptions, and that system is an integrated one. Ideas in the same direction were earlier expressed by Spinoza (1677), the concept of God-Nature as a coherent entity.

In a more recent version, the Gaia-Hypothesis by James Lovelock (1979), also sees the earth as an integrated system. The earth exists in a form of homeostasis: the eco-system creates the atmosphere, the environment in which it feels well, and the system contains numerous, delicate feedback mechanisms to keep the balance, a kind of capacity of control. However, we should be careful to call the earth a living system. Although the earth does show an important aspect of living: not to be in a static state, a kind of equilibrium, it fails to have another important aspect: reproduction, to bring forth offspring.

31.3 Science Questions with the Focus on Emissions

A number of science questions/challenges for the future will be described here. These challenges can only be addressed in an adequate way by earth system models. This requires the development of an integrated modelling system, with special attention to the biogenic emissions.

The claim is that we know-almost- sufficient about meteorology, but not enough about emissions, anthropogenic, but most specifically concerning biogenic as well as geogenic emissions.

Emissions are the key uncertainty in chemical transport modelling, and consequently in earth system modelling; they are more crucial/uncertain than meteorology, and further development in earth system modelling should be more focused on emissions than on meteorology. We should not forget that the emissions are the driving force for atmospheric chemistry, the meteorology is "just" the transport.

The uncertainty in emissions is both in anthropogenic as well as with biogenic and geogenic emissions. Special attention needs to be given to the influence of meteorology on these emissions. This holds for both anthropogenic as well as biogenic and geogenic emissions.

Some recent examples will be given here.

A clear improvement in the modelling of SO2-concentrations over Europe could be shown by taking into account the impact of outdoor temperature on SO2-emissions- "heating degree days" (Mues et al. 2014).

A relatively small, but significant improvement is shown in the modelling of NH3 concentrations when the effect of soil water content on effective NH3-emissions is taken into account. Also the effect of the temperature influence on the NH3-emissions by stables is important.

More impact of meteorology than on anthropogenic emissions can be seen with biogenic and geogenic emissions. Recent studies of the modelling of aerosols by the VBS-approach seem to indicate that the current methods to calculate the quantity and the temperature dependence of terpene emissions are inadequate and need improvement.

Another science question is whether with the help of earth system modelling the information concerning the chemical composition of the natural atmosphere can be calculated. This seems to be possible concerning the natural O3-concentrations, most likely in the order of 15 ppb, with rather small fluctuations over the year, and maybe also for PM10, in the order of 10 ugr/m3, with remarkable small spatial gradients (Builtjes and Kranenburg 2012).

Concerning the natural concentration of NH3, there is evidence that this might be in the order of 1 ugr/m3, obviously with large spatial and temporal gradients. The current concentration of NH3 is in the order of 8 ugr/m3. This order of a factor 8 is in line with the best estimates concerning the global ammonia estimates, which show a ratio of about 10 of anthropogenic versus natural ammonia emissions (Sutton et al. 2015). In Sutton et al. (2015), the estimate is given that due to climate change and increasing emissions this factor might increase till 25 by 2100.

Proper modelling of land biosphere dynamics should take place in the context of earth system modelling. As mentioned the plants and forest are much more intelligent than we assume: they do react- although on often on a somewhat slower time scale then we as humans- on external forces, and this should be taken into account. An example is the increase in terpene emissions from forests at elevated O3-concentrations, in order to "abate" the high O3-concentrations.

The study of feedback mechanisms does also require the earth system modelling approach. Especially the interactive representation of aerosols and ozone is essential (see Raes et al. 2010).

One of the most challenging questions you might ask from earth system models are whether these models can help to determine what is the resilience- the quality or property of recovering of the original state after being pulled- of the earth system/atmosphere? The natural background of tropospheric ozone is about 15 ppb, harmfully effects for eco-systems already appear at values of about 30 ppb, which is-only- a factor 2. A recent report by the German Board for Environmental Questions, SRU (2015), advocated a yearly limit value for PM 10 of 20 ugr/m3, also a factor 2 above the natural background. Whether this factor 2 can be supported by earth system modelling would require a very complete and accurate modelling of land biosphere dynamics. Although this factor 2 might seem a very tight limit value, it should not be forgotten that harmful concentrations for human health are-too often- based on the male population around 40 years, and not on the not yet born children (Klein 2014 and references therein). The consequence of the factor 2 above the natural background would lead, in case the trace gas is not present in the natural atmosphere, to the fact that these kind of trace gases would not be allowed at all—which would have been a clever idea for CFC's anyhow.

31.4 Side Remark: The Atmospheric Boundary Layer

Although the main uncertainties in earth system modelling will be in the uncertainties in emissions, the weakest point in meteorological modelling needed for earth system modelling is the Atmospheric or Planetary Boundary Layer, ABL or PBL. I do realize that others might claim that clouds are more uncertain and more important, but I will focus here on the ABL because of its intimate relation with the biosphere.

Many studies show the problems in chemical transport modelling due to the difficulties concerning the description of the stable boundary layer, see Stern et al. (2008) as an example. Also, experimental studies as well as modelling studies including LES have been carried out recently (see Holtslag et al. 2013; Bosveld et al. 2014). These studies show that the current NWP's which are used as input to chemical transport models do include stable boundary layer descriptions which are not stable enough. However, including in these NWP's more stable descriptions

leads to lower scores in weather predictions at the larger scales of hundreds of kilometers. It seems that a lot of small scale effects, which doesn't have to be turbulent effects but might be associated with gravity waves or surface roughness changes, are still unknown and consequently not described (Holtslag 2015).

31.5 Application Issues

In fact chemical transport models and also earth system models are reasonably well advanced, which means advanced enough to be used in application studies like the analyses of abatement strategies, source apportionment and related policy questions. The problem often is to ask the good questions to the models.

For application studies it is essential that models have gone through an evaluation procedure. Recently much progress has been made in this area. It is important that models can be trusted to give the best answer possible at the moment, and it is also important that modelers can be trusted.

A very important issue is the use of data assimilation, the combination of models and observations. Chemical data assimilations is used more often, but a real breakthrough seems not to be the case yet. This is partly due to the large computer resources required, and to the rather subjective choice which parameters to use in the model to decrease the difference between model results and observations. Often, the uncertainty is given to the emissions, most likely correctly, but not really objective. In case more complete earth system models would be available, it might well be that, because such a model is more complete and contains the proper feedbacks, data assimilation will become more objective.

31.6 Ten Rules/Suggestions/Directions to Live a Happy and Fruitful Modelling Live

- Do not believe in your model—it is just a coherent collection of current knowledge (do not believe in observations either).
- Never perform modelling without combining it with observations (data assimilation) and never perform observations without data-analysis/modelling.
- Be aware that accurate emissions are more essential for good model results than accurate meteorology (emissions are the driving force for air quality, meteorology is "just" transport).
- Always take into account in air pollution modelling, on a global, a regional and also on a local scale, biogenic and natural emissions- so move towards earth system modeling.

- Improving meteorology should focus on better descriptions of the PBL, and better representation of clouds. Especially the importance of the PBL is underrated in climate modelling.
- Take the impact of meteorology into account concerning anthropogenic emissions.
- The biogenic emission modelling should not only take meteorology into account, but should move in the direction of active plant/ecosystem modelling, including the reaction of the eco-system to changes in CO2 and other trace gases like O3.
- Models should be evaluated, models should be reliable models, used by reliable modelers.
- Accept that there are limitations to modelling, there will always be an inherent uncertainty, how many big data and computer resources you might have.
- Always remember that modelling is fun, and that modelling should be carried out with the purpose to create a more healthy and better atmosphere.

Question and Answers

Questioner: Valerie Garcia
Question: Regarding your remark always combining observations with modelling, are there not some applications where care should be taken? For example "correcting" the model in areas where you have data causing inconsistent bias, which affects the ability to discern a signal in health studies.

Answer: You are right, you should always be careful which observations you want to include, or not in your data-assimilation. My remarks was meant as: always use observations, unless..etc.

Questioner: Wouter Lefebvre
Question: How can we combine: 1) Including plants/biogenic reactions/feedbacks with 2) Do not make your model overcomplicated?

Answer: Good point. We should try to include plants and feedbacks as simply as possible, but we should include them. And always try to do that in a balanced way: not to include in one part of the model system a complicated process description, and at the other hand have rather uncertain input data to that process.

Questioner: Heinke Schluenzen
Question: If emissions are more relevant than meteorology, how are good emissions data that depend on meteorology ever achieved? Should not both be well described?

Answer: Of course, both should be well described. I meant to say that we know already a lot about meteorology, and many scientist are working in that area. We know still less about emissions, and we need more effort and people for the area of the science of emissions.

Questioner: Ivanka Stajner
Question: Emissions are essential for accurate AQ-modelling. Data assimilation for air quality is limited by availability of sufficient quality and type of observations. Another issue limiting progress in chemical data assimilation are model biases such as those due to the emissions.

Answer: I agree with you. However this should not lead to not to perform chemical data assimilation, we can still learn a lot by applying it, but with care.

Questioner: S.T.Rao
Question: Isn't it obvious that emissions are more important than meteorology. You can control and abate emissions, but not meteorology

Answer: I cannot agree more

References

Bosveld F et al (2014) The third CABLS Intercomparison case study for evaluation of boundary layer models. Bound. Layer Meteo. doi:10.1007/S10546-014-9919-1
Benson W (2012) Kingdom of plants: a journey through their evolution, London
Builtjes P, Kranenburg R (2012) Modelling clean air. In: Proceedings of Air Pollution Modelling and its Application XXXII, ITM, Utrecht
Flato G et al (2013) Evaluation of climate models in Climate Change 2013, WG1 AR5, Chapter 9
Holtslag A (2015) Personal Communication
Holtslag A et al (2013) Stable atmospheric boundary layer diurnal cycles: challenges for weather and climate models. Bull Amer Meteo Soc 94:1691–1706
Klein M (2014) This changes everything, Capitalism vs. The Climate, Simon and Schuster
Lovelock J (1979) Gaia: a new look at life on earth. Oxford University Press, Oxford
Morton O (2008) Eating the sun: how plants power the plant. Garland Science, New York
Mues A et al (2014) Sensitivity of air pollution simulation with LOTOS-EUROS to the temporal distribution of emissions. ACOP 14:939–953
Raes F et al (2010) Atmospheric chemistry-climate feedbacks. J Geophys Res 115:D12121
Schopenhauer A (1844) The world as will and representation
Spinoza B (1677) Ethica
SRU-Sachverständigenrat für Umweltfragen (2015) Nitrogen, Solution strategies for a pressing Environmental Problem (in German)
Stern R et al (2008) A model-intercomparison study focussing on episodes with elevated PM 10 concentrations. Atmos Environ 42:4567–4588
Sutton MA et al (2015) Towards a climate-dependent paradigm of ammonia emission and deposition. Phil Trans R Soc B 368:20130166
van Kesteren B et al (2013) Measuring H2O and CO2 fluxes at the field scale with scintillometry. Part II-Validation and application of 1- min. flux estimates. Agric Forest Meteorol 178–179: 88–105

Chapter 32
International Workshop on Air Pollution, Climate Change, Human Health, and Extreme Weather

Sushil K. Dash, Mahendra P. Singh and S. Trivikrama Rao

Abstract Despite the substantial progress in addressing air quality problems, air pollution is still a serious concern in the developing and developed countries. There is now scientific consensus that atmospheric loading of greenhouse gases has been contributing to climate change. The 2014 IPCC report reiterated the need to address climate change on a global basis. It is also recognized that atmospheric composition can profoundly influence weather and climate directly by changing the atmospheric radiation budget or indirectly by affecting cloud formation and precipitation. Given the ever increasing computational power and ground and satellite-based observations, it is feasible to conduct observational and modeling investigations to improve our understanding of the role of aerosols on the monsoon dynamics and extreme events under changing climate. To address the above mentioned challenges, a three-day workshop was held during January 12–15, 2015 in Delhi, India bringing together scientists in air quality, weather, and climate fields from India, Europe, Japan, and North America to discuss the current state-of-science, identify research gaps, and prepare a research agenda to help improve our understanding of air quality and climate change interactions, and operationalize atmospheric modeling methods to better forecast the monsoon dynamics. Following the workshop, a small team of scientists from India, USA, Canada, and Europe met for a day to prepare an action plan for implementing recommendations of the workshop. It is envisioned that lead scientists identified from different countries will coordinate this research effort. This paper presents a summary of the recommendations made by the workshop participants and actions being taken at the national and international levels.

It is well known that population growth and unsustainable growth path followed for the last so many years have been contributing to the unprecedented increase in

S.K. Dash
Indian Institute of Technology Delhi, New Delhi, India

M.P. Singh
Ansal Institute of Technology and Management, Lucknow, India

S. Trivikrama Rao (✉)
North Carolina State University, Raleigh, NC, USA
e-mail: strao@ncsu.edu

D.G. Steyn and N. Chaumerliac (eds.), *Air Pollution Modeling and its Application XXIV*, Springer Proceedings in Complexity,
DOI 10.1007/978-3-319-24478-5_32

Greenhouse Gases and other pollutants in the atmosphere. Global warming together with the dangerous chemicals and particulate matters emitted to the air have lead to weather extremes and threat to the human health. So far as the Indian scenario is concerned, air pollution and climate change can lead to devastating impacts on the Indian monsoon dynamics and extreme weather events. Examination of archived temperature data of India indicates rise in surface air temperature (Dash et al. 2007). There are some robust signals of warming over India; especially the number of cold nights in the winter months of December to February has been decreasing (Dash and Mamgain 2011). The weather and climate of India is dominated by the summer monsoon circulation which occurs during June to September and this phenomenon contributes about 80 % of the total annual rainfall. Studies indicate that although the total rainfall has not changed much, the characteristics of rainfall has undergone changes in terms of its temporal and spatial distribution. In the recent past, the occurrence of heavy intensity rain events with short duration has shown increasing tendency (Dash et al. 2009, 2010) which is statistically significant. In India, the change in the characteristics of rainfall differs from region to region. The spatial and temporal distribution of aerosols in India might have some clue to the changes in the characteristics of rainfall observed over India.

Comparison of aerosols simulated by the models used in CMIP5 shows that none of the global models is able to simulate aerosol distribution as observed over India. Over India some studies have been successfully conducted with the use of the Abdus Salam International Centre for Theoretical Physics (ICTP) regional climate model RegCM4.1 coupled to its dust aerosol module. The atmospheric variables in RegCM4.1 are driven by six hourly lateral boundary conditions from NCEP/NCAR reanalysis data sets at 2.5° × 2.5° resolution. The surface elevation data used are obtained from the United States Geological Survey (USGS). Optimum interpolated weekly sea surface temperature gridded data at 1° × 1° resolution have been obtained from the National Oceanic and Atmospheric Administration (NOAA). The emission flux of SO_2 is fed into the model from the global emission inventory data of EDGAR (Emission Database for Global Research). In this regard more information is available in Solmon et al. (2006). The Black Carbon (BC) and Organic Carbon (OC) values are taken from the inventory described in Junker and Liousse (2008). The calculation of fossil fuel emissions of BC and OC aerosols are based on methodology followed by Cooke et al. (1999). The biomass burning emissions of BC and OC are from forest, agricultural and domestic fire sources described in Liousse et al. (1996). Das et al. (2013) have used RegCM4.1 to simulate the space-time distribution of dust aerosols and associated direct radiative forcing due to mineral dust over the Indian subcontinent for the year 2009. Results show that this model captures the seasonality in dust transport appreciably well when compared with remote sensing and AERONET datasets. However, a low bias in coarse mode in model-simulated dust optical depth (τ_d) is observed, because the model does not account for the local dust sources. Dust is transported across the Indo-Gangetic Basin and accumulated at 700–850 hPa altitude against the Himalayan foothills during the pre-monsoon season, of which >80 % particles are in fine mode. Enhanced dust loading ($\tau_d > 0.5$) over the oceans surrounding the

subcontinent in the monsoon season, previously reported by satellite observations, further validates the capability of RegCM4.1 in examining long-range dust transport. Further, RegCM4.1 has been utilized to examine (Das et al. 2014a) the dynamic impacts of large aerosol radiative forcing on the atmospheric circulation in India during the contrasting monsoon (Jun–Sep) seasons of 2009 and 2010. During the above normal monsoon of 2010, a larger dust load has been simulated as compared to the weaker monsoon in 2009. This can be explained by the stronger low level winds in 2010 as compared to that in 2009. Results show that RegCM4.1 is sensitive to the anthropogenic aerosol load in terms of the radiative effect and hence the simulated surface temperature. Integrating RegCM4.1 during the period 2001–2010, Das et al. (2014b) have shown that there is decrease in the surface (2 m) air temperature over the Indo Gangetic Basin and east coast of India by more than 0.2 °C due to dimming effect of anthropogenic aerosols. Based on the results of this study, it may be hypothesised that the aerosol induced cooling leads to an increase in surface pressure over the region which eventually inhibits moisture transport from the Bay of Bengal and Arabian Sea towards the Indian landmass. In turn there may be enhancement in precipitation over the Bay of Bengal and some parts of the east coast of India. These results demonstrate the direct radiative impacts of anthropogenic aerosols on the Indian monsoon circulation and encourage for future studies combining the dynamical and microphysical impacts.

Realising the importance of such studies in India, an international workshop entitled "Assessing the Impacts of Aerosols and Changing Climate on Monsoon and Extreme Events" was held in Ansal University, Gurgaon during January 12–15, 2015. This workshop was supported by the Centre for Atmospheric Sciences, Indian Institute of Technology (IIT) Delhi and was sponsored by the Department of Science and Technology (DST) and Ministry of Earth Sciences (MoES), Government of India. The objective of this workshop was to bring together some key scientists and stakeholders from India and other countries to discuss and develop a research strategy for assessing the impacts of aerosols and climate change on monsoon dynamics, precipitation patterns, and extreme events. The deliberations were categorised under the following broad themes relevant to India.

1. Aerosols and Monsoon Dynamics
2. Weather Extremes in Changing Climate
3. Impact of Air Quality and Climate Change on Human Health
4. Climate Geoengineering

There were 31 presentations by eminent scientists from USA, Canada, Europe, Japan and India. In addition to discussions after each session, there were separate panel discussions on each of the four themes where the respective chairmen summarised the important scientific findings from each theme area and initiated discussion amongst the scientists. The workshop provided plenty of opportunities for interaction among participants. Following the panel discussions, a small team of scientists from India and abroad drafted theme wise recommendations which were presented by four scientists for further discussion and modifications. Finally, a set of four recommendations on thematic areas Aerosols and monsoon dynamics,

Weather extremes in changing climate, Impact of air quality and climate change on human health and Climate geo-engineering were approved by the participants. On the last day of the workshop, the recommendations were deliberated upon by a select group of experts from India and abroad for the following action plan:

It was realised that adequate emphasis has been given in India on the research related to climate science and climate change. The Government of India agencies such as the DST and MoES (including IMD) are successfully promoting and carrying out operational activities as well as research on the topics of discussion in the workshop such as Aerosols, Monsoon, Extremes, Air quality and Human health. However, due to the global changes occurring today, there are a number of important issues which cannot be attended to by the existing Centres of excellence in the field of weather and climate. There is necessity of a Centre of excellence which will exclusively deal with the matters related to Aerosols, Climate change, Extremes and Human health in a holistic manner.

The experts felt that the proposed Centre should be established in Public-Private-Partnership (PPP) mode where international scientists can also join hands in a collaborative manner. The Department of Science and Technology, the Ministry of Earth Sciences, Government of India will be approached to provide initial funding based on which private companies from India and abroad with keen interest on climate science and environment will be requested to fund the Centre. This proposed Centre will primarily encourage scientists from India and abroad to work under its umbrella in a collaborative manner on front-end climate research having societal benefits.

To start with, the proposed Centre will concentrate on the following two topics:

1. Understanding monsoon-aerosol interaction in the context of extremes.
2. Impact of climate change on public health.

In order to realise the above goals, it is essential to develop a modelling system with the inclusion of aerosols which can simulate rainfall distribution very close to the actual observed distribution. Simultaneously, it is required to conduct nation-wide co-ordinated experiments in order to relate weather extremes to health related episodes.

References

Cooke WF, Liousse C, Cachier H, Feichter J (1999) Construction of a 1 × 1 fossil fuel emission data set for carbonaceous aerosol and implementation and radiative impact in the ECHAM4 model. J Geophys Res 104(D18):22137–22162. doi:10.1029/1999JD900187

Das S, Dey S, Dash SK (2014a) Impacts of aerosols on dynamics of Indian summer monsoon using a regional climate model. Clim Dyn 1–13 doi:10.1007/s00382-014-2284-4

Das S, Dey S, Dash SK (2014b) Direct radiative effects of anthropogenic aerosols on Indian summer monsoon circulation. Theo Appl Clim. doi:10.1007/s00704-015-1444-8

Das S, Dey S, Dash SK, Basil G (2013) Examining mineral dust transport over the Indian subcontinent using the regional climate model RegCM4.1. Atmos Res 134:64–76

Dash SK, Mamgain Ashu (2011) Changes in the frequency of different categories of temperature extremes in India. J Appl Meteor Climatol 50:1842–1858. doi:10.1175/2011JAMC2687.1

Dash SK, Jenamani RK, Kalsi SR, Panda SK (2007) Some evidence of climate change in twentieth-century India. Clim Change 85:299–321

Dash SK, Kulkarni MA, Mohanty UC, Prasad K (2009) Changes in the characteristics of rain events in India. J Geophys Res 114:D10109. doi:10.1029/2008JD010572

Dash SK, Nair AA, Kulkarni MA, Mohanty UC (2010) Changes in the long and short spells of different rain intensities in India. Theo Appl Clim. doi:10.1007/s00704-011-0416-x

Junker C, Liousse C (2008) A global emission inventory of carbonaceous aerosol from historic records of fossil fuel and biofuel consumption for the period 1860–1997. Atmos Chem Phys 8:1195–1207. doi:10.5194/acp-8-1195-2008

Liousse C, Penner JE, Chuang C, Walton JJ, Eddleman H, Cachier H (1996) A global three-dimensional model study of carbonaceous aerosols. J Geophys Res 101 (D14):19411–19432. doi:10.1029/95JD03426

Solmon F, Giorgi F, Liousse C (2006) Aerosol modelling for regional climate studies: application to anthropogenic particles and evaluation over a European/African domain. Tellus B 58 (1):51–72

Chapter 33
Future Climate and Air Quality of the Brussels Capital Region for the 2050s Under A1B Scenario

A.W. Delcloo, R. De Troch, O. Giot, R. Hamdi, A. Deckmyn and P. Termonia

Abstract Within the framework of the ACCEPTED project (an Assessment of Changing Conditions, Environmental Policies, Time-activities, Exposure and Disease), a high-resolution urban dynamical downscaling technique has been applied for the Brussels Capital Region. First, regional climate simulations were performed with a new version of the limited-area model of the ARPEGE-IFS system running at 4-km resolution called ALARO coupled with the Town Energy Balance scheme (TEB). Then, to further downscale the regional climate projections to an urban scale, at 1 km resolution, a stand-alone surface scheme was employed in offline mode. Downscaling simulations of present and future urban climate of the Brussels areas are conducted. The downscaling strategy was first evaluated for a 10-years period [2001–2010] using ERA-INTERIM re-analysis data. In a next step, a downscaling simulation for the period 2046−2055 under the A1B scenario was performed. Results from our simulations indicate that while both urban and rural areas warm substantially for the 2050s horizon (1.5 °C), climate change will have a neutral impact on annual mean urban heat island (UHI) intensity. The most important increase is noted for the nocturnal UHI during the winter (+15 %) and the most important decrease is noted for the daytime UHI during the summer (−43 %). However, the model projects an increase of stable situations in the lower atmosphere during winter which may tend to keep pollutants concentrated over urban areas, with the associated health effects. Two approaches have been used to examine meteorological conditions that are unfavorable for the dispersion of air pollution under climate change conditions: (i) a transport index, based on the wind

A.W. Delcloo (✉) · R. De Troch · O. Giot · R. Hamdi · A. Deckmyn · P. Termonia
Royal Meteorological Institute of Belgium, Brussels, Belgium
e-mail: Andy.Delcloo@meteo.be

R. De Troch · P. Termonia
Department of Physics and Astronomy, Ghent University, Ghent, Belgium

O. Giot
Plant and Vegetation Ecology (PLECO), University of Antwerp, Antwerp, Belgium

D.G. Steyn and N. Chaumerliac (eds.), *Air Pollution Modeling and its Application XXIV*, Springer Proceedings in Complexity,
DOI 10.1007/978-3-319-24478-5_33

speed and Brunt-Väisälä frequency, that characterizes a typical length of horizontal and vertical transport, (ii) state-of-the-art chemistry transport models CHIMERE coupled to the 4 km regional climate simulations. The results from both approaches will be compared to assess future concentrations at the urban scale.

33.1 Introduction

For the first time ever, the majority of the world's population lives in a city and this proportion will continue to grow in the future. By 2050, 7 out of 10 people will live in a city. The urban climate is therefore becoming the dominant environment for most of humanity. Within the framework of the ACCEPTED project (an Assessment of Changing Conditions, Environmental Policies, Time-activities, Exposure and Disease), an observational and modeling approach is set up to improve our understanding of future exposure situations and their impact on health to a mid-century horizon 2050s accounting for the effects of a changing urban climate. With applications in several large European cities, including Brussels, the project will study the impact of several alternative adaptation scenarios on urban air-quality and human health. This study focuses on the first part of the ACCEPTED project where simulations of present and future urban climate over the Brussels Capital Region will be conducted and used as input for the regional air-quality model CHIMERE. In this project, the high-resolution urban dynamical downscaling technique presented in Hamdi et al. (2014) will be applied: (i) on the 10-years period 2001–2010, considered as the warmest period on record since modern meteorological records began around the year 1850, (ii) on the period 2046–2055, which is more relevant for local policy makers who are stakeholders for the ACCEPTED project.

33.2 Results and Discussion

33.2.1 Urban Micro-Climate

Results from our simulations indicate that while Brussels Capital Region warm substantially for the 2050s horizon (1.6°C), climate change will have a neutral impact on annual mean urban heat island (UHI) intensity. The biggest and statistically significant change of nocturnal (daytime) UHI is noted during winter (summer) season with an increase (decrease) of +0.2°C (−0.1°C). During summer, the decrease in daytime UHI is directly connected to soil drying over rural areas, while the increase in nocturnal UHI during the winter can be explained by the projected decrease of wind speed.

33.2.2 Urban Air Quality

33.2.2.1 CHIMERE

The chemical transport model CHIMERE (Vautard et al. 2001) has been coupled to the ARPEGE/ALARO NWP model at a spatial resolution of 7 km × 7 km (Delcloo et al. 2014). For the air quality simulations we will ingest the high resolution NWP data from ALARO, using the SURFEX- and TEB (Town Energy Balance) scheme, into the chemical transport model

CHIMERE (Delcloo et al. 2014).

The different data sets we consider are the following:

- ERA-INTERIM driven run (2005–2008)
- Historical control run (1990–1999)
- A1B scenario run (2046–2055)

For all the simulations, the same emissions from TNO/GEMS (2004) are used (Visschedijck et al. 2007). This gives us the opportunity to verify if the changes in meteorological conditions will actually lead to a change in observed PM10 and ozone pattern, especially for the cities.

To validate the skills of our model setup, the simulations for the time period 2005–2008 have been validated, using ERA-INTERIM data for the downscaling. Figure 33.1 shows the day-to-day variability in averaged daily PM10 concentrations, observed at the Uccle station for this time period under consideration. The observational data (PM10 and O_3) are obtained by IRCELINE. The figure shows a good correlation and low bias between the observations and modelled PM10 concentrations. This indicates that our model strategy succeeds to correctly reproduce observed PM10 concentrations for Uccle.

For the climate simulations we have compared the averaged PM10 concentrations calculated from 10 years of modelled data for the time period 1990–1999 to the modelled averaged PM10 concentrations derived from the A1B simulations, covering the time period 2046–2055.

This relative difference shows a general increase of 3.5 % in modelled PM10 concentrations for the city of Brussels. Since the same emissions have been used for both time periods under consideration, it is interesting to verify what could be the cause of this increase.

Therefore another proxy for identifying in an objective way stable meteorological situations which are not favorable for the dispersion of pollutants will be used, i.e. the transport index.

33.2.2.2 Transport Length

The transport index gives a measure of the horizontal and vertical transport of nonreactive pollutants in stable atmospheric conditions and has been proposed and

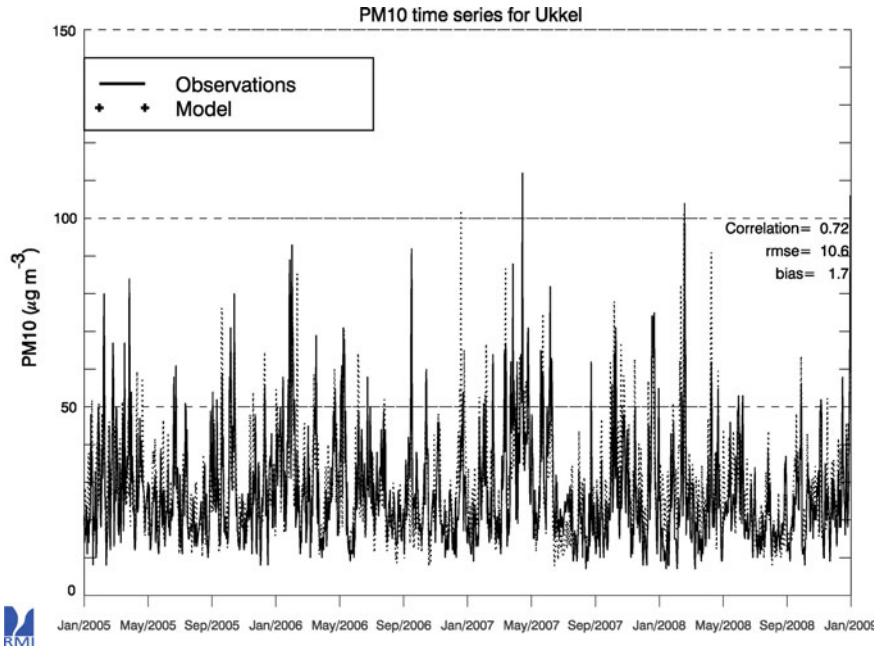

Fig. 33.1 Time series of observed- and modelled averaged daily particulate matter (PM10) concentrations for the time period 01/01/2005–31/12/2008 for the station of Ukkel

tested by Termonia and Quinet (2004). It gives a characteristic length scale l which is the ratio of the mean horizontal wind speed and the Brunt-Väisälä frequency.

In this way low values for this index l (smaller than 100 m) in the lower part of the boundary layer during an extended time span of 12 h, correspond to calm situations and a stable atmosphere and thus indicate unfavorable conditions for the dispersion of air pollutants. The index is calculated for both historical control and future scenarios for the grid point of Uccle.

When we compare the number of exceedances of this threshold value (100 m) between both simulations an increase of about 27 % has been observed, confirming that more stable situations will occur in the future. Also calculations have been made for the stations of Hasselt and Houtem where we found respectively an increase of about 28.3 and 26.2 %.

From a policy maker's view, it is interesting to know the number of times the EU threshold value for daily mean particulate matter (PM10) following the air quality directive 2008/EC/50 may exceed 50 micrograms per cubic metre (μg/m3) in the current climate simulations compared to the A1B future simulations.

Therefore a selection has been made of three locations from the inner domain to investigate the time series of daily mean PM10 concentrations for those stations

Table 33.1 Changes in exceedances in transport length (%) compared with changes in exceedances (%) for the daily averaged EU-threshold value for PM10 concentrations (50 µg/m^3) at three stations

City	Change in exceedances (%) transport length < 100 m	Change in exceedances (%) (PM10 > 50 µg/m^3)
Ukkel	26.8	17.3
Houtem	26.2	28.9
Hasselt	28.3	20.6

against both scenarios. The stations are representative for a sub-urban (Ukkel, Hasselt) and rural (Houtem) station type. A general increase in exceedance of this EU threshold value for daily mean PM10 concentrations is shown in Table 33.1 and varies between 17 and 29 %.

33.3 Conclusion

The results, obtained for daily mean PM10 concentrations, show a clear increase in modelled PM10 concentrations related to changes in meteorological conditions. More stable situations are observed within the future climate simulations. Since stable meteorological situations during winter are the main cause for the initiation of pollution episodes, it will be important for policy makers to make sure that the reduction in anthropogenic emissions will continue.

Acknowledgments The authors would like to thank IRCELINE for providing the ozone and PM10 data.

References

Delcloo A, Hamdi R, Deckmyn A, De Backer H, Forêt G, Termonia P, Van Langenhove H (2014) A one year evaluation of the CTM CHIMERE using SURFEX/TEB within the high resolution NWP models ALARO and ALADIN for Belgium, air pollution modeling and its application XXIII. NATO Sci Peace Secur Ser C: Environ Secur 495–498. doi: 10.1007/978-3-319-04379-1_81

Hamdi R, Van de Vyver H, De Troch R, Termonia P (2014) Assessment of three dynamical urban climate downscaling methods: Brussels's future urban heat island under an A1B emission scenario. Int J Climatol 34(4):978–999. doi: 10.1002/joc.3734

Termonia P, Quinet A (2004) A new transport index for predicting episodes of extreme air pollution. JAM 43:631–640. doi: 10.1175/1520-0450(2004)043<0631:ANTIFP>2.0.CO

Vautard R, Beekmann M, Roux J, Gombert D (2001) Validation of a deterministic forecasting system for the ozone concentrations over the Paris area. Atmos Environ 35:2449–2461

Visschedijk AJH, Zandveld PYJ, Denier van der Gon HAC (2007) A high resolution gridded European database for the EU integrate project GEMS, TNO-report 2007-A-R0233/B

Chapter 34
Impact of Climate Change on the Production and Transport of Sea Salt Aerosol on European Seas

Joana Soares, Mikhail Sofiev, Camilla Geels, Jesper H. Christensen, Camilla Anderson, Joakim Lagner and Svetlana Tsyro

Abstract The impact of climate change on sea salt concentration over the European seas is studied using four CTMs driven by the same global projection of future climate over the control (1990–2009) and future (2040–2059) period. This study shows how model formulation for sea salt production dependency on water surface temperature and salinity can influence surface concentrations estimations. According to this study, sea salt concentration is overall increasing between control and future periods due to expected increase of water temperature and more frequent local storms, mostly visible over the Mediterranean and Black Seas.

34.1 Introduction

Sea salt aerosol (SSA) is a dominant aerosol type over oceans and affects the Earth radiation budget, atmospheric chemistry and cloud processes. The impact of climate change on SSA over the European seas is studied using three offline regional chemical transport models (EMEP MSC-W, MATCH and SILAM) and one hemispheric (DEHM) driven by the same global projection of future climate over the control (1990–2009) and future (2040–2059) period is show in the study.

J. Soares (✉) · M. Sofiev
Finnish Meteorological Institute, Helsinki, Finland
e-mail: joana.soares@fmi.fi

C. Geels · J.H. Christensen
Swedish Meteorological and Hydrological Institute, Norrköping, Sweden

C. Anderson · J. Lagner
Department of Environmental Science, Aarhus University, Roskilde, Denmark

S. Tsyro
EMEP MSC-W, Norwegian Meteorological Institute, Oslo, Norway

D.G. Steyn and N. Chaumerliac (eds.), *Air Pollution Modeling and its Application XXIV*, Springer Proceedings in Complexity,
DOI 10.1007/978-3-319-24478-5_34

34.2 Methodology

This study uses the same basic model chain as in the study of Langner et al. (2012) and Simpson et al. (2014). We focus on the comparison of SSA simulations from three European-scale CTMs: EMEP MSC-W, MATCH and SILAM, and one hemispheric CTM, DEHM. The horizontal grid for these CTMs was identical to the RCA3 grid, while the vertical discretization was left free to each model.

34.2.1 Climate-Meteorology

Results of the global-scale ECHAM5/MPIOM general circulation model (Roeckner et al. 2006), driven by emissions from the SRES A1B scenario (Nakicenovic 2000), were downscaled over Europe with the RCA3 (Samuelsson et al. 2011; Kjellstrom et al. 2011). The global ECHAM5/MPIOM version used is defined in spectral grid with truncation T63, which at mid-latitudes corresponds to a horizontal resolution of ca. 140 km (ca. 140 × 210 km^2). The horizontal resolution of RCA3 was 0.44° × 0.44° (ca. 50 × 50 km^2) on a rotated latitude-longitude grid, and data were provided with 6-hourly resolution.

34.2.2 Chemical Boundary Conditions

Lateral and top boundaries were provided by the hemispheric DEHM model, which was also driven by the global ECHAM5-r3 meteorology. The boundary values taken from DEHM were updated every 6 h and interpolated from the DEHM resolution to the respective geometry of each regional CTM.

34.2.3 SSA Production

The models used in this study have been introduced in our preceding multi-model study: Langner et al. (2012) and Simpson et al. (2014). Production of SSA is mainly based on two parameterization schemes describing the bubble-mediated sea spray production of fine fraction based on Mårtensson et al. (2003), while for the larger sizes the Monahan et al. (1986), with both including a dependency on wind speed ($U^{3.41}$). The main difference between the models is the source dependence on water surface temperature and salinity. DEHM, MATCH (Foltescu et al. 2005) and SILAM (Sofiev et al. 2011) depend both on salinity and temperature; EMEP on temperature (Tsyro et al. 2011).

34.3 Results and Discussion

Typically, higher SSA concentrations are at open sea followed by the Mediterranean (Fig. 34.1, left). This study shows that concentration can substantially differ from model to model; the differences are manly driven by the SSA formation dependence on temperature/salinity. SSA concentration increase between control and future periods is expected due to estimated increase of water temperature in southern latitudes, and more frequent local storms: e.g. North of Iceland and Gulf of Bothnia (Fig. 34.1, right). The concentrations in the Mediterranean and Black Seas correlate very well with the increase of seawater temperature expected and also the wind dependency. SILAM seems to be the most sensitive model to the future climate, in particular where the temperature increase is higher—crucial for particle formation. EMEP, on the other hand, seems less sensitive. DEHM show difficulties on resolving the inner seas due to the coarser resolution. Trend analysis (Fig. 34.2) indicates that regional patterns are commonly paired: DEHM and EMEP versus MATCH and SILAM, showing some disagreement in terms of future-climate signal. Nevertheless, there is a clearer positive trend for the Mediterranean and Black Seas, closely related with increase of water surface temperature. Future climate suggests a large increase on the Baltic Sea's surface water temperature but the low salinity levels will not allow massive production of SSA particles, not reflecting on mass concentration levels.

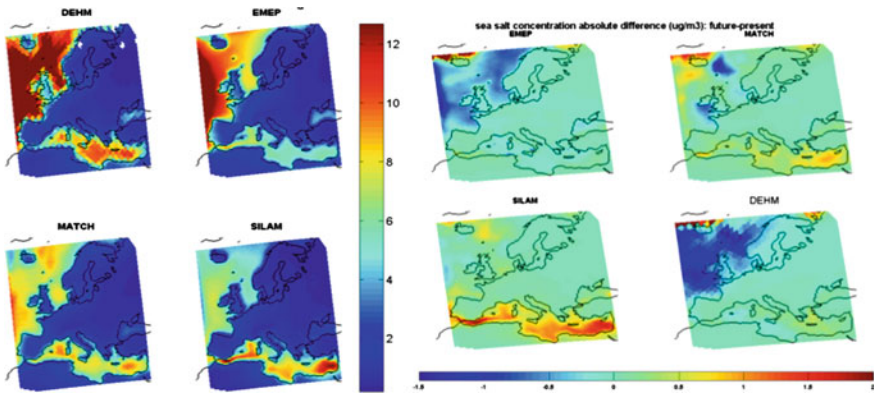

Fig. 34.1 Sea salt concentration (μg/m^3): average present period (*left*); absolute difference between present and future

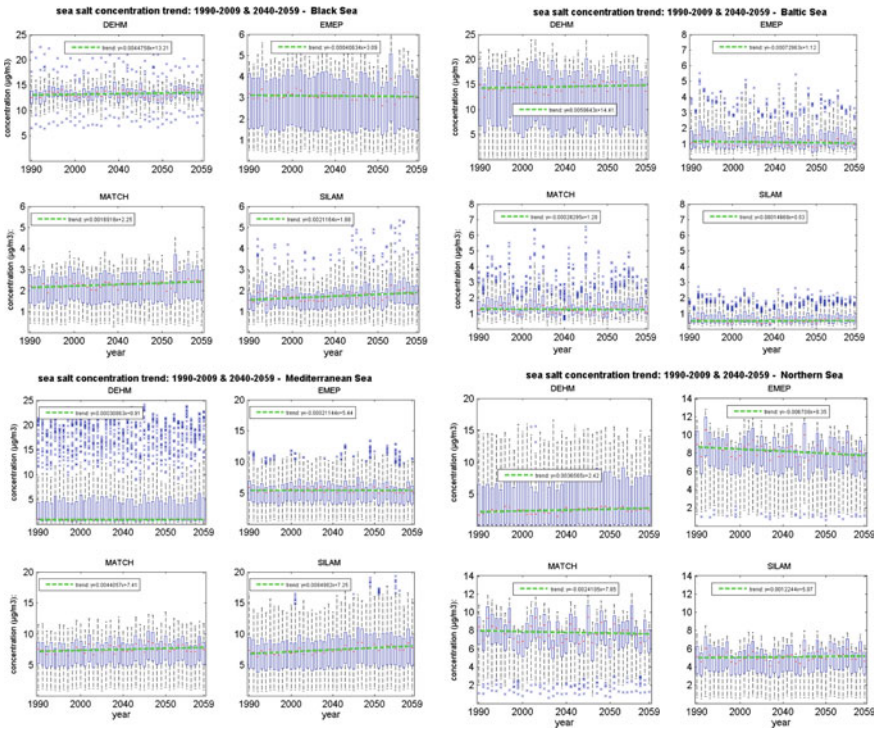

Fig. 34.2 Sea salt concentration trend ($\mu g/m^3$)

34.4 Conclusion

This study shows how important it is the dependence of sea salt production on temperature and salinity on model formulation. Increases in seawater temperatures between 1990 and 2059 drive a preferential production of sea salt aerosol, which are most visible over the Mediterranean and Black Seas.

Acknowledgments This study was supported by the Nordic Council of Ministers (EnsCLIM project no: KoL-1004).

Questions and Answers

Questioner: Paul Makar
Question: The flux formulae change between the models, but do the models use the fluxes in the same way in their formulation of the rates of change of sea salt mass? For example, do all of the models use the flux as a boundary condition on the diffusion equation?

If so, do they all have the same predicted (1) vertical resolution, (2) diffusivity coefficients, and (3) atmospheric stability?

Answer: All the models use the flux as a boundary condition on the diffusion equation. They do have different vertical resolution that may be significant for the mixing, deposition, etc. The atmospheric stability prediction is based on NWP model and turbulent diffusivity coefficients, with the latter having some differences in computation from model to model. The approach of taking multiple models is intentional, so we are aware of the differences in the description of physical processes in the different models and why we suggested the ensemble approach: a single model might be insufficient to represent, as correctly as possible, the state of the atmosphere and the sea salt aerosol flux.

Questioner: Tony Dore
Question: Have you been performing any model-measurement comparison?

Answer: Very little was show in the oral presentation about the model-measurement comparison. Nevertheless this was done with EMEP data considering sea salt concentration and deposition data available at the EBAS database (ebas.nilu.no). The comparison is done by: (i) considering only the station that are representative (75 % of the hourly data is available in an annual basis); (ii) observation and model data monthly averages are compared.

References

Foltescu VL, Pryor SC, Bennet C (2005) Sea salt generation, dispersion and removal on the regional scale. Atmos Environ 39:2123–2133

Kjellström E, Nikulin G, Hansson U, Strandberg G, Ullerstig A (2011) 21st century changes in the European climate: uncertainties derived from an ensemble of regional climate model simulations, Tellus

Langner J, Engardt M, Baklanov A, Christensen JH, Gauss M, Geels C, Hedegaard GB, Nuterman R, Simpson D, Soares J, Sofiev M, Wind P, Zakey A (2012) A multi-model study of impacts of climate change on surface ozone in Europe. Atmos Chem Phys 12:10423–10440. doi:10.5194/acp-12-10423-2012

Monahan EC, Spiel DE, Davidson KL (1986) A model of marine aerosol generation via whitecaps and wave disruption. In: Monahan EC, MacNiochaill G (eds) Oceanic whitecaps, D. Reidel, Norwell, pp 167–193

Mårtensson EM, Nilsson ED, de Leeuw G, Cohen LH, Hansson H-C (2003) Laboratory simulations and parameterization of the primary marine aerosol production. J Geophys Res 108 (D9):4297. doi:10.1029/2002JD002263

Nakićenović N (2000) Global greenhouse gas emissions scenarios: integrated modeling approaches. Tech Forecast Soc Change 63:105–109

Roeckner E, Brokopf R, Esch M, Giorgetta M, Hagemann S, Kornblueh L, Manzini E, Schlese U, Schulzweida U (2006) Sensitivity of simulated climate to horizontal and vertical resolution in the ECHAM5 atmosphere model. J Clim 19:3771–3791. doi:10.1175/JCLI3824.1

Samuelsson P, Jones CG, Willén U, Ullerstig A, Gollvik S, Hansson U, Jansson C, Kjellström E, Nikulin G, Wyser K (2011) The rossby centre regional climate model RCA3: model description and performance. Tellus A 63:4–23. doi: 10.111/j.1600-0870.2010.00478.x

Simpson D, Andersson C, Christensen JH, Engardt M, Geels C, Nyiri A, Posch M, Soares J, Sofiev M, Wind P, Langner J (2014) Impacts of climate and emission changes on nitrogen deposition in Europe: a multi-model study. Atmos Chem Phys 14:6995–7017. doi:10.5194/acp-14-6995-2014

Sofiev M, Soares J, Prank M, de Leeuw G, Kukkonen J (2011) A regional-to-global model of emission and transport of sea salt particles in the atmosphere. J Geophys Res 116:D21302. doi:10.1029/2010JD014713

Tsyro S, Aas W, Soares J, Sofiev M, Berge H, Spindler G (2011) Modelling of sea salt concentrations over Europe: key uncertainties and comparison with observations. Atmos Chem Phys 11:10367–10388. doi:10.5194/acp-11-10367-2011

Chapter 35
European Air Quality Simulations in the Context of IMPACT2C, Focus on Aerosol Concentrations

G. Lacressonnière, L. Watson, M. Engardt, M. Gauss, C. Andersson, M. Beekmann, A. Colette, G. Foret, B. Josse, V. Marécal, A. Nyiri, G. Siour, S. Sobolowski and R. Vautard

Abstract In the context of the IMPACT2C project, one of the objectives is to estimate the pan-European impacts of a global 2-degree increase in temperature on human health, including change in air pollution. Climate change will affect atmospheric dispersion, biogenic and fire emissions, chemistry, and the frequency of extreme weather situations such as heat waves. These changes will have an impact on air quality with subsequent health consequences that must be evaluated. In order to evaluate how climate change will potentially affect the efficiency of emission abatement policies and how this will potentially affect health, several simulations have been conducted using different chemistry-transport models (CTMs): CHIMERE (IPSL), EMEP MSC-W (MET.NO), MATCH (SMHI), and MOCAGE (Météo-France). The use of four CTMs provide an estimate of the uncertainty in

G. Lacressonnière (✉) · M. Beekmann · G. Foret · G. Siour
Laboratoire Interuniversitaire des Systèmes Atmosphériques (LISA), Université Paris Est et 7, CNRS, Créteil, France
e-mail: gwendoline.lacressonniere@lisa.u-pec.fr

M. Beekmann
e-mail: matthias.beekmann@lisa.u-pec.fr

L. Watson · B. Josse · V. Marécal
CNRM-GAME, Météo France/CNRS, Toulouse, France

M. Engardt · C. Andersson
SMHI, Norrköpping, Sweden

M. Gauss · A. Nyiri
EMEP MSC-W, Norwegian Meteorological Institute, Oslo, Norway

A. Colette
INERIS, Verneuil-en-Halatte, France

S. Sobolowski
UNI Research, The Bjerknes Centre for Climate Research, Bergen, Norway

R. Vautard
Laboratoire des Sciences du Climat et de l'Environnement, LSCE, CEA-CNRS-UVSQ, Gif-sur-Yvette, France

D.G. Steyn and N. Chaumerliac (eds.), *Air Pollution Modeling and its Application XXIV*, Springer Proceedings in Complexity,
DOI 10.1007/978-3-319-24478-5_35

projections with the spread between models and driving meteorological data. To compare with future climate, the first step is to perform air quality simulations for the current climate: HINDCAST (CTMs forced by reanalysis boundary forcing ERA Interim) and HISTORICAL (global climate model boundary forcings). The comparisons between HINDCAST and HISTORICAL simulations allow to evaluate how global climate models modify climate hindcasts by boundary conditions inputs. In this study, we focus on particulate matter (PM10 and PM2.5) and its chemical composition. We first analyze whether the chemical composition of PM is affected by the use of climate models. We then investigate the contributions of the changes in meteorological parameters (frequency of precipitation, 2-m temperature, etc.) as well as emissions and depositions processes on surface PM. These results are the basis for analyzing future 2° warming climates. Under the RCP4.5 scenario, simulations have been performed in order to calculate the effect of climate change on emission reduction scenarios, the climate penalty, as well as the effect of emission mitigation. This analysis also provide uncertainties associated to future AQ projections.

35.1 Methodology

35.1.1 Participating Models

The CTMs involved in this study are CHIMERE (Bessagnet et al. 2004; Menut et al. 2013), EMEP (Berge and Jakobsen 1998; Simpson et al. 2012), MATCH (Robertson et al. 1999; Andersson et al. 2007) and MOCAGE (Peuch et al. 1999; Josse et al. 2004). The characteristics of the CTMs are presented in Table 35.1.

35.1.2 Regional Air Quality Simulations

For the current climate, two types of simulations (Table 35.2) have been performed: HINDCAST (CTMs forced by RCM simulations with a common reanalysis boundary forcing) and HISTORICAL (global climate model forcing of RCMs).

Table 35.1 Description of the model chains used, from GCM simulations to regional CTMs

Institute	CTM	Driving GCM	RCM used for downscaling	Chemical boundary conditions
CNS-IPSL	CHIMERE	IPSL-CM5A-MR	WRF	LMDz-INCA
MET.NO	EMEP	NorESM	WRF	LMDz-INCA
SMHI	MATCH	EC-EARTH	RCA4	LMDz_INCA
Météo-France	MOCAGE	ARPEGE-Climat	N/A	MOCAGE (global)

Table 35.2 Description of the simulations performed for the current (HINDCAST, HISTORICAL)

Name	Climate	Boundary conditions	Emissions
HINDCAST	1989–2008	2005	ECLIPSE V4a 2005 CLE[a]
HISTORICAL	1971–2000	2005	ECLIPSE v4a 2005 CLE[a]

[a]Current legislation emissions

The ECLIPSE anthropogenic precursor emissions were used in all four models [http://eclipse.nilu.no/, Klimont et al. (2015)]. This inventory has a spatial resolution compatible with our models, and we have chosen data representative of the year 2005. These data comprise the gridded annual sums of the emissions of black carbon, CO, NH3, nonmethane hydrocarbons, NOx, organic carbon and SOx.

35.2 Results

35.2.1 Statistics of PM and Secondary Inorganic Aerosols

In order to evaluate the models, EMEP and AirBase databases have been used and compared to our HINDCAST simulations. We focus on particulate matter with a diameter smaller than 10 µm (PM10) and 2.5 µm (PM2.5). The measurements of nitrate, ammonia and sulphate from EMEP will serve for the analyses of particulate matter.

A common underestimation of PM10 is observed for the MOCAGE, EMEP and MATCH models. For CHIMERE, PM10 levels are slightly overestimated from October to December and underestimated for the rest of the year. However, the seasonal cycles are well reproduced by the CHIMERE, EMEP and MATCH models. The statistical scores of PM10 and PM2.5 display satisfactory performances compared to other studies.

35.2.2 Differences Between HINDCAST and HISTORICAL Simulations

Figure 35.1 shows the differences of PM2.5 between HISTORICAL and HINDCAST. In winter, PM2.5 levels simulated by CHIMERE are lower over western Europe in HISTORICAL. Changes in MATCH are smaller over the continental Europe while the decreases or increases are in the range of 30 % in MOCAGE and EMEP. In summer, the CHIMERE, MOCAGE and EMEP models display higher PM2.5 in HISTORICAL over central part of Europe up to 35 %.

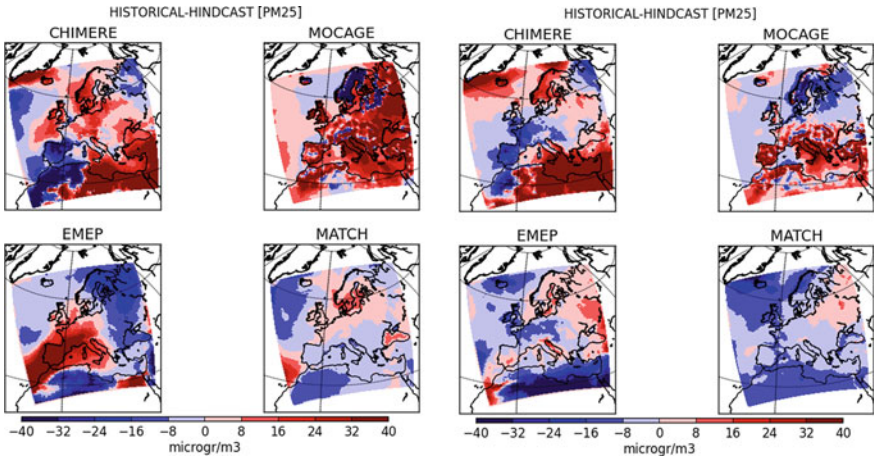

Fig. 35.1 Differences in average PM2.5 concentrations between HISTORICAL and HINDCAST simulated by CHIMERE, MOCAGE, EMEP and MATCH for summer (*left*) and winter (*right*) seasons

We compared the chemical composition of aerosols in PM10 over the continental Europe (North Africa excluded and sea surface excluded), between HINDCAST and HISTORICAL simulations for the CHIMERE, EMEP and MATCH models.

Among the secondary inorganic aerosols, sulfate makes up the largest proportion in CHIMERE (up to 22.5 %) and MATCH (up to 21.3 %) by comparison to nitrate and ammonium, while the fractions of sulfate and nitrate have a similar importance (up to 20.4 %) in EMEP. On average, the comparisons in chemical composition display a similar distribution of aerosols between the two simulations. We show that the use of meteorological forcing from a regional climate model doesn't affect the chemical composition of PM.

Our results allow to conclude that the differences in summer primary components, simulated in the south of the domain, are dominated by the changes in dust levels, due to changes in precipitation, relative humidity, as well as wind speed and direction. While the differences over northwestern Europe are due to the sea salt levels, as wind speed and direction change. In winter season, we find that changes in PBL height, precipitation and wind speed contribute to explain the differences in secondary aerosols. Similar to the summer season, differences in dust levels mainly explain the changes in primary components over southern Europe, while the changes over north-west Europe are attributed to sea salt.

References

Andersson C, Langner J, Bergstrom R (2007) Interannual variation and trends in air pollution over Europe due to climate variability during 1958–2001 simulated with a regional CTM coupled to the ERA40 reanalysis. TELLUS B 59:77–98

Berge E, Jakobsen HA (1998) A regional scale multilayer model for the calculation of longterm transport and deposition of air pollution in Europe. TELLUS B 50:205–223

Bessagnet B, Hodzic A, Vautard R, Beekmann M, Cheinet S, Honoré C, Liousse C, Rouïl L (2004) Aerosol modeling with CHIMERE-preliminary evaluation at the continental scale. Atm Env 38:2803–2817

Josse B, Simon P, Peuch V-H (2004) Radon global simulation with the multiscale chemistry transport model MOCAGE. Tellus 56:339–356

Klimont Z, Hoglund L, Heyes Ch, Rafaj P, Schoepp W, Cofala J, Borken-Kleefeld J, Purohit P, Kupiainen K, Winiwarter W, Amann M, Zhao B, Wang SX, Bertok I, Sander R (2015) Global scenarios of air pollutants and methane: 1990–2050. In preparation for ACPD

Menut L, Tripathi OP, Colette A, Vautard R, Flaounas E, Bessagnet B (2013) Evaluation of regional climate simulations for air quality modelling purposes. CDYN 40

Peuch V-H, Amodei M, Barthet T, Cathala M-L, Michou M, Simon P (1999) MOCAGE, MOdéle de Chimie Atmosphèrique à Grande Echelle. In: Proceedings of Météo France: workshop on atmospheric modelling, Toulouse, France, pp 33–36

Robertson L, Langner J, Engardt M (1999) An Eulerian limited-area atmospheric transport model. J Appl Meteor 38:190–210

Simpson D, Benedictow A, Berge H, Bergstrom R, Emberson LD, Fagerli H, Flechard CR, Hayman GD, Gauss M, Jonson JE, Jenkin ME, Nyiri A, Richter C, Semeena VS, Tsyro S, Tuovinen J-P, Valdebenito A, Wind P (2012) The EMEP MSC-W chemical transport model technical description. ACP 12:7825–7865. doi: 10.5194/acp-12-7825-2012

Chapter 36
Cloud Processing of Aerosol Particles: Consequences for Precipitation?

Andrea I. Flossmann and W. Wobrock

Abstract Are clouds able to modify the ambient aerosol particle spectrum so that the number concentration is reduced and the size and chemical composition of the particles is changed? Can they do it in such a way that the cloud forming on these particles will finally be able to precipitate and remove the water and pollution from the atmosphere?

36.1 Introduction

One of the greatest uncertainties in current climate model is connected to aerosol particles through their direct and indirect effect. In addition, the increased drop concentration is suspected to modify cloud properties resulting in modified lifetimes and precipitation (second indirect effect). Some groups suggest that pollution can, thus, be at the origin of droughts in a future climate, as the numerous small drops will prevent the formation of precipitation-sized particles.

This concept seems in contradiction to the fact that the capacity of the atmosphere to hold water (vapour or condensed) is limited and even simple forecast models that don't consider the effect of aerosol particles on hydrometeor formation and treat water in a bulk form are able to roughly reproduce precipitation quantities.

The topic of our studies is to discuss the apparent contradiction and suggest pathways to resolve this contradiction. The key hypothesis here is that the capacity of drops and ice crystals to process and modify aerosol particles during a cloud passage will be the regulating process.

A.I. Flossmann (✉) · W. Wobrock
Laboratoire de Météorologie Physique, Université Clermont Auvergne, Université Blaise Pascal, 63000 Clermont-Ferrand, France
e-mail: A.Flossmann@opgc.univ-bpclermont.fr

A.I. Flossmann · W. Wobrock
CNRS, INSU, UMR 6016, LaMP, TSA 60026, 4 av. Blaise Pascal, 63178 Aubière, France

D.G. Steyn and N. Chaumerliac (eds.), *Air Pollution Modeling and its Application XXIV*, Springer Proceedings in Complexity,
DOI 10.1007/978-3-319-24478-5_36

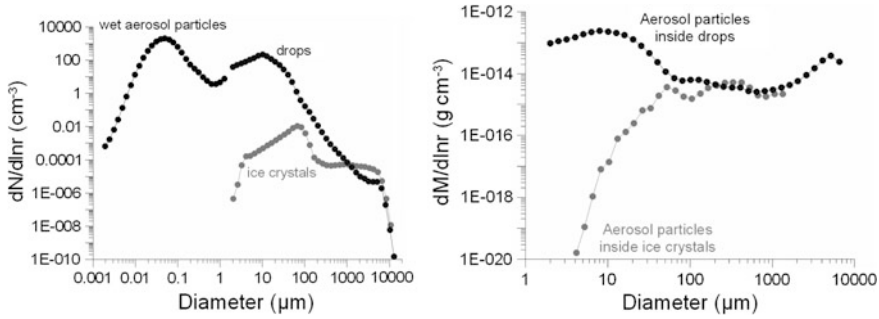

Fig. 36.1 The grid resolution of the different distribution functions treated by DESCAM 3D

36.2 The Model

The 3D model with detailed (bin) microphysics used herein couples the 3D non-hydrostatic model of Clark and Hall (1991) with the Detailed Scavenging Model DESCAM (Flossmann and Wobrock 2010a) for the microphysical package. It follows 5 density distribution function: the number distribution function for the aerosol particles $f_{AP}(m_{AP})$, for drops $f_d(m)$ and for the ice particles $f_i(m_i)$, as well as the mass density distribution function for aerosol particles in the drops $g_{AP,d}(m)$ and in the ice crystals $g_{AP,i}(m_i)$. For their size range and grid resolution see Fig. 36.1.

A discussion of the different processes considered in the microphysics code can be found in Flossmann and Wobrock (2010a).

36.3 Results

In Flossmann and Wobrock (2010b) we already studied the processing of particles in individual clouds and short time cloud fields. From the simulations we noted that inside cloud (LWC > 0.1 gm^{-3}) about 20 % of the area were subsaturated suggesting a strong cycling of the cloud volumes.

Varying particle number concentration could suppress precipitation for individual clouds. For cloud fields and longer simulations times, we noted a strong temporal and spatial variability. Some locations showed an inverse behaviour from the overall trend at some time. The differences between the simulations using different particle number concentrations seemed to decrease in the course of time.

We concluded that the air parcel concept generally overpredicts the reaction of the cloud to the initial parameters. The complex dynamics and microphysics installs a non-linear feedback. Great caution is, thus, advised before making climate relevant conclusions imposing that more research is needed to confirm the behaviour of cloud fields on aerosol particle evolution for longer periods and larger scales.

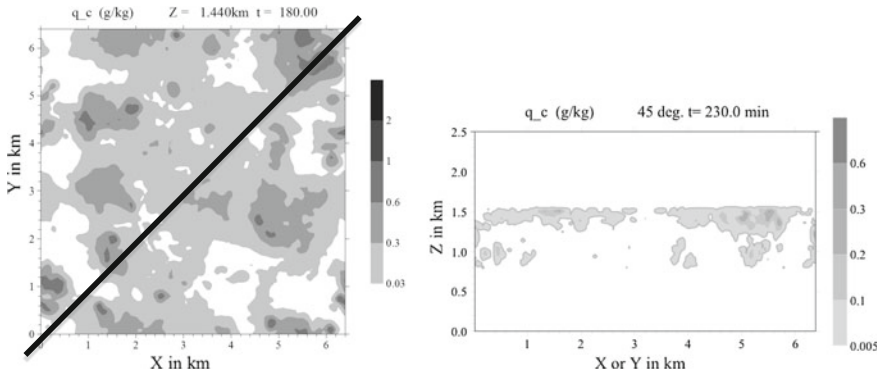

Fig. 36.2 A horizontal (*left*) and vertical (*right*) cross-section through the simulated cloud water in g/kg at 3 h and almost 4 h

Below results are presented to continue the study of the cycling of aerosol particles in cloud fields. As a "sandbox"-type scenario (6 km*6 km*2.5 km) we selected to simulate the processes in a marine stratocumulus cloud as observed during the VOCALS-Rex campaign in 2008 over the remote subtropical southeast Pacific (Wood et al. 2011).

Initializing the simulations with an observed sounding and an aerosol particle spectrum that resemble the observed ones yields cloud fields with 20–60 drops/cm^3. Figure 36.2 shows a horizontal cross section at 1.4 km altitude at 3 h and a vertical cross section along the indicated black line at almost 4 h. Cloud cover stays around 55 % during this time in the evolving stratocumulus field.

After 230 min, a second number density distribution function for processed aerosol particles was added in the model that allows separating the "pristine" particles from particles that went through several cloud cycles of successive condensation/evaporation periods.

Figures 36.3 and 36.4 show the aerosol particles in the ambient air (Fig. 36.3) and the aerosol particles that formed drops (Fig. 36.4), separating between "pristine" particles that never entered cloud drops (for the particles in air, Fig. 36.3, left) or formed drops for the first time (Fig. 36.4, left) and "processed" particles that lived several cloud cycles (right figures).

We note from Fig. 36.3 that after 40 simulated minutes of cloud lifetime (between 230 and 270 min in this simulation) locally up to 20 % of the aerosol particle number concentration has already been in a previous cloud cycle. The processed particles spread over the entire boundary layer and do not stay confined to the cloud region (compare Fig. 36.2).

All of these particles (pristine or processed) can nucleate drops when again entering supersaturated conditions. Figure 36.4 shows that about 30 % of the drops formed on processed particles that had already formed drops during previous cloud passages but that had been evaporated in sub-saturated regions.

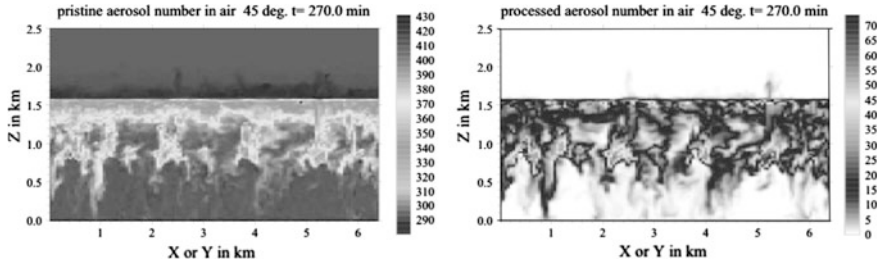

Fig. 36.3 Vertical cross section of the aerosol particle number concentration in the air in cm^{-3}, after 40 min of cloud evolution for pristine (*left*) and processed (*right*) particles

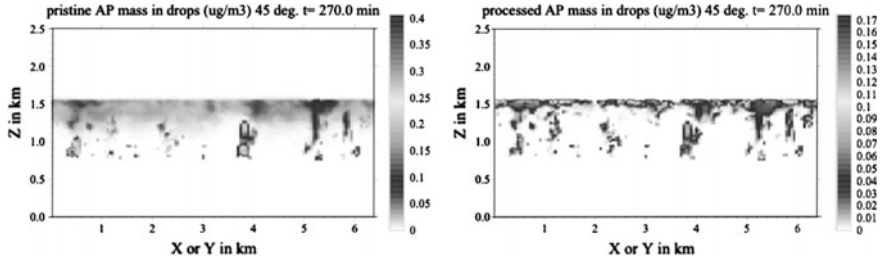

Fig. 36.4 Vertical cross section of the aerosol particle mass contained in cloud drops for "pristine" particles (*left*) and "processed" particles (*right*)

36.4 Conclusion

This is the first study that explicitly tracks aerosol particles forming cloud drops and being evaporated after leaving cloud boundaries and follows the fate of these processed particles in detail. We note that even for a period as short as 40 min around 30 % of the cloud drops formed on such previously "processed" particles. In the studied case for a rather shallow stratocumulus the cloud residence times of the drops were quite short and an observed broadening of the particle spectrum was quite small. Also, the considered domain was kept small in order to keep computer time costs reasonable. More studies of this kind for larger cloud systems and longer times need to be performed to confirm the importance of cloud cycling of ambient aerosol particles.

Acknowledgments The calculations for this study have been done on computer facilities of IDRIS, CNRS at Orsay and CINES in Montpellier, under the project 940180. The authors' acknowledgement with gratitude the hours of computer time and the support provided.

References

Clark TL, Hall WD (1991) Multi-domain simulations of the time dependent Navier-Stokes equation: benchmark error analysis of some nesting procedures. J Comput Phys 92:456–481

Flossmann AI, Wobrock W (2010a) A review of our understanding of the aerosol—cloud interaction from the perspective of a bin resolved cloud scale modelling. Atmos Res. doi: 10.1016/j.atmosres.2010.05.008

Flossmann AI, Wobrock W (2010b) Will pollution reduce precipitation? In: Steyn DG, Castelli ST (eds) Air pollution modeling and its application XXI. Springer, Netherlands, pp 549–557. doi: 10.1007/978-94-007-1359-8_92

Wood R, Bretherton CS, Leon D, Clarke AD, Zuidema P, Allen G, Coe H (2011) An aircraft case study of the spatial transition from closed to open mesoscale cellular convection over the Southeast Pacific. Atmos Chem Phys 11:2341–2370. doi:10.5194/acp-11-2341-2011

Chapter 37
Assessment of Tropospheric Ozone Increase in Future Climate Change Scenarios

Matteo Michelotti, Irene Chiesa, Ennio Tosi, Giovanni Bonafè, Rodica Tomozeiu, Giulia Villani and Fausto Tomei

Abstract This work aims to assess the impact of climatological increment of temperature on the tropospheric ozone concentration in the Po Valley (Italy). Creation, destruction, and transport of ozone is not only governed by the sun, via photochemical reactions, but also by atmospheric conditions. Air quality is therefore significant, and its connection with climate change important. With a statistical downscaling of data from different General Circulation Models (GCMs), and the application of a Weather Generator (WG), it was possible to generate data series of daily temperature in the future (2021–2050). These were compared to data from the past (1961–1990, from the *Agroscenari* project), and the present (2000–2013, measured in six stations), showing how temperatures are bound to increase. We calibrated a simple statistical model based on a stratified sampling technique over a dataset of measured ozone and temperature, predicting the summer ozone daily maximum distribution. This allowed us to determine changes in ozone concentration over the years as a consequence of temperature increase. The results suggest that the last decade can be viewed as a projection of the future "ozone climate" in the Po Valley.

37.1 Introduction

In the troposphere, ozone is harmful to humans and vegetation (Ainsworth et al. 2012; Schlink et al. 2006) even in low concentration. Its origin is both anthropogenic and natural, and it requires the interaction of other substances (*precursors*, primarily VOC and NO_x) with the solar radiation in order to form. While creation and destruction of ozone are mainly dependent on exposure to the sun, they also

M. Michelotti (✉) · G. Bonafè · R. Tomozeiu · G. Villani · F. Tomei
ARPA, Bologna, Italy
e-mail: matteo.michelotti@outlook.com

I. Chiesa · E. Tosi
University of Bologna UNIBO, Bologna, Italy

D.G. Steyn and N. Chaumerliac (eds.), *Air Pollution Modeling and its Application XXIV*, Springer Proceedings in Complexity,
DOI 10.1007/978-3-319-24478-5_37

depend, as well as its transport, on meteorological conditions. Therefore, changes in climate that affect these conditions can alter air quality (Jacob and Winner 2009; Meleux et al. 2007).

We focused our attention on the correlation between ozone concentration and surface temperature during the summer (May–September) in the Po Valley (Italy). This region is a semi-closed basin surrounded by complex orography: a perfect "container" for pollutants, where they can distribute but not easily disperse.

37.2 Data and Methods

The observational data (over the period 2000–2013) consists of time series of daily maximum temperature and daily maximum ozone concentration (T_{max} and O_3^{max}), taken at six locations distributed across the Po Valley. In each location, two nearby stations were identified for temperature and ozone respectively. Data has been collected by the offices of ARPA-SIMC in Bologna, Italy. The control data consists of time series of daily maximum temperature (T_{max}) from the *Agroscenari* project (www.agroscenari.it), defined at a regular grid with a spatial resolution of 35 km, over the period 1961–1990. On the same grid, a statistical downscaling of data from different AOGCMs, followed by the application of a weather generator, produced data of daily maximum temperature over the period 2021–2050 (Tomozeiu et al. 2007).

For this study, we used six General Circulation Models, part of the ENSEMBLES project (for the A1B scenario): ECHAM5-MPI-OM (*Max Plank Institute, Germany*), FUB-EGMAM run1 and run2 (*Freie Universitaet Berlin, Germany*), IPSL-CM4 (*Institute Pierre Simon Laplace, France*), INGV-SINTEX-G (*INGV-CMCC, Italy*), METO-HC (*Met Office's Hadley Centre, UK*).

37.2.1 Model Calibration and Validation

In order to assess the concentration of ozone relative to any given temperature series, we calibrated a statistical model based on a stratified sampling technique. Initially, we randomly divided the conjoined data set of measured temperature and ozone in two groups (70 and 30 %), using the first as calibration for the model and the second as a validation group. We split the calibration group into 20 intervals (I_1, I_2 … I_{20}), separated by an evenly spaced sequence of percentiles of T_{max} ($P_{5\%} < P_{10\%} < \cdots < P_{95\%}$).

For any given day d, the forecasted $O_3^{max}(d)$ is determined by the $T_{max}(d)$ of that day, which belongs to the ith interval I_i in the calibration group: from this interval, 1 day is randomly selected and the forecasted $O_3^{max}(d)$ is the one of that day. Such stratified random selection is iterated many times for each day of the validation

group, and the statistical features of the produced data set have been compared to the same statistical features of the observed data. We also calculated the number of exceedance days per year of the 180 μg/m^2 threshold (called *information threshold*), defined as the point at which the population must be alerted to possibly dangerous levels of pollutant. Then, the same technique is applied to the future climate scenarios, i.e. to the Weather Generator time series based on the downscaled AOGCM output (2021–2050), and to the control series in the past (1961–1990).

We used this construct to evaluate the distribution of concentration of ozone for the past and the future, so as to assess how the concentration of this pollutant changed over time (Fig. 37.1).

37.2.2 Stations Cross-Calibration

We used the calibration data of each station to evaluate the ozone concentration of the remaining stations. This attempt aimed to prove the independence of the statistical method from the specific location, therefore showing that the underlying mechanism linking surface temperature and ozone concentration can be considered to act on a larger scale. The result, obtained taking as calibration the station of Cittadella (Parma), is shown in Fig. 37.2.

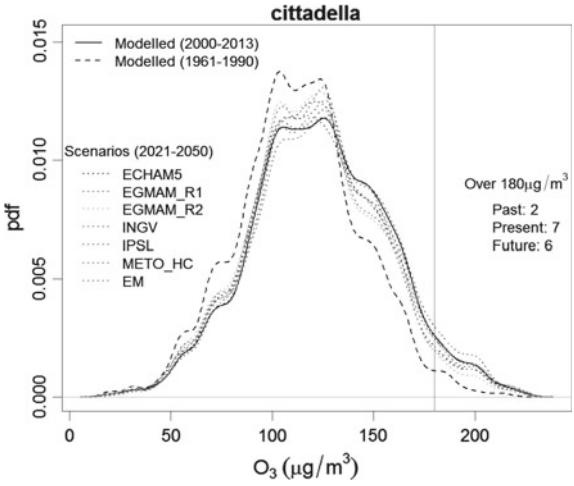

Fig. 37.1 Ozone distributions modelled for the past (1961–1990), present (2000–2013) and future (2021–2050). The different results for each model used in the study are also shown, including their Ensemble Mean (EM). The exceedance days per year of the 180 μg/m^3 information threshold are indicated in the R.H.S. of the graph. The value for the future is referred to the EM of the models

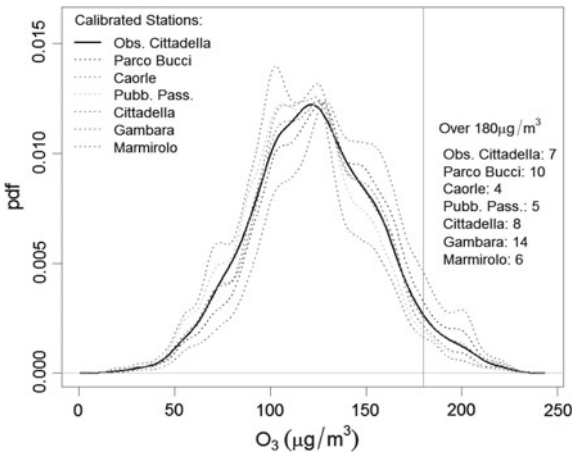

Fig. 37.2 Ozone distribution of observed data (*bold line*) and modelled data (*dotted lines*) for the station of Cittadella (Parma) over 2000–2013. The modelled data was produced using the calibration set of the Cittadella station applied on the sets of the other stations. The exceedance days per year of the 180 $\mu g/m^3$ information threshold are indicated in the R.H.S. of the graph

37.3 Conclusions

In this study, we developed a statistical model based on a stratified sampling technique in order to assess the increment of tropospheric ozone concentration in the Po Valley due to climate change. In this simplified model we assumed no variation of emissions (both natural and anthropogenic) of the pollutant from the calibration levels. The model was applied to temperature data from the past (1961–1990), the present (2000–2013), and the future (2021–2050).

The results show an increase of the average ozone concentration with respect to the period 1961–1990 and the present comparable with the increase between the reference period and the future 2021–2050. Other parameters calculated from the temperature and ozone data showed the same behavior (e.g. exceedance days of the information threshold, or the frequency and duration of heat waves, not shown in this paper), suggesting that the last decade can be considered as a projection of the future "ozone climate" in the Po Valley.

References

Ainsworth EA, Yendrek CR, Sitch S, Collins WJ, Emberson LD (2012) The effects of tropospheric ozone on net primary productivity and implications for climate change. Annu Rev Plant Biol 63:637–661

Jacob DJ, Winner DA (2009) Effect of climate change on air quality. Atmos Environ 43(1):51–63

Meleux F, Solmon F, Giorgi F (2007) Increase in summer European ozone amounts due to climate change. Atmos Environ 41(35):7577–7587

Schlink U, Herbarth O, Richter M, Dorling S, Nunnari G, Cawley G, Pelikan E (2006) Statistical models to assess the health effects and to forecast ground-level ozone. Environ Model Softw 21(4):547–558

Tomozeiu R, Cacciamani C, Pavan V, Morgillo A, Busuioc A (2007) Climate change scenarios for surface temperature in Emilia-Romagna (Italy) obtained using statistical downscaling models. Theor Appl Climatol 90(1–2):25–47

Part V
Regional and Intercontinental Modeling

Chapter 38
Sensitivity-Based VOC Reactivity Calculation

Sergey L. Napelenok and Deborah Luecken

Abstract Volatile Organic Compound (VOC) reactivity scales are used to compare the ozone-forming potentials of various compounds. The comparison allows for substitution of compounds to lessen formation of ozone from paints, solvents, and other products. Current reactivity scales for VOC compounds were first developed using 1-D trajectory/box models for short pollution episodes several decades ago. In this study, they are updated using the 3-D air quality model CMAQ instrumented with DDM-3D. DDM-3D sensitivities are used to update relative reactivity metrics of a number of VOCs over more meaningful timescales. Using sensitivity calculation in the context of an air quality model for reactivity calculations avoids the issues of trajectory assumptions inherent in the 1-D calculations and allow for calculation of regional representative metrics.

38.1 Introduction

Thousands of Volatile Organic Compounds (VOCs) are continuously emitted into the troposphere from natural and anthropogenic sources. Each species has different chemical and physical properties and thus behaves differently once emitted. Of particular interest is a compound's potential to react in the atmosphere in the presence of nitrogen oxides (NO_x) and other precursors to form ozone (O_3). O_3 is widely known to have an adverse impact on human and ecosystem health. Abatement strategies have been developed focusing on regions in the world where this pollutant's ambient concentrations have been found to be exceeding concentration thresholds above which damage occurs. Strategies have been developed depending on meteorological and chemical conditions of a controlled region. In most cases, chemical transport models (CTMs) have been used as a testbed to develop the control strategies.

S.L. Napelenok (✉) · D. Luecken
Atmospheric Modeling and Analysis Division, National Exposure Research Laboratory, U.S. Environmental Protection Agency, RTP, Durham, NC, USA
e-mail: napelenok.sergey@epa.gov

D.G. Steyn and N. Chaumerliac (eds.), *Air Pollution Modeling and its Application XXIV*, Springer Proceedings in Complexity,
DOI 10.1007/978-3-319-24478-5_38

Traditional VOC controls have focused on total emitted mass without regard for speciation. However, controls would be more effective and cost efficient if VOCs that are more conductive to ozone formation could be identified and removed first. Thus, there has been a need to identify the most reactive VOCs and to quantify their ozone forming potential. The majority of such efforts have been based on box model estimates, where initial conditions of the chemical constituents are adjusted to achieve various end points (such as the large amount of ozone formed) (Carter 1994). Once developed, box models can be an efficient platform to test many compounds quickly. More recent VOC reactivity calculations have been based on CTM simulations in order to account for more representative (non-ideal) ozone precursor conditions and more realistic variability in ozone formation in time and space (Hakami et al. 2004). Here, CTM-based VOC reactivity calculations are revisited and a demonstration is applied for ten sample major VOC species in terms of both emissions and reactivity.

38.2 Model Simulations and Observations

The Community Multiscale Air Quality Model (CMAQ) version 5.0.2 was used as the based model configured with the SAPRC07tc chemical mechanism (Hutzell et al. 2012). The species of interest represent a sample of different structure and were: m-xylene, ethene, propene, formaldehyde, 2-methyl-2-butene, n-butane, 2-methylpentane, ethane, benzene, and ethanol. For the case of 2-methyl-2-butene (BUT2ME2), n-butane (NC4), and 2-methylpentane (C5ME2), additional reactions were added to the SAPRC07tc mechanism from the detailed SAPRC07 mechanism (Carter 2010) as these species are not included in the condensed version. The added reactions were as follows:

$$\begin{aligned} \mathrm{NC4} + \mathrm{OH} &= 1.334 * \mathrm{RO2C} + 0.079 * \mathrm{RO2XC} + 0.079 * \mathrm{zRNO3} + 0.921 * \mathrm{xHO2} \\ &\quad + 0.632 * \mathrm{xCCHO} + 0.12 * \mathrm{xRCHO} + 0.485 * \mathrm{xMEK} + \mathrm{yROOH} \\ \mathrm{K} &= 1.63\mathrm{E} - 12 \end{aligned}$$

$$\begin{aligned} \mathrm{C5ME2} + \mathrm{OH} &= 1.671 * \mathrm{RO2C} + 0.185 * \mathrm{RO2XC} + 0.185 * \mathrm{zRNO3} + 0.815 * \mathrm{xHO2} \\ &\quad + 0.001 * \mathrm{xHCHO} + 0.003 * \mathrm{xCCHO} + 0.657 * \mathrm{xRCHO} \\ &\quad + 0.343 * \mathrm{xACETONE} + 0.006 * \mathrm{xMEK} + 0.16 * \mathrm{xPROD2} + \mathrm{yR6OOH} \\ \mathrm{K} &= 5.20\mathrm{E} - 12 \end{aligned}$$

$$\begin{aligned} \mathrm{BUT2ME2} + \mathrm{OH} &= 0.935 * \mathrm{RO2C} + 0.065 * \mathrm{RO2XC} + 0.065 * \mathrm{zRNO3} + 0.935 * \mathrm{xHO2} \\ &\quad + 0.935 * \mathrm{xCCHO} + 0.935 * \mathrm{xACETONE} + \mathrm{yR6OOH} \\ \mathrm{K} &= 1.92\mathrm{E} - 11 \end{aligned}$$

$$\begin{aligned}\mathrm{BUT2ME2} + \mathrm{O3} = {} & 0.862 * \mathrm{OH} + 0.051 * \mathrm{HO2} + 0.213 * \mathrm{MEO2} + 0.7 * \mathrm{RO2C} \\ & + 0.162 * \mathrm{CO} + 0.093 * \mathrm{CO2} + 0.7 * \mathrm{CCHO} + 0.3 * \mathrm{ACETONE} \\ & + 0.045 * \mathrm{CCOOH} + 0.7 * \mathrm{xMECO3} + 0.7 * \mathrm{xHCHO} + 0.7 * \mathrm{yR6OOH} \\ \mathrm{K} = {} & 6.51\mathrm{E} - 15\end{aligned}$$

$$\begin{aligned}\mathrm{BUT2ME2} + \mathrm{NO3} = {} & 0.935 * \mathrm{RO2C} + 0.065 * \mathrm{RO2XC} + 0.065 * \mathrm{zRNO3} \\ & + 0.935 * \mathrm{xNO2} + 0.935 * \mathrm{xCCHO} + 0.935 * \mathrm{xACETONE} \\ & + \mathrm{yR6OOH} \\ \mathrm{K} = {} & 9.37\mathrm{E} - 12\end{aligned}$$

Furthermore, software was created to automatically generate a chemical Jacobean of the updated SAPRC07tc chemical mechanism. The Jacobean of the photochemical mechanism was then used as a part of the decoupled direct method in three dimensions (DDM-3D) extension to CMAQ in order to calculate sensitivity coefficients of O_3 to uniform emissions fields of each compound of interest. The simulation was carried out for the month of July 2011 (with 10 days in June as discarded spin-up) over the continental United States at 12 km grid resolution.

Hourly Maximum Ozone Incremental Reactivity (MOIR) was then defined as the O_3 sensitivity coefficient at the location where maximum O_3 concentration occurred during the hour $\left(MOIR_i \approx \frac{\partial O_3}{VOC}\Big|_{max(O_3)} \right)$. In order to perform spatial comparisons, the domain was divided into six geographic regions: Pacific, Rocky Mountain, Southwest, Midwest, Southeast, and Northeast. Also, in order to facilitate comparison between different VOCs, MOIRs were normalized by those of ethene chosen as an arbitrarily low reactivity species.

38.3 Results and Discussion

Reactivity of the ten compounds was found to vary in both space and time (e.g, ethene in Fig. 38.1), but when averaged over the entire episode, was mostly in line with previously calculated box-model and CTM-based estimates (Carter 2009; Hakami 2004). Episode-long averages by region for reactivity are summarized in Table 38.1. M-xylene was found to be the most reactive compound and benzene was found to be the least. In some regions, benzene indicated negative reactivity meaning that increasing emissions actually led to less ozone produced. This is likely due to the removal of radicals from the ozone formation mechanism. In the hourly results, most species exhibited a consistent diurnal profile with reactivity peaking during the part of the day with the greatest amount of photolysis activity.

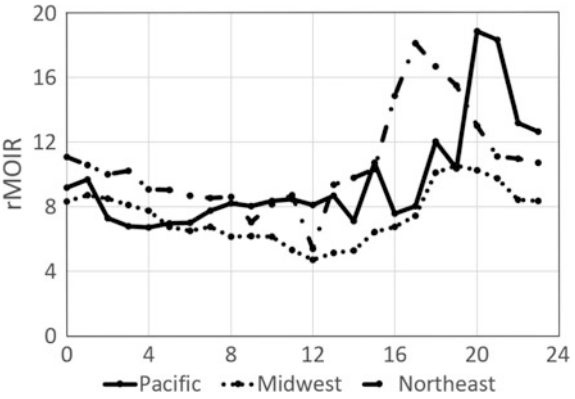

Fig. 38.1 Relative (to ethane) maximum ozone incremental reactivity of ethene in three geographic regions

Table 38.1 Episode-long averaged reactivity normalize by that of ethane

Species	Pacific	Rocky mountain	Southwest	Midwest	Southeast	Northeast
m-xylene	18.0	11.4	4.6	15.3	8.1	19.9
ethene	9.6	9.1	6.6	7.4	5.6	10.6
propene	11.8	9.6	5.0	8.3	6.0	11.2
formaldehyde	4.0	2.8	1.1	2.4	1.4	3.8
2-methyl-2-butene	14.5	10.6	4.4	12.8	8.9	17.7
n-butane	4.7	4.0	3.3	4.0	3.8	4.5
2-methylpentane	7.8	5.7	4.9	6.3	5.5	7.5
ethane	1.0	1.0	1.0	1.0	1.0	1.0
benzene	1.2	2.4	1.2	−0.7	−1.8	−0.1
ethanol	4.6	3.7	3.1	3.6	3.0	3.9
O_3 (ppm)	78.0	77.8	81.9	87.0	91.2	85.1

Disclaimer Although this work has been reviewed and approved for publication by the U.S. Environmental Protection Agency, it does not necessarily reflect the views and policies of the agency.

Questions and Answers

Questioner: S. Arunachalam
Question: You mentioned lower formaldehyde reactivity calculated with ddm-based model compared to box-model. Why? What is the mechanism that causes this difference?

Answer: Formaldehyde and other aldehydes are more reactive in box model (resulting in higher reactivity quantifications), because the residence time considered doesn't allow for carryover of products that continue to be chemically active in the CTM.

Questioner: A. Hakami
Question: How did you prepare your individual VOC emissions?

Answer: VOC emissions for the sensitivity calculations where set to 0.0001 mol/s for each species constant over the entire domain. This was a quantity sufficiently small compared to total VOC emissions to not impact base model ozone concentrations.

References

Carter WPL (1994) Development of ozone scales for volatile organic compounds. J Air Waste Manage Assoc 44:881–899

Carter WPL (2009) Updated chemical mechanisms for airshed model applications. Report to California air resources board. Contract no. 03-318, 06-408, 07-730

Carter WPL (2010) Development of the SAPRC-07 chemical mechanism. Atmos Environ 44:5324–5335

Hakami A, Harley R, Milford JB, Odman MT, Russell AG (2004) Regional, three-dimensional assessment of the ozone formation potential of organic compounds. Atmos Enivorn 38:121–134

Hutzell WT, Luecken DJ, Appel KW, Carte WPL (2012) Interpreting predictions from the SAPRC07 mechanism based on regional and continental simulations. Atmos Environ 46:417–429

Chapter 39
Multiscale Modeling of Multi-decadal Trends in Ozone and Precursor Species Across the Northern Hemisphere and the United States

Rohit Mathur, Jia Xing, Sergey Napelenok, Jonathan Pleim, Christian Hogrefe, David Wong, Chuen-Meei Gan and Daiwen Kang

Abstract Multi-decadal model calculations for the 1990–2010 period are performed with the coupled WRF-CMAQ modeling system over a domain encompassing the northern hemisphere and a nested domain over the continental U. S. Simulated trends in ozone and precursor species concentrations across the U.S. over the past two decades are compared with those inferred from available measurements during this period. The model results suggest large and contrasting changes in tropospheric composition over the northern hemisphere with significant reductions in air pollution over North America and Western Europe and increase in large portions of Asia. The model is able to capture the changing seasonal distributions in surface O_3 in the U.S. during 1990–2010 arising from changing emissions and long-range transport.

39.1 Introduction

Air pollutants near the Earth's surface can be convectively lofted to higher altitudes where strong winds can efficiently transport them from one continent to another, thereby impacting air quality on intercontinental to global scales. Thus, strategies for reduction of pollution levels of surface air over a region are complicated not only by the interplay of local emissions sources and several complex physical, chemical, dynamical processes in the atmosphere, but also hemispheric background levels of pollutants. Contrasting changes in emissions of a variety of air pollutants

R. Mathur (✉) · J. Xing · S. Napelenok · J. Pleim · C. Hogrefe · D. Wong · C.-M. Gan
Atmospheric Modeling and Analysis Division, National Exposure Research Laboratory, U.S. Environmental Protection Agency, RTP, Durham, NC, USA
e-mail: napelenok.sergey@epa.gov

D. Kang
Computer Sciences Corporation, RTP, Durham, NC, USA

D.G. Steyn and N. Chaumerliac (eds.), *Air Pollution Modeling and its Application XXIV*, Springer Proceedings in Complexity,
DOI 10.1007/978-3-319-24478-5_39

have occurred across the northern hemisphere in response to implementation of control measures in some regions and population and economic growth in others, likely resulting in changes in long-range pollutant transport patterns and hemispheric background pollution levels. In the U.S., implementation of emission control measures over the past two decades has resulted in significant reductions in ambient levels of O_3 and precursor species. Possible tightening of the O_3 National Ambient Air Quality Standard (NAAQS) also places increasing emphasis on quantifying the relative contribution of background pollution to ambient levels both regionally and locally. Thus a need exists to understand and accurately model the trends in contributions of local, regional pollution, and long-range to the ambient O_3 levels.

39.2 Model Setup

The coupled WRF-CMAQ modeling system (Wong et al. 2012) was exercised for a 21-year period spanning 1990–2010 to simulate changes in tropospheric O_3 resulting from changes in anthropogenic emissions during this period. Model simulations were performed over two domains: an outer hemispheric scale domain covering the Northern hemisphere, set on a polar stereographic projection and discretized with a horizontal resolution of 108 km (cf. Mathur et al. 2012, 2014) and a nested 36 km resolution grid covering the Continental U.S. and portions of Canada and Mexico. Year specific emissions for the northern hemispheric domain were derived from the EDGARv4.2 global emission inventory (Xing et al. 2015). The regional 36 km resolution calculation employed emission estimates from recently developed inventory for 1990–2010 in which state-level anthropogenic emissions of SO_2, NO_x, CO, NMVOC, NH_3, PM_{10} and $PM_{2.5}$ for a total of 49 sectors were estimated based on several long-term databases containing information about activity and emission controls (Xing et al. 2013). The CB05 chemical mechanism was used to represent gas-phase photochemistry. In addition, O_3 mixing ratios in the top most model layer ($\sim$50 mb) were modulated based on scaling of the spatially and temporally varying potential vorticity fields to represent possible effects associated with stratosphere-troposphere exchange (Mathur et al. 2008).

39.3 Results and Discussion

Figure 39.1 presents spatial plots of simulated trends in the daily maximum 8-hour average surface O_3 (DM8hr O_3) mixing ratios for the 1990–2010 period across the North American domain. Trends are estimated at different percentiles of the O_3 mixing ratio range as well as for different seasons to examine how changing emissions within the domain as well as possible changes in O_3 imported into the region impact the distribution of ambient O_3 across the domain. Large declining

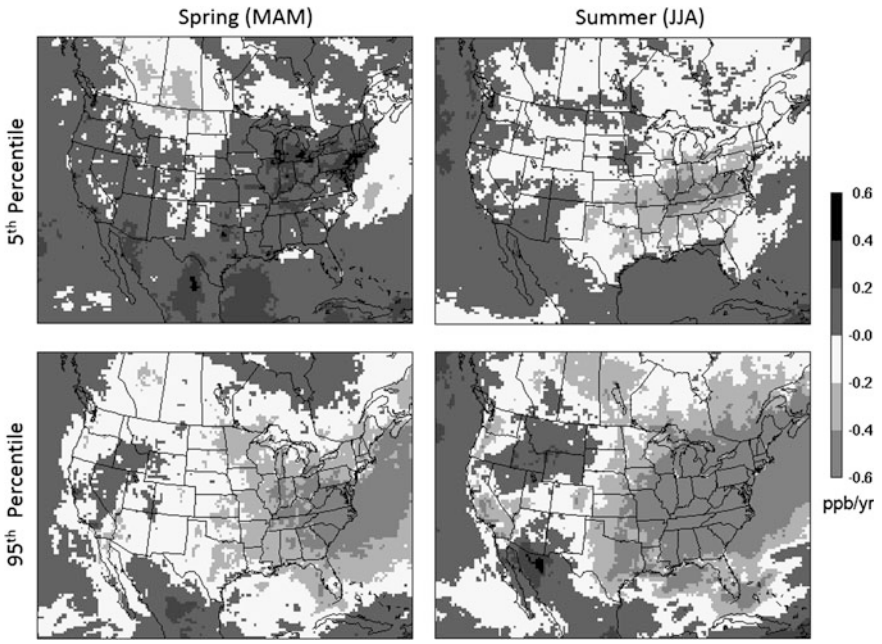

Fig. 39.1 Simulated trends in ambient DM8hr O_3 mixing ratios during 1990–2010 for different seasons and at different percentiles of the surface O_3 mixing ratio distribution

trends in 95th percentile surface O_3 are noted during both spring and summer along the industrial northeast corridor, urban areas across the country, and downwind of the major electric generation units in the Ohio River Valley, resulting from the significant reductions in precursor NO_x and VOC emissions over the past two decades. Stronger declining trends are evident in summer. In contrast, at the lower end of the O_3 mixing ratio range (5th percentile), increasing trends are noted during spring. Stronger increasing trends are noted in the urban and high NO_x emission cells and result from the reduced titration of O_3 by declining NO_x emissions. Also evident during spring are increasing trends in the 5th percentile O_3 in rural areas as well as in the western U.S., indicative of the possible impact of increasing pollution import associated with long-range transport of increasing pollution from Asia across the Pacific.

Figure 39.2 presents comparisons of these model estimated trends at different percentiles of the DM8hr O_3 with corresponding trends inferred from observations at the AQS monitors across the U.S. During spring, both model and observations show increasing trends at the lower end of the DM8hr O_3 distribution at majority of the sites. Observed summertime trends at the median mixing ratio range show decreases across majority sites, while the spring time trends at median mixing ratio range still show increases at many locations; these seasonal contrasts in trends are replicated by the model at many locations. At the upper end (95th percentile) of the

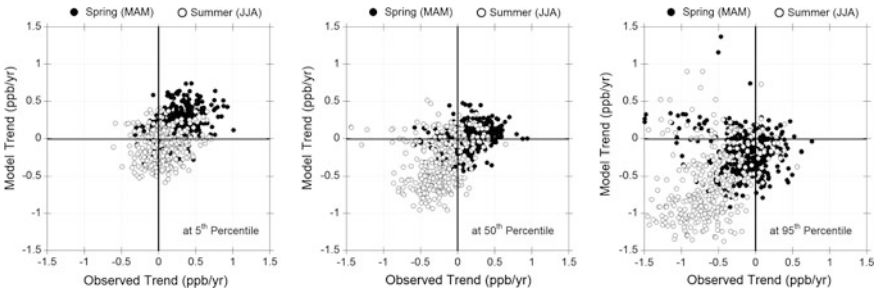

Fig. 39.2 Comparison of model and observed trends at different percentiles of the DM8hr O_3 distribution and for different seasons during 1990–2010

DM8hr O_3 distribution, decreasing trends are noted at most locations both during summer and spring in the observations, and these are captured by the model. Discrepancies between model and observed trends are however noted at some locations and likely result from the relatively coarse spatial resolution (36 km) employed here that is unable to adequately represent sub-grid variability in air pollution in many urban locations.

These comparisons suggest that the model is able to capture the changing seasonal distributions of surface level O_3 in the U.S. during 1990–2010 arising from changing emissions and long-range pollutant transport. The results also suggest that changing emission patterns across the northern hemisphere will impact background pollution levels in a region. The WRF-CMAQ modeling system provides a framework to examine the seasonal variations in this background pollution as well potentially varying source contributions.

Disclaimer: Although this work has been reviewed and approved for publication by the U.S. Environmental Protection Agency, it does not necessarily reflect the views and policies of the agency.

Question and Answer

Questioner: S. Arunachalam
Question: Did the emission inventory differ in the nested 36-km domain and the North American portion of the hemispheric domain?

Answer: Yes, the emission over the North American portion of the nested regional and hemispheric domain differ in these calculations. The hemispheric domain used the year specific EDGAR4.2 estimates, while the regional 36 km resolution calculation used our recently developed estimates multi-decadal inventory described in Xing et al. (2013). Ideally, we would have used the Xing et al. estimates for North America also in the hemispheric run. However due to staging of the runs that was not possible.

Questioner: I. Stajner
Question: How is stratospheric O_3 at the model top specified? How is meteorology constrained for these two decade long runs?

Answer: We specify the O_3 mixing ratios at the top of our model domain using a potential vorticity (PV) scaling. In these simulations we used 20 ppb O_3 per PV unit. We are now refining the scheme to develop a scaling that varies by season and latitude. The meteorology is constrained via nudging to the NCEP/NCAR reanalysis. Weak nudging was performed only above the PBL. NCEP ADP Operational Global Surface Observations were used for surface reanalysis which is used for indirect soil moisture and temperature nudging in the PX-LSM employed in our model configuration.

References

Mathur R, Lin H-M, McKeen S, Kang D, Wong D (2008) Three-dimensional model studies of exchange processes in the troposphere: use of potential vorticity to specify aloft O_3 in regional models. In: 2008 CMAS conference. http://www.cmascenter.org

Mathur R, Gilliam R, Bullock OR, Roselle S, Pleim J, Wong D, Binkowski F, Streets D (2012) Extending the applicability of the community multiscale air quality model to hemispheric scales: motivation, challenges, and progress. In: Steyn DG, Trini Castelli S (eds) Air pollution modeling and its applications, XXI. Springer, Dordrecht, pp 175–179

Mathur R, Roselle S, Young J, Kang D (2014) Representing the effects of long-range transport and lateral boundary conditions in regional air pollution models. In: Steyn DG et al (eds) Air pollution modeling and its application XXII. Springer, Dordrecht, pp 303–308. doi:10.1007/978-94-007-5572-2_51

Wong DC, Pleim J, Mathur R, Binkowski F, Otte T, Gilliam R, Pouliot G, Xiu A, Young JO, Kang D (2012) WRF-CMAQ two-way coupled system with aerosol feedback: software development and preliminary results. Geosci Model Dev 5:299–312. doi:10.5194/gmd-5-299-2012

Xing J, Pleim J, Mathur R, Pouliot G, Hogrefe C, Gan C-M, Wei C (2013) Historical gaseous and primary aerosol emissions in the United States from 1990 to 2010. Atmos Chem Phys 13:7531–7549. doi:10.5194/acp-13-7531-2013

Xing J, Mathur R, Pleim J, Hogrefe C, Gan C-M, Wong DC, Wei C, Gilliam R, Pouliot G (2015) Observations and modeling of sir quality trends over 1990–2010 across the Northern Hemisphere: China, the United States and Europe, 2015. Atmos Chem Phys 15:2723–2747. doi:10.5194/acp-15-2723-2015

Chapter 40
Global and Regional Modeling of Long-Range Transport and Intercontinental Source-Receptor Linkages

Christian Hogrefe, George Pouliot, Jia Xing, Johannes Flemming, Shawn Roselle, Rohit Mathur and Stefano Galmarini

Abstract In this study, we compare air quality over North America simulated by the C-IFS global model and the CMAQ regional model driven by boundary conditions from C-IFS against surface and upper air observations. Results indicate substantial differences in model performance for surface ozone between the two models. Above the boundary layer, differences are least pronounced in the free troposphere but increase in the upper troposphere and lower stratosphere. In addition, we also compare the impacts of perturbed emissions in East Asia and North America on air quality over North America simulated by CMAQ and C-IFS.

40.1 Introduction

Many previous observational and modeling studies have been performed to quantify intercontinental transport of air pollution and its impact on local air quality. Much of this work has informed the 2010 report of the Task Force on Hemispheric Transport of Air Pollution (TF-HTAP) (HTAP 2011). TF-HTAP is currently conducting a new round of modeling and analysis activities to refine estimates of intercontinental transport. One approach for doing so is to include both global and linked global-regional modeling approaches in which output from global models is used as input to regional models over specific source and/or receptor

C. Hogrefe (✉) · G. Pouliot · J. Xing · S. Roselle · R. Mathur
Atmospheric Modeling and Analysis Division, National Exposure Research Laboratory, U.S. Environmental Protection Agency, RTP, Durham, NC, USA
e-mail: hogrefe.christian@epa.gov

J. Flemming
European Centre for Medium-Range Weather Forecasts, Reading, UK

S. Galmarini
European Commission Joint Research Centre, Ispra, Italy

D.G. Steyn and N. Chaumerliac (eds.), *Air Pollution Modeling and its Application XXIV*, Springer Proceedings in Complexity,
DOI 10.1007/978-3-319-24478-5_40

regions. The contributions for some of the regional modeling activities are coordinated through the third phase of the Air Quality Model Evaluation International Initiative (AQMEII3). The specific science questions to be addressed through AQMEII3 are (a) in which aspects does model performance over North America and Europe differ between global and regional models? and (b) how do source/receptor linkages differ between global models and linked global/regional models? In this study, we provide illustrative examples of these analyses using datasets that have been generated to date.

40.2 Model Simulations and Observations

The 2010 regional air quality simulations analyzed in this study were performed with version 5.0.2 of the Community Multiscale Air Quality (CMAQ) modeling system (Byun and Schere 2006). Meteorological fields were prepared using version 3.4 of the Weather Research and Forecasting (WRF) model (Skamarock and Klemp 2007). The 2010 emission inputs are described in Pouliot et al. (2015). The CMAQ simulations were performed with a horizontal grid spacing of 12 km over the continental U.S. with a vertical extent to 50 mb using 35 vertical layers. Chemical boundary conditions were prepared from global concentration fields estimated by the European Center for Medium Range Weather Forecasts (ECMWF) Composition—Integrated Forecast System (C-IFS) model (Flemming et al. 2015). The C-IFS simulations were performed on a T255 grid with a horizontal resolution of roughly 80 km and 60 vertical levels ranging from the surface to 0.1 mb. For the analysis presented in this study and to facilitate future comparisons to additional simulations performed by other AQMEII participants, both the CMAQ and C-IFS fields were interpolated to a common analysis grid with a horizontal resolution of 0.25 × 0.25° and the CMAQ vertical structure. A comparison of the CMAQ and C-IFS vertical structure shows that CMAQ places more emphasis on high vertical resolution in the planetary boundary layer (PBL) while C-IFS uses a slightly coarser resolution in the PBL but significantly finer resolution in the tropopause region as well as the stratosphere. Hourly ozone observations retrieved from the U.S. Environmental Protection Agency (U.S. EPA) Air Quality System (AQS) database were used to derive daily average ozone mixing ratios. Ozonesonde observations at six sites in the analysis domain were obtained from the World Ozone and UV Data Center (WOUDC). In addition to the CMAQ and C-IFS simulations described above, simulations with perturbed emissions were also performed. For the first sensitivity simulation (labeled "EAS" hereafter), East Asian emissions for all pollutants and all anthropogenic sectors were reduced by 20 % in the C-IFS simulations. The corresponding CMAQ simulations used boundary conditions derived from these C-IFS EAS simulations. For the second sensitivity simulation (labeled "NAM" hereafter), North American (i.e. U.S. and Canadian) emissions for all

pollutants and all anthropogenic sectors were reduced by 20 % in the C-IFS simulations. The corresponding CMAQ simulations used boundary conditions derived from these C-IFS NAM simulations and also reduced U.S. and Canadian anthropogenic emissions by 20 %.

40.3 Results and Discussion

Figure 40.1 shows annual time series of daily average ozone from observations, CMAQ, and C-IFS averaged over all AQS monitors in the analysis domain. The figure shows that C-IFS underestimates observed mixing ratios in winter and overestimates observed mixing ratios during summer. CMAQ is almost unbiased during winter and displays a positive bias during summer, though this positive bias is less pronounced than for C-IFS. The summertime ozone overestimation by C-IFS is consistent with the findings for other global models reported by Fiore et al. (2009) who attributed it to uncertainties in the representation of NO_x-O_3-isoprene chemistry.

We also compared simulated vertical ozone profiles against measurements taken by ozonesondes. Figure 40.2 shows a composite of these profiles across six ozonesonde stations in the analysis domain and across all soundings taken in 2010. This figure indicates that both CMAQ and C-IFS tend to underestimate ozone in the free troposphere. In addition, the graphs also suggest that the differences between the two simulations are smallest in the free troposphere while they increase in the PBL and in the upper troposphere/lower stratosphere. To extend this analysis beyond the location of the ozonesonde stations, differences between CMAQ and C-IFS were computed at each grid point of the common analysis grid and each vertical layer and then averaged over the entire year. The resulting vertical profile of differences is shown in Fig. 40.3 and confirms that the relative model-to-model differences are smallest in the free troposphere and larger in the PBL and especially the upper troposphere/lower stratosphere region. The differences in the PBL likely are caused by differences in horizontal grid resolution and the resulting differences

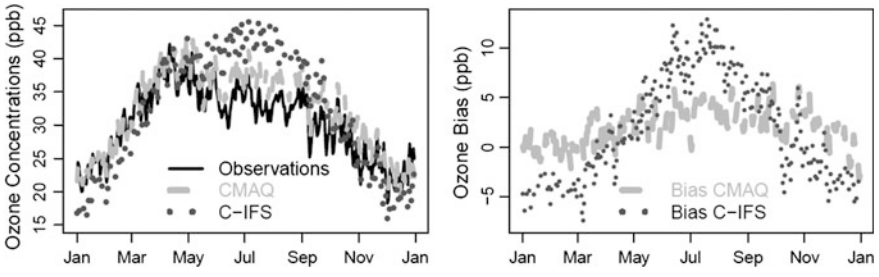

Fig. 40.1 Time series of observed and modeled ozone mixing ratios (*left*) and differences between model simulations and observations (*right*), spatially averaged over all monitors

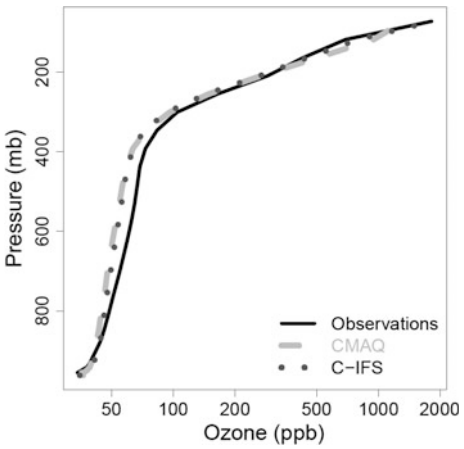

Fig. 40.2 Observed and modeled ozone profiles average across all launches at six ozonesonde sites in 2010

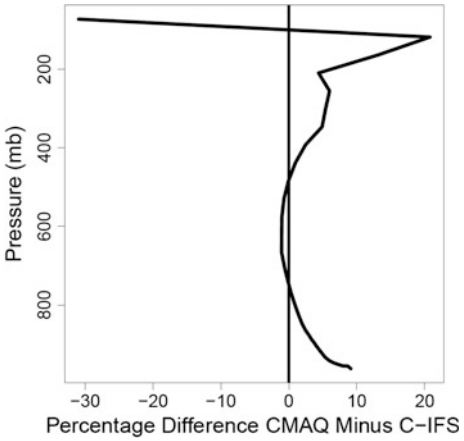

Fig. 40.3 Percent difference between CMAQ and C-IFS vertical ozone profiles average across all grid cells and hours in 2010

in the representation and dilution of emission sources and near-source chemistry. The small differences in the free troposphere likely reflect the fact that the CMAQ ozone mixing ratios in this region are dominated by horizontal advection from the lateral boundaries and the fact that vertical gradients of ozone are small. The differences in the upper troposphere and lower stratosphere, a region of large vertical gradients in ozone, likely are caused by differences in the vertical resolution between the two models in this region as discussed above. The positive sign of the differences suggests that the coarser vertical resolution used in CMAQ led to more downward mixing of elevated stratospheric ozone mixing ratios compared to C-IFS.

The second objective of AQMEII3 and HTAP is to compare the source/receptor linkages simulated by global and linked global/regional modeling systems. In Fig. 40.4, we present the results of the C-IFS and CMAQ NAM and EAS simulations. The Figures show the differences between the reduced emissions case and

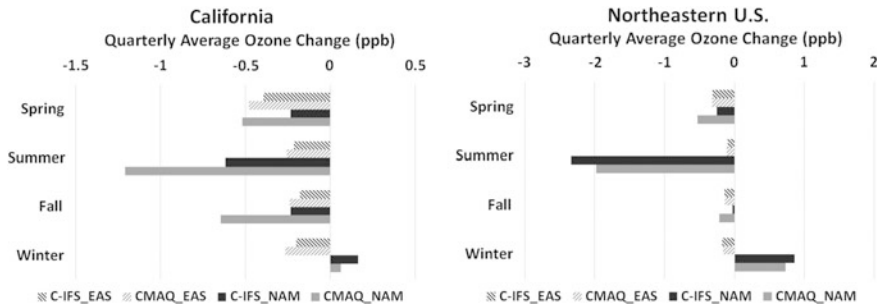

Fig. 40.4 Impact of East Asian (EAS) and North American (NAM) emission reduction on seasonal average ozone simulated by C-IFS and CMAQ over California (*left*) and the Northeast (*right*)

the base case as quarterly averages spatially averaged over California and the Northeastern U.S. The results show that the differences between C-IFS and CMAQ are small for the EAS case in all seasons, consistent with the notion that the impact of this emission perturbation is via transport in the free troposphere which shows small differences between the two modeling approaches. In contrast, the differences are more pronounced for the NAM case in which emissions over North America are perturbed, pointing to the effects of horizontal grid resolution on the representation of emissions and near-source chemistry.

40.4 Summary

AQMEII Phase 3 focuses on evaluating and intercomparing regional and linked global/regional modeling systems by collaborating with HTAP. This study provided initial examples of the planned analyses by comparing results from the global C-IFS and regional CMAQ modeling systems over North America for both the base case and two emission perturbation cases. Future work will be directed at expanding this analysis to Europe as well as to other modeling systems.

40.5 Disclaimer

Although this work has been reviewed and approved for publication by the U.S. Environmental Protection Agency, it does not necessarily reflect the views and policies of the agency.

Question and Answer

Questioner: P. Lee
Question: The vertical structure of the AQMEII is largely refined. At NOAA AQ forecasting team is learning what your team at EPA is doing carefully. With NOAA's involvement in the recent DISCOVER-AQ measurement campaigns with flight and lidar, strata about PBL may be subject to shallow convection venting of pollutants from the PBL. Therefore NOAA's forecasting system is now increasing from its current 22 layers to 35 layers. We intend to refine both the layers where shallow convection and tropospheric-stratospheric exchange may happen. We hope to learn and share our experience with the EPA team. On your sub-grid variability plot, the difference at the surface over California is standing out. I wonder if the emission harmonization still allows differences stemming from resolution differences.

Answer: We agree with your comment on the need to carefully consider the vertical resolution used in our model to adequately represent the dynamic processes affecting the vertical distribution of ozone. Differences in horizontal resolution likely are indeed the main contributor to the subgrid variability noticeable in urban areas, causing differences in both the dilution of primary emissions into the grid cell volume and the resulting non-linearities in the formation of secondary pollutants.

References

Byun DW, Schere KL (2006) Review of the governing equations, computational algorithms, and other components of the models-3 community multiscale air quality (CMAQ) modeling system. Appl Mech Rev 59:51–77

Fiore AM et al (2009) Multimodel estimates of intercontinental source-receptor relationships for ozone pollution. J Geophys Res 114:D04301. doi:10.1029/2008JD010816

Flemming J et al (2015) Tropospheric chemistry in the integrated forecasting system of ECMWF. Geosci Model Dev 8:975–1003. doi:10.5194/gmd-8-975-2015

HTAP (2011) Hemispheric transport of air pollution 2010: Part A—ozone and particulate matter. Economic Commission for Europe, United Nations, 304 pp, Sept 2011. ISBN 13: 9789211170436

Pouliot et al. (2015) Analysis of the emission inventories and model-ready emission datasets of Europe and North America for phase 2 of the AQMEII project. Atmos Env. doi:10.1016/j.atmosenv.2014.10.061

Skamarock WC, Klemp JB (2007) A time-split nonhydrostatic atmospheric model for research and NWP applications. J Comp Phys 227(7):3465–3485 (Special issue on environmental modeling)

Chapter 41
Calculation of Sensitivity Coefficients for Individual Airport Emissions in the Continental UnitedStates Using CMAQ-DDM3D/PM

Scott Boone, Stefani Penn, Jonathan Levy and Saravanan Arunachalam

Abstract Previous estimates of aviation contributions to ground-level ozone and fine particulate matter concentrations have either offered domain- and sector-wide estimates or focused on a few airports. Using the decoupled direct method (DDM), an advanced sensitivity analysis module for the CMAQ air quality modeling suite, we calculate per-airport sensitivity coefficients allowing quantification of 66 individual airports' impact on air quality in the United States. Preliminary results show that these airports, collectively representing about 76 % of aviation activity by fuel burn in the US, are responsible for about 0.04 % of nationwide $PM_{2.5}$ concentrations; near-airport concentrations are proportionately much higher. Peak annual average contributions from individual airports vary from 0.018 to 0.0001 $\mu g/m^3$; secondary $PM_{2.5}$ has effects at distances of up to 700 km downwind while primary $PM_{2.5}$ affects only the immediate vicinity of the airport. Complete results detailing specific air quality and health impacts of each airport will be presented at the ITM conference in May.

41.1 Background

Aviation is a critical segment of the U.S. transportation sector, growing year-over-year in both absolute and relative terms. Between 2001 and 2011, the share of domestic passenger-miles traveled by air increased from 9.5 to 11.8 %

S. Boone (✉) · J. Levy · S. Arunachalam
University of North Carolina, Chapel Hill, NC, USA
e-mail: stboone@unc.edu

S. Arunachalam
e-mail: sarav@unc.edu

S. Penn
Boston University, Boston, MA, USA

D.G. Steyn and N. Chaumerliac (eds.), *Air Pollution Modeling and its Application XXIV*, Springer Proceedings in Complexity,
DOI 10.1007/978-3-319-24478-5_41

compared to terrestrial and marine modes. Over the same period, air carriers saw growth of about 17 %, with nearly 578 billion domestic passenger miles traveled in 2013 (Bureau of Transportation Statistics 2014).

Fine particles are emitted directly from aircraft in the form of soot and dust, while oxidation of emitted nitrates, sulfates and organic compounds leads to the formation of both O_3 and secondary particulate matter. Human exposure to O3 and fine particulates (i.e., particles of size less than 2.5 microns, collectively known as $PM_{2.5}$) can cause chronic and acute disease in the form of asthma, bronchitis, cardiopulmonary disease and cancer. Large-scale cohort studies have found that 10 $\mu g/m^3$ increase in $PM_{2.5}$ concentrations is associated with a ten percent increase in all-cause mortality (Pope III et al. 2002).

Previous estimation of aviation's contribution to O_3 and $PM_{2.5}$ showed that in 2005, about 0.05 % of average ambient $PM_{2.5}$ levels could be linked to aircraft landing and takeoff operations (LTO), with this value rising to 0.11 % by 2025 (Woody et al. 2011). However, impacts near airports are significantly higher, with proportion of ambient $PM_{2.5}$ attributable to aircraft LTO approximately doubling compared to regions located more distantly from an airport. Model-based estimations of annual excess mortality from LTO have estimated that in 2005, 75 premature deaths were caused by aircraft LTO at 99 major US airports, a number expected to rise to 460 in 2025 (Levy et al. 2012).

Eulerian Chemical Transport Models (CTMs) function by modeling the atmosphere as a series of well-mixed three-dimensional grid cells. At each modeled time step, the effects of meteorological, solar, chemical, and physical processes are evaluated within and between grid cells, giving discrete values for the chemical concentrations of each modeled species. These values are then aggregated to provide estimates of air quality and health impacts of atmospheric pollutants.

Sensitivity analysis of CTMs forms the heart of model-based air quality analysis. A number of methods for sensitivity analysis exist, each balancing computational complexity, flexibility, and precision of results. Popular methods of sensitivity analysis include the brute force method (also known as the subtractive or zero-out method), regression-based methods (Box and Draper 1987; Lee et al. 2012), tagged-species methods (Kwok et al. 2013) and direct calculation of sensitivity coefficients (Dunker 1984; Napelenok et al. 2006, 2008) (Fig. 41.1).

Of these methods, the decoupled direct method, or DDM, offers a few advantages. DDM allows for calculation of multiple sensitivity coefficients in a single model run. Use of the DDM allows for sensitivity coefficients to be calculated "up-front", allowing varying emissions scenarios to be evaluated without requiring a re-running of the model. While the per-run computational costs of DDM are substantial, the decreased number of total runs and greater flexibility allowed compare favorably to similar analyses conducted using brute force or regression-based methods.

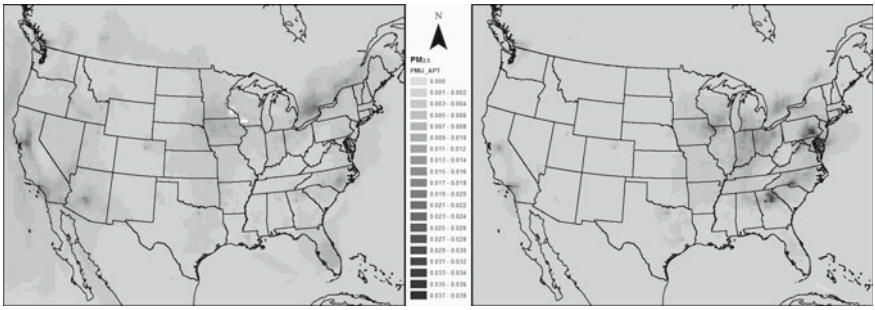

Fig. 41.1 January (*left*) and July (*right*) $PM_{2.5}$ sensitivities to emissions from all airports in the continental US

41.2 Methodology

A modeling framework was created to quantify the contributions of individual airports during the year 2005 and generate sensitivity coefficients to evaluate the impacts of variations in these emissions. The model was run for 1 month each in January and July, with a ten-day spin-up period used to generate initial conditions.

Airports were selected for modeling in order to capture as much of US aviation activity as possible, both in terms of spatial coverage and absolute emissions. Because each additional sensitivity parameter represents a linear increase in processing time, airports distant enough to not create overlapping sensitivity plumes were combined into sensitivity groups where possible. In total, 66 airports were chosen and allocated among 30 sensitivity groups, each group containing between one and four airports. These airports represent 77 % of annual fuel burn as reported by the FAA's Aviation Emission Design Tool (AEDT) (Roof et al. 2007; Wilkerson et al. 2010). An additional group was created containing emissions from all airports in the continental united states, for a total of 31 groups.

For each airport group, six precursor species groups (NO_x, SO_2, VOCs, PSO_4, PEC and POC) were designated as sensitivity input parameters, for a total of 186 sensitivity parameters. Flight segment data from AEDT were processed into gridded emission rate files using AEDTProc (Baek et al. 2012). Emissions were capped at 3,000 ft (about 914 m) in order to only capture landing and takeoff operations. Background emission rates from EPA's National Emissions Inventories (NEI-2005) were processed into grid-based emissions using the Sparse Matrix Operator Kernal Emissions (SMOKE) (U.S. Environ-mental Protection Agency 2005). Meteorology for 2005 was obtained from the Weather Research and Forecasting model (WRF), with outputs downscaled from NASA's Modern-Era Retrospective Analysis for Research and Applications data (MERRA) (Rienecker et al. 2011). CMAQ v4.7.1 with first-order DDM-3D was used to generate sensitivity and concentration output files (Byun and Schere 2006; Napelenok et al. 2006).

41.3 Results

Results compare favorably with previous estimations of sector contribution (Woody et al. estimate a total proportional contribution of 0.05 %, where we find a value of 0.04 %), but give the added capability of disaggregating impacts on an airport-by-airport basis (Fig. 41.2). Total average annual $PM_{2.5}$ sensitivity for all airports in the US was 0.87 μg/m^3 for primary (i.e., directly-emitted) $PM_{2.5}$ and 14.64 μg/m^3 for secondary (i.e., formed via chemical reaction) $PM_{2.5}$ (Table 41.1). Impacts near airports were substantially higher, with monthly $PM_{2.5}$ sensitivities reaching as high as 0.029 μg/m^3 near Atlanta's Hartsfield-Jackson international airport during July (Fig. 41.3). Primary $PM_{2.5}$ sensitivities show a largely monotonic decrease as distance from the airport increases; in contrast, peaks in secondary particulate concentration are often located up to 700 km from the airport site.

The aggregated group of thirty individual DDM runs captured about 94 % of primary and 72 % of secondary $PM_{2.5}$ relative to the sector-wide DDM model run; recall that our group of thirty runs comprised about 76 % of fuel burn. When results are compared with sector-wide brute force runs conducted with the same input data, the DDM model shows a sector-wide over-prediction in O_3 and both primary and

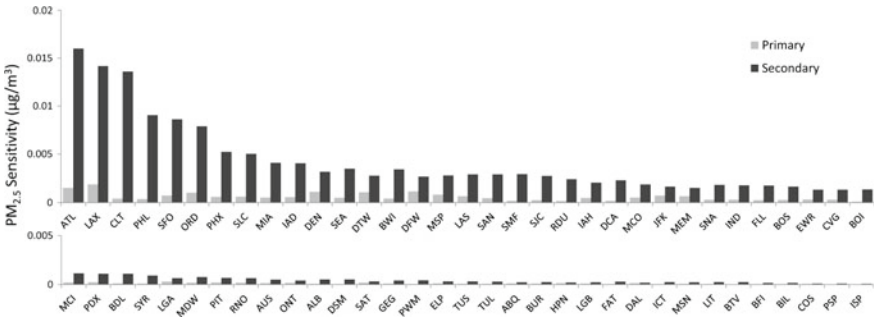

Fig. 41.2 Sixty-six individually modeled airports by mean peak primary (*blue*) and secondary (*red*) $PM_{2.5}$ sensitivities. Each value represents the annual average peak sensitivity found within a twenty-cell radius (about 720 km) of the cell containing the airport. Airports are listed by their four-letter ICAO designation, sans the US-specific "K" prefix

Table 41.1 Domain-wide total and per-grid-cell average annual sensitivities over the continental US (left, all thirty DDM runs combined; center, single sector-wide DDM run) and zero-out contributions (right, sector-wide brute force run)

	DDM (30 runs)		DDM (All apts.)		Brute force	
	Avg.	Total	Avg.	Total	Avg.	Total
O_3 (ppbV)	0.00071	11.75	0.00124	20.54	0.00069	11.52
Pri. $PM_{2.5}$ (μg/m^3)	0.00005	0.82	0.00005	0.87	0.00003	0.55
Sec. $PM_{2.5}$ (μg/m^3)	0.00064	10.58	0.00088	14.64	0.00065	10.78

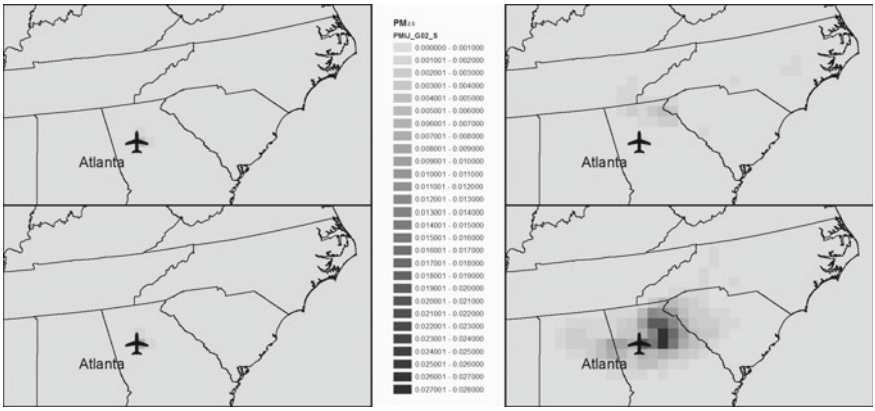

Fig. 41.3 Clockwise from *top left*: primary January, secondary January, secondary July, and primary July sensitivities to emissions from Atlanta's Hartsfield-Jackson International Airport

secondary $PM_{2.5}$. When disaggregated by species, these differences are largely due to over-predictions in sensitivities to NO_x emissions, especially far downwind from emissions sites. Modeling sensitivity of secondary nitrogen-based $PM_{2.5}$ species (e.g. nitrate and ammonium species) using DDM is difficult, but could potentially be improved with the use of higher-order DDM (Koo et al. 2009). Model results are being used to calculate air quality impacts and health impacts per quantity of emitted pollutants, which will be presented at the ITM conference in May.

Acknowledgments The authors thank M Reed, UNC ITS; C Coats, BH Baek, M Woody, P Vennam and SY Chang, UNC IE; and M Serre, UNC ESE. This work used the Extreme Science and Engineering Discovery Environment (XSEDE), which is supported by National Science Foundation grant number ACI-1053575. This work was funded by PARTNER under grants to UNC. PARTNER is funded by FAA, NASA, Transport Canada, US DOD, and EPA. The aviation emissions inventories used for this work were provided by US DOT Volpe Center and are based on data provided by the US FAA and EUROCONTROL in support of the objectives of the ICAO Committee on Aviation Environmental Projection CO2 Task Group. Any opinions, finding, and conclusions or recommendations expressed in this material are those of the author(s) and do not necessarily reflect the views of the US DOT, Volpe Center, the US FAA, EUROCONTROL, ICAO or PARTNER.

Questions and Answers

Questioner: Peter Builtjes, Talat Oldman
Question: What is the rationale behind using 3000 ft as a kind of average mixing height? In reality the mixing height varies in time and space. How do you allocate take-off emissions in the vertical? Do you consider ground equipment emissions?

Answer: The 3,000 ft emissions cutoff is not meant to correspond to any atmospheric condition; rather, it is an operations-based distinction between landing and takeoff (LTO) operations and cruise operations. The emissions processing sequence is primarily based on the operations mode provided as part of the aviation activity and emissions inventory from the Federal Aviation Administration (FAA)™s Aviation Environmental Design Tool (AEDT). In this dataset, spatiotemporal aircraft activity is provided from which emissions are calculated and gridded (in three dimensions) for use in CMAQ. One attribute of this database is emissions mode, which corresponds to one of ten sequential aircraft operation types, from taxiing to takeoff to climb to cruise, and finally descent to landing. Modes 1–3 correspond to taxi and takeoff modes and assigned to the departure airport, while modes 7–10 correspond to arrival and taxi modes and assigned to the arrival airport. Modes 4–6, corresponding to cruise activity, are not included in the modeling process. These chorded segments by activity mode for each flight path are then gridded into the corresponding CMAQ grid-cells based upon the relevant flight paths that fall in each grid-cell, as described in Baek et al. (2012). The AEDT only provides activity information for aircraft, and thus non-aircraft emissions (such as those from airport ground service vehicles) are not included. Thus, while a hard ceiling of 3,000 ft is built into the system, a soft cap based on aircraft operation mode limits emissions to a much lower altitude. And finally, EDMS (the precursor model to AEDT for preparing airport emissions inventories) uses a value of 3,000 ft as the default mixing height and the vertical extent of aircraft operations during LTO activities, and this provided the key motivation for us to define LTO activity in the vertical. However, the mixing height used in CMAQ predictions is based upon the WRF model, and truly varies in time and space.

Questioner: Talat Odman
Question: Would you consider verifying your results for one large and one small airport by modeling their domain of influence with higher resolution (e.g., 4-km grid size)?

Answer: One of the primary challenges of this work was balancing model runtime (CPU-hours) and quantity of disk space required against domain size. Certainly, a 4-km grid (a grid with 81 times the resolution of our 36-km grid) would provide a higher-resolution idea of the sensitivities caused by aircraft operations, which would give a more spatially-resolved indication of where impacts are located. Arunachalam et al. (2006) gives a good overview of the impact of grid size on model performance, with statistically significant differences between 36- and 4-km grid cells; further in a subsequent airport-specific grid-resolution investigation of air quality and health impacts, Arunachalam et al. (2011) showed that in spite of significant differences in maximum concentrations attributable to aviation emissions due to differing grid resolutions, total population health risks over the entire model domain were largely unaffected by model resolution. Thus, the need for higher model resolution is dependent on the objective of the study.

References

Arunachalam S (2011) Effect of chemistry-transport model scale and resolution on population exposure to $PM_{2.5}$ from aircraft emissions during landing and takeoff. Atmos Environ 45(19):3294–3300

Arunachalam S, Holland A, Do B, Abraczinskas M (2006) A quantitative assessment of the influence of grid resolution on predictions of future-year air quality in North Carolina, USA. Atmos Environ 40(26):5010–5016

Baek BH, Arunachalam S, Woody M, Vennam P, Omary M, Binkowski F, Fleming G (2012) A new interface to model global commercial aircraft emissions from the FAA Aviation Environmental Design Tool (AEDT) in air quality models. In: Proceedings of the 11th annual CMAS conference

Box GE, Draper NR (1987) Empirical model-building and response surfaces. Wiley, New Jersey

Bureau of Transportation Statistics (2014) National transportation statistics. http://www.transtats.bts.gov/. Accessed May 2014

Byun D, Schere KL (2006) Review of the governing equations, computational algorithms, and other components of the models-3 community multiscale air quality (CMAQ) modeling system. Appl Mech Rev 2:51–77

Dunker AM (1984) The decoupled direct method for calculating sensitivity coefficients in chemical kinetics. J Chem Phys 81:2385–2393

Koo B, Wilson G, Morris R, Dunker A, Yarwood G (2009) Comparison of source apportionment and sensitivity analysis in a particulate matter air quality model. Envir Sci Tech 43:6669–6675

Kwok R, Napelenok S, Baker K (2013) Implementation and evaluation of $PM_{2.5}$ source contribution analysis in a photochemical model. Atmos Environ 80:398–407

Lee K, Ashok A, Yim S, Barrett S (2012) Response surface model (RSM) v.3: CMAQ performance evaluation and hypotheses test results

Levy J, Woody M, Baek BH, Shankar U, Arunachalam S (2012) Current and future particulate-matter-related mortality risks in the United States from aviation emissions during landing and takeoff. Risk Anal 32:237–249

Napelenok S, Cohan DS, Odman M, Tonse S (2008) Extension and evaluation of sensitivity analysis capabilities in a photochemical model. Environ Modell Softw 23(8):994–999

Napelenok S, Cohan DS, Hu Y, Russell AG (2006) Decoupled direct 3D sensitivity analysis for particulate matter (DDM-3D/PM). Atmos Environ 40(32):6112–6121

Pope CA III, Burnett RT, Thun MJ, Calle EE, Krewski D, Ito K, Thurston GD (2002) Lung cancer, cardiopulmonary mortality, and long-term exposure to fine particulate air pollution. JAMA 287(9):1132–1141

Rienecker MM, Suarez MJ, Gelaro R, Todling R, Bacmeister J, Liu E, Bosilovich MG, Schubert SD, Takacs L, Kim GK (2011) MERRA: NASA's Modern-Era retrospective analysis for research and applications. J Climate 24(14):3624–3648

Roof C, Hansen A, Fleming G, Thrasher T, Nguyen A, Hall C, Grandi F, Kim B, Usdrowski S, Hollingsworth P (2007) Aviation Environmental Design Tool (AEDT) system architecture. Doc# AEDT-AD-01

U.S. Environmental Protection Agency (2005) National Emissions Inventory (NEI). http://www.epa.gov/ttn/chief/eiinformation.html

Wilkerson JT, Jacobson MZ, Malwitz A, Balasubramanian S, Wayson R, Fleming G, Naiman AD, Lele SK (2010) Analysis of emission data from global commercial aviation: 2004 and 2006. Atmos Chem Phys 10(13):6391–6408

Woody M, Baek BH, Adelman Z, Omary M, Lam YF, West J, Arunachalam S (2011) An assessment of aviation's contribution to current and future fine particulate matter in the United States. Atmos Environ 45:3424–3433

Chapter 42
Regional Scale Dispersion Modelling of Amines from Industrial CCS Processes with COSMO-MUSCAT

Ralf Wolke, Andreas Tilgner, Roland Schrödner, Claus Nielsen and Hartmut Herrmann

Abstract Both detailed chemical process model studies are performed in order to develop a reduced chemical mechanism for MEA and complex 3D dispersion model investigations with COSMO-MUSCAT were carried out focusing mainly on the chemical fate and lifetime of MEA and its reaction products such as nitramines and nitrosamines as well as their removal. In conclusion, the present dispersion model study has revealed that based on the available emissions and the meteorological conditions the proposed guidelines for long-term exposure in air should be not exceeded. Overall, the model results might allow future evaluations of possible environmental impacts and human health effects of pollutants emitted from CCS processes.

42.1 Introduction and Motivation

The CO_2 capture and store (CCS) technologies are designed to reduce anthropogenic CO_2 emissions into the atmosphere. At present, amine-based post-combustion CO_2 capture techniques of power plants will release discharged air into the environment, which will contain a small but still significant amount of amines and their oxidation products (Karl et al. 2014). Moreover, it is known that the atmospheric oxidations of amines can lead to the formation of harmful (potentially carcinogenic) compounds such as nitramines and nitrosamines (Nielsen et al. 2012). Thus, an improved knowledge on the tropospheric chemical fate and physical removal processes of released amines and its oxidation products is required in order to assess the environmental impact and risks resulting from

R. Wolke (✉) · A. Tilgner · R. Schrödner · H. Herrmann
Leibniz Institute for Tropospheric Research (TROPOS), Permoserstrasse, 15, 04303 Leipzig, Germany
e-mail: wolke@tropos.de

C. Nielsen
University of Oslo, Postboks 1033 Blindern, 0315 Oslo, Norway

D.G. Steyn and N. Chaumerliac (eds.), *Air Pollution Modeling and its Application XXIV*, Springer Proceedings in Complexity,
DOI 10.1007/978-3-319-24478-5_42

amine-based capturing operations. Recent box model studies performed at TROPOS (Herrmann et al. 2011) have implicated the importance of multiphase chemical interactions for the tropospheric processing of emitted amines from CCS techniques. However, complex chemical interactions were not yet considered in former simple dispersion modelling.

The present air pollution study focuses mainly on the regional scale modelling of the tropospheric fate and deposition of monoethanolamine (MEA) and its oxidation products using the modelling system COSMO-MUSCAT. The present modelling work was specifically designed to investigate conditions and impacts at the planned CO_2 capture power plant at Mongstad (Norway) and the surrounding area. The primary amine MEA was selected as test amine for the amine-based post-combustion facility at Mongstad. Complex dispersion model simulations were carried out focusing on the lifetime and removal of MEA as well as its reaction products such as nitramines and nitrosamines. The study is aimed to provide detailed and conclusive concentration/deposition charts. These charts provide details on the regional fate of MEA and its oxidation products, the regional distribution of such pollutants and characterize locally the potential input of those pollutants into other environmental compartments. The performed annual simulations were attended by extensive sensitivity and process studies to evaluate the associated uncertainties. For this study, realistic concentrations of reactants (OH, NO_3, NO_2) for MEA chemistry were provided by applying the RACM chemistry and anthropogenic emission inventories The physical loss processes of dry and wet deposition are described in dependence on meteorological conditions and land use properties.

42.2 Regional Dispersion Modelling

Setup. The modelling department of the TROPOS has developed the state-of-the-art multiscale model system COSMO-MUSCAT (Wolke et al. 2012; Renner and Wolke 2010). It is qualified for process studies as well as the operational forecast of pollutants in local and regional areas. The model system consists of two online-coupled codes. The operational forecast model COSMO is a non-hydrostatic and compressible meteorological model and solves the governing equations on the basis of a terrain-following grid (Schättler et al. 2013). Driven by the meteorological model, the chemistry transport model MUSCAT treats the atmospheric transport as well as chemical transformations for several gas phase species and particle populations. The transport processes include advection, turbulent diffusion, sedimentation, dry and wet deposition.

Transport and Deposition of MEA. The dynamics of the plume was analysed for different situations, where rotating, alternating, retrograde, and fast variable wind leads to very complex structures like evasion of the mountains, advance into the fjords, transport of former plume fractions, and oscillating plumes. Not only the spatial resolution plays an important role in a realistic simulation of the plumes, but also the (fast) temporal development of the meteorological situation. Such changes,

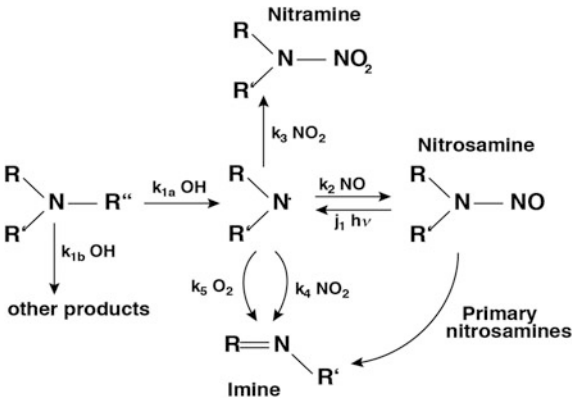

Fig. 42.1 Generalized atmospheric photo-oxidation scheme for amines (modified after Nielsen et al. 2012)

e.g. of the dynamic stability of the atmosphere, can occur abruptly, which necessarily affords an online-coupled combined treatment of all processes as is implemented in the applied model system.

Formation of Nitramines and Nitrosamines. The nitramine concentrations modelled by the explicit MEA chemistry mechanism were compared with two simplified schemes, which provide upper limits for the nitramine concentrations. In the first approach (BFe1), the product of the OH-reaction (see Fig. 42.1) gives an upper limit. In the second approach (BFvar), the branching by the NO_x and O_2 reaction pathways of the product is also taken into account.

As expected, the explicit mechanism produces the smallest concentrations. The values are 10–30 % smaller than for the BFvar scheme and reduce the simple BFe1 estimation by a factor about 10. Dry and wet depositions are equally important for the tropospheric removal. Dry deposition is closely correlated to the land-use data. The pattern of wet deposition is due to the occurrence of precipitation and high concentration in the same region at the same time (Figs. 42.2 and 42.3).

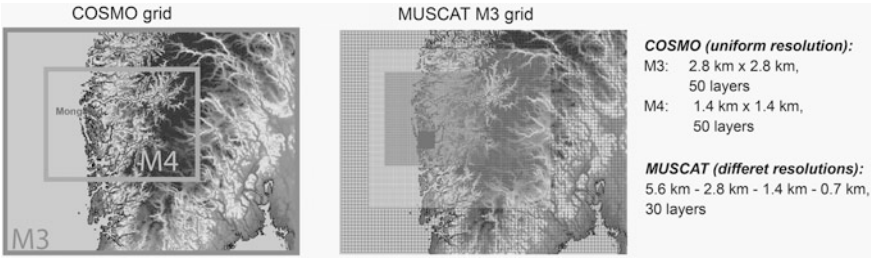

Fig. 42.2 COSMO and MUSCAT grids for the M3 model simulations

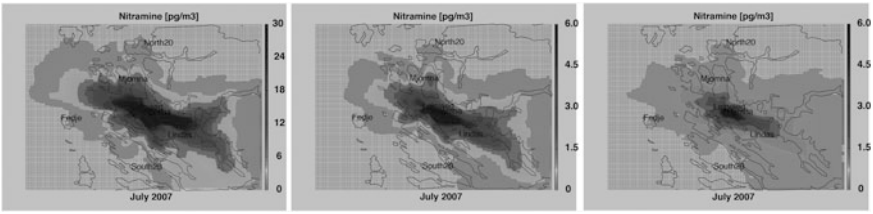

Fig. 42.3 Modelled monthly mean concentration of nitramine (pg/m^3) at ground level for July 2007: branching factor equal to 1 (*left column*); variable branching factor in dependence on NO_x concentration (*center column*); explicit MEA gas phase chemistry (*right column*)

42.3 Multiphase MEA Chemistry Modelling

Detailed process studies revealed the importance of both clouds and aqueous particles for the multiphase chemical processing of MEA and its products (Herrmann et al. 2011). Due to the shifted partitioning of MEA towards the aqueous phase, the model investigations implicate that aqueous oxidation by OH radicals represents the main sink for MEA under daytime cloud summer conditions. Reaction flux analyses have indicated that under aqueous particle conditions, the Cl radical represents also an important oxidant. Moreover, the simulations showed that the aqueous formation of N-nitroso-MEA is an irrelevant process under tropospheric conditions. MEA oxidations are quite restricted under low photochemical winter conditions leading to much longer tropospheric residence times. Additionally, the model simulations implicated that the aqueous phase reduces substantially the formation of harmful compounds such as MEA-nitramine in the gas phase. Thus, simulations without aqueous phase chemistry treatment were characterised by much higher concentrations of MEA-nitramine implicating that pure gas phase simulations provide elevated "worst case concentrations" and might be used for "upper limit" estimations of harmful MEA production.

To provide a condensed mechanism applicable for regional scale dispersion modelling, a manual mechanism reduction was performed. The developed reduced mechanism contains just 303 gas and 112 aqueous phase reactions and describes adequately the chemical fate of MEA and its key oxidation products. Performed comparison of the full and reduced mechanism showed relatively small deviations for MEA and its main oxidation products.

42.4 Summary and Conclusions

Based on the results of the process model studies, further COSMO-MUSCAT studies were aimed at the examination of the importance of tropospheric gas phase oxidations for the fate of MEA, the production of harmful compounds such as nitramines and the dispersion of MEA and its products including their regional

concentration levels. In conclusion, the present dispersion model study has revealed that based on the available emissions and the meteorological conditions in the Mongstad region, the proposed guidelines for long-term exposure in air for MEA and also the total amount of nitrosamines and nitramines should be not exceeded. Moreover, the modelled annual deposition rates of MEA are also below the critical deposition. However, for nitrosamines and nitramines, this conclusion cannot be safely given due to the large uncertainties about residence times of these compounds in the soil water. Additionally, the model simulations implicated that the aqueous phase reduces substantially the formation of harmful compounds such as MEA-nitramine in the gas phase. Thus, simulations without aqueous phase chemistry treatment were characterised by much higher concentrations of MEA-nitramine implicating that pure gas phase simulations provide elevated "worst case concentrations" and might be used for "upper limit" estimations of harmful MEA production.

Acknowledgments This project was gratefully funded by the Technology Centre Mongstad (TCM, http://www.tcmda.com). Furthermore, the ZIH Dresden and the NIC Jülich supported this work. We gratefully acknowledge the DWD Offenbach for good cooperation.

References

Herrmann H et al (2011) Atmospheric chemistry—aqueous phase chemistry multiphase modelling. Tel-Tek report 2211030-AQ07 v2.Rep

Karl M et al (2014) Uncertainties in assessing the environmental impact of amine emissions from a CO_2 capture plant. Atmos Chem Phys 14:8533–8557

Nielsen CJ et al (2012) Atmospheric degradation of amines (ADA): summary report from atmospheric chemistry studies of amines, nitrosamines, nitramines and amides. University of Oslo, Oslo

Renner E, Wolke R (2010) Modelling the formation and atmospheric transport of secondary inorganic aerosols with special attention to regions with high ammonia emissions. Atmos Environ 44:1904–1912

Schättler U, Doms G, Schraff C (2013) A description of the nonhydrostatic regional COSMO-Model. Part I: Users guide. Deutscher Wetterdienst, Offenbach. http://www.cosmo-model.org

Wolke R, Schroder W, Schrodner R, Renner E (2012) Influence of grid resolution and meteorological forcing on simulated European air quality: a sensitivity study with the modeling system COSMO-MUSCAT. Atmos Environ 53:110–130

Chapter 43
Contribution of Ship Emissions to the Concentration and Deposition of Pollutants in Europe: Seasonal and Spatial Variation

Sebnem Aksoyoglu, A.S.H. Prévôt and U. Baltensperger

Abstract We studied the effects of ship emissions on the annual and seasonal concentrations and depositions of pollutants in Europe using the regional air quality model CAMx with and without ship emissions for 2006. Ship emissions cause a decrease in annual ozone mixing ratios around the English Channel and the North Sea, whereas they lead to an increase (4–14 %) in the Mediterranean region. They also cause an increase in $PM_{2.5}$ concentrations over the Mediterranean Sea (up to 80 %) and in the North Sea and Baltic Sea as well as along the coastal areas (10–15 %). Increased concentrations of the primary particles are predicted only along the shipping routes, whereas concentrations of the secondary pollutants are affected over a larger area. Particulate sulfate concentrations increase in the Mediterranean and the North Sea while elevated particulate nitrate levels are found especially around the Benelux area and northern Italy where there are high NH_3 land-based emissions. Our model results show that not only the air concentrations of pollutants are affected by ship emissions, but also depositions of nitrogen and sulfur compounds increase significantly along the shipping routes, especially in the Mediterranean Sea. The effects are found to be larger in summer.

43.1 Introduction

Increases in population and mobility are associated with emissions of pollutants from transport sectors such as road, air traffic and international shipping; these emissions affect the air quality and climate (Eyring et al. 2010). There have been many studies and future projections on the effects of air and road traffic emissions, but relatively little detailed work has been done on the impacts of ship emissions

S. Aksoyoglu (✉) · A.S.H. Prévôt · U. Baltensperger
Laboratory of Atmospheric Chemistry, Paul Scherrer Institute,
5232 Villigen PSI, Switzerland
e-mail: sebnem.aksoyoglu@psi.ch

D.G. Steyn and N. Chaumerliac (eds.), *Air Pollution Modeling and its Application XXIV*, Springer Proceedings in Complexity,
DOI 10.1007/978-3-319-24478-5_43

(Dalsoren et al. 2009; Hodnebrog et al. 2011; Johansson et al. 2013; Jonson et al. 2015). The marine transport sector contributes significantly to air pollution, particularly in coastal areas (Marmer et al. 2009). Ship emissions are continuously growing, while land-based emissions are gradually decreasing. The Regulations for the Prevention of Air Pollution from Ships (Annex VI) aim to minimize airborne emissions from ships and their contribution to local/global air pollution (http://www.imo.org). In Europe, maximum sulphur content of the fuels is limited to 0.1 % as of 1 January 2015 in the Sulphur Emission Control Areas (SECAs) which cover the Baltic Sea, the English Channel and the North Sea (http://ec.europa.eu/environment/air/transport/ships.htm). We report here the effects of ship emissions in Europe on the spatial and seasonal distributions of pollutant concentration and deposition in 2006.

43.2 Method

We used the CAMx (Comprehensive Air quality Model with extensions, Version 5.40, http://www.camx.com) and WRF (The Weather Research and Forecasting Model, Version 3.2.1, http://wrf-model.org/index.php) models. The model domain covered Europe with a horizontal resolution of 0.250° × 0.125°. The gridded TNO/MACC for 2006 was used as the basic anthropogenic emission inventory (Denier van der Gon et al. 2010). Other details of the model input and parameterization are described in Aksoyoglu et al. (2014). Concentrations and dry/wet deposition of pollutants were calculated for the entire year 2006, with and without ship emissions.

43.3 Results

Our results suggest that ship emissions cause a decrease (2–18 %) in annual ozone mixing ratios in the English Channel and the North Sea, but an increase (4–14 %) in the Mediterranean Sea (Fig. 43.1, left); the effects are larger in summer. $PM_{2.5}$ concentrations increase in the Mediterranean Sea (up to 80 %), the North Sea and the Baltic Sea (10–15 %), as well as along the coastal areas (10–15 %) due to ship emissions (Fig. 43.1, right). The contribution of emissions from naval engines is predicted to be smaller in winter and larger in summer (Fig. 43.2).

Ship emissions lead to an increase in the concentrations of particulate sulfate in the Mediterranean and along the northern coast while concentrations of particulate nitrate increase especially around the Benelux area and northern Italy where there are high NH_3 emissions (Fig. 43.3). Primary organic aerosol and elemental carbon concentrations increase only along the shipping routes. Contribution to the

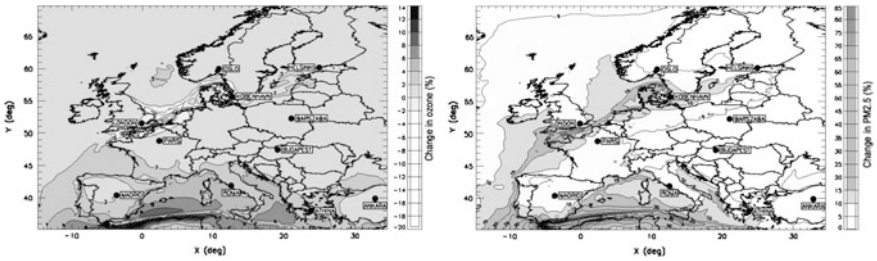

Fig. 43.1 Relative contribution of ship emissions (%) to annual ozone (*left*) and $PM_{2.5}$ (*right*)

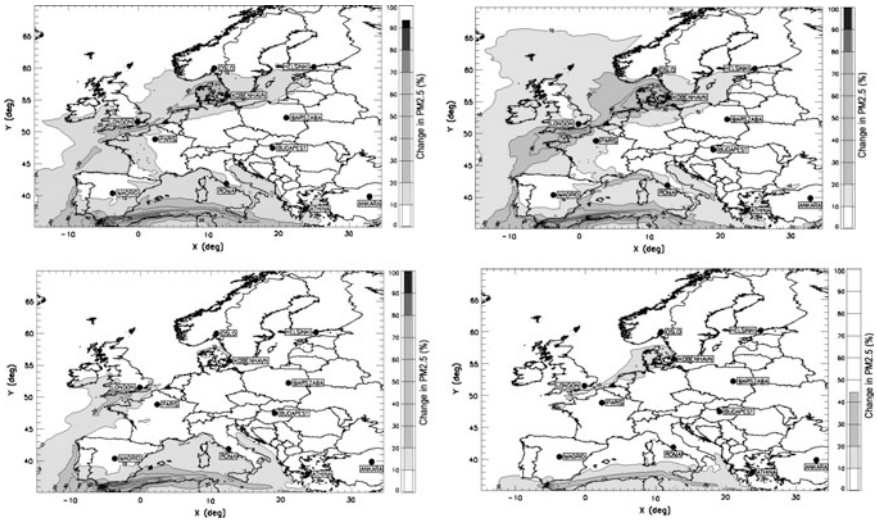

Fig. 43.2 Relative change in $PM_{2.5}$ (%) due to ship emissions in spring (*top left*), summer (*top right*), fall (*bottom left*), and winter (*bottom right*)

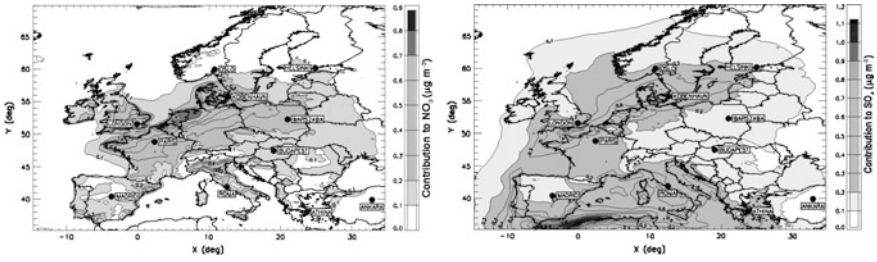

Fig. 43.3 Contributions of ship emissions to annual particulate nitrate (*left*) and sulfate (*right*)

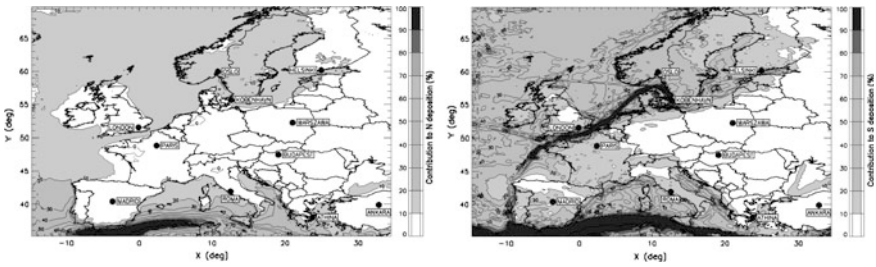

Fig. 43.4 Contributions of ship emissions (%) to deposition of N (*left*) and S compounds (*right)*

secondary organic aerosols on the other hand, is less than 10 %. Ship emissions also cause an increase in the deposition of nitrogen (mainly oxidized N) and sulfur (mainly dry deposition of SO_2) along the shipping routes (Fig. 43.4).

43.4 Conclusions

Our model study using the emissions in 2006 suggests that ship emissions decrease (2–18 %) annual ozone mixing ratios in the English Channel and the North Sea, but they lead to an increase (4–14 %) in the Mediterranean Sea. They also cause an increase in $PM_{2.5}$ concentrations in the Mediterranean (up to 80 %), the North Sea, Baltic Sea as well as along the coastal areas (10–15 %). Increased concentrations of primary organic aerosols and elemental carbon occur only along the shipping routes. All effects of ship emissions are larger in summer. The most significant effect is on the secondary inorganic aerosols; the secondary organic aerosol concentrations increase by not more than 10 %. Ship emissions increase the concentrations of the particulate sulfate in the Mediterranean as well as along the northern coast while concentrations of particulate nitrate increase around the Benelux area and northern Italy where there are high NH_3 land emissions. Ship emissions lead to an increase in the deposition of nitrogen (mostly deposition of oxidized N) and sulfur compounds (mainly dry deposition of SO_2) along the shipping routes, especially in the Mediterranean region.

Acknowledgments This study was funded by the Competence Center Energy and Mobility CCEM-CH). We are grateful to ECMWF, TNO and AQMEII for providing us with data.

Questions and Answers

Questioner Name: T. Dore
Q: You mentioned Sulphur Emission Control Areas. Nitrogen Emission Control Areas are also being discussed for shipping. How is current and planned policy

likely to affect the contribution of shipping to PM formation and N and S deposition in the future?
A: According to the EEA, NO_x emissions from international shipping in European waters could be equal to land-based sources from 2020 onwards. On the other hand IMO NOx limits refer only to new ships, therefore the impact of these regulations is limited at present and near future. In addition, land-based NH_3 emissions are critical for PM formation. Since they are not expected to decrease significantly, particulate nitrate formation would not decline. Regulations of ship emissions would certainly help reducing oxidized nitrogen and S deposition in the future; it would take some time to see their impacts, though.

Questioner Name: Jukka-Pekka Jalkanen
Q: How is the temporal variation of ship emissions included in your work?
A: Monthly, daily and hourly emission factors for each SNAP sector are provided by TNO to scale the annual emissions. Temporal variation of emission factors for ships shows a slight increase in summer.

Questioner Name: S. Arunachalam
Q: How were shipping emissions represented in your model? If area sources on the ground, is that realistic since ships have tall stacks that give high plume rise?
A: We treated the ship emissions provided by TNO as area sources (in the first layer) due to limited information. If enough data is available, one can distribute these emissions to the vertical layers of the model. Most of them would be then injected to the first two layers.

References

Aksoyoglu S, Keller J, Ciarelli G, Prévôt ASH, Baltensperger U (2014) A model study on changes of European and Swiss particulate matter, ozone and nitrogen deposition between 1990 and 2020 due to the revised Gothenburg protocol. Atmos Chem Phys 14:13081–13095. doi:10.5194/acp-14-13081-2014

Dalsoren SB, Eide MS, Endresen O, Mjelde A, Gravir G, Isaksen ISA (2009) Update on emissions and environmental impacts from the international fleet of ships: the contribution from major ship types and ports. Atmos Chem Phys 9(6):2171–2194

Denier van der Gon H, Visschedijk A, van de Brugh H, Droege R (2010) A high resolution European emission data base for the year 2005. A contribution to UBA-Projekt: "Strategien zur Verminderung der Feinstaubbelastung" – PAREST: Partikelreduktionsstrategien—Particle Reduction Strategies Rep. TNO-034-UT-2010-01895_RPT-ML, TNO, Utrecht (NL)

Eyring V, Isaksen ISA, Berntsen T, Collins WJ, Corbett JJ, Endresen O, Grainger RG, Moldanova J, Schlager H, Stevenson DS (2010) Transport impacts on atmosphere and climate: shipping. Atmos Environ 44(37):4735–4771

Hodnebrog O, Berntsen TK, Dessens O, Gauss M, Grewe V, Isaksen ISA, Koffi B, Myhre G, Olivié D, Prather MJ, Pyle JA, Stordal F, Szopa S, Tang Q, van Velthoven P, Williams JE, Odemark K (2011) Future impact of non-land based traffic emissions on atmospheric ozone and OH—an optimistic scenario and a possible mitigation strategy. Atmos Chem Phys 11(21):11293–11317

Johansson L, Jalkanen JP, Kalli J, Kukkonen J (2013) The evolution of shipping emissions and the costs of regulation changes in the northern EU area. Atmos Chem Phys 13(22):11375–11389

Jonson JE, Jalkanen JP, Johansson L, Gauss M, Denier van der Gon HAC (2015) Model calculations of the effects of present and future emissions of air pollutants from shipping in the Baltic Sea and the North Sea. Atmos Chem Phys 15:783–798. doi:10.5194/acp-15-783-2015

Marmer E, Dentener F, Aardenne Jv, Cavalli F, Vignati E, Velchev K, Hjorth J, Boersma F, Vinken G, Mihalopoulos N, Raes F (2009) What can we learn about ship emission inventories from measurements of air pollutants over the Mediterranean Sea? Atmos Chem Phys 9: 6815–6831

Chapter 44
Development of an Approximate Method for Advection of Sensitivity Fields

Pedram Falsafi and Amir Hakami

Abstract Although advection equation is linear in time and space, positive definite and mass conservative advection schemes in chemical transport models (CTMs) behave nonlinearly mostly due to discontinuous (conditional) operations in discretization. A new approach is developed to indirectly simulate the advection process in CTMs. Instead of integrating the continuity equation directly for various species, advection equations for various pollutants are solved in relations to advected air densities. Our approach relies on the run-time estimation of the Jacobian of the advection operator, and can be based on the native advection algorithm in any CTM. The estimated transport Jacobian for air densities are then applied to other species with corrections that would ensure consistency with the underlying scheme. Since our proposed method is truly linear in species concentration, it is not suspect to complications associated with advecting sensitivities as experienced with nonlinear advection schemes. We implement our advection method in CMAQ 5.0 using its native Piecewise Parabolic Method (PPM) advetion scheme. Our preliminary results show good consistency with the PPM scheme, and potential for truly linear advection of sensitivity fields.

44.1 Introduction

Community Multiscale Air Quality (CMAQ) modelling system (Byun and Schere 2006) currently employs Piecewise Parabolic Method (PPM) scheme (Colella and Woodward 1984) to solve one-dimensional (i.e. split) horizontal advection equations for all species. Advection is a linear process, and it is desirable for an advection scheme to preserve the linearity of the process. PPM is a nonlinear scheme, and as a consequence, it does not behave similarly for pollutants with

P. Falsafi · A. Hakami (✉)
Department of Civil and Environmental Engineering, Carleton University, Ottawa, Canada
e-mail: amir_hakami@carleton.ca

D.G. Steyn and N. Chaumerliac (eds.), *Air Pollution Modeling and its Application XXIV*, Springer Proceedings in Complexity,
DOI 10.1007/978-3-319-24478-5_44

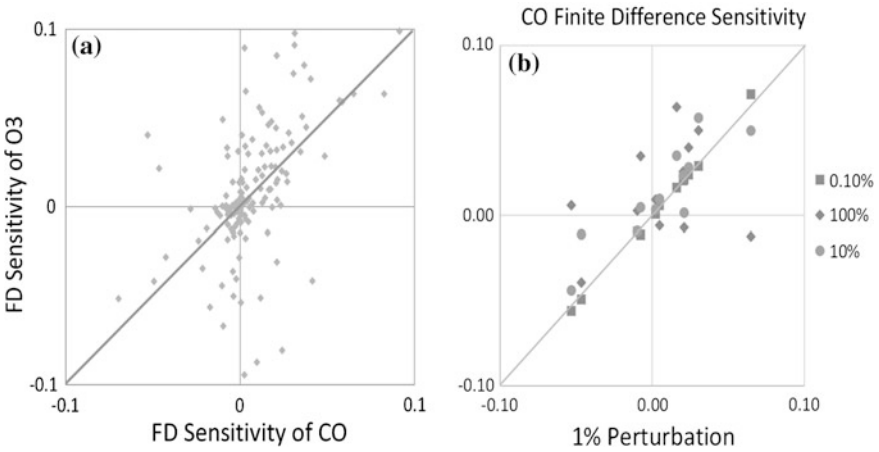

Fig. 44.1 Comparison of finite difference sensitivity coefficients for **a** various species (with different spatial distributions), and **b** with different perturbation levels

different spatial distributions. For example, at one grid point, different species may have various sensitivities to the same perturbations in their concentrations (Fig. 44.1a) or different levels of perturbation may not generate similar sensitivities (Fig. 44.1b), while the sensitivity coefficient for this linear process should be independent of concentration profile or perturbation level.

It can also be seen in Fig. 44.1 that there are points with negative sensitivities, indicating an increase in concentration of one point due to a decreased initial concentrations; an outcome that is physically meaningless for the advection process. Furthermore, as PPM depends on the sign of the advective flux for various species, it may also behave differently for species with negative and positive sensitivities, even as they are advected within the same wind field.

Here, we revert to the fact that advection is due to the bulk air motion; thus, advection of air acts as the governing process in transport of all other species. The main objective of this study is to provide a linear solution to the advection problem, which would maintain the mass conservation properties of the underlying advection scheme. The most important advantage of this approach, however, is in its use for advecting derivatives/sensitivities in forward (i.e. decoupled direct method, DDM) or backward (adjoint) sensitivity analysis applications.

44.2 Methodology

One dimensional continuity equation for species in the atmosphere in the flux form as used in CMAQ is:

$$\frac{\partial C_x}{\partial t} + \nabla \cdot (uC_x) = 0 \tag{44.1}$$

where C_x is pollutant's mass/number concentration and u is the wind velocity. In Linear Sensitivity Advection Method (LSAM), we advect the air density using the native CMAQ advection scheme (i.e. PPM). After each time-step, the fraction of air mass in each cell that is transported to other cells can be evaluated by tracking the effect of density field on the mass flux that enters or exits each cell. As a result air density for a grid point j can be expressed as:

$$\rho_j^{n+1} = \sum_{i=i_0}^{i_n} \rho_i^n \times \mathcal{J}_{ij}^n \tag{44.2}$$

where ρ is the air density and $\mathcal{J}_{ij}^n$ is the mass fraction of air in cell i which transports to cell j, so $\mathbf{J^n} = [\mathcal{J}_{ij}^n]$ can be considered as the Jacobian of advection operator. The Jacobian of the advection operator constitutes a contribution matrix, and can be estimated by various approaches, such as single-cell perturbation of density fields. Applying the PPM scheme leads to transport of air up to two neighbor cells on each side so ρ_j^{n+1} will be only sensitive to ρ_{j-2}^n to ρ_{j+2}^n. Equation 44.2 then can be reduced to:

$$\rho_j^{n+1} = \sum_{i=j-2}^{j+2} \rho_i^n \times \mathcal{J}_{ij}^n \tag{44.3}$$

The advection process of other species is governed by the bulk motion of air, and therefore, the portion of air mass that is transported from cell i to cell j is equal to the fraction of other species advected from cell i to cell j. Consequently, $\mathcal{J}_{ij}^n$ coefficients (i.e., contribution coefficients) in 44.2 can be used to evaluate the concentration of other species.

$$C_j^{n+1} = \sum_{i=j-2}^{j+2} C_i^n \times \mathcal{J}_{ij}^n \tag{44.4}$$

Here C_i^n is the pre-advection concentration of pollutant. We note that for a linear scheme, this approach would be equivalent to solving the continuity equation for individual species. In this method, contribution coefficients ($\mathcal{J}_{ij}^n$) are independent of pollutants concentrations and only depend on meteorological data (i.e. velocity field and air density). Since integration of the advection equation for individual pollutants is not necessary, this approach may be computationally less demanding.

44.3 Results and Discussion

To evaluate the proposed method, we compare full simulation outputs with the original CMAQ 5.0 over a 36 km continental domain for contiguous U.S. and for a period of 8 days. The difference between pollutants concentration in these two cases is calculated as a measure of error in adopting LSAM instead of native PPM. Temporal and spatial contrasts are considered for various pollutants such as O_3 and CO.

Figures 44.2 and 44.3 compare daily maximum concentration of species at day 4 (a) and 8 (b) for O_3 and CO, respectively. The model outputs are in acceptable agreement with original CMAQ for pollutants of concern and their differences are

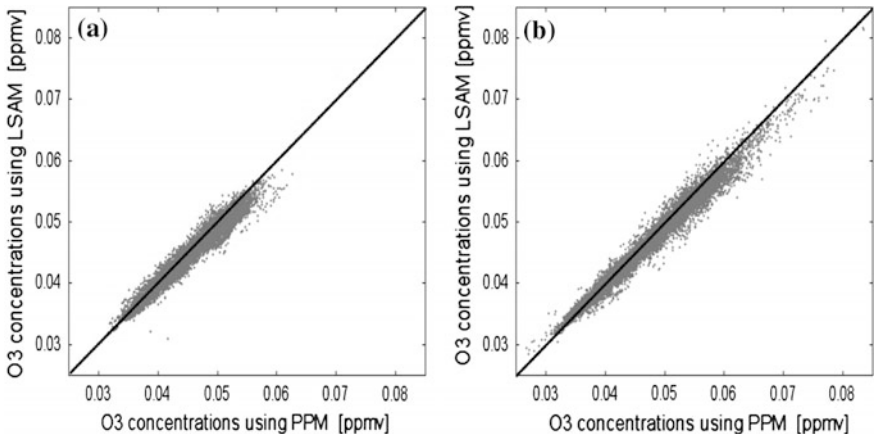

Fig. 44.2 Comparison of ozone concentrations over the domain for the first layer **a** after 4 days R-squared = 0.946 and **b** after 8 days of simulation R-squared = 0.965

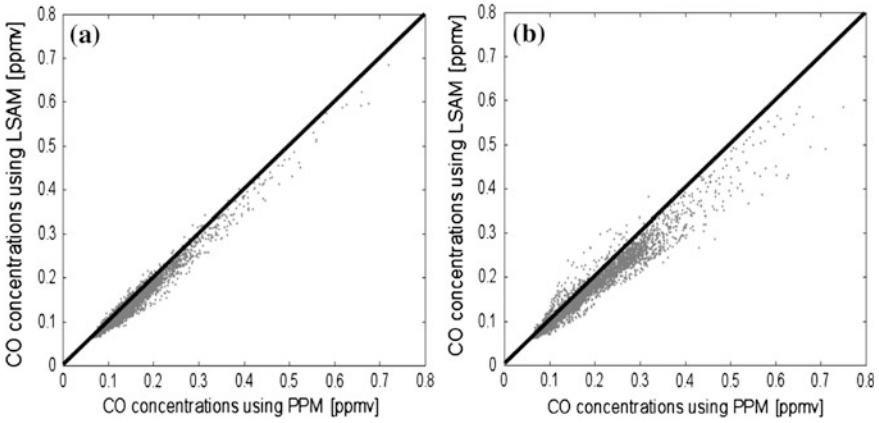

Fig. 44.3 Comparison of CO concentrations over the domain for the first layer **a** after 4 days R-squared = 0.969 and **b** after 8 days of simulation R-squared = 0.948

not growing significantly over time. Note that since our approach is an approximate method, some level of discrepancy with the underlying is to be expected.

44.4 Conclusions

The method proposed in this work is computationally efficient, as it does not integrate the continuity equation for individual species. Because of this computational saving, the CTM can afford to take advantage of a more accurate and expensive algorithm as the underlying advection scheme for the transport of air densities.

Furthermore, this approach provides a truly linear and mass conservative solution to the advection problem that is reliable for advecting derivatives. Current advection algorithms are designed to advect positive concentrations, and may behave erroneously when advecting sensitivities that can be negative. In future work, we will evaluate how LSAM performs for the advection of sensitivity fields. As the suggested approach is an approximate method, we do not recommend using this approach for advecting concentrations, unless further improvements make the results more comparable with the underlying advection scheme. However, we consider this method to hold potentially significant advantage in advecting sensitivity fields of different shapes and signs.

Question and Answer

Questioner: Clemens Mensink
Question: Would it be interesting to simply go to higher order or more accurate schemes?

Answer: More accurate schemes are obviously desirable, but increased accuracy often is accompanied by artificial non-linearity, as well as additional computational cost. We believe that it is physically inconsistent to advect sensitivities of different species (or for that matter their concentrations), differently while they are all advected in the same wind field. This approach aims to address that underlying problem.

References

Byun DW, Schere KL (2006) Review of the governing equations, computational algorithms, and other components of the models-3 community multiscale air quality (CMAQ) modeling system. Appl Mech Rev 59:51–77

Colella P, Woodward PR (1984) The piecewise parabolic method (PPM) for gas-dynamical simulations. J Comput Phys 54(1):174–201

Chapter 45
Modeling and Chemical Analysis Used as Tools to Understand Decade-Long Trends of Ozone Air Pollution in the Lower Fraser Valley, British Columbia, Canada

Nadya Moisseeva, Bruce Ainslie, Roxanne Vingarzan and Douw Steyn

Abstract The Lower Fraser Valley (LFV) B.C., a largely deindustrialized region with emissions dominated by the transportation sector, has experienced large reduction in precursor emissions over the last 20 years. While these reductions have resulted in concomitant changes in summertime ambient ozone concentrations, the changes have not been uniform across the region, with trends in long term behavior differing noticeably between the eastern and western portions of the valley. In this work, we draw upon previous modeling, observational and experimental studies to infer how the sensitivity of ground-level ozone to precursor emissions has changed over the last two decades. This work is notable for several reasons. First we establish not only VOC- and NO_x-ozone sensitivities during summertime ozone episodes, but across the full range of summertime meteorological conditions. Next, we examine how these sensitivities have changed over the last two decades. We also examine how these sensitivities vary spatially across the LFV and finally we use the above findings to explain observed summertime ozone trends in terms of changing ozone sensitivities and changing emission rates.

45.1 Introduction

Over the last three decades LFV has witnessed significant emission reductions due to federal regulations targeting vehicle and fuel emissions, the implementation of a successful provincial Air Care program and two regional air quality management

N. Moisseeva (✉) · D. Steyn
The University of British Columbia, Vancouver, Canada
e-mail: nmoisseeva@eos.ubc.ca

B. Ainslie · R. Vingarzan
Environment Canada, Vancouver, Canada

D.G. Steyn and N. Chaumerliac (eds.), *Air Pollution Modeling and its Application XXIV*, Springer Proceedings in Complexity,
DOI 10.1007/978-3-319-24478-5_45

plans (AQMPs) in 1994 and 2005. Consequently it has seen dramatic changes in the emissions of precursor pollutants, which has altered the spatiotemporal characteristics of ozone distribution. Substantial (40–50 %) but localized reductions in precursor emissions have been reported (GVRD 2007), highlighting the importance of identifying air quality trends in both space and time. Earlier work on the subject was primarily focused on episodic ozone pollution. Approaching the issue using both statistical (Ainslie and Steyn 2007) and numerical (Ainslie et al. 2013) methods, it was shown that summertime ozone episodes exhibit variable spatial patterns and VOC- and NO_x-ozone sensitivities. The current work aims to expand these findings and establish sensitivity regimes for the full range of meteorological conditions in the LFV, rather than restricting the analysis to episodic events.

Given the nature of the large scale emission reductions, the fact that LFV does not seem to be influenced by up-stream urban sources of ozone and its precursors and that the fixed monitoring network has been operating over the emission reductions timeframe, a trend analysis of the monitoring data offers an insightful window into the local nature of air quality. Furthermore, photochemical and dispersion modeling can be used to complement the observational datasets and offer the ability to directly explore source- receptor relationships and ozone-precursor sensitivities.

45.2 Methods

For the present analysis, we consider trends only over the 1992–2012 period to be relevant from a policy point of view. The start of this period is marked by the implementation of federal regulations on fuels and vehicles (1991) and a local in-use and maintenance (IM) vehicle emissions program (AirCare 1991).

Data were obtained from the Greater Vancouver Regional District (GVRD) fixed monitoring network. Our study makes use of 21 years (1992–2012) of hourly ambient ozone, NO and NO_2 measurements (from over 39 stations); 21 years of 24 h averaged speciated VOC measurements from (15 stations); observations of "clean" upwind ozone concentrations; emission inventories and previous modeling work.

Using 1-h averaged NO_x data, we have calculated temporal trends in both maxima and percentiles for years 1992–2012. One-in-six day, 24-h averaged VOC measurements were examined for trends for all available stations for the same time period. Further, we have selected 20 station locations, for which consistent hourly ozone data were available. The ozone trend analysis was performed in the context of Canada Wide Standards (CWS) for $PM_{2.5}$ and O_3 (CCME 2000), using 1 and 8 h ozone concentrations. Temporal trends in maximum and background (percentile) concentrations were calculated for the period 1992–2012. We have also examined the changes in summer diurnal ozone concentration profiles, by comparing the current and pre-AQMP patterns. Joint comparison of trends in precursor concentrations and

ambient ozone measurements were used to approximate the spatial distribution of sensitivity regimes in the valley.

CMAQ model output from the Steyn et al. (2013) and Ainslie et al. (2013) retrospective modeling studies are used to understand how emission reductions have changed the spatial behavior of ozone sensitivity to NO_x and VOC emissions within the LFV.

45.3 Discussion and Results

We have found declining trends in both measured NO_x and VOC across the valley, suggesting that emission reductions have led to lower concentrations of these precursor pollutants throughout the region. However, these large-scale reductions in ozone precursors have not led to uniform decrease in ozone concentrations throughout LFV. Moreover, the emission reductions were more efficient in decreasing peak hourly ozone concentrations than maximum 8 h concentrations. The nature of this inhomogeneity in the effects of precursor reductions on ozone concentrations was examined from spatial, temporal and metric perspectives.

As suggested by earlier modeling work (Ainslie et al. 2013) the LFV has an east-west split in ozone sensitivity. Our present study suggests that this split is subject to the particular ozone metric (percentile) used. For peak concentrations, the western LFV appears to be VOC-limited, while the eastern LFV is NO_x-limited. VOC emission reductions appear to have been more efficient, i.e. NO_x-efficiency has increased. For 95th and lower percentiles, the whole LFV is VOC-limited and responds the same way to emission reductions, consistent with previous unpublished findings by Environment Canada. One possible explanation for this difference is that, outside of peak summer days, there is insufficient solar insolation and VOC emissions to process all NO_x emissions resulting in VOC-limited conditions everywhere in the airshed.

Over the two-decade time period, there has been a notable reduction in number and severity of exceedances of CWS, and an overall consistent decline in maximum ozone concentrations throughout the region. However, the analysis showed a dramatic increase in background ozone (with 95 % percentiles showing significant positive trends throughout the network), consistent with recent estimates for Western North America by Jaffe and Ray (2007) and Chan and Vet (2010).

Comparing trends in the diurnal profiles of eastern and western measurement sites provides and insight into the spatial variability of changes in ozone sensitivity. Higher summer-averaged peak ozone over the 2000–2010 period (compared to 1985–1995 baseline) in the western end of the valley suggests reduced NO_x-inhibition in a VOC-limited regime. In contrast, lower summer-averaged peak ozone over the same timeframes in eastern part of the valley suggests reduced ozone formation in a NO_x-limited region.

There is evidence of overall widening of the diurnal summer ozone profiles likely indicating increased NO_x efficiency. The profiles show increased nighttime

ozone concentrations, which are likely a result of reduced ozone titration by NO_x emissions (mainly as NO). Furthermore, we have found the O_3 concentrations show a slower decline in the afternoon when compared to the baseline time period indicating, similarly, slower titration. In contrast, there was no apparent change in the onset time of ozone build-up, suggesting that the processes controlling O_3 formation (rush hour, sea-breeze onset, vertical mixing) remained unchanged for the entire 1985–2012 period.

Photochemical modeling suggests that in many cases, and depending on local mesoscale circulation patterns, peak ozone concentrations occur outside of the spatial area sampled by the fixed monitoring network. This presents an additional complexity that needs to be taken into consideration when interpreting the observational dataset analysis. Finally, photochemical modeling shows that there can be large amounts of advection of ozone and its precursors across the US-Canada border, which bisects the LFV. This is another consideration to be accounted for because emission reduction trends have not been the same across the two parts of the LFV.

Acknowledgments Air quality monitoring data were provided by Metro Vancouver. Funding for the research was derived from CREATE-IACPES and NSERC grants to Douw Steyn. The project was guided by Environment Canada, Meteorological Services of Canada, Prediction and Services West.

Question and Answer

QUESTIONER: S.Aksoyoglu
QUESTION: You mentioned that background O_3 increased. Did you check if there is any increase in radiation of the last decades due to decreasing particles, leading to increased production of O_3?
ANSWER: We have looked at the effects of summertime temperatures on O_3, as a proxy for insolation (shown in trend plots on the presentation slides). It appears to be responsible for much of the scatter in the maximum ozone values, however, has little effect below 95th percentile. Unfortunately, the Metro Vancouver air quality network is not equipped to collect long-term incoming solar radiation data.

QUESTIONER: Lucas Hennem
QUESTION: I have concerns over defining the lowest percentile of ozone as the "background", since without local anthropogenic emissions it is unlikely that that ozone concentrations would go to the very low values observed in urban centers.
ANSWER: Using solely statistical trend analysis to define "background" is certainly a very limiting approach. The values are inevitably tied to local emission sources. However, as we see from summertime diurnal ozone profiles, there is an approximately equal increase in nighttime levels of O_3 present for both urban West LFV and rural East LFV over the more recent years as compared to pre-AQMP years, indicating a large-scale change, rather than a local response.

QUESTIONER: Amir Hakami
QUESTION: How did you evaluate your VOC or NO_x-limited areas, and would it be possible to compare those with model-based DDM chemical regimes?
ANSWER: We used Sillman indicators to establish the connection between changing ozone sensitivity and the long-lived indicator $[O_3]/[NO_y]$. The model indicates that when the 8-h average afternoon $[O_3]/[NO_y]$ concentration is below 7.0, the airmass is VOC-sensitive, otherwise it is NO_x-sensitive. It would certainly be interesting to compare our results with those obtained using a DDM-based method.

References

Ainslie B, Steyn D (2007) Spatiotemporal trends in episodic ozone pollution in the Loer Fraser Valley, British Columbia, in relation to mesoscale atmospheric circulation patterns and emissions. J Appl Meteorol Climatol 46:1631–1644

Ainslie B, Steyn DG, Reuten C, Jackson PL (2013) A retrospective analysis of ozone formation in the Lower Fraser Valley, British Columbia, Canada. Part II: Influence of emissions reductions on ozone formation. Atmos Ocean 51(2):170–186

Canadian Council of Ministers of the Environment (2000) Canada-wide standards for particulate matter (PM) and ozone. Technical report, CCME, Quebec City, PQ

Chan E, Vet RJ (2010) Baseline levels and trends of ground level ozone in Canada and the United States. Atmos Chem Phys 10:8629–8647

Greater Vancouver Regional District (2007) 2005 Lower Fraser Valley air emissions inventory and forecast and backcast. Technical report, GVRD Policy and Planning Department, Burnaby, BC

Jaffe D, Ray J (2007) Increase in surface ozone at rural sites in the Western US. Atmos Environ 41:5452–5463

Steyn DG, Ainslie B, Reuten C, Jackson PL (2013) A retrospective analysis of ozone formation in the Lower Fraser Valley, British Columbia, Canada. Part I: Dynamical model evaluation. Atmos Ocean 51(2):153–169

Chapter 46
A Source-Receptor Analysis of NO_x Emissions in the Lower Fraser Valley, B. C.

Annie F. Seagram, Bruce Ainslie and Roxanne Vingarzan

Abstract Though the Lower Fraser Valley (LFV) has generally good air quality (AQ), ozone episodes may occur under a narrow set of synoptic and mesoscale conditions. These conditions give rise to complex flow systems, which further complicate the chemical sensitivity of the airshed. In this study, we use the MLDP0 dispersion model to investigate source-receptor relationships between NO_x emissions and receptor locations (AQ stations) subject to high ozone concentrations in the NO_x-limited portion of the valley.

46.1 Introduction

The LFV has generally good AQ due to the lack of heavy industry and relatively modest total emissions (e.g. Steyn et al. 1997). However, the region occasionally experiences severe ozone episodes, where the highest hourly ozone values are often observed in the eastern NO_x-limited portion of the valley, e.g. at Abbotsford, Chilliwack, or Hope (see Fig. 46.1a). Ainslie and Steyn (2007) identified four mesoscale Circulation Regimes (CRs) of ozone episodes: two with northwesterly daytime winds (CR I and II), and two with southerly daytime winds (CR III and IV) at the coast. However, advection of NO_x emissions from the western valley, where NO_x emissions are highest, to the NO_x-limited eastern LFV is a poorly understood process due to the valley's coastal location and complex terrain, which give rise to

A.F. Seagram (✉) · B. Ainslie · R. Vingarzan
Air Quality Research Unit, Meteorological Service of Canada,
Environment Canada, 401 Burrard Street, Vancouver, BC V6C 3S5, Canada
e-mail: aseagram@eos.ubc.ca

B. Ainslie
e-mail: bruce.ainslie@ec.gc.ca

R. Vingarzan
e-mail: roxanne.vingarzan@ec.gc.ca

D.G. Steyn and N. Chaumerliac (eds.), *Air Pollution Modeling and its Application XXIV*, Springer Proceedings in Complexity,
DOI 10.1007/978-3-319-24478-5_46

thermo-topographically forced flows. The purpose of this modelling study is to identify potential source regions of NO_x emissions that likely impact the eastern NO_x-limited portion of the LFV, and to examine their variability during meteorological conditions typical of summertime ozone episodes.

46.2 Study Approach

Eighty summer candidate ozone days between 2001–2012 were identified, whose meteorological conditions correspond to one of the four CRs of ozone episodes, totaling 20 cases of each CR. The meteorology of each day was modelled using Environment Canada's (EC) Global Environmental Multiscale—Limited Area Model (GEM-LAM) v. 4.4.0 (Côté et al. 1998), with 2.5 km horizontal grid spacing and 58 vertical levels. Output fields were saved every 2 min modelled timestep. GEM-LAM fields were then used to perform backward dispersion simulations using EC's *Modèle Lagrangien de Dispersion de Particules d'ordre 0* (MLDP0) model (D'Amours et al. 2015). Using a unit hourly emission rate beginning at 1800 local time (approximate time of peak observed ozone), 100 000 inert Lagrangian particles initiated at 10 m agl were tracked for 12 h (the photochemical period, and on the order of the lifetime of NO_x) from the location of eastern AQ monitoring stations (receptors) (see Fig. 46.1a). The resulting particle concentration fields on the GEM-LAM grid between 0-500 m agl (average depth of the daytime boundary layer) represent the source-receptor sensitivity (SRS) coefficients which can be folded with a spatially gridded emission inventory to calculate linear NO_x transport from individual grid cells (sources) to the receptor, as described by Wotawa et al. (2003). Average hourly SRS fields (n = 20) were used. A NO_x emissions inventory for a single representative day generated by SMOKE (Houyoux and Vukovich 1999) was used to investigate the influence of meteorological conditions on source-receptor (SR) relationships, rather than the effect of changing emissions over the study period.

46.3 Results and Discussion

Here, we present only the results of backward dispersion runs and SR analysis initiated at Chilliwack (T12) during CR I and IV conditions.

Due to prevailing northwesterly winds during CR I, transport to T12 is most favourable from over water in the early morning and from within tributary valleys (not shown). However, NO_x emissions in these areas are negligible. By midday, SRS coefficients are highest over municipalities along the coast, where NO_x emissions are also highest. T12 is most sensitive to transport from Surrey and northern Whatcom County at 1400 (Fig. 46.1a). Peak potential NO_x contributions from this time are up to 10^{-1} µg m^{-3} (Fig. 46.1c). From 1500 onwards, transport is

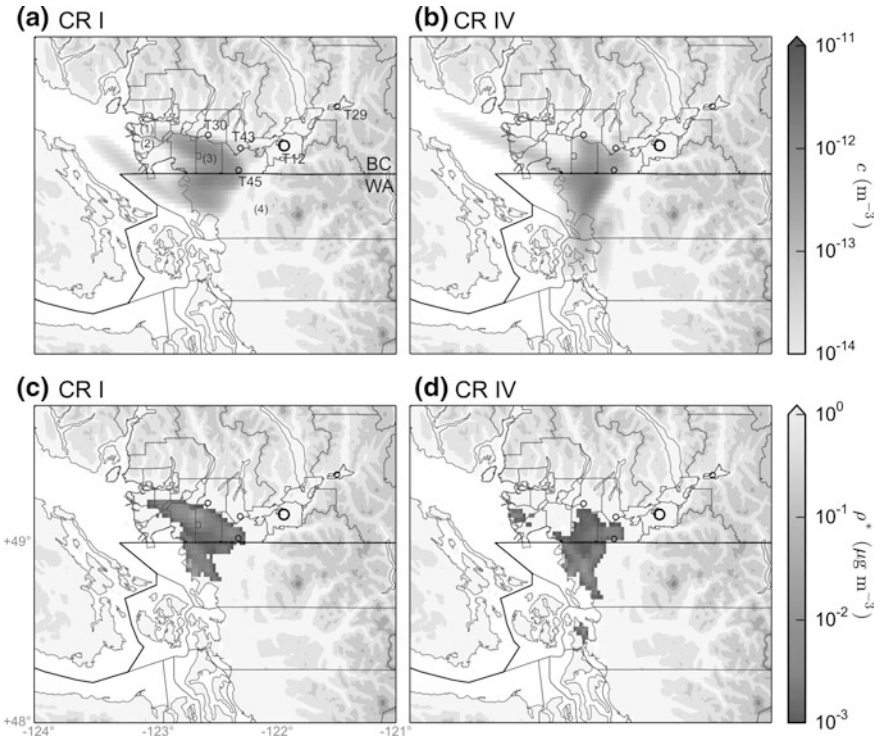

Fig. 46.1 Backward simulation transport to Chilliwack (T12) (*large open circle*) arriving at 1800 local time during CR I (**a**, **c**) and CR IV (**b**, **d**) conditions. (*top row*) Source-receptor sensitivity coefficients (**c**) calculated between 0–500 m agl. (*bottom row*) Corresponding hourly potential NO_x contribution fields (ρ^*). All fields are valid at 1400 local time, and are an average of 20 cases. Elevation contours (*grey fill*) are every 600 m asl, starting from sea level. Other receptor locations in this study are denoted by small open circles: Maple Ridge (T30), Mission (T43), Abbotsford (T45), and Hope (T29). Canadian municipalities and US counties are outlined in grey. Additional census divisions are numbered for reference: Vancouver (1), Richmond (2), Surrey (3), Whatcom County (4). The US-Canadian border between British Columbia (BC) and Washington (WA) is also drawn (*black line*)

most favourable from Abbotsford, since it is located directly upwind (not shown). Overall, the SR relationship for T12 under CR I conditions is complicated, where coastal urbanized areas may be important NO_x sources in the morning, but contributions from Whatcom County and Abbotsford dominate later in the day.

During CR IV, SRS coefficients are again highest over water in the early morning (not shown). However, owing to strong southerly wind components during this regime, midday transport to T12 is favourable along the Washington coast (e.g. Figure 46.1b). Due to the presence of high NO_x emissions from mobile and point sources in this region, there is considerable total potential NO_x transport to T12 (Fig. 46.1d). Later in the day, SRS coefficients and potential NO_x transport are

again highest from Whatcom County and Abbotsford due to their proximity upwind (not shown).

It is interesting to note that transport from Vancouver (proper) to T12 is negligible during either CR. This agrees with previous modelling studies (e.g. Seagram 2014) and forward dispersion runs also performed in this study (not shown). In general, late in the day, potential NO_x source regions for T12 are the same during all CRs (e.g. Whatcom County, Abbotsford). This is not surprising given that flow is channeled at T12 and wind vectors are oriented along the valley axis (southwest to northeast). That is, there is only one direction that air (and pollutants) can arrive at Chilliwack in the afternoon because of the surrounding topographic constraints.

46.4 Conclusion

Overall, linear SR relationships of NO_x emissions in the LFV are influenced by meteorological variability (i.e. CR) and time of day during ozone episodes. Interestingly, pollutants originating from the vicinity of Vancouver do not likely contribute to poor AQ in the eastern LFV. An important potential source of NO_x emissions impacting the eastern NO_x-limited LFV is located along the coast in the center of the valley (including, but not limited to, northern Washington, Abbotsford, and Surrey) under all CRs. This will have important implications on trans-boundary management plans. The results found here can be used to inform, and should be confirmed with, a follow-up photochemical modelling study.

Acknowledgments This project was contracted and funded by Metro Vancouver. The authors would like to thank the members of the Regional Ground-Level Ozone Strategy Steering Committee (RGLOSSC) for their involvement. The modelling and analysis support from Nils Ek, Jean-Philippe Gauthier, and Alain Malo of the Canadian Meteorological Center (CMC) is greatly appreciated.

Disclaimer The views expressed in this report are those of the authors and do not necessarily reflect the views or policies of Environment Canada or Metro Vancouver.

Questions and Answers

Questioner: Jaakko Kukkonen
Q: How did you evaluate the uncertainties of your modelling system in the course of the selected episodes? e.g. you could possibly use a different meteorological model and/or a different transport model to illustrate the variability of results in terms of the selected models.
A: First, we performed a brief evaluation of the meteorological fields and emission inventory compared to observed timeseries and recorded inventory totals, respectively. Results were satisfactory. However, our focus was not to explain NO_x transport or reconstruct pollutant timeseries during specific episodes, but to develop

a generalized understanding of SR relationships in the LFV. For this reason, all hourly particle concentration fields are an average of 20 cases within the same CR.

Questioner: Paul Makar
Q: What about recirculation events? Do you plan to check for these in the future?
A: Lagrangian particles may recirculate within the 12 h of simulation time, which would affect SRS coefficients (though particle age is not accounted for). However, day-to-day carryover could not be accounted for, as extending the simulation time beyond 12 h is less representative of the lifetime of NO_x in a polluted airmass. The process of recirculation was investigated in a trajectory modelling study (see Seagram 2014), but it would be interesting to determine the magnitude of possible impacts of precursor recirculation on ozone formation using a photochemical model. The results from this study may help inform such targeted modelling exercises.

References

Ainslie B, Steyn D (2007) Spatiotemporal trends in episodic ozone pollution in the Lower Fraser Valley, British Columbia, in relation to mesoscale atmospheric circulation patterns and emissions. J Appl Meteorol Climatol 46(10):1631–1644

Côté J, Gravel S, Methot A, Patoine A, Roch M, Staniforth A (1998) The operational CMC-MRB global environmental multiscale (GEM) mode. Part 1: design considerations and formulation. Mon Weather Rev 126:1373–1395

D'Amours R, Malo A, Flesch T, Wilson J, Gauthier J-P, Servranckx R (2015) The Canadian Meteorological Center's Atmospheric transport and dispersion modelling suite. Atmos Ocean. doi:10.1080/07055900.2014.1000260

Houyoux MR, Vukovich JM (1999) Updates to the sparse matrix operator kernel emissions (SMOKE) modeling system and integration with Models-3. The Emissions Inventory: Regional Strategies for the Future, 1461

Seagram AF (2014) Atmospheric recirculation during ozone episodes in the Lower Fraser Valley, B. C. Master's Thesis. 128 pp. The University of British Columbia, Vancouver, Canada. http://hdl.handle.net/2429/50834

Steyn DG, Bottenheim JW, Thomson RB (1997) Overview of tropospheric ozone in the Lower Fraser Valley, and the Pacific'93 field study. Atmos Environ 31(14):2025–2035

Wotawa G, De Geer L-E, Denier P, Kalinowski M, Toivonen H, D'Amours R, Desiato F, Issartel J-P, Langer M, Seibert P, Frank A, Sloan C, Yamazawa H (2003) Atmospheric transport modelling in support of CTBT verification– overview and basic concepts. Atmos Environ 37:2529–2537

Chapter 47
Modelling Photochemical Air Pollutants from Industrial Emissions in a Constrained Coastal Valley with Complex Terrain

Benjamin Weinstein, Douw Steyn and Peter Jackson

Abstract In order to assess the potential change in ambient concentrations of ozone and its precursors that may arise from the construction of large industrial facilities in the Terrace-Kitimat valley (TKV), we conducted a study using the WRF, SMOKE and CAMx models for two periods in 2010. We developed and applied control and test cases for each period, the former for model evaluation and the latter to assess pollutant change. Model evaluation showed that CAMx is able to emulate O_3 peaks in an adjacent valley (where monitoring occurred) for both the spring and summer periods. Results for the spring period suggest that the addition of NO_X from industrial sources may lead to modest O_3 production outside of the main plume trajectory and on valley walls during afternoon hours as well as overnight O_3 titration along low elevations of the TKV upwards of 80 km downwind of sources. Results from the summer period suggest that the addition of O_3 precursors may at times contribute to a greater than 100 % increase in O_3 production under certain meteorological conditions up to 50 km downwind of sources.

47.1 Introduction

The Terrace-Kitimat valley (TKV), located at the head of the Douglas Channel in northwest British Columbia (BC), is poised to be the centre of large industrial expansion in the next 5 years. In addition to the pending construction of a new

B. Weinstein (✉) · D. Steyn
Department of Earth, Ocean and Atmospheric Sciences, The University of British Columbia, Vancouver, BC, Canada
e-mail: bweinste@eos.ubc.ca

P. Jackson
Environmental Science and Engineering Program, University of Northern British Columbia, Prince George, BC, Canada

D.G. Steyn and N. Chaumerliac (eds.), *Air Pollution Modeling and its Application XXIV*, Springer Proceedings in Complexity,
DOI 10.1007/978-3-319-24478-5_47

aluminum smelter there is also the potential for construction of a bitumen-condensate export-import terminal, four natural gas liquefaction (LNG) facilities and an oil refinery. The cumulative effects of airborne emissions from existing and potential sources were the subject of a large government study however it was limited in scope to SO_2 and NO_2 exposure as well as sulphur and nitrogen deposition. Absent was an evaluation of primary particulate matter (PM) and secondary pollutants. In addition, despite high projected emissions of photochemical oxidant precursors (mainly from LNG and marine transportation sources) to date no proponent has been required to investigate the potential generation of photochemical air pollutants as part of their environmental assessments. Without an understanding of the total change in atmospheric pollutant concentrations it is not possible to make final conclusions regarding the risk(s) from any combination of new sources. Our research aims to address this shortcoming by modelling emissions in the TKV with the chemical and dispersion model CAMx. If successful this approach can be applied to other airsheds with complex coastal terrain subject to industrial expansion where proposed projects emit photochemical precursor pollutants.

47.2 Methods

Output from the Weather Research and Forecasting model (WRF ARW v3.6) was developed. Each 34-h WRF run was initialized at 00:00 GMT using the North American Mesoscale Forecast System at 32 km resolution. Files were created for a parent and series of nested grids with horizontal resolutions of 36, 12, 4 and 1.3 km. The Sparse Matrix Operator Kernel Emissions model (SMOKE v3.5.1) was employed for emissions processing. Emissions data were derived from a series of reports accessed through the BC Ministry of Environment as well as the National Pollutant Release Inventory (NPRI). The control case consisted of emissions from an existing aluminum smelter as well as mobile and biogenic sources. The test case consisted of emissions from an aluminum smelter, four LNG facilities, an oil refinery, as well as mobile, marine and biogenic sources. Test case emissions represent full construction of all proposed industrial projects. Biogenic emissions were created using the Model of Gases and Aerosols from Nature (MEGAN v2.10). The Comprehensive Air Quality Model with Extensions (CAMx v6.10) was used for the photochemical modelling. 24-h CAMx runs from 00:00 to 00:00 PST were completed, with output concentrations from 1 day used as input concentrations for the following day. Results from the first day of each period were discarded as model spin-up. The carbon bond version 5 (CB05) gas phase chemical mechanism and the

course-fine (CF) aerosol option were selected, while point sources were treated with the GREASED plume-in-grid option (described by (Karamchandani et al. 2011) as best used for large NO_X sources).

47.3 Model Evaluation

As there is no O_3 monitoring in the TKV, model evaluation was conducted in the nearest community with measured O_3 (Smithers, BC). This location is outside of the finest (1.3 km) domain but well within the 4 km domain. Control case emissions for this area included mobile and biogenic sources as well as point sources contained in the NPRI. Further inventory development was not completed. Results from the evaluation indicate that CAMx was capable of consistently reproducing O_3 maximums for both the spring and summer periods, with a stronger performance in the spring. Without accounting for all NO_X emissions in Smithers, CAMx was less able to replicate overnight O_3 reduction by NO.

47.4 Effect of Industrial Emissions on Photochemical Air Pollutant Production

Spring Period. The spring period was selected to investigate whether new NO_X sources would exacerbate naturally elevated springtime O_3 as is commonly found in the northern hemisphere (Monks 2000). Results indicate that additional NO_X emissions may at times lead to modest O_3 production outside the main plume trajectory and along valley walls. Also suggested is a reduction in overnight O_3 concentrations along low elevations in the TKV upwards of 80 km downwind. These O_3 reductions mirror an increase in near field NO_2. An example of this O_3 titration is found in Fig. 47.1 (left).

Summer Period. Similar to other findings, results from the summer period suggest that in the near field O_3 titration will occur (Castell et al. 2010). Results also suggest that under certain meteorological conditions these emissions may contribute to a greater than 100 % increase in O_3 production in areas up to 50 km downwind of the main sources. This was especially evident during a two-day sea breeze event where the mixing height did not exceed the height of the surrounding mountains. An example of this result is presented in Fig. 47.1 (right).

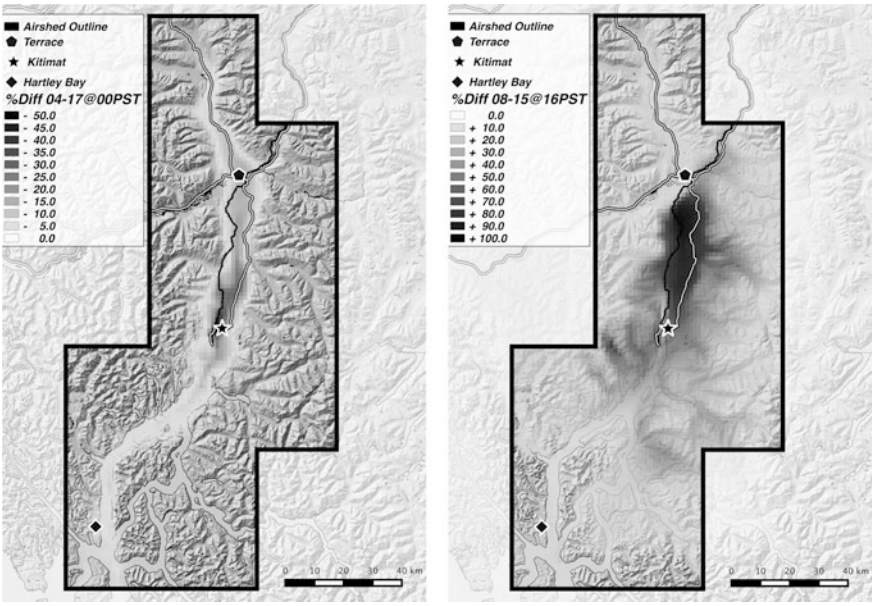

Fig. 47.1 Modelled examples of springtime O_3 titration at 00:00 PST on April 17, 2010 (*left*) and summertime O_3 production at 16:00 PST on August 15, 2010 (*right*) in the TKV airshed. Shading represents percent change from the control to the test cases

47.5 Summary and Conclusion

We used a combination of WRF-SMOKE-CAMx in order to assess the potential change in ambient concentrations of ozone and its precursors that may arise from the construction of large industrial facilities in the Terrace-Kitimat valley (TKV). A spring and a summer model period were selected and control and test emission inventories were developed. Model evaluation demonstrated the ability of CAMx to recreate daily O_3 peaks for both periods. Results suggest that the emission of photochemical precursor pollutants in the spring may lead to modest O_3 production outside the main plume trajectory and along valley walls as well as a reduction in overnight O_3 concentrations along low elevations upwards of 80 km downwind. In the summer these emissions may, under certain meteorological conditions, contribute to a greater than 100 % increase in O_3 production up to 50 km downwind. This approach can be applied to other airsheds with complex coastal terrain subject to industrial expansion, where proposed projects emit photochemical precursor pollutants.

Acknowledgments We would like to thank RWDI staff Jeff Lundgren and Martin Gautier for their mentoring and ideas. Also, GIS support from Morgan Hite (http://hesperus-wild.org/) and Dave Amirault (BC Ministry of Forests, Lands and Natural Resource Operations) was critical to the success of this research. We acknowledge the Natural Sciences and Engineering Research Council of Canada (NSERC) Collaborative Research and Training Experience—Atmospheric Aerosol Program (CREATE-AAP) for funding this research.

Questions and Answers

QUESTIONER: S. Aksoyoglu
QUESTION: You showed diurnal variation of CAMx results for O_3 failing to represent overnight O_3 mixing ratios. Did you check NO_X? How is the resolution?

ANSWER: For the control case presented, both modelled NO and NO_2 mixing ratios did not adequately represent measured mixing ratios. A series of sensitivity tests have since been conducted and it has been concluded that the original emissions inventory did not reasonably capture NO_X emissions.

QUESTIONER: S. Aksoyoglu
QUESTION: In spite of high biogenic emissions (especially isoprene) in summer, O_3 are lower than in spring. What is the reason for that?

ANSWER: Elevated springtime O_3 in northern latitudes has been observed and studied for may years however the definitive cause has yet to be determined. Some argue that the O_3 is stratospheric in origin while others argue that it is produced in-situ from the thermal degeneration of PAN and other NMHCs. A detailed summary of this debate is presented in (Monks 2000).

QUESTIONER: G. Kallos
QUESTION: What are characteristic widths of the valleys in your high-resolution domain? You mentioned horizontal grid resolution of 1.2 km. I think this is not adequate to resolve flow along the narrow valleys there. CAMx is using Kv (eddy diffusivity coefficients). This kind of parameterization is not considered adequate to resolve dispersion within valleys there.

ANSWER: The horizontal resolution of the fine grid is 1.333 km. At its narrowest the TKV is less than 3 km wide yet for the most part the valley is wider than this. Indeed the bulk of the valley is wider then 6.666 km (equivalent of 5 grid cells). As well, it should be noted that valley width increases with height, in many places quite rapidly. By the second model layer (200 m AGL) the entire valley is typically 5 cells wide. Also, the main flow is north-south along the length of the valley (> 100 km). For these reasons 1.333 km grid cells can be considered adequate to capture eddy diffusivity in the TKV.

References

Castell N, Mantilla E, Salvador R, Stein A, Millan M (2010) Photochemical model evaluation of the surface ozone impact of a power plant in a heavily industrialized area of southwestern Spain. J Environ Manage 91(3):662–676

Karamchandani P, Vijayaraghavan K, Yarwood G (2011) Sub-grid scale plume modelling. Atmosphere 2:389–406

Monks PS (2000) A review of the observations and origins of the spring ozone maximum. Atmos Environ 34:3545–3561

Chapter 48
Diagnosis of Transboundary Mass Fluxes from Modelled North American Regional Sulphur and Nitrogen Deposition Fields

Michael D. Moran, Chul-Un Ro, Robert Vet and Qiong Zheng

Abstract Vet and Ro (Atmos Environ 42:2518–2529, 2008) developed an observation-based acid deposition model consisting of a conceptual regional mass-balance framework and inputs of mean area-integrated emissions data and wet deposition measurements over eastern North America. They then applied this model to estimate multi-year transboundary mass fluxes of sulphur and oxidized nitrogen between eastern Canada and the eastern United States during the 1990s. In this paper their approach is extended to use gridded emissions and deposition fields obtained from a numerical acid deposition model as inputs in place of measurements in order to diagnose transboundary fluxes of sulphur, oxidized nitrogen, and reduced nitrogen from model-predicted annual wet, dry, and total deposition fields. By following this approach, additional information of interest can also be inferred from an acid deposition model simulation after the simulation has been completed.

48.1 Introduction and Previous Work

Acid deposition has been recognized as an environmental issue in eastern North America (ENA) since the 1970s (e.g., Likens et al. 1979). While many numerical acid deposition models have been applied since that time to study acid deposition over North America, including statistical, Lagrangian, and Eulerian models (e.g., Clark et al. 1989; Karamchandani and Venkatram 1992), Vet and Ro (2008: hereafter VR08) developed a novel, *observation-based* acid deposition model consisting of a conceptual regional mass-balance framework and inputs of mean area-integrated emissions data and wet deposition measurements over eastern North America. They then applied this simple algebraic model to estimate multi-year transboundary mass fluxes of sulphur (S) and oxidized nitrogen (N_{ox}) between

M.D. Moran (✉) · C.-U. Ro · R. Vet · Q. Zheng
Air Quality Research Division, Environment Canada, 4905 Dufferin Street, Toronto, ON, Canada
e-mail: mike.moran@canada.ca

D.G. Steyn and N. Chaumerliac (eds.), *Air Pollution Modeling and its Application XXIV*, Springer Proceedings in Complexity,
DOI 10.1007/978-3-319-24478-5_48

eastern Canada (EC) and the eastern United States (EUS) during two periods in the 1990s.

The two 5-year periods considered were 1990–94 and 1996–2000. For each period they calculated SO_2 and NO_x mean annual regional emissions over EC and EUS based on state and province-level emissions inventories. VR08 also calculated mean annual wet deposition estimates of nitrate (NO_3^-) and non-sea-salt sulphate (nss-SO_4^{2-}) for each period for the two regions as follows. First, they calculated mean annual station values of NO_3^- and nss-SO_4^{2-} wet deposition from daily or weekly measurements made at a set of 176 irregularly-spaced precipitation-chemistry stations in EC and EUS. They then applied universal Kriging to calculate gridded mean annual deposition fields on a grid consisting of 45-km by 45-km grid cells covering ENA and summed these fields over the EC and EUS regions to obtain mean regional wet deposition totals.

The simple two-region mass-balance model used by VR08 to estimate transboundary contributions to regional wet deposition had the following form:

$$WD_{\mathrm{ec}} = A_{\mathrm{ec}} * E_{\mathrm{ec}} + B_{\mathrm{ec}} * E_{\mathrm{eus}},\ F_{\mathrm{ec}} = B_{\mathrm{ec}} * E_{\mathrm{eus}}/WD_{\mathrm{ec}}, \tag{48.1}$$

$$WD_{\mathrm{eus}} = A_{\mathrm{eus}} * E_{\mathrm{eus}} + B_{\mathrm{eus}} * E_{\mathrm{ec}},\ F_{\mathrm{eus}} = B_{\mathrm{eus}} * E_{\mathrm{ec}}/WD_{\mathrm{eus}}, \tag{48.2}$$

where

WD denotes regional wet deposition, *E* denotes regional emissions, the
A factor gives the fraction of internal regional emissions contributing to "self" or internal deposition (i.e., *A* x E_{internal}), the
B factor gives the fraction of external emissions contributing to internal deposition (i.e., *B* x E_{external}), and the
F value gives the fraction of wet deposition contributed by transboundary transport (i.e., by external emissions).

To make use of this mass-balance model the following assumptions were made:

- EC emissions that are not wet deposited in EC are either dry deposited in EC or transported out of EC; the same assumptions apply equally to EUS;
- Inflows of anthropogenic and natural S and N_{ox} into ENA are small relative to the emissions of S and N_{ox} within ENA and can be neglected;
- Transboundary fluxes (in both directions) are implicit in the *B* terms (i.e., transboundary transport precedes wet deposition).

Note that the two regional mass-balance equations do not have a unique solution for the four coefficients A_{ec}, B_{ec}, A_{eus}, and B_{eus}, but reasonable lower and upper bounds can be determined for these coefficients by trial and error. VR08 assumed that A_{ec} and A_{eus} would have values in the range 0.2–0.4 and then calculated the corresponding *B* and *F* values from 48.1 and 48.2. They found that the mass-balance

equation for the EUS is very sensitive to the choice of the A coefficient (i.e., self-deposition): a large value for A results in a negative B coefficient (i.e., fraction of EC emissions deposited in the EUS), which is impossible.

48.2 Extension of Methodology

Given that VR08 employed gridded wet deposition fields as an intermediate step to calculate area-integrated deposition totals, the use of gridded emissions and deposition fields from a numerical, source-based acid deposition model is a natural extension of their methodology. In fact there are a number of advantages to the use of acid-deposition-model outputs in the mass-balance analysis:

- Gridded model values are available even in areas where no measurement stations are located.
- Acid deposition models also predict the dry deposition of sulphur and nitrogen species, for which routine network measurements are not available.
- Dry and wet deposition fields predicted by the model are consistent with the emissions fields used by the model, allowing the same approach to be used with output from future-year emissions-scenario simulations for which no observations are available.
- The transboundary flux calculation allows flexibility in the choice of boundary to be considered, such as the boundary between EC and EUS, between western Canada (WC) and the western U.S. (WUS), between ENA and western North America (WNA), and so on.
- Analysis of the WNA ENA regional pair will allow VR08's assumption that external contributions are negligible for ENA to be assessed.

The main disadvantage of this extension is of course that model predictions are not measurements and are limited by model skill and uncertainty.

To implement this extension, 48.1 and 48.2 are generalized by replacing WD with D (deposition), where D can represent dry deposition (d), wet deposition (w), or total deposition (t), and by replacing regions "ec" and "eus" with generic regions 1 and 2. We thus consider six equations with 12 unknown coefficients: Ad_1, Ad_2, Bd_1, Bd_2, Aw_1, Aw_2, Bw_1, Bw_2, At_1, At_2, Bt_1, and Bt_2. However, it also follows that $At = Ad + Aw$ and $Bt = Bd + Bw$, which provide another four equations.

Next, to calculate the one-way transboundary transport flux into a region (T), if we assume that emissions transported into a region from outside are deposited in the same proportion as emissions internal to a region that self-deposit, it then follows that

$$T_1 = B_1 * E_2/A_1 = F_1 * D_1/A_1, \tag{48.3}$$

$$T_2 = B_2 * E_1/A_2 = F_2 * D_2/A_2. \tag{48.4}$$

Moreover, the fact that T must have the same value regardless of whether it is calculated based on dry, wet, or total deposition values imposes two strong constraints:

$$T_1/E_2 = Bw_1/Aw_1 = Bd_1/Ad_1 = Bt_1/At_1, \tag{48.5}$$

$$T_2/E_1 = Bw_2/Aw_2 = Bd_2/Ad_2 = Bt_2/At_2. \tag{48.6}$$

Thus, if both dry and wet deposition are considered, the system of equations will have a unique solution for the 12 coefficients listed above.

48.3 Results and Discussion

The extended methodology described in the previous section was applied to output from the AURAMS acid-deposition model (e.g., Gong et al. 2006; Moran et al. 2008). Gridded annual SO_2, NO_x, and NH_3 emissions fields and annual dry and wet deposition fields for a large set of S and nitrogen (N) species were obtained from a 1-year North American simulation for 2006 on a 45-km grid (Makar et al. 2009). The deposition fields included SO_2, p-SO_4, NO_2, HNO_3, organic NO_3, p-NO_3, PAN, NH_3, and p-NH_3 dry deposition and SO_4^{2-}, NO_3^-, and NH_4^+ wet deposition; Fig. 48.1a shows a sample annual dry deposition field for SO_2. A GIS package was then used to calculate area-integrated annual values of emissions and dry and wet deposition of these species for four regions: WC, EC, WUS, and EUS (see Fig. 48.1b). Unit conversions were then performed and species combined to arrive at a set of emissions and dry and wet deposition values for S, N_{ox}, and N_r (reduced nitrogen). Lastly, the mass-balance equations were solved iteratively to arrive at a self-consistent set of values for Ad_1, Ad_2, Bd_1, Bd_2, Aw_1, Aw_2, Bw_1, Bw_2, At_1, At_2, Bt_1, Bt_2, F_1, F_2, T_1, and T_2 for S, N_{ox}, and N_r for 4 different pairs of regions: EC and EUS; WC and WUS; C and US, and ENA and WNA. Note that, following VR08, emissions sources external to each pair of regions were assumed to be negligible (although further generalization of 48.1 and 48.2 is possible to account for the contribution of such external emissions).

Table 48.1 shows mass-balance calculation results for the four pairs of regions for total sulphur. Some interesting similarities, differences, and patterns are evident in this table:

- All four pairs of regions have a "lopsided" S emissions distribution where S emissions from one region are considerably larger than emissions from the other member of the pair. The range is from roughly a factor of two for the WC:WUS pair to a factor of 12 for the EC:EUS pair.
- Because Ad values are smaller than Aw values and Bd values are smaller than Bw values for all eight analysis regions, the magnitude of wet S deposition must be larger than that of dry S deposition in all regions.

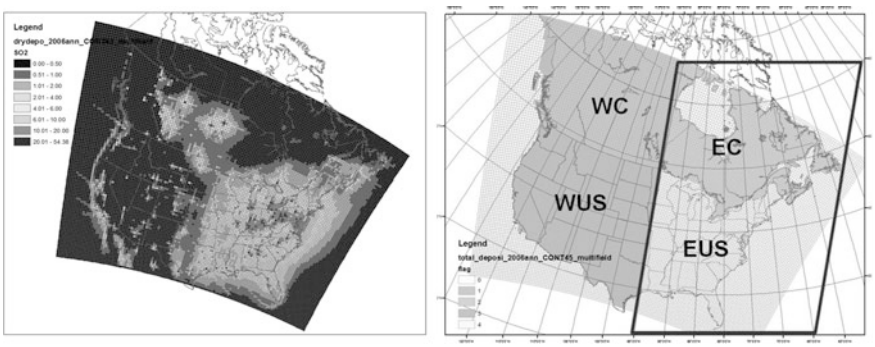

Fig. 48.1 Plots of (*left*) predicted annual SO_2 dry deposition field (kg SO_2 ha^{-1}) and (*right*) AURAMS 45-km North American grid with four analysis regions indicated by labels and different shading. The trapezoid marks the regions considered by VR08

Table 48.1 Values of *A, B, F,* and *T* coefficients determined iteratively for 4 pairs of regions from area-integrated annual sulphur emissions and dry and wet deposition values calculated from 2006 AURAMS annual simulation. Units of emissions and transboundary fluxes are MT S y^{-1}

Analysis region	Sulphur emissions	Dry deposition (DD)				Wet deposition (WD)			
		A	B	F	T	A	B	F	T
EC	0.47	0.06	0.03	0.85	2.702	0.22	0.11	0.86	2.794
EUS	5.55	0.17	0.15	0.07	0.420	0.21	0.19	0.07	0.428
WC	0.49	0.14	0.10	0.61	0.777	0.32	0.23	0.61	0.783
WUS	1.08	0.15	0.12	0.26	0.381	0.28	0.21	0.26	0.373
C	0.96	0.08	0.04	0.79	3.639	0.25	0.13	0.79	3.517
US	6.63	0.17	0.15	0.11	0.850	0.22	0.18	0.11	0.788
ENA	6.02	0.17	0.12	0.15	1.073	0.275	0.18	0.15	1.048
WNA	1.57	0.15	0.03	0.41	1.073	0.31	0.05	0.40	1.036

- As expected from 48.5 and 48.6 the *T* values obtained independently from the dry and wet S deposition calculations are identical within the precision of the iterative calculations. For example, T_{ena}, the annual one-way transboundary flux from WNA to ENA, was estimated to be 1.073 MT S y^{-1} using dry deposition values vs. 1.048 MT S y^{-1} using wet deposition values.
- Different pairs of regions have different deposition characteristics. For example, for the three Canadian analysis regions (EC, WC, C), the dry self-deposition factor *Ad* ranges from 0.06 to 0.14 while the wet self-deposition factor *Aw* ranges from 0.22 to 0.32. For the three U.S. regions (EUS, WUS, US) the corresponding ranges are 0.15–0.17 and 0.21–0.28. Note that the assumption made by VR08 that *Aw* will have a value between 0.20 and 0.40 holds for all six regions for this 2006 example. In terms of the fraction of dry and wet deposition contributed by transboundary transport (*F*), for the three Canadian regions *F* ranges from 61 to 86 %, whereas for the three U.S. regions *F* ranges from 7 to 26 %. The greater

contribution of transboundary transport for the Canadian regions is consistent with the U.S. member of each regional pair having higher S emissions
- It can be seen from the bottom of Table 48.1 that ENA is moderately impacted by WNA S emissions (i.e., $T_{ena} = \sim 1$ MT is ~ 17 % of $E_{ena} = 6$ MT) compared to the assumption by VR08 that this source could be neglected.

Questions and Answers

Questioner: Amir Hakami
Q: How sensitive are your results with respect to where you draw the line on west/east separation?
A: There is sensitivity to the magnitude of the emissions associated with each region. For example, if a region is made larger without enclosing more emissions sources (e.g., extending EC further north), then the results will be very similar.
Questioner: Steven Hanna
Q: Can most of the difference in deposition/emissions be explained by the observed distribution in annual wind roses of stations along the US-Canada border?
A: Mean transport climatology plays an important role for dry deposition but southwest-to-northeast transport associated with cyclonic storm systems is favoured for wet deposition.

References

Clark TL, Voldner EC, Dennis RL, Seilkop SK, Alvo M, Olson MP (1989) The evaluation of long-term sulfur deposition models. Atmos Environ 23:2267–2288

Gong W, Dastoor AP, Bouchet VS, Gong S, Makar PA, Moran MD, Pabla B, Ménard S, Crevier L-P, Cousineau S, Venkatesh S (2006) Cloud processing of gases and aerosols in a regional air quality model (AURAMS). Atmos Res 82:248–275

Karamchandani PK, Venkatram A (1992) The role of non-precipitating clouds in producing ambient sulfate during summer: results from simulations with the Acid Deposition and Oxidant Model (ADOM). Atmos Environ 26:1041–1052

Likens GE, Wright RF, Galloway JN, Butler TJ (1979) Acid rain. Sci Amer 241:43–51

Makar PA, Moran MD, Zheng Q, Cousineau S, Sassi M, Duhamel A, Besner M, Davignon D, Crevier L-P, Bouchet VS (2009) Modelling the impacts of ammonia emissions reductions on North American air quality. Atmos Chem Phys 9:7183–7212

Moran MD, Zheng Q, Pavlovic R, Cousineau S, Bouchet VS, Sassi M, Makar PA, Gong W, Stroud C (2008) Predicted acid deposition critical-load exceedances across Canada from a one-year simulation with a regional particulate-matter model. In: 15th Joint AMS/A&WMA Conference on Applications of Air Pollution Meteorology, New Orleans, January, American Meteorological Society, Boston, 20 pp. http://ams.confex.com/ams/pdfpapers/132916.pdf

Vet R, Ro C-U (2008) Contribution of Canada-United States transboundary transport to wet deposition of sulphur and nitrogen oxides - A mass balance approach. Atmos Environ 42:2518–2529

Chapter 49
Modelling Regional Air Quality in the Canadian Arctic: Impact of North American Wildfire and Arctic Shipping Emissions

Wanmin Gong, Stephen R. Beagley, Junhua Zhang, Sophie Cousineau, Jack Chen, Mourad Sassi, Rodrigo Munoz-Alpizar, Heather Morrison, Lynn Lyons and Pascal Bellavance

Abstract Air quality model simulations were carried out for the 2010 northern shipping season over a regional Arctic domain. Preliminary evaluation of the base model simulation shows that the model is able to capture the general trends of the observed ambient ozone and $PM_{2.5}$ in the northern region. Analysis on relative contributions from North American wildfires and Arctic marine/shipping to ambient concentrations of various pollutants and their depositions in the Canadian Arctic and northern regions was conducted.

49.1 Introduction

The Arctic is recognized as one of the key areas of the globe, both in terms of its sensitivity to climate change, and by the increasing economic activity associated with the opening up of Arctic waters in a warming climate. Environment Canada is

W. Gong (✉) · S.R. Beagley · J. Zhang · H. Morrison
Air Quality Research Division, Environment Canada, Toronto, ON, Canada
e-mail: wanmin.gong@canada.ca

S.R. Beagley · S. Cousineau · J. Chen · M. Sassi · R. Munoz-Alpizar
National Prediction Operations, Meteorological Service of Canada, Environment Canada, Montreal, Canada

J. Chen
Marine and Ice Service, Meteorological Service of Canada, Environment Canada, Ottawa, Canada

L. Lyons · P. Bellavance
Transportation Division, Environment Stewardship Branch, Environment Canada, Gatineau, Canada

D.G. Steyn and N. Chaumerliac (eds.), *Air Pollution Modeling and its Application XXIV*, Springer Proceedings in Complexity,
DOI 10.1007/978-3-319-24478-5_49

undertaking an initiative to develop an air quality prediction capacity for the Canadian North and Arctic region, in the context of assessing the impacts of the current and future air contaminant emissions from shipping and other sources on the northern environment and human health.

In this study, using an on-line air quality prediction model GEM-MACH, simulations were carried out for the 2010 northern shipping season (April–October) over a regional Arctic domain. North American wildfire emissions and detailed marine shipping emissions were developed and included in the simulations. The base-case simulation (including all emissions) was evaluated against available observations from existing air quality monitoring networks. Additional model simulations were carried out excluding the ship emissions or wild fire emissions, respectively. Relative contributions from these different sources to the ambient concentrations of various pollutants and their deposition in the Canadian Arctic and northern regions were analyzed based on comparing these scenario simulations with the base-case simulation.

49.2 The Model and Simulation Setup

GEM-MACH (Global Environmental Multi-scale model—Modelling Air quality and CHemistry) is an on-line chemistry transport model embedded within GEM. A limited area version of GEM-MACH has been in use as Environment Canada's operational air quality prediction model since 2009 (Moran et al. 2010; Ménard et al. 2014). The model has comprehensive representations of air quality processes, such as gas-phase, aqueous-phase, and heterogeneous chemistry and aerosol processes.

For this study, model simulations were conducted over a domain with a rotated lat-lon grid projection at 15 km horizontal resolution (see Fig. 49.2). The domain is centered over the Canadian Arctic with its southern boundary extending south of the Canada-US border. Eighty vertical, unevenly spaced, hybrid coordinate levels were used to cover between the surface and 0.1 hPa. Several model upgrades and special considerations were made for this study:

Representation of sea ice and snow cover in dry deposition: Dynamic sea ice and snow cover fractions were introduced to the dry deposition module to adjust the land-use covers in order to account for ice-snow cover conditions. In addition, a greater surface resistance was used in this study for treating dry deposition of ozone over ice surfaces following Helmig et al. (2007).

Chemical lateral boundary conditions: For this study, the MACC-IFS chemical reanalysis for 2010 (Inness et al. 2013), available 3-hourly, was used to build daily chemical boundary condition files for the GEM-MACH Arctic domain. In addition, the southern boundary condition was enhanced by using the operational GEM-MACH archives for the simulation time period in order to better represent the transport from the south.

North American wildfire emissions: Daily hotspot data for 2010 was used to generate the North American wildfire emissions; the BlueSky methodology (O'Neill et al. 2003) was used to estimate the daily emissions per fire hotspot. Several fire plume injection methodologies were tested.

Canadian shipping emissions: A detailed marine emission inventory for ships sailing in Canadian waters including the Canadian Arctic was developed for 2010, based on vessel movement data supplied by the Canadian Coast Guard (CCG). The link-based emission data was processed into monthly major point source files for input to the model.

Other anthropogenic emissions included in the model simulations are based on the 2010 Canadian and the 2012 (projected) U.S. anthropogenic emission inventories. Biogenic emissions were estimated on-line using the BEIS v3.09 algorithms. The simulations were carried out for the time period of March–October, 2010; the first month of the simulation is counted as spin-up and not included in the analysis.

49.3 Results and Discussion

49.3.1 Model Evaluation

Comprehensive model evaluation against available observations from existing air quality monitoring networks was carried out. Figure 49.1 shows examples of the model-observation comparison of ozone and $PM_{2.5}$ for sites north of 55 N for the months of August. The model is able to capture the general trends of the observed ambient ozone and $PM_{2.5}$ in the northern region. Modelled ozone has a small positive mean bias of 1–2 ppbv (or about 5–10 % in relative terms) and a smaller diurnal range than observed in this region. Modelled $PM_{2.5}$ has an overall negative bias, mostly driven by the under-prediction of background concentration levels in early summer and lower predicted peak values (compared to observations) during some of the pollution events.

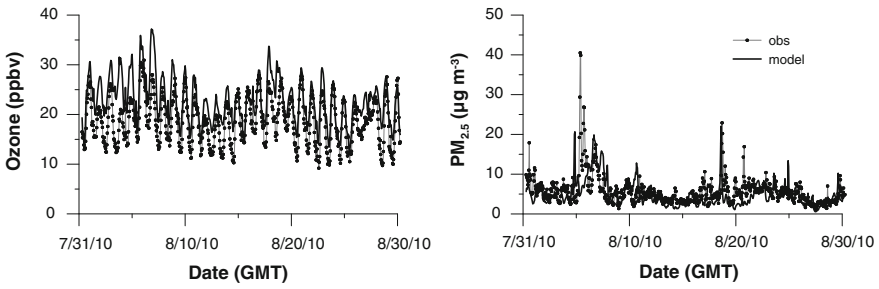

Fig. 49.1 Time series of modelled and observed ground-level ozone (in ppbv; *left*) and $PM_{2.5}$ (in µg m^{-3}; *right*) averaged over the monitoring sites located north of 55 N, for the month of August, 2010

49.3.2 Impact of Different Emission Sources to the Canadian Arctic and Northern Environment

The impact of the shipping and North American (NA) wild fire emissions is illustrated in Fig. 49.2. The examples shown are relative differences (in percent) in monthly averaged ambient ozone and $PM_{2.5}$ concentrations as well as monthly accumulated total deposition of sulfur (for the month of August).

The relative impact from shipping emissions over the northern regions is stronger in the east, from shipping activities over the east coast and Arctic waters. The impact on ambient ozone extends to a wider area, while the impact on ambient $PM_{2.5}$ is more localised along the shipping channel. The shipping emissions also make a significant contribution to sulfur and nitrogen (not shown) depositions in the northern regions particularly over eastern Nunavut and northern Quebec.

In comparison, the impact from wildfire emissions is more strongly felt on the west, due to the fact that most of fires in summer of 2010 were over northern British Columbia, Alaska, and northern Prairies. The impact on ambient $PM_{2.5}$ from fire emissions is considerably more significant than on ambient ozone over the northern regions, partly due to lower background concentration levels. The impact from fire emissions on deposition of sulfur also extends to the High Arctic.

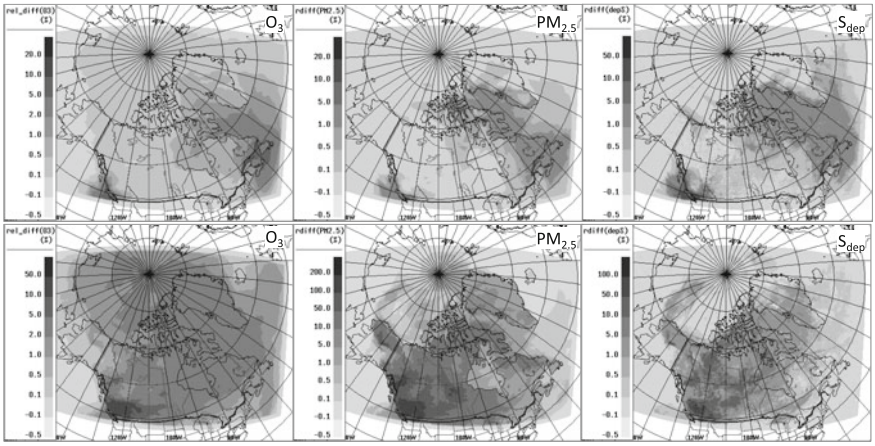

Fig. 49.2 Modelled relative contribution from shipping (*top panel*) and NA wildfire emissions (*bottom panel*) to monthly averaged ozone (*left*) and $PM_{2.5}$ (*centre*) at ambient level and to accumulated total sulfur deposition (*right*), all for the month of August, 2010

49.4 Conclusions

Current shipping emissions do contribute to the air pollution levels in the Canadian Arctic and Northern regions. In terms of relative contribution, shipping emissions have a more significant impact on ambient $PM_{2.5}$ levels than on ambient ozone levels. The impacts from shipping on depositions in the northern regions are also significant particularly over eastern Canadian Arctic. Wildfire emissions have a widespread impact on air quality in the Canadian northern regions particularly from the northern boreal forest fires.

Acknowledgments The authors would like to acknowledge The MACC-II project and Xiaobo Yang (ECMWF) for processing the MACC-IFS-MOZART reanalysis data. The support from the EC GEM-MACH development team is much appreciated. We would also like to acknowledge NATChem for providing data from North American air quality monitoring networks.

Question and Answer

Questioner: Annie Seagram
Q: Other than (perhaps) for political reasons, what is the purpose in the context of this research of comparing the impacts of fire emissions and shipping emissions?
A: We know that the Arctic is often impacted by long-range transport of pollutants, particularly during winter and spring seasons. During summer (also the Arctic shipping season), while the transport from mid-latitudes is reduced due to weaker polar circulation, the North American wildfire emissions are still able to reach the Arctic (as shown in this study). In contrast to the long-range transport which often happens at elevated levels, the emissions from Arctic shipping activities are delivered to the Arctic at levels much closer to the surface. It is important to look at both of these major pollution sources and understand the roles they play in affecting the Arctic air quality and environment.

References

Helmig D et al (2007) The role of ozone atmosphere-snow gas exchange on polar, boundary-layer tropospheric ozone—a review and sensitivity analysis. Atmos Chem Phys 7:15–30. doi:10.5194/acp-7-15-2007

Inness A et al (2013) The MACC reanalysis: an 8 yr data set of atmospheric composition. Atmos Chem Phys 13:4073–4109. doi:10.5194/acp-13-4073-2013

Menard S et al (2014) Current and future developments in numerical air quality forecasting in Canada. In: Steyn DG, Mathur R (eds) Air pollution modelling and its application XXIII. Springer, Dordrecht, pp 629–632

Moran MD et al (2010) Particulate-matter forecasting with GEM-MACH15, a new Canadian air-quality forecast model. In: Steyn DG, Rao ST (eds) Air pollution modelling and its application XX. Springer, Dordrecht, pp 289–292

O'Neill SM et al (2003) The BlueSky smoke modeling framework. In: 5th symposium on fire and forest meteorology. American Meteorological Society, Orlando, FL. www.blueskyrains.org

Chapter 50
LEO: Combination of a Plume and Grid Model in the Netherlands

Eric van der Swaluw, Richard Kranenburg, Wilco de Vries, Ferd Sauter, Roy Wichink Kruit, Jan Aben, Astrid Manders, Guus Velders, Martijn Schaap and Addo van Pul

Abstract We present the chemistry transport model LEO: a hybrid model, which combines the Eulerian grid model **L**OTOS-**E**UROS with the Gaussian plume model **O**PS. LEO is a new model under development in the Netherlands, which combines high resolution plume calculations around sources with large-scale transport and chemistry from a Eulerian grid model. In this way, we combine the best of both worlds into a new state-of-the-art model. The aim of LEO is to have a new calculation tool available in the Netherlands at a high resolution (typically 1×1 km^2), which can (among others) deliver data input for the yearly produced maps of concentrations and deposition over the Netherlands. In the presentation a brief overview of the LEO model is given, and results of calculations are presented for calculating annual averaged concentrations of pollutants and deposition of acidifying and eutrophying components over the Netherlands. Furthermore, preliminary results are shown for LEO in its Plume-in-Grid (PinG) configuration, i.e., the transport of the mass released from a number of point sources is initially calculated with a plume description, after which the mass of the plumes is dumped into the grid. We will illustrate the performance of LEO by analysing existing multi source situations for ammonia with high time resolution measurements of ammonia.

50.1 Introduction

In the Netherlands large-scale concentration maps of pollutants over its surface area are calculated and presented on an annual basis at a resolution of 1×1 km (Velders et al. 2014). These calculations are performed with OPS, which combines a Gaussian plume model approach for local applications with a Lagrangian trajectory

E. van der Swaluw (✉) · W. de Vries · F. Sauter · R. Wichink Kruit · J. Aben · G. Velders · A. van Pul
RIVM, PO Box 1, 3720 Bilthoven, BA, The Netherlands
e-mail: Eric.van.der.Swaluw@rivm.nl

R. Kranenburg · R. Wichink Kruit · A. Manders · M. Schaap
TNO, PO Box 80015, 3508 Utrecht, TA, The Netherlands

D.G. Steyn and N. Chaumerliac (eds.), *Air Pollution Modeling and its Application XXIV*, Springer Proceedings in Complexity,
DOI 10.1007/978-3-319-24478-5_50

model for long range transport. OPS has a good performance on local scales (1 × 1 km), in particular in areas close to sources. Large-scale chemistry in the OPS model is parameterized, and therefore less robust than for example a Eulerian chemistry transport model. In this paper we present the LEO model, which combines the **L**OTOS-**E**UROS model with the **O**PS model, in this way combining the best of both worlds: a good performance of large-scale chemistry (LOTOS-EUROS), without losing the high resolution near the areas with sources (OPS). We present two variants of the LEO model, i.e. an off-line version in which the results from both models are combined, but not coupled, *and* an on-line version in which the models run simultaneously as a Plume-in-Grid (PinG) configuration. We discuss the first variant in Sect. 2, and the second variant in Sect. 3. Section 4 gives a summary and outlook.

50.2 LEO Using Source Apportionment

In the decoupled variant of LEO, both models run independently with source apportionment, a module available for both LOTOS-EUROS and OPS. In order to calculate concentrations of pollutants over the Netherlands in this LEO configuration, we tag emissions in both models using two labels: emissions from the Netherlands (label I) and emissions outside of the Netherlands (label II). Subsequently, a LEO (annual averaged) concentration map over the Netherlands is constructed *after* calculations with both models have been performed. This is done by adding the calculated OPS concentrations due to Dutch emissions (label I) *and* the LOTOS-EUROS concentrations due to non-Dutch emissions (label II). In this way the high resolution (1 × 1 km) on local scales is maintained, while at the same time the large-scale chemistry due to emissions from abroad is also taken into account. Notice that in the LOTOS-EUROS calculations both Dutch and non-Dutch emissions are included, so the chemistry is completely described (without omissions) in the calculations. However, because of the use of source apportionment module, at the end of the simulation, the concentrations from label II in LOTOS-EUROS are selected for usage in the constructed LEO map.

The calculations have been performed for a range of pollutants, i.e. PM_{10}, $PM_{2.5}$, EC, NH_3, NO_x, and SO_2. Compared to OPS calculations, an improvement occurs in the LEO maps in particular for secondary inorganic aerosols (SIAs), due to the more realistic chemistry scheme taking into account large-scale transport. Compared to LOTOS-EUROS calculations, components like NH_3 and NO_x are represented more accurate in the LEO model due to the higher resolution near source regions.

Figure 50.1 shows the LEO map of the annual averaged NH_3 map, in which the mass contribution from Dutch emission sources (and hence OPS calculations) are dominating. A comparison with the measurements of NH_3 in the Netherlands shows a very good agreement (regression coefficient close to unity, and a correlation coefficient of order 0.9).

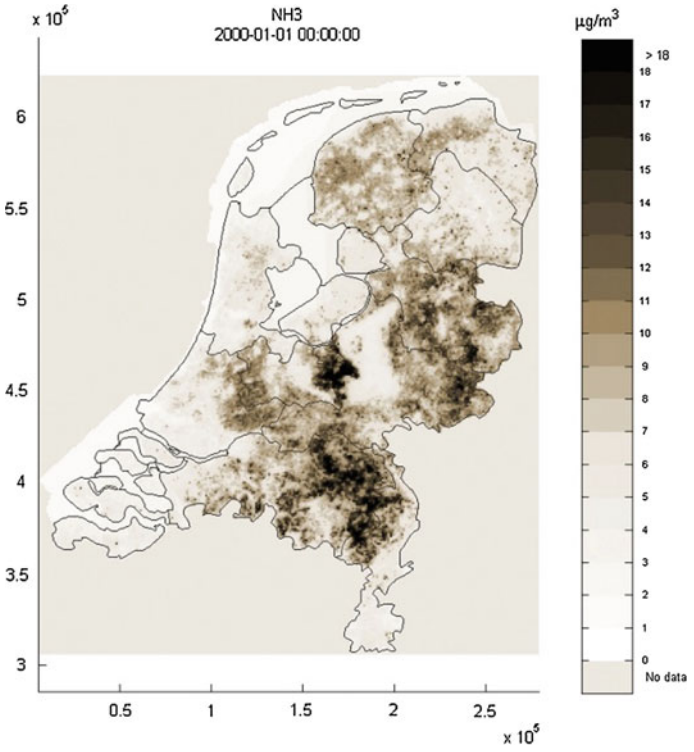

Fig. 50.1 The annual averaged concentration map of NH_3 as calculated by the LEO model for the year 2009

50.3 LEO in PinG Configuration

In the coupled variant of LEO, both models are run simultaneously in PinG configuration. Close to point sources, the dispersion is calculated hour-to-hour with the Gaussian plume model OPS. After approximately 2–3 h, the mass of the plume is dumped into the grid of the LOTOS-EUROS model, which commences its dispersion at later times. The LEO PinG model is currently working for passive tracers (no deposition, no chemistry) with multiple (point) sources. Dumping of the mass from the plume model to the grid model occurs when the width of the plume is comparable with the horizontal grid size ($\sim$7 km) of the Eulerian model (see for example (Korsakissok and Mallet 2010)). As yet no dumping criteria based on chemical equilibrium have been considered, since the model currently uses passive tracers.

Currently we have LEO PinG running in which multi-source passive tracers are modelled with ECMWF meteo as input. An example of concentrations as calculated with LEO PinG with one source is depicted in Fig. 50.2.

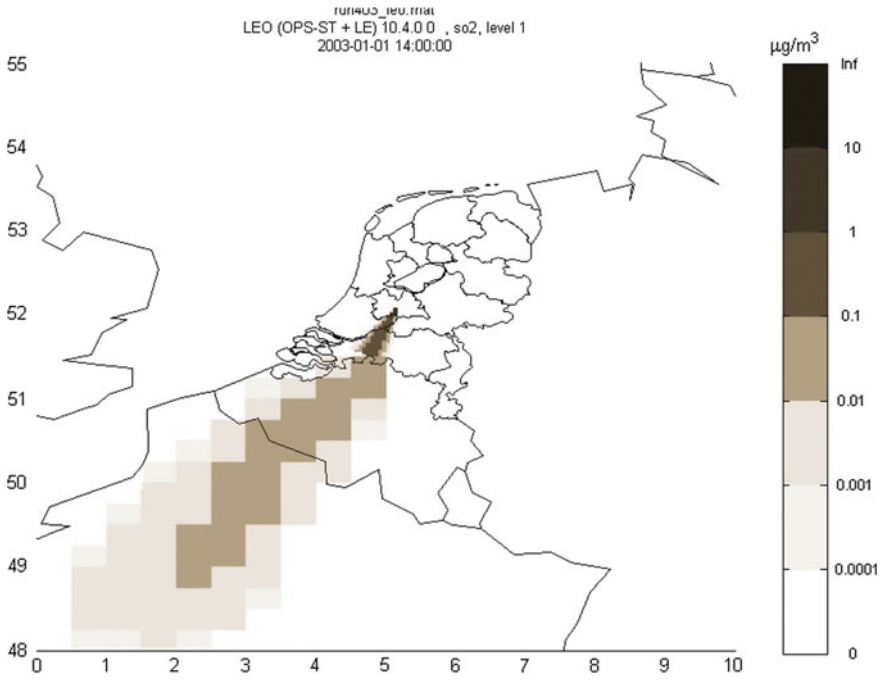

Fig. 50.2 Preliminary result of LEO PinG in which a single plume (passive tracer) is modelled

50.4 Conclusions and Outlook

The LEO model is presented in this paper in its two variants: one is applicable for calculating annual averaged concentration maps over the Netherlands, the PinG version of the model is applicable for hour-to-hour calculations over the Netherlands. This approach combines high resolution plume calculations around sources with OPS with large-scale transport and chemistry from the Eulerian grid model LOTOS-EUROS.

The first application of LEO PinG will be on NH_3 in *De Peel* region in the Netherlands: this is a region in the Southeastern part of the Netherlands with intensive agricultural activity. A convergence study will be performed in which an increasing number of point sources will be added to the PinG model calculation, this in contrast with a calculation in which all sources will be modelled in a *Eulerian way* with the LOTOS-EUROS model.

Questions and Answers

Questioner: T. Dore
Question: The use of 'colors' in LOTOS-EUROS suggests that source attribution can be calculated in a single model run. How flexible is the model assignment of colors regarding contributions from different numbers of country or sector emissions?

Answer: Indeed, the LOTOS-EUROS model can calculate a different numbers of country or sector emissions *in a single model run*. The number of 'colors' which can be used in a single model run is not limited by the source apportionment module itself: obviously computation time increases as one increases the number of 'colors'.

Questioner: B. Carissino
Question: You mention that the plume chemistry is linear, presumably mixing with the background. How does that impact the results and is it possible to improve it by adding first order non-linear effects such as HDMR?

Answer: Large-scale chemistry in the OPS model is parameterized. The LEO model improves this by combining the **L**OTOS-**E**UROS model with the **O**PS model, such that one yields a good performance of large-scale chemistry (LOTOS-EUROS), without losing the high resolution near the areas with sources (OPS). Nevertheless we indeed will look in a later stage into the possibility of adding simple first-order reaction schemes.

Questioner: S. Hanna
Question: You mentioned that a Gaussian plume model is used in the near field. Is it a straight-line model or does it bend or curve its trajectory?

Answer: The OPS model is a Gaussian plume model approach for local applications with a Lagrangian trajectory model for long range transport. This means that for example a change in wind direction over time is taken into account by the OPS model, such that one obtains curved trajectories. The OPS model used in the LEO model can hence be considered as a segmented plume model, and not as a straight-line model.

References

Korsakissok I, Mallet V (2010) Development and application of a reactive plume-in-grid model: evaluation over Greater Paris. Atmos Chem Phys 10:8917–8931

Velders GJM, Aben JMM, Geilenkirchen GP, den Hollander HA, Noordijk H, van der Swaluw E, de Vries WJ, Wesseling J, van Zanten, MC (2014) Large-scale concentration and deposition maps the Netherlands report 2014. RIVM report 680363002

Chapter 51
Increasing the Number of Allergenic Pollen Species in SILAM Forecasts

Marje Prank, Mikhail Sofiev, Pilvi Siljamo, Mari Kauhaniemi and European Aeroallergen Network

Abstract SILAM has been among the first regional dispersion models to develop the ability to compute pollen emission and dispersion. For previous seasons forecasts have been provided for birch, grasses, olive and ragweed. For the current season this list has been extended by alder and mugwort. The growing number of modelled species makes it possible to draw conclusions from the existing experiences, related to the features of the input data and algorithms applied to describe the pollen emission. We demonstrate, that the currently available options in SILAM allow adding new pollen species with minimal development effort and limited input data, to allow forecasts with comparable quality to the previously developed taxa.

51.1 Introduction

Due to raising allergy levels among European population, modelling of allergenic pollen has become an important part of air quality forecasting. SILAM has been among the first models to develop the ability to compute pollen emission and dispersion. For previous seasons forecasts have been provided for birch (Sofiev et al. 2013), grasses, olive and ragweed (Prank et al. 2013). For coming seasons this list has been extended by alder and mugwort. This paper discusses the experiences obtained while developing the source terms for these pollen species.

51.2 Methods

Pollen emission model requires two main components: a habitat map and a flowering model specifying the dependencies of the season timing on external forcings.

M. Prank (✉) · M. Sofiev · P. Siljamo · M. Kauhaniemi · European Aeroallergen Network
Finnish Meteorological Institute, Helsinki, Finland
e-mail: marje.prank@fmi.fi

D.G. Steyn and N. Chaumerliac (eds.), *Air Pollution Modeling and its Application XXIV*, Springer Proceedings in Complexity,
DOI 10.1007/978-3-319-24478-5_51

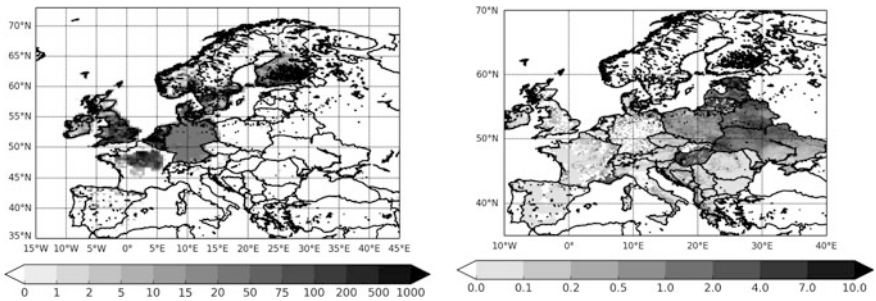

Fig. 51.1 Distribution maps of mugwort (Global Biodiversity Information Facility, *left*) and alder (European Forest Institute, *right*)

Several data sources exist for plant habitat maps. Land cover and forest inventories can contain either the required land use type (e.g. olive plantations or grasslands) or a surrogate type that needs to be scaled for the specific species (e.g. broadleaf forest for birch or alder). The more detailed data sources, such the Global Biodiversity Information Facility (GBIF, www.gbif.org) that provides data on observations of specific species or European Forest Institutes (EFI) database on tree species (Brus et al. 2011) have not proven very useful, as the observation practices differ noticeably between regions. For instance, the distribution of mugwort in the GBIF (Fig. 51.1a) shows clear differences between countries and very few observations of the plant in the Eastern Europe, where the plant is known to be common. According to the EFI alder map (Fig. 51.1b), Finland is almost free of alder, which is not true, and country borders are again visible. Thus, it has proved more useful to use the more general land-use maps, such as broadleaf forest or grasslands and croplands, and scale them with pollen observations.

SILAM currently allows several parameters to influence the flowering, e.g. accumulated temperature, soil humidity and photoperiod. All trees are represented as temperature sum dependent species, while the flowering of the annuals such as ragweed is assumed to mainly depend on photoperiod. For grasses—a family of species with different features—a simplified model is used where the flowering time is taken as the average observed season. The calibration of the flowering model would ideally be based on phenological observations; however, these are not available for all species. In this case, the pollen observations can be used.

Substantial research efforts were needed for introducing the first four pollen species to SILAM. In order to study the necessary complexity of pollen modelling, the development of the source terms for the two added species was made with minimal input data and simplest models. The broadleaf forest map and temperature sum based flowering model was taken as a starting point for the alder source term. All human influenced land-uses (roads, urban areas, etc.) were assumed as the mugwort habitat and the flowering was assumed to start and end on fixed calendar

days. This first guess model was run for 5 years (2008–2012), after which the habitat maps and flowering parameters were updated based on the model-measurement differences. This procedure was repeated for 3 times.

51.3 Results and Discussion

The comparison of the quality of the SILAM predictions for the six species is shown in Table 51.1. The best modelled species is ragweed, with the spatial correlation of the seasonal pollen index (SPI, sum of daily mean pollen concentrations over the pollen season) of 0.91 and the modelled season start within 3 days from the observed in 54 % of the cases. Season start is also well reproduced for birch, the only species where the flowering model has been calibrated based on phenological observations, not pollen counts. The newly added species do not lose much in modelling quality to the older models. The worst scores are shown for grass pollen, where the correlation is almost zero and a large bias exists for the SPI. This stresses the need of calibration of the habitat map with the pollen observations, to take into account the plants pollen productivity in different climatic zones, but also correct errors in the underlying land-use data. The end of the season is reproduced by the model with lower quality than the beginning, with noticeable biases for several species. However, the accuracy of the forecasts of season end is much less relevant for the allergy patients than the accuracy of predicting the start of the season, in order to start the medications in time.

One of the reasons for the low quality in predicting the seasons end is that in the model the season is assumed to have a single peak. However, in the observations

Table 51.1 Model performance

	Birch	Grass	Olive	Ragweed	Mugwort	Alder
Seasonal pollen index						
Correlation	0.52	0.02	0.66	0.91	0.72	0.65
Norm bias	−0.19	1.53	−0.06	0.08	0.02	−0.09
Start 5 % day						
Bias (days)	0.31	4.60	−9.51	3.02	4.49	−0.47
<3Day	0.50	0.25	0.28	0.54	0.39	0.35
<7Day	0.73	0.46	0.46	0.81	0.69	0.55
End 95 % day						
Bias (days)	2.25	−2.00	−18.89	−1.53	−5.69	−13.11
<3Day	0.38	0.20	0.19	0.45	0.27	0.23
<7Day	0.61	0.40	0.36	0.77	0.51	0.40

Norm. bias—bias normalized with the observed average concentration
Correlation—spatial correlation of observed and modelled SPI values over the stations
Season start, end—day when 5 % or 95 % of the total SPI is reached
<*nDays*—Fraction of cases when SILAM is within n days from the observed season start or end

seasons with multiple peaks are relatively common. This can be caused by several species with somewhat different flowering times producing indistinguishable pollens. Another reason for errors in the flowering time can be temperature accumulation in unresolved mountain terrains and seaside, where the large model grid cell covers microenvironments with noticeably different conditions.

The future plans in SILAM pollen modelling include further extensions of the species list, also considering allergenic fungal spores. Regarding the species already in the model, it will be relevant to start modelling the inter-annual variations in the plant pollen production—currently the same plant is assumed to produce exactly the same amount of pollen every year and this is known to lead to large errors in the forecast. Another possible development foreseen in the future is to start accounting for the variable potency of pollen grains—as shown by Buters et al. (2012, 2015) and Galan et al. (2013), the amount of allergen in birch, grass and olive pollen can vary noticeably from day to day.

Acknowledgments This research was performed within the scope of the TEKES-SmartPollen, Academy of Finland APTA and FP-7 MACC-II projects. We would like to thank the European Aeroallergen Network for kindly providing the pollen observations and helpful insights to the life of the plants.

Questions and Answers

Questioner: K.H. Schluenzen.
Question: How do you intend to determine the inter-annual change in the total amount of pollen emitted, which depends on year and space?
Answer: Some ideas exist about the processes causing the inter-annual variations. For example, in case of birch, the development of the pollen starts already in the previous summer, and thus the production of the current year seeds competes directly for the resources with the preparation of the next year's pollen, causing well noticeable biannual variations, while for the annual species the pre-flowering conditions, such as temperature, solar radiation and soil humidity determine the plant growth.

Questioner: D. Neumann.
Question: There are pollen forecasts available—for example in Germany. Are these forecasts mainly based on measurements (spatial interpolation of measured concentrations) or are there more groups working on pollen emission and transport modelling?
Answer: There do exist a few examples of other pollen forecast models. The COSMO-ART model is used to forecast birch and ragweed pollen in Germany and Swizerland. In Denmark the ENVIRO-HIRLAM model is applied for pollen forecasts. Also, SILAM source term for birch has been implemented in the models of the MACC regional multi-model ensemble. However, majority of the public pollen forecasts in Europe rely currently on pollen and phenological observations.

In Finland we are working currently on a project that would allow the duty forecasters to correct manually the SILAM forecasts based on the observations before making them available to public.

Questioner: S. Hanna.
Question: Does your model account for the gravitational settling velocity of the pollen?
Answer: Yes, pollen is treated like standard aerosol in SILAM, with large size but relatively lower density. However, sometimes pollen grains are of complex shapes, evolved to increase their flight distances, making it non-trivial to guess their aerodynamic diameters from their physical size. The pollen aerodynamic diameters have been measured for only a few species, which does increase the uncertainties in modelling the pollen deposition.

References

Brus D, Hengeveld G, Walvoort D, Goedhart P, Heidema A, Nabuurs G, Gunia K (2011) Statistical mapping of tree species over Europe. Eur J For Res V131(1):145–157

Buters J, Thibaudon M, Smith M, Kennedy R, Rantio-Lehtimaki A, Albertini R, Reese G, Weber B, Galan C, Brandao R, Antunes C, Jaeger S, Berger U, Celenk S, Grewling L, Jackowiak B, Sauliene I, Weichenmeier I, Pusch G, Sarioglu H, Ueffing M, Behrendt H, Prank M, Sofiev M, Cecchi L (2012) Release of Bet v 1 from birch pollen from 5 European countries. Results from the HIALINE study. Atmos Environ V55:496–505

Buters J, Prank M, Sofiev M, Pusch G, Albertini R, Annesi-Maesano I, Antunes C, Behrendt H, Berger U, Brandao R, Celenk S, Galan C, Grewling Ł, Jackowiak B, Kennedy R, Rantio-Lehtimäki A, Reese G, Sauliene I, Smith M, Thibaudon M, Weber B, Cecchi L (2015) Variation of the group 5 grass pollen allergen content of airborne pollen in relation to geographic location and time in season. J Allergy Clin Immunol. ISSN 0091-6749. doi:10.1016/j.jaci.2015.01.049

Galan C, Antunes C, Brandao R, Torres C, Garcia-Mozo H, Caeiro E, Ferro R, Prank M, Sofiev M, Albertini R, Berger U, Cecchi L, Celenk S, Grewling L, Jackowiak B, Jaeger S, Kennedy R, Rantio-Lehtimaki A, Reese G, Sauliene I, Smith M, Thibaudon M, Weber B, Weichenmeier I, Pusch G, Buters JT (2013) Airborne olive pollen counts are not representative of exposure to the major olive allergen Ole e 1. Allergy 68:809–812

Prank M, Chapman D, Bullock J, Belmonte J, Berger U, Dahl A, Jäger S, Kovtunenko I, Magyar D, Niemelä S, Rantio-Lehtimäki A, Rodinkova V, Sauliene I, Severova E, Sikoparija B, Sofiev M (2013) An operational model for forecasting ragweed pollen release and dispersion in Europe. Agric For Meteorol 182–183:43–53

Sofiev M, Siljamo P, Ranta H, Linkosalo T, Jaeger S, Rasmussen A, Rantio-Lehtimaki A, Severova E, Kukkonen J (2013) A numerical model of birch pollen emission and dispersion in the atmosphere. Description of the emission module. Int J Biometeorol 57:45–48

Chapter 52
PM Modelling over Nepal with WRF-Chem

A. Mues, A. Lauer and M. Rupakheti

Abstract Very high particulate matter (PM) and black carbon (BC) concentrations are observed in the Kathmandu Valley, Nepal. With an aim of gaining a better understanding of the dynamics of these air pollutants, PM and BC simulations with the WRF-Chem model have been performed. The comparison of the simulation results with measurements shows that the model strongly underestimated the measured PM and BC levels. It is concluded that this is mainly due to missing up-to-date high resolution information on emissions in the valley.

52.1 Introduction

The urban area of the Kathmandu Valley in Nepal has been rapidly growing over the last two decades; this went along with a rapidly expanding urban sprawl and a constantly increasing traffic volume and resulted in a visible degradation of the air quality. Ambient measurements from the year 2013 identified particulate matter (PM) as the dominant air pollutant in the Kathmandu Valley with a high share of black carbon (BC). Because of the significant impact of PM and BC on public health and particularly of BC on climate the focus of this study is on these air pollutants.

The above mentioned measurements were taken during the 6 month SusKat-ABC (Sustainable Atmosphere for the Kathmandu Valley-Atmospheric Brown Cloud) field campaign in the Kathmandu Valley and surrounding regions which was organized as a part of the new initiative SusKat led by the Institute for Advanced

A. Mues (✉) · A. Lauer · M. Rupakheti
Institute for Advanced Sustainability Studies, Potsdam, Germany
e-mail: andrea.mues@iass-potsdam.de

A. Lauer
Deutsches Zentrum für Luft- und Raumfahrt (DLR), Institut für Physik der Atmosphäre, Oberpfaffenhofen, Germany

M. Rupakheti
Himalayan Sustainability Institute, Kathmandu, Nepal

D.G. Steyn and N. Chaumerliac (eds.), *Air Pollution Modeling and its Application XXIV*, Springer Proceedings in Complexity,
DOI 10.1007/978-3-319-24478-5_52

Sustainability Studies (IASS) (Rupakheti et al. 2016). SusKat is aiming at improving the understanding of and addressing air pollution in Nepal with a special focus on the Kathmandu Valley. During the campaign high quality meteorological and air quality data were collected at several sites in the Kathmandu Valley and the surrounding regions. In order to support the analysis and interpretation of the measurement data as well as to improve the understanding of the meteorological and chemical processes leading to the observed high pollution levels in the valley, model experiments with the Weather Research and Forecasting (WRF) model (Skamarock et al. 2008) including chemistry and aerosols (WRF-Chem) (Grell et al. 2005) are being performed. Because of the complex topography of the Himalayan Mountains and foothills the modeling of this region is very challenging and requires an adequate set of input data and parameterizations (model configuration) as well as a careful evaluation of both simulated meteorology and air quality.

52.2 Method

Three simulations are performed with the WRF model (meteorology only) for this study over South Asia (15 × 15 km^2 horizontal resolution) and nested simulations over Nepal (3 × 3 km^2) and the Kathmandu Valley (1 × 1 km^2) (Fig. 52.1) covering the time period December 2012–June 2013. In order to evaluate the simulations observational data from various sources are compared with the simulation results.

In addition, a WRF-Chem simulation with domains 1 and 2 has been performed covering the time period December 2012–February 2013. The schemes used for chemistry and aerosols as well as the input data used are given in Table 52.1. To date, no high resolution emission inventory exists for the region, and therefore the EDGAR HTAP emissions (based on the Regional Emission inventory in ASia (REAS) with a resolution of 0.25°) (Janssens-Maenhout et al. 2012) were used for the model simulations.

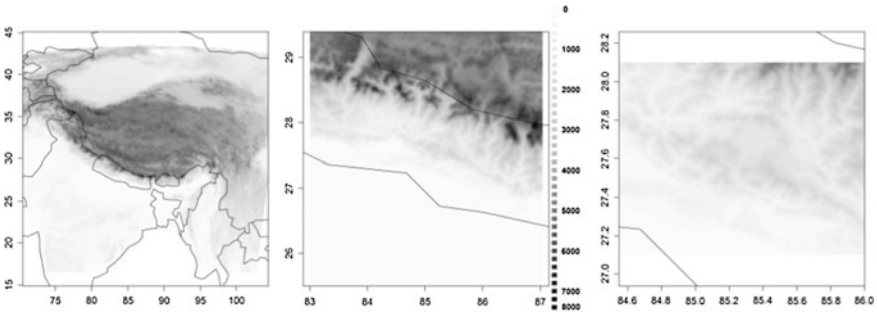

Fig. 52.1 Schematic overview of the WRF/WRF-Chem model domains with 15 km^2 (domain 1), 3 km^2 (domain 2) and 1 km^2 (domain 3) horizontal resolution. Exemplary shown is the topographic height in m

Table 52.1 Input data and schemes used for the WRF-Chem simulations

Input data	
Boundary cond. chemistry	MOZART-4/GEOS-5 (Global CTM) (Emmons et al. 2010)
Anthropogenic emissions	EDGAR HTAP v2.2 (resolution 0.1°, based on 0.25° REAS)
Fire emission	NCAR FINN v1.0 (Wiedinmyer et al. 2011)
Biogenic emissions	MEGAN (online)
Parameter	Scheme
Chemistry	RADM2+CMAQ aqueous phase chem.
Aerosols	MADE/SORGAM
Dust	GOCART on-line dust emissions (AFWA modifications)

52.3 Results

The results show that the meteorological parameters in general are reasonably well reproduced by the model although the mismatch in the model and the real elevation of several stations leads to, for instance, too high or low 2 m temperatures and pressure values compared with the measurements. Especially during night time the observed wind speed is overestimated by the model. A good temporal correlation of modeled and observed meteorological variables suggests that the most important key processes are captured by the model. For most parameters, the increase in horizontal resolution in the nested model domains gives only little benefit with the exception of wind speed and direction, which generally improve with increasing horizontal resolution. This demonstrates that high-resolution simulations also require adequate high-resolution input data such as land classification data or surface albedo.

The results of the WRF-Chem simulation show peak concentrations of PM10 in the area of the Taklamakan desert (mineral dust) and in urban areas in India (up to 500 μg/m^3 averaged over simulation period). The daily average PM10 concentrations monitored at the Bode station in the Kathmandu Valley are between 100–200 μg/m^3 in February 2013. These measured PM10 concentrations are highly underestimated (factor of three) by both model simulations with slightly higher concentrations in the nested domain 2 in which the temporal variability is also slightly different compared to the outer domain 1. In the model, PM10 mainly consists of secondary inorganic aerosols and organic matter at Bode. The measured PM2.5 concentrations at this station are better reproduced by the model compared with PM10. This suggests that especially in the aerosol fraction between PM10 and PM2.5 a substantial part of mass is missing and/or that the size of the particles is underestimated in the model requiring more detailed information on the particles size distribution of the emissions.

The simulated BC shows highest concentrations in urban areas in India with values of up to 30 μg/m^3 (Fig. 52.2a), average concentrations in Nepal are typically between 2 and 8 μg/m^3. Observed concentrations of BC at the Bode station are

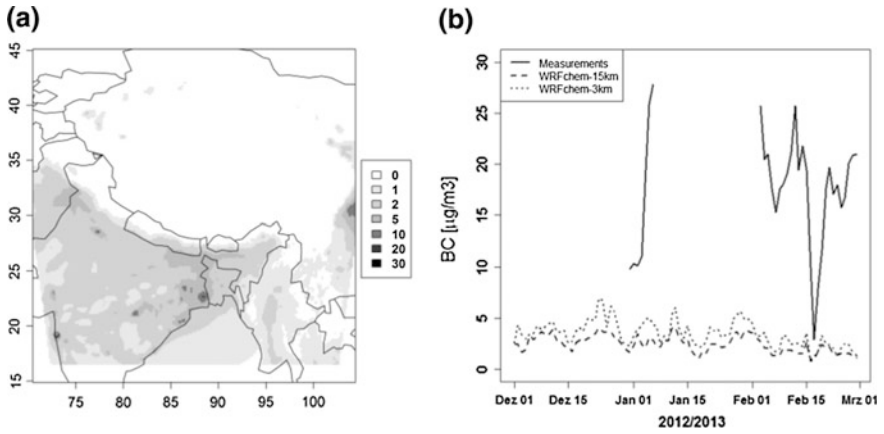

Fig. 52.2 Geographical distribution of the modeled near-surface BC concentrations averaged over the whole modeling period (**a**), and comparison of measured and simulated daily mean BC concentrations in the Kathmandu Valley (**b**)

highly underestimated by the model as shown in Fig. 52.2b. Measured BC daily mean concentrations at stations located in the surroundings of the valley are typically between 2 and 10 $\mu g/m^3$ in January and February 2013, which is substantially lower than at stations inside the valley. Although still underestimated, the BC concentrations at the stations outside of the valley are better reproduced by the WRF-Chem model. The averaged diurnal cycle of BC at the Bode stations shows a clear underestimation of measured concentrations by the model which is most prominent during the night and morning hours. In contrast, the model simulations reproduce nicely the temporal pattern of the observed mean diurnal cycle.

For both PM10 and BC the increase of the horizontal resolution leads to slightly higher PM10 and BC concentration and also a change in the temporal variability (e.g. Fig. 52.2b).

52.4 Conclusions

The fact that the measured BC concentrations at stations in the outskirts of the valley are better reproduced by the model than at stations in the urban areas of the valley together with the finding that similarly high BC and PM concentrations as measured in the valley are simulated in other parts of the model domain clearly suggests that adequate and up-to date local emission inventories are crucial. This stresses the need for an improved emission inventory for this rapidly changing region in order to assess properly current air quality issues in the Kathmandu Valley with high-resolution modeling.

References

Emmons LK, Walters S, Hess PG, Lamarque JF, Pfister GG, Fillmore D, Granier C, Guenther A, Kinnison D, Laepple T, Orlando J, Tie X, Tyndall G, Wiedinmyer C, Baughcum SL, Kloster S (2010) Description and evaluation of the Model for Ozone and Related chemical Tracers, version 4 (MOZART-4). Geosci Model Dev 3:43–67

Grell GA, Peckham SE, McKeen S, Schmitz R, Frost G, Skamarock WC, Eder B (2005) Fully coupled "online" chemistry within the WRF model. Atmos Environ 39:6957–6975

Janssens-Maenhout G, Dentener F, van Aardenne J, Monni S, Pagliari V, Orlandini L, Klimont Z, Kurokawa J, Akimoto H, Ohara T, Wankmüller R, Battye B, Grano D, Zuber A, Keating T (2012) EDGAR-HTAP: a harmonized gridded air pollution emission dataset based on national inventories. European Commission, Joint Research Centre, Institute for Environment and Sustainability, Report

Rupakheti M, Panday AK, Lawrence MG, Kim SW, Sinha V, Kang SC, Naja M, Park JS, Hoor P, Holben B, Sharma RK, Gustafsson Ö, Mahata K, Bhardwaj P, Sarkar C, Rupakheti D, Regmi RP, Pandit AK et al (2016) Atmospheric pollution in the Himalayan foothills: overview of the SusKat-ABC field campaign in Nepal. In preperation for Atmos Chem Phys

Skamarock WC, Klemp JB, Dudhia J, Gill DO, Barker DM, Duda MG, Huang X-Y, Wang W, Powers JG (2008) A description of the advanced research WRF version 3. NCAR/TN–475 +STR NCAR Technical Note

Wiedinmyer C, Akagi SK, Yokelson RJ, Emmons LK, Al-Saadi JA, Orlando JJ, Soja AJ (2011) The Fire INventory from NCAR (FINN): a high resolution global model to estimate the emissions from open burning. Geosci Model Dev 4:625–641

Chapter 53
Impact of Temporal Resolution of Dry Deposition Velocities on Air Quality Modeling

Joaquim Arteta, Beatrice Josse, Mathieu Joly, Virginie Marecal and Matthieu Plu

Abstract In the framework of global atmospheric composition and air quality forecasting, accurate modeling of atmospheric chemical species redistribution and evolutions in numerical weather and air quality prediction models has become an important challenge in terms of research and developments. Such model developments are a part of the MACCII and MACCIII projects (EU-FP7) done to extend ECMWF's integrated forecast system (IFS) by adding modules for chemistry, deposition and emission of reactive gases. It is now well known that deposition of chemical species, and especially dry deposition, is a major sink of pollutant in the atmospheric boundary layer. Several parameterizations have been developed in the last decades, while the resistances approach proposed by Wesely (1989) is the most commonly used. However, modeling of dry deposition is confronted to a lack of validation data. Indeed, this kind of parameterization is highly sensible to physical inputs like meteorological and surface fields. Currently, most of models use monthly-means values for dry deposition. It is thus impossible to take into account rapid transitions that can be observed on this inputs and can maybe leads to large biases on the short term forecasts. To investigate impacts of temporal resolution of dry deposition fields on air quality modeling, long simulations were done with the MOCAGE CTM developed at Météo-France, four type of temporal resolution (monthly-means, daily-means, mean daily-cycle, dynamic velocities) have been used, and results have been evaluated at regional and global scale. They shows important impacts in low-levels atmospheric composition locally, but also at global scale.

53.1 Methodology

Two set of 4 global and regional air quality simulations (DYN, CYC, DCSTE and MCSTE), covering year 2006 and 2008 have been performed using dry deposition velocities for chemical species with different time evolutions (hourly dynamically

J. Arteta (✉) · B. Josse · M. Joly · V. Marecal · M. Plu
CNRM-GAME/Météo-France, Toulouse, France
e-mail: Joaquim.Arteta@meteo.fr

D.G. Steyn and N. Chaumerliac (eds.), *Air Pollution Modeling and its Application XXIV*, Springer Proceedings in Complexity,
DOI 10.1007/978-3-319-24478-5_53

Table 53.1 Summary of model setup

	DYN	DCSTE	CYC	MCSTE
Dry deposition velocities	Calculated online	Daily mean value	Monthly mean daily cycle	Monthly mean value
Spatial resolution	Global 2° × 2° + Europe 0.2° × 0.2° 47 layers up to 5 hPa (7 in ABL)			
Meteorological driver	ARPEGE IFS			
Chemical scheme	RACMOBUS (RACM + REPROBUS)			
Emissions	IPCCv4 + GEIA			
Timestep	1 h for advection			
	15 min for physical processes			
	15 min to 20 s for chemistry, depending of vertical level			
Dry deposition velocities temporal resolution	1 h			
Dry deposition velocities parameterization	Wesely (1989), Wesely and Hicks (2000), Ganzeveld et al. (1998)			

driven, monthly mean cycle, daily mean and monthly mean). The overall configuration of the experiments is given below (Table 53.1). Simulations were performed using the MOCAGE-CTM semi-lagragian model developed at Météo-France.

53.2 Results

Dry deposition velocities, spatially integrated over Europe for 2006, show a huge variability seasonally, daily and hourly. This is related to the local variability of the meteorological fields, especially for reactive species like HCHO (Fig. 53.1).

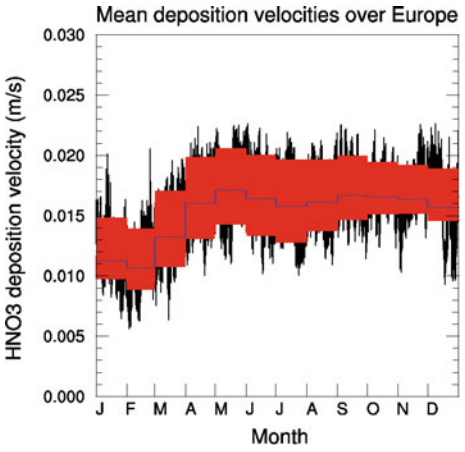

Fig. 53.1 Evolution of dry deposition velocities averaged over Europe for HNO3 for year 2006 (DYN in black; CYC in red; MCSTE in blue)

In the DYN simulation (black curve), this variability can reach 50 % locally between 2 consecutive days, even if variability is low at regional scale.

Since CYC experiment (red curve) uses "monthly mean" diurnal cycles, the daily variability is not represented. In this case, some high or low deposition velocities can be respectively under or over-estimated compared to the DYN simulation. This error can reach 25 %.

In the MCSTE experiment (blue curve), only variability at the monthly scale is present. All the effects of local meteorology is lost, leading to huge over/underestimations depending on the considered daytime compared to the DYN simulation.

DCSTE (not shown in figure 53.1) experiment slightly counterbalances this by adding the daily variability, even if most of the bias is still due to the lack of diurnal cycle.

The impact of the temporal evolution of dry deposition on atmospheric gas concentrations is important. The concentration difference between DYN and CYC is low, because the diurnal cycle is present even if the daily variability of deposition velocities is not modeled. Without diurnal cycle (DCSTE and MCSTE), depending on the species, the impact can be extremely low (HNO_3: mainly because concentrations are low) or important, as for ozone. For ozone, concentration is around 5 ppbv higher in DYN at nighttime, due to lower deposition velocities, and up to 10 ppb lower at daytime (Fig. 53.2). Such difference values are not negligible while using models for air quality forecasting purposes. This can lead to changes in chemical equilibria.

At the global scale (Fig. 53.3), absolute differences for O_3 can go up to 3 ppbv (0.5 for HNO_3) when using a mean cycle, and up to 10 ppbv with a mean value compared to dynamical dry depositions. The concentrations in DYN are lower during daytime and higher during nighttime, as already shown in Fig. 53.2. When focusing on particular days, this impact can be much higher, around 30 ppb (not

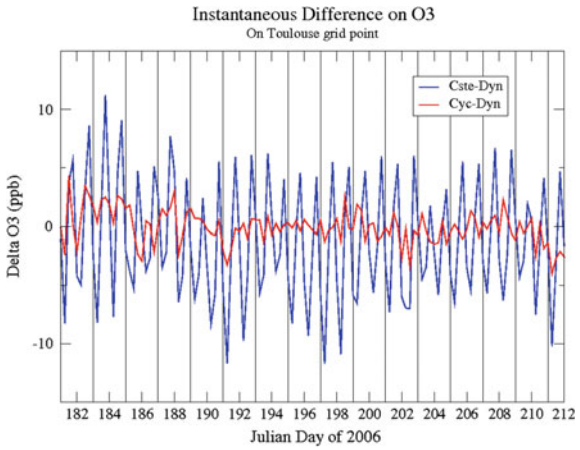

Fig. 53.2 Instantaneous absolute differences of O_3 concentration between DYN & MCSTE, and DYN & CYC runs, for June 2006, over Toulouse

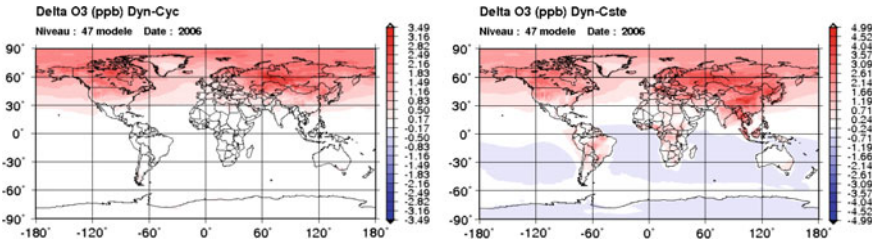

Fig. 53.3 Absolute mean differences of O_3 concentrations between DYN & MCSTE, and DYN & CYC runs, for year 2006, averaged in time

shown here). Moreover, using a high temporal resolution for deposition velocities also has an impact on the global budget of chemical species. When averaging hourly over all days of the year, we got from 3.5 to 5 ppbv more ozone over the northern hemisphere (Fig. 53.3).

53.3 Conclusion

Since the dry deposition velocities can be highly variable in space and time, using high temporal resolution fields can lead to a better estimation of chemical concentrations in the atmospheric boundary layer. In the framework of air quality forecasting, absolute differences up to 10 ppb for ozone concentrations can be responsible of missing some threshold overtaking or false alarms. This preliminary work shows that using constant monthly mean values is not suitable for air quality modeling. We show that at least monthly mean diurnal cycles could be used. This analysis, mainly focused on ozone, should be extended to other reactive and non-reactive species like NO_x, PAN, OH, etc.

References

Ganzeveld L, Lelieveld J, Roelofs G-J (1998) A dry deposition parameterization for sulfur oxides in a chemistry and general circulation model. J Geophys Res 103(D5):5679–5694

Wesely ML (1989) Parameterization of surface resistance to gaseous dry deposition in regional-scale numerical models. Atmos Environ 23(6):1293–1304

Wesely ML, Hicks BB (2000) A review of current status of knowledge on dry deposition. Atmos Environ 34:2261–2282

Chapter 54
Modelling of Pollen Emission Process for Dispersal Simulation of Birch Pollen

Shigeto Kawashima, Satoshi Kobayashi and Keita Tanaka

Abstract The number of patients of pollinosis caused by airborne pollen is increasing rapidly in the world. From a global perspective, pollinosis from birch is a serious problem in Europe, North America, and Northeast Asia. Our aim in this research is to generalize the principle of our pollen emission model developed for cedar. We observed temporal variations in airborne pollen concentrations of birch in Hokkaido, Japan, by using a Hirst-type pollen sampler. Relationship between airborne birch pollen and meteorological conditions during the main dispersal period was analyzed. Our results indicate that airborne pollen concentrations are related to changes in air temperature and solar radiation. The derivative of air temperature is most important and effective factor than the air temperature itself. The air temperature change for shorter time was related to the pollen emission of birch compared with the case of cedar. The amount of birch pollen emitted from the flowering birch forest was formulated using the algorithm summarized from the analysis.

54.1 Introduction

The number of patients of pollinosis caused by airborne pollen is increasing rapidly in the world. There are a number of ways to ameliorate the allergy, such as treatment with anti-allergic drugs, but the most important is to minimize contact with the substances that cause the allergy in the first place. For sufferers to appropriately organize their activities, it will be necessary to develop techniques to estimate pollen concentrations that are more detailed temporally and spatially. Much research has been undertaken to clarify the diffusion process of pollen in the atmosphere. For pollen emission amounts, measurements and estimates based on measurements have been used. There has been very little detailed investigation of

S. Kawashima (✉) · S. Kobayashi · K. Tanaka
Kyoto University, Kitashirakawa Oiwakechou, Sakyo, Kyoto, Japan
e-mail: sig@kais.kyoto-u.ac.jp

D.G. Steyn and N. Chaumerliac (eds.), *Air Pollution Modeling and its Application XXIV*, Springer Proceedings in Complexity,
DOI 10.1007/978-3-319-24478-5_54

modeling of pollen emissions. We had investigated methods of estimating the amount of pollen emitted per unit time per unit area of flowering cedar forest, treating meteorological factors as explanatory variables. From the results of our studies, we constructed pollen emission models for cedar forest. The aim in this research is to generalize the principle of our pollen emission model. In this article, we formulate the relationships between amounts of airborne birch pollen and meteorological factors, and we present a prototype of a birch pollen emission model that we have constructed in accordance with those relationships.

54.2 Materials and Methods

54.2.1 Analyzed Data

We conducted this research in the city of Sapporo, in the island of Hokkaido, northern Japan. Observations of airborne pollen were performed at the Hokkaido Institute of Public Health in Sapporo. For meteorological data, we used values observed at a weather monitoring station of the Sapporo District Meteorological Observatory. Birch woods and forests are spread through the urban areas of Sapporo and the nearby hills. We used the vegetation map provided by the Ministry of the Environment. The objective of the analysis was modeling of pollen emission amounts, so where possible we wanted to analyze changes in airborne pollen which had not been travelling for a long time from emission. We selected early period in pollen dispersal season, the middle in May.

54.2.2 Pollen Emission Model

We have previously proposed a model for evaluating flux of cedar pollen emitted per unit time per unit area of cedar forest (Kawashima and Takahashi 1995, 1999). With our data on airborne birch pollen, we conducted an analysis similar to the one we conducted for the cedar pollen emission model. A point to note is that the airborne pollen data at the Institute of Public Health located in the urban area of Sapporo cannot simply be treated as emission data, not being data observed within a birch forest. Nevertheless, in the early period in pollen dispersal season, almost all the airborne birch pollen observed in Sapporo is to be dispersed from birch woods in the nearby hills and mountains and on the plain. We studied the relationships between the airborne birch pollen data from Sapporo and the meteorological data and meteorological fluctuation components, using different values of the averaging period, and we established the meteorological factors and their fluctuation components that affected birch pollen emission amounts. Working from the results of this analysis, we selected the meteorological factors to be used in the construction of our pollen emission model.

54.3 Results and Discussion

The correlation analysis between airborne pollen concentrations and the meteorological factors were done for the early stage of birch pollen season in Sapporo. Based on the results of the correlation analysis and previous researches (Kawashima and Takahashi 1995, 1999), we combined air temperature fluctuation, wind speed fluctuation, and insolation values to create the following equation for the pollen emission model.

$$P = a\Delta T + b\Delta W + cS + d \tag{54.1}$$

where P is the pollen emission potential from a uniformly flowering forest, T is air temperature (°C), W is wind speed (m s^{-1}), S is insolation (MJ m^{-2}), Δ is operator for temporal deviation, and a, b, c, and d are constants. The parameters a, b, c, and d relate to the types of tree and quantities of male flowers. If the estimated value of P is negative, then P is set to zero.

A comparison between pollen emission concentrations estimated by this model and actually measured airborne pollen concentrations is shown in Fig. 54.1. This figure shows that our model can satisfactorily estimate patterns of change in pollen emission by using common meteorological factors. A particular point to note is that, in the case of birch pollen as in the case of cedar pollen, it is clear that, rather than simple values of temperature and wind speed, pollen emission amounts correlate with fluctuations in temperature and wind speed obtained as differences from average values over certain previous periods. We have made an improvement to the pollen emission model by adding insolation, which did not show a high correlation in the case of cedar, as a descriptive factor. It is suggested that this principle is generalized to the pollen emission from various plants.

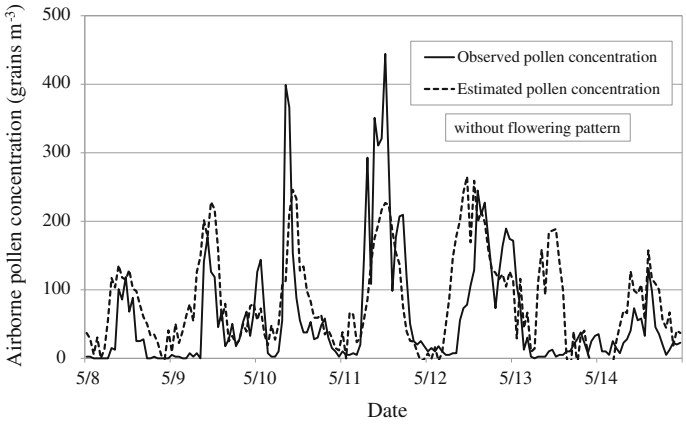

Fig. 54.1 Observed and estimated changes in the airborne pollen concentration

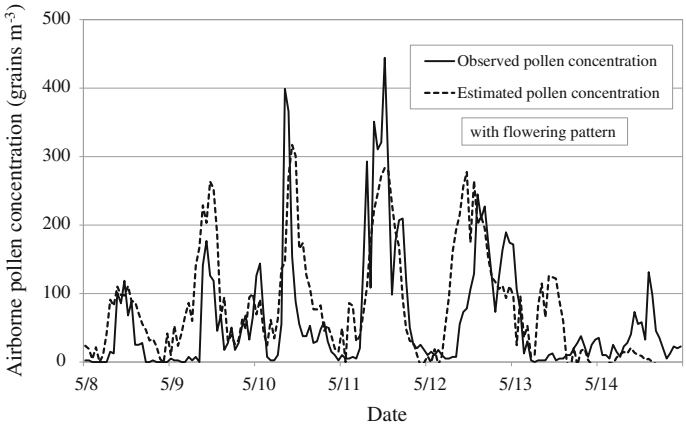

Fig. 54.2 Observed and estimated changes in the airborne pollen concentration with time using the flowering condition

The equation of the pollen emission model given above is for evaluating the potential amount of pollen emitted per unit of time per unit of area of uniformly flowering forest. For a pollen dispersal prediction simulation, data of forest density D of birches in each cell of a land area divided by a grid system is needed. If the proportion of birches flowering in a unit area of forest is F, the pollen emission amount Q to be used in a simulation can be found by the following equation.

$$Q = DFP \tag{54.2}$$

We estimated the change of birch flowering condition F during the flowering period. We then multiplied the pattern of change over time in the flowering proportion by the pollen emission potential to find birch pollen emission concentrations through the whole season. Figure 54.2 shows the observed and estimated changes in the airborne pollen concentration with time using the flowering pattern. The use of a flowering pattern allowed the estimation of birch pollen emission to reproduce very well the daily and overall changes in the number of airborne cedar pollen grains at the early period in the birch pollen season.

References

Kawashima S, Takahashi Y (1995) Modelling and simulation of mesoscale dispersion processes for airborne cedar pollen. Grana 34:142–150

Kawashima S, Takahashi Y (1999) An improved simulation of mesoscale dispersion of airborne cedar pollen using a flowering-time map. Grana 38:316–324

Chapter 55
May Weather Types and Wind Patterns Enhance Our Understanding of the Relationship Between the Local Air Pollution and the Synoptic Circulation?

Antonella Morgillo, Giovanni Bonafè, Enrico Minguzzi, Isabella Ricciardelli, Gian Paolo Gobbi, Luca Di Liberto, Federico Angelini, Tony C. Landi, Michele Stortini and Davide Dionisi

Abstract Aim of this work is to better understand the connections between synoptic circulation patterns, local wind regimes and air pollution in the Po Valley which is a densely populated and heavily industrialized area. In this study we present a classification of weather types (WTs) in the Alps region performed with an objective method (COST Action 733 "Harmonization and Applications of Weather Type Classification for European regions") based on hierarchical cluster analysis followed by a k-means cluster analysis, which is applied to the daily 500hPa time series from ERA INTERIM reanalysis. In order to take in account the strong influence of the regional wind regime on the local air quality, a classification of surface wind pattern (WPs) is performed as well with a cluster analysis technique. The link between WTs and WPs is investigated, and the statistical properties of pollutants concentration, aerosol chemical composition and dimensional distribution are analyzed in connection with WTs and WPs.

A. Morgillo (✉) · G. Bonafè · E. Minguzzi · I. Ricciardelli · M. Stortini
ARPA Emilia-Romagna, Bologna, Italy
e-mail: amorgillo@arpa.emr.it

G.P. Gobbi · L. Di Liberto · D. Dionisi
ISAC-CNR, Rome, Italy

F. Angelini
ENEA UTAPRAD-DIM, Frascati, Italy

T.C. Landi
ISAC-CNR, Bologna, Italy

D.G. Steyn and N. Chaumerliac (eds.), *Air Pollution Modeling and its Application XXIV*, Springer Proceedings in Complexity,
DOI 10.1007/978-3-319-24478-5_55

55.1 Introduction

The Po valley in Northern Italy is a semi-closed basin surrounded by complex orography. Surface winds are very weak, and strong temperature inversions are often observed near the ground and in the boundary layer. Since Po Valley is a densely populated and heavily industrialised area, air pollution is a major issue. Aim of this work is to better understand the connections between synoptic circulation patterns, local wind regimes and air pollution in the Po Valley.

55.2 Method

To perform the analysis, two meteorological classifications have been used: a synoptic pressure patterns classification and a local wind patterns classification. Moreover, hourly data of h_{ABL}, estimated by an Automated Lidar Ceilometer, have been used.

The classification of **synoptic pressure patterns** (SPPs) was performed in a domain covering Italy and the Alps, with an objective method (Philipp et al. 2014), using as input the time series of daily geopotential height at 500 hPa (Jan1985–Dec2014) provided by ERA-Interim. The CAP (Cluster analysis of Principal Component) method is applied, a two steps procedure comprising first a principal component analysis, then a clustering procedure. Classification is obtained with an agglomerative hierarchical cluster analysis (Ward Jr 1963), followed by a k-means (non-hierarchical) cluster analysis. Nine SPPs have been produced; their short names identify the prevailing geostrophic flux in the domain: (1) NW; (2) NW strong; (3) W weak; (4) flat; (5) SW strong; (6) NNE weak; (7) NNW strong; (8) SSW weak; (9) W.

Moreover, a **local wind patterns** (LWPs) classification is performed with a cluster analysis technique (Jiménez et al. 2009) over the Po Valley. Hourly time series (Jan2005–Dec2014) of wind speed and direction, observed at 10 m above the ground by 17 anemometers have been used. First, wind data are daily averaged and normalized in space and in time. Then, the Euclidean distance was calculated between each day, and used for a two-step cluster analysis: (1) agglomerative nesting in order to identify the optimal number of clusters; (2) final classification, performed with the technique of the partition around medoids. Nine LWPs have been produced; their short names identify the prevailing surface wind in the domain: (1) W, (2) N to NW, (3) NE, extended, (4) NE, limited, (5) E, (6) S, (7) SE, (8) incoherent, (9) SW.

Automated lidar ceilometer (ALC) observations have been performed at S. Pietro Capofiume[1] over a 3 year period (Jan2012–Dec2014) by means of a Jenoptik CHM15 Nimbus system.[2] The h_{ABL} is derived by an operator-driven analysis of

[1]A rural site in the central-eastern Po Valley.

[2]Time resolution: 5 min; vertical resolution: 15 m; altitude range: 200 m to 15 km.

daily plots of atmospheric backscatter and relevant gradients and variance (Angelini et al. 2009; Haeffelin et al. 2012).

55.3 Results

SPPs 1, 3 and 4 are the most frequent. SPPs 2 and 7 are typical of the winter months. All SPPs are persistent: in 50–60 % of the days the SPP is the same as the day before. LWPs are less persistent: in 20–30 % of the days the LWP is the same as the day before. The contingency table between SPPs and LWPs show no strong connection, suggesting that local wind regimes in the Po Valley are to some extent decoupled from the synoptic situation (Fig. 55.1).

Concentrations of PM10, O_3 and NO_2 measured at 10 urban background sites in Emilia Romagna have been compared with SPPs and LWPs for a 10 yrs period. SPPs with prevailing W–NW geostrophic fluxes lead to high concentration of PM10 and NO_2 in Oct–Mar, and so does LWP 1 (W), while LWPs with prevailing S wind component lead to high concentrations of O_3. Moreover the link between SPPs and LWPs and PM2.5 chemical composition is investigated (Fig. 55.2).

Finally, the h_{ABL} evaluated by ALC was compared with the h_{ABL} simulated by two models, the non-hydrostatic meteorological model COSMO-I7 (Steppeler et al. 2003) and the mass-consistent pre-processor CALMET (Scire et al. 2000). CALMET overestimates h_{ABL} in the afternoon, with a sudden decrease after sunset, when it switches from the mixed to the stable layer scheme. COSMO performs quite good during the day. Both models perform good in identifying SPP 7 (strong fluxes from NNW) and 2 (strong fluxes from NW) as associated to a lower daily h_{ABL}, but they wrongly associate to SPP 1 (fluxes from NW) a higher daily h_{ABL}. As

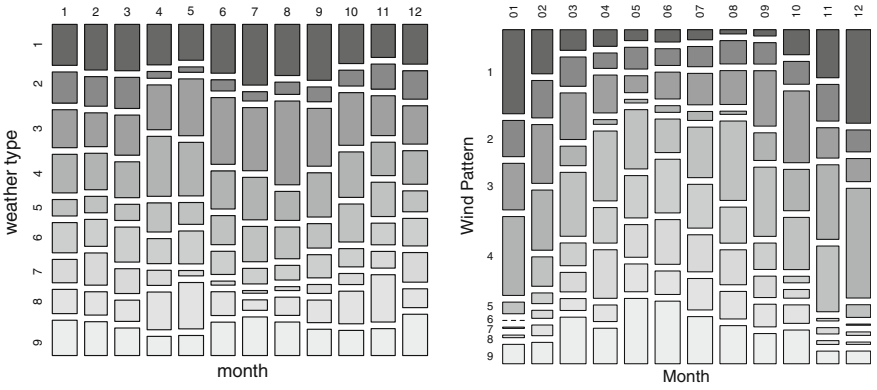

Fig. 55.1 Monthly relative occurrences of daily synoptic pressure patterns (*left*) and local wind patterns (*right*)

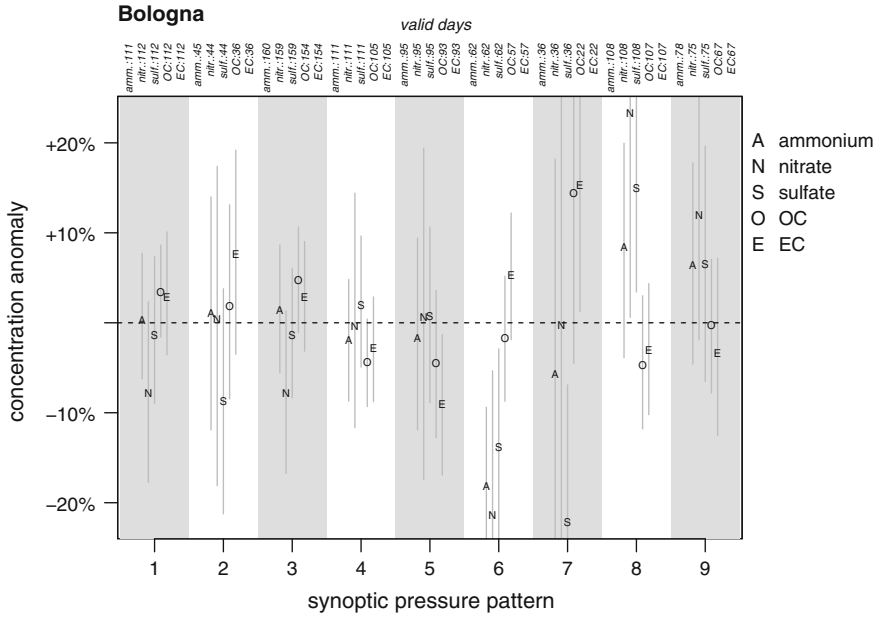

Fig. 55.2 Concentration anomaly of nitrate, sulfate, ammonium, elemental and organic carbon measured in the PM2.5 in a background site in Bologna, Italy (Nov2011–May2014). To filter out the seasonality, the relative anomaly with respect to the monthly average is considered. *Letters* relative anomalies, averaged for each Synoptic Pressure Pattern. *Vertical lines* intervals of confidence of the mean

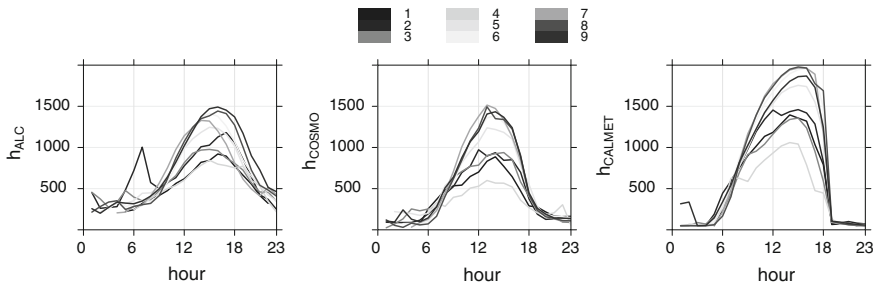

Fig. 55.3 Daily evolution of h_{ABL}, averaged for each Local Wind Pattern. *Left* ALC-derived; *center* simulated by COSMO; *right* simulated by CALMET

expected, both models associate the highest h_{ABL} with the LWPs which are more common in summer. In average, COSMO underestimates h_{ABL} only with LWP 4 (wind from NE, limited to the Adriatic coast). (Fig. 55.3)

55.4 Conclusions

Classification algorithms permit to objectively identify synoptic circulation patterns and local wind regimes in the Po Valley. Some of this regimes show a systematic link with high pollution levels, or with anomalies in the aerosol chemical composition, or with weaknesses in h_{ABL} simulations. The occurrence of specific weather types has a small but clear effect on air quality; their analysis can be a useful support in AQ assessment and management.

Acknowledgments This research was carried out in the framework of the "Supersito" project, supported by Emilia-Romagna Region and ARPA Emilia-Romagna.

References

Angelini F, Barnaba F, Landi TC, Caporaso L, Gobbi GP (2009) Study of atmospheric aerosols and mixing layer by lidar. Radiat Prot Dosimetry 137(3–4):275–279

Haeffelin M, Angelini F, Morille Y, Martucci G, Frey S, Gobbi G, Lolli S, O'dowd C, Sauvage L, Xueref-Rémy I et al (2012) Evaluation of mixing-height retrievals from automatic profiling lidars and ceilometers in view of future integrated networks in Europe. Bound-Layer Meteorol 143(1):49–75

Jiménez PA, González-Rouco JF, Montávez JP, Garca-Bustamante E, Navarro J (2009) Climatology of wind patterns in the northeast of the Iberian Peninsula. Int J Climatol 29 (4):501–525

Philipp A, Beck C, Huth R, Jacobeit J (2014) Development and comparison of circulation type classifications using the COST 733 dataset and software. Int J Climatol

Scire JS, Robe FR, Fernau ME, Yamartino RJ (2000) A user's guide for the CALMET Meteorological Model. Earth Tech, USA

Steppeler J, Doms G, Schättler U, Bitzer H-W, Gassmann A, Damrath U, Gregoric G (2003) Meso-gamma scale forecasts using the non-hydrostatic model LM. Meteorol Atmos Phys 82:75–96

Ward JH Jr (1963) Hierarchical grouping to optimize an objective function. J Am Stat Assoc 58(301):236–244

Chapter 56
Sensitivity of Ground-Level Ozone to NO_x Emission During a High Ozone Episode in SW Poland

Kinga Wałaszek, Maciej Kryza, Małgorzata Werner and Hanna Ojrzyńska

Abstract Sensitivity of ozone formation to NO_x and VOC emission is important in terms of implementing control strategies for photochemical pollutants, helping to determine the most effective way to limit O_3 concentrations and population exposure to high levels of O_3. In this study, the role of NO_x emissions on hourly O_3 concentrations is examined in order to determine whether NO_x is the driver or limiting factor of ozone formation in SW Poland in high-ozone situations. In order to assess that, four scenarios are analyzed: baseline, with no modification of the available emission inventory, a 10, 20 and 30 % decrease in anthropogenic emission of NO_x. The simulations were performed for an episode with high O_3 concentrations. Both spatial and temporal changes in ozone concentrations for all scenarios have been analyzed. Preliminary results show that reducing NO_x emission is associated with higher O_3 concentrations, however, further research is needed to assess the role of VOC.

56.1 Introduction

Tropospheric ozone, which is a secondary atmospheric pollutant formed in photolysis processes involving mainly volatile organic compounds (VOC) and nitrogen oxides (NO_x), has become one of the main reasons of poor air quality in the summer in Poland over the last few decades (Jarosławski 1993; Rozbicka and Rozbicki 2014). The formation of tropospheric ozone is controlled mainly by the concentration of its two main precursors—nitrogen oxides (NO and NO_2) and volatile

K. Wałaszek (✉) · M. Kryza · M. Werner · H. Ojrzyńska
Department of Climatology and Atmosphere Protection, University of Wroclaw, Wroclaw, Poland
e-mail: kinga.walaszek@uwr.edu.pl

M. Werner
National Pollen and Aerobiology Research Unit, University of Worcester, Worcester, UK

D.G. Steyn and N. Chaumerliac (eds.), *Air Pollution Modeling and its Application XXIV*, Springer Proceedings in Complexity,
DOI 10.1007/978-3-319-24478-5_56

organic compounds (VOC). Because of the variety of factors influencing ozone formation, including both emissions and meteorological conditions, emission abatements may not directly cause reduction in ozone concentration (Wilson et al. 2012). Depending on meteorological and chemical conditions, the regime of ozone formation and destruction is either NO_x-sensitive or VOC-sensitive (NO_x-saturated). Because of that, many studies have been devoted to the analysis of ozone concentration sensitivity to NO_x and VOC emissions, both on a regional and continental scale, mainly based on surface measurements, 1D chemistry models and 4D chemical transport models (e.g. Aksoyoglu et al. 2012; Derwent et al. 2014; Spirig et al. 2002). In this study, the WRF-Chem model is applied for the area of SW Poland to determine how sensitive ozone concentration is to NO_x emission reduction during a high ozone episode. This work will be followed by similar study regarding ozone sensitivity to VOC emissions.

56.2 Data and Methods

The analysis is made for Lower Silesian Voivodeship, which is located in SW Poland. Due to a lot of sunshine hours and high temperatures, episodes with high concentration of ground-level ozone are not uncommon, especially during late spring and summer. One of those episodes is July 3rd to August 3rd, 2006, which is a test period of this study. Maximum hourly O_3 concentrations reached 180 μg m^{-3} at 2 stations out of 9 located in the study region. The highest maxima were observed at urban and suburban measurement sites, where ozone daily cycles are driven mainly by its production in situ, and where largest population exposure to high O_3 concentrations is observed.

The model used in this study is the Weather Research and Forecasting v. 3.5 running with chemistry module (Grell et al. 2005). The simulation was initiated with the ERA–Interim meteorological data (Dee et al. 2011) and TNO MACC II emission inventory (Kuenen et al. 2014). Four simulations were performed for the study period with 2 day spin up time. All model settings remained the same for all model runs and the only variable changing was the anthropogenic emission of nitrogen oxides. The first was a base simulation with no modification of the emission inventory. For the remaining three, the emission of NO_x was reduced by 10, 20 and 30 %.

56.3 Results

The results of the simulations were analyzed spatially by averaging O_3 concentrations over time for each grid point for each simulation. Then, the differences between the map for base simulation and those with reduced NO_x emissions were calculated. In order to determine any diurnal cycles in the response of ozone concentrations to NO_x emissions, the same procedure was applied to selected hours

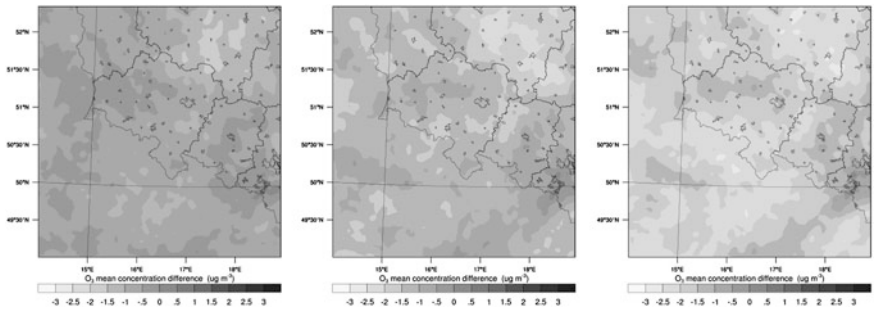

Fig. 56.1 Differences in average O_3 concentration between base simulation and NO_x reduced by 10 % (*left*), 20 % (*middle*) and 30 % (*right*)

of the day. Because maximum ozone concentration in urban areas falls on the afternoon and minimum—just before dawn, differences between simulations at 3:00 am and 3:00 pm UTC are shown. For most of the model domain the reduction of NO_x emission causes a decrease in ozone concentration, although the change is very small and does not exceed 3 μg m^{-3}. The only region where ozone levels are higher is the densely populated and industrialized area of Upper Silesia in the southeast. However, this difference disappears almost completely for the simulation with 30 % reduction of NO_x, which may be influenced by the trends in neighboring areas (Fig. 56.1).

Figure 56.2 presents ozone concentration differences averaged for 3:00 am and 3:00 pm UTC for the entire study period. The map for 3:00 am shows a general tendency of decreased O_3 for reduced NO_x emissions. However, there are some

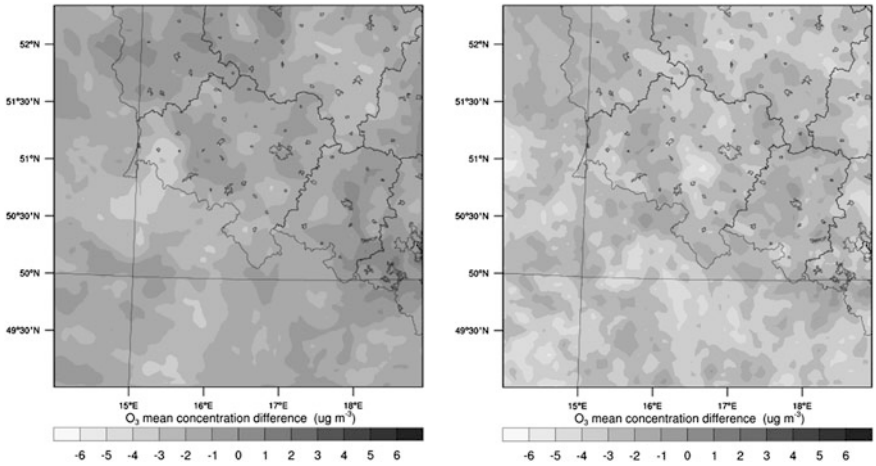

Fig. 56.2 Differences in average O_3 concentration for 3:00 am (*left*) and 3:00 pm (*right*) between base simulation and NO_x emission reduced by 30 %

areas with elevated O_3 concentrations, which include mostly highly populated areas, such as mentioned above Upper Silesian conglomeration. For the afternoon, there is no significant spatial pattern. Moreover, O_3 concentrations are lower for the whole domain, up to 5 μg m^{-3} less than the base model run.

56.4 Summary

The main findings of this work are that in Lower Silesian voivodeship, when O_3 concentrations are high, anthropogenic NO_x emissions abatements may not be sufficient to reduce it. NO_x is most likely the limiting factor for ozone formation in the region, with the exception of highly industrialized areas. The most increase is observed for afternoon hours, whereas at nighttime ozone concentrations are lower in some areas. However, the change associated with the reduction of NO_x emission by 30 % is small. For a more complete analysis, there is a need to evaluate the role of VOC emissions on O_3 concentrations as well.

Acknowledgments The study was supported by the Polish National Science Centre project no. UMO-2013/09/B/ST10/00594. The project was financed with means of the European Union under the Financial Instrument LIFE+ and co-financed by the National Found of Environmental Protection and Water Management. Calculations were carried out in the Wrocław Centre for Networking and Supercomputing (http://www.wcss.wroc.pl), Grant No. 170.

References

Aksoyoglu S, Keller J, Oderbolz DC, Barmpadimos I, Prévôt ASH, Baltensperger U (2012) Sensitivity of ozone and aerosols to precursor emissions in Europe. Int J Environ Pollut 50 (1):451–459. doi:10.1504/IJEP.2012.051215

Dee DP, Uppala SM, Simmons AJ, Berrisford P, Poli P, Kobayashi S, Vitart F et al (2011) The ERA-Interim reanalysis: configuration and performance of the data assimilation system. Q J R Meteorol Soc 137(656):553–597. doi:10.1002/qj.828

Derwent R, Beevers S, Chemel C, Cooke S, Francis X, Fraser A, Vieno M et al (2014) Analysis of UK and European NOx and VOC emission scenarios in the Defra model intercomparison exercise. Atmos Environ 94:249–257. doi:10.1016/j.atmosenv.2014.05.036

Grell G, Peckham S, Schmitz R (2005) Fully coupled "online" chemistry within the WRF model. Atmos Environ 39:6957–6975. doi:10.1016/j.atmosenv.2005.04.027

Jaroslawski J (1993) Measurements of surface ozone at Belsk, Poland, vol 2047, pp 202–206. doi:10.1117/12.163484

Kuenen JJP, Visschedijk AJH, Jozwicka M, Denier van der Gon HAC (2014) TNO-MACC_II emission inventory; a multi-year (2003–2009) consistent high-resolution European emission inventory for air quality modelling. Atmos Chem Phys 14(20):10963–10976. doi:10.5194/acp-14-10963-2014

Rozbicka K, Rozbicki T (2014) Spatiotemporal variations of tropospheric ozone concentrations in the Warsaw Agglomeration (Poland). Ann Warsaw Univ Life Sci Land Reclam 46(3):247–261

Spirig C, Neftel A, Kleinman LI, Hjorth J (2002) NOx versus VOC limitation of O_3 production in the Po valley: local and integrated view based on observations. J Geophys Res: Atmos 107 (D22):8191. doi:10.1029/2001JD000561

Wilson RC, Fleming ZL, Monks PS, Clain G, Henne S, Konovalov IB, Menut L et al (2012) Have primary emission reduction measures reduced ozone across Europe? An analysis of European rural background ozone trends 1996–2005. Atmos Chem Phys 12(1):437–454. doi:10.5194/acp-12-437-2012

Chapter 57
Using a Dynamical Approach for Implementing Ammonia Emissions into WRF-Chem Over Europe

Małgorzata Werner, Camilla Geels, Maciej Kryza and Carsten Ambelas Skjøth

Abstract This paper presents the influence of an emission approach applied (fixed and dynamical) on calculated ammonia concentration and model performance. We simulated with the WRF-Chem model a winter (January) and an early spring period (March) of 2012 for the entire Europe. Regardless of a relatively coarse resolution (36 km × 36 km) of the WRF-Chem simulations and the Europe-wide default settings applied in the dynamic ammonia model, the modelled concentrations are improved significantly by applying a dynamical emission instead of using a fixed emission profile.

57.1 Introduction

Ammonia (NH_3) is a climate dependent gas and the main alkaline component in the atmosphere (Skjøth and Geels 2013). Ammonia affects air quality, e.g. through particle formation (Xu and Penner 2012) which again affects overall climate

M. Werner (✉) · C.A. Skjøth
National Pollen and Aerobiology Research Unit, University of Worcester, Worcester, UK
e-mail: malgorzata.werner@uwr.edu.pl

C.A. Skjøth
e-mail: c.skjoth@worc.ac.uk

C. Geels
Department of Environmental Science, Aarhus University, Aarhus, Denmark
e-mail: cag@envs.au.dk

M. Werner · M. Kryza
Department of Climatology and Atmosphere Protection, University of Wrocław, Wrocław, Poland
e-mail: maciej.kryza@uwr.edu.pl

D.G. Steyn and N. Chaumerliac (eds.), *Air Pollution Modeling and its Application XXIV*, Springer Proceedings in Complexity,
DOI 10.1007/978-3-319-24478-5_57

through feedback processes. According to IPCC the integrated effect of these processes are poorly understood (IPCC 2013). The emissions are however challenging to simulate with atmospheric models due to the strong climate dependency on the emissions (Sutton et al. 2013). It is therefore difficult to obtain a spatial and temporal profile of the atmospheric ammonia concentration and the resulting effects on the environment. It is important to capture the dynamic and episodic nature of NH_3 emissions, including the influence of meteorology, air-surface exchange, and human activities (Bash et al. 2013). Danish studies have shown significant improvements in model performance by replacing static seasonal variations by a dynamic approach which is accounting for physical processes like volatilization of NH_3 (Skjøth et al. 2011). Results presented by Werner et al. (2015) suggest that implementing this dynamical approach improves simulations even in areas with limited information about location of the agricultural fields, livestock and agricultural production methods.

Here, we implemented the dynamic ammonia emission calculated with the approach developed by Skjøth et al. (2011) into the atmospheric transport model WRF-Chem and use this to study the impact on Harwell (UK) by comparing the results with measured ammonia concentrations and with a simpler approach that uses fixed emissions from the TNO MACC data set.

57.2 Data and Methods

The main tools used in the study are the WRF-Chem model version 3.5 (Grell et al. 2005) and the Europe-wide dynamic ammonia emission model (Skjøth et al. 2011). The WRF-Chem model was run for the entire Europe with a resolution of 36 km × 36 km and for the year 2012. In the first step we run the WRF-Chem simulation (called later BASIC) using the TNO MACC II emission data set with 1/8° × 1/16° spatial resolution without a temporal variation (Pouliot et al. 2012). In the second step we run the WRF-Chem model with hourly variations in ammonia emissions for the entire year 2012 (DYNAMIC) by using the same approach as for the Danish Eulerian Hemispheric Model (Geels et al. 2012), where the ammonia emission model uses gridded hourly meteorology, calculated with WRF, to simulate the emission variations. The ammonia concentrations from the two simulations were compared with 1 h measurements aggregated into daily values from a representative agricultural EMEP station, in this case Harwell in the UK and focusing on January and March as these months had near complete observational data set (Fig. 57.1 and Table 57.1).

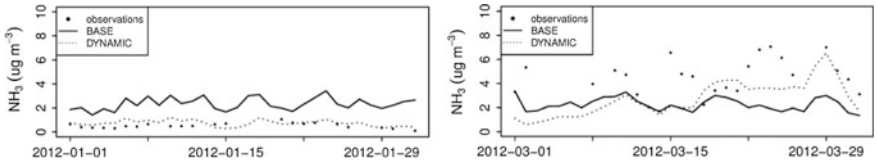

Fig. 57.1 Time series of modelled (simulation BASE and DYNAMIC) and measured ammonia concentration for Harwell for January and March 2012

Table 57.1 Model performance for the BASE and DYNAMIC simulation based on daily values[a]

Month	Simulation	FAC2	MB	NMB	RMSE
January	BASE	0.05	1.69	3.27	1.76
	DYNAMIC	0.68	0.20	0.38	0.36
March	BASE	0.46	−2.20	−0.49	2.74
	DYNAMIC	0.71	−1.53	−0.34	2.22

[a]*FAC2* Factor of two, *MB* Mean bias, *MNB* Mean normalised bias, *RMSE* Root mean square error

57.3 Results

Mean ammonia concentration measured at Harwell station in January 2012 is 0.52 μg m^{-3}. Corresponding value based on the WRF-Chem calculations is equal to 2.29 and 0.71 μg m^{-3} for the BASE and DYNAMIC simulation, respectively. The BASE simulation overestimates measured concentrations for the entire analyzed period. Application of the dynamical ammonia emission in WRF-Chem improves model performance. All statistical parameters improve substantially, e.g. MB decreases about a factor of nine and RMSE about a factor of five (Table 57.1). Mean ammonia concentration measured at the station in March 2012 is 4.50 μg m^{-3}. Both corresponding values based on WRF-Chem calculations are lower and equal to 2.29 and 2.77 for the BASE and DYNAMIC simulation, respectively. For March, model performance is also better for the DYNAMIC simulations in comparison to BASE and with similar NMB to January.

Maps of daily mean NH_3 concentrations for two selected days of the study period (22 January and 22 March) are presented in Fig. 57.2. For January, there is a large difference in spatial distribution of ammonia concentration between the simulations and for most of the land area, concentrations from the BASE simulation are more than 60 % higher than from DYNAMIC. For March, the DYNAMIC simulation provides higher concentrations for several regions in Europe, e.g. most parts of the UK, Poland, Spain or Italy but simultaneously there are some regions with higher values (by about 30–40 %) provided by BASE (e.g. part of Germany, France and Scandinavia).

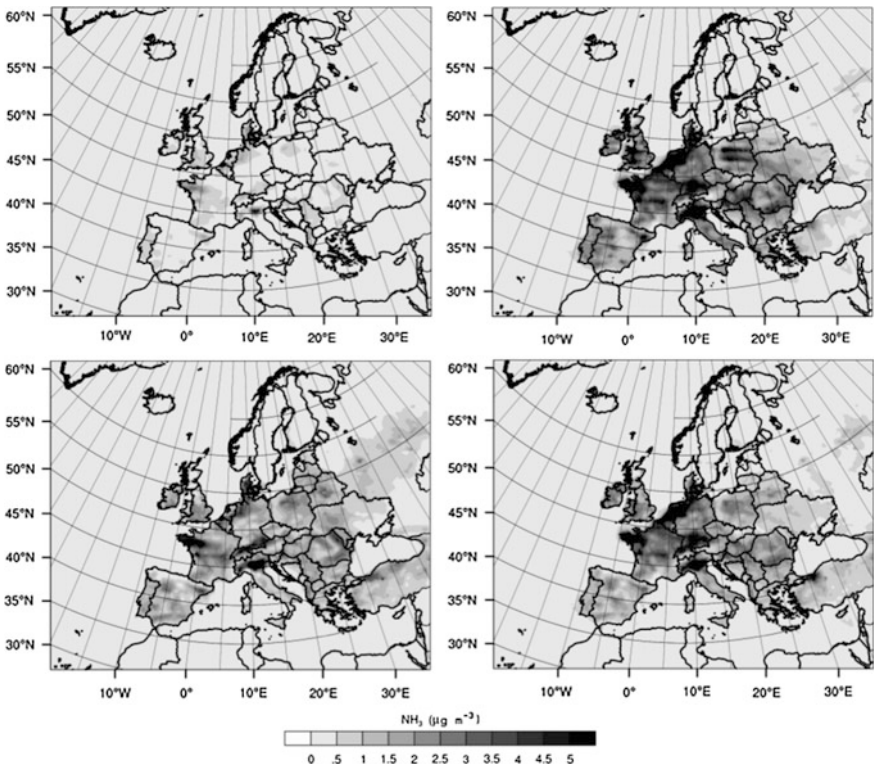

Fig. 57.2 Spatial distribution of simulated mean daily NH_3 concentrations for January 22 (*left*) and March 22 (*right*) for the dynamic (*top*) and static approach (*bottom*)

57.4 Summary and Conclusion

This paper presents the influence of temporal resolution of emission on calculated ammonia concentration and model performance. We simulated with WRF-Chem a winter (January) and an early spring period (March) of 2012 for the entire Europe. The main results are summarized below:

- Regardless of the relatively coarse resolution (36 km × 36 km) of the WRF-Chem simulations and the Europe-wide default settings applied in the dynamic ammonia model (Skjøth et al. 2011), the model results are improved by applying a dynamical emission instead of using a fixed emission profile. This suggests that for regional modelling of NH_3 in Europe it will be an advantage to move from a static to a dynamic approach, even if limited information is available in the target region.
- The dynamical emission approach works well with the TNO MACC emission, which is the default emission data set for many European air quality models. The approach can be implemented in on-line models as WRF-Chem, off-line

Gaussian models and trajectory models (e.g. Skjoth et al. 2011, and reference therein). The method takes into account both changes in overall climatic conditions from year to year (e.g. Skjøth and Geels 2013) and differences within a country. As such the emission method is therefore more advanced than both a fixed profile and a fixed monthly profile for individual countries and can be used over large areas that have no established monthly profile. This suggests flexibility, which coupled with open-source code, can be a suitable method for improving the emission of ammonia in many different models over large geographical areas.

Acknowledgments We are grateful to the ECLAIRE project for providing access to the TNO MACC emission data set. This study addresses some of the objectives in the ECLAIRE project, in particular the further development of a dynamical ammonia emission model for use in regional scale Chemistry Transport Models. Preparation of the emissions data to the WRF-Chem model were supported by the Polish National Science Centre project no. UMO-2013/09/B/ST10/00594.

References

Bash JO, Cooter EJ, Dennis RL, Walker JT, Pleim JE (2013) Evaluation of a regional air-quality model with bidirectional NH_3 exchange coupled to an agroecosystem model. Biogeosciences 10:1635–1645. doi:10.5194/bg-10-1635-2013

Geels C, Andersen HV, Ambelas Skjøth C, Christensen JH, Ellermann T, Løfstrøm P, Gyldenkærne S, Brandt J, Hansen KM, Frohn LM, Hertel O (2012) Improved modelling of atmospheric ammonia over Denmark using the coupled modelling system DAMOS. Biogeosciences 9:2625–2647. doi:10.5194/bg-9-2625-2012

Grell G, Peckham SE, Schmitz R, McKeen SA, Frost G, Skamarock WC, Eder B (2005) Fully coupled "online" chemistry within the WRF model. Atmos Environ 39:6957–6975. doi:10.1016/j.atmosenv.2005.04.027

IPCC (2013) Climate change 2013: the physical science basis. In: Stocker TF, Qin D, Plattner G-K, Tignor M, Allen SK, Boschung J, Nauels A, Xia Y, Bex V, Midgley PM (eds) Contribution of working group I to the fifth report of the intergovernmental panel on climate, 1535 pp

Pouliot G, Pierce T, Denier van der Gon H, Schaap M, Moran M, Nopmongcol U (2012) Comparing emission inventories and model-ready emission datasets between Europe and North America for the AQMEII project. Atmos Environ 53:4–14. doi:10.1016/j.atmosenv.2011.12.041

Skjøth CA, Geels C (2013) The effect of climate and climate change on ammonia emissions in Europe. Atmos Chem Phys 13:117–128. doi:10.5194/acp-13-117-2013

Skjøth CA, Geels C, Berge H, Gyldenkærne S, Fagerli H, Ellermann T, Frohn LM, Christensen J, Hansen KM, Hansen K, Hertel O (2011) Spatial and temporal variations in ammonia emissions—a freely accessible model code for Europe. Atmos Chem Phys 11:5221–5236. doi:10.5194/acp-11-5221-2011

Sutton MA, Reis S, Riddick SN, Dragosits U, Nemitz E, Theobald MR, Tang YS, Braban CF, Vieno M, Dore AJ, Mitchell RF, Wanless S, Daunt F, Fowler D, Blackall TD, Milford C, Flechard CR, Loubet B, Massad R, Cellier P, Personne E, Coheur PF, Clarisse L, Van Damme M, Ngadi Y, Clerbaux C, Skjøth CA, Geels C, Hertel O, Wichink Kruit RJ, Pinder RW, Bash JO, Walker JT, Simpson D, Horváth L, Misselbrook TH, Bleeker A,

Dentener F, de Vries W (2013) Towards a climate-dependent paradigm of ammonia emission and deposition. Philos Trans R Soc Lond B Biol Sci 368:20130166. doi:10.1098/rstb.2013.0166

Werner M, Skjøth CA, Kryza M, Dore AJ (2015) Understanding emissions of ammonia from buildings and application of fertilizers: an example from Poland. Biogeosciences Discuss 12:2021–2061. doi:10.5194/bgd-12-2021-2015

Xu L, Penner JE (2012) Global simulations of nitrate and ammonium aerosols and their radiative effects. Atmos Chem Phys 12:9479–9504. doi:10.5194/acp-12-9479-2012

Chapter 58
Application of the WRF-Chem Model for Air Pollution Forecasting in Poland

Małgorzata Werner, Maciej Kryza, Carsten Ambelas Skjøth, Hanna Ojrzyńska, Kinga Wałaszek and Anthony J. Dore

Abstract This paper presents the first step in the development of a forecasting system for air pollution concentrations for the south-west region of Poland. We simulated a winter (January) and a summer (July) period of 2014 with WRF-Chem. The focus has been on studying different chemical options during the two simulation periods, therefore keeping emissions constant, except for natural sources. The authors have found that different model setups increase model performance for gases and particulate matter and that there is no clear dependence between forecast lead time and model performance.

M. Werner (✉) · C.A. Skjøth
National Pollen and Aerobiology Research Unit, University of Worcester, Worcester, UK
e-mail: malgorzata.werner@uwr.edu.pl

C.A. Skjøth
e-mail: c.skjoth@worc.ac.uk

M. Werner · M. Kryza · H. Ojrzyńska · K. Wałaszek (✉)
Department of Climatology and Atmosphere Protection, University of Wrocław, Wrocław, Poland
e-mail: kinga.walaszek@uwr.edu.pl

M. Kryza
e-mail: maciej.kryza@uwr.edu.pl

H. Ojrzyńska
e-mail: hanna.ojrzynska@uwr.edu.pl

A.J. Dore
Centre for Ecology and Hydrology, Edinburgh, UK
e-mail: todo@ceh.ac.uk

D.G. Steyn and N. Chaumerliac (eds.), *Air Pollution Modeling and its Application XXIV*, Springer Proceedings in Complexity,
DOI 10.1007/978-3-319-24478-5_58

58.1 Introduction

Air pollution can have an adverse impact on human health (Kampa and Castanas 2008), on the ecosystem (Bell et al. 2011; Lovett et al. 2009) and on climate (Forkel et al. 2012). The adverse impact on human health depends largely on the chemical composition of pollution. The health damaging components include traditional pollution such as CO, NO_2, O_3, PM (both 2.5 and 10 μm fractions) and SO_2 but also organic compounds with toxic properties or heavy metals.

In Poland, high concentrations of PM and SO_2 appear especially during the winter season caused by a high coal consumption used for residential heating and meteorological conditions preventing mixing and dilution of air pollutants (Werner et al. 2015). In contrast high O_3 concentrations appear during the summer season often caused by a long range transport. The areas that are affected in Poland are also determined by the relief of the landscape (e.g. valleys with strong inversions during winters) and land use (e.g. urban areas). Spatial and explicit mapping of air pollution is therefore highly useful for Poland.

There are no high spatial and temporal resolution air quality forecasts for south-west Poland, an area known to have harmful concentrations of air pollution (Krynicka and Drzeniecka-Osiadacz 2013; Werner et al. 2015). This paper focuses on comparison of forecasted concentrations for: (1) two different chemical approaches available in WRF-Chem, (2) two leads time (3) two seasons and against measurements.

58.2 Data and Methods

WRF-Chem version 3.5 (Grell et al. 2005) is used with one-way nested domains (36, 12 and 4 km), where the highest resolution is used for forecasting over south-west Poland with a 48 h lead time. Details of the model configuration are provided by Werner et al. (2015). Emissions are the TNO MACC II data set with 1/8° × 1/16° spatial resolution (Pouliot et al. 2012). Temporal variations in emissions are restricted to emissions from nature (sea salt aerosol emission, wind blown dust and biogenic emission), while the TNO MACC II emissions are assumed constant during the entire simulation. The first 48-h forecast uses a 2-week spin-up, with the model simulations initialized with the GFS meteorology for initial and boundary conditions. Thereafter, the model uses chemistry cycling, and the WRF-Chem simulation from the last hour on the previous day is used to initialize the next day's forecast. Two sets of simulations were run for each forecast cycle: (1) simulations with simplified wet deposition processes and no aqueous reactions (Chem_2) and (2) simulations which include aqueous reactions (Chem_41, Table 58.1). Simulations were carried out for January (winter) and July (summer) 2014 and the

Table 58.1 Model configuration used in WRF-Chem simulations[a]

Category	Model setup
Grid scale wet deposition	Chem_2 (Simple), Chem_41 (Easter04)
Conv. wet dep	Chem_2 (Yes), Chem_41 (Yes)
Grid scale aq. chem	Chem_2 (No), Chem_41 (WT86)
Conv. aq. chem	Chem_2 (WT86), Chem_41 (WT86)
Chem_opt	Chem_2 (2), Chem_41 (41)

[a]Please refer to the WRF and the WRF-Chem user's guides for a complete description of the options

results from both sets of simulations were compared with measured 1-h air concentration of SO_2, NO_2, O_3 and PM_{10} for both periods. Observations were gathered by the Voivodeship Inspectorate of Environmental Protection in the Lower Silesia region in SW Poland with the following numbers of sites: SO_2 (6 sites), NO_2 (6 sites), O_3 (4 sites) and PM_{10} (1 site). All 1 h observations were available as integers for the simulation period and did not include information about water content in PM10 measurements. This means that the model output of PM_{10} concentration (dry mass) is compared with observed PM10 (total mass). The model performance was summarized with the following statistics: Factor of Two (FAC2), Mean Bias (MB), Normalized Mean Bias (NMB) and Normalized Mean Gross Error (NMGE) and compared using the Taylor diagrams.

58.3 Results

Mean modelled concentration (simulation Chem_2) of SO_2, NO_2, O_3, and PM_{10} for the study domain is 2.8, 16.7, 40.4 and 25.2 μg m^{-3} during winter and 2.5, 11.7, 70.5 and 18.0 μg m^{-3} during summer period, respectively. The highest concentrations of primary gases are related to emission sources—e.g. urban areas, point sources (e.g. copper works), communication tracks. Increased PM10 concentrations appear in larger distances to emission sources, often several tens of kilometers from the origin. An inverse concentration distribution in comparison to primary pollutants is observed for ozone, which is mainly due to the Leighton relation between NO, NO_x and O_3. Therefore the highest concentrations are observed in the mountainous area (Sudety Mountains).

There are no clear dependencies between lead time and the model performance for the investigated chemical compounds. For PM_{10} and O_3 a slightly better performance is obtained for 48 h lead time compared to 24 h. With respect to the model configuration, option 41 (includes aqueous reactions), provides better model performance for gasses than option 2 (without aqueous reactions)—the better

Table 58.2 Model performance for 24 and 48 h lead time, separately for two chemical options (Chem_2 and Chem_41) and months (January and July 2014)

			FAC2		MB		NMB		NMGE	
	Season and compound	N	24 h	48 h	24 h	48 h	24 h	48 h	24 h	48 h
Chem_2	July SO_2	4170	0.39	0.36	−0.12	−0.43	−0.04	−0.15	0.95	0.92
	January SO_2	3782	0.14	0.14	−9.82	−9.94	−0.75	−0.75	0.77	0.78
	July NO_2	5090	0.48	0.46	−2.27	−2.25	−0.13	−0.12	0.74	0.74
	January NO_2	4016	0.68	0.68	−5.77	−5.92	−0.21	−0.21	0.48	0.47
	July O_3	2969	0.76	0.76	9.49	8.82	0.15	0.14	0.39	0.39
	January O_3	2795	0.55	0.57	15.28	14.30	0.63	0.58	0.76	0.70
	July PM_{10}	696	0.43	0.48	−14.31	−13.00	−0.42	−0.37	0.65	0.59
	January PM_{10}	647	0.53	0.55	−21.43	−22.07	−0.44	−0.45	0.56	0.56
Chem_41	July SO_2	4170	0.40	0.37	−0.20	−0.41	−0.07	−0.14	0.93	0.90
	January SO_2	3782	0.20	0.21	−8.81	−8.91	−0.67	−0.68	0.71	0.71
	July NO_2	5090	0.47	0.45	−2.46	−2.55	−0.14	−0.14	0.74	0.76
	January NO_2	4016	0.68	0.69	−5.13	−5.26	−0.18	−0.19	0.48	0.48
	July O_3	2969	0.78	0.77	3.30	5.11	0.05	0.08	0.39	0.38
	January O_3	2795	0.59	0.60	11.20	11.04	0.46	0.44	0.65	0.61
	July PM_{10}	696	0.25	0.37	−23.94	−20.82	−0.70	−0.60	0.71	0.65
	January PM_{10}	647	0.15	0.17	−37.05	−36.31	−0.77	−0.75	0.80	0.78

N number of observations

performance was obtained for SO_2 and O_3 for both periods and also for most NO_2 statistics during winter. Simultaneously, model performance for PM_{10} decreased significantly for Chem_41 simulation. Irrespective of the chemical option used, the model tends to underestimate measured concentrations of SO_2, NO_2 and PM_{10} for both months (January and July) and winter underestimation is higher than summer. For O_3, modelled concentrations are higher than measured, with larger overestimations during winter (Table 58.2).

The correlation coefficient between model and measurements of SO_2 and NO_2 is below 0.5 for both seasons, with a slightly better performance during winter for SO_2 and summer for NO_2. In case of ozone the modelled results are better correlated with observations during July (Fig. 58.1) than January. For both seasons the standard deviation of modelled O_3 concentrations are about two times lower than measured.

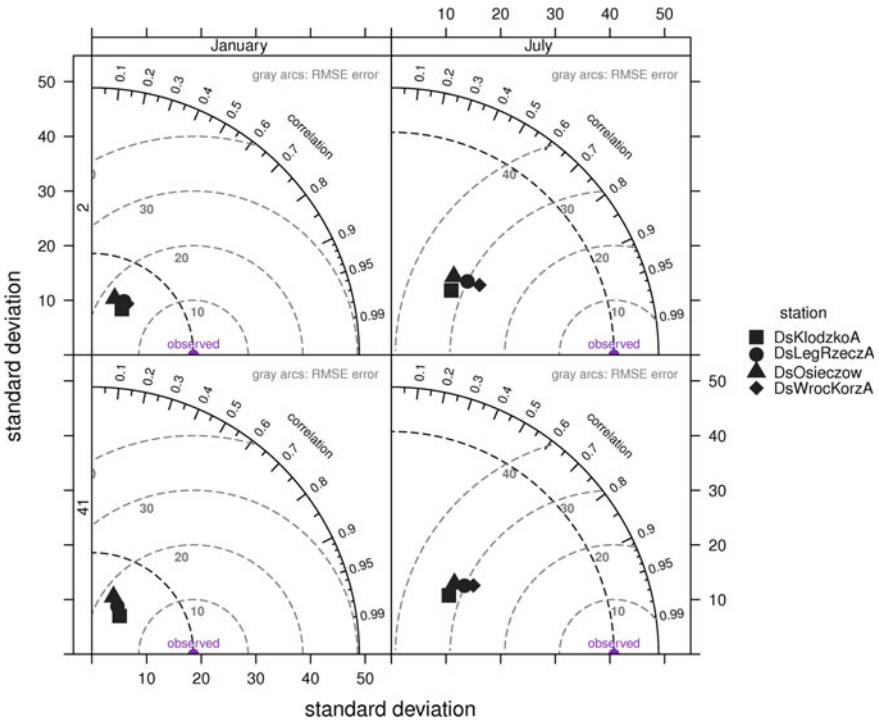

Fig. 58.1 Taylor diagrams of ozone concentration for Chem_2 (*upper row*) and Chem_41 (*lower row*) and two seasons: January (*left*) and July (*right*)

58.4 Summary and Conclusion

This paper presents the first step in the development of a forecasting system for air pollution concentrations for the south-west region of Poland. We simulated a winter (January) and a summer (July) period of 2014 with WRF-Chem. The focus has been on studying different chemical options (Chem_2 and Chem_41) during two simulation periods (winter and summer), therefore keeping emissions constant, except for natural sources. The main results are summarized below:

- The more advanced chemical option which includes aqueous reactions provides better results for primary gases and worse results for particulate matter. The latter confirms the results obtained with WRF-Chem by Saide et al. (2012). In that study the authors suggest that observed aerosol mass and number are usually closer to WRF-Chem simulations when wet deposition removal is excluded. It should here be noted, that the comparisons of PM_{10} is based on dry mass from WRF-Chem and total mass from the observations, where the latter has no information about water content as suggested by Werner et al. (2014).

- The simulated concentrations of SO_2, NO_2 and PM_{10} are always underestimated, with the largest underestimations during winter. This underestimation is most likely related to a simplified approach in the emission (no temporal variation for the study period). It should here be noted that 1 h observations have limited numerical accuracy, which inevitably will cause a decreased correlation and differences in the value of standard deviations between modelled and measured data.
- There is no clear dependence between forecast lead time and model performance. This means that forecasts 48 h ahead are sensible, if the model is able to capture the overall variability throughout the area.

Acknowledgments The study was supported by the Polish National Science Centre project no. UMO-2013/09/B/ST10/00594 and the LIFE+, project LIFE12 ENV/PL/000056. The authors acknowledge the Voivodeship Inspectorate of Environmental Protection in Wrocław for providing observations of air pollution concentrations.

References

Bell JNB, Power SA, Jarraud N, Agrawal M, Davies C (2011) The effects of air pollution on urban ecosystems and agriculture. Int J Sustain Dev World Ecol 18:226–235. doi:10.1080/13504509.2011.570803

Forkel R, Werhahn J, Hansen AB, McKeen S, Peckham S, Grell G, Suppan P (2012) Effect of aerosol-radiation feedback on regional air quality—a case study with WRF/Chem. Atmos Environ 53:202–211. doi:10.1016/j.atmosenv.2011.10.009

Grell G, Peckham SE, Schmitz R, McKeen S, Frost G, Skamarock WC, Eder B (2005) Fully coupled "online" chemistry within the WRF model. Atmos Environ 39:6957–6975. doi:10.1016/j.atmosenv.2005.04.027

Kampa M, Castanas E (2008) Human health effects of air pollution. Environ Pollut 151:362–367. doi:10.1016/j.envpol.2007.06.012

Krynicka J, Drzeniecka-Osiadacz A (2013) Analysis of variability in PM10 concentration in the Wroclaw agglomeration. Polish J Environ Stud 4:22

Lovett GM, Tear TH, Evers DC, Findlay SEG, Cosby BJ, Dunscomb JK, Driscoll CT, Weathers KC (2009) Effects of air pollution on ecosystems and biological diversity in the eastern United States. Ann N Y Acad Sci 1162:99–135. doi:10.1111/j.1749-6632.2009.04153.x

Pouliot G, Pierce T, Denier van der Gon H, Schaap M, Moran M, Nopmongcol U (2012) Comparing emission inventories and model-ready emission datasets between Europe and North America for the AQMEII project. Atmos Environ 53:4–14. doi:10.1016/j.atmosenv.2011.12.041

Saide PE, Spak SN, Carmichael GR, Mena-Carrasco M, Yang Q, Howell S, Leon DC, Snider JR, Bandy R, Collett JL, Benedict KB, de Szoeke SP, Hawkins LN, Allen G, Crawford I, Crosier J, Springston SR (2012) Evaluating WRF-Chem aerosol indirect effects in Southeast Pacific marine stratocumulus during VOCALS-REx. Atmos Chem Phys 12:3045–3064. doi:10.5194/acp-12-3045-2012

Werner M, Kryza M, Dore AJ (2014) Differences in the spatial distribution and chemical composition of PM10 between the UK and Poland. Environ Model Assess 19:179–192. doi:10.1007/s10666-013-9384-0

Werner M, Kryza M, Ojrzyńska H, Skjøth CA, Wałaszek K, Dore AJ (2015) Application of WRF-Chem to forecasting PM10 concentration over Poland. Int. J. Environ Pollut (In review)

Chapter 59
The LAPMOD_SA Modelling System for Source Attribution

Giovanni Bonafè, Roberto Bellasio and Roberto Bianconi

Abstract A source attribution tool, based on a Lagrangian dispersion model, is proposed for an intermediate scale, when turbulent, small-scale and also synoptic phenomena are relevant for the fate of the emitted pollutant. The tool is applied to better understand the causes of a peak of fine particulate, rich in ammonium nitrate, observed in the Po Valley.

59.1 Introduction

To analyze air quality data and to better understand the causes of events of pollution, source attribution tools are needed. While backtrajectories are suitable to analyze long-range transport with negligible contribution of small-scale and turbulent phenomena, "pollution roses" are often useful when the distance between sources and receptor is small (less than some km).

In this work a source attribution tool is proposed and tested for an intermediate scale, when turbulent, small-scale and also synoptic phenomena are relevant for the fate of the emitted pollutant.

59.2 The Modelling System

LAPMOD_SA is a modelling system for source attribution, allowing to assess the origin of air masses at a given location. LAPMOD_SA is based on the LAPMOD Lagrangian particle model (Bellasio and Bianconi 2012) and thus it can be applied up to several hundreds of kilometers of distance between sources and receptors.

G. Bonafè (✉)
Arpa Emilia-Romagna, Bologna, Italy
e-mail: gbonafe@arpa.emr.it

R. Bellasio · R. Bianconi
Enviroware Srl, Concorezzo, Italy

D.G. Steyn and N. Chaumerliac (eds.), *Air Pollution Modeling and its Application XXIV*, Springer Proceedings in Complexity,
DOI 10.1007/978-3-319-24478-5_59

Lagrangian particle models simulate the dispersion of a pollutant in the atmosphere through a number of computational particles, each representing a fraction of the emitted mass. These models are particularly useful in presence of non-homogeneous meteorological fields, as in presence of complex terrain, coastal areas and large domains, as well as under stagnation and recirculation conditions. LAPMOD is coupled with the meteorological preprocessor CALMET (Scire et al. 2000), initialized with COSMO-I7 meteorological model (Steppeler et al. 2003) and using additional observations provided by the local network.

LAPMOD_SA is a tool for identifying the origin of a polluted air mass arriving at a single receptor. The basic idea of LAPMOD_SA is to perform a set of simulations and to determine the concentration due to each of them at a specific location. The analysis of the results allows to individuate in probabilistic terms the possible position and the release time interval of the sources with major contributions at the receptor.

LAPMOD_SA performs three basic operations[1]:

1. Starting from a series of KML files produced by the user, identifying the possible areas containing the sources, it creates the source file for LAPMOD, distributing the sources over a regular grid with specific resolution.
2. Using the automatically generated source file and a specified CALMET output file, launches a LAPMOD simulation.
3. Analyzes the simulated concentrations due to the different sources at the receptor of interest and create a KML file with source contributions.[2] During this step a new refined source file may also be created by discarding sources below a specific threshold and thickening the remaining ones.

59.3 Case Study

LAPMOD_SA was applied to investigate the origin of the air masses during a heavy episode of PM10 pollution in the Po Valley, Italy. In particular, a sudden peak of fine particulate matter, rich in ammonium nitrate, was observed in Bologna February 16 2012 (Fig. 59.1). Already in the afternoon of February 15, when "Föhn" wind flowed across the plain from the Alps through Lombardy, reaching Bologna and the southern part of the plain, the concentration of fine particles begin to increase (Fig. 59.2).

While NO_x emissions are ubiquitous in the Po Valley, due to the urban sprawl and the dense road network of that region, the emissions of ammonia are mainly

[1]the tool has been developed in Perl language, therefore it can be used on any operating system.
[2]contributions may be determined considering the average or maximum concentration over the simulation period, or using the concentration value at a specific output time.

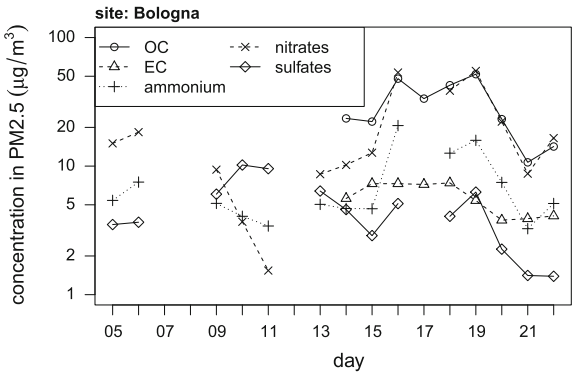

Fig. 59.1 Ionic and carbonaceous components of the PM2.5 measured in a background site in Bologna. On February 16 a sudden increase of the concentrations of ammonium and nitrates was observed

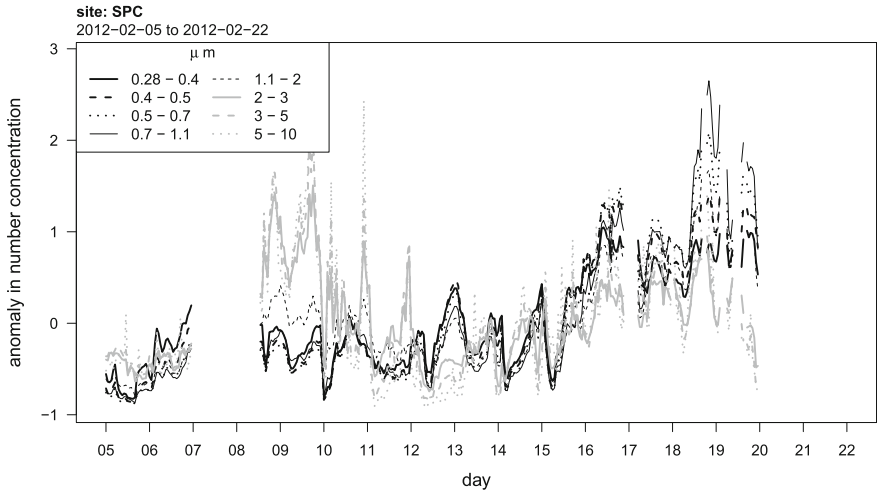

Fig. 59.2 Number of particles counted in a rural background site near Bologna. During the afternoon of February 15 the concentration of fine particles begins to increase

(about 97 %, according to the emission inventories) attributable to livestocks and fertilization, with peaks during manure spreading. In February 2012 manure spreading was not allowed in the southern part of the Po Valley, covered by snow. Therefore, the "candidate" emission area, where ammonia observed in Bologna was likely to come from (delimited by dashed line in Fig. 59.3), was defined as the region, not covered by snow, with annual average emission larger than 4 Mg/km^2.

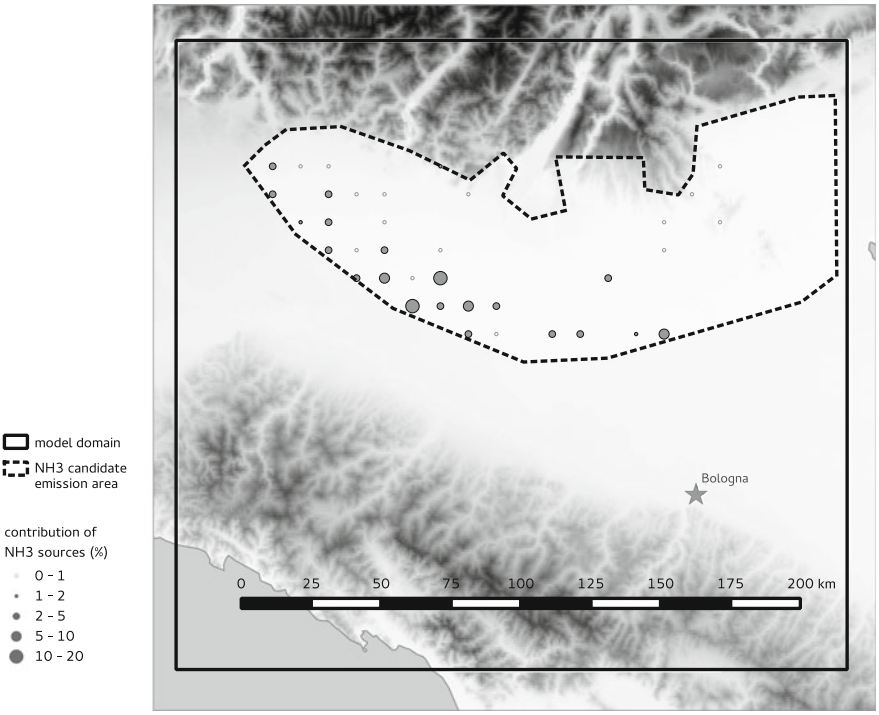

Fig. 59.3 Results of the application of LAPMOD_SA on the episode. The size of the *grey circles* represents the probability of each cell to contribute to the impact on the receptor point located in Bologna

A constant emission rate is assigned to each 5 km cell included in the "candidate" emission area, after February 15, the first day of year 2012 when manure spreading was permitted.

59.4 Results

For each cell of the "candidate" emission area, LAPMOD_SA assessed the probability to contribute to the impact on the receptor point, located in Bologna, during the period when the peak was observed (15 Feb 14:00–16 Feb 23:59 UTC).

The model identified as probable origin of ammonia a flat rural area in Lombardy (Fig. 59.3).

Acknowledgments Part of this research was carried out in the framework of the "Supersito" Project, which was supported and financed by Emilia-Romagna Region and Regional Agency for Prevention and Environment.

References

Bellasio R, Bianconi R (2012) Il sistema modellistico LAPMOD per la simulazione dell'inquinamento atmosferico in orografia complessa. Ingegneria Ambientale 61(6):492–500

Scire JS, Robe FR, Fernau ME, Yamartino RJ (2000) A user's guide for the CALMET Meteorological Model. Earth Tech, USA

Steppeler J, Doms G, Schättler U, Bitzer H-W, Gassmann A, Damrath U, Gregoric G (2003) Meso-gamma scale forecasts using the non-hydrostatic model LM. Meteorol Atmos Phys 82:75–96

Part VI
Local and Urban Scale Modelling

Chapter 60
Near-Field Pollutants Dispersion in a Stratified Surface Layer: Comparison of Numerical Study and Field Measurements of SIRTA

Xiao Wei, Eric Dupont, Bertrand Carissimo, Eric Gilbert and Luc Musson-Genon

Abstract In order to study pollutants dispersion in a stable atmospheric boundary layer, an experimental program consisting in measuring turbulence fluctuations and pollutants dispersion in a stratified surface layer and in near field is being conducted on the site 'SIRTA' in the southern suburb of Paris. Turbulence is characterized to be strongly anisotropic in a stable surface layer. Forest to the north of experiment field induces a strong wind directional shear between 3 m and 30 m levels and a wind speed decrease. Numerical simulation in RANS mode with k-ε turbulence closure and a canopy model enables to reproduce the observed wind channeling effect of forest on the mean flow and turbulence kinetic energy. A preliminary simulation taking into account the real pollutants flow rate has been performed and compared with measurements.

60.1 Introduction

Pollutants dispersion in a stable atmospheric boundary layer and in complex environment is still a phenomenon that is relatively poorly described by modeling and difficult to reproduce in a wind tunnel. Nevertheless, this topic is of major interest in the field of air pollution from human activities, as stable conditions induce large fluctuations of pollutants concentrations with possible occurrence of very high values. An experimental program consisting in measuring pollutants dispersion in a stratified surface layer and in near-field (less than 200 m) is carried out on the site SIRTA (Instrumental Site Research by Atmospheric Remote Sensing), about 20 km south of Paris. The aim of this experimental program is to

X. Wei (✉) · E. Dupont · B. Carissimo · E. Gilbert · L. Musson-Genon
Research and Teaching Center in Atmospheric Environment (CEREA),
EDF R&D, 6 Quai Watier, Chatou, France
e-mail: xiao.wei@edf.fr

D.G. Steyn and N. Chaumerliac (eds.), *Air Pollution Modeling and its Application XXIV*, Springer Proceedings in Complexity,
DOI 10.1007/978-3-319-24478-5_60

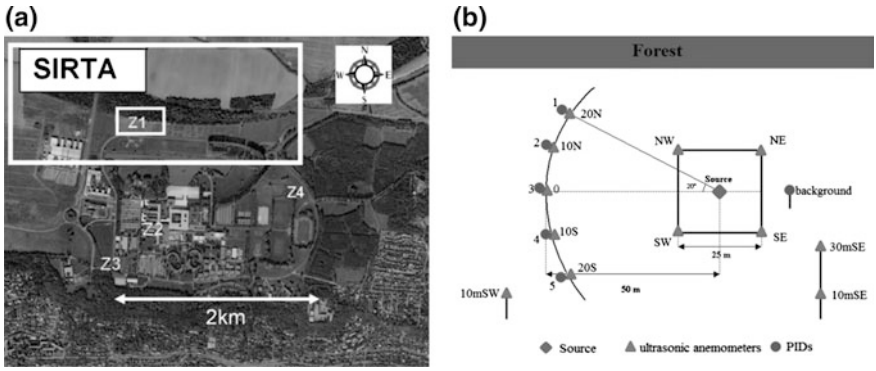

Fig. 60.1 **a** Whole measurement area in the SIRTA field (big *rectangular*: modelling area; *small rectangular*: instrumental area) and **b** sensors positions in Zone 1

characterize the fine structure of turbulence and associated dispersion through high temporal and spatial resolution collocated measurements in a real site, and to find expected relationships between concentration fluctuations and passage of turbulence structure particularly in a stable atmospheric boundary layer.

Figure 60.1a shows the different measurement areas of the SIRTA site. Our campaign is carried out in Zone 1, which is limited in the north by a forest and in the south by a road. Figure 60.1b shows position of sensors used for this experiment. We have 12 ultrasonic anemometers measuring wind components (*u, v, w* in meteorological reference) and sound velocity (from which is derived the "sonic" air temperature *T*) at 10 Hz, and 6 photo-ionization detectors (PIDs) measuring tracer gas (propylene) concentration at 50 Hz. Turbulence is measured at three levels (3, 10 and 30 m height) with an intensive network at 3 m, and concentration is measured only at height of 3 m. Turbulence measurements have been recorded continuously for more than 2 years (since April 2012), while concentration measurements have been performed only during short (about 1 h) gas releases for specific meteorological conditions (tracer tests). Main characteristics of the program, meteorological conditions during tracer tests, devices information and sensors positions have been all described in details in Wei et al. (2014a).

Intensive observation periods (IOPs) with gas releases have been performed since March 2012, an IOP on 5 June 2013 (from 18:48 to 20:17) has been chosen to present the results because of better quality in PIDs measurements.

60.2 Data Analysis

For sonic data processing and analysis, procedures are explained in Wei et al. (2014a). Statistical analysis for 2 years of continuous measurements of turbulence fluctuations and for the IOP on 5 June 2013 is presented in Wei et al. (2014b).

Concentration data processing and statistical analysis for the same IOP are described in Wei et al. (2014c).

Analyses of 2 years of data show that the forest to the north of experiment field induces a strong wind directional shear and a wind speed deceleration below the forest height. During the IOP on 5 June 2013, wind is slightly southeast with velocity around 1.5 m/s at height of 3 m. Positives values of L_{MO} indicate a stable surface layer. Turbulence strong anisotropy is quantified by different orders of magnitude between variances of the 3 wind components (σ_a^2, σ_b^2, σ_w^2) and integral length scales (L_{aa}, L_{bb}, L_{ww}), where a and b represent streamwise and crosswind components of velocity. Wind direction and velocity have always a lag between measurements from anemometers in the north and in the south due to the perturbation from the forest to the north of Zone 1. During this IOP, the PIDs worked correctly except PID 4 which could not detect gas concentration. We observe that PIDs 1, 2, and 3 detected most of the concentration peaks, and mean concentrations C are found to have higher values for PID located in the north, which are consistent with the south-easterly wind measured at height of 3 m.

60.3 Numerical Simulations

Numerical simulations are performed by using an open source CDF code Code_Saturne co-developed by CEREA and Electricity de France (EDF). An area of dimension 1600 m × 700 m × 200 m in Zone 1 has been chosen for modelling (see modelling area in Fig. 60.1a) with a progressive three-dimensional mesh refined in the instrumental area and near the ground. Numerical procedures are described in Wei et al. (2014c). Simulations are made in RANS mode with standard k-ε turbulence model. Stable thermal stratification and tracer gas release flow rate during the IOP on 5 June are taken into consideration. A drag porosity model introduced in Zaïdi et al. (2013) has been applied to model the forest area. Pollutants dispersion has been modelled by a transport equation model described in Milliez and Carissimo (2008).

We found that Code_Saturne is able to reproduce correctly the mean flow and turbulence on measurements site. Simulation results show that the forest changes wind direction and slows down wind velocity below its height, and generates higher TKE above it. Simulations also show a divergent flow in the instrumented area and reproduce the difference on wind direction and velocity and TKE as shown in measurements of anemometers in the north and in the south. Overall they are in good agreement with measurements but underestimate wind velocity and the wind rotation below the forest height for this IOP. As for the dispersion, Fig. 60.2a shows an example of simulated mean concentration C with the leaf area density $\alpha = 0.9$. Figure 60.2b compares means concentration between measurements and simulations for $\alpha = 0.9$ and 2. Mean concentrations are in the same order of magnitude between simulations and measurements. The peak values of C in simulations appears to be more south than measurements, which can be explained by the

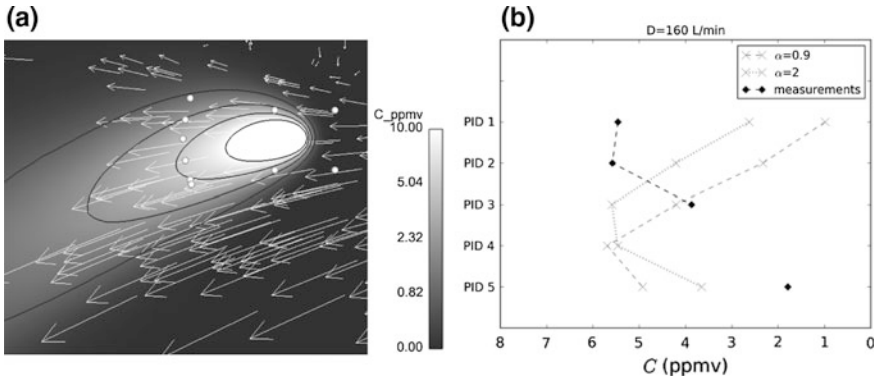

Fig. 60.2 Simulation results for the IOP on 5 June 2013 at 3 m height: **a** mean concentration for α = 0.9 (*white fleches* represent horizontal mean wind velocity), **b** comparison of mean concentration between measurements and simulations with α = 0.9 (*dashed line*) and 2 (*dotted line*)

underestimation of the wind rotation at height of 3 m by simulations. With increasing the leaf area density α in the simulation, the wind turns more to the north inside the instrumented area, and the agreement is better with the measured concentrations. Simulations overestimate the concentration fluctuations σ_C with the dissipation model described in Milliez and Carissimo (2008).

60.4 Conclusion

Simulations have been run for zone 1 domain with a canopy model and standard k-ε closure in stable condition for the IOP on 5 June 2013. Comparisons between measurements and simulations show that Code_Saturne is able to reproduce correctly the mean flow, the impact of forest and pollutants dispersion in the experiment area. Differences in specific values between simulations and measurements are possibly due to an inaccurate inlet profile, which are not measured and therefore have to be built with theoretical profiles and measurements inside the simulation domain. Simulations will be continued for other IOPs and with a second-order turbulence closure (R_{ij}-ε). Comparison between measurements and numerical study will be made for more variables such as second order moments.

Question and Answer

Questioner: A. Manor
Question: How did you model the dissipation time scale for the concentration fluctuations? Is it constant?

Answer:
According to Milliez and Carissimo (2008), we applied a simple model for the dissipation terms in transport equation of concentration variance

$$2D\overline{\frac{\partial c'}{\partial x_i}\frac{\partial c'}{\partial x_i}} = \rho\varepsilon_c = \frac{\rho}{R_f}\overline{c'^2}\frac{\varepsilon}{k}$$

where we assume that the ratio of the dissipation time scale T_k of the turbulent kinetic energy k to the dissipation time scale T_c of the concentration variance $\overline{c'^2}$ is a constant R_f:

$$\frac{T_c}{T_k} = \frac{\overline{c'^2}/\varepsilon_c}{k/\varepsilon} = R_f$$

Questioner: S. Hanna
Question: What is the averaging time that you use for your wind and concentration simulations and observations? Do your account for horizontal meandering of the upstream flow, with typical time scales of several minutes?

Answer:
For the continuous measurements over 2 years, the data is averaged every 10 min. For the measurements during the IOP on 5 June 2013 (both wind and concentration), the averaging period is 60 min.

For now, we run the simulations in RANS mode, thus we test only the capacity of Code_Saturne to reproduce the mean flow in a stable condition. In the future, we will perform simulations in LES which will allow taking into account the horizontal meandering of the upstream flow and see how it will affect the dispersion of the tracer gas.

References

Milliez M, Carissimo B (2008) Computational fluid dynamical modeling of concentration fluctuations in an idealized urban area. Boundary-Layer Meteor 127:241–259

Wei X, Dupont E, Carissimo B, Gilbert E, Musson-Genon L (2014a) A preliminary analysis of measurements from a near-field pollutants dispersion campaign in a stratified surface layer. Int J Environ Pollut 55:183–191

Wei X, Dupont E, Carissimo B, Gilbert E, Musson-Genon L (2014b) Turbulence measurements for a near-field pollutants dispersion campaign in a stratified surface layer. In: Paper presented at 21th Symposium on Boundary Layers and Turbulence, 8B.4, Leeds, UK, 9–13 June 2014

Wei X, Dupont E, Carissimo B, Gilbert E, Musson-Genon L (2014c) Experimental and numerical study of a near-field pollutants dispersion campaign in a stratified surface layer. In: Paper presented at 16th International conference on Harmonisation within Atmospheric Dispersion Modelling for Regulatory Purposes, H16-8, Varna, Bulgaria, 9–11 Sept 2014

Zaïdi H, Dupont E, Milliez M, Musson-Genon L, Carissimo B (2013) Numerical simulations of the microscale heterogeneities of turbulence observed on a complex site. Boundary-Layer Meteor 147:237–259

Chapter 61
Cool Cities—Clean Cities? Secondary Impacts of Urban Heat Island Mitigation Strategies on Urban Air Quality

Joachim Fallmann, Renate Forkel and Stefan Emeis

Abstract Cities are the predominant places for human beings to settle down, thus becoming more vulnerable to extreme weather events aggravating phenomena like heat stress and decreasing air quality aroused by inner city pollution. The excessive warming of impervious surfaces and additional release of anthropogenic heat promotes urban heat island (UHI) formation. Human activities lead to an increase of emissions of air pollutants which in turn influences the chemical composition of urban air. In this study, the mesoscale chemical transport model WRF-Chem is used for the urban area of Stuttgart to simulate the effect of UHI mitigation strategies such as urban greening and high albedo materials on the concentration of primary and secondary pollutants.

61.1 Introduction

Urban Heat Island (UHI) describes the tendency for an urbanized area, because of its radiative and geometrical features, to remain warmer than its rural surroundings and thus generating its own microclimate (Oke 1982). Specific urban planning strategies like green roofs or facades and highly reflective materials are able to reduce the negative effects of the UHI and mitigate future problems (Taha 1997). The urban atmosphere can be described as a reaction chamber within which chemical reactions between anthropogenic pollutants and biogenic compounds take place under specific urban conditions such as higher temperature, higher turbulence, less humidity and modified radiation. Altering the characteristics of the urban surface promote changes in the energy and radiation budgets which modify the accumulation and dilution of primary compounds and the formation of secondary

J. Fallmann (✉) · R. Forkel · S. Emeis
Institute for Meteorology and Climate Research (IMK-IFU) of the Karlsruhe Institute of Technology (KIT),
Kreuzeckbahnstr 19, 82467 Garmisch-Partenkirchen, Germany
e-mail: joachim.fallmann@kit.edu

D.G. Steyn and N. Chaumerliac (eds.), *Air Pollution Modeling and its Application XXIV*, Springer Proceedings in Complexity,
DOI 10.1007/978-3-319-24478-5_61

compounds. This study aims to investigate the feedback of the abovementioned mitigation strategies on urban air quality by using the mesoscale chemical transport model WRF-Chem on regional scale, coupled to a multi-layer urban canopy parameterization scheme (Chen et al. 2011). The urban area of Stuttgart acts as test bed for the modelling of an extreme case scenario (2003 European Heat Wave).

61.2 Data and Methods

For representing urban sub-grid scale processes in WRF-Chem, the multi-layer urban canopy model BEP is applied (Martilli et al. 2002). By using a 33 classes CORINE data set, urban land cover is divided into three sub-classes (high- and low density residential and commercial). Each sub-class inherits specific geometrical and physical characteristics, which are to be defined within an urban parameter table (Fallmann et al. 2014). The innermost model domain covers an area of 600 × 450 km with a horizontal resolution of 3 km and 36 vertical levels. Anthropogenic emissions are retrieved from the MACC 7 km emission inventory, biogenic emissions from the global MEGAN emission database. MOZART lateral chemical boundary conditions are used and the RADM2 scheme is applied for calculating the gas-phase chemistry, aerosol dynamics and chemistry is described with the module MADE/SORGAM. The modelled time period ranges from August 9 to August 18 2003. Model setup for the meteorological part is documented by Fallmann et al. (2014).

Two scenarios are conducted with WRF-Chem representing urban greening ('Park') and increased albedo ('Albedo'). Results are compared with the base case ('Control'). With regard to the urban greening scenario, four urban grid cells in the centre of Stuttgart, accounting for 15 % of the total urban area, are replaced to grassland. An increased albedo is simulated by changing the roof albedo in the urban canopy parameter table from 0.2 to 0.7 for the entire urban area, not distinguishing between different urban classes. Dry deposition models have to be adapted in WRF-Chem in order to account for the three urban classes.

61.3 Results and Discussion

Changing the radiative or geometrical properties of urban surfaces has an effect on the dynamic structure of the urban boundary layer, thus resulting in a modification of turbulent mixing. The effect of reduced temperature on the concentration of primary and secondary pollutants can be quantified by the difference between scenario run and base case ('Control'). Results are presented for an area of 13 × 13 grid cells for the lowest model level (∼8.5m) (Fig. 61.1).

While the effect on primary pollutants is most pronounced for the albedo scenario (Fig. 61.1a), with a maximum mean concentration increase of 32 ppb (8.7 %)

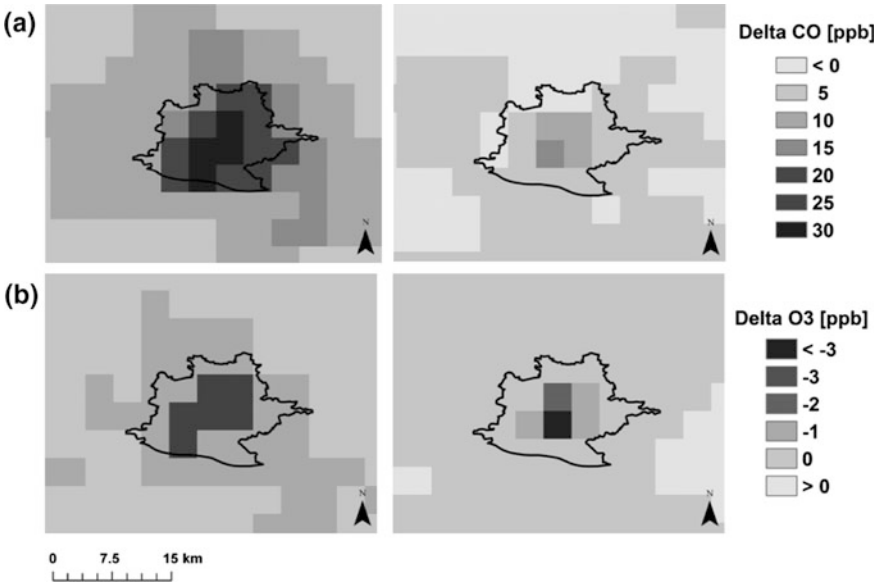

Fig. 61.1 Difference between scenario run and base case for simulated mean CO (**a**) and ozone (**b**) in the lowest model level. The 'Albedo' scenario is shown on the *left* and the 'Park' scenario on the *right* of each figure. Values are displayed in mean modelled concentration differences [ppb] with dark colours representing the major effect

the situation is reversed for ozone (Fig. 61.1b) with a maximum mean decrease of 3.7 ppb (9.2 %) for the 'Park' scenario. For ozone, the urban greening scenario locally has the bigger impact on average concentrations.

The different impact of reduced temperature on primary and secondary compounds as shown in Fig. 61.1 can be explained by two basic mechanisms. A decrease of turbulent kinetic energy (TKE) due to a lower temperature (Fig. 61.2a) leads to a lower rate of turbulent mixing and a decrease of the mixing layer height, thus slowing down the removal rate of primary pollutants such as CO

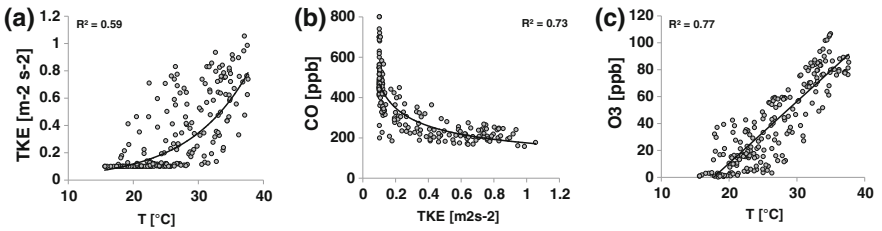

Fig. 61.2 Correlation between grid cell simulated hourly mean values of temperature and turbulent kinetic energy TKE [m-2 s-2] (**a**), TKE and CO (**b**) and temperature and ozone (**c**) in the lowest model level with regard to an urban grid cell

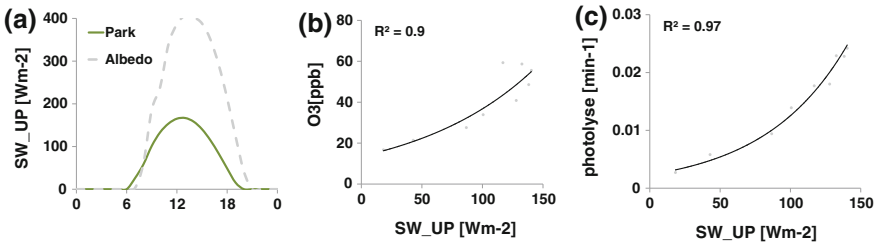

Fig. 61.3 Mean diurnal profile of short wave upwelling radiation SW_UP [wm^{-2}] for 'Albedo' and urban greening scenario (**a**), correlation between SW_UP and ozone concentrations [ppb] (**b**) and photolysis rates [min^{-1}] (**c**)

(Fig. 61.2b). The decrease of ozone particularly is related to a temperature dependency of photochemical reaction rates (Fig. 61.2c).

The impact on mean ozone concentration is lower for the albedo than for the urban greening scenario (Fig. 61.1b), which basically can be explained by the additional part of reflected short wave radiation of high reflective materials (Fig. 61.3a). This aspect in turn leads to higher ozone concentrations during peak hours (3b), due to an increase of photolysis rates (3c).

61.4 Conclusion

This study shows that common urban planning strategies to mitigate UHI formation can have both positive and negative impacts on the urban air quality. Model results reveal that the concentration of primary pollutants is largely dependent on the dynamical structure of the urban boundary layer, being responsible for turbulent exchange and vertical mixing. Ozone formation instead is mainly driven by temperature and intensity of shortwave radiation. Finding sustainable strategies for future urban planning has to consider both, meteorological and air chemical aspects. It should further account for both primary and secondary compounds and impacts.

Questions

Questioner: Prof. Builtjes
Question
Do you intend to take PM 10 into account in your future work?
Answer: In our study we observed a large negative bias between model and measurement which we cannot explain in detail yet. We have to figure out if the problem mainly lies in the model configuration or the selection of measurement data. Yes, we intend to discuss PM as well for future studies.

Questioner: Dr. Lenartz:
Question
What is the effect of solar panels on the albedo (and consequently on temperature and air quality)?

Answer:
We have not tested that special case, but I suppose the black surface of the solar panels could have a negative effect on urban temperature and heat island. With regard to the results of our study, the effect on primary pollutants however could be positive.

Questioner: Dr. Carissimo:
Question
On the slide where you compare the effect of different heat island mitigation measures there are areas of increased temperature?

Answer:
With regard to the albedo scenario, also buildings in the surrounding area are changed, that's why the effect well extends to outer areas. With regard to the urban greening case, these dots are model errors.

Question
Your conclusion discusses only the effect at 8 pm. In early morning effects could be different?

Answer:
Yes, you are right. I have chosen to discuss this time step, because on the one hand I wanted to see the effect on the urban heat island which is more pronounced in the evening/night-time and on the other hand I wanted to look at a time of the day, where most of the urban population is still active.

References

Chen F et al (2011) The integrated WRF/urban modelling system: development, evaluation, and applications to urban environmental problems. Int J Climatol 31(2):273–288

Fallmann J, Emeis S, Suppan P (2014) Mitigation of urban heat stress - a modelling case study for the area of Stuttgart. DIE ERDE - J Geogr Soc Berlin 144(3–4):202–216

Martilli A, Clappier A, Rotach M (2002) An Urban Surface Exchange Parameterisation for Mesoscale Models. Bound-Layer Meteorol 104(2):261–304

Oke TR (1982) The energetic basis of the urban heat island. Quart J R Meteorol Soc 108 (455):1–24

Taha H (1997) Urban climates and heat islands: albedo, evapotranspiration, and anthropogenic heat. Energy Buildings 25(2):99–103

Chapter 62
Deposition Following Accidental Releases of Chlorine from Railcars

Steven Hanna, Joseph Chang, John Hearn, Bruce Hicks, Shannon Fox, Mark Whitmire, Thomas Spicer, David Brown, Michael Sohn and Tetsuji Yamada

Abstract Chlorine releases to the atmosphere due to accidents involving railcars can be extremely hazardous to health, the environment, and man-made materials. Since the chlorine is released as a mixture of reactive gas and small (median diameter of 20–100 μm) aerosols, and the initial cloud has a very high concentration (>10,000 ppm), deposition to the surface can be important. The various mechanisms include dry deposition caused by chemical reactions between the gas and the surface (ground, vegetation, or materials), dry or wet deposition of small aerosols, and gravitational settling and impaction of larger aerosols. The state-of-the art in gas deposition modeling is based on the resistance analogy, which has been widely used in deposition modeling of a variety of air pollutants. The resistance

S. Hanna (✉)
Hanna Consultants, 7 Crescent Ave., Kennebunkport, ME, USA
e-mail: hannaconsult@roadrunner.com

J. Chang
HSSAI, Falls Church, VA, USA

J. Hearn
Lee University, Cleveland, TN, USA

B. Hicks
MetCorps, Norris, TN, USA

S. Fox
DHS S&T CSAC, Aberdeen Proving Ground, Aberdeen, MD, USA

M. Whitmire
Noblis, Falls Church, VA, USA

T. Spicer
University of Arkansas, Fayetteville, AR, USA

D. Brown
ANL, Argonne, IL, USA

M. Sohn
LBNL, Berkeley, CA, USA

T. Yamada
YSA, Santa Fe, NM, USA

D.G. Steyn and N. Chaumerliac (eds.), *Air Pollution Modeling and its Application XXIV*, Springer Proceedings in Complexity,
DOI 10.1007/978-3-319-24478-5_62

formula is reviewed and it is shown that, even though chlorine is relatively reactive, its deposition may be inhibited by the increased aerodynamic resistance in the very stable cloud. A method is suggested for parameterizing the effect of the dense cloud on the aerodynamic resistance. Deposition measurement methods planned for the Jack Rabbit II (JR II) chlorine release field experiments are reviewed, where up to 10 tons of pressurized liquefied chlorine will be released in several field trials.

62.1 Introduction

Chlorine has a relatively large rate of reaction with many natural surfaces. Consequently it is possible that, during the downwind transport of a chlorine cloud released to the atmosphere in an accident, a significant amount could be deposited to the ground surface (Dillon 2009; Hearn et al. 2013). This can adversely affect the surface, but has the positive effect of reducing concentrations (and hence potential health effects) in the air farther downwind. Thus there is great interest in improving knowledge of the deposition of chlorine and incorporation of this knowledge in operational transport and dispersion models used for emergency response.

For large releases of pressurized liquefied chlorine, the resulting initial cloud is characterized by a strong momentum jet consisting of about 20 % gas and 80 % liquid (by mass), in the form of aerosol (drops) with a broad size range but a mass median diameter of about 20–100 μm (Britter et al. 2011). Due to chlorine's relatively large saturation vapor pressure, the aerosol drops tend to evaporate fairly quickly, perhaps within a minute or so. It is difficult to measure this in an actual large chlorine release, though, partly because, at the same time the chlorine drops are evaporating, entrained ambient water vapor is condensing (due to the low (−34 °C) temperature in the initial cloud).

The Jack Rabbit (JR) field experiments are investigating the behavior of chlorine releases from pressurized tanks. JR I, which took place in 2010, used one and two ton releases from a tank mounted about 1 m above ground, with the initial jet pointed downward. JR II is planned for 2015 and 2016 and will release up to ten tons of chlorine, with different jet orientations.

Videos during the JR I experiments clearly show the two phase chlorine momentum jet striking the ground and deflecting into a donut-shaped dense wall jet (Hanna et al. 2012; Bauer 2013). However, the deposition of chlorine aerosol due to impaction and/or gravitational settling to the underlying surface can not be easily seen. After the cloud moved away, investigators found evidence of liquid chlorine having penetrated into the desert surface, mainly through cracks, but the amount could not be quantified. Hearn et al. (2013) set out pails of various types of soils flush with the surface during JR I, at distances out to about 50 m, and analyzed the chloride ion in the samples to estimate the deposition to the surface. They found significant deposition, especially to organic and/or moist soils, and hypothesized

that over half of the chlorine in the cloud could be removed by deposition within about 50 m of the source. Thus there is great interest in making further measurements of deposition during JR II.

62.2 General Approaches to Calculating Deposition

Gas and small aerosol (diameter < about 10 μm) deposition is caused by chemical reactions with the surface (soil, vegetation, or whatever) or Brownian motion (of aerosols). This is called "dry deposition" and is often parameterized by a deposition velocity, v_d. When measurements of mass deposition rate per unit surface area F and ambient air concentration C are available, $v_d = F/C$. Clearly v_d is larger for gases that are reactive. Inert gases have v_d of essentially zero, while reactive gases such as chlorine have v_d of about 5 cm/s. Intermediate reactive chemicals such as SO_2 and ozone have v_d of about 1 cm/s.

For aerosols with diameters much larger than 10 μm, gravitational settling is dominant. Well-established physical laws such as "Stokes Law" apply and allow the gravitational settling velocity v_g to be estimated as a function of aerosol density and diameter. For example, v_g is about 1 m/s for aerosols with diameters of 200 μm. This is sufficient to remove most of the particles of that size from a ground-based cloud within the first 100 m of travel. Gravitational settling is also called "rainout" for pressurized liquefied gas releases, although impaction (by a downward-pointing jet) can also contribute. Rainout is difficult to measure in a 5–10 ton chlorine release as planned for JR II.

Another type of deposition is due to ambient water drops (rain) falling through the cloud, collecting the pollutant (gas or aerosol), and bringing it to the ground surface. Many complicated approaches have been developed for modeling this "wet deposition", with parameterizations for raindrop sizes and shapes versus gas composition or aerosol sizes and shapes. However the needed details are seldom known and wet deposition is often parameterized in operational models by a simple "wet deposition" time scale, T_w, used in the simple formula $dC/dt = C/T_w$, giving $C(t) = C(t = 0)e^{-t/Tw.}$ This implies that, after a travel time of $t = T_w$, the concentration is reduced by about 60 %. T_w = 1000 s (about 15 min) for moderate rain rates is a default used in some operational models, although it actually depends on rain rate and aerosol or gas characteristics. Some models parameterize T_w as proportional to rain rate raised to some power.

As mentioned earlier, a complicating factor for chlorine releases is that the visible aerosol initially is likely to be almost 100 % chlorine, but the composition changes over time so that the aerosol is 100 % ambient water after a few minutes of travel. This transition should occur within a few hundred meters of the source, since the liquid chlorine rapidly evaporates at the same time that ambient water vapor is rapidly condensing in the very cold (−34 °C) cloud. Our currently-available instruments can measure the aerosol size distribution but not the chlorine vs condensed water vapor fractions.

The remainder of this manuscript addresses gas deposition, which can be measured by available methods during JR II.

62.3 Chlorine Gas Deposition as Estimated by the Resistance Theory

In most state-of-the-art atmospheric transport, dispersion, and deposition models, the calculation of deposition mass flux to the surface uses the resistance analogy (Dyer and Hicks 1970; Wesely and Hicks 1977; Hicks et al. 1979; Dillon 2009).

$$F = C/R \quad \text{where } R = R_a + R_b + R_c \tag{62.1}$$

C is gas concentration near the surface and R is the resistance to deposition. Thus $v_d = 1/R$. As Hicks et al. (1979) explain, the resistance terms are defined as upper case (as above) when the deposition from the atmosphere to an integrated area is of concern, and are defined as lower case when the deposition to a particular surface is of concern (e.g., a house roof or a garden of tomato plants).

The aerodynamic resistance R_a is associated with the atmospheric turbulent flux towards the surface, between the height at which C is measured and the surface. R_b (the "quasi-laminar resistance") is the overall consequence of the very-near-surface boundary-layer resistances of all of the individual receptor surfaces, and R_c (the capture resistance) is the net effect of surface uptake effectiveness. The following parameterizations of the resistance components are made:

$$R_a = \left(u(z_r)/u*^2\right) f(z/L) \tag{62.2}$$

where u* is the ambient air friction velocity, $u(z_r)$ is the wind velocity at reference height z_r, L is Monin-Obukhov length, and f (the stability term) = 1 during neutral conditions

$$R_b = (u * B)^{-1} \tag{62.3}$$

where B is a dimensionless constant that is the ratio of the Prandtl and Schmidt numbers and can be set equal to one as an approximation. Note that, for f and B = 1.0, and assuming a typical ratio of u*/u = 0.1, both R_a and R_b are proportional to 1/u*, although R_a is about ten times larger than R_b. Thus R_a has a larger effect on deposition than R_b. In the above discussions, for application to a chlorine cloud release, u* and L are the values for the ambient boundary layer upwind of the release location.

The capture resistance, R_c, depends on the surface characteristics, such as leaf stomata openings or chemical constituents at the ground or material surface. This is where the relative chemical reactivity with the surface is important, because even if the material is brought down to the surface by turbulent transport, it will not deposit

unless it reacts or is ingested or otherwise is absorbed by the surface. Conversely, even if the material may react quickly with the surface, it will not deposit significantly unless there is adequate turbulent transport to bring material to the surface.

There are theoretical formulas for estimating capture resistance, but in practice, it is usually determined by measurements in controlled well-mixed chambers. For example, a layer of grass sod can be placed in a chamber and chlorine is introduced and is well-mixed above the sod (i.e., R_a and R_b are very small, so R_c dominates deposition). Thus a set of R_c values are determined for various underlying surfaces.

62.4 Modifications to the Aerodynamic Resistance, R_a, for a Dense Cloud

In 62.2, the turbulent transport speed is parameterized by the ambient friction velocity u*. However, because a dense chlorine cloud can have a temperature as low as −34 °C near the source, there may be a very stable layer near the surface with reduced turbulent transport in the vertical and effective u* (in the cloud). To modify u* for this increased stability very near the surface, we suggest using Briggs et al.'s (2001) formulation for the vertical entrainment velocity, w_e, which parameterizes the rate of entrainment of ambient air into a dense cloud. Several dense gas dispersion models use the empirical formula:

$$w_e = au^*/(1 + bRi^*) \tag{62.4}$$

where a and b are "constants" and Ri* is the Richardson number of the local cloud:

$$Ri^* = (g(\rho_c - \rho_a)/\rho_a)h/u^{*2} \tag{62.5}$$

where g is the acceleration of gravity, h is the local cloud depth, ρ_c is local cloud density, and ρ_a is ambient density (Hanna and Chang 2001). Briggs et al. (2001) analyzed data from three wind tunnels and found that, for Ri* up to 20, the observations showed reasonable agreement with the following relation:

$$w_e = 0.65u^*/(1 + 0.2Ri^*) \tag{62.6}$$

We propose that this same correction be made to the u* value in the R_a formula, so that u* is multiplied by 1.0/(1.0 + 0.2Ri*). This will effectively increase the aerodynamic resistance and therefore decrease the rate of deposition, as expected from basic physics principles.

62.5 Jack Rabbit II Deposition Measurements

JR II will focus on extensive measurements of air concentrations of chlorine gas, on sampler arcs at downwind distances from 50 m to 11 km. Some measurements of aerosol sizes will be made in the near field (x < about 100 m). There will be about 20 locations with deposition measurements made next to gas concentration samplers. The methodology is still under discussion. It is likely that cores will be taken in the hard playa surface and analyzed in a laboratory for total chloride mass. It is also likely that, as done in JR I (Hearn et al. 2013), a few buckets of other substances (e.g., organic-rich soil) will be sunk flush with the surface and analyzed in a similar way as the natural playa. Additional measurements are planned with X-Ray Fluorescence (XRF) devices, which detect the chlorine at the surface. Other ideas for deposition measurements are being considered, but the final plan has not been resolved.

Indoor deposition experiments are also being planned as part of the chlorine release experiments in a Mock Urban Array, where about half of the JR I releases will occur. This is a 100 m by 100 m array of CONEX's and small trailers, where about six of the structures will be modified to be more like normal residences and office buildings with HVAC systems. Chlorine transport, dispersion, and deposition will be studied inside the structures. Deposition to surfaces such as carpets, sheetrock, and chairs, etc., with various orientations, will be investigated.

Companion laboratory experiments, using well-mixed chambers, are currently underway at Argonne National Laboratory for natural surfaces and soils. These efforts are aimed at direct specification of the capture resistance, R_c, for several types of substances and surfaces. During JR II, separate chamber studies are planned at the field site and at several laboratories employing both well-mixed chambers and flow chambers (e.g., recirculating wind tunnels).

Questions and Answers

Questioner: P. Builtjes
Question: In your experiments regarding R_c, are you going to use artificial surfaces?
Answer: Yes, several types of soils, artificial surfaces, and vegetation will be placed out on the desert surface. The artificial surface coverage will be about 1 m^2 and as level with the natural surface as possible. These artificial surfaces will be located close to one of the chlorine concentration samplers.

Questioner: Enrico Ferraro
Question: Do you plan to perform turbulence measurements for dispersion model applications inside the small buildings?
Answer: Mean flow observations will be made inside the small buildings. Because the indoor model being tested is a rather simple model, no turbulence observations are currently planned.

Questioner: Jaakko Kukkonen
Question: Such experimental field studies are rarely organized. I feel therefore that this new campaign will probably provide valuable new results. Could you elaborate whether the measured datasets will be publicly available in the future, and whether there will be an international model evaluation exercise?

Answer: Several international modeling groups are already participating by running their models for a few prescribed worst-case scenarios. The results are being used to better plan the positioning of concentration samplers. The modelers are also invited to attend the field experiment and test their model in real time. It is expected that the field experiment data archive will be made available to the modeling community for future evaluations.

Questioner: Douw Steyn
Question: You use cloud depth h as a length scale for the Richardson number. Surely this is too large if you are interested in deposition at cloud base?
Answer: The length scale h is used to evaluate the bulk negative buoyancy of the total chlorine cloud. This is then used to calculate the cloud Richardson number and hence the effective turbulent transport velocity in the chlorine cloud. The reduction in the turbulent transport velocity affects the deposition through the aerodynamic resistance term R_a.

References

Bauer TJ (2013) Comparison of chlorine and ammonia concentration field trial data with calculated results from a Gaussian atmospheric transport and dispersion model. J Hazard Mater 254–255:325–335

Briggs GA, Britter RE, Hanna SR, Havens JA, Robins AG, Snyder WH (2001) Dense gas vertical diffusion over rough surfaces: results of wind-tunnel studies. Atmos Environ 35:2265–2284

Britter RE, Weil J, Leung J, Hanna SR (2011) Toxic Industrial Chemical (TIC) source emission model improvements for pressurized liquefied gases. Atmos Environ 45:1–26

Dillon M (2009) The role of deposition in limiting the hazard extent of dense-gas plumes. J Hazard Mater 164:1293–1303

Dyer AJ, Hicks BB (1970) Flux-gradient relationships in the constant flux layer. Q J R Meteorol Soc 96:715–721

Hanna SR, Chang JC (2001) Kit fox dense gas dispersion field experiment and HEGADAS model testing. Atmos Environ 35:2231-2242

Hanna SR, Britter R, Chang J, Argenta E (2012) The Jack Rabbit chlorine release experiments: implications of dense gas removal from a depression and downwind concentrations. J Hazard Mater 213–214:406–412

Hearn JD, Weber R, Nichols R, Henley M, Fox S (2013) Deposition of Cl_2 on soils during outdoor releases. J Hazard Mater 252–253:107–114

Hicks BB, Hess GD, Wesely ML (1979) Analysis of flux profile relationships above tall vegetation, an alternative view. Q J R Meteorol Soc 105:1074–1077

Wesely ML, Hicks BB (1977) Some factors that affect the deposition rates of sulfur dioxide and similar gases on vegetation. J Air Poll Control Assoc 27:1110–1116

Chapter 63
A Community-Scale Modeling System to Assess Port-Related Air Quality Impacts

Vlad Isakov, Timothy Barzyk, Saravanan Arunachalam, Michelle Snyder and Akula Venkatram

Abstract Near-port air pollution has been identified by numerous organizations as a potential public health concern. Based upon multiple near-road and near-source monitoring studies, both busy roadways and large emission sources at the ports may impact local air quality within several hundred meters of the ports. As the volume of trucking and freight movement increases, near-road air quality along transportation routes could be affected well outside port boundaries. Health effects have been associated with near-road exposures and proximity to large emission sources, so characterizing emission sources is important for understanding potential health effects. To address this need, we have developed a new community-scale tool called C-PORT to model emissions related to all port-related activities—including, but not limited to ships, trucks, cranes, etc.—and predict concentrations at fine spatial scales in the near-source environment. C-PORT represents one of the first efforts to develop a reduce-form modeling system that is optimized for community-scale applications. The modeling system includes dispersion algorithms for area, point, and line sources related to port activities, and emissions from the port terminals. The use of the reduced-form approach in C-PORT enables us to examine what-if scenarios of changes in emission volume, such as due to changes in traffic counts, fleet mix, speed, or in port emissions due to equipment or vehicles in near real-time,

V. Isakov (✉)
Atmospheric Modeling and Analysis Division, National Exposure Research Laboratory, U.S. Environmental Protection Agency, RTP, Durham, NC, USA
e-mail: Isakov.Vlad@epa.gov

T. Barzyk
Human Exposure and Atmospheric Sciences Division, National Exposure Research Laboratory, Office of Research and Development, U.S. EPA, Research Triangle Park, Durham, NC, USA

S. Arunachalam · M. Snyder
Institute for the Environment, University of North Carolina, Chapel Hill, NC, USA

A. Venkatram
Department of Mechanical Engineering, University of California, Riverside, CA, USA

D.G. Steyn and N. Chaumerliac (eds.), *Air Pollution Modeling and its Application XXIV*, Springer Proceedings in Complexity,
DOI 10.1007/978-3-319-24478-5_63

using a web-based easy-to-use interface. The C-PORT model can be used to examine different scenarios of air quality impacts in order to identify potentially at-risk populations located near emission sources, and the effects that port expansion may have on them. We present an illustrative example of the near-port modeling assessment focusing on the Port of Charleston in South Carolina, USA, to complement a field-study that was conducted during spring 2014 to take air quality measurements in residential neighborhoods in the port vicinity.

63.1 Introduction

Many Ports are important drivers for some regional economies. As regional ports and infrastructure agencies prepare for additional freight, nearby communities voice concerns about increased emissions and air pollution exposure. As has been established in near-road and near-source monitoring studies, busy roadways and large emission sources may impact local air quality within several hundred meters of the source. A significant portion of this traffic is related to the freight transportation system that moves containers with heavy-duty diesel trucks. These trucks, in addition to the large commercial marine vessels that transport these goods in and out of ports are a significant source of pollution in the immediate vicinity of the port. As the volume of trucking and freight movement increases, near-road air quality along transportation routes could be affected well outside port boundaries (Hagler et al. 2013). Health effects have been associated with near-road exposures and proximity to large emission sources, so characterizing emission sources is important for understanding potential health effects. However, there is a lack of tools that can be applied to study near-source pollution in an easy manner, and explore the benefits of improvements to air quality and exposures—either due to voluntary or mandatory programs. Screening-level or reduced-form air quality modeling is a useful tool for examining what-if scenarios of changes in emission volume, such as those due to changes in traffic counts, fleet mix, or speed, or changes in port emissions due to equipment or vehicles. Examining various scenarios of air quality impacts in this way can identify potentially at-risk populations located near emission sources, and the effects that port expansion may have on them. To address this need for a systems approach, we have developed a new community-scale tool called C-PORT to model emissions related to all port-related activities (including, but not limited to ships, trucks, cranes, etc.), and predict concentrations at fine spatial scales in the near-source environment.

63.2 Community-Scale Modeling Tool C-Port

C-PORT represents one of the first efforts to develop a reduce-form modeling system that is optimized for community-scale applications. The modeling system includes dispersion algorithms for area, point, and line sources related to port activities, and emissions from the port terminals. C-PORT incorporates modeling algorithms developed through research and development of the R-LINE model on pollutant transport and dispersion from roadways (Snyder et al. 2013). The use of the reduced-form approach in C-PORT enables us to examine what-if scenarios of changes in emission volume, such as due to changes in traffic counts, fleet mix, speed, or in port emissions due to equipment or vehicles in near real-time, using a web-based easy-to-use interface (Barzyk et al. 2015). The C-PORT model can be used to examine different scenarios of air quality impacts in order to identify potentially at-risk populations located near emission sources, and the effects that port expansion may have on them. Key model features include the ability to select and change model inputs (roadway sources, area sources, ships at the terminal and ships in transit), perform the analysis, and visualize the results. An example of C-PORT, a computer screen snapshot, is shown in Fig. 63.1. The figure illustrates how the model results (e.g. near-road pollutant gradients) are visualized for a selected scenario.

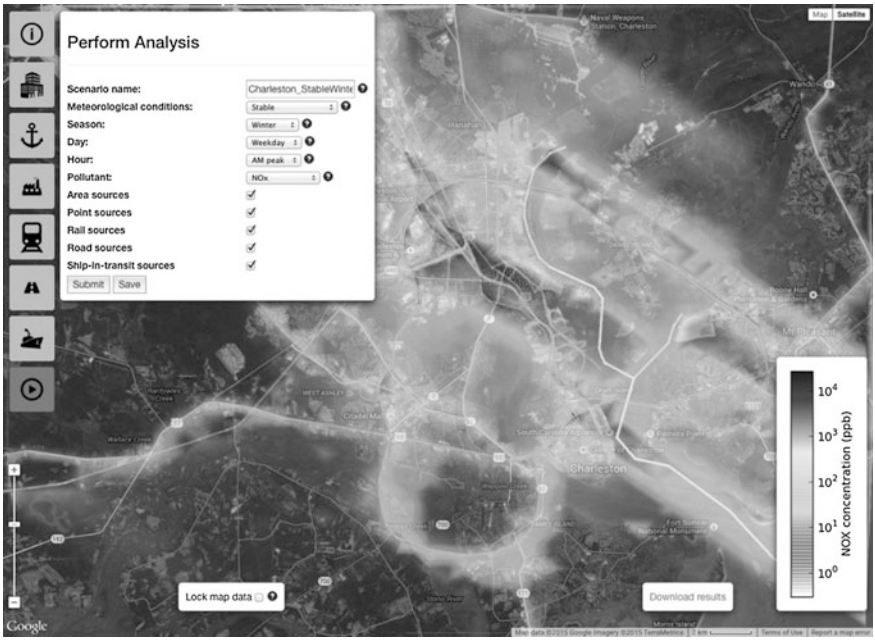

Fig. 63.1 Computer screen snapshot of the C-PORT model

63.3 Illustrative Example of C-PORT Application in Charleston, SC

We applied the C-PORT model as a part of the near-port modeling assessment in Charleston, South Carolina, USA. Figure 63.2 show a map of the study area. We have also conducted a field-study during spring 2014 to take air quality measurements in residential neighborhoods in the port vicinity. High-resolution monitoring using EPA's Geospatial Monitoring of Air Pollution (GMAP) vehicle was performed along driving routes near several port terminals and rail yard facilities, recording geospatial coordinates and measurements of pollutants including black carbon (BC), size-resolved particle count ranging from ultrafine to coarse, carbon monoxide (CO), carbon dioxide (CO_2), and nitrogen dioxide (NO_2). Additionally, a portable meteorological station was used to characterize local meteorology. Port activity data was provided by the Port Authority of Charleston and includes counts of ships and trucks, and port service operations such as cranes and forklifts during the sampling time periods. These data are analysed in order to characterize the impact of the port activity on local scale air quality. Preliminary analysis shows the

Fig. 63.2 Map of the study area showing locations of port terminals in Charleston, SC

highest concentrations are found along major roadways. Modeling provides relative contributions of traffic emissions, emissions from port terminals, and emissions from ships to the total concentrations at model receptors. Further analysis will be performed to use the model-based estimates of relative contributions of various port-related source categories in order to isolate the effect of port-related activity on local communities. The C-PORT modeling application will help to identify potentially at-risk populations located near emission sources at the port terminals, and the effects that change in port-related activities may have on them.

Disclaimer Although this work has been reviewed and approved for publication by the U.S. Environmental Protection Agency, it does not necessarily reflect the views and policies of the agency.

Questions and Answers

Questioner: Stefano Alessandrini
Question: Does your model treat the buoyant plumes as independent? An interaction could eventually enhance the rise compared to what can happen treating them separate.

Answer: We agree with your comment on the need to carefully consider the interaction of plumes in the model to adequately represent the complex processes affecting the plume behavior. However, the C-PORT model is based on a steady-state Gaussian dispersion model formulations and therefore doesn't consider plume interactions. Increasing complexity of model formulations to account for plume interactions might not be feasible for a web-based, real-time reduced-form models such as C-PORT.

Questioner: Jukka-Pekka Jalkanen
Question: How do you estimate the axillary engine usage of ships at berth? This is an area of large uncertainty in port emissions modeling.

Answer: We agree with your comment on the need to accurately characterize ship emissions. We provide default emissions for all ship emissions at 17 ports in southeastern US, and we recognize that the uncertainty in these default ship emissions could be high. However, for a reduced-form model such as C-PORT, an ability to provide quick calculations and bound the uncertainty in ship emissions. The user can change these emissions and run C-PORT to calculate a difference in resulting concentrations for low and upper bounds of emission estimates in order to understand the impact of uncertainty in emission inputs on modeled concentrations.

References

Barzyk TM et al (2015) A near-road modeling system for community-scale assessments of mobile-source air toxics: the community line source (C-Line) modeling system. Environ Model Softw 66:46–56. doi:10.1016/j.envsoft.2014.12.004

Hagler G et al (2013) Panama Canal expansion illustrates need for multimodal near-source air quality assessment. Environ Sci Technol 47:10102–10103. doi:10.1021/es403145x

Snyder MG et al (2013) RLINE: a line source dispersion model for near-surface releases. Atmos Environ 77:748–756. doi:10.1016/j.atmosenv.2013.05.074

Chapter 64
Recent Advances in Modeling of the Atmospheric Boundary Layer and Land Surface in the Coupled WRF-CMAQ Model

Jonathan Pleim, Robert Gilliam, Wyat Appel and Limei Ran

Abstract Advances in the land surface model (LSM) and planetary boundary layer (PBL) components of the WRF-CMAQ coupled meteorology and air quality modeling system are described. The aim of these modifications was primarily to improve the modeling of ground level concentrations of trace chemical species such as nitrogen oxides (NO_x), carbon monoxide (CO), particulate matter (PM), and ozone (O_3) during the evening transition and overnight. However, evaluation of both meteorological and air quality quantities shows that the advanced algorithms added to the PX LSM and the ACM2 PBL schemes improved results both day and night. Modeling experiments at various grid spacings (1, 4, and 12 km) and for different years and seasons all show significant improvements. The revised versions of these components have already been released in WRFv3.7 and will be released in the fall of 2015 in CMAQv5.1.

64.1 Introduction

Air quality models have been shown to have persistent tendencies for high biases in near surface concentrations of ground level emitted chemical species (e.g. NO_x, CO, primary PM) and, conversely, low biases in ozone during the evening transition and overnight on many days. Meteorology models often show similar tendencies to over-predict ground level water vapor mixing ratios during evening

J. Pleim (✉) · R. Gilliam · W. Appel
Atmospheric Modeling and Analysis Division, U.S. EPA,
Research Triangle Park, Durham, NC 27711, USA
e-mail: Pleim.jon@epa.gov

L. Ran
Institute for the Environment, University of North Carolina, Chapel Hill
NC 27599, USA

D.G. Steyn and N. Chaumerliac (eds.), *Air Pollution Modeling and its Application XXIV*, Springer Proceedings in Complexity,
DOI 10.1007/978-3-319-24478-5_64

transition times. Such biases suggest that PBL models become too stable too early in the evening, particularly in developed areas where most of the pollutant emissions are located. Model errors in either surface heat flux and/or the parameterization of PBL turbulent mixing may be contributing to these biases. Several approaches have been used to diagnose and correct these model errors. Note that these errors are typically mitigated in air quality models through the use of artificially large minimum values for eddy diffusivities in chemical transport models. In some models, the large values are only used in urban areas, following the logic that meteorology models have inadequate treatment of urban heat island effects. Thus, improvements to urban parameterizations, particularly increased surface heat capacity and the addition of anthropogenic heating, can reduce premature and excessive stabilization. Also, it has recently been shown that there is usually a time lag after the sign reversal in surface buoyancy flux for the development of stable virtual potential temperature profiles in the surface layer.

64.2 Advancements to the Pleim-Xiu Land Surface Model

In order to diagnose overpredictions of chemical concentrations during the evening transition, it is useful to find a meteorological parameter that behaves in a similar way to the chemical concentrations so that WRF simulations could be evaluated against surface meteorological measurements that are far more extensive than air quality surface measurements. Since the flux of water vapor rises from the surface during daytime and into the early evening due to evapotranspiration, water vapor mixing ratio is often overpredicted in the meteorology model in a similar way to surface emitted chemical species (e.g. NO_x, CO, primary PM). Thus modifications to the land surface model that shift some of the available surface energy flux from latent heat flux to sensible heat flux as the sun sets in the evening have the desirable effect of reducing over prediction of water vapor mixing ratio during the evening and into the early nighttime. Towards this end, the original stomatal conductance function for photosynthetically active radiation (PAR) that was based on Noilhan and Planton (1989) is replaced with a new empirical function that was fitted to gross primary productivity (GPP) versus PAR measurements shown by Clark et al. (2011). The biggest difference is that the new function has significantly lower magnitude when surface short wave radiation values are less than 350 W m^{-2} which results in reduced latent heat flux and enhanced sensible heat flux, causing a delay in surface stabilization during the evening transition. Note that these empirical functions for stomatal conductance will be replaced once a photosynthesis modeling approach, which is currently being developed, is added to the PX LSM. Other modifications to the PX LSM include an updated (reduced) value for the heat capacity of vegetation, which has the effect of reducing overpredictions of minimum 2-m temperature occurring around dawn and underpredictions during the post-dawn morning hours.

64.3 Modifications to the Asymmetric Convective Model Version 2

The Asymmetrical Convective Model version 2 (ACM2) is a combined local and non-local closure PBL scheme that is used in both WRF and CMAQ for consistent PBL transport of meteorology and chemistry (Pleim 2007a, b). Two major revisions have been made to ACM2. For the WRF application, the ACM2 now estimates and applies different eddy diffusivities for momentum (K_m) and heat (K_h) which means that Prandtl number is no longer assumed to be unity ($Pr = K_m/K_h \neq 1$). The eddy diffusivity model in ACM2 uses the maximum of two formulations: one that follows a commonly used boundary layer scaling approach (e.g. Brost and Wyngaard 1978; Troen and Mahrt 1986; Holtslag et al. 1990):

$$K_{h,m} = kz\frac{u_*}{\phi_{h,m}}\left(1-\frac{z}{h}\right)^p \tag{64.1}$$

where k is von Karman's constant, u_* is the surface friction velocity, $\phi_{h,m}$ is the Monin Obukhov similarity stability functions for heat and momentum, h is the PBL height and the exponent p is taken to be 2. The second eddy diffusivity form is essentially an empirical formulation that combines wind shear, length scale, and a stability function:

$$K_{h,m} = K_{\min} + \left|\frac{\partial u}{\partial z}\right| l^2 f_{h,m}, l = \frac{kz\lambda}{kz+\lambda}, \lambda = 80\,\mathrm{m} \tag{64.2}$$

Thus, for (64.1), which is usually dominant in the unstable boundary layer, the Prandtl number is given by $Pr = \phi_h/\phi_m$, while for (64.2), which is usually dominant in stable conditions both within the PBL and above, Pr is set to 0.8.

The other major modification to ACM2 is that new stability functions have been developed for both heat and momentum for use in 64.2:

$$\begin{aligned} f_h &= \left(1 + 10\mathrm{Ri} + 50\mathrm{Ri}^2 + 5000\mathrm{Ri}^4\right)^{-1} + 0.0012 \\ f_m &= \mathrm{Pr} * f_h + 0.00104 \end{aligned} \tag{64.3}$$

where Ri is the gradient Richardson number. These functions were derived based on a database of 80 LES for neutral and stable conditions compiled and presented by Esau and Byrkjedal (2007). The changes were extensively tested in a single column model (SCM) version of ACM2 for the GABLS3 experiment that was based on measurements from the Cabauw tower in the Netherlands for July 1, 2006. Figure 64.1 shows that while the new ACM2 still overpredicts water vapor mixing ratio for the whole period the much greater overprediction seen for the old ACM2 in the evening transition is much reduced.

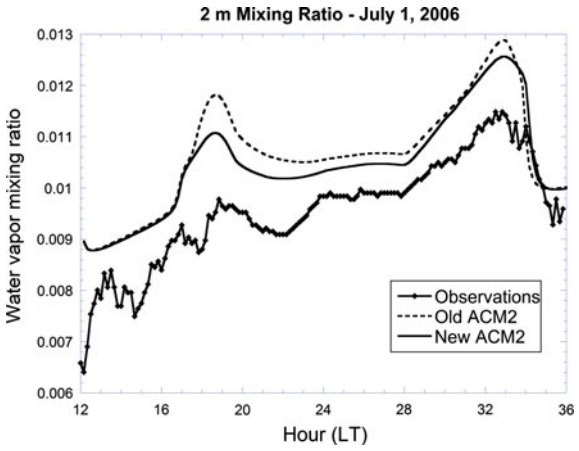

Fig. 64.1 Comparison of water vapor mixing ratios from new and old versions of ACM2 compared to measurements from the GABLS3 experiment for 1 July 2008

64.4 Effects of Upgrades to LSM and PBL on WRF and CMAQ Results

We tested the new versions of the PX LSM and ACM2 in the WRF-CMAQ model at various grid resolutions ($\Delta x = 12, 4, 1$ km) and for different seasons. The changes to the LSM and PBL components of WRF-CMAQ significantly improved statistical comparisons to observations for 2-m temperature (2mT) and 2-m water vapor mixing ratio (2mQ). For example, over the entire CONUS domain with 12-km grid spacing, the mean biases for 2mT and 2mQ decreased from 0.415 to 0.163 and 0.506 to 0.359, respectively, while mean absolute errors decreased from 1.52 to 1.45 and 1.31 to 1.24, respectively. Similarly, daily 8-h max O_3 mixing ratio decreased on the average over the whole domain for every day of the simulation (Fig. 64.2).

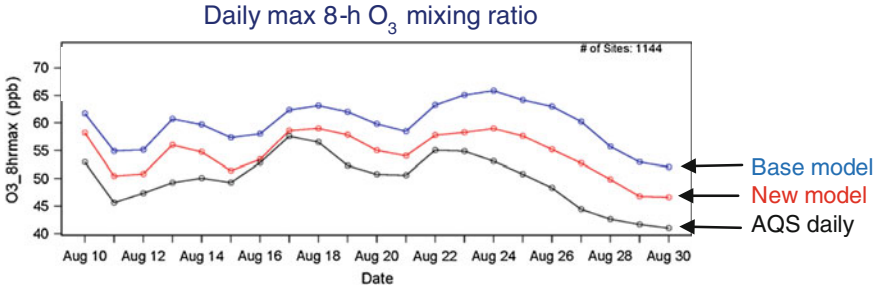

Fig. 64.2 Daily max 8-h O_3 mixing ratio averaged over the entire 12 km WRF/CMAQ CONUS domain for 10–30 August 2006

64.5 Conclusions

Both meteorology and chemical parameters simulated by the WRF-CMAQ coupled modeling system were significantly improved compared to observations when the PX LSM and the ACM2 PBL model were upgraded. The initial motivation was to increase PBL mixing during the evening transition to reduce overprediction of ground-emitted chemical species and 2mQ and underprediction of ozone during these times, which was achieved. However, initial testing has shown reduced error and bias in ozone for most hours of the day and reduced overprediction of $PM_{2.5}$ in winter months overnight. Note that many of these results are not shown here due to the brevity of this document, but they were shown in the presentation. The changes for PX LSM and ACM2 have already been released in the latest version of WRF (v3.7). Updates to ACM2 in CMAQ to be consistent with the changes in WRF will be released in CMAQv5.1 in the fall of 2015.

Acknowledgments and Disclaimer Although this work has been has been reviewed by EPA and approved for publication, it does not necessarily reflect their policies or views.

Questions and Answers

Questioner Name: Steve Hanna
Q: Are your modifications to the PBL formulations in the WRF version used by EPA transferred to the basic WRF maintained by NCAR?
A: Yes. All the modifications to the ACM2 and PX LSM discussed in this presentation have been released in WRFv3.7 from NCAR.

Questioner Name: S. Arunachacam
Q: Previously, CMAQ overpredicts nighttime O_3 and the recommended fix to make K_z = f(PURB), and have a variation as function of land-cover. With your new updates to PX LSM and ACM2, did you also vary K_z, or are these compensating errors? Can you comment on the overall effect of these three (PX LSM and ACM2, and K_z min) on model performance?
A: We did not alter the CMAQ minimum K_z that is set to a higher value according to the fraction of urban land use. Note that this algorithm affects only very small areas in cities. The effects of the changes to the ACM2 and PX LSM are far more widespread.

References

Brost R, Wyngaard JC (1978) A model study of the stably stratified boundary layer. J Atmos Sci 8:1427–1440

Clark DB, Mercado LM, Sitch S, Jones CD, Gedney N, Best MJ, Pryor M, Rooney GG, Essery RLH, Blyth E, Boucher O, Harding RJ, Huntingford C, Cox PM (2011) The Joint UK

Land Environment Simulator (JULES), model description—part 2: carbon fluxes and vegetation dynamics. Geosci Model Dev 4:701–722. doi:10.5194/gmd-4-701-2011

Esau I, Byrkjedal Ø (2007) Application of large eddy simulation database to optimization of first order closure for neutral and stably stratified boundary layers. Bound Layer Meteorol 125: 207–225

Holtslag AAM, De Bruijn EIF, Pan HL (1990) A high resolution air mass transformation model for short-range weather forecasting. Mon Weather Rev 118:1561–1575

Noilhan J, Planton S (1989) A simple parameterization of land surface processes for meteorological models. Mon Weather Rev 117:536–549

Pleim JE (2007a) A combined local and nonlocal closure model for the atmospheric boundary layer. Part I: model description and testing. J Appl Meteor Climatol 46:1383–1395

Pleim JE (2007b) A combined local and nonlocal closure model for the atmospheric boundary layer. Part II: application and evaluation in a mesoscale meteorological model. J Appl Meteor Climatol 46:1396–1409

Troen I, Mahrt L (1986) A simple model of the atmospheric boundary layer: sensitivity to surface evaporation. Bound Layer Meteor 37:129–148

Chapter 65
A Coupled Experimental-Modelling Approach to Estimate Black Carbon Concentrations at Urban Level

Fabian Lenartz, Olivier Brasseur, Priscilla Declerck and Luc Bertand

Abstract Mobile measurements of black carbon are made in the city center of Liège (Belgium) to evaluate the contribution of this, not yet regulated pollutant, to the ambient air particulate matter level. By means of the $CANS_{BC}$ model, we intend to determine the part due to traffic and, furthermore, to make the distinction between direct emissions and recirculation, depending on meteorological and geometric parameters, in street canyons. Background concentrations are, on one hand, directly measured at one station, and on the other hand, estimated via the Lagrangian Austal2000 model, fed with domestic heating emissions. Short-term experiments, led at six selected sites, are used to calibrate the model, which will be further extended to the whole city.

65.1 Context

Black carbon (BC) is a component of particulate matter (PM) generated by incomplete combustion of fossil fuels, biofuels, and biomass (EPA 2012). In urban environments, the two main sources of this atmospheric pollutant are domestic heating and traffic. It is not sure yet whether health effects due to PM or BC exposure are different, however the latter is thought to operate as a universal carrier of a wide variety of chemical constituents of varying toxicity (WHO 2012). As it is, BC is inert and therefore an excellent candidate for modelling experiments.

Its measurement relies on filter-based optical techniques. In Belgium, aethalometers from Magee Scientific or multi-angle absorption photometers from

F. Lenartz (✉) · L. Bertand
Institut Scientifique de Service Public, Rue du Chéra 200, 4000 Liège, Belgium
e-mail: f.lenartz@issep.be

O. Brasseur · P. Declerck
Brussels Environment, Gulledelle 100, 1200 Brussels, Belgium

D.G. Steyn and N. Chaumerliac (eds.), *Air Pollution Modeling and its Application XXIV*, Springer Proceedings in Complexity,
DOI 10.1007/978-3-319-24478-5_65

Thermo Scientific are used at the fixed stations of the three regional monitoring networks. For the assessment of personal exposure, the portable devices from AethLabs are commonly used throughout the country. When synchronized with a GPS tracker, and after appropriate data treatment, the latter allow one to pinpoint hot spots.

The ExTraCar (*Exposition, trafic et carbone noir*) project aims at mapping and assessing BC concentrations in the city of Liège, by using data analysis and modelling.

65.2 Material and Method

An intensive campaign, covering the city center, started in April 2014 and is going to end in December 2015. BC concentrations are recorded by means of AE51 aethalometers, at a frequency of 1 Hz, along six pre-defined tracks all around the city (see Fig. 65.1), while DG200 GPS recorders from GlobalSat are used to keep track of the operators' movements at the same time rate. Repetitions are expected to be performed ten times, during morning and evening rush hours, and under three different dispersion conditions (unstable, neutral and stable atmosphere). Further off-hours measurements are made to evaluate off-peak concentrations during several "10-h of measurements" days. These assessments will provide us with a snapshot of pollution levels in Liège and will be compared with the ones measured at three nearby fixed stations. The latter are located in the inner city, and at the southwestern and northeastern boundaries of Liège. All information is stored in a georeferenced PostgreSQL/PostGIS data base, which allows one to easily retrieve pollution levels in a specific area where we ride our bikes.

A street canyon model, namely $CANS_{BC}$, based on OSPM's equations (Operational Street Pollution Model) and implemented at Brussels Environment (Brasseur et al. 2014), is used to evaluate BC concentrations in a limited number of streets. The model input arguments are wind direction and velocity above building height, geometrical characteristics of the street canyon, vehicle counts and emission rates. Care is taken to have the most precise input parameters: wind is measured continuously in the valley and on top of the hill at several heights, street geometry is available via the PICC (*Projet Informatique de Cartographie Continue*), traffic density was evaluated both via a Doppler radar from ICOMS Detections and manual counts. The best choice for emission rates is still under investigation; presently we are using ones available from HBEFA for France. As they are expressed in g of PM2.5 per km, one has to convert them in g of BC per km using a factor of 0.66 (Lefebvre et al. 2011).

The cross sections where the model is run are selected in such a way that a range of H/W ratios (building height over street width) and street orientations is covered (see Fig. 65.1). Hence, afterwards, results can be extrapolated on the mere basis of geographical and traffic information. This model provides at the same time the

Fig. 65.1 Tracks and sections selected, respectively, for the experimental and modelling approach

direct contribution of traffic to the observed concentrations, as well as that due to recirculation. In order to compare the results with on-field measurements, one needs to take into account the background concentrations. For summertime simulations, they are simply estimated via the measurements at the more distant fixed stations; for wintertime simulations, the Lagrangian model Austal2000 (UBA 2014) is used to evaluate the contribution of domestic heating.

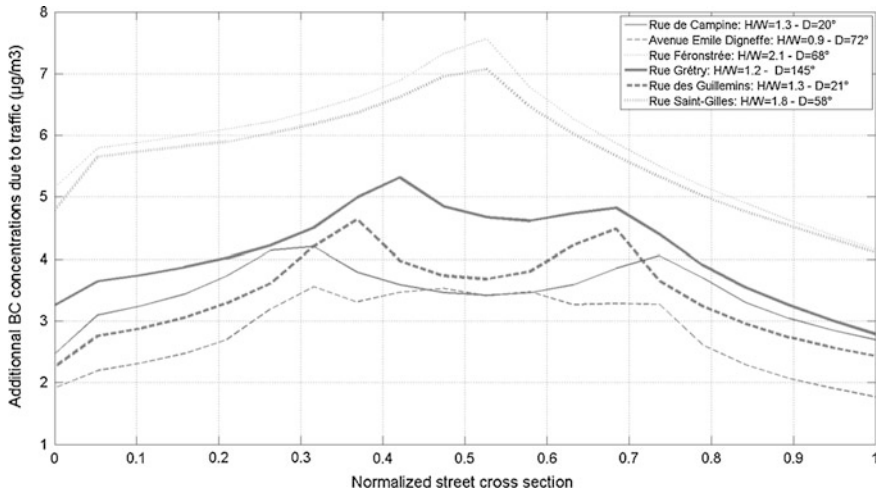

Fig. 65.2 Impact of the geometric characteristics on the BC concentrations

65.3 Results

At this early stage of the work, we only ran a limited number of test cases. The model, which already displayed good performance in terms of monthly averages and diurnal evolutions (Brasseur et al. 2014), is also able to reproduce convincingly time patterns in short-term simulations. For a given traffic pattern, we have simulated the impact of street geometry on the BC concentrations (see Fig. 64.2). First, one can observe a factor of about 2 between the levels from a street with a relatively high (~ 2) and a relatively low (~ 1) H/W ratio. Secondly, one can see that the broader multi-lane streets (also the ones with the lower H/W ratios) present a flatter cross-section profile than the one-way streets. Thirdly, for a similar aspect ratio the more perpendicular to the wind the street is, the higher the pollution. In our case, section 22, which is almost aligned with the southwestern winds, presents lower levels than section 11. From these first tests, one has also noticed—and this is no surprise—that the model displays an important sensitivity to traffic counts and emission rates.

References

Berkowicz R et al (2008) Evaluation and application of OSPM for traffic pollution assessment for a large number of street locations. Environ Model Softw. doi:10.1016/j.envsoft.2007.04.007

Brasseur O, Declerck P, Heene B, Vanderstraeten P (2014) Modelling Black Carbon concentrations in two busy street canyons in Brussels using CANSBC. Atmos Environ. doi:10.1016/j.atmosenv.2014.10.049

Lefebvre W, Vercauteren J, Schrooten L, Janssen S, Degraeuwe B, Maenhaut W, de Vlieger I, Vankerkom J, Cosemans G, Mensink C, Veldeman N, Deutsch F, Van Looy S, Peelaerts W, Lefebre F (2011) Validation of the MIMOSA-AURORA-IFDM model chain for policy support: modelling concentration of elemental carbon in Flanders. Atmos Environ. doi:10.1016/j.atmosenv.2011.08.033

Umwelt Bundesamt (German Federal Environmental Agency) (2014) Austal2000—program documentation of Version 2.6. http://www.austal2000.de. Accessed 16 Mar 2015

United States Environmental Protection Agency (2012) Report to congress on black carbon. http://www.epa.gov/blackcarbon/2012report/fullreport.pdf. Accessed 16 Mar 2015

World Health Organization Regional Office for Europe, (2012) Health effects of Black Carbon. http://www.epa.gov/blackcarbon/2012report/fullreport.pdf. Accessed 16 Mar 2015

Chapter 66
Exposure Assessment to High-Traffic Corridors in Bogota Using a Near-Road Air Quality Model

Jorge E. Pachón, Constanza Saavedra, María P. Pérez, Boris R. Galvis and Saravanan Arunachalam

Abstract Vehicular traffic in Bogota is one of the main causes of air pollution, therefore it is necessary to estimate concentration levels at which the population is exposed near roads. This work summarizes the implementation of the near-road air quality model R-LINE in Bogota. Emissions from vehicles were calculated for 12,725 road links (912 km of principal roads) and assigned to the model in ($g\ m^{-1}s^{-1}$) units. Meteorological information was obtained from the Bogota's Air Quality Monitoring Network (BAQMN) stations. Evaluation of model was performed by comparing modeling outputs against pollutant observations from the BAQMN. Results suggest a good model performance and potential to use the model to evaluate personal exposure and assess/develop emission reduction strategies for improving air quality in a large metropolitan area.

66.1 Introduction

Bogotá, Colombia, has experienced rapid economic growth in recent years, which has led to a deterioration of air quality from increased vehicle, industrial and commercial emissions. It is estimated that most of the emissions of NO_x, CO, CO_2, SO_2 and VOCs in the city are from mobile sources, whereas PM is almost equally emitted by mobile and point sources. However, mobile sources are ubiquitous in the city and contribute to air pollution in the Bogota metropolitan area. The local environmental authority in Bogota (SDA) is interested to test emission reduction strategies for mobile sources in main vehicle corridors and assess their impacts on

J.E. Pachón (✉) · C. Saavedra · M.P. Pérez · B.R. Galvis
Environmental Engineering Department, Universidad de La Salle, Bogotá, Colombia
e-mail: jpachon@unisalle.edu.co

S. Arunachalam
Institute for the Environment, University of North Carolina, Chapel Hill, NC, USA

D.G. Steyn and N. Chaumerliac (eds.), *Air Pollution Modeling and its Application XXIV*, Springer Proceedings in Complexity,
DOI 10.1007/978-3-319-24478-5_66

air quality and human exposure. Therefore, the application of a near-road air quality model such as R-LINE (Snyder et al. 2013) is desirable.

66.2 Methods

66.2.1 Emissions by Pollutant

The emissions used in the model were prepared using the information from the main road network in the city preforming an individual calculation for each of the 12,725 road links that add up to 912 km. Information on annual average daily traffic (AADT) was processed from 40 traffic monitoring points throughout the city. Emissions factors consisted of a compilation of previous work developed in the city from 2009 through 2014 (Rodríguez and Behrentz 2009; Peñaloza and Rojas 2010; SDA and UNAL 2013). Following a bottom-up approach, the emissions inventory was calculated using 66.1:

$$E_i = FE_{ij} * F_{jk} \tag{66.1}$$

Were E_i (g $m^{-1}s^{-1}$) is the total emission of pollutant *i*, FE_{ij} (g/m-veh) is the emission factor for pollutant *i* for vehicular category *j* and F_{jk} (veh/s) is the vehicle flux for the vehicular category *j* in the road network category *k*.

Once the emissions per link were calculated a text file (.txt) was generated with the beginning and ending coordinates of the main road links in UTM coordinate system using QGIS 2.4. This text file was used as source input to the model.

66.2.2 Receptor Selection

The receptors selected to estimate the concentration of pollutants and subsequently evaluate the model performance were located in the stations of the Bogota's Air Quality Monitoring Network (BAQMN). Although the monitoring equipment at each station has different height above ground, all the points were evaluated at the same elevation. The receptors were input in R-LINE in a text (.txt) file.

66.2.3 Meteorological Information

The meteorological pre-processor AERMET was implemented to estimate Monin-Obukhov length, surface friction velocity, mechanical and convective mixing generated height and PBL characteristics required for R-LINE and implemented through a surface (.sfc) file.

66.2.4 Model Execution and Evaluation

Once the input files (source, receptor, meteorological) were prepared, R-LINE was executed during two periods of fifteen days each during February and October 2012. Output concentrations were obtained at the selected receptors points and then the background concentration was added to compare against BAQMN records. Evaluation was performed for CO and NO_x.

66.3 Results

66.3.1 Emissions by Pollutants

PM emissions are mainly from heavy-duty diesel vehicles (buses and trucks). Passenger vehicles and motorcycles contribute to CO, CO_2, NO_x, SO_2 and VOCs and are the fastest growing fleet in the city. Spatial distribution of PM emissions in the city is highlighted in Fig. 66.1.

66.3.2 Receptor Selection

In total 12 receptors were evaluated, where the distances between the monitoring stations and nearest main roadway source ranged from 16 to 1615 m (Table 66.1).

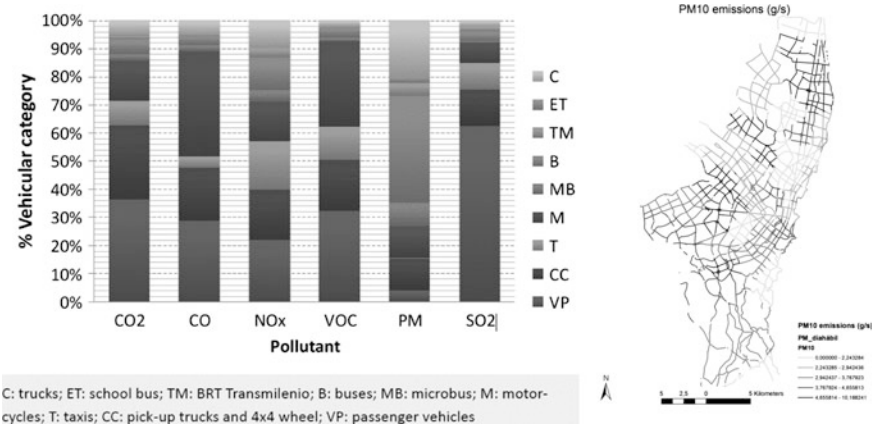

Fig. 66.1 Emission by pollutant and by vehicular category in Bogota (*left*) and spatial distribution of PM emissions (*right*)

Table 66.1 Receptor distance to nearby roads (m)

Receptor location	Distance to nearby roads (m)			
	Roads N	Roads S	Roads E	Roads W
1—Guaymaral	490,9	470,5	340,8	1.615,17
2—Kennedy	1.002,2	77,9	109,3	857,1
3—Tunal	43,9	681,6	48,2	119,5
4—San Cristóbal	333,3	230,6	454,9	503,6
5—Parque S.B.	342,6	359,5	722,3	442,5
6—Usaquén	185,6	859,8	175,4	256,9
7—Las Ferias	841,4	16,7	111,2	218,3
8—Fontibón	225,1	674,4	542,2	358,6
9—Puente Aranda	433,1	381,8	648,5	417,9
10—Suba	168,0	544,0	251,7	955,1
11—Carvajal	607,9	41,3	337,0	372,6
12—Sagrado Corazón	757,1	451,5	119,4	218,7

66.3.3 Meteorological Evaluation

The most important meteorological parameters are the Monin-Obhukov length, surface friction velocity and the height of mechanically-generated boundary layer.

66.3.4 Model Execution and Evaluation

The R-LINE model is able to reproduce the daily variability of CO and NO_x (Fig. 66.2) from the BAQMN records. Morning and afternoon rush hour peaks are visible in the plots with larger values in the AM due to characteristics of the PBL.

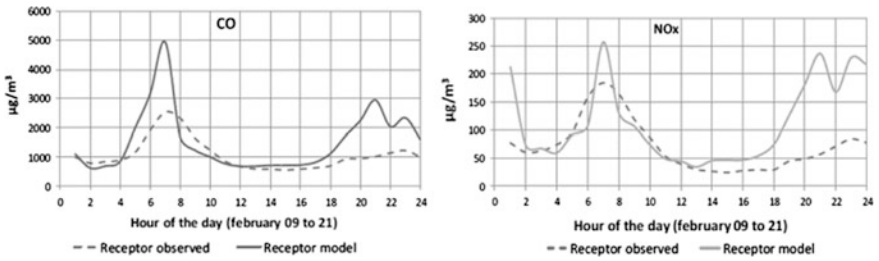

Fig. 66.2 Concentrations of CO and NO_x predicted by RLINE

66.4 Conclusions

R-LINE was implemented for the first time in Bogtoa, and evaluated against AQ records showing a good performance. Bogota has a complex terrain and challenging meteorology that greatly impact air quality model results. Further research is needed to improve AQ modeled fields used in this study.

Sources, receptors and meteorological input files were prepared with local information to reproduce AQ fields close to main roads and demonstrated the potential to use this modeling system to further assess/develop emissions reductions strategies for improving air quality in Bogota.

Acknowledgments This project was funded by Secretaria de Ambiente de Bogota SDA under Contract 1467/2013. The authors thank the School of Engineering and the Research Division at Universidad de la Salle, and the University of North Carolina for their support.

References

Peñaloza NE, Rojas NY (2010) Distribución espacial y temporal del inventario de emisiones provenientes de las fuentes móviles y fijas de la ciudad de Bogotá D.C. Universidad Nacional de colombia

Rodríguez PA, Behrentz E (2009) Actualización del inventario de emisiones de fuentes móviles para la ciudad de Bogotá a través de mediciones directas. Universidad de los Andes

SDA and UNAL (2013) Informe del Contrato Interadministrativo 013 de 2012. Bogotá D.C

Snyder MG, Venkatram A, Heist DK, Perry SG, Petersen WB, Isakov V (2013) RLINE: a line source dispersion model for near-surface releases. Atmos Environ 77:748–756

Chapter 67
Atmospheric Plume Modeling with a Three-Dimensional Refinement Adaptive Grid Method

M. Talat Odman, Yongtao Hu and Fernando Garcia-Menendez

Abstract We present a three-dimensional fully-adaptive grid algorithm for chemical transport models. The method is designed to refine vertical and horizontal resolution by dynamically concentrating grid nodes within a region of interest. Exceptionally high grid resolution can be achieved in Eulerian air quality models using the method. Here the algorithm's main operations are described. In addition, advection tests are used to demonstrate the algorithm's ability to better capture concentration gradients in atmospheric plumes.

67.1 Introduction

Adaptive grids can be used to enhance the multiscale capabilities of grid-based air quality models (Garcia-Menendez and Odman 2011). The technique is used to increase solution accuracy by dynamically refining the modeling grid in response to a model variable or parameter. Nearly all prior adaptive grid air quality modeling has been limited to horizontal refinement and vertical adaptation has not yet been explored in operational models. However, full three-dimensional adaptation would be valuable in simulations featuring concentrated plumes in the free troposphere, as well as plumes near inversions or the top of the boundary layer. Here a three-dimensional adaptive grid algorithm designed for chemical transport models is presented. The mesh-moving (r-refinement) method allows vertical and horizontal refinement to occur simultaneously yet retains a grid's original structure, enhancing compatibility with existing air quality models.

M. Talat Odman (✉) · Y. Hu
School of Civil and Environmental Engineering, Georgia Institute of Technology, Atlanta, GA 30332-0512, USA
e-mail: odman@gatech.edu

F. Garcia-Menendez
Center for Global Change Science, Massachusetts Institute of Technology, Boston, MA 02139-4307, USA

D.G. Steyn and N. Chaumerliac (eds.), *Air Pollution Modeling and its Application XXIV*, Springer Proceedings in Complexity,
DOI 10.1007/978-3-319-24478-5_67

67.2 Methodology

The three-dimensional adaptive grid method described extends on the two-dimensional algorithm presented in Srivastava et al. (2000) and implemented into the Community Multi-scale Air Quality (CMAQ) modeling system in Garcia-Menendez et al. (2010). Grid nodes are allowed to freely move across the three-dimensional modeling domain to regions calling for increased resolution. However, the total number of nodes and their connectivity remain constant throughout the simulation. Grid adaptation is achieved through an iterative process consisting of four key operations: (1) estimating a three-dimensional weight field; (2) grid node repositioning in relation to the weight field; (3) redistribution of concentration fields onto the newly adapted grid; and (4) examining grid convergence criteria to continue or terminate the process.

Node movement is driven by a three-dimensional weight field. A discrete approximation of the Laplacian is used to evaluate numerical error and assign adaptation weights to each cell. We estimate adaptation weights as $w = \mid \nabla^2 c \mid$, where the Laplacian, ∇^2, is approximated using a seven-point stencil derived from the gridded concentrations, c, of any atmospheric species. To conserve the nonuniform vertical layering typically used in air quality models, a minimum value that is a function of the cell's vertical layer is added onto each estimated weight. The new location of each node is determined from the weight and centroids of the eight cells that share the node. The formulation prevents nodes from crossing cell borders and moving into nonadjoining cells, therefore retaining grid connectivity. A local interpolation algorithm is used to estimate solution fields on the new grid after nodes are repositioned. A maximum displacement of 10 % for grid nodes with respect to initial cell spacing and an upper limit of 10 adaptation iterations were selected as convergence criteria to halt adaptation and advance the model solution in time using the repositioned grid. To use the model's original solution algorithms on an irregular grid, a local coordinate transformation from the model's original space (x, y, z) to a boundary-conforming curvilinear coordinate system (ξ, η, ζ) is applied. The transformation allows converting a nonuniform grid in physical space into a grid featuring unit dimensions in computational space (Fig. 67.1).

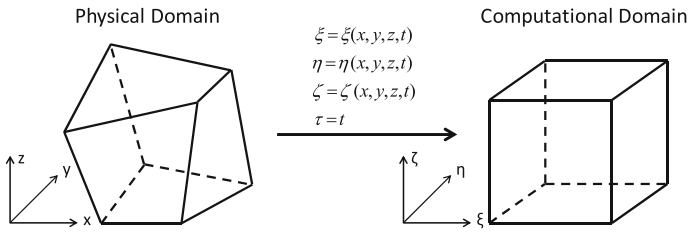

Fig. 67.1 Grid cell transformation from Cartesian (x, y, z, t) to boundary-conforming curvilinear coordinates (ξ, η, ζ, τ)

67.3 Results

To explore the three-dimensional algorithm's performance several tests were performed using CMAQ. In one test adaptation was used to simulate the advection of a pollutant puff under a three-dimensional wind field generated with the Weather Research and Forecasting Model (WRF). A fine particulate matter puff was instantaneously injected into a single grid cell 2500 m above the ground. Figure 67.2 illustrates the grid's response to the pollutant puff being advected across the domain. The puff is depicted as a three-dimensional iso-surface bounded by 10 μg m^{-3} concentration. Within the plots, intersecting grid planes along *X* and *Y* are shown at different times and include grid lines and predicted concentrations along each plane. Three-dimensional adaptation is apparent in the sequence: grid cells along the X and Y planes are initially regular and uniform; while the puff crosses the intersection, grid resolution is refined around the puff; as the puff moves beyond the plane intersection, refinement persists prior to returning to the original grid configuration. The adaptive grid performs as expected, simultaneously refining both horizontal and vertical resolution in response to pollutant concentrations.

A similar test was used to simulate the transport of a pollutant puff in a wind field and the results produced with fixed and adaptive grids were compared. Here an elemental carbon (EC) pollutant puff was instantaneously injected into a WRF-generated wind field approximately 2000 m above the ground. The grids initially featured 4 km horizontal grid resolution and 34 vertical layers. The pollutant was injected into a single grid cell approximately 400 m tall. The emissions instantaneously increased EC concentration within the cell to 1000 μg m^{-3}. Pollutant dispersion was simulated for several hours. No initial concentrations or additional emissions sources were included and only horizontal and vertical advection were modeled. In the simulations, the puff rapidly dispersed as it was

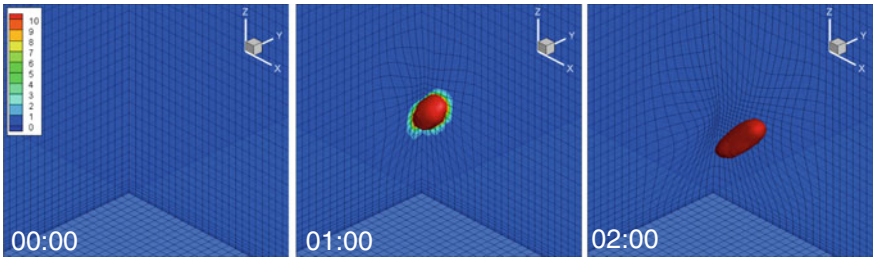

Fig. 67.2 Pollutant puff shown as a three-dimensional iso-surface bounded by $PM_{2.5}$ concentration equal to 10 μg m^{-3} crossing an intersection of *X* and *Y* grid planes. Grid lines and concentrations (μg m^{-3}) along planes are also included

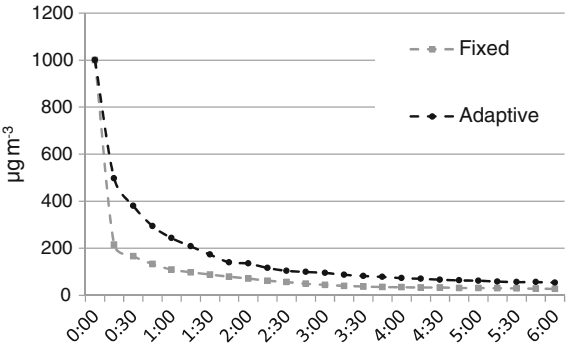

Fig. 67.3 Decrease in maximum EC concentration predicted by fixed and adaptive grid simulations for dispersion of an instantaneous pollutant puff

advected across the domain. Under the adaptive grid, the puff remains more compact. Figure 67.3 compares the decrease in maximum EC concentrations during the 6 h following the puff's release. In both simulations, the initial EC concentration falls abruptly after emissions are injected. However, the drop is attenuated by the adaptive grid. In addition, 6 h into the simulation the maximum concentration estimated in the adaptive grid simulation (54 µg m^{-3}) is twice as large as that predicted using a fixed grid (27 µg m^{-3}).

67.4 Conclusion

A three-dimensional adaptive grid algorithm applicable to Eulerian air quality models has been developed. The mesh-moving algorithm may be especially well-suited for chemical transport models developed under the assumption of structured grids. Additionally, a coordinate transformation can be used to apply solution algorithms designed exclusively for uniform or symmetrical grids on an irregular refined grid. The algorithm is the first adaptive grid method designed for regional-scale air quality models to simultaneously refine horizontal and vertical grid resolution. Three-dimensional refinement would improve simulations featuring concentrated plumes and may ultimately aid in eliminating subgrid scale treatments and embedded models, designed to capture small-scale processes relevant to atmospheric plumes, from regional-scale chemical transport models.

Acknowledgments This research was supported by the Strategic Environmental Research and Development Program (RC-1647), Joint Fire Science Program (08-1-6-04 & 12-3-01-6) and US EPA's Science to Achieve Results Program (RD83521701). The statements made here do not represent the official views of US EPA or any other funding agency.

References

Garcia-Menendez F, Odman MT (2011) Adaptive grid use in air quality modeling. Atmosphere 3:484–509

Garcia-Menendez F, Yano A, Hu Y, Odman MT (2010) An adaptive grid version of CMAQ for improving the resolution of plumes. Atmos Pollut Res 1:239–249

Srivastava RK, McRae DS, Odman MT (2000) An adaptive grid algorithm for air-quality modeling. J Comput Phys 165:437–472

Chapter 68
Modelling the Dispersion of Particle Numbers in Five European Cities

Jaakko Kukkonen, Matthias Karl, Menno P. Keuken, Hugo A.C. Denier van der Gon, Bruce R. Denby, Vikas Singh, John Douros, Astrid Manders, Zissis Samaras, Nicolas Moussiopoulos, Sander Jonkers, Mia Aarnio, Ari Karppinen, Leena Kangas, Susanne Lützenkirchen, Tuukka Petäjä and Ranjeet S. Sokhi

Abstract We have presented an overview of the modelling of particle number concentrations (PNC's) in five major European cities, namely Helsinki, Oslo, London, Rotterdam and Athens, in 2008. We have presented emission inventories of particle numbers both on urban and European scales, atmospheric dispersion modelling of PNC's in the cities and on a European scale, and evaluated the predicted results against available measured PNC's. The concentrations of PN in the selected cities were mostly influenced by the emissions from local vehicular traffic. However, harbor and airport activities can also have a substantial influence on the PN concentrations. There was a substantial variation in the performance of the models from site to site, when compared with the available measurements, both regarding the annual average concentrations, and the temporal correlation of the

J. Kukkonen (✉) · M. Aarnio · A. Karppinen · L. Kangas
Finnish Meteorological Institute, Helsinki, Finland
e-mail: jaakko.kukkonen@fmi.fi

M. Karl · B.R. Denby
Norwegian Institute for Air Research, Kjeller, Norway

M.P. Keuken · H.A.C.D. van der Gon · A. Manders · S. Jonkers
TNO, Netherlands Organization for Applied Research, Utrecht, The Netherlands

V. Singh · R.S. Sokhi
Centre for Atmospheric and Instrumentation Research (CAIR),
University of Hertfordshire, Hatfield, UK

J. Douros · Z. Samaras · N. Moussiopoulos
Aristotle University of Thessaloniki, Thessaloniki, Greece

S. Lützenkirchen
City of Oslo—Agency for Urban Environment, Oslo, Norway

T. Petäjä
University of Helsinki, Helsinki, Finland

D.G. Steyn and N. Chaumerliac (eds.), *Air Pollution Modeling and its Application XXIV*, Springer Proceedings in Complexity,
DOI 10.1007/978-3-319-24478-5_68

hourly time series. In the future, more accurate emission inventories and emission factors will be needed for the relevant source categories. More long-term measurements of PNC's will also be needed in various urban locations.

68.1 Introduction

While a large base of scientific information exists on particle mass, there are substantially less studies on particle number (PN). This is particularly true on modelling the dispersion of PN in city environments. The rapid transformation processes of PN after emissions in ambient air, such as condensation/evaporation, coagulation, dry deposition and dilution pose challenges for dispersion modelling, especially on an urban scale. Although much attention on the health effects of particulate matter has been focused on particle mass fractions, a number of studies are indicating that UFP's may have specific health effects.

The aim of this article is to present an overview of the modelling of PNC's on an urban scale in five major European cities. The target cities represent megacities, such as London (population of approximately 8.3 million) and Athens (we address here Greater Athens, 3.5 million), and other major cities, such as Helsinki Metropolitan Area, Oslo and Rotterdam (populations of 1.0, 0.6 and 0.6 million, respectively). The primary year used in the computations is 2008.

68.2 Modelling Methods

All of the urban emission and dispersion modelling systems were locally or nationally developed ones; these were different for each city. However, the regional background concentrations for all the urban scale modelling systems were computed with the same model, the LOTOS-EUROS chemical transport model (Schaap et al. 2008). The TRANSPHORM project emission database was used on an urban scale in three of the target cities.

Two urban modelling systems applied a meteorological pre-processing model, two others other meteorological models, and one modelling system applied directly measured data. All the models included the emissions from vehicular traffic, and some of the models included also the emissions from major and/or small-scale stationary sources and other sources. The shipping emissions were explicitly included in the computations of Oslo and Athens, and the importance of primary shipping emissions was separately evaluated for Helsinki. Measured PNC data was available in four of the cities, in three of these for a complete year; however, only at one or two measurement stations for each city. A new European-scale emission inventory was compiled for the EU-wide transport activities, supplemented by non-transport activities (Denier van der Gon et al. 2005).

68.3 Predicted Concentration Distributions in the Target Cities

The predicted annually averaged spatial concentration distributions in the target cities are presented in Fig. 68.1a–e. For Oslo, the roads with average daily traffic higher than 1000 vehicles per day are shown. In the case of Rotterdam, the following roads have been marked: the motorways around the city centre and major

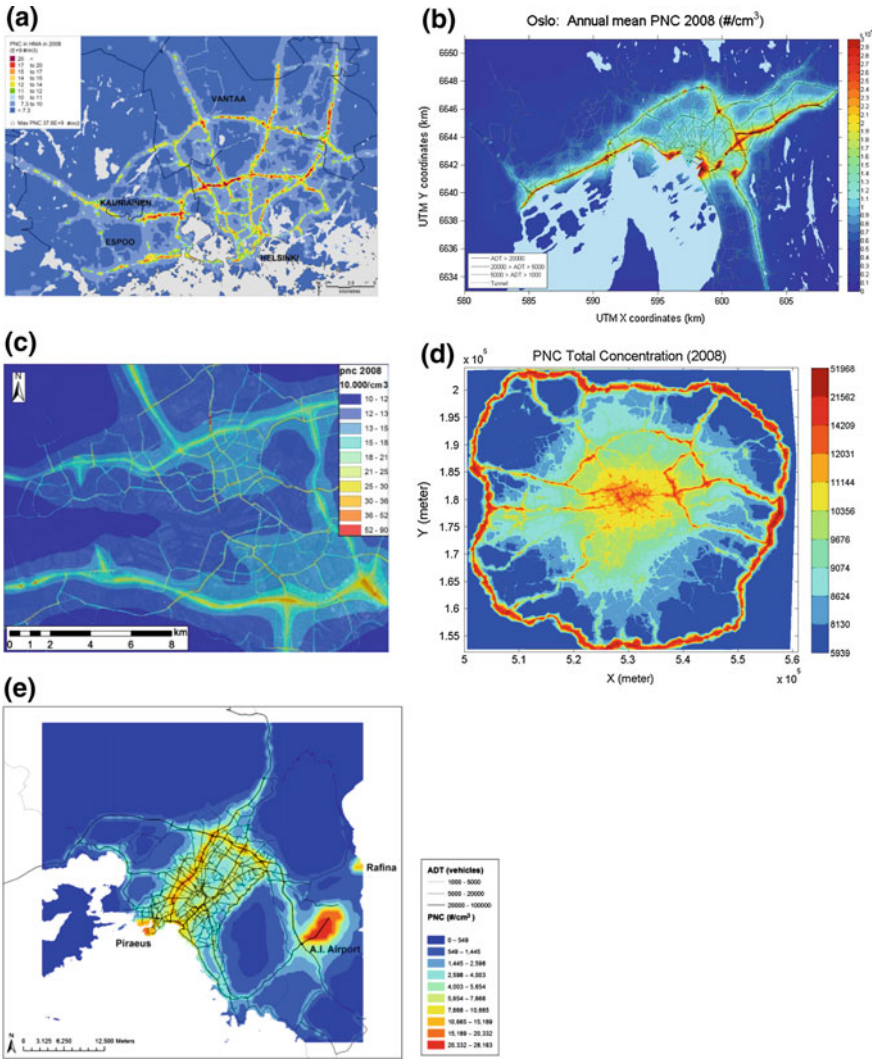

Fig. 68.1 **a–e** The predicted spatial PNC distributions in the target cities in 2008. ADT is the average daily traffic. The concentration unit is particles per cm^3

inner urban roads that have a traffic volume higher than 10 000 vehicles per day. For Athens, a few key locations have also been marked in the figure.

In all cities, the spatial distributions of PNC are dominated by road traffic emissions; the major traffic networks are clearly visible. Especially in Helsinki and London, the main ring roads surrounding the city are clearly visible. In Oslo, the PNC's are enhanced near road tunnel entrances and in the harbor region. In Athens, there are substantially elevated PNC's near the Athens International Airport and near the harbour regions (Piraeus and Rafina).

68.4 Conclusions

We have presented the results of the modelling of PNC's in five major European cities in 2008; such a compilation of PNC's for several cities has not previously been presented. Novel emission inventories of particle numbers have been compiled both on urban and European scales. The concentrations of PN in the selected cities were mostly influenced by the emissions from local vehicular traffic, and harbor and airport activities. There was a substantial variation in the performance of the models from site to site, when compared with the available measurements. The influence of aerosol processes on PNC's was studied on an urban scale in one of the cities (Oslo), and with the help of dedicated measurement campaigns.

Acknowledgments This work was mainly funded by EU Seventh Framework Programme—(ENV.2009.1.2.2.1) project TRANSPHORM.

References

Denier van der Gon HAC, Visschedijk A, van der Brugh H, Dröge R (2005) A high resolution European emission data base for the year 2005, a contribution to UBA—Projekt PAREST: particle reduction strategies, TNO report TNO-034-UT-2010-01895_RPT-ML, Utrecht, 2010b

Schaap M, Timmermans RMA, Roemer M, Boersen GAC, Builtjes PJH, Sauter FJ, Velders GJM, Beck JP (2008) The LOTOS-EUROS model: description, validation and latest developments. Int J Environ Pollut 32(2):270–290

Chapter 69
Development of a Screening Tool for Quick Environmental Assessment of Mobility Scenarios

Wouter Lefebvre, Bino Maiheu, Stijn Vranckx and Stijn Janssen

Abstract Large mobility projects, for example, construction of new highways, have attracted an increased interest from the public at large. Pressure groups and environmental activists often propose their own alternatives for the planned projects. The vast amount of scenarios that are proposed in this way lead to an enormous increase of work related to the environmental assessment. Therefore, a new screening tool is proposed that can serve as a first phase in the environmental assessment procedure for air pollution. The tool enables users to quickly estimate the impact of a scenario on local air quality. Only scenarios which show promising results in this screening tool are then to be discussed in the normal environmental assessment procedure which is much more time-consuming. There are several requirements in order to have a successful approach: the screening tool needs to be fast, it needs to provide results which are close to the detailed environmental assessment procedure and it needs to enable calculations for the major pollutants (NO_2, PM_{10}, EC/BC, …) including fast ozone chemistry. Such a screening tool is presented here. It determines annual average concentrations of the major pollutants (NO_2, PM_{10}, $PM_{2.5}$, EC, C_6H_6) in a short calculation time of only some 10 min on 1 CPU, compared to calculations of 2 days on 24 CPUs for the detailed assessment procedure. The speed-up is obtained by using lookup tables of pre-simulated situations, which are then combined into the large-scale scenario. For instance, the effect of a 100 m road segment from north to south with a unit emission strength is calculated beforehand. If such a segment occurs in the input, this result is then used with the emissions scaled according to need. The tool does not calculate absolute concentrations (therefore, a standard model is still used) but only differences between scenarios. For some scenarios both the screening tool and the regular assessment procedure have been applied and results are compared. Comparing for both methods the screening tool with the full model yields small biases (−0.0022–0.0075 $\mu g/m^3$), a small RMSE (0.02–0.21 $\mu g/m^3$), a high R^2 of (0.75–0.87) and a slope of the regression curve close to 1 (1.01–1.18), showing that for screening purposes the tool is well capable of making the cut between good and bad scenarios.

W. Lefebvre (✉) · B. Maiheu · S. Vranckx · S. Janssen
VITO, Boeretang 200, 2400 Mol, Belgium
e-mail: wouter.lefebvre@vito.be

D.G. Steyn and N. Chaumerliac (eds.), *Air Pollution Modeling and its Application XXIV*, Springer Proceedings in Complexity,
DOI 10.1007/978-3-319-24478-5_69

69.1 Introduction

Regional and city authorities are often coping with substantial delays in essential urban transport infrastructure developments, not seldom a direct result of public opposition. Pressure groups and environmental activists often propose their own alternatives for the planned projects. The vast amount of scenarios that are proposed in this way lead to an enormous increase of work related to the environmental assessment. Therefore, a new screening tool is proposed that can serve as a first phase in the environmental assessment procedure. Only scenarios which show promising results in this screening tool are then to be discussed in the normal environmental assessment procedure which is much more time-consuming.

There are several requirements in order to have a successful approach: the screening tool needs to be fast, it needs to provide results which are close to the detailed environmental assessment procedure and it needs to enable calculations for the major pollutants (NO_2, PM_{10}, EC/BC, …) including fast ozone chemistry.

69.2 The Screening Tool

69.2.1 Preparation

Before using the screening tool, a series of preliminary calculations should be performed. On the one hand, the base case scenario has to be simulated using the full and complex model chain (e.g. Lefebvre et al. 2013), as the screening tool will only provide differences between scenarios. On the other hand, a series of lookup tables with pre-simulated situations are made. For instance, the effect of a 100 m road segment from north to south with a unit strength is calculated and the effect of this road segment on the concentrations in its vicinity are stored in the lookup table. Similar calculations are performed for road segments at slightly different angles and at different heights (to represent bridges). In addition, if needed, series of point sources can be simulated beforehand too, in order to be able to apply them in the screening tool. In the table, only passive pollutants are stored, for instance for PM, only the primary fraction is simulated (the secondary fraction is ignored in the screening tool, as the pollution is formed at longer time and spatial scales than we wish to represent in the tool). Furthermore, in order to perform the NO_2-calculations, only NO_x-calculations are stored in the database and the transformation of NO_x to NO_2 is done in postprocessing.

69.2.2 The Screening Tool

The screening tool is fed with the line segments of the base case scenario and the scenario that one wants to screen. The line segments in both scenarios are split up in segments of 100 m long. The corresponding concentrations in the look-up tables are then combined upon a regular grid of 25 m resolution, while scaling the results with the ratio of the emissions of the road segment and the unit strength emission applied in calculating the look-up tables. The transformation from NO_x to NO_2 is done as in the Dutch law (Rbl 2007).

69.3 Results

The resulting concentration differences were calculated for two different scenarios, for two pollutants (NO_2 and EC), for a domain around the city of Antwerp, Belgium. The calculations using the standard model chain took about 2 days on 24 CPUs per scenario, while the calculation time with the screening tool took somewhat less than 10 min on 1 CPU. Both results were then interpolated to the same 50 × 50 m^2 resolution grid and point-wise compared. Differences larger than 10 µg/m^3 between the scenario and the base-case were ignored as they were only found close to tunnel exits (Fig. 69.1). The differences at these locations between the screening tool and the full model results were quite large, due to different model grids, leading to different interpolations and large interpolation errors in these large gradient areas. As can be seen in Table 69.1, the number of points on which this applies is very small, at maximum 0.06 % of the total number of points.

Comparing for both methods the screening tool with the full model yields small biases (−0.0022–0.0075 µg/m^3), a small RMSE (0.02–0.21 µg/m^3), a high R^2 of (0.75–0.87) and a slope of the regression curve close to 1 (1.01–1.18), showing that for screening purposes the tool is well capable of differentiating between scenarios with a positive and less positive air quality impact.

69.4 Conclusions

The presented methodology can be applied when a large range of mobility scenarios are proposed for a transport infrastructure development, raising the need for a first screening prior to a full assessment of the most promising scenarios. The validity of using a screening tool, and the development of such a tool, for making the cut between good and bad scenarios in impact assessment analyses has been demonstrated. The methodology can be implemented in the future for other air quality modelling application where the request for short computation times rules out the use of standard air quality models.

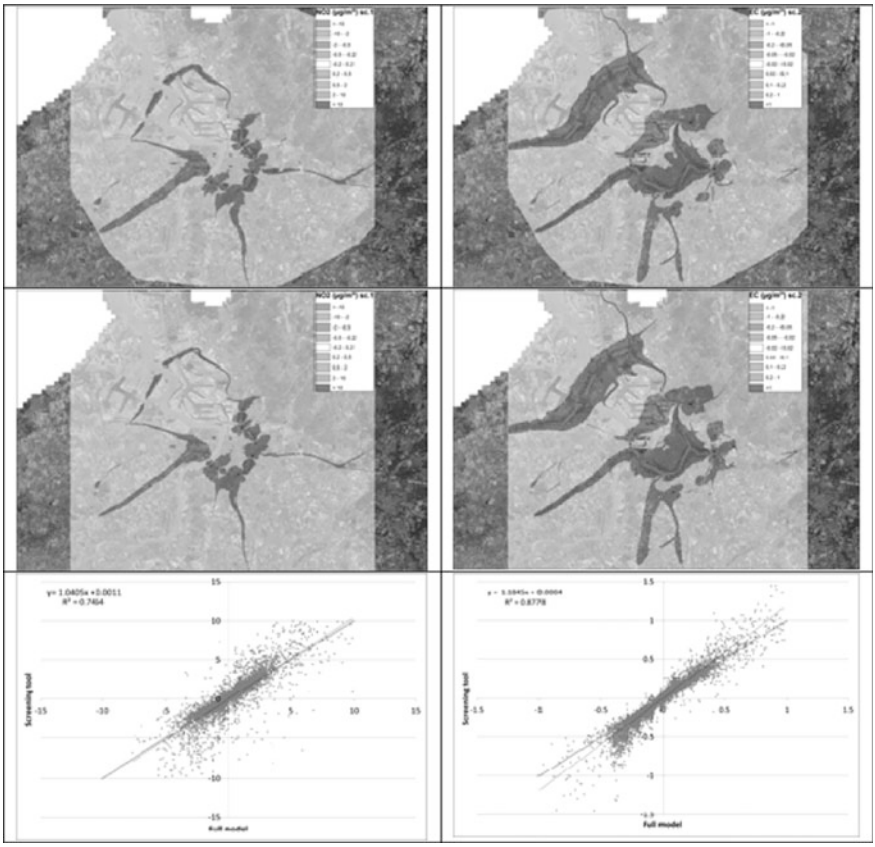

Fig. 69.1 The results of concentration differences with the respective base case for NO_2 for scenario 1 (*left column*) and for EC for scenario 2 (*right column*). *Upper part* full model. *Middle part* screening tool. *Lower part* scatter plot comparing both

Table 69.1 Validation parameters of the screening tool on the full model for concentration differences between each scenario and the base case

Scenario	Sc.1	Sc.1	Sc.2	Sc.2
Pollutant	NO_2	EC	NO_2	EC
Bias ($\mu g/m^3$)	−0.0022	−0.0001	0.0075	0.0001
RMSE ($\mu g/m^3$)	0.16	0.02	0.21	0.02
R^2	0.75	0.74	0.78	0.87
Slope	1.04	1.16	1.05	1.18
Number of points	386843 (99.94 %)	386903 (99.96 %)	386962 (99.98 %)	386918 (99.96 %)

References

Lefebvre W, Van Poppel M, Maiheu B, Janssen S, Dons E (2013) Evaluation of the RIO-IFDM-street canyon model chain. Atm Env 77:325–337

Regeling boordeling luchtkwaliteit (2007) Bijlage 2 Standaardrekenmethode 2, 3.a, http://wetten.overheid.nl/BWBR0022817/Bijlage2/geldigheidsdatum_29-01-2015

Chapter 70
Assessing Climate Change in Cities Using UrbClim

Hans Hooyberghs, Bino Maiheu, Koen De Ridder, Dirk Lauwaet and Wouter Lefebvre

Abstract The urban heat island effect, in which air temperatures tend to be higher in urban environments than in rural areas, is known to exacerbate the heat impact on population health. We introduce a new urban climate model, further referred to as UrbClim, designed to study the urban heat island effect at a spatial resolution of a few hundred metres. Despite its simplicity, UrbClim is found to be of the same level of accuracy as more sophisticated models, while also being much faster than high-resolution mesoscale climate models. Because of that, the model is well suited for long time integrations, in particular for applications in urban climate projections. In this contribution, we present temperature maps for London, including an assessment of the present-day climate, and projections for the future (2081–2100).

70.1 Introduction

There is increasing concern regarding the impact of global climate change on cities. Together with drought and flooding, extreme heat stress is perceived as a problem that may turn really bad if no action is taken (IPCC 2014). Indeed, climate projections indicate that extreme heat waves, as that occurring in 2003 in Europe, are expected to become more commonplace towards the end of the century (Meehl et al. 2004; Schär et al. 2004).

Cities experience an additional heat stress due the urban heat island (UHI) effect, in which air temperatures tend to be higher in urban environments than in rural areas. Moreover, during heat waves the urban heat island appears to increase (De Ridder et al. 2011; Li et al. 2013), and hence the heat-related impact on population health is exacerbated in urban areas. Including urban heat island effects in the

H. Hooyberghs (✉) · B. Maiheu · K. De Ridder · D. Lauwaet · W. Lefebvre
VITO, Flemish Institute for Technological Research, Urban Climate Team,
Boeretang 200, 2400 Mol, Belgium
e-mail: hans.hooyberghs@vito.be

D.G. Steyn and N. Chaumerliac (eds.), *Air Pollution Modeling and its Application XXIV*, Springer Proceedings in Complexity,
DOI 10.1007/978-3-319-24478-5_70

formulation of heat warnings and climate change adaptation plans is therefore essential and part of a sustainable urban development in general.

Yet, little or no information is available regarding future urban climate. Especially, climate projections at the scale of urban agglomerations are lacking, which is in part related to the computational constraints fine-scale climate models are facing. In order to remedy this, a new urban climate model (UrbClim) was developed. In this study, this new UrbClim model simulates the urban climate for a reference period (1986–2005) and a far future period (2081–2100) for eight cities under the strongest climate scenario of the IPCC (RCP8.5), by coupling it to the model output of eleven global climate models.

70.2 The UrbClim Model

An important difficulty often encountered with typical numerical climate models is the limited resolution and long integration time, making them difficult to use when studying urban and intra-urban variations especially in the context of climate change. In this contribution, we will present a new urban climate model, further referred to as UrbClim, designed to cover agglomeration-scale domains at a spatial resolution of a few hundred metres (De Ridder et al. 2014). The model scales large-scale weather conditions down to agglomeration-scale and computes the impact of urban development on the most important weather parameters, such as temperature and humidity. UrbClim is composed of a land surface scheme describing the physics of energy and water exchange between the soil and the atmosphere in the city, coupled to a 3D atmospheric boundary layer module. The atmospheric conditions far away from the city centre are fixed by meteorological input data, while local terrain and surface data influences the heat fluxes and evaporation within the urban boundaries. The primary output consists of hourly air temperature and apparent air temperature maps with a spatial resolution of 250 or 500 m.

Despite its simplicity, UrbClim is found to be of the same level of accuracy as more sophisticated models. The model has been subjected to exhaustive validation, and model results have been compared with hourly temperature measurements for, amongst other, London (UK), Bilbao (Spain) and Paris (France) (De Ridder et al. 2011, 2014b; Keramitsoglou et al. 2012). At the same time, the urban boundary layer climate model is faster than high-resolution mesoscale climate models by at least two orders of magnitude. Because of that, the model is well suited for long time integrations, in particular for applications in urban climate projections.

70.3 Urban Climate Projections

Within the EU RAMSES and NACLIM projects, urban climate projections have been set up for eight cities on three different continents (Almada/Lisbon, Antwerp, London, Bilbao, Berlin, New York, Rio De Janeiro and Skopje) (Hooyberghs et al. 2015). The methodology consists of a two-step process, in which at first the current urban climate in these cities is assessed, and only thereafter the climate projections are implemented.

To assess the current-day situation, the UrbClim model is coupled to ERA-Interim reanalysis data for the period 1986–2005. Since we are mainly interested in warm episodes, we make maps of the temperature during hot summer nights or days. As an example, in Fig. 70.1 we show the 95th percentile of the minimal temperature during the period 1986–2005, i.e. the temperature that is exceeded on average during four nights each year, for the city of Antwerp (Belgium). In this way, we identify the city districts which are, at present, most vulnerable to excess heat stress.

Furthermore, a coupling has been established between UrbClim and the output of global climate models, allowing the assessment of the urban heat island effects under future climate conditions. Within this study, we employed the business-as-usual RCP8.5 scenario of the IPCC and used the output of 11 global climate models to assess the climatic conditions in cities at the end of the current century. The coupling is described in detail in Lauwaet et al. (2015). Figure 70.2 compares the current and the future climate in London, by showing the 95th percentile of the minimal temperature for both the reference period (1986–2005) and

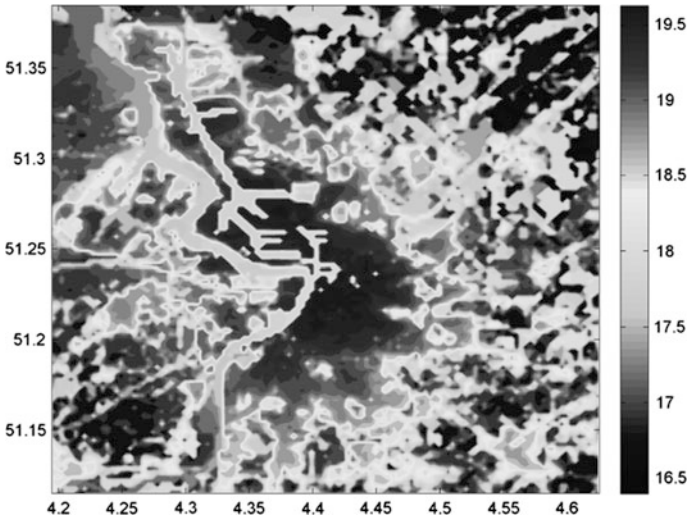

Fig. 70.1 95th percentile of the minimal temperature in Antwerp during the period 1986–2005. Higher temperatures are observed in the city centre (dark spots in the middle of the figure), while lower temperatures are observed in the rural areas (dark spots close to the edges of the figure)

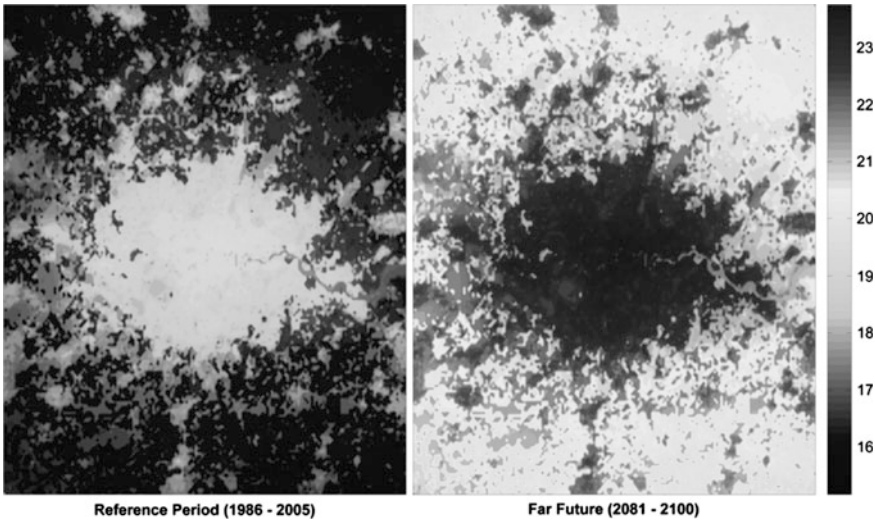

Fig. 70.2 95th percentile of the minimal temperature in London during the period 1986–2005 and during the period 2081–2100. Temperatures in the city centre are around 20 °C during the reference period and rise to 23 °C at the end of the 21th century

the far future (2081–2100). Clearly, there is a large temperature increase: future rural temperatures are comparable to current urban temperatures, while the future urban temperatures are unprecedented in London. On the other hand, the UHI-effect is almost the same in current and future conditions, and also the spatial pattern remains more or less unchanged, indicating that city districts more prone to urban heating in the present, are also expected to be more prone to heating in the future.

70.4 Conclusions

We have modelled and analysed the current and future urban climate in eight cities using the UrbClim model. By coupling the model to ERA-Interim reanalysis meteorological data, we identify city districts which are, at present, most prone to urban heating effects. The influence of global warming on the urban climate at the end of the current century (2081–2100) has been assessed by coupling the model to the output of 11 global climate models.

Acknowledgments The research leading to these results has received funding from the European Community's Seventh Framework Programme under Grant Agreement No. 308497 (Project RAMSES).

Questions and Answers

Questioner: K.H. Schlünzen

Question: How is the bias correction done? How do you ensure it is physically consistent for e.g. temperature and humidity?

Answer: The bias correction between the runs with ERA-Interim data and the runs with GCM-data for the reference period is described in Lauwaet et al. (2015). Hence, we refer the questioner to this article for a detailed description of the procedure and its influence on the data. Since only the temperature results of the GCM-runs are used, the bias correction only deals with the temperatures.

Questioner: J. Plein

Question: Please describe the model. What are the driving factors of the UHI-effect?

Answer: The model is described in De Ridder et al. (2015). Hence, we refer the questioner to this article full a detailed description. The main driving factor of the UHI-effect during the late afternoon and the evening is the release of heat that has been stored in the buildings and artificial structures in the city.

Questioner: D.G. Steyn

Question: What effect will changes in the UHI have on air quality?

Answer: There are numerous studies that focussed on the close link between air quality and climate change. Most of these studies, however, do not specifically look at the effects of urban climate. We think that the change in (urban) temperatures has a limited influence on air quality, but also that other elements of urban climate, like a reduced wind speed, have larger influences.

References

De Ridder K, Sarkar A (2011) The urban heat island intensity of Paris: a case study based on a simple urban surface parameterisation. Bound Layer Meteorol 138:511–520

De Ridder K, Acero JA, Lauwaet D, Lefebvre W, Maiheu B, Mendizabal M (2014b) Validation of agglomeration-scale climate projections, RAMSES project report D4.1

De Ridder K, Lauwaet D, Maiheu B (2015) UrbClim—a fast urban boundary layer climate model. Urban Clim 12:21–48

Hooyberghs H, de Ridder K, Lauwaet D, Lefebvre W, Maiheu B, de Ridder K, González-Aparicio I, Mendizabal M (2015) Agglomeration-scale urban climate and air quality projections, RAMSES project report D4.2

Keramitsoglou I, Daglis IA, Amiridis V, Chrysoulakis N, Ceriola G, Manunta P, Maiheu B, de Ridder K, Lauwaet D, Paganini M (2012) Evaluation of satellite-derived products for the characterization of the urban thermal environment. J Appl Remote Sens 6:061704

Lauwaet D, Hooyberghs H, Maiheu B, Lefebvre W, Driesen G, van Looy S, De Ridder K (2015) Detailed Urban Heat Island projections for cities worldwide: dynamical downscaling CMIP5 global climate models. Climate 3(2):391–415

Li D, Bou-Zeid E (2013) Synergistic interactions between urban heat Islands and heat waves: the impact in cities is larger than the sum of its parts. J Appl Meteorol Climatol 52:2051–2064

Meehl GA, Tebaldi C (2004) More intense, more frequent, and longer lasting heat waves in the 21st Century. Science 305:994–997

Schär C, Vidale PV, Lüthi D, Frei C, Häberli C, Liniger MA, Appenzeller C (2004) The role of increasing temperature variability in European summer heatwaves. Nature 427:332–336

Part VII
Model Assessment and Verification

Chapter 71
Is It Now Possible to Use Advanced Dispersion Modelling for Emergency Response? The Example of a CBRN-E Exercise in Paris

Patrick Armand, Christophe Duchenne and Luc Patryl

Abstract It is now generally admitted by the first responders and decision-makers that atmospheric dispersion modelling and health impact assessment can be of help in an emergency implying the release of Chemical, Biological, Radiological or Nuclear species, possibly preceded by an Explosion (CBRN-E). Such an event may be of accidental or malevolent origin and is likely to occur in a built industrial, harbour or urban environment. Thus, a modelling and decision-support tool should be able to deal with several types of threats and scenarios and give the possibility to run flow and dispersion models adapted to complex environments. Moreover, such a tool should produce in a limited amount of time (maximum of 15 min) 2D/3D simulation results directly useable by the civilian security to protect the population. These are precisely the specifications of CERES® CBRN-E software which is developed at CEA with the aim to transfer R&D advances to operational applications. This paper first comments on the advantages of advanced dispersion models. It presents the main features of CERES® and its use in connection with the civilian security by way of the "Toxic 2014" exercise done in "La Defense" district near Paris. Finally, the paper condenses the major lessons learnt from this exercise regarding the future development of CERES® as a decision-support tool.

71.1 Introduction and Context

CBRN-E threats have numerous expressions among which deleterious atmospheric releases originating from industrial accidents or malicious activities (sabotage, terrorist attack…) may lead to numerous civilian or military victims. Dispersion and health impact of potentially toxic gaseous or particulate species are thus a major concern shared by the rescue teams and public authorities. Among these emergency

P. Armand (✉) · C. Duchenne · L. Patryl
CEA, DAM, DIF, 91297 Arpajon, France
e-mail: patrick.armand@cea.fr

D.G. Steyn and N. Chaumerliac (eds.), *Air Pollution Modeling and its Application XXIV*, Springer Proceedings in Complexity,
DOI 10.1007/978-3-319-24478-5_71

actors, it is increasingly deemed that dispersion modelling is not only "of interest", but a main component of emergency preparedness and management.

During the last decades, physical modelling of air flow and dispersion at the meso-scale and local scale has experienced impressive improvements (see a discussion in Benamrane et al. (2013) about the evolution in the use of models from Chernobyl to Fukushima). The development of advanced 4D (3D space plus time) computational tools has been motivated (among other reasons) by the need of models adapted to complex environments like industrial sites or urban districts (definitely the places where CBRN-E events may arise). This development has been accompanied by the rapid and steep increase of the computational capabilities from standard laptops to multiple-cores parallelized machines making 3D meshed computations on very large domains now possible (Oldrini et al. 2013).

Moreover, a major trend is to integrate models in decision support systems. It is worth noticing that these systems are intended to satisfy the comparable needs of civilian security and military authorities to protect the population or the troops on the battlefield. To reinforce emergency response tools and foster good practices for using them, three conditions are to be met:

(i) The models must be deeply validated on an experimental basis;
(ii) The results must be available in a short time consistent with the crisis;
(iii) The results must adequately fit the needs of their end-users.

The French Atomic and alternative Energies Commission (CEA) has a long and strong experience in developing modelling and decision support systems adapted to CBRN-E threats (Armand et al. 2013a, b, 2014). This paper is organised in three parts and intended to illustrate this statement. Firstly, the urgent need of advanced dispersion models is exemplified; secondly, the main features of CERES® CBRN-E modelling system are presented; thirdly, a major civilian security exercise at "La Defense" district near Paris, implying the release of a toxic industrial chemical and using the capabilities of CERES® CBRN-E is described.

71.2 The Interest of Advanced Dispersion Models

While scientists are aware of the pros and cons of the various types of flow and dispersion models, emergency responders and decision makers are more receptive to practical considerations and illustrative examples. The following computations carried out at CEA have been shown as of the year 2007 to security services in France and certainly contributed to make the emergency responders now more and more take account of recent models capabilities.

Figure 71.1a, b represent the distribution of the inhalation dose (for an adult) resulting from the fictitious dispersion of a radionuclide (3 TBq of ^{137}Cs) in "La Bastille" district (in Paris). This event is hypothetically generated by the explosion

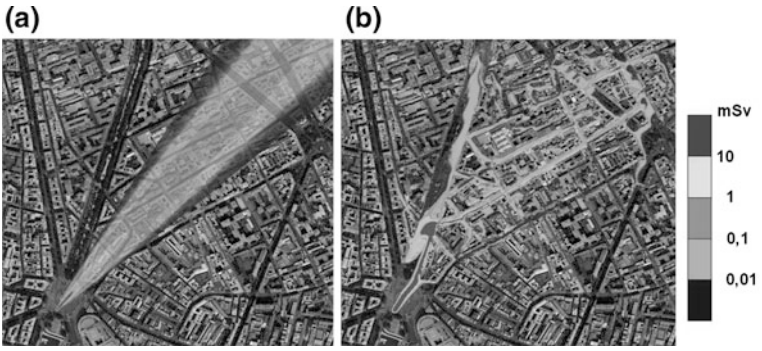

Fig. 71.1 Inhalation dose due to a release of ^{137}Cs at La Bastille in Paris as computed by a Gaussian model (**a**) and a diagnostic flow & LPDM model (**b**)

of a "dirty bomb". The radiological exposure is representative of the contaminant integrated concentration. The results are drawn in a horizontal section near the ground (where the population and first responders breathe). The 3D computations were done using two of the dispersion solvers implemented in CERES® CBRN-E (see the description of this tool in the next section), a Gaussian model in Fig. 71.1a and the combination of a diagnostic flow (influenced by the buildings) and a Lagrangian Particle Dispersion Model (LPDM) in Fig. 71.1b.

Indeed, the differences among the models are obvious. As expected, the angular sector impacted by the release is much larger and the contaminant distribution is channelled by the streets' network (which is not in line with the South-West wind) in the LPDM calculation compared to the Gaussian one. Not visible on the snap-shots, the travel time of the plume through the simulation domain (square of 1 km edge) and its residence time in the streets and courtyards are much longer as obtained from the LPDM. Thus, even if these results were not compared against measurements (what was done in other situations), the results issued by the LPDM are both more realistic and more relevant in this configuration than the Gaussian results. Moreover, it is essential to point out that (at least in the chosen meteorological conditions) the Gaussian model is not conservative: see the most affected zone in both cases and the avenue to the West which does not seem to be impacted by the contamination if the Gaussian model were trusted.

Last, the computational time of the Lagrangian model was no more than 5 min on a quad-core server (versus about 10 s for the Gaussian model), thus an acceptable duration for a much detailed prediction of the dispersion and exposure assessment of the release. This example could be supplemented by numerous ones evidencing the interest, if not the necessity, to switch to advanced flow and dispersion modelling.

71.3 CERES® CBRN-E as a Unified Modelling System

Since 2005, CEA has been mandated to coordinate and run the French inter-ministerial R&D program dedicated to CBRN-E threats. Modelling and simulation bring a transverse contribution to the topics included in this research program: prevention, detection, alert, intervention, mitigation… In this framework, CERES® CBRN-E (shortened CERES® in the follow-up of the paper) is a new operational modelling and decision-support system which is being developed in collaboration between CEA and academic research partners.

CERES® software is devoted to model the atmospheric dispersion of potentially hazardous materials and to assess their impact on both the environment and the human health. CERES® has a dual application as it can deal with the authorized emissions of industrial facilities (in routine operations) and the noxious releases resulting from moderate to serious accidents on industrial (nuclear or non-nuclear) sites, transport accidents, or any kind of malevolent activities. CERES® can be used for regulatory purpose safety studies and/or emergency preparedness and handling. When applied in an emergency, the software is committed to deliver operational results (like danger or counter-measures zones…) to decision-makers in less than 15 min whatever the situation, so that the modelling system is by design oriented towards the urgency response.

The main characteristics of CERES® are to be modular and flexible.

1. It deals with 3D dispersion computations at local or regional scale in natural or complex built environments (industrial sites or urban areas).
2. It handles various categories of threat agents (radionuclides, chemicals or biological pathogenic agents).
3. It allows a large panel of non-energetic or energetic scenarios (leakage from a tank or a pipe, evaporation from a pool, fire, explosion…) with simplified or advanced models to describe the source terms.
4. It includes a Gaussian puff model, an advanced urbanized Gaussian model and, farsighted and R&D oriented (see the next section), a LPDM using 3D diagnostic or prognostic models of the turbulent wind. Associated with the dispersion models, meteorological data are adaptive from basic data at one or more meteorological stations to vertical profiles or meso-scale forecasting.
5. It proposes endpoint models adapted to the consequences assessment of C, B or R-N agents on the population and first responders health.

It is worth noticing that CERES® is provided with data bases including terrain elevation, buildings data, physicochemical data, transfer coefficients through the soil and biota, radiological dose conversion coefficients, toxicological reference values, etc. The fate of the C, B or R-N agents in the atmosphere is taken into account: indeed, the radioactive decay chains, the chemical reactions if any, and the bio-agents degradation depending on the met conditions are considered.

CERES® results are disseminated in a tried and tested ergonomic graphical user interface and can be visualized in the Geographic Information System (GIS) of the

software or exported in formats adapted to other GIS, e.g. ArcGIS® as a support to intervention and decision processes. All the developments in CERES® have been validated using experimental wind tunnel and/or field data. Various applications have been carried out for realistic accidental and intentional releases (see some examples of them in Patryl et al. 2013a, b, 2014).

While CERES® was first aimed at the CEA own safety needs, its interest for more users was quickly identified. For more than 5 years, CERES® has been licensed to the French nuclear industry. More recently, it has been distributed to civilian security services for experimentation and feedback. In this context, the following section is devoted to the presentation of an innovative use of CERES® CBRN-E in the frame of a major civilian security exercise named "Toxic 2014".

71.4 "Toxic 2014" or How an Advanced Dispersion Model Has Been Applied to a Crisis Exercise?

End of 2013, a collaboration between CEA, Paris Fire Brigade, the public body in charge of the security of "La Defense" business district (located North-West of Paris) and the local public authorities (called "Prefecture" in France) was launched with the objective to evaluate the adequacy of the modelling and decision-support tools with the actual needs of the urgency actors. This common work included the organization of an exercise named "Toxic 2014" held on 22 May 2014 to test the new safety procedures plan of "La Defense" district in case of a toxic release.

The involvement of CEA in "Toxic 2014" exercise included two phases:

1. Contribution to the development of the toxic release scenario;
2. Contribution to the exercise by providing expertise and modelling regarding atmospheric dispersion and health impact assessment.

In the follow-up, the paper documents these two phases and the simulations that have been produced for the preparedness and response to the emergency.

71.5 Elaboration of the "Toxic 2014" Scenario

Proposal for scenarios—In September 2013, the CEA was mandated by the Prefecture to develop realistic scenarios taking account of a number of requests. For the release, chemicals should be preferred as a "dirty bomb" exercise had been carried out the year before. Meteorological conditions should be chosen in order to affect a large part of "La Defense". The danger zones should be quite large in order to simulate a serious event and to train the first-responders and decision-makers.

Considering these constraints, the CEA proposed several plausible CBRN-E events corresponding to either accidents or malevolent actions. In order to obtain a

large panel of situations, different weather situations, locations of the release, and toxic chemicals were presented. For each possible place of the release, realistic scenarios and operating modes were built up.

Final choice of the exercise scenario—In December 2013, a meeting was held gathering all actors implied in the future exercise (municipalities and Prefecture authorities, fire-fighters, police, health service, public transport operators…). The CEA presented the 3D modelling results of the fictitious toxic releases and their potential consequences on the population. On this basis, the scenario of the CBRN-E exercise was eventually decided.

The chosen event was a hazardous material transport accident consisting in a breach in a tanker-vehicle containing liquefied ammonia. This scenario was considered as appropriate by all the emergency actors as ammonia was a usual species compared to the other proposed chemicals. Moreover, it could be related to both an accidental event and a malevolent action (tanker hijacking). The location was taken on the circular boulevard, to the West of the district, quite aligned with the esplanade of "La Defense".

Then, the CEA was in charge to finalize the features of the scenario, choosing them as realistic as possible and obeying the following requests: to respect the protocols and intervention times of the fire-fighters and to make the Prefecture command center work in anticipation by considering a change in the wind direction before the end of the release, thus a variation of the impacted areas that could be predicted during the exercise.

Final inputs for "Toxic 2014"—In March 2014, the CEA presented the detailed conditions of the scenario to the animation teams of the exercise regarding the evolving meteorological conditions (wind blowing from North-West then from South-West), the source term ($\sim$10 tons of ammonia with 15 % instantaneously released and 85 % evaporating in 45 min), and the mock-up of the urban district (based on the topography, the explicit description of the buildings at 1 m resolution and the rugosity for the small elements not described in the obstacles files).

71.6 Participation in the "Toxic 2014" Exercise

Progress of the exercise—The exercise began on May 22, 2014 at 1 pm. The Prefecture was alerted at 1:15 pm to an accident which had occurred at "La Defense" and implied a tanker-vehicle. The command center and the security procedures plan were activated at 1:25 pm simultaneously with the information about the victims and the probable chemical risk.

The CEA involvement during the exercise was decided in agreement with the Prefecture and Paris Fire Brigade. The CEA was informed at 1:30 pm by the Fire Brigade and received the input (place of the event and estimate of the source term) necessary to launch dispersion calculations taking account of the buildings.

Results were obtained in about 20 min and sent by e-mails both to the Fire Brigade operational center (in Paris) and the command center of the Prefecture. Meanwhile, a CEA representative was called and requested to join the command center where this person arrived at 2:00 pm. The exercise implied many decisions relating to the population protection, the transport, the hospitals, the schools, etc. In the follow-up, only the main facts are discussed, when the modelling and the expertise were of help for the Fire Brigade and the Prefecture in decision-making.

Beginning of the exercise—The question of the population sheltering or evacuation arose very quickly. It was discussed by the representatives of the Fire Brigade, the medical emergency team, the Prefecture, and the expert using the map views of the complex dispersion pattern (see below) displayed on the computers terminals of the command center. At 2:03 pm, the Fire Brigade recommended the confinement of the skyscrapers rather than their evacuation. As a precaution, the Prefecture decided to confine the whole district waiting for a more accurate evaluation of the situation.

At 2:23 pm, the CEA debated the plume dispersion simulation results with the Fire Brigade. From a video of the dispersion, it was clear that at this time, the release was over and the plume diluted with concentrations below any adverse effects on the human health. Then, the map of the toxic load (presented after the plume crossed all the area) was used to delimitate the sanitary consequences zones (see below). While the most severe effects were limited to "La Defense" esplanade, it was probable that due to a low olfaction threshold, numerous people may have detected the abnormal presence of the ammonia in many localities at the North of the district. This was considered as very important information by the Fire Brigade.

First update of the situation—At 2:39 pm, the arrival of the Prefecture cabinet director triggered the first situation update. The representative of the Prefecture briefly described the event. The Fire Brigade indicated with a map the presence of the rescue teams on the spot and the measures taken to confine the population. The floor was given to the CEA which presented the simulation results: the plume dispersion on a video and the assessment of the health consequences (cumulated from the beginning of the release to the update time). The Fire Brigade explained that at this time, the risk did not evolve anymore and that a confirmation was expected from the field.

The medical emergency team updated the number of casualties and the hospitals taking care of them. It also stressed the saturation problem which could happen if people smelling the ammonia headed to the hospitals (see the olfaction area shown on the map below). The round table went on with all emergency actors: public transport, roads, schools, municipalities…

End of the first update of the situation—The first update continued with further examination of the measures taken in the municipalities at the North of the district. Firstly, it was noticed that buildings aeration could be advised as the plume had left this sector. Secondly, measurements in the field were now available and indicated that the concentration levels were very low consistently with the modelling.

Second update of the situation—At 4:00 pm, the arrival of the Prefect at the command center triggered the second situation update. A discussion was

under-taken about the nature of the event, the population protection measures, and the progressive annulment of the confinement measures. Once more, to supplement the Fire Brigade and the health emergency service reviews, the CEA was requested to present the ammonia dispersion simulation and the consequences assessment. The full termination of the security measures all over "La Defense" district was declared at 4:30 pm.

71.7 Numerical Simulations in the "Toxic 2014" Exercise

Computations details—The simulations were performed utilizing Parallel-Micro-SWIFT-SPRAY (PMSS) which is developed by ARIA Technologies, MOKILI, and the CEA (Tinarelli et al. 2013). PMSS is the third dispersion solver set up in CERES®. It is devoted to advanced modelling solutions testing. PMSS is nested by a meso-scale weather forecast system based on WRF and operated routinely by CEA (resolution of 5 km above France and 1.6 km over Paris region). Then, PMSS solves the 3D local urban flow and dispersion at a resolution of 1 to 5 meters.

In the case of "Toxic 2014", PMSS simulations were carried out on a domain with dimensions 4.2 km × 6.3 km and a horizontal mesh size of 3 meters. This large domain was sub-divided in 24 tiles of maximum 351 × 351 points. The vertical meshing had 37 levels from the ground to a height of 800 m. The flow was run with P-SWIFT on 25 processors and the dispersion was carried out with P-SPRAY using a maximum number of 64 processors. All the simulations were performed in less than 15 min (duration consistent with the emergency management).

Numerical results—Fig. 71.2a–d illustrates the plume propagation and the volumetric concentration near the ground at successive times after the triggering of the hypothetical release. The ammonia concentration field is presented with a gradual fading of the same color. It was decided not to adopt the most usual colors of the danger zones to avoid any confusion between the concentration and the health consequences when providing the Fire Brigade and Prefecture command centers with maps.

Assessment of the toxic loads—The health consequences of the ammonia release were evaluated on the basis of the reference toxicological values applicable in France (given by the INERIS for usual industrial gases) in case of an accidental acute exposure by inhalation. As the concentration was not time constant, the toxic load was evaluated at each point of the simulation domain and compared to the threshold values. The ammonia sensorial perception (SP) by olfaction was also considered. This is a concentration which is between 3.5 and 35 $mg.m^{-3}$ depending on the individuals, does not result in any health effect and it is not associated with a duration. The maximum concentration at each point was compared to the SP to identify the area where the olfaction threshold was exceeded.

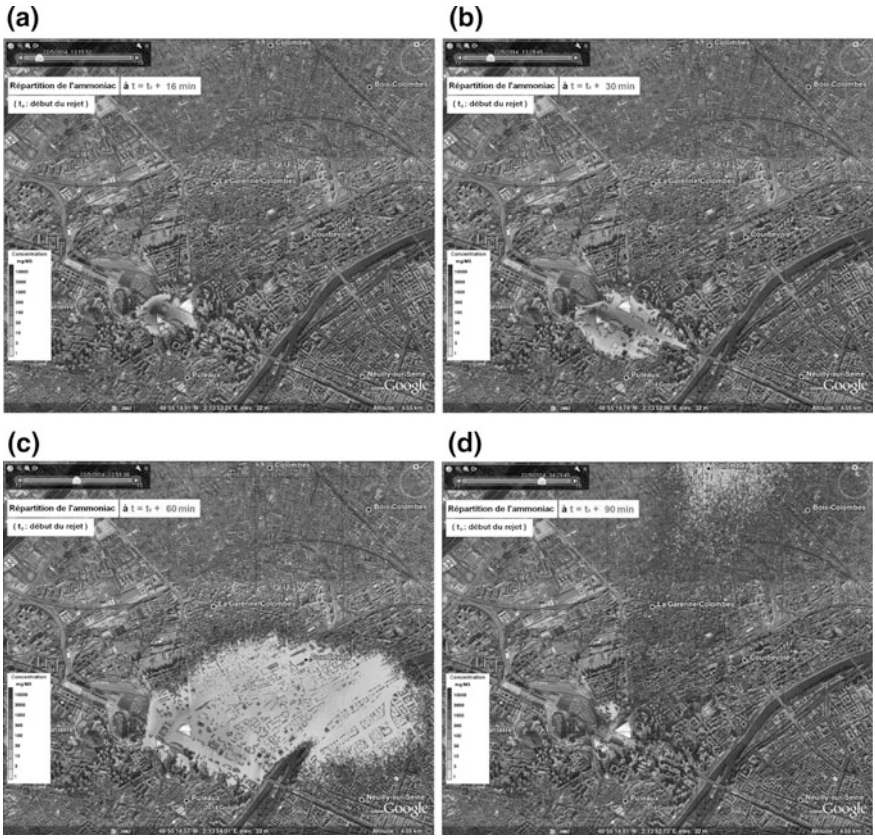

Fig. 71.2 Ammonia volumetric concentration distribution at t_0 + 16 min (**a**), t_0 + 30 min (**b**), t_0 + 60 min (**c**), and t_0 + 90 min (**d**)

Numerical results—Fig. 71.3a–d presents the danger zones associated with the health effects of the toxic plume at four times after the beginning of the release to show the extent of the perimeters with the ammonia plume progression. Using original colors, the zone of significant (5 %) lethal effects (SELS) was in dark red; the zone of first (1 %) lethal effects (SPEL) in red; the zone of irreversible health effects (SEI) in orange and the zone of reversible effects (SER) in yellow. The area in which ammonia smelling may have been detected by the population from the beginning of the release to the considered time frame was originally colored in blue. It covers a much extended territory around municipalities East and North of "La Defense". Here, the illustrations have been transformed to grey-scale figures.

ALOHA is the hazard software of the CAMEO modelling system developed by the US-EPA (Jones et al. 2013). It is widespread in the USA with the firemen and

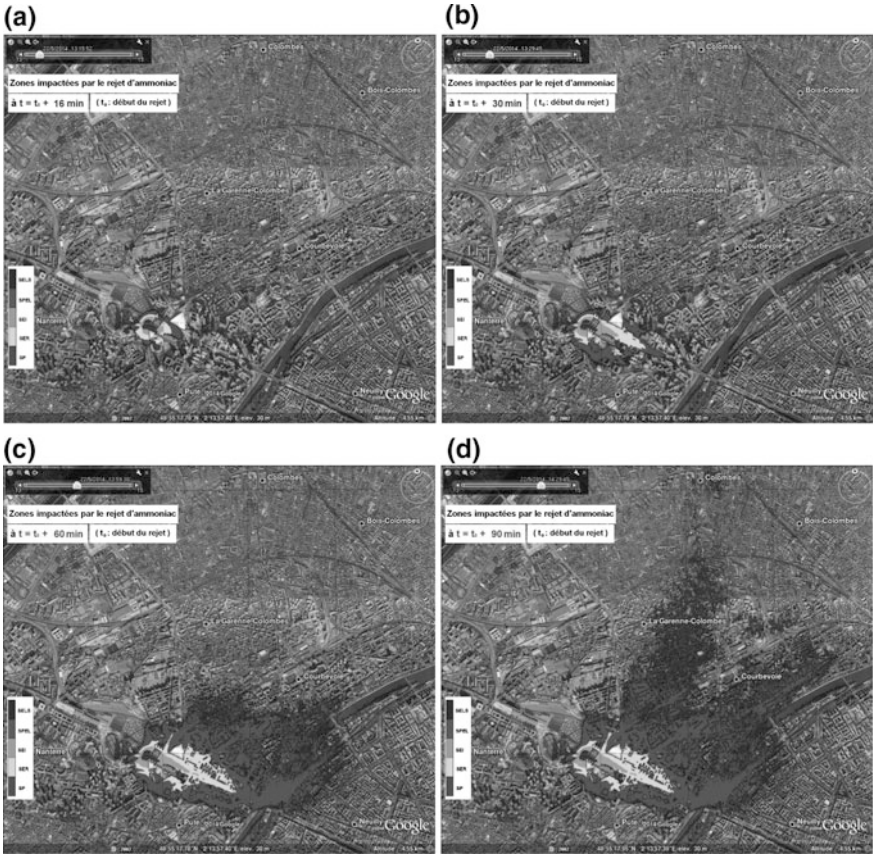

Fig. 71.3 Danger zones and olfactory perception area at t_0 + 16 min (**a**), t_0 + 30 min (**b**), t_0 + 60 min (**c**), and t_0 + 90 min (**d**)

also popular in France. Although this tool is equipped with a Gaussian dispersion model not taking account of the topography and buildings, it was used for a comparison with PMSS as shown in Fig. 71.4. Given the model limitations, ALOHA results (smooth ellipses) are quite consistent with PMSS results. The main difference is that the plume progression is contained by the buildings what can be predicted by PMSS and not by ALOHA. Moreover, 30 min after the beginning of the release, the wind changes its direction and the Eastern part of "La Defense" is not affected by the toxic plume. This is predicted by PMSS and cannot be foreseen by ALOHA. Finally, due to the complex met conditions and air flow in between the buildings, PMSS can predict contaminated areas upwind what ALOHA cannot do.

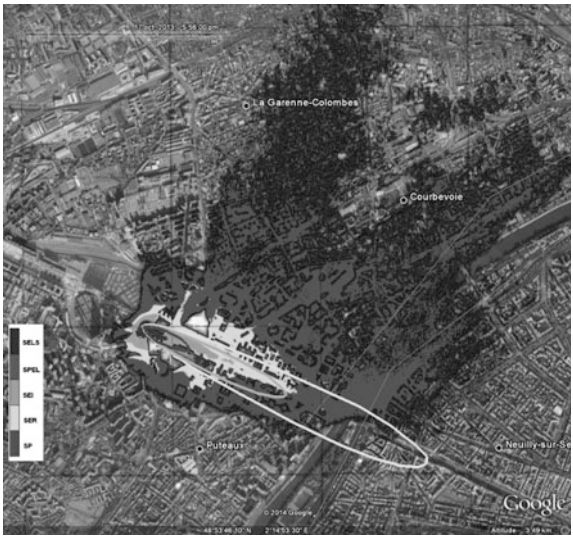

Fig. 71.4 Comparison of the danger zones predicted by PMSS and ALOHA

71.8 Conclusions and Perspectives

This paper addresses the promising capacities of dispersion modelling and health consequences assessment in the frame of emergency preparedness and response. First of all, the need of advanced 3D air flow and dispersion models in complex built environments (industrial sites or urban districts) is highlighted. Secondly, the main characteristics of CERES® CBRN-E are presented. CERES® is a recent computational tool developed by CEA and research partners. It is designed for emergency issues—both conventional accidents and emergent CBRN-E risks—resulting in releases of deleterious materials. Thirdly, the support brought by the advanced modelling in the course of an emergency is analyzed in the frame of a civilian security exercise implying a fictitious chemical release in "La Defense" district (near Paris). In this exercise called "Toxic 2014", flow and dispersion results taking account of both the buildings and the local meteorological conditions were produced in around 20 min at a metric resolution by PMSS embedded in CERES®. These results were post-processed to deduce the danger zones and transmitted to Paris fire-fighters and the local authorities (Prefecture).

"Toxic 2014" demonstrated two essential benefits in providing simulation results and expertise in the course of a deleterious atmospheric release.

1. The results are relevant to enhance a common understanding of the space-and-time distribution of the species what helps in making decisions and taking adapted measures for the population protection.
2. The results may be used to foster the communication to the authorities and all emergency actors what helps in generating a shared representation of the situation and an optimal coordination of the command center.

The main lesson was the synergy between the rescue teams' first actions which are irreplaceable for short and medium duration releases and the simulations done to diagnose the situation and anticipate its evolution. Even if the performance in real life would be diminished as it is uneasy to determine the source term, the early visualization of the dispersion pattern and plume is undoubtedly of interest to support the response first phase. Another lesson was the importance to share the modelling results between the security organization services even if their missions and time responses differ. For example, simulation results were transmitted to the French operational inter-ministerial emergency management center which was not concerned by "Toxic 2014" exercise but expressed its interest for the CEA results and integrated them directly in its Geographical Information System (GIS).

Some other aspects of "Toxic 2014" feedback are summarized hereafter.

Concerning the scenario elaboration, the key points to keep in mind are:

1. The better knowledge between the experts in dispersion modelling and the civilian security services through preparatory meetings and exchanges;
2. The evaluation of a full panel of malicious CBRN-E events hypothetically targeting "La Defense" and a much better apprehension of the resulting human and organizational impact (to our knowledge, this was a "premiere" in terms of CBRN-E risk analysis for a business district);
3. The development of a realistic scenario, technically more precise than usual present practices (this relevant release scenario allowed the involved services to work in-depth the time sequence for this table top exercise).

Concerning the in-situ participation, the key points to keep in mind are:

1. The relevance of the modelling which was effectively utilized by the services in charge of the population protection. The simulation results were helpful to identify the dispersion processes in the built environment, adapt the first actions of the rescue teams and anticipate the event follow-up;
2. The interest of the static and dynamic presentation of the results: the CEA maps were used all along the exercise for communication purpose and to help in sharing a collective view during the situation updates;
3. The interest of this experience for CEA to further improve and adapt the results provided by the computational tools to better fit the needs and missions of the civilian security organization.

In the past few years, R&D performed at CEA in the field of atmospheric dispersion and health impact assessment has not only focused on the physical modelling, but also encompassed the decision-support tools adequacy with the organization and missions of the civilian security. It increasingly seems to us that this approach is essential to promote the usage of scientific 3D models inside of operational computational tools accepted by practioners.

Questions and Answers

Questioner: A. Manor

Question: Non-expert end-users have a tendency to take the model's results as "the truth". However, this is completely untrue. The models have significant uncertainties. Can you comment about this, please?

Answer: When modeling results are provided (especially in emergency), they have to be explained and commented on by a technical "expert". It is the responsibility of the modeler not to communicate his or her results if he or she is not confident in them. Quantification of the uncertainties is a very active current field of research. It could be a benefit to give results assorted with an interval of confidence, but only if the modeler is able to present them in a way they can be easily understood and utilized by practitioners. This will be a further step in the dissemination of modeling results.

Questioner: S. Galmarini

Question: My comment is exactly the contrary. Sometimes, decision makers do not want to use modeling results. How to deal with this?

Answer: Both attitudes of an excessive trust or mistrust can be observed among the practitioners facing modeling results. From my experience, better and closer relationships with first responders and decision makers should favor a rational use of modeling for emergency preparedness and response. In this field, education and training are essential as a mutual respect of the expertise held respectively by modelers and by practitioners.

References

Armand P, Duchenne C, Benamrane Y, Libeau C, Le Nouëne T, Brill F (2013a) Meteorological forecast and dispersion of noxious agents in the urban environment—application of a modelling chain in real-time to a fictitious event in Paris city. In: Proceedings of the Harmo'15 conference, Madrid, Spain, pp 724–728, 6–9 May 2013a

Armand P, Patryl L, Lamaison G, Soulhac L, Deguillaume L, Chaumerliac N (2013b) CERES® CBRN—a unified modelling and decision support system to assess the dispersal and health impact of hazardous releases in urban or open-field environments. In: Proceedings of the Harmo'15 conference, Madrid, Spain, pp 172–177, 6–9 May 2013b

Armand P, Duchenne C, Bouquot E (2014) Atmospheric dispersion modelling and health impact assessment in the framework of a CBRN-E exercise in a complex urban configuration. In: Proceedings of the Harmo'16 conference, Varna, Bulgaria, 8–11 Sept 2014

Benamrane Y, Wybo J-L, Armand P (2013) Chernobyl and Fukushima nuclear accidents: What has changed in the use of atmospheric dispersion modeling? J Environ Radioact 126 (2013):239–252

Jones R, Lehr W, Simecek-Beatty D, Reynolds RM (2013) ALOHA® (Areal Locations of Hazardous Atmospheres) 5.4.4 technical documentation. In: NOAA technical memorandum NOS OR&R 43, November 2013

Oldrini O, Nibart M, Armand P, Olry C, Moussafir J, Albergel A (2013) Multi-scale build-up area integration in Parallel SWIFT. In: Proceedings of the Harmo'15 conference, Madrid, Spain, pp 485–489, 6–9 May 2013

Patryl L, Duchenne C, Armand P, Soulhac L, Lamaison G (2013a) Validation of the urban modelling in CERES® CBRN by comparison with a Lagrangian code for complex cases. In: Proceedings of the NATO/SPS international technical meeting on air pollution modelling and its application, ITM 2013, Miami, Florida, USA, 26–30 Aug 2013a

Patryl L, Long Y, Deguillaume L, Armand P, Chaumerliac N (2013b) Improvements of the chemical reactivity module in CERES® CBRN software and sensitivity study for various complex cases. In: Proceedings of the NATO/SPS international technical meeting on air pollution modelling and its application, ITM 2013, Miami, Florida, USA, 26–30 Aug 2013b

Patryl E, Lapebie SH, Armand P (2014) New capabilities of CERES® CBRN-E decision support tool in the fields of explosion modelling and source term estimation. In: Proceedings of the Harmo'16 conference, Varna, Bulgaria, 8–11 Sept 2014

Tinarelli G, Mortarini L, Trini-Castelli S, Carlino G, Moussafir J, Olry C, Armand P, Anfossi D (2013) Review and validation of Micro-SPRAY, a Lagrangian particle model of turbulent dispersion. In: Lagrangian modeling of the atmosphere, geophysical monograph, Vol. 200, pp. 311–327. AGU, May 2013

Chapter 72
Typical Performances of Mesoscale Meteorology Models

K. Heinke Schlünzen, Kristina Conrady and Christopher Purr

Abstract Reliable meteorological model results are one pre-condition for a good air quality simulation. The achievable quality of the meteorological information determines how accurate a concentration simulation can be. Many meteorological services as well as research institutions perform model evaluations on a routine basis, but the outcomes are not always published in refereed journals and little is known on typical model performances. This paper summarizes results of quantitative model evaluations that were published in refereed journals by statistically analyzing the published values for *bias*, root mean square error, *rmse,* as well as correlation coefficient, *r*. The 50 percentile of the quality measures *rmse* and *r* is used as threshold to derive typical performances. For *r* the 50 percentile is 0.47, 0.62, 0.89 and 0.87 for wind direction, wind speed, temperature and specific humidity, respectively. While *bias* values are small compared to their average values, *rmse* values are large.

72.1 Introduction

Mesoscale models for concentration and air quality simulation, hereafter referred to as AQ simulation, solve the Reynolds-averaged equations. Thus, besides advection also vertical and horizontal diffusion have a relevant impact on pollution dispersion, and on the pollutant's mixing ratios and thereby on chemical reactions. Furthermore, "…. photochemical reactions increase with increasing radiation. Some aerosol reactions are accelerated in a humid atmosphere. Thus, for a reliable AQ

K.H. Schlünzen (✉) · K. Conrady · C. Purr
Meteorological Institute, CEN, University of Hamburg, Hamburg, Germany
e-mail: heinke.schluenzen@uni-hamburg.de

Present Address:
K. Conrady
Department of Earth Sciences, Uppsala University, Uppsala, Sweden

D.G. Steyn and N. Chaumerliac (eds.), *Air Pollution Modeling and its Application XXIV*, Springer Proceedings in Complexity,
DOI 10.1007/978-3-319-24478-5_72

simulation with an atmospheric dispersion model, reliable meteorological data are necessary" (Schlünzen 2002). The achievable quality of a meteorology simulation considerably determines how good an AQ simulation can become. Even though a reliable AQ simulation depends on many parameters, the meteorological values are among the (most) relevant drivers.

It can be expected that model performances considerably differ for different meteorological situations. However, it is not easy to decide, if the results of a specific model evaluation are typical or exceptional with respect to the received model performance. Therefore, the knowledge on the range of typical model performances is relevant not only if meteorological data are used in the frame of AQ simulations, but also if meteorology simulations are in the sole focus of the model user. Meteorological services as well as research institutions evaluate results of meteorological models on a routine basis. However, the evaluations are not summarized in a statistical way themselves. To get an idea of typical model performances, a literature survey was performed by Conrady (2010), starting with publications of the year 2000. Her survey included mostly evaluations of wind, temperature and humidity; Purr (2013) added evaluations of atmospheric boundary layer heights.

In the present paper evaluations are included that were published in refereed journals in year 2000 and thereafter; 80 journal articles were analyzed. A full citation list is not given here but can be found in Schlünzen et al. (2016). The publications were selected with focus on those that summarize evaluations of several models or of several model set-ups for one and the same case, focusing on surface measurements. Some single model evaluations were added to broaden the variety of models and cases considered to determine typical model performances. Therefore, for some meteorological parameters more than 80 evaluations are available for a specific quality measure. However, for some quality measures and/or meteorological parameters only very few published evaluations were found. The analyses therefore focus on those meteorological parameters and quality measures for which at least 25 quantitative evaluations can be included (Sect. 72.2). The results for the typical model performances are given in Sect. 72.3 and conclusions drawn in Sect. 72.4.

72.2 Analyses Method

A diagnostic evaluation (Dennis et al. 2010) of an AQ simulation should aim at evaluating processes to be right for the right reason. For AQ simulations this would mean to evaluate the relevant meteorological processes as well. As a proxy for these, the most relevant meteorological parameters are taken here. Based on expert voting, Schlünzen and Sokhi (2008) suggest the following order of meteorological parameters with respect to their relevance for AQ simulations: atmospheric boundary layer height (ABL height), wind direction, atmospheric stability, short

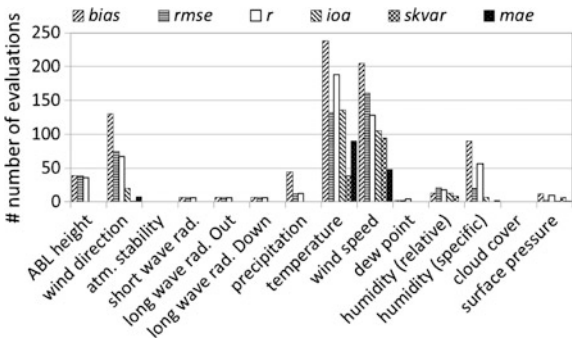

Fig. 72.1 Number of evaluations per quality measure *bias*, *rmse*, *r*, *ioa*, *skvar*, *mae* (meaning see text) for the different meteorological parameters

wave radiation, precipitation, cloud cover, temperature,[1] wind speed, dew point temperature/relative humidity/specific humidity, mean sea level pressure. The evaluation survey performed has shown that the most relevant meteorological parameters, like ABL height, atmospheric stability or precipitation, are not the ones most frequently evaluated (Fig. 72.1). Most evaluations were found for temperature and wind speed. This is resulting from the typical use of meteorology model results: mostly they are needed for weather forecast (NWP), and evaluations are done for that purpose. For NWP temperature and wind speed are very relevant parameter, while ABL height is of little interest to the normal NWP customer. Furthermore, data on temperature and wind speed are more easily available than those for vertical mixing or ABL height. For ABL height 36–39 evaluations were found, but they are based on two publications only (Lemonsu et al. 2006; Vautard et al. 2012). This needs to be considered when drawing conclusions on results for the typical performance of models simulating ABL heights.

Wind direction is frequently evaluated. Wind direction is of relevance for NWP and for AQ simulations. Different measures for humidity are typically evaluated, but relative humidity is rarely chosen. This is disadvantageous for AQ simulations, since many chemical reactions depend on relative humidity. Specific humidity and mixing ratio are more frequently evaluated. They are analyzed together here since their values are similar for surface measurements.

Precipitation is also a relevant meteorological parameter for AQ simulations, but not often found in the selected evaluations. One reason is the quality measures used for evaluation of precipitation, which are quantiles with miss/success rates. Since the categorization is not harmonized, it is very difficult to give a summary of typical model performances as intended in the present paper. Furthermore, even though sufficient precipitation data are available, they have a low spatial representativeness.

[1]Temperature was originally rated least relevant; however, since many chemical reactions and biogenic emissions depend on temperature, it is rated to be more relevant in this paper.

To overcome this, long sampling times of measurements and model results would be required (Bohnenstengel et al. 2011).

These analyses focus on the quality measures correlation coefficient *r*, *bias* and root mean square error, *rmse*, because these quality measures turned out to be most frequently used in the literature (Fig. 72.1). Index of agreement (*ioa*), skill variance (*skvar*) and mean absolute error (*mae*) are all used less and are not considered here.

Each evaluation results in a specific quality value Q_i, where index *i* refers to the different evaluations. *N* evaluation results are used to determine typical model performances. For each of the quality measures several percentiles are calculated per meteorological parameter, where *Px* is the value, below which *x*% of the Q_i lie. *P25* is the value for which 25 % of the Q_i are below or equal to *P25,* and *P75* describes the value for which 25 % of the Q_i are higher than *P75* (75 % are below or equal *P75*). *P50* describes the *median*; it is chosen to characterizes the typical model performance, if a quality measure has only positive values, e.g. correlation coefficient *r*, or root mean square error *rmse*. For *bias* positive and negative values can occur. Again, 50 % of the evaluation results are chosen to be typical, which determines the range between *P25* and *P75*. All percentile values are calculated using Microsoft Excel, Version 14.0.

72.3 Performance of Models for the Different Meteorological Parameters

Of large relevance for a realistic simulation of pollutant concentrations is the vertical mixing and, as a quality measure for it, the height of the atmospheric boundary layer (ABL). If pollutants are trapped in the night-time residual layer above the ABL they can be mixed into the ABL at nighttime, e.g. above still heated urban areas. These entrained pollutants may considerably impact near-surface concentrations (Zhang and Rao 1999). The height of the ABL has a very pronounced diurnal cycle; high correlation coefficients should be expected. A value of $r = 0.58$ (*P50*) is small for this (Table 72.1). The relative uncertain simulation of the ABL height is reflected in much larger values for *rmse* compared to *bias*. In addition, the *bias* is large compared to average ABL heights: 50 % of the model results lie between -287 m (*P25*) and 26 m (*P75)*. Supported by *P50*, a majority of the models underestimates ABL heights. If the underestimation is a daytime or nighttime feature cannot be derived from the present analyses. However, assuming the correct ABL height would be (on average) underestimated by 126 m for an average boundary layer height of 800 m, the concentrations resulting from surface emitters would be overestimated by 19 % in the model compared to those concentrations that were calculated with the correct ABL height. This error is non-negligible for AQ simulations. It needs to be kept in mind that only two publications and very few evaluation approaches were considered here. Furthermore, the ABL height is difficult to determine not only from model results but also from measurements.

Table 72.1 Typical performances of mesoscale meteorological models for parameters given in the Table in order of priority

Meteorological parameter	*r*		*bias*				*rmse*	
	#	*P50*	#	*P25*	*P75*	*P50*	#	*P50*
ABL height	36	0.58	39	−287 m	+26 m	−126 m	39	403 m
Wind direction	67	0.47	130	−13°	+10°	−1°	75	71°
Atm. stability	<25	–	<25	–	–	–	<25	–
Atm. radiation	<25	–	<25	–	–	–	<25	–
Precipitation amount	<25	–	44	−1 mm	+28 mm	+8 mm	<25	–
Temperature	188	0.89	238	−1.1 K	+0.3 K	−0.3 K	132	2.5 K
Wind speed	128	0.62	205	−0.2 m/s	+0.7 m/s	0.1 m/s	161	1.8 m/s
Dew point t.	<25	–	<25	–	–	–	<25	–
rel. humidity	<25	–	<25	–	–	–	<25	–
spe. humidity	56	0.87	90	−0.2 g/kg	+0.3 g/kg	0.0 g/kg	<25	–

The threshold determining the 50 % best evaluation results is given by *P50* for correlation coefficient *r* and root mean square error *rmse* and by the *P25–P75* range for *bias*. Values are only given if at least 25 different mesoscale model evaluations were found in refereed journals, published since year 2000. The total number (#) of single evaluations used in this summary is given per quality measure. Atm., t., rel. and spe. short for Atmospheric, temperature, relative and specific, respectively

Wind direction has a *P50* for the correlation coefficient of 0.47 (Table 72.1), but the diurnal pattern is not very pronounced so that high values cannot be expected. While the *bias* is relatively small (50 % of model evaluations show a *bias* between −13° and 10°; *P50* = −1°), *rmse* is large (*P50* = 71°). This means the wind direction cannot be simulated well in detail. Thus, there might be an inherent uncertainty in the wind simulations or in their measurement. Assuming, the WMO (2014) uncertainty goal of 0.5 m/s for wind speed measurements is achieved, wind directions are wrong by 10° for moderate winds (3 m/s); thus, at least the *bias* for the 50 % best evaluation results cannot be much improved due to the measurement data uncertainties. These relative small errors, nonetheless, result in a lateral offset of a plume by 18 km from its real position 100 km downwind a source (Schlünzen et al. 2015), which can result in wrong chemical reactions due to an incorrect mixture of aged and pristine air masses. To overcome this problem the uncertainty of the measurements needs to be emulated by the models by performing, for instance, ensemble simulations with respect to wind direction and delivering probability distributions for the concentrations.

The model performance for precipitation is again based on only two publications (Vautard et al. 2012; Wu et al. 2008), and needs to be interpreted with care. It seems the precipitation values are overestimated by the models. If this result could be confirmed by more studies, this would mean that close to sources wet deposition might be overestimated, while deposition and concentrations in remote areas might be underestimated.

As mentioned, most evaluations were performed for temperature. Correlation coefficients are high (r = 0.89 for *P50*), not surprisingly for a meteorological

parameter with a well pronounced diurnal and annual cycle. 50 % of the model evaluations have a *bias* between −1.1 and 0.3 K. Values for *P50* (−0.3 K) are negative for *bias*, suggesting a frequent underestimation of the observed temperatures by models. Uncertainty is very large with *P50* = 2.5 K for the *rmse*. Since measurement accuracy is high (target to be 0.5 K with a 1 km resolution; WMO 2014), there seems to be room for improvement in the models.

Wind speed seems to be well simulated considering the measurement uncertainty. 50 % of the model evaluations show a *bias* between −0.2 and 0.7 m/s. *P50* confirms that the models overestimate wind speeds. The correlation coefficient is higher than for wind direction. Again, *P50* of *rmse* values are large compared to those of *bias* suggesting little agreement in detail—or the impact of uncertain measurements as suggested for wind direction.

Specific humidity has high correlation coefficients (*P50* = 0.87), and 50 % of the model evaluations result in a *bias* between −0.2 and 0.3 g/kg (Table 72.1). Thus, the agreement seems to be quite good, but *rmse* values are not available. Furthermore, for AQ simulations relative humidity would be the more relevant meteorological parameter.

72.4 Conclusions

Dependent on the meteorological parameter, the quality measures reflecting the best 50 % of the model results reach different levels. While a correlation coefficient of 0.43 and higher is already a *P50* value for wind direction, for temperature and specific humidity this threshold is 0.89 and 0.87, respectively. The *bias* values for the 50 % best model evaluation values are—except for ABL height- small compared to the actually measured values. However, *rmse* values are large and the 50 % best models have values up to 403 m, 71°, 2.5 K, 1.8 m/s for ABL height, wind direction, temperature and wind speed, respectively. This means that the actual timing and spacing are less well simulated than the average values (characterised by *bias*) for each of the meteorological parameters. For AQ simulations this is of specific relevance, since the emissions also depend on time and space, and the meteorological parameters need to be simulated not only well on average but well at the right time and place.

A drawback of the currently used quality measures is that they neglect any uncertainty in the comparison data. To overcome this, it is advantageous to use the hit rate *H* (72.1) as suggested by Cox et al. (1998). For *K* absolute and relative differences of model results, M_j, and measurements, O_j, the fraction below the absolute, *A,* or relative deviation, *D, is* determined:

$$\mathrm{H} = \frac{1}{K} \sum_{j=1}^{K} \begin{cases} 1 \; for \; |M_j - O_j| < A, \; or \; \left|\frac{M_j - O_j}{O_j}\right| < D \\ 0 \; else \end{cases} \tag{72.1}$$

Table 72.2 Recommended absolute, *A*, and relative, *D*, deviations for surface measurements to calculate hit rate *H* (72.1)

Meteorological parameter	A	D (%)
Component of wind vector[1]	0.35 m/s	10
Wind speed	0.50 m/s	10
Temperature[2]	0.5 K	0.2
Specific humidity[3]	0.2 g/kg	2

[1]Based on values for wind speed (0.5 m/s; WMO 2014), the components are correspondingly smaller. The percentage is calculated based on average wind speeds at surface level (10 m)
[2]Based on values given by WMO (2014). D is calculated based on about 300 K at 2 m level
[3]Values of WMO (2014) for specific humidity are given in %. This is recalculated to *A* values

H is a distribution independent quality measure. In order to come up with a similar summary as in the present paper in the near future, it is essential the same values for *A* and *D* are used in the community. Table 72.2 suggests values based on targeted accuracies for high spatial and temporal resolution (WMO 2014) and suggested in a guideline on mesoscale wind field model evaluation (VDI 2015).

The values suggested in Table 72.2 are smaller than those used by Cox et al. (1998), or other authors (Schlünzen and Katzfey 2003; Ries and Schlünzen 2009; Grawe et al. 2013). They might need to be adjusted, if non-routine comparison data are used, as done by Dierer et al. (2005), who compared model results and aircraft data and considered their uncertainty in the comparison. However, if the same *A* and *D* values are used for surface measurements in future in the scientific community (Table 72.2), then the different evaluations will be comparable again.

The results on performance are robust for some meteorological parameters, but too few evaluations have been found for ABL height or precipitation. More evaluations are also needed to determine dependencies on, e.g. the year of publication. Nonetheless, this summary of different model evaluations should already help to increase the knowledge on typical model performances. It also helps a model user to determine, if the results of a specific model simulation are within the range of typical model performances.

Acknowledgments This research is supported through the Cluster of Excellence 'CliSAP' (EXC177) and the research project UrbMod funded by the state of Hamburg, Germany.

Questions and Answers

Questioner: Jose M. Baldasano

Question: It is very good to define quantitative values for the models, but what is your opinion about the spatial representativeness of the meteorological observations?

Answer: The spatial representativeness is not considered in the measures used for evaluation and analysed here. Spatial representativeness is in part included in the quality objectives (parameters A, D given in Table 72.2); the instrumental accuracy itself would be higher. However, the given values assume perfect instrumental set-up, homogeneous terrain and are objectives for domains of ~ 1 km^2. Especially the homogeneity is not fulfilled e.g. in urban areas, where the representativeness is small (see an example in Schlünzen et al. 2003, for wind speed). For the evaluation we need more information on the spatial and temporal representativeness.

Questioner: Peter Builtjes

Question: You stated that evaluation of rain data/precipitation is not possible/useful. Can you say a bit more about it?

Answer: It is useful and possible, but one has to be very careful evaluating precipitation *amounts* from in situ *data*. Even daily values measured by rain gauges are hardly representative in a distance of more than 10 km (4 km: Buytaert et al. 2006; $\sim$10 km: Bohnenstengel et al. 2011). One has to be aware that large deviations in amounts are to be expected especially at short time scales (e.g. 10 min), since the measurements are not representative for large areas. The longer the precipitation data are integrated, the larger the spatial representativeness of every single in situ station. Bohnenstengel et al. (2011) found for an area in North-East Germany that differences of precipitation sums can be a factor of 3.3, 2, 1.4 for daily, weekly, monthly amounts, respectively, when using one gauge for an area of 25×25 km^2 compared to the area average value. The representativeness of rain *occurrence* is compared to the representativeness of the amounts relatively large in space and in time.

The data quality can be improved in future by merging in situ precipitation and remote sensing data (currently 0.25° for monthly values, 1° for daily values; gpcc.dwd.de, last accessed 01.09.2015).

Questioner: Bertrand Carissimo

Question: I'm concerned about the choice of ABL height for comparison with model results because it is sometimes ill defined, for example in the residual layer seen by lidar observation in a narrow valley. Can you comment on the choice and discuss possible better alternatives to characterise the mixing layer.

Answer: ABL height is indeed a difficult variable to determine. For the time being it seems to be the only parameter for which we might receive any values at all. They are uncertain and derived from other data like temperature or from remote sensing measurements (lidar). Also in models the ABL height is difficult to determine. It would be much better if we had measurements on the turbulence and the mixing process in the atmosphere and thus compare with what is calculated in the models. These data are rare. There are, however, several towers (plus remote sensing systems) with flux measurements up to about 200 m. If these data would be made available on a routine basis, they could be a very valuable source for evaluation of models, once the uncertainty and representativeness of the data is assessed.

Questioner: Paul Makar

Question: Are the wind speed errors which increase as you go to smaller wind speeds a concern given that the spatial scale of the resulting motion would be smaller than the resolution of most grids?

Answer: For coarse grids the problem is indeed small: Considering the wind speed error in Table 72.2 (0.5 m s^{-1}), and focusing on very small wind speeds (0.5 m s^{-1}), the distance error is 10 km, if the low wind situation lasts for 6 h, as might be the case during night-time. This is not very relevant for models of 10 km resolution. However, for models of $\sim$1 km resolution or even higher resolution this uncertainty is of large relevance. Since models of this resolution are already used and will be used more and more, the uncertainty becomes even more relevant in evaluations in the future.

Questioner: Clemens Mensink

Question: Did you find any scaling effects in the results? In other words: Does it help to go to higher resolution approaches?

Answer: The dependence on model resolution is difficult to determine since very few evaluations are published for coarse grids and short time periods. Mostly, averaging over weeks or even a year is performed. This time averaging is the signal found in the model performances: The longer the model results are averaged, the smaller is e.g. the bias (most visible for temperature). At first glance the temperature bias seems to be grid independent, but it is the averaging time which "improves" the performance for coarse grids. Evaluations for different horizontal grids but for the same (short) periods show that model performance can be better for smaller grid sizes (e.g. Schlünzen and Katzfey 2003).

Questioner: Mikhail Sofiev

Question: I would like to continue from Peter's note on precipitation and general conclusion on absence of improvement with increased resolution. Are we in an area where deterministic solutions do not work anymore? The above problems may suggest different criteria -distribution functions, percentiles, probability of exceedances, etc.,—but not usual scatter plots, *RMSE* and correlations?

Answer: The improvement with increasing resolution is to be expected (e.g. resolving buildings instead of parameterising the effect) and was found in model evaluations (see answer to Clemens). However, we cannot conclude in general if model performance improves for smaller grid sizes, since the published evaluations are not done for the same time periods. Instead, coarser resolving models are mostly longer integrated and thus evaluated for longer time periods. This time averaging leads to smaller errors, especially in the bias.

Since spatial and temporal representativeness of data impact the performance, we should include these in the evaluation measures and also aim at measures independent of averaging time. This could be the hit rate (72.1), which allows for both. Going to distribution functions or percentiles in the evaluation will not help to consider representativeness and data uncertainty. Concerning scatter plots, *RMSE*,

correlation coefficients etc., they are helpful to detect strange behaviours at first glance (scatter plots) and to continue the history of evaluation (*RMSE, r*). However, they should not be the only measures used since they might lead to positive/negative judgements on model performance for wrong reasons.

Questioner: Douw Steyn

Question: Because wind direction is a circular variable, calculations of correlation coefficient (and other metrics) can be tricky. Can you be sure all authors in your study got this right?

Answer: One cannot be sure the published values are correctly calculated. We had to take them as given in the literature for our summary. For our calculation of the wind direction uncertainty we considered the circularity. Again, if we would go to hit rates this problem would be reduced, since a deviation has to be calculated and this can easily be assessed to be smaller than 180°. We will elaborate on the possible error function for wind direction in Schlünzen et al. (2016).

References

Bohnenstengel SI, Schlünzen KH, Beyrich F (2011) Representativity of in-situ precipitation measurements—a case study for the LITFASS area in North-Eastern Germany. J Hydrol 400 (3–4):387–395

Buytaert W, Celleri R, Willems P, Bievre B De, Wyseure G (2006) Spatial and temporal rainfall variability in mountainous areas: a case study from the south Ecuadorian Andes. J Hydrol 329 (3–4):413–421

Conrady K (2010) Typische Werte statistischer Maßzahlen zur Evaluierung mesoskaliger Modelle. Bachelor thesis meteorology, University of Hamburg, Germany

Cox R, Bauer BL, Smith T (1998) Mesoscale model intercomaprison. Bull Am Meteorol Soc 87:167–196

Dennis R, Fox T, Fuentes M, Gilliland A, Hanna S, Hogrefe C, Irwin J, Rao ST, Scheffe R, Schere K, Steyn D, Venkatram A (2010) A framework for evaluating regional-scale numerical photochemical modeling systems. Environ Fluid Mech 10:471–489

Dierer S, Schlünzen KH, Birnbaum G, Brümmer B, Müller G (2005) Atmosphere–sea ice interactions during a cyclone passage investigated by using model simulations and measurements. Mon Weather Rev 133:3678–3692

Grawe D, Schlünzen KH, Pascheke F (2013) Comparison of results of an obstacle resolving microscale model with wind tunnel data. Atmos Environ 79:495–509

Lemonsu A, Pigeon G, Masson V, Moppert C (2006) Sea-town interactions over Marseille: 3D urban boundary layer and thermodynamic fields near the surface. Theoret Appl Climatol 84:171–178

Purr C (2013) Übersicht und Vergleich von Evaluationen der Grenzschichthöhe und weiterer meteorologischer Größen in mesoskaligen Modellen. Bachelor thesis meteorology, University of Hamburg, Germany

Ries H, Schlünzen KH (2009) Evaluation of a mesoscale model with different surface parameterisations and vertical resolutions for the Bay of Valencia. Mon Weather Rev 137:2646–2661

Schlünzen KH (2002) Simulation of transport and chemical transformations in the atmospheric boundary layer–review on the past 20 years developments in science and practice. Meteorol Z 11:303–313

Schlünzen KH, Katzfey JJ (2003) Relevance of sub-grid-scale land-use effects for mesoscale models. Tellus 55A:232–246

Schlünzen KH, Sokhi RS (eds) (2008) Overview of tools and methods for meteorological and air pollution mesoscale model evaluation and user training. Joint report of COST Action 728 and GURME. GAW Report No. 181, 115 p

Schlünzen KH, Hinneburg D, Knoth O, Lambrecht M, Leitl B, Lopez S, Lüpkes C, Panskus H, Renner E, Schatzmann M, Schoenemeyer T, Trepte S, Wolke R (2003) Flow and transport in the obstacle layer—first results of the microscale model MITRAS. J Atmos Chem 44:113–130

Schlünzen KH, Builtjes P, Deserti M, Douros J, Galmarini S, Miranda AI, Palau JL, Schere K (2015) Evaluating the performance of mesoscale meteorology models used for air quality simulations. In: Sokhi RS, Baklanov A, Schlünzen KH (eds) Mesoscale meteorological modelling for air pollution and dispersion applications, in preparation

Schlünzen KH, Conrady K, Purr C, Fischereit J (2016) Performance of high-resolution meteorology models. In: Preparation

Vautard R, Moran MD, Solazzo E, Gilliam RC, Matthias V, Bianconi R, Chemel C, Ferreira J, Geyer B, Hansen AB, Jericevic A, Prank M, Segers A, Silver JD, Werhahn J, Wolke R, Rao ST, Galmarini S (2012) Evaluation of the meteorological forcing used for the Air Quality Model Evaluation International Initiative (AQMEII) air quality simulations. Atmos Environ 53:15–37

VDI (2015) VDI 3783 sheet 7: environmental meteorology—prognostic mesoscale wind field models—evaluation for dynamically and thermodynamically induced flow fields. In: review. http://www.beuth.de/

WMO (2014) Oscar variables. http://www.wmo-sat.info/oscar/variables/view/11. Accessed 11 Nov 2014

Wu S-Y, Krishnan S, Zhang Y, Aneja V (2008) Modeling atmospheric transport and fate of ammonia in North Carolina—part I: evaluation of meteorological and chemical predictions. Atmos Environ 42:3419–3436

Zhang J, Rao ST (1999) The role of vertical mixing in the temporal evolution of the ground-level ozone concentrations. J Appl Meteorol 38:1674–1691

Chapter 73
The Effect of Wood Burning on Particulate Matter Concentrations in Flanders, Belgium

Wouter Lefebvre, Frans Fierens, Charlotte Vanpoucke, Nele Renders, Kaat Jespers, Jordy Vercauteren, Felix Deutsch and Stijn Janssen

Abstract Since 2010, new estimations of the particulate matter emissions in Flanders have been made by using a tier-II approach. By means of a survey, the quantity of the wood by households, buildings (services sector), industry and agricultural sector consumption in Flanders has been estimated. A survey is necessary as not all consumed wood is purchased, e.g. some of the wood is sourced locally or waste wood is used. These surveys also provided data on the installation stock in Flanders, such as the type (fireplaces, pellet stoves, …) and age of the heating installation. Besides the wood consumption and use patterns, emission factors of particulate matter per type of wood and per type and age of heating installation were also updated based on international, recent literature on emission factors. Both new estimations resulted in an actualization of the particulate matter emissions of the residential wood burning in Flanders. Overall, the estimations were a factor 13 higher than the old estimations. This factor 13 is due to a factor 4 increase in the average emission factor and a factor of 3.4 in the wood consumption. As a result, heating in residential sector is estimated to be the most important emission source for primary particulate matter (37 % of all primary emissions) in Flanders. To confirm these results a comparison was carried out with the estimates of the contribution of wood burning to ambient PM10 concentrations based on measurements of levoglucosan. It was shown that about 10 % of the particulate matter concentrations in winter were due to wood burning, while in summer this amounted only 2–3 %. In the next step, a dispersion model has been used in order to check the consistency of both results. It is shown that the increased emissions are consistent with the measured particulate matter concentrations due to wood burning. Indeed, the increase in emissions by a factor 13 is needed to understand the

W. Lefebvre (✉) · N. Renders · K. Jespers · F. Deutsch · S. Janssen
VITO, Boeretang 200, 2400 Mol, Belgium
e-mail: wouter.lefebvre@vito.be

F. Fierens · C. Vanpoucke
IRCEL/CELINE, Kunstlaan 10-11, 1210 Brussels, Belgium

J. Vercauteren
VMM, Kronenburgstraat 45, 2000 Antwerp, Belgium

D.G. Steyn and N. Chaumerliac (eds.), *Air Pollution Modeling and its Application XXIV*, Springer Proceedings in Complexity,
DOI 10.1007/978-3-319-24478-5_73

high levoglucosan concentrations in ambient air in Flanders. Finally, the large changes that have been made to the Belgian SNAP-2 emission inventory due to the results of this study, raise questions about the homogeneity (both spatial and temporal) of the European emission inventory for this sector. Adjustments to this sector could possibly decrease the modelled PM-gap quite substantially.

73.1 Introduction

Recently, wood burning by Flemish households was discussed quite intensively in Flemish press and also in the Flemish parliament. The attention for this environmental topic originated from interesting, new estimations of PM emissions and concentrations in the ambient air. Three major studies have been done and are discussed in this paper. Firstly, new estimations of wood burning particulate matter emissions in Flanders have been made. Secondly, measurements of levoglucosan in ambient air have been done. Finally, a dispersion model has been used to check the consistency of the results of the two previous studies.

73.2 Emission Estimates

Since 2010, new estimations of the particulate matter emissions in Flanders have been made by using a tier-II approach (Renders et al. 2011; Aernouts et al. 2013a, b). By means of a survey, the quantity of the wood consumption by households, buildings (services sector), industry and agricultural sector in Flanders has been estimated. A survey is necessary as not all consumed wood is purchased, e.g. some of the wood is sourced locally or waste wood is used. These surveys also provided data on the installation stock in Flanders, such as the type (fireplaces, pellet stoves, …) and age of the heating installation.

Besides the wood consumption and use patterns, emission factors of particulate matter per type of wood and per type and age of heating installation were also updated based on international, recent literature on emission factors (Renders et al. 2011). Both new estimations resulted in an actualization of the particulate matter emissions of the residential wood burning in Flanders. Overall, the estimations were a factor 13 higher than the old estimations (591–7991 ton/year). This factor 13 is due to a factor 4 increase in the average emission factor (128–510 ton/PJ) and a factor of 3.4 in the wood consumption (4.6–15.6 PJ). As a result, heating in residential sector is estimated to be the most important emission source for primary particulate matter (37 % of all primary emissions) in Flanders (Fig. 73.1) (Vanpoucke et al. 2013).

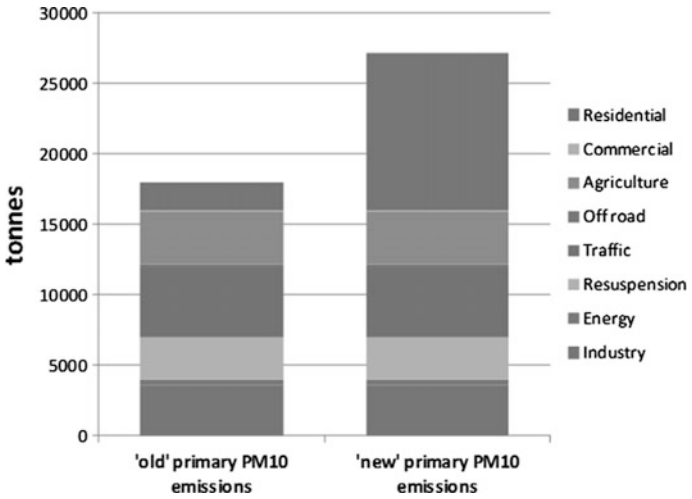

Fig. 73.1 Primary PM_{10} emissions (tonnes/year) for the different sectors before (*left*) and after (*right*) the application of the new wood use and emission factor data in the Flemish Emission Inventory

73.3 Levoglucosan Measurements in Ambient Air

To confirm these results a comparison was carried out with the estimates of the contribution of wood burning to ambient PM10 concentrations based on measurements of levoglucosan. (VMM 2011, 2013), in order to estimate the contribution of wood burning in the ambient concentrations (all sectors). Sampling was done for 24 h with a Leckel SEQ47/50 instrument that samples 55 m^3 of air on a filter. After sampling the filters were reweighed in the lab to determine the total PM10 concentration in the air. Then one 1 cm^2 punch of the filter was sent to the Antwerp University for the determination of levoglucosan. This product is an oxidation product of cellulose or starch and is a good tracer of wood burning emissions. Based on Austrian research (Schmidl et al. 2008; Caseiro et al. 2009) the PM contribution of wood burning was estimated to be equal to 10.7 times the levoglucosan concentrations. This factor is well within the range of values in European studies albeit somewhat low to the average value (Maenhaut et al. 2012). Two 12-month measurement campaigns were performed (February 2010–February 2011 and June 2011–July 2012) at in total 10 Flemish locations. Sampling was done every 4th day in both campaigns.

Using these measurements, it was shown that about 6–10 % of the particulate matter concentrations in winter were due to wood burning, while in summer this amounted only 2–3 %. Furthermore, it is important to note that on days that the PM10 daily limit of 50 $\mu g/m^3$ was exceeded, the average contribution, during the first campaign, was even higher (almost 6 $\mu g/m^3$). It was estimated that a significant part of the exceedences of the European daily limit value would be avoided if no wood burning would be present.

73.4 Dispersion Modelling

In a final step, a dispersion model has been used in order to check the consistency of both results (Veldeman et al. 2013). Therefore, the bi-gaussian IFDM-model was applied, using emissions estimated with the new wood consumption and before and after applying the new emission factors. Only emissions within Flanders were taken into account. To account for emissions outside of Flanders, an average background concentration of 0.2 μg/m^3 was imposed. The spatial distribution of the emissions was based on the population distribution and the rural/urban characteristics. The temporal distribution of the emissions was based on the system of degree days with a limit value for the daily average temperature of 15 °C. It is shown that the increased emissions are consistent with the measured particulate matter concentrations due to wood burning. Indeed, the increase in emissions by a factor 13 is needed to understand the high levoglucosan concentrations in ambient air in Flanders (Fig. 73.2).

The large amount of scatter, both on the spatial validation and temporal validation was to be expected. First of all, the emissions were spread as surface sources at a 1 × 1 km^2 scale. However, wood burning has a strong local component which is not known. Secondly, wood burning is in principal not used as primary heating source in Flanders, but is used in many cases at places where other heating systems are present. As a result, the use of degree days will not represent the inherent variability in wood burning. Furthermore, some of the outliers on Fig. 73.2 can be explained. The locations closest to the frontiers (N029, RT01 and somewhat less LR02) are in general underestimated, which was to be expected as the contribution due to regions outside of Flanders is expected to be larger, but was kept constant.

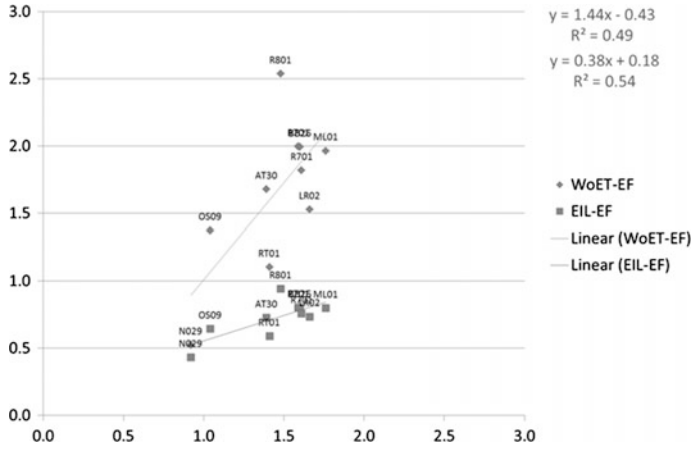

Fig. 73.2 Comparison of the modelled and measured PM10-concentrations attributed to wood burning. *Upper part* spatial validation, on the X-axis: measurements (in μg/m^3), on the Y-axis: model data (in μg/m^3). Every dot represents the average over time of one measurement location; diamonds using the new emission estimates, squares using the new wood consumption data but the old emission factors

73.5 Conclusions

Based on new estimations of emissions, ambient air measurements of levoglucosan and a modelling study confirming these, new estimations of particulate matter wood burning emissions were presented to the Flemish Government. The differences between the current estimations and the previous ones were quite large, amounting to a factor 13. If such differences in emission inventories persist in Europe, validating regional models using measurement data could lead to wrong conclusions.

Questions and Answers

Questioner: S. Aksoyoglu

Question: You compare modelled PM10 from wood burning with measurements to validate wood burning emissions. What is the uncertainty in the measurements?

Answer: The uncertainty in the measurements is quite large, mainly from the factor used to transform levoglucosan measurements into PM10. However, it will not approach the factor 3 to 4 which we want to demonstrate, showing that the comparison as made in the paper is valid.

Questioner: J. Kukkonen

Question: I totally agree with you on the uncertainty of small-scale combustion emissions. I would like to mention one additional source of levoglucosan as a tracer of wood combustion, i.e., wild-land fires. In case of Belgium, these pollutants are regionally or long-range transported.

Answer: The question is valid, as long-range transport of smoke from wildfires would also influence the levoglucosan measurements. However, the spatio-temporal variability in the measurements and the seasonal variation (winter $\gg$ summer) discard this source as a major pollution source for Belgium.

References

Aernouts K, Jespers K, Dams Y (2013a) Energiebalans Vlaanderen 2011, 2013/TEM/R/XXX, maand 2013

Aernouts K, Jespers K, Dams Y (2013b) Energiebalans Vlaanderen 2012 (voorlopig), 2013/TEM/R/XXX, maand 2013

Caseiro A et al (2009) Wood burning impact on PM10 in three Austrian regeions. Atmos Environ 43:2186–2195

Maenhaut W, Vermeylen R, Claeys M, Vercauteren J, Matheeussen C, Roekens E (2012) Assessment of the contribution from wood burning to the PM10 aerosol in Flanders, Belgium. Sci Total Environ 437:226–236

Renders N, de Weedt Y, Gijsbers M, Jespers K, van Esch L, Wevers M (2011) Emissies door houtverbranding—Sectoren gebouwenverwarming en landbouw, 2011/TEM/R/158

Schmidl C et al (2008) Chemical characterisation of fine particle emissions from wood stove combustion of common woods grown in mid-European Alpine regions. Atmos Environ 42:126–141

Vanpoucke C, Fierens F, Lefebvre W (2013) Domestic wood burning emissions in Flanders: underestimated? Wood Burning Workshop Ghent. http://www.joaquin.eu/03/MyDocuments/Woodburning_emissions.pdf. Accessed 2–3 Dec 2013

Veldeman N, Janssen L, Viaene P, Deutsch F, Maiheu B, Lefebvre W, Vankerkom J, Vranckx S, Janssen S (2013) Rapport activiteit in 2013 uitgevoerd in kader van de referentietaak 12 "Kenniscentrum Luchtkwaliteitsmodellering", 2013/RMA/R/XXX

VMM (2011) Chemkar PM10, Chemische karakterisering van fijn stof in Vlaanderen—2010

VMM (2013) Chemkar PM10, Chemische karakterisering van fijn stof in Vlaanderen, 2011–2012

Chapter 74
Diagnostic Evaluations of the CHIMERE Model: Local Versus Advected Contributions of Fine Particles and Nitrate Formation Regime in the Paris Megacity

Herve Petetin, M. Beekmann, J. Sciare, M. Bressi, A. Rosso, O. Sanchez, V. Ghersi, R. Sarda-Estève and J.-E. Petit

Abstract Chemistry transport models (CTMs) are a powerful tool to investigate various features of the aerosol pollution in megacities, including its geographical origin or its sensitivity to anthropogenic emissions changes (scenario analysis). However, due to the numerous uncertainties still at stake in CTMs, assessing the reliability of the results obtained in these two common exercises remains a challenging task that usually requires specific observations and methodologies. In our work, we have taken advantage of some recent campaigns in the Paris region—PARTICULES and FRANCIPOL—to run a diagnostic evaluation of the

Key topics: Model assessment and verification (and in some extent Aerosol in the atmosphere).

H. Petetin (✉) · M. Beekmann
LISA/IPSL, Laboratoire Interuniversitaire des Systèmes Atmosphériques, UMR CNRS 7583, Université Paris Est Créteil (UPEC) et Université Paris Diderot (UPD), Paris, France
e-mail: hervepetetin@gmail.com; herve.petetin@lisa.u-pec.fr

M. Beekmann
e-mail: matthias.Beekmann@lisa.u-pec.fr

J. Sciare · M. Bressi · R. Sarda-Estève · J.-E. Petit
LSCE, Laboratoire des Sciences du Climat et de l'Environnement, CNRS-CEA-UVSQ, Gif-sur-Yvette, France
e-mail: jean.sciare@lsce.ipsl.fr

M. Bressi
e-mail: michael.bressi@jrc.ec.europa.eu

R. Sarda-Estève
e-mail: Roland.Sarda-Esteve@lsce.ipsl.fr

J.-E. Petit
e-mail: Jean-Eudes.Petit@lsce.ipsl.fr

D.G. Steyn and N. Chaumerliac (eds.), *Air Pollution Modeling and its Application XXIV*, Springer Proceedings in Complexity,
DOI 10.1007/978-3-319-24478-5_74

CHIMERE model regarding these two issues. The first substantive point is to assess in what extent the model is able to retrieve the correct share between local production and regional advection of aerosol pollution in the Paris agglomeration. During a whole year, daily measurements of the fine particulate matter ($PM_{2.5}$) and its main chemical constituents (elemental and organic carbon, nitrate, sulfate and ammonium) are available at various stations both in and around Paris (PARTICULES project). Based on back-trajectory data, we can locate the upwind station, from which the concentration is identified as the import, the local production being deduced from the urban concentration by subtraction. Uncertainties on these contributions are quantified. Small biases in urban background $PM_{2.5}$ simulations (+16 %) hide significant error compensations between local and advected contributions, as well as in $PM_{2.5}$ chemical compounds. In particular, wintertime OM imports appear strongly underestimated (potentially explained by uncertain continental woodburning emissions and missing SOA pathways) while local OM and EC production are overestimated all along the year (likely to be related to uncertainties in emissions and dynamics). A statistically significant local formation of nitrate is also highlighted from observations, but missed by the model. Together with the overestimation of nitrate imports, it leads to a bias of +51 % on the local $PM_{2.5}$ contribution. In parallel to inorganic aerosols measurements, gaseous nitrate precursors (nitric acid and ammonia) have also been measured (FRANCIPOL project), which offers the opportunity to investigate the regime of nitrate formation in Paris and its sensitivity to precursor changes and to assess, again, the ability of the CHIMERE model to retrieve the observed sensitivity. Experimental data clearly point to NH_3-rich conditions in the city (as indicated by high gas ratio values), but a quite similar sensitivity of nitrate concentrations to changes in nitric acid and ammonia. However, simulation results indicate that the model highly overestimates the sensitivity of nitrate to ammonia changes. Thus, while overall particulate matter levels are well reproduced by the model, differences with observations are much larger for local versus advected contributions, and the sensitivity of nitrate formation with respect to gaseous precursors.

A. Rosso · O. Sanchez · V. Ghersi
AIRPARIF, Agence de surveillance de la qualité de l'air, Paris, France
e-mail: amandine.rosso@airparif.asso.fr

O. Sanchez
e-mail: olivier.sanchez@airparif.asso.fr

V. Ghersi
e-mail: veronique.ghersi@airparif.asso.fr

H. Petetin
CNRS and Université Paul Sabatier, Laboratoire d'Aérologie, Toulouse, France

74.1 Introduction

Chemistry transport models (CTMs) are a powerful tool to investigate various features of aerosol pollution in megacities, including its geographical origin or its sensitivity to anthropogenic emissions changes (scenario analysis). However, due to the numerous uncertainties still at stake in CTMs, assessing the reliability of the results obtained in these two common exercises remains a challenging task that usually requires specific observations and methodologies. In this work, we will take advantage of two recent campaigns in the Paris region—PARTICULES and FRANCIPOL—to run a diagnostic evaluation of the CHIMERE model regarding these two issues. This evaluation is motivated by the fact that CHIMERE is a state of the art CTM widely used by the scientific community for process and budget studies, and by the air quality management community for scenario calculations and pollution forecast (Menut et al. 2013).

74.2 Local Versus Advected Contributions to $PM_{2.5}$ in Paris

We first investigate the ability of the CHIMERE model to reproduce the share between regional imports and local production in the Paris megacity for both $PM_{2.5}$ and its main chemical constituents (organic matter (OM), elemental carbon (EC) and secondary inorganic aerosols (SIA)).

The PARTICULES campaign. In the framework of the PARTICULES project, daily filter measurements are performed during a whole year (from 10 September 2009 to 9 September 2010) at one urban background site in the center of Paris (so-called PAR) and three rural background sites at around 50 km north-east, south and north-west from the city (so-called RNE, RUS and RNW, respectively). Various chemical analysis described in detail in Bressi et al. (2013) are performed to get $PM_{2.5}$, OM, EC, nitrate, sulfate and ammonium concentrations at all sites.

Determination of advected and local $PM_{2.5}$ contributions. In order to discriminate regional imports from the local production in Paris, 40 back-trajectories simulations are performed each day with the FLEXTRA model during the PARTICULES campaign. This allows identifying the upwind rural background site, the concentration of which is considered as the advected contribution, the Paris local one being then deduced from the urban background concentration by subtraction.

As various errors may arise from such a simple procedure, in particular due to the regional background heterogeneity (i.e. what is measured at the upwind rural site is not exactly what is advected toward the urban site), the exact value of imports is assumed to lie within the maximal concentration range among all three rural sites,

this range being finally used as a (daily) estimation of the uncertainties affecting advected contributions.

Results and discussion. Fine particulate matter pollution in Paris appears dominated by imports (71 %, around 10 μg m^{-3}) which consist equally of OM and SIA, although with significant seasonal differences, OM being particularly high in winter while SIA dominate in late winter/spring. The local increment (29 %, around 4 μg m^{-3}), mainly composed of OM and to a lesser extent EC, varies much less all along the year (Fig. 74.1).

At the yearly scale, the CHIMERE model shows a reasonable positive bias on $PM_{2.5}$ (+16 %). However, results highlight significant error compensations on the seasonal variability, the chemical speciation and the share between imports and local production. In terms of imports, CHIMERE dramatically fails at reproducing the very high wintertime OM import episodes, leading to an underestimation of $PM_{2.5}$ of almost a factor of two in January and February. These negative biases largely exceed uncertainties on advected contributions, as well as possible measurement artefacts, and are thus likely due to errors in woodburning emissions and/or secondary organic aerosol (SOA) formation pathways. The importance of woodburning pollution is confirmed by levoglucosan measurements at both PAR and RUS sites. In addition, an unexpected negative bias also affects wintertime sulfate imports, that may be related to transport errors and/or heterogeneous formation pathways.

In terms of local contribution, CHIMERE significantly overestimates the EC production, and to a lesser extent OM. Errors on these two co-emitted compounds suggest an overestimation of their emissions in the center Paris probably combined to an erroneous representation of the boundary layer over the city. The local SIA formation remains low in Paris, except during fog events in January where their fast production is missed by the CHIMERE model.

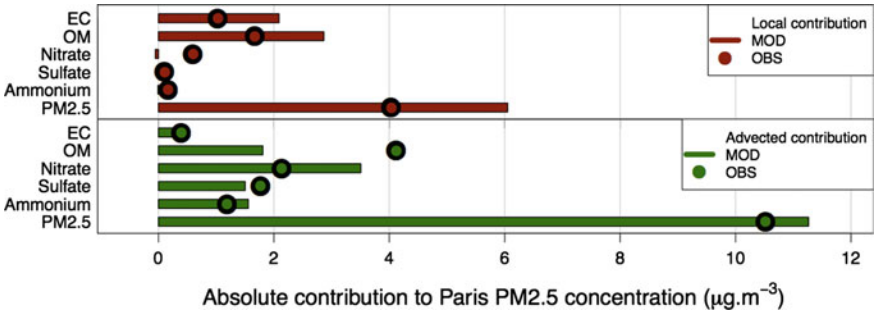

Fig. 74.1 Observed and modelled local (*top panel*) and advected (*bottom panel*) contributions to Paris urban background $PM_{2.5}$ from September 2009 to September 2010 (*source* Petetin et al. 2014)

74.3 Nitrate Formation Regime

As shown in the previous section, SIA highly contribute to the Paris $PM_{2.5}$ urban background. Despite a reasonably good knowledge about the thermodynamics of inorganic compounds, uncertainties persist on (i) the formation regime of ammonium nitrate in Paris, in terms of limited species among its gaseous precursors, nitric acid (HNO_3) and ammonia (NH_3), and (ii) its representation in the CHIMERE model. In this section, we take benefit from measurements of these two compounds to investigate the sensitivity to emissions changes.

The FRANCIPOL campaign. In the framework of the FRANCIPOL project, real-time measurements of HNO_3 and NH_3 have been performed at an urban background site close to the aforementioned PAR site, from April to December 2010. Albeit not colocated, both gaseous and aerosol measurements can be reasonably considered as such since both sites are less than 3 km apart and nitrates have been proven to be mostly advected, thus ensuring a rather good homogeneity over the Paris megacity.

Results. Significant NH_3 concentrations (4 ppb on average) are observed in Paris, with episodic large values during late spring and early summer, concomitantly with intense agricultural emissions Petetin et al. (2015). Conversely, despite high NO_x emissions, HNO_3 concentrations remain low in Paris, whether because the dominant form is particulate nitrate (imports in spring) or because the oxidation of NO_x is too slow to produce HNO_3 within the city (in summer). This leads to a clear NH_3-rich regime, with gas ratio (GR) of 12.6 ppb ppb^{-1}.

Concerning the CHIMERE results, significant biases are found on both NH_3 and HNO_3 during the FRANCIPOL campaign (−75 and +195 %, respectively). Errors on NH_3 clearly points out an erroneous representation of agricultural emissions (in terms of intensity and both spatial and temporal distribution). The high errors on HNO_3 were not expected, and sensitivity tests suggest that they may mainly originate from an overestimation of OH radical concentrations, although further investigations are required. Both errors leads to a significant underestimation of GR (1.2 ppb ppb^{-1} on average), the simulated regime oscillating now between NH_3- and HNO_3-rich regime.

Nitrate sensitivity coefficients, as defined by Takahama et al. (2004), are calculated with the ISORROPIA thermodynamic model for various decreases (−10, −25, −50 and 90 %) of total TNH_3 (=NH_3 + NH_4^+) and TNO_3 (=HNO_3 + NO_3^-) reservoirs. Results indicate that CHIMERE significantly overestimates the sensitivity to moderate decreases of TNH_3 (by a factor of 2–3).

74.4 Discussion and Conclusion

In this study, we have taken benefit from an original and complementary dataset to perform a diagnostic evaluation of the CHIMERE model in the Paris megacity, with a focus on $PM_{2.5}$ chemical constituents and some of its gaseous precursors. Several

major biases have been highlighted in the PARTICULES program, with error compensations in the simulation of $PM_{2.5}$ Paris urban background operating at several levels: the geographic origin (advected versus local), season (winter versus other seasons) and chemical speciation (OM versus SIA in autumn). These results clearly underline the usefulness of such an original approach for evaluating a CTM over a large megacity as Paris. Concerning ammonium nitrate, important findings from FRANCIPOL concern the significant negative and positive biases on NH_3 and HNO_3, respectively, leading to an overestimated sensitivity of the CHIMERE model to NH_3 emissions reductions.

These results have important implications on the use of CHIMERE for scenario analysis, as expected benefits from some emissions reductions at the scale of the Paris region may be overestimated (due to the underestimated advected contribution and the too high sensitivity to NH_3 decreases). This study thus provides valuable information on priority directions for model improvement in the near future.

Acknowledgments This work has been funded by a PhD DIM grant from the Ile-de-France region. The PARTICULES project has been funded by the French state, the Ile-de-France region and the Paris city. The FRANCIPOL project has received funding from PRIMEQUAL, CNRS, CEA, the Ile-de-France region, ACTRIS and DIM R2DS.

References

Bressi M, Sciare J, Ghersi V, Bonnaire N, Nicolas JB, Petit J-E, Moukhtar S, Rosso A, Mihalopoulos N, Féron A (2013) A one-year comprehensive chemical characterisation of fine aerosol (PM2.5) at urban, suburban and rural background sites in the region of Paris (France). Atmos Chem Phys 13(15):7825–7844

Menut L, Bessagnet B, Khvorostyanov D, Beekmann M, Blond N, Colette A, Coll I, Curci G, Foret G, Hodzic A, Mailler S, Meleux F, Monge J-L, Pison I, Siour G, Turquety S, Valari M, Vautard R, Vivanco MG (2013) CHIMERE 2013: a model for regional atmospheric composition modelling. Geosci Model Dev 6:981–1028

Petetin H, Beekmann M, Sciare J, Bressi M, Rosso A, Sanchez O, Ghersi V (2014) A novel model evaluation approach focusing on local and advected contributions to urban PM2.5 levels—application to Paris, France. Geosci Model Dev 7(4):1483–1505

Petetin H, Sciare J, Bressi M, Rosso A, Sanchez O, Sarda-Estève R, Petit JE, Beekmann M (2015) Assessing the ammonium nitrate formation regime in the Paris megacity and its representation in the CHIMERE model. Atmos Chem Phys Discuss 15:23731–23794

Takahama S, Wittig AE, Vayenas DV, Davidson CI, Pandis SN (2004) Modeling the diurnal variation of nitrate during the Pittsburgh Air Quality Study. J Geophys Res 109(D16) D16S06

Chapter 75
AQMEII 1, 2 and 3: Direct and Indirect Benefits of Community Model Evaluation Exercises

S. Galmarini, E. Solazzo, U. Im and I. Kioutsioukis

Abstract Now that the third model evaluation exercise has been launched, a critical review of the activities performed under the Air Quality Model Evaluation International Initiative (AQMEII) is presented. Attention will be focused on the scientific results obtained by individual modeling groups and by the overall community activity. In particular, we critically review the contributions of AQMEII to operational, diagnostic, dynamic, and probabilistic model evaluation. In addition, the role of community collaborations around coordinated modeling activities will be analyzed. Aspects considered in this analysis are the coverage of multiple topics and research interests, the distribution of the workload among several players, the exploitation of web technology for data exchange, the rationalization of the organization of information, and the exploitation of existing data from emission inventory to niche ad hoc and operational monitoring data. Finally, we discuss the channeling of efforts towards the collaboration with other international activities such as the LTRAP Task Force on Hemispheric Transport of Air Pollutant (TF-HTAP) thus multiplying the benefits for the community.

75.1 Introduction

The Air Quality Model Evaluation International Initiative (AQMEII, Rao et al. 2011) is now in its 3rd phase. Started with the aim of finding and exercising new and common model evaluation practices for the regional scale air quality modeling

S. Galmarini (✉) · E. Solazzo
European Commission—DG Joint Research Centre, Institute for Environment and Sustainability, Ispra, Italy
e-mail: stefano.galmarini@jrc.ec.eiuropa.eu

U. Im
Department of Environmental Science, Aarhus University, Roskilde, Denmark

I. Kioutsioukis
Physics Department, Laboratory of Atmospheric Physics, University of Patras, 26500 Rio, Greece

D.G. Steyn and N. Chaumerliac (eds.), *Air Pollution Modeling and its Application XXIV*, Springer Proceedings in Complexity,
DOI 10.1007/978-3-319-24478-5_75

communities in Europe and North America, AQMEII has achieved interesting results that will be presented briefly herewith. These are results that strictly relate to the model evaluation practice but also in terms of organization, data logistics and community effort. The AQMEII activities are based on the model evaluation framework presented by Denis et al. (2010). The four model evaluation modalities identified as: operational, diagnostic, dynamic and probabilistic have been exercised through the different phases of AQMEII on several tens of model results, the North American and European continents and for 2 years (2006 and 2010).

75.2 Phase 1, 2 and 3

75.2.1 Phase 1

The first phase of AQMEII was run for the year of 2006, collecting over 20 modelling contributions. Operational analysis was performed to gauge the ability of models to simulate the time series of ozone, particulate matter, CO, NO_2 at surface and in the troposphere. The analysis revealed that, although able to mimic the trend of pollutants, modelled gaseous species still suffer from too large biases due to emissions and boundary conditions (especially in winter and near the borders) and stable boundary layers (mostly affecting nighttime concentration). Modelled CO, in particular, demonstrated severe limitations in the variability at surface and in the whole troposphere as well as in magnitude. Particulate matter was largely underestimated on account of poor emission inventories concerning wind-blown dust and re-suspension and missing modelled processes, both physical and chemical.

75.2.2 Phase 2

The phase II ensemble consists of models with, compared to phase I, generally improved skill for NO_2, worse skill for PM_{10} and similar skill for O_3. The phase II ensemble as a whole demonstrates smaller *skill differences* between models for all species. Last, increased *error dependence* is evidenced in phase II, arising primarily from the fact that 50 % of the ensemble members run the same model with differences arising only from the choice of different physical or chemical parameterizations. The modulation of the ensemble mean skill owing to the changes in its properties across the two phases is now examined.

The skill of the multi-model mean has been compared against the skill of the best available deterministic model, independently evaluated at each monitoring site (Kioutsioukis and Galmarini 2014). If models were behaving like i.i.d., the probabilities of being best would be roughly equal ($\sim$1/M) for all models. As can be inferred from Table 75.1, the proportion of *equally good models* has increased in phase II for O_3 and NO_2, where the number of models with probability equal to 1/M

Table 75.1 Interpretation of the differences between phase I and phase II through selected indicators including the expectations of the quantities 'MSE(best)/<MSE>' and 's_m explained variation', the fraction of stations where mme outscores the locally best deterministic model and the number of best models at specified probability

	O_3 (I)	O_3 (II)	NO_2 (I)	NO_2 (II)	PM10 (I)	PM10 (II)
E[MSE(best)/< MSE >]	0.68	0.76	0.61	0.70	0.72	0.77
E[s_m expl variation]	71.1	77.9	65.3	69.1	74.2	79.1
Fraction(MSE_{MME}/ $MSE_{BESTMODEL}$ < 1)	*52.1*	*49.1*	*38.6*	*63.5*	*38.1*	*42.0*
Pr(1/M)	4	6	3	7	3	4

contains half of the models compared to one third in phase I. This is not however true for the Phase II PM_{10} simulations, where one model outscores the others at 50 % of the stations, implying a missing process in the majority of the models.

The geographical distribution of the ratio $MSE_{MME}/MSE_{BESTMODEL}$ does not exhibit any longitudinal or latitudinal dependence. Moreover, the number of extreme cases where the *mme* skill was notably inferior to the best model has dropped dramatically. The statistical distribution of the indicator (Table 75.1) shows:

- no major differences exist for O_3, with the *mme* outscoring the best model at half of the stations. Extreme values of the indicator at both tails are trimmed in phase II;
- a clear improvement is evident for NO_2, with the *mme* providing more skilled forecasts at 63 % of the sites, compared to 38 % in the previous phase. All ranges exhibit improvement, indicating a distribution shift;
- a mild improvement is also evident for PM_{10}, where the number of stations where *mme* performs better increased from 38 to 42 %. Extreme values of the indicator at both tails are increased in phase II.

The reason behind the behaviour of *mme* is given in Fig. 75.1 for NO_2 and emerges from the joint distribution of skill difference and error dependence (functions inversely proportional to accuracy and diversity). Skill difference decreased for all species and error dependence increased for all species. It is their relative change that modulates *mme* skill (Table 75.1). For O_3, both are altered by a comparable amount, resulting in similar *mme* skill across phase I and II. For NO_2, skill difference was improved more than error dependence was worsened, yielding a net improvement of *mme*. For PM_{10}, the situation is similar to NO_2 though with a milder relative difference.

The area below the diagonal corresponds to monitoring sites with disproportionally low diversity under the current level of accuracy. Seen from another angle, this area of the chart indicates high spread in skill difference and relatively highly dependent errors. This situation practically means a limited number of skilled models with correlated errors, which in turn denotes a small N_{EFF} value. The

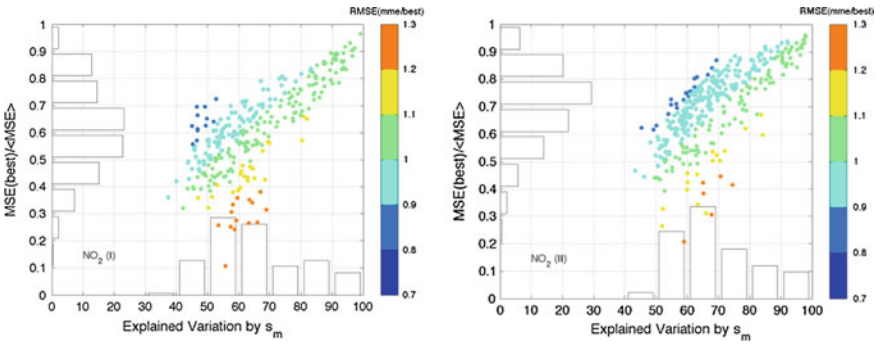

Fig. 75.1 The explanation behind the mme skill against the best local deterministic model with respect to skill difference and error dependence

opposite state is true for the area above the diagonal. It corresponds to locations that are constituted from models with comparable skill and relatively independent, reflecting a high N_{EFF} value. This is the desired synthesis for an ensemble.

75.2.3 Phase 3

In this that is the current phase of AQMEII a synergy has been created with the Long Range Transport of Air Pollution UN-ECE program and in particular with the Task Force on Hemispheric Transport of Air Pollution (HTAP). The task force is in charge of studying the transport across continents of air pollution, the influence on the global and regional backgrounds. AQMEII will then use the results produced by hemispheric simulations to run detail regional assessments on Europe and North America.

75.3 Benefits for the Community at Large

The success of the three phases of AQMEII is proving that the model set up can be taken as raw model for international model evaluation exercises. The organization of the activity with distribution of tasks such as data gathering and harmonization and their organization in a centralized repository such as the JRC ENSEMBLE system (Galmarini et al. 2012) are crucial elements of the success of the activity. This in fact provides the possibility:

- To the modeling:
  - groups to concentrate on the simulations;
  - to rely on a vast amount of different types of monitoring data (in terms of species, spatial a temporal coverage);

  - the data are harmonized, geo-referenced and directly coupled with the modeling data once the latter are also uploaded to the ENSEMBLE platform.

- To the activity at large;
  - to collect and harmonize data that otherwise would not be used by anyone simple because it would require to many resources to organize them;
  - to collect a variety of data and provide the possibility of a comprehensive evaluation of the models across chemistry, meteorology and spatial representativity;
  - to organize modeling and modeling data in a way that can be used again in time.

The definition of a common grid for model output and common format for the modeling data delivered has also been an important key element that guarantees comparability and speed in data acquisition and analysis. All three activities have been and are being beneficial to many groups. Several tens of scientific publications have been produced and improvements in model performance are obtained.

References

Galmarini S, Bianconi R, Appel W, Solazzo E, Mosca S, Grossi P, Moran M, Schere K, Rao ST (2012) ENSEMBLE and AMET: two systems and approaches to a harmonized, simplified and efficient facility for air quality models development and evaluation. Atmos Environ 53:51–59

Kioutsioukis I, Galmarini S (2014) De praeceptis ferendis: good practice in multi-model ensembles. Atm Chem Phys 14:11791–11815

Trivikrama Rao S, Stefano Galmarini, and Keith Puckett (2011) Air quality model evaluation international initiative (aqmeii): advancing the state of the science in regional photochemical modeling and its applications. Bull AmerMeteor Soc 92:23–30. http://dx.doi.org/10.1175/2010BAMS3069.1

Dennis R, Fox T, Fuentes M, Gilliland A., Hanna S, Hogrefe C, Irwin J, Rao ST, Scheffe R, Schere K, Steyn D, Venkatram A (2010) A Framework for Evaluating Regional-Scale Numerical Photochemical Modeling Systems. Environ Fluid Mech 10:471–489

Chapter 76
Sensitivity of Modelled Land Use Specific Nitrogen Deposition Fluxes to Improved Process Descriptions

Sabine Banzhaf, Martijn Schaap, Roy Wichink Kruit, Richard Kranenburg, Astrid Manders and Carlijn Hendriks

Abstract In this study, the chemistry transport model (CTM) LOTOS-EUROS is used to calculate the deposition fluxes of eutrophying and acidifying reactive nitrogen (Nr) to ecosystems in Germany. In the last years important developments have been made for the modelling of the budget of Nr. The new model version has changed the spatial explicit budget calculations across Germany and was thoroughly evaluated with respect to pollutants concentrations and deposition fluxes. The results revealed that the balance between dry and wet deposition is sensitive to the updates in the process descriptions impacting the pollutants transport distances. A comparison to observations showed an improvement of the new model version compared to the pre-developments model version.

76.1 Introduction

European terrestrial ecosystems are strongly affected by the deposition of nitrogen and sulphur, which is a major driver for biodiversity loss and ecosystem dysfunction. CTMs provide a means to assess the dispersion, transformation and removal of air pollutants released into the atmosphere. The concentrations of the pollutants are determined by their lifetime against removal or conversion. The LOTOS-EUROS CTM is used to calculate the deposition fluxes of eutrophying and acidifying components to ecosystems in Germany within the PINETI projects

S. Banzhaf (✉)
Institute of Meteorology, Freie Universität Berlin, Carl-Heinrich-Becker Weg 6-10, 12165 Berlin, Germany

M. Schaap · R. Wichink Kruit · R. Kranenburg · A. Manders · C. Hendriks
Department Climate, Air Quality and Sustainability, TNO, Princetonlaan 6, 3508 Utrecht, TA, The Netherlands

R. Wichink Kruit
RIVM, Antonie van Leeuwenhoeklaan 9, 3721 Bilthoven, MA, The Netherlands

D.G. Steyn and N. Chaumerliac (eds.), *Air Pollution Modeling and its Application XXIV*, Springer Proceedings in Complexity,
DOI 10.1007/978-3-319-24478-5_76

funded by the Federal Environment Agency (UBA). In the last years important developments have been made for the modelling of the budget of Nr. The aim of this study is to provide an assessment of the impact of the model developments on Nr deposition distributions across Germany. For this purpose a sensitivity study was performed to assess the impacts of the individual developments. Moreover, the results of the new model version were compared to available observations.

76.2 Simulation Description

76.2.1 Model Description LOTOS-EUROS

The model employed in this study is the 3-D regional CTM LOTOS-EUROS, which simulates air pollution concentrations solving the advection-diffusion equation on a regular lat-lon-grid with variable resolution over Europe. The model is of intermediate complexity in the sense that the relevant processes are parameterized in such a way that the computational demands are modest enabling hour-by-hour calculations over extended periods of several years within acceptable CPU time. The model is extensively described in Schaap et al. (2008). In the last years the model has been upgraded by the implementation of (i) the compensation point for ammonia (NH_3) (Wichink Kruit et al. 2012), (ii) the co-deposition effect between NH_3 and sulphur dioxide (SO_2), (iii) the description for the dry deposition of aerosols following Zhang et al. (2001), (iv) a pH-dependent cloud chemistry (Banzhaf et al. 2012), (v) below and in-cloud scavenging considering droplet saturation (Banzhaf et al. 2012), (vi) the inclusion of CORINE2006 land use database instead of CORINE2000 and (vii) an update of the deposition and land use related parameter roughness length (z_0), friction velocity (u*) and quasi-laminar resistance (R_B).

76.2.2 Model Setup

The model simulations were performed on a domain covering Germany (47 N-55 N; 1E-15.7E) with a grid resolution of 0.125° longitude × 0.0625° latitude for the year 2009. Simulations covering a European domain on a resolution of 0.50° longitude × 0.25° latitude provided the boundary conditions for the German scale simulations. In the vertical, the model extends to 3.5 km a.s.l. and uses the dynamic mixing layer approach to determine the model vertical structure. The model is driven by short-range meteorological forecasts (0–12 h) from the ECMWF Operational Data stream. The emissions for Germany were taken from a national inventory for the year 2005. National emission totals were scaled to those reported for 2009 at SNAP 1 level. The temporal variation of the emissions is represented by monthly, day-of-the-week and hourly time factors for each source category. With

this set-up, a run using the pre-developments model version v1.7, a run using the new version v1.10 (= base) and 9 sensitivity simulations, excluding either one of the new developments from model version v1.10, were performed.

76.3 Results

Figure 76.1 shows the annual total deposition distributions of dry and wet deposition for Nr for the base run. Averaged over Germany and all ecosystems the deposition totals 909 eq ha^{-1} a^{-1}. On average, the division between dry and wet deposition is about equal. However, the ratio shows variability as in source areas for Nr the dry deposition dominates. In more natural regions the wet deposition is about two times more important than the dry flux. Dry and wet deposition of Nr maximises in the north west of the country and in the south east, coinciding with the main regions with the main agricultural areas in Germany. Near the Alpine range in Bavaria increased wet deposition is modelled due to high precipitation amounts.

In Fig. 76.2a we summarize the average dry, wet and total deposition of Nr to the German territory for the base case, all sensitivity calculations and the pre-developments model version. For the total nitrogen flux it is striking that the average flux is within about 6 % of the base case for all sensitivity simulations. This means that for a relatively large country as Germany the sensitivity simulations do not have a significant impact on net import or export of Nr. Inspection of the contributions to the total deposition shows that the ratio between wet and dry deposition is significantly affected by the sensitivity simulations. Especially the change in aerosol deposition velocity (ZHANG-OFF) and the introduction of the compensation point (COMP-OFF) cause an increase of modelled wet deposition at the cost of the dry deposition flux. In Fig. 76.2b the combined effects of all developments on modelled total N deposition is shown. The spatial signature is dominated by the impact of including the compensation point for NH_3. In the base

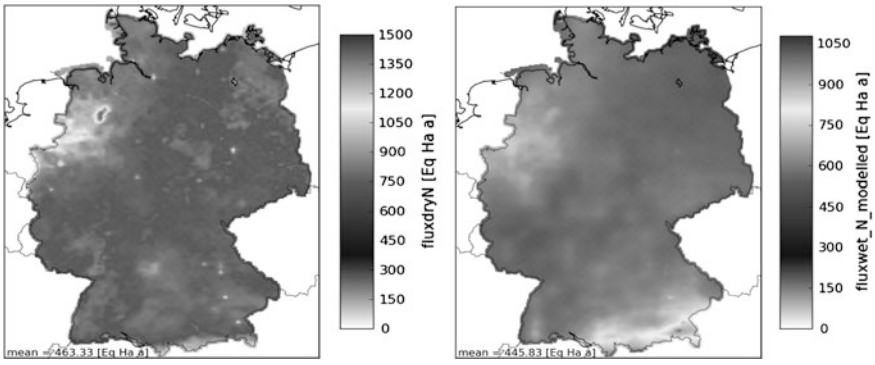

Fig. 76.1 Annual total deposition distributions (eq ha^{-1} a^{-1}) of dry (*left*) and wet (*right*) deposition for Nr

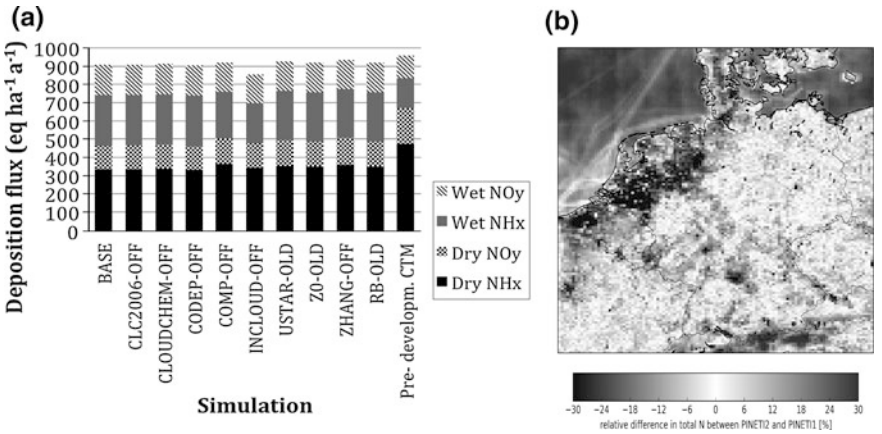

Fig. 76.2 **a** Comparison of the wet, dry and total deposition of NHx and NOy to Germany for all simulations performed in the sensitivity analysis and **b** relative difference (to base case) in NHx dry deposition due to the incorporation of the compensation point of NH_3

case the latter causes lower deposition within the major source regions in the northwest and southeast of the country. As a consequence, the concentrations of NH_3 increase causing more effective wet deposition as well as larger transport distances. The latter results in increased dry deposition fluxes of N in the central part of the country including the forested areas of the black forest and Harz of about 10–20 %. The new model version v1.10 (NEW) was also evaluated against available observations and compared to results of the pre-developments version v1.7 (OLD). Figure 76.3 shows an example of this evaluation exercise. Evaluation

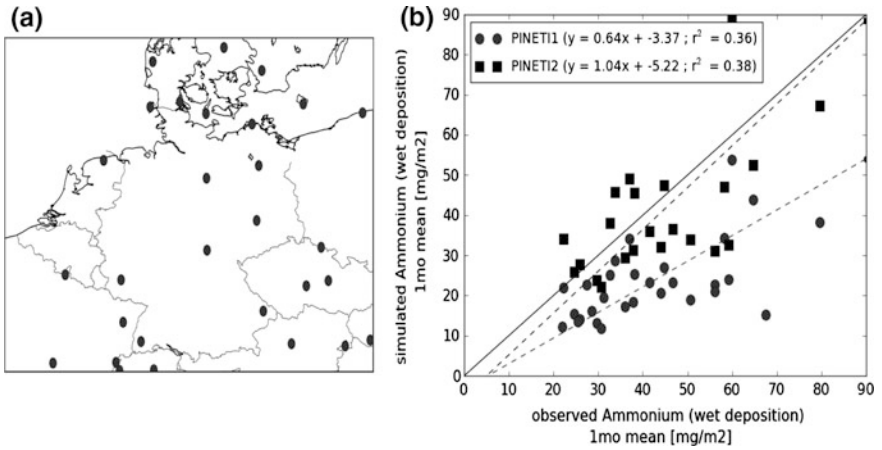

Fig. 76.3 **a** Wet deposition measurement locations and **b** modelled versus measured wet deposition fluxes for the base case (PINETI2) and the pre-developments CTM (PINETI1)

of the total deposition is hampered by the fact that there are hardly any measurements of dry deposition fluxes. Hence, here we confront the modelled NHx wet deposition fluxes to those measured. An increased wet deposition is observed for the new model version as a consequence of the model developments. The results of the new model version compare better to observed fluxes than the pre-developments version. Comparison of the rain amounts (not shown here) has shown that the differences in rain amounts are small. Improvements were also found for NOy wet deposition fluxes and air concentrations of Nr when using the new model version (not shown here).

76.4 Conclusions

The new model version has changed the spatial explicit budget calculations of Nr across Germany. The results revealed that the balance between dry and wet deposition is sensitive to the updates in the process descriptions. Especially the introduction of the compensation point and the revision of the particle dry deposition scheme caused a shift from dry to wet deposition impacting the pollutants transport distances. The comparison to observations showed an improvement of the new model version compared to the pre-developments model version.

Question and Answer

Questioner: Camilla Geels

Question: How is the concentration of NH_3 in the plants determined and how sensitive is the dry deposition of NH_3 to this?

Answer: The stomatal concentration is modelled following Wichink Kruit et al. (2012). It is dependent on the leaf surface temperature and the ratio between the apoplastic molar NH_4^+ and H^+ concentration. The latter ratio is computed dependent on the 'long-term' ammonia concentration to account for the pollution climate and the leaf surface temperature to account for seasonal variation.

In LOTOS-EUROS we use the 2 m temperature instead of the leaf surface temperature after a sensitivity study deriving the leaf surface temperature from longwave outgoing radiation has shown, that the impact on the stomatal concentration was small. For the 'long-term' ammonia concentration as indication for the pollution climate we use the mean ammonia concentration of the last month. Furthermore, for the consideration of the external leaf pathway also the ammonia concentration of the previous hour is used. Hence, the effect of the compensation point on model results is sensitive to modelled ammonia concentrations and therewith to the assumed seasonal cycle of atmospheric ammonia. Due to the latter we are currently working on improving the ammonia emission timing in the model.

References

Banzhaf S et al (2012) Implementation and evaluation of pH-dependent cloud chemistry and wet deposition in the chemical transport model REM-Calgrid. Atmos Environ 49:378–390

Schaap M et al (2008) The LOTOS-EUROS model: description, validation and latest developments. Int J Environ Pollut 32(2):270–290

Wichink Kruit RJ et al (2012) Modeling the distribution of ammonia across Europe including bi-directional surface-atmosphere exchange. Biogeosciences 9(12):5261–5277

Zhang L et al (2001) A size-segregated particle dry deposition scheme for an atmospheric aerosol module. Atmos Environ 35:549–560

Chapter 77
A Comprehensive CTM Assessment Over an Highly Polluted Area

Tony C. Landi, Michele Stortini, Giovanni Bonafé, Enrico Minguzzi, Paolo Cristofanelli, Matteo Rinaldi, Stefania Gilardoni, Stefano Decesari, Isabella Ricciardelli, Antonella Morigillo, Gian Paolo Gobbi and Paolo Bonasoni

Abstract Photochemistry, particles formation and cycling, and aerosol optical properties predicted by a deterministic modeling system have been evaluated through both in-situ and satellite measurements. The three-dimensional air quality modeling system NINFA/AODEM was implemented over the Po valley for the entire year 2012 with the aim to characterize the atmospheric conditions, in terms of meteorological parameters and chemical composition. In addition, NINFA/AODEM has been deeply evaluated by using measurements of size-segregated aerosol samples collected on hourly basis at the 3 different sampling sites representative of urban background (Bologna), rural background (San Pietro Capofiume) and remote high altitude station (Monte Cimone 2165 ma.s.l.).

77.1 Introduction

Photochemistry, particles formation and cycling, and aerosol optical properties predicted by a deterministic modeling system on seasonal basis have been evaluated against both in situ and satellite measurements. In particular, observations

T.C. Landi (✉) · P. Cristofanelli · M. Rinaldi · S. Gilardoni · S. Decesari · P. Bonasoni
CNR-ISAC, Via Gobetti 101, Bologna, Italy
e-mail: t.landi@isac.cnr.it

M. Stortini · G. Bonafé · E. Minguzzi · A. Morigillo
ARPA-SIMC, Viale Silvani 6, Bologna, Italy

I. Ricciardelli
ARPA, Via Rocchi 19, Bologna, Italy

G.P. Gobbi
CNR-ISAC, Roma Tor Vergata, Via Fosso del Cavaliere 100, Roma, Italy

D.G. Steyn and N. Chaumerliac (eds.), *Air Pollution Modeling and its Application XXIV*, Springer Proceedings in Complexity,
DOI 10.1007/978-3-319-24478-5_77

performed during intensive field campaigns carried out in the framework of projects SUPERSITO (for whole 2012) and PEGASOS (for summer season) over three sampling sites of Emilia Romagna region were used for the model verification.

77.2 Modeling Setup

A three-dimensional air quality modeling system NINFA/AODEM over the Po valley for entire 2012 with the aim to characterize the atmospheric conditions, in terms of meteorological parameters and chemical composition, was implemented. NINFA (Stortini et al. 2007) is based on the chemical transport model CHIMERE (Bessagnet et al. 2008), driven by COSMO-I7 (Steppeler et al. 2003), the meteorological Italian Limited Area Model. Boundary conditions have provided by Prev'air data, and emissions data input are based on regional, national and European inventories. Besides, we implemented a post-processing tool for aerosol optical properties calculation, called AODEM (Landi 2013).

77.3 Observational Datasets

AirBase[1] was used for a model verification at ground level over an high polluted area such as the Po basin. Aerosols and gas concentrations on daily and hourly basis were considered for these investigations. Only the stations with data coverage exceeding 75 % were considered for these comparisons. Since the model simulations were performed by using an horizontal resolution of 5 km, only the stations classified as background were taken into account (i.e. we did not consider the traffic and industrial zones). Neverthless, a comprehensive CTM assessment requires the vertical resolved and columnar measurements of atmospheric compounds, thus model's outputs were verified by using LiDaR[2] and satellite[3] observations for t he entire 2012. Furthermore, we focused on the major aerosols species, which were measured during the intensive field campaigns carried out in the framework of SuperSito[4] and PEGASOS[5] projects.

[1] http://www.eea.europa.eu/data-and-maps/data/airbase-the-european-air-quality-database-8.

[2] see G. Bonafé and G, P. Gobbi et al., (34_ITM_Giovanni_Bonafé_919.pdf).

[3] MODIS terra and aqua platforms, ftp://ladsweb.nascom.nasa.gov/allData/6.

[4] http://www.arpa.emr.it/index.asp?idlivello=1459.

[5] http://pegasos.iceht.forth.gr/.

77.4 Results

The model verification is presented in this work by following three steps: firstly we compare the AOD (i.e. Aerosol Optical Depth measured by MODIS Terra and Aqua platforms) calculated by the modeling system NINFA/AODEM both overall the northern Italy and for two sampling sites (i.e. data collected by NASA sun-photometers installed at Ispra 45.80N–8.62E, 235 m.a.s.l. and Venise 43.31N–12.50E, 10 m.a.s.l.). Secondly, we show an assessment of aerosols and gas at ground level over NINFA domain for two fourty-days periods, during winter and summer of 2012 respectively. Thirdly, we argue about a more specific verification of speciated aerosols by using the measurements collected at three sampling sites located in Emilia Romanga region, representative of urban background (BOL, Bologna 44.50N–11.35E, 54 m.a.s.l.), rural background (SPC, San Pietro Capofiume, 44.65N–11.64E, 11 m.a.s.l.), and remote high altitude station (MTC, Mt. Cimone, 44.19N–10.70E, 2165 m.a.s.l.).

Assessment of calcualted AOD values highlights that (i) the spatial distribution of AOD observed by MODIS is partially reproduced by the model, (ii) the largest discrepancy was found over the southern part of Adriatic coast and over the eastern part of the domain (Piedmont region), (iii) the model displays a smoother AOD gradient at land-sea interface over the northern Adriatic coast.

About the comparisons carried out for the two sampling sites, the underestimate ranges between a factor 4 for Ispra and a factor 2.6 for Venise. The linear correlation in time is slightly better for Ispra than for Venise, even if it is lower than 0.5.

However, encouraging results was found for the aerosols and gases assessment at ground level over the NINFA's domain, except for sulphate dioxide. In Table 77.1 are reported the basic statistics for PM_{10} and $PM_{2.5}$ (calculated for both cold and warm season of 2012) for the background stations of northern Italy.

In Table 77.2 as for the Table 77.1, but for O_3, NO_2 and SO_2.

Table 77.1 Basic statistics calculated by using daily values (in the Table indicated by *N)* for bulk mass of particulate matter (i.e. (PM_{10}) and its fine fraction (i.e. ($PM_{2.5}$) for summertime and wintertime of 2012 overall the background stations

	PM_{10} [$\mu g\ m^{-3}$]					$PM_{2.5}$ [$\mu g\ m^{-3}$]				
Summer	Obs.	Model	MB	P.Corr.	N	Obs.	Model	MB	P.Corr.	N
All stations	22.9	12.2	−10.8	0.55	46	13.5	6.9	−6.6	0.41	45
Rural	18.0	10.3	−7.7	0.47	46	12.6	6.6	−5.9	0.32	44
Suburban	23.8	12.6	−11.2	0.54	46	13.1	6.7	−6.2	0.29	41
Urban	21.9	12.5	−9.4	0.56	46	13.0	7.1	−5.9	0.45	45
Winter	Obs.	Model	MB	P.Corr.	N	Obs.	Model	MB	P.Corr.	N
All stations	32.6	15.9	−16.9	0.56	39	26.6	13.6	−12.9	0.55	39
Rural	24.2	14.2	−9.9	0.53	38	26.4	16.3	−10.2	0.45	38
Suburban	33.0	16.8	−16.2	0.55	39	24.8	12.5	−12.2	0.57	32
Urban	34.7	17.2	−17.5	0.53	40	28.1	15.4	−12.7	0.52	40

Table 77.2 Basic statistics calculated by using hourly levels (in the Table indicated by *N)* of major gases, such as ozone (O_3), nitrogen dioxide (NO_2), and sulphate dioxide (SO_2) for summertime and wintertime of 2012 overall the background stations

	O_3 [μg m^{-3}]					NO_2 [μg m^{-3}]					SO_2 [μg m^{-3}]				
Summer	Obs.	Model	MB	P.Corr.	N	Obs.	Model	MB	P.Corr.	N	Obs.	Model	MB	P.Corr.	N
All stations	85.5	101.9	16.5	0.70	1102	19.9	9.0	−10.8	0.25	1063	4.0	2.5	−1.5	**0.01**	930
Rural	91.7	103.7	12.0	0.70	1107	8.5	6.8	−1.7	0.30	1039	4.4	0.9	−3.5	**−0.03**	706
Suburban	81.5	102.2	20.7	0.70	1098	15.2	8.1	−7.1	0.30	1037	5.7	1.9	−3.8	**−0.01**	1051
Urban	86.3	100.5	14.2	0.70	1128	17.2	9.4	−7.8	0.30	1096	3.4	2.5	−0.9	**0.01**	1000
Winter	Obs.	Model	MB	P.Corr.	N	Obs.	Model	MB	P.Corr.	N	Obs.	Model	MB	P.Corr.	N
All stations	22.4	31.5	9.0	0.47	916	38.8	16.2	−22.6	0.42	942	4.6	5.4	0.8	**0.15**	817
Rural	34.8	38.3	3.4	0.46	915	20.7	12.4	−8.4	0.38	943	3.5	1.9	−1.6	**0.07**	627
Suburban	18.9	31.0	12.1	0.48	914	33.3	15.8	−17.4	0.43	954	5.1	5.4	0.3	**0.10**	829
Urban	16.1	26.4	10.3	0.47	941	41.0	18.1	−22.9	0.43	948	4.8	6.3	1.5	**0.16**	882

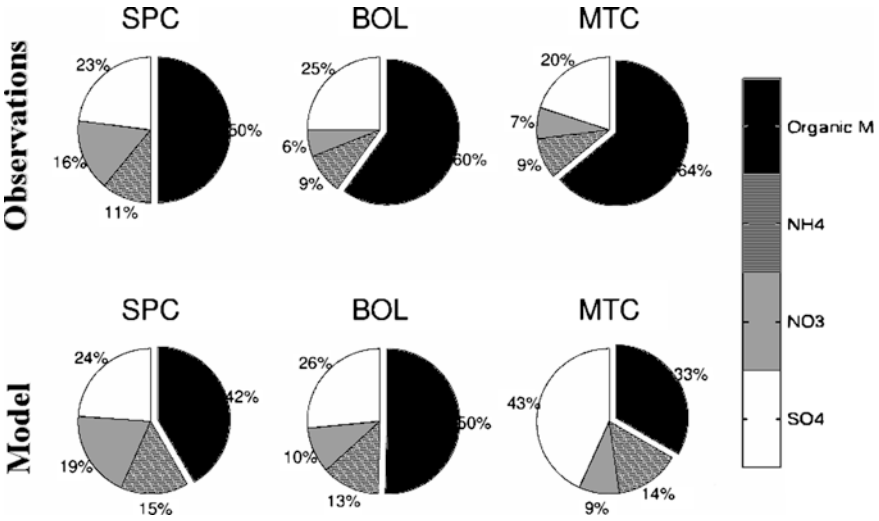

Fig. 77.1 Composition of non-refractory part of PM_1, (i.e. sulphate, nitrate, ammonium, and oragnic compounds) as observed (*upper pies*) and modeled by NINFA modeling system (*lower pies*) for the simpling sites of SPC, BOL, and MTC

By focusing on the PEGASOS field campaign (12 June–13 July 2012), Aerosol Mass Spectrometer (AMS) measurements were used for a more specific model verification. Figure 77.1 shows the comparison of non-refractory part of PM_1 (i.e. SIA, secondary inorganic aerosols, and OM, organic matter) for the sampling sites of SPC, BOL, and MTC. Model reproduces quite well these compounds of aersols fine fraction; even if the organics decrease moving towards high altitude station of MTC, conversly to what pointed out by the observations. It suggests the need to improve the model description of secondary organic aerosol formation.

Acknowledgments Part of this research was carried out in the framework of the ``Supersito'' Project, which was supported and financed by Emilia-Romagna Region and Regional Agency for Prevention and Environment.

Questions and Answers

Questioner: P.J.H. Builtjes

Question: Could the underestimation of PM_{10} be due to wood-burnings emissions in houses?

Answer: Yes, of course. Currently in Italy there is a project for the emissions harmonization over national domain to refine and give more accurate estimation of each emission sector, even if uncertainties of black carbon emission remain.

References

Bessagnet B, Menut L, Curci G, Hodzic A, Guillaume B, Liousse C, Moukhtar S, Pun B, Seigneur C, Schulz M (2008) Regional modeling of carbonaceous aerosols over europe-focus on secondary organic aerosols. J Atmos Chem 61(3):175–202

Landi TC (2013) AODEM: a post-processing tool for aerosol optical properties calculation in the Chemical Transport Models. Book published by LAP—Lambert Academic Publishing ISBN: 978-3-659-31802-3

Steppeler J, Doms G, Schttler U, Bitzer HW, Gassmann A, Damrath U, Gregoric G (2003) Meso-gamma scale forecasts using the nonhydrostatic model LM. Meteorol Atmos Phys 82(1–4):75–96

Stortini M, Deserti M, Bonafé G, Minguzzi E (2007) Long-term simulation and validation of ozone and aerosol in the Po Valley. In: Borrego C, Renner E (eds) Developments in environmental sciences, vol 6, pp 768–770. Elsevier

Chapter 78
Application of a Hybrid Chemical Transport-Receptor Model to Develop Region-Specific Source Profiles for $PM_{2.5}$ Sources and to Assess Source Impact Changes in the United States

Cesunica E. Ivey, Heather A. Holmes, Yongtao Hu, James A. Mulholland and Armistead G. Russell

Abstract A novel, hybrid chemical transport/receptor model approach is used to develop spatial fields of daily source impacts. The spatial-hybrid (SH) method uses source impact fields obtained from CMAQ simulations, which are then adjusted to better match species-specific observations. Specifically, the SH method assimilates modeled 36-km source impact estimates from CMAQ and ground observations from the Chemical Speciation Network (CSN) to produce source impacts that better reflect observed data. New source profiles are generated using source impact results from the SH method. The new source profiles reflect modeled and observed concentrations and also reflect secondary formation processes that are captured by CMAQ. Results of the application of this method suggest that the default source profiles used in emissions inventories may be inconsistent with observations. In this work, we present SH source impact fields over the year 2006. These results are then used to develop updated source profiles for fine particulate matter sources for the contiguous U.S. The profiles characterize the composition of 22 particulate matter species, including major ions, carbon species, and 17 metals. Sources analyzed include fossil fuel combustion, mobile sources, sea salt, biogenic emissions, biomass burning, as well as livestock operations, agricultural activities, metals processing, and solvents. Source profiles are evaluated by comparing results for two locations Atlanta, GA, and St. Louis, MO to previous studies.

C.E. Ivey (✉) · Y. Hu · J.A. Mulholland · A.G. Russell
School of Civil and Environmental Engineering,
Georgia Institute of Technology, Atlanta, GA, USA
e-mail: sunni.ivey@gmail.com

H.A. Holmes
Department of Physics, University of Nevada Reno, Reno, NV, USA

D.G. Steyn and N. Chaumerliac (eds.), *Air Pollution Modeling and its Application XXIV*, Springer Proceedings in Complexity,
DOI 10.1007/978-3-319-24478-5_78

78.1 Introduction

Source impact estimates quantify the contribution of emissions sources on ambient concentrations of air pollutants. Of interest in several research disciplines, such as earth sciences, engineering, and epidemiology, is determining source impacts on fine particulate matter ($PM_{2.5}$) concentrations over spatial domains encompassing cities, states, or sub-regions. Two main source apportionment techniques are source-oriented and receptor-oriented approaches. In this work, both approaches are combined for optimal source impact estimation that takes into account observations, chemistry, and physics. Source profiles are used in receptor modeling to determine fractional source contributions of $PM_{2.5}$ species. Source profiles are uncertain because contributions are estimated near source and do not take into account long-range transport or chemical evolution of emitted species. Methods presented here take secondary processes into account when developing source profiles.

78.2 Methods

In this work, a novel hybrid source apportionment model along with a spatial extension is used to estimate source impacts for 20 distinct sources of $PM_{2.5}$. The model uses a nonlinear optimization approach to minimize discrepancy between observed concentrations and modeled source impacts and to produce source impact adjustment factors, R (Hu et al. 2014). Modeled source impacts are generated using the Community Multiscale Air Quality (CMAQ) model. Observations of total $PM_{2.5}$ mass, major ions, carbon species, and 35 trace metals are obtained from the Chemical Speciation Network (CSN). Equation 78.1 is applied at monitors with available speciated $PM_{2.5}$ data.

$$X^2 = \sum_{i=1}^{N} \left[\frac{\left[\left(c_i^{obs} - c_i^{sim} - \sum_{j=1}^{J} SA_{i,j}^{base} (R_j - 1) \right) \right]^2}{\sigma_{i,obs^2} + \sigma_{i,CTM^2}} \right] + \Gamma \sum_{j=1}^{J} \frac{ln(R_j)^2}{\sigma_{ln(R_j)^2}} \quad (78.1)$$

X^2 is the error to be minimized, c is observed or simulated concentrations, SA are modeled source impacts, σ is uncertainty in observations, modeled concentrations, and source strengths, and Γ is a numerical weighting term. The model is extended by spatially kriging hybrid adjustment factors for full coverage over the spatial domain (Ivey et al. 2015). Improved concentrations (c^{adj}) are reconstructed over the domain using hybrid results in 78.2.

$$c_i^{adj} = c_i^{sim} + \sum_{j=1}^{J} SA_{i,j}^{base} (R_j - 1) \quad (78.2)$$

Further, source profiles are estimated by minimizing the discrepancies between hybrid-adjusted concentrations and observations, and by optimizing f using 78.3:

$$X^2 = \sum_{i=1}^{I} \frac{\left[c_i^{obs} - f_{ij}\left[\sum_{i=1}^{I} SA_{i,j}^{base} R_j\right]^T\right]^2}{\sigma_{i,obs^2}} \tag{78.3}$$

f_{ij} is a matrix of mass fractions of species i from sources j. Initial conditions for f_{ij} are derived from an emissions study by Reff et al. (2009). In this work, source profiles are optimized for one winter and one summer month in 2006 for two urban monitors with available speciated $PM_{2.5}$ data.

78.3 Results

The spatial hybrid method is applied for the year 2006, and results are analyzed for seasonal and regional trends. Coal combustion impacts are most dominant in eastern U.S. and peak in the summer (Fig. 78.1). Lowest impacts are estimated in

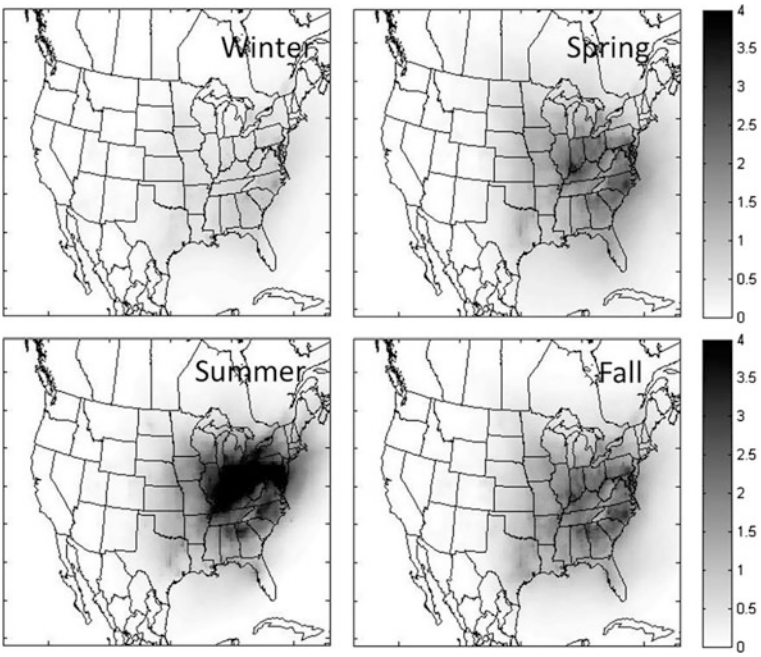

Fig. 78.1 Seasonally-averaged coal combustion impacts on $PM_{2.5}$ in 2006

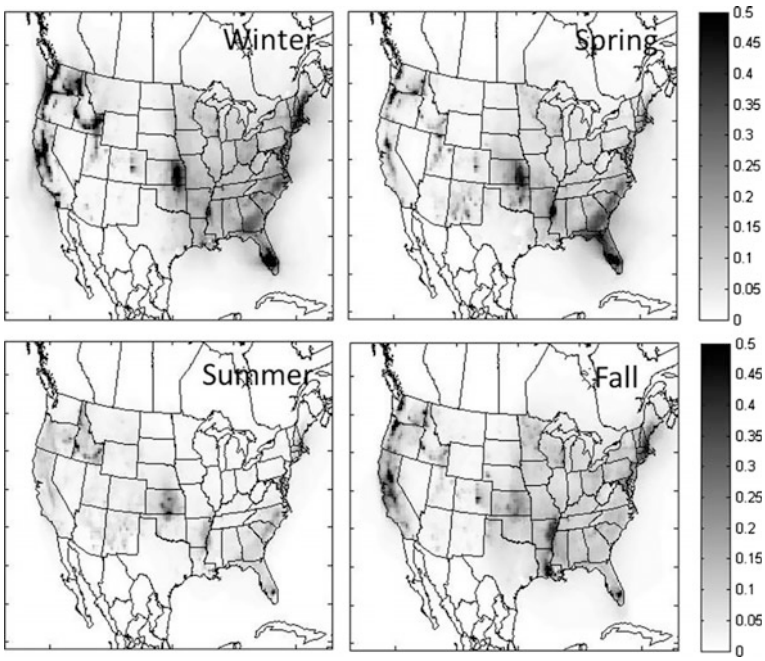

Fig. 78.2 Seasonally-averaged biomass burning impacts on $PM_{2.5}$ in 2006

winter, most likely due to stack heights being above wintertime PBL heights. The southeastern U.S. has highest impacts for biomass burning during winter, consistent with the typical burn season for the region (Fig. 78.2). Burn impacts peak in the Four Corners region during summer, which is consistent with wildfire activity in the summer. California and the Pacific Northwest experience heavy burning impacts throughout much of the year. Biogenic impacts are dominant in the Southeast throughout much of the year, peaking in summer, consistent with the region's heavily forested land cover (Reff et al. 2009) (Fig. 78.3). Summertime biogenics are also high in the western U.S. (west of the Rocky Mountains). Future work includes applying these methods to other years and determining trends over time.

A summer source profile is estimated for light-duty gasoline vehicles (LDGV) in Atlanta, GA and a winter biomass burning source profile is estimated for St. Louis, MO. Results are compared with profiles estimated by previous studies that implement an ensemble-based approach (Balachandran et al. 2012; Maier et al. 2013). For the gasoline profile, both the ensemble and hybrid methods list organic and elemental carbon as the top two species fractions (Fig. 78.4). For the wintertime biomass burning profile, ensemble and hybrid estimates are comparable. Moreover, the hybrid method apportions mass to cooper, manganese, lead, and selenium, which was unapportioned in the ensemble profile (Fig. 78.5). Further evaluation includes implementing the hybrid-based profiles in CMB and comparing to CMB results from previous studies.

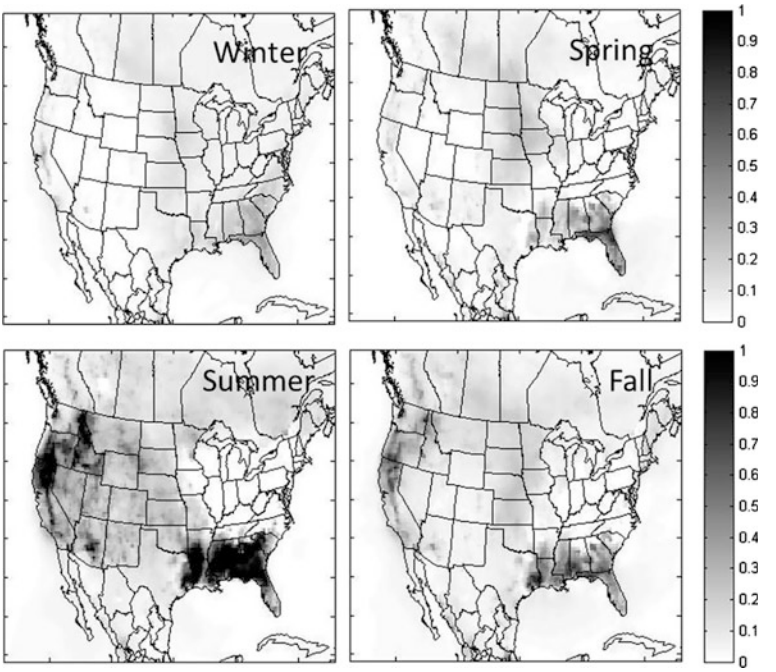

Fig. 78.3 Seasonally-averaged biogenic impacts on $PM_{2.5}$ in 2006

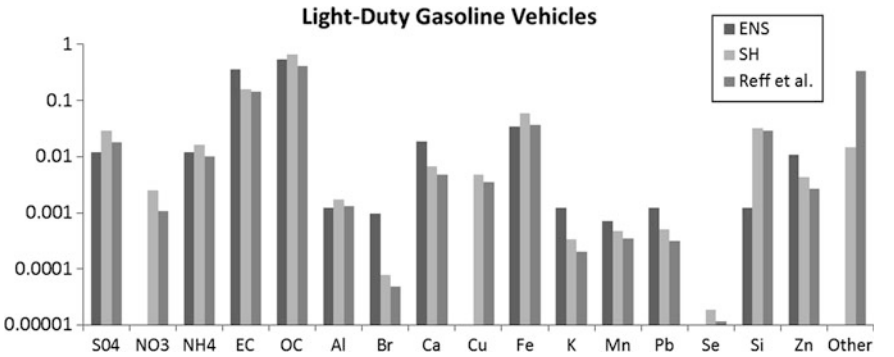

Fig. 78.4 Ensemble-based (ENS) and spatial hybrid (SH) summertime source profiles for light-duty gasoline vehicles in Atlanta, GA

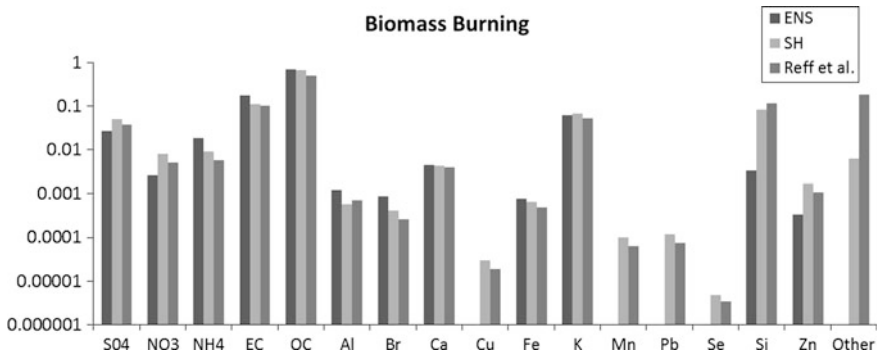

Fig. 78.5 Ensemble-based (ENS) and spatial hybrid (SH) wintertime source profiles for biomass burning in St. Louis, MO

Questions and Answers

Questioner: Wouter Lefebvre

Question: How do you explain more impact from coal burning in the summer compared to the winter?

Answer: In the summer time, higher temperatures lead to less sulfate uptake and by ammonium, as compared to winter time.

Questioner: Amir Hakami

Question: Are you able to estimate uncertainties for your optimized source profiles?

Answer: Currently, the standard deviation of source contributions (daily contributions averaged over time) serve as a proxy for source profile uncertainties. Other methods are currently being explored to estimate source contribution uncertainty.

Questioner: S. T. Rao

Question: Can you please comment on how your study results in health assessment analysis?

Answer: Resulting spatial fields can be used as human exposure surrogates in health studies that seek to find correlations between sources and adverse health effects at the neighborhood or census scale.

References

Balachandran S et al (2012) Ensemble-trained source apportionment of fine particulate matter and method uncertainty analysis. Atmos Environ 61:387–394

Hu Y et al (2014) Fine particulate matter source apportionment using a hybrid chemical transport and receptor model approach. Atmos Chem Phys 14(5415–5431):2014

Ivey CE et al (2015) Development of PM2.5 source impact spatial fields using a hybrid source apportionment air quality model. Geosci Model Dev Discuss 8:645–671. doi:10.5194/gmdd-8-645-2015

Maier ML et al (2013) Application of an ensemble-trained source apportionment approach at a site impacted by multiple point sources. Environ Sci Technol 47:3743–3751

Reff A et al (2009) Emissions Inventory of PM2.5 Trace Elements across the United States. Environ Sci Technol 43:5790–5796. doi:10.1021/Es802930x

Chapter 79
Evaluation of Local-Scale Models for Accidental Releases in Built Environments: Results of the Modelling Exercises in Cost Action ES1006

Silvia Trini Castelli, Kathrin Baumann-Stanzer, Bernd Leitl, C. Maya Milliez, Eva Berbekar, Aniko Rakai, Vladimir Fuka, Antti Hellsten, Anton Petrov, George Efthimiou, Spyros Andronopoulos, Gianni Tinarelli, Richard Tavares, Patrick Armand, Claudio Gariazzo, Klara Jurcakova, Goran Gašparac and all COST ES1006 Members

Abstract A main research task of COST Action ES1006 is the evaluation of atmospheric dispersion models by their comparison against test data from qualified field and laboratory experiments and by a model inter-comparison. The model

S. Trini Castelli (✉)
Institute of Atmospheric Sciences and Climate, National Research Council, Turin, Italy
e-mail: s.trinicastelli@isac.cnr.it

K. Baumann-Stanzer
Central Institute for Meteorology and Geodynamics, Vienna, Austria

B. Leitl
Meteorological Institute, University of Hamburg, Hamburg, Germany

C.M. Milliez
Univ. Paris Est Electricite de France, Chatou Cedex, France

E. Berbekar · A. Rakai
Budapest University of Technology and Economics, Budapest, Hungary

V. Fuka
Faculty of Mathematics and Physics, Department of Meteorology and Environment Protection, Charles University, Prague, Czech Republic

A. Hellsten
Finnish Meteorological Institute, Helsinki, Finland

A. Petrov
National Institute of Meteorology and Hydrology-Bulgarian Academy of Sciences, Sofia, Bulgaria

D.G. Steyn and N. Chaumerliac (eds.), *Air Pollution Modeling and its Application XXIV*, Springer Proceedings in Complexity,
DOI 10.1007/978-3-319-24478-5_79

comparison and evaluation carried out for three test cases is presented, addressing the performance of the different modelling approaches, quantifying the scatter of results when different models are applied and assessing the effect of uncertainties.

79.1 Introduction

Three case studies were considered as modelling exercises for the evaluation activity performed in COST ES1006 Action: (1) the Michelstadt exercise, based on data gathered in a wind-tunnel flow and dispersion experiment where an idealized Central-European urban environment was modelled and both continuous and puff releases were reproduced; (2) a real-field campaign, then reproduced also in the wind tunnel, with continuous and puff releases in a European city with a harbour, named as CUTE case, and (3) a real industrial accident occurred in a European Country, named as AGREE case.

The available models applied to the modelling exercises ranged from Gaussian type (Type 1), to Lagrangian (Type 2) and advanced Eulerian CFD (Type 3) ones. In all cases, 'blind tests' were conducted, that is only the minimum flow information was provided to the modellers. In our approach, it was assumed that a typical emergency response model has already been validated with regard to local-scale dispersion modelling. Thus, the existing model evaluation and validation strategies are extended towards task- and application-specific measures for

G. Efthimiou
University of Western Macedonia, Kozani, Greece

G. Efthimiou · S. Andronopoulos
National Centre for Scientific Research "Demokritos", Aghia Paraskevi, Greece

G. Tinarelli
ARIANET Srl, Milan, Italy

R. Tavares
Laboratory of Hydrodynamics, Energetics and Atmospheric Environment and Institute for Research on Urban Sciences and Techniques, Nantes, France

P. Armand
CEA, DAM, DIF, Arpajon, France

C. Gariazzo
INAIL Research Center, Monteporzio Catone, Italy

K. Jurcakova
Institute of Thermomechanics AS CR, Prague, Czech Republic

G. Gašparac
Gekom—Geophysical and Ecological Modeling Ltd., Zagreb, Croatia

all COST ES1006 Members
http://www.elizas.eu/

accidental release scenarios. In case of continuous release, maximum concentrations, dosages and especially the area affected by values above a relevant threshold usually are the information expected from an emergency response model. In case of one or several puff releases, additional information may be of interest, e.g. the arrival time of the puff at given locations, the duration of the puff passage there, the peak concentration values. Here we discuss a few illustrative examples and outline the major conclusions. For the full description of the results we refer to the official report (Baumann-Stanzer et al. 2015) that will be available on the COST ES1006 Action website http://www.elizas.eu.

79.2 Test Cases, Results and Discussion

In **Michelstadt** test case, a typical European urban site is reproduced (Fig. 79.1), designed to characterise the neighbourhood-scale urban areas across Europe. Data were gathered in a wind-tunnel flow and dispersion experiment at Hamburg University: several continuous and puff releases in different locations were reproduced. For the modelling exercise, both non-blind and blind tests were performed.

CUTE test case regards both a field experiment and its reproduction in the wind tunnel (Fig. 79.1). Continuous and puff releases from a boat towards the harbour area were carried out. The concentration was detected by 20 measurement stations located at different positions in the field experiment, while more than 30 recording stations were used in the wind tunnel.

AGREE test case refers to a real accident where Vinyl Chloride Monomer was released inside a building in a liquid state and partially evaporated causing high concentrations in the air outside the building. Measurements were collected by the local VCM automatic monitoring network (more than 50 samplers) installed around the plant, causing an alarm state and the intervention of Firemen. The accident was managed and closed after about 50 min .

We note that in complex built environments, the model performance is influenced by the location of the source and of the receptor points, since an appropriate and accurate description of the geometry of the surrounding buildings becomes

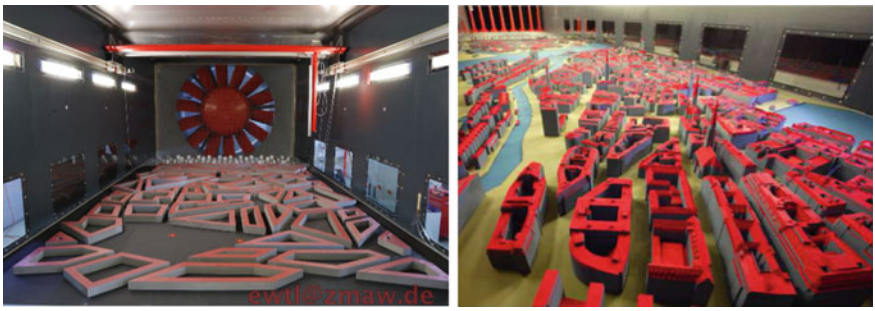

Fig. 79.1 Michelstadt (*left*) and CUTE (*right*) test cases as reproduced in the wind tunnel

fundamental for reproducing the plume separations and the concentration pattern. Even small deviations of the plume due to a not perfect reproduction of the flow inside the buildings may compromise the model performance at a measuring point in street canyons or crossings.

From the Michelstadt and CUTE wind-tunnel experiments we have learnt that, as expected, the model performance increases with increasing model complexity, that is the level of physical description. The improving trend in accuracy when going from the simpler to the more sophisticated models was observed qualitatively from scatter plots (Fig. 79.2) and quantitatively by comparing the validation

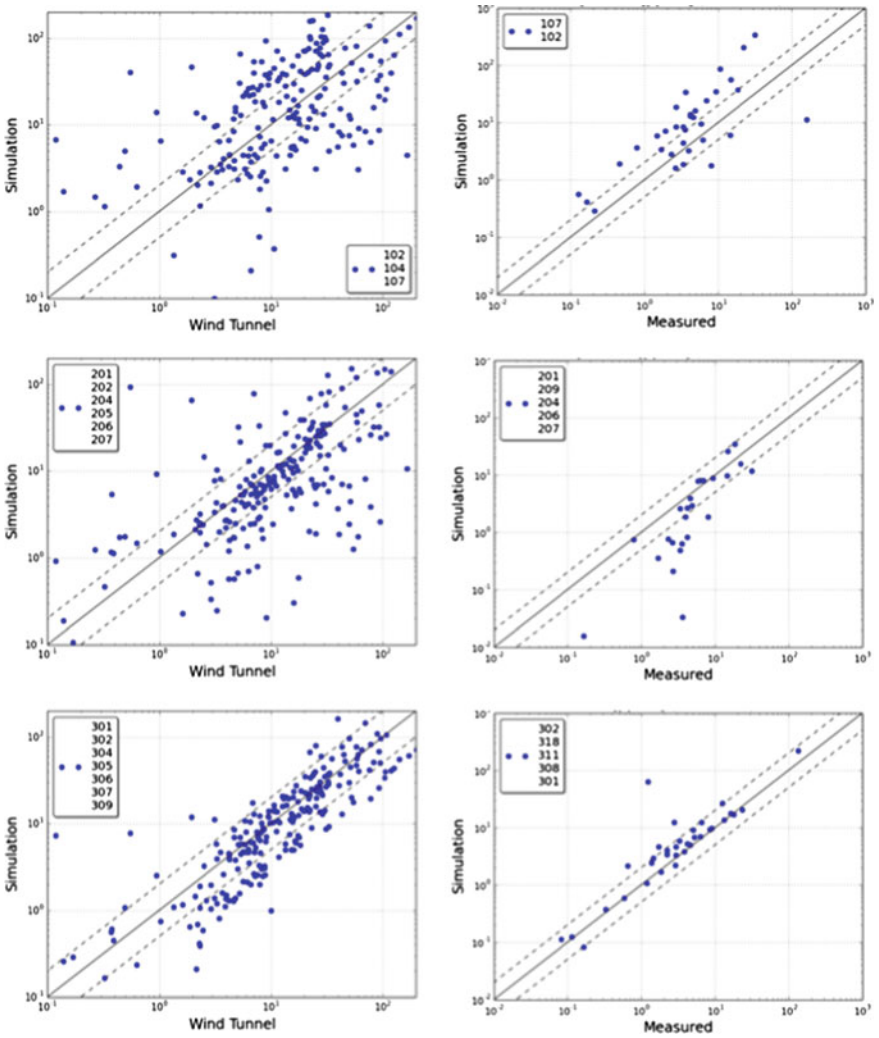

Fig. 79.2 Scatter plots of the observed mean concentrations versus the ensemble averaged modelled mean concentrations for Michelstadt (*left*) and CUTE (*right*) continuous release, for models Type 1 (*top*), Type 2 (*middle*) and Type 3 (*bottom*)

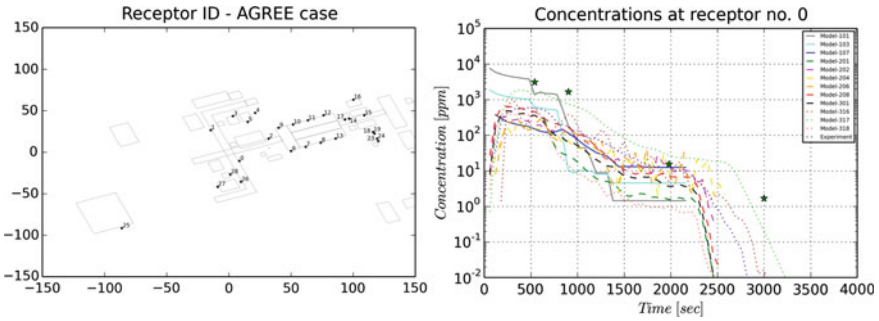

Fig. 79.3 Sketch of the AGREE site (*left*) and comparison between time-dependent concentrations observed and modelled at a receptor nearby the emission point (*right*)

metrics. In particular, we noticed that the Type 1 models are not adequate for correctly reproducing puff releases, due to large underestimation of the measured concentrations. On the other hand, Type 3 models still need long computation and preparation time and are not yet directly usable in the emergency phase during the response, where a fast answer is requested. In this case, Type 2 models are significantly faster than Type 3 ones, they render a satisfying agreement with measurements and could be used with a certain confidence. Within the Michelstadt exercise the issue of blind versus non-blind test was also addressed. Even if in the continuous-release test the acceptance limits for the metrics are better matched for the non-blind case, in general the quality of the results shows no clear systematic difference between the non-blind and the blind test. This suggests that the performance of the models might be well established and assures the same performance also when the information related to the input is very limited and the evolution of the dispersion is unknown. This is confirmed by the results obtained for the AGREE case, for which the models show reasonable results even in such difficult, complex and uncertain situation, as in the example of Fig. 79.3.

Question and Answer

Questioner: S. Hanna

Question: In view of the uncertainties in modelled and observed wind and plume directions that you showed, shouldn't we advise emergency responders that we are not sure which way the plume will go?

Answer: In the cases where modellers can rely on good quality input data (for example, in monitored industrial sites), we think that an information of the direction of the plume and the consequent affected areas can and should be given to emergency responders with a certain confidence, using adequately advanced and

evaluated modelling tools. An estimation of the related uncertainty of the modelled affected area would add additional value, although this is at present typically not required by decision makers. The estimation of this uncertainty is an open and debated research field.

Reference

Baumann-Stanzer K, Trini Castelli S, Stenzel S (eds) (2015) COST ES1006 model evaluation case studies: approach and results. http://www.elizas.eu

Chapter 80
High Resolution Model Simulations of the Canadian Oil Sands with Comparisons to Field Study Observations

P.A. Makar, C. Stroud, J. Zhang, M. Moran, A. Akingunola, W. Gong, S. Gravel, B. Pabla, P. Cheung, Q. Zheng, G. Marson, S.-M. Li, J. Brook, K. Hayden, J. Liggio, R. Staebler and A. Darlington

Abstract The governments of Canada and Alberta are implementing a joint plan for oil sands monitoring that includes investigating emissions, transport and downwind chemistry associated with the Canadian oil sands region. As part of that effort, Environment Canada's Global Environmental Multiscale—Modelling Air-quality And CHemistry (GEM-MACH) system was reconfigured for the first time to create nested forecasts of air quality at model grid resolutions down to 2.5 km, with the highest resolution domain including the Canadian provinces of Alberta and Saskatchewan. The forecasts were used to direct an airborne research platform during a summer 2013 monitoring intensive. Subsequent work with the modelling system has included an in-depth comparison of the model predictions to monitoring network observations, and to field intensive airborne and surface supersite observations. A year of model predictions and monitoring network observations were compared, as were model and aircraft flight track values. The relative impact of different model versions (including modified emissions and feedbacks between weather and air pollution) will be discussed. Model-based predictions of indicators of human-health (i.e., Air Quality Health Index) and ecosystem (i.e. deposition of pollutants) impacts for the region will also be described.

P.A. Makar (✉) · C. Stroud · J. Zhang · M. Moran · A. Akingunola · W. Gong · S. Gravel · B. Pabla · P. Cheung · Q. Zheng · G. Marson · S.-M. Li · J. Brook · K. Hayden · J. Liggio · R. Staebler · A. Darlington
Air Quality Research Division, Environment Canada, 4905 Dufferin Street, Toronto, ON M3H 5T4, Canada
e-mail: paul.makar@ec.gc.ca

D.G. Steyn and N. Chaumerliac (eds.), *Air Pollution Modeling and its Application XXIV*, Springer Proceedings in Complexity,
DOI 10.1007/978-3-319-24478-5_80

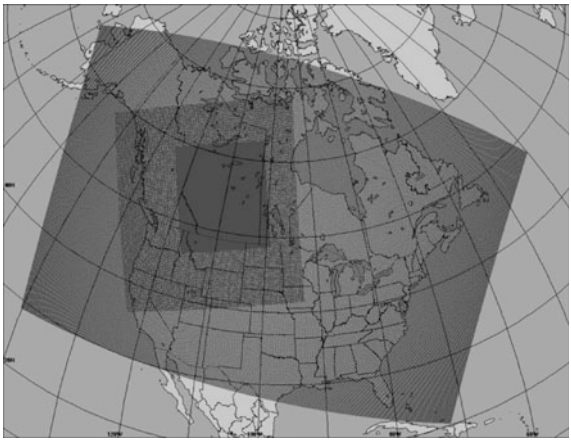

Fig. 80.1 Three-level nested grid of GEM-MACH used in environment Canada oil sands simulations

80.1 GEM-MACH

The model used by Environment Canada for the simulation of air quality in the oil sands region is the on-line Global Environmental Multiscale—Modelling Air-quality and CHemistry (GEM-MACH) system. GEM-MACH was first described in Moran et al. (2010); for a detailed description of the model and comparisons with peer-models and observations see Makar et al. (2014a, b). The model includes detailed chemistry (gas and aqueous phase, inorganic and organic secondary particle formation, 2-or-12-bin sectional aerosol microphysics, with eight particle species (sulphate, nitrate, ammonium, secondary organic aerosol, primary organic aerosol, elemental carbon, sea-salt and crustal material). A three-level nesting setup was used here (Fig. 80.1): 10 km/36 h continental forecasts feeding 10 km/30 h W. Canada/NW USA, feeding the 2.5 km/24 h Alberta/Saskatchewan domain.

Annual and 1-month simulations using the 2-bin and 12-bin model versions, respectively, have been carried out; the latter are being compared to aircraft and ground-based monitoring intensive observations from the summer of 2013 to evaluate the impact of new emissions data and other model improvements on the model performance. Both sets of simulations include outputs which can be used to estimate potential human health (e.g. Air Quality Health Index) and ecosystem impacts (e.g. deposition of sulphur and nitrogen to ecosystems within the 2.5 km domain). The model output is also being used to develop methodologies to evaluate the effectiveness of the spatial placement of monitoring site locations.

80.2 Monitoring Data

Two types of observation data are being compared to model output; (a) hourly AIRNOW monitoring network data, with 40 stations across the high-resolution domain, for a simulation from October 1, 2013 through September 30th, 2014, and

(b) aircraft and ground-based monitoring intensive data, for the period August 10th through September 10th, 2013). The latter provides more process-oriented model evaluation.

80.3 Comparisons to Observations—Examples

Table 80.1 presents 2-bin model domain-wide annual average statistics for the above period. Ozone (O_3) and fine particulate matter ($PM_{2.5}$) have the best performance for normalized mean bias and errors, while nitrogen oxides (NO_x) have the best correlation coefficient though with a positive bias of 45 %. Sulphur dioxide (SO_2) performance is relatively poor in comparison to the other species. Figure 80.2 shows the corresponding surface maps for these species, as well as total volatile organic compounds (TVOC), annual deposition of total sulphur, total nitrogen, and their sum, and the Air Quality Health Index (AQHI). The deposition totals will be used in future calculation of exceedences of critical loads, a measure of ecosystem damage. The AQHI is a measure of short term human health impacts and is a nonlinear function of the concentrations of O_3, nitrogen dioxide (NO_2) and $PM_{2.5}$.

An example of a comparison between model and aircraft observations for one of the 22 flights that comprised the summer 2013 monitoring intensive is shown in Fig. 80.3. The flight track (yellow line) for this measurement flight is shown in Fig. 80.3a, around one of the oil sands facilities (solid coloured regions shows property boundaries and ownership for different facilities). Figure 80.3b shows the model-predicted SO_2 concentrations in the column during the flight, overlaid with the observed values as dots with the same colour scale. The model-predicted magnitudes were reasonable for this flight, but the model consistently over-predicted the height of the SO_2 plume. Initial analysis indicates the stack volume flow rates and temperatures from continuous emissions monitoring for this source are lower than those in the emissions inventory used for the simulations. The

Table 80.1 Annual average comparisons, 2.5 km domain AIRNOW stations

	O_3 (ppbv)	NO_x (ppbv)	$PM_{2.5}$ (ug m^{-3})	SO_2 (ppbv)
Number of stations	38	38	40	44
FAC2[a]	1.00	0.76	0.85	0.09
NMB	−0.01	0.45	−0.05	2.25
NMGE	0.12	0.57	0.36	2.89
RMSE	4.11	10.02	3.12	6.68
R	0.58	0.72	0.49	−0.09

[a]*FAC2* Fraction of model values within a factor of two of observations. *NMB* Normalized mean bias. *NMGE* Normalized mean gross error. *RMSE* Root mean square error. *R* Pearson's correlation coefficient

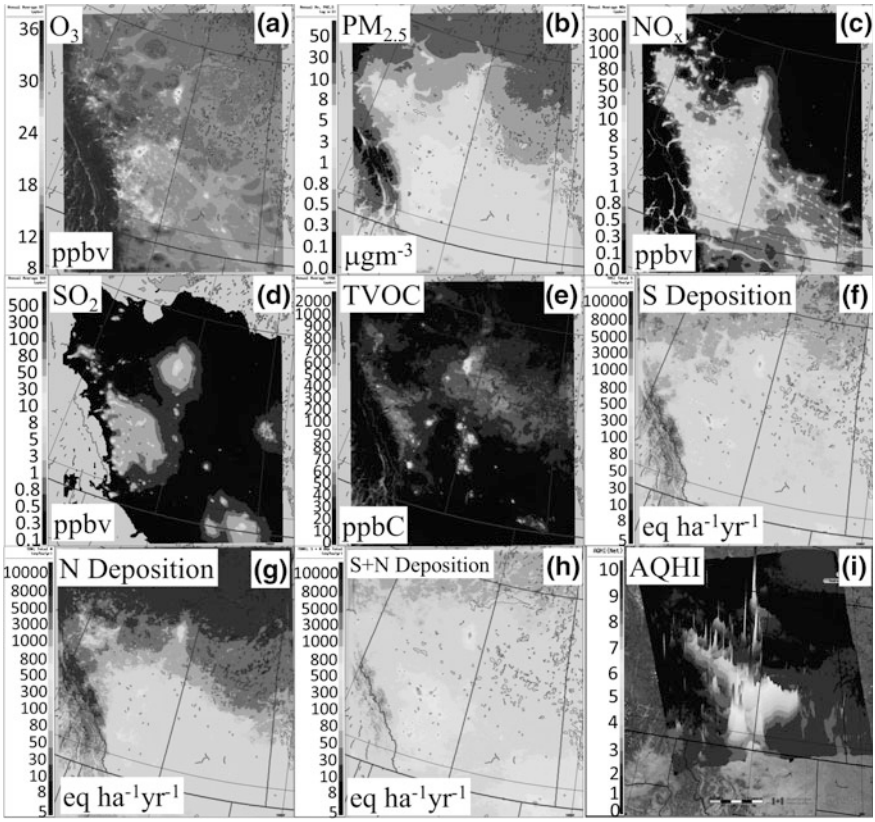

Fig. 80.2 **a**–**h** Annual averages of O_3, $PM_{2.5}$, NO_x, SO_2, TVOC, S deposition, N deposition, S+N deposition. **i** Example AQHI prediction for 19UT August 23rd, 2013

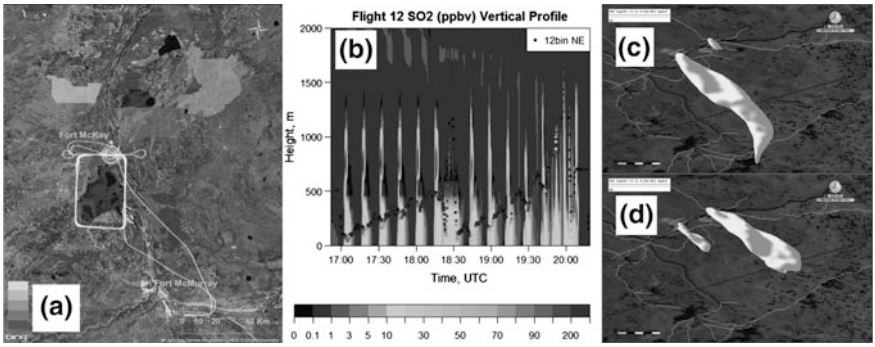

Fig. 80.3 **a**, **b**: Flight track and model versus observations SO_2 comparison, flight 12. **c**, **d**: Older inventory and new CEM emission impacts on SO_2 plumes

use of the Alberta Continuous Emissions Monitoring System (CEMS) data for emissions input is being investigated under current work. Figure 80.3c, d contrast the model's 3 ppbv SO_2 3D contour envelope for older inventory (c) and more accurate (CEMS and other information-based) emissions (d), respectively. The use of the updated emissions information has a substantial impact on the location and distribution of the plumes.

Further examples of additional model simulations (e.g. weather/ air pollution feedback effects, scenarios using revised anthropogenic and biogenic emissions, special studies using revised model parameterizations, critical load estimates), etc., will be presented at the meeting.

80.4 Question and Answer

Questioner: S.T. Rao

Question: Would you care to comment on the subgridscale variability of the monitoring network data used in the model evaluation? Do you have any plans to examine this?

Answer: This is actually the subject of investigation within the current fiscal year. We are hoping to analyze both the model output and the observation data in order to determine the extent to which specific stations may influence the model performance statistics, as well as use the model as a proxy for determining the optimum locations for possible future monitoring stations.

Questioner: C. Hogrefe

Question: Do you plan to do longer-term runs for feedbacks?

Answer: Longer term runs at lower resolution were carried out under the AQMEII-2 model/observation intercomparison program, see above references. For the high resolution simulations carried out here, the difficulty is the requisite processing time. We have carried out high resolution runs with the 2 particle bin version of the model as an on-going forecast, but these are not in feedback mode (and the 2 particle bin version of the model does not provide adequate particulate size resolution to simulate feedback effects properly). The 12-bin version of the model has been used here for 3 simulations (no-feedback, direct-effect only, and direct + indirect effect), each with 3 levels of nesting and each of 1 month duration, and each nested simulation takes place at about ½ real time. A longer term simulation with 12-bin version of the model isn't practical with the current level of computer resources, but may be so in the future.

References

Makar PA, Gong W, Milbrandt J, Hogrefe C, Zhang Y, Curci G, Zabkar R, Im U, Balzarini A, Baro R, Bianconi R, Cheung P, Forkel R, Gravel S, Hirtl M, Honzak L, Hou A, Jimenez-Guerrero P, Langer M, Moran MD, Pabla B, Perez JL, Pirovano G, San Jose R, Tucella P, Werhahn J, Zhang J, Galmarini S (2014a). Feedbacks between air pollution and weather, Part 1: effects on weather. Atmos Environ (in press)

Makar PA, Gong W, Hogrefe C, Zhang Y, Curci G, Zabkar R, Milbrandt J, Im U, Balzarini A, Baro R, Bianconi R, Cheung P, Forkel R, Gravel S, Hirtl M, Honzak L, Hou A, Jimenez-Guerrero P, Langer M, Moran MD, Pabla B, Perez JL, Pirovano G, San Jose R, Tucella P, Werhahn J, Zhang J, Galmarini S (2014b). Feedbacks between air pollution and weather, Part 2: effects on chemistry. Atmos Environ (in press)

Moran MD, Menard S, Talbot D, Huang P, Makar PA, Gong W, Landry H, Gravel S, Gong S, Crevier L-P, Kallaur A, Sassi M (2010) Particulate-matter forecasting with GEM-MACH15, a new Canadian air-quality forecast model. In: Steyn DG, Rao ST (eds) Air pollution modelling and its application XX. Springer, Dordrecht, pp 289–292

Chapter 81
Uncertainties of Top-Down Fire Emission Estimates at Regional and Global Scales

M. Sofiev, J. Soares, J. Vira, M. Prank and R. Kouznetsov

Abstract Top-down emission estimation via inverse dispersion modelling is frequently used for estimation of emission from wild-land fires. The approach, efficiently constraining the emission from fires, also has major uncertainties, which are illustrated here with a few examples of the Integrated System for wild-land Fires (IS4FIRES).

81.1 Integrated System for Wild-Land Fires (IS4FIRES)

IS4FIRES generates the smoke emission and injection profile from MODIS and SEVIRI active-fire radiative energy observations. The emission calculation includes two steps: (i) top-down calibration of emission factors via inverse dispersion problem solution that is made once, (ii) application of the obtained emission coefficients to individual-fire radiative energy observations, thus leading to bottom-up emission compilation.

Based on Kaufman et al. (1998) and Ichoku and Kaufman (2005) it is possible to relate the energy of the fire with the rate of biomass consumption and derive a relationship between the release of radiative energy by the fire, the so-called fire radiative power (FRP), and its emission fluxes.

$$E_i = C_{ia} * FRP \tag{81.1}$$

Here C_{ia} is the emission coefficient [kg MJ^{-1}]. Its assessment for each type of the fire, land use, environmental conditions, etc., is the goal of the top-down system calibration. Having the set of coefficients C_{ia} determined during the top-down step, the emission calculation turns into scaling of the observed fire radiative energy (the bottom-up inventory construction step).

M. Sofiev (✉) · J. Soares · J. Vira · M. Prank · R. Kouznetsov
Finnish Meteorological Institute, Erik Palmenin Aukio 1, Helsinki, Finland
e-mail: mikhail.sofiev@fmi.fi

D.G. Steyn and N. Chaumerliac (eds.), *Air Pollution Modeling and its Application XXIV*, Springer Proceedings in Complexity,
DOI 10.1007/978-3-319-24478-5_81

81.2 Major Contributors into Emission Uncertainties

For the procedure outlined above, the uncertainties include both the errors coming from the calibration top-down step and of the bottom-up inventory compilation. In particular: (i) imperfect information on fires, (ii) simplifications in the fire description, (iii) inaccuracies in the smoke observations and modelling, (iv) inaccuracies of the inverse problem solution.

Detailed analysis of these uncertainties can be found in Soares et al. (2015). Here, we summarise the findings and extend the analysis with the most-recent results.

The emission estimation methodology based on FRP observations has both strong and weak points. It avoids using the extremely uncertain parameters, such as the fuel load and combustion efficiency, as well as the guess-work on the fire intensity, its temporal evolution, injection height, etc. The utilization of the direct fire power observations, especially if they are made several times a day, provides more information.

The main weak points originate from the instant character of the FRP observations, which lead to strong under-sampling of the dataset (e.g. Wooster et al. 2005; Schultz et al. 2008; Kaufman, et al. 1998). The second major contributor to the uncertainty of the coefficients is the high sensitivity of PM emission to burning characteristics.

The above main uncertainties, if left unconstrained, result in substantial and poorly determined biases in the total emission estimation. The only possibility to constrain them is the calibration step: the dispersion calculations integrate the fire emission and mix-up the plumes from many fires. The subsequent comparison with observations and adjustment of the coefficients then incorporates all errors into the optimised EFs.

The IS4FIRES calibration relies on SILAM modelling of plume dispersion and increase of atmospheric optical density (AOD), which is then compared with MODIS observations. The SILAM computations of AOD incorporate a number of simplifications, e.g. aerosol size distribution, chemical composition and hygroscopy, limited list of species considered, etc.

Thus, recent observations of the fire smoke size distributions suggested much wider range with substantial concentrations than anticipated before—and also large fraction of small particles even in mass-weighted distribution (Fig. 81.1).

Discussion

Question (Amir Hakami)
Can you comment on the impact of over-pass time on your top-down estimates?
Answer:
Indeed, the effect of the overpass time can be very substantial: both MODIS-loaded satellites have sun-synchronous orbits, i.e. they fly over each area at the same local

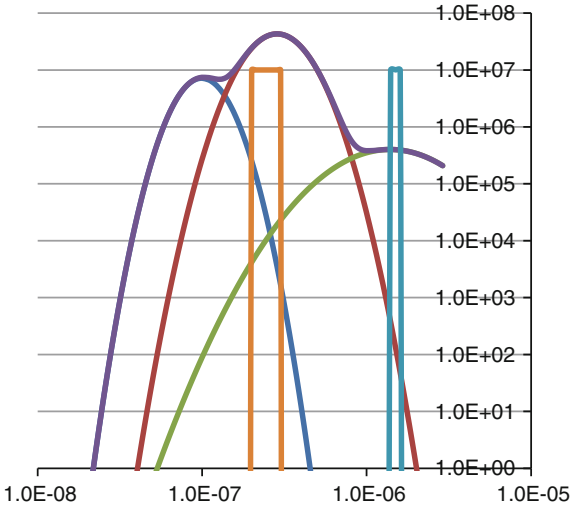

Fig. 81.1 Fit of the mass-weighted observed distribution (Virkkula et al. 2014) with 3 log-normal functions, IS4FIRES v.1 PM2.5 distribution (*blue rectangular*) and Reid et al. (2005) distribution (*orange rectangular*)

time every day. Since fires have strong diurnal variation, there is a correlation, which can lead to significant biases in the total emission estimates made by the top-down approach. To reduce this effect, we included the mean diurnal variation of the fire intensity, as observed by SEVIRI geostationary satellite for the three main types of the land-use: grasses, forests, and mixed vegetation. The observed MODIS FRP is then scaled with the SEVIRI-based diurnal variation. This does not give us much information on an individual fire but is quite efficient in the mean bias reduction.

Question (Talat Odman)
AOD indicates smoke while FRP indicates fire. The smoke from the same fire may be in different locations. When you try to determine the uncertainty by comparing AOD (top-down approach) to FRP (bottom-up), how do you reconcile for this difference? You mentioned dispersion modelling; what kind of additional uncertainties does the model introduce?

Second, there are reliable ground-based information on fires in certain parts of the world. Could those available data be used to determine the uncertainty in different global fire emission inventories, or at least to get an idea of which ones are more accurate?
Answers:
About AOD vs FRP. Indeed, the fire smoke is transported over substantial distances and AOD is affected over quite large areas downwind from the fire. To connect these two pieces together, we use dispersion model SILAM, which is an Eulerian chemistry transport model equipped with the wild-land fire source term. It accounts for the plume elevation due to buoyancy, mixing due to turbulence, transport and chemical and physical transformations of the smoke. It also computes AOD as a standard output. Since the model can tag the species, it is straightforward to

associate specific AOD contribution with the fire sources, thus being able to select the areas where AOD is mainly determined by the fires. Only those areas are used for the system calibration. The uncertainties are the standard ones for such types of models. The most-significant impact comes from the wind direction and precipitation fields. The latter one is of particular importance because of strong convective activity in summer, which leads to chaotically located convective precipitation events. In large-scale weather models they can form a "wall of rain", which completely washes out the plume—whereas in reality it passes between the individual events. One can deal with it either increasing the resolution or introducing some rain porosity parameterizations.

About in situ data on the fires. Such data are very welcome but, unfortunately, they refer to the areas, where the fires are by no means the biggest ones: information on vast fires in Africa, Siberia, Amazonia, and even Canada and Alaska is almost exclusively satellite-born. But wherever possible, such data can be and are being used for evaluation of the remote-sensing inventories. The problem is just that such comparison constrains only specific types of fires and only in specific regions.

References

Ichoku C, Kaufman YJ (2005) A method to derive smoke emission rates from MODIS fire radiative energy measurements. IEEE Trans Geosci Remote Sens 43(11):2636–2649. doi:10.1109/TGRS.2005.857328

Kaufman YJ, Justice CO, Flynn LP, Kendall JD, Prins EM, Giglio L, Ward DE, Menzel WP, Setzer AW (1998) Potential global fire monitoring from EOS-MODIS. J Geophys Res-Atmos 103(D24):32215–32238

Schultz MG et al (2008) FREEVAL final report: p 139

Soares J, Sofiev M, Hakkarainen J (2015) Uncertainties of wild-land fires emission in AQMEII phase 2 case study. AtmosphEnviron. doi:10.1016/j.atmosenv.2015.01.068

Virkkula A et al (2014) Prescribed burning of logging slash in the boreal forest of Finland: emissions and effects on meteorological quantities and soil properties. Atmos Chem Phys 14 (9):4473–4502, doi:10.5194/acp-14-4473-2014

Wooster MJ, Roberts G, Perry GLW, Kaufman YJ (2005) Retrieval of biomass combustion rates and totals from fire radiative power observations: FRP derivation and calibration relationships between biomass consumption and fire radiative energy release. J Geophys Res 110(D24311) doi:10.1029/2005JD006318

Chapter 82
Inherent Uncertainties in Atmospheric Models: Weather and Air Pollution

Marina Astitha, Jaemo Yang, Huiying Luo and S.T. Rao

Abstract It is well known that there are reducible and irreducible uncertainties in both uncoupled and coupled meteorology-atmospheric chemistry models. Reducible (i.e., structural and parametric) uncertainties are attributable to our incomplete or inadequate understanding of the relevant atmospheric processes (e.g. chemical mechanism, PBL evolution, modeling domain, grid resolution, cloud treatment) and errors in model input data (e.g., emissions, boundary conditions). Inherent or irreducible uncertainties stem from our inability to properly characterize the atmosphere with appropriate initial conditions. When the initial state of the atmosphere is unknown, its future state cannot be predicted with great accuracy. There is an emerging need to properly assess these types of modeling uncertainties in order to improve the prediction accuracy of modeling systems. This work focuses on the assessment of inherent uncertainties in atmospheric and air quality modeling systems by estimating the impacts of various options for initial conditions on weather parameters and their consequent effect on atmospheric pollutant concentrations. Support for the modeling efforts is given by data collected from surface measurement networks for the meteorological and air quality parameters. We focus on the changes in atmospheric variables that strongly affect the fate and transport of air pollutants like ozone and aerosols.

M. Astitha (✉) · J. Yang · H. Luo
Department of Civil & Environmental Engineering, University of Connecticut, Storrs-Mansfield, CT 06269, USA
e-mail: astitha@engr.uconn.edu

S.T. Rao
Department of Marine, Earth & Atmospheric Sciences, North Carolina State University, Raleigh, NC, USA

D.G. Steyn and N. Chaumerliac (eds.), *Air Pollution Modeling and its Application XXIV*, Springer Proceedings in Complexity,
DOI 10.1007/978-3-319-24478-5_82

82.1 Introduction

The scientific discussion on model uncertainty reduction goes back more than two decades with the current practice including model evaluation, data assimilation and ensemble modeling techniques (Hogrefe et al. 2000, 2001; Gilliam et al. 2012 among others). Nevertheless, the inherent uncertainty cannot be eliminated since our inability to properly characterize the initial state of the atmosphere will prevent the accurate prediction of its future state (Porter et al. 2015). This complex topic is addressed in this work using three model initialization fields from global model analyses outputs. Four Dimensional Data Assimilation (FDDA) is implemented in the gridded domain (analysis nudging) and the uncertainty is quantified for cloud formation, precipitation, wind speed and atmospheric pollutant concentrations (gases and aerosols) for continental and Northeastern US. The results indicate that the most impacted atmospheric fields are precipitation, cloud cover, ventilation coefficient, and sea salt loading. The predicted daily maximum ozone concentration has shown substantial variability, ranging from 10 to 40 %, during the simulation period.

82.2 Methodology

In this work we assess the inherent uncertainty by keeping the model configuration and physics the same and change the initial conditions through analysis nudging using the atmospheric modeling system RAMS/ICLAMS. The coupled meteorology-chemistry modeling system RAMS/ICLAMS is based on RAMSv.6 (Cotton et al. 2003) with the implementation of atmospheric gases and aerosols (Solomos et al. 2011; Kushta et al. 2014). RAMS/ICLAMS includes the following modules and capabilities: Online production of desert dust and sea salt emissions; Rapid Radiative Transfer Model (RRTM); Desert dust and sea-salt radiative effects as a function of size and water content; Explicit treatment of desert dust and sea salt as CCN, GCCN and IN particles; Cloud microphysics: Two-moment bulk scheme with 5 ice condensates species. For the air quality simulations we used anthropogenic emissions for 2005 on 0.1 × 0.1° resolution (EDGAR-JRC); gas, aqueous and aerosol phase chemistry (CB-V, ISORROPIA); dry and wet deposition modules.

Three simulations were conducted for the period 10–19 June 2006 by utilizing different initial conditions: the NCEP Global Forecast System (GFS) Analyses (1 × 1°), the NCEP FNL (Final) Operational Global Analyses data (1 × 1°) and the European Center for Medium-Range Weather Forecasts (ECMWF) Analyses (1 × 1°). The variability of atmospheric variables was examined by estimating the standard deviation and coefficient of variation (as stdev/mean) for the three simulations. Also, we examined the hourly RMSE for those variables where measurements were available. The focus of this work is primarily in NE U.S. and results are

discussed for wind speed at 850 hPa (steering level), ventilation coefficient (wind speed@10 m*mixing height), cloud cover, precipitation, sea salt and maximum ozone concentration.

82.3 Results and Discussion

We have focused on the inherent uncertainty in coupled atmospheric-air quality models by examining the impact of various initial conditions on weather variables. Preliminary results have showed that the most impacted atmospheric fields are ventilation coefficient (Fig. 82.1), precipitation, cloud cover (Fig. 82.2), and sea salt load (Fig. 82.3).

Ozone daily maximum concentration has shown substantial variability throughout the simulation. As expected, the variability caused by changing initial conditions is more pronounced during the first days of the simulation. Figure 82.4 illustrates the changes in wind speed and temperature variability in the hourly RMSE. Nevertheless, the variability of daily maximum ozone concentration is non-negligible throughout the simulation as a result of the variability in

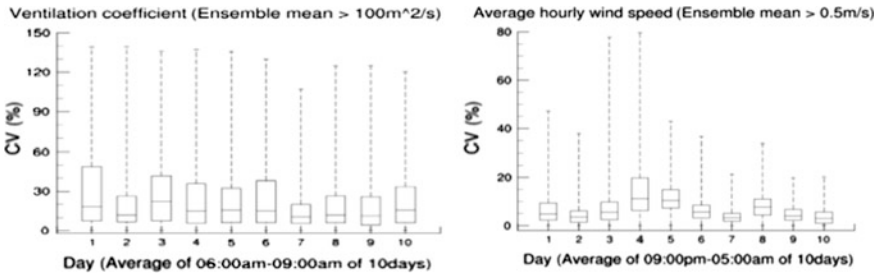

Fig. 82.1 Coefficient of variation (CV) for daytime ventilation coefficient (*left*); nighttime wind speed at 850 hPa (*right*) for the simulation period June 10–19, 2006

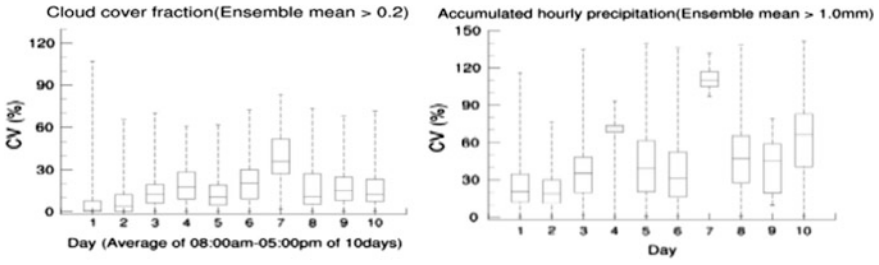

Fig. 82.2 CV for cloud cover fraction (*left*) and accumulated precipitation (*right*)

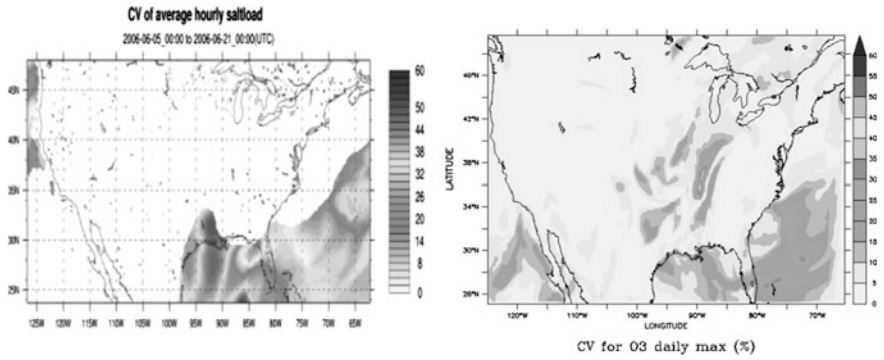

Fig. 82.3 CV for sea salt load (*left*) and daily maximum ozone concentration (06/18; *right plot*)

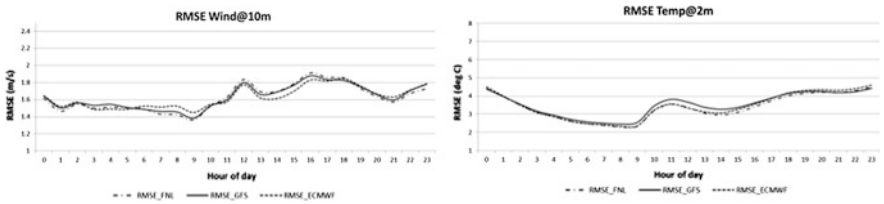

Fig. 82.4 Hourly RMSE for wind speed at 10 m (*left*) and temperature at 2 m (*right*) for 10–19 June 2006, for NE US

atmospheric variables that control the production (shortwave radiation, clouds) and fate (wind speed, precipitation) of atmospheric chemical species.

In general, the preliminary results indicate that the inherent uncertainty in characterizing the atmospheric fields (meteorological and air pollution) is substantial, ranging from 10 to 100 % for some variables. Further research is needed to quantify the confidence that can be placed for policy analysis and regulatory assessments. Future research includes the examination of inherent uncertainty from longer time period simulations to understand seasonal variation and the impact of changing emissions on air quality variables; include additional initialization fields (i.e. NAM, NARR, SREF) in model simulations; determine the influence of inherent uncertainty on concentrations of additional atmospheric pollutants.

Acknowledgments This work is partially supported by the Northeast Utilities (NU) project "Damage Modeling and Forecasting System of the NU Center Bridge-Funding", Northeast Utilities and Department of Civil and Environmental Engineering, School of Engineering, University of Connecticut. Part of this work was also supported by the Center for Environmental Science and Engineering (CESE) at the University of Connecticut (www.cese.uconn.edu) through the PhD fellowship for Jaemo Yang.

Question and Answer

Questioner: D.G. Steyn
Question: I wonder about the validity of averaging the ventilation coefficient from 0600-0900, especially in the coastal zone where both u and z_i are changing so rapidly in time (and space)?
Answer: The rationale for choosing the 6–9 am EDT is that emissions, predominantly from mobile sources since utility sector emissions are trapped aloft in the residual layer, are injected into the atmosphere. The variation in emissions loading and mixing height is not that great during these early morning hours; the mixing height usually grows very rapidly after 9 am EDT. The fate of reactive pollutants depends on the ventilation coefficient, which represents the amount of dilution of the emissions injected into the atmosphere. The efficacy of emission control strategies depends on whether the chemicals are allowed to react first and then diluted or diluted first and then allowed to react (see "Effects of Uncertainties in Meteorological Inputs on Urban Airshed Model Predictions and Ozone Control Strategies, G. Sistla, N. Zhou, J.Y. Ku, W. Hao, S.T. Rao, R. Bornstein, F. Freedman, P. Thunis, Atmos. Environ., 30: 12, 1996; "Numerical Investigation of the Effects of Boundary-Layer Evolution on the Predictions of Ozone and the Efficacy of Emission Control Strategies in the Northeastern United States" by M. Ku, K. Zhang, H. Mao, K. Civerolo, S.T. Rao, C.R. Philbrick, R. Clark, B. Doddridge, Environ. Fluid Mech.,1(2), 2001; "Summertime Characteristics of the Planetary Boundary Layer over the Eastern United States and Relationships to Ambient Ozone Levels" by S.T. Rao, J.Y. Ku, S. Berman,K. Zhang, H. Mao, Pure and Applied Geophysics., 160:21–55, 2003; "Spatial and Temporal Variations in Mixing Heights over the Northeastern United States" by S. Berman, J.Y. Ku, S.T. Rao, J. Appl. Meteor., 1999; "The Role of Vertical Mixing in the Temporal Evolution of the Ground-level Ozone Concentrations" by J. Zhang and S.T. Rao, J. Appl. Meteor., 1999). We agree that averaging the ventilation coefficient over the morning hours (6–9am) smoothens out the results. Even with the smoothened results, we see that the variability can be significant near the coast and inland, caused by the different initialization states.

Questioner: Pavel Kishcha
Question: Do you use data assimilation using available meteorological observations? This could reduce significantly differences in the initial meteorological conditions from the three different sources used.

Answer: The simulations were performed with four dimensional data assimilation using an analysis nudging scheme; a scheme where the domain is nudged toward a gridded data analysis (the global model analyses fields). The global model analyses fields have incorporated a variety of observations from in situ stations, radars, radiosondes etc. In that sense, the simulations were performed with the best-of-knowledge initial and boundary conditions but the inherent uncertainty we discuss in this work goes beyond the usage of this and similar nudging techniques. The initial state will always be uncertain since the geographic coverage of the

observations cannot match the area of any model domain and, thus, the initialization will be one realization of possible initial states. Our work attempts to quantify this uncertainty and provide confidence limits in the model predictions that focus on regulatory applications.

References

Cotton WR et al. (2003) RAMS 2001: Current status and future directions. Meteorol Atmos Phys 82:5–29. doi:10.1007/s00703-001-0584-9

Gilliam RC, Godowitch JM, Rao ST (2012) Improving the horizontal transport in the lower troposphere with four dimensional data assimilation. Atmos Environ 53:186–201

Hogrefe C, Rao ST, Zurbenko IG, Steven Porter P (2000) Interpreting the information in ozone observations and model predictions relevant to regulatory policies in the Eastern United States. Bull Am Meteorol Soc 81:9

Hogrefe C, Rao ST, Kasibhatla P, Hao W, Sistla G, Mathur R, McHenry J (2001) Evaluating the performance of regional-scale photochemical modeling systems: Part II—ozone predictions. Atmos Environ 35:4175–4188

Kushta J, Kallos G, Astitha M, Solomos S, Spyrou C, Mitsakou C, Lelieveld J (2014) Impact of natural aerosols on atmospheric radiation and consequent feedbacks with the meteorological and photochemical state of atmosphere. J Geophys Res 119(3). doi: 10.1002/2013JD020714

Porter SP, Rao ST, Hogrefe C, Gego E, Mathur R (2015) Methods for reducing biases and errors in regional photochemical model outputs for use in emission reduction and exposure assessments. Atmos Environ 112:178–188

Solomos S, Kallos G, Kushta J, Astitha M, Tremback C, Nenes A, Levin Z (2011) An integrated modeling study on the effects of mineral dust and sea salt particles on clouds and precipitation. Atmos Chem Phys 11:873–892. doi:10.5194/acp11-873-2011

Chapter 83
Diagnostic Evalutation of Bromine Reactions on Mercury Chemistry

Johannes Bieser, Volker Matthias, Oleg Travnikov, Ian M. Hedgecock, Christian Gencarelli, Francesco De Simone, A. Weigelt and Jialei Zhu

Abstract This model study about the influence of chemical reactants on the transport of mercury is part of an international mercury model inter-comparison (MMTF) coordinated by the EU-FP7 Research Project GMOS (Global Mercury Observation System). GMOS focuses on the improvement and validation of mercury models to assist establishing a global monitoring network and to support the implementation of the Minamata Convention. For the model inter-comparison, several global and regional Chemistry Transport Models (CTM) were used to simulate the influence of reactants on mercury oxidation. For this, gas and aqueous phase reactions of mercury with bromine were implemented into the models. As reactants, precalculated bromine concentrations were taken from the global bromine models P-TOMCAT and GEOS-CHEM. The modelled concentrations of oxidized mercury were compared to observations from GMOS measurement stations, and air craft campaigns. It was found that, even outside of polar regions, bromine plays an important role in the oxidation of mercury. Moreover, the chosen reactant influenced the vertical distribution of mercury in the atmosphere. While little difference was found for GOM concentrations at the surface level, the bromine reaction was able to explain the elevated concentration of GOM observed in the free troposphere.

J. Bieser (✉) · V. Matthias · A. Weigelt
Helmholtz-Zentrum Geesthacht, Institute of Coastal Research, Max-Planck-Strasse 1, 21502 Geesthacht, Germany
e-mail: johannes.bieser@hzg.de

J. Bieser
DLR—Deutsches Luft und Raumfahrtzentrum, Münchener Straße 20, 82234 Weßling, Germany

O. Travnikov
Meteorological Synthesizing Center-East of EMEP, 2nd Roshchinsky proezd, 8/5, Moscow 115419, Russia

I.M. Hedgecock · C. Gencarelli · F. De Simone
CNR—Istituto Inquinamento Atmosferico, U.O.S. di Rende, UNICAL-Polifunzionale, 87036 Rende, Italy

J. Zhu
Nanjing University, 22 Hankou Road, Nanjing, China

D.G. Steyn and N. Chaumerliac (eds.), *Air Pollution Modeling and its Application XXIV*, Springer Proceedings in Complexity,
DOI 10.1007/978-3-319-24478-5_83

83.1 Introduction

Mercury is a toxic substance that is ubiquitous in the environment. In the atmosphere mercury exists in three forms: Gaseous Elemental Mercury (GEM), Gaseous Oxidized Mercury (GOM), and Particle Bound Mercury (PBM). GOM and PBM make up only 1 % of the total. But deposition, which is the only sink for atmospheric mercury, is dominated by these two species. Therefore, oxidation processes are key to understand the behaviour of mercury in the atmosphere. However, in the scientific community a consensus on the importance of oxidizing reactants, namely ozone, hydroxy radicals, and halogens, has not been reached yet.

This study is a continuation of the work presented at the 33rd ITM (Bieser et al. 2014). The main advancement is the implementation of bromine chemistry into the regional chemistry transport model (CTM) CMAQ and the comparison with newly available observations of GOM in the free troposphere.

83.2 Model Set-up and Domain

The regional models were set up for a domain covering the whole of Europe with a 24 × 24 km2 grid.

We used two independent air quality modelling systems. The first one is based on CMAQ version 5.0.1 using the multi pollutant gas phase chemistry mechanisms with additionally implemented bromine chemistry. The model was driven by meteorological fields from the COSMO-CLM model. Boundary conditions for mercury were obtained from the GLEMOS global model. The second regional model used is WRF-CHEM which was forced with boundary conditions from the ECHMERIT global model, while meteorology was calculated online by WRF. The models were used to calculate mercury concentrations for 2013 using ozone, OH, H_2O_2, and bromine respectively as the only oxidant for GEM. Additionally, different precalculated bromine fields from the P-TOMCAT and GEOS-CHEM model were used for the bromine runs.

83.3 Ground Based Observations

Looking at GOM concentrations at the surface level ozone and bromine gave very similar results. Figure 83.1 depicts results from CMAQ for the year 2009 compared to observations at Waldhof. (Please note that this is the same figure as shown in Air Pollution Modeling and its Application XXIII but with the addition of the bromine run). While the statistics are slightly betterfor the bromine run, the difference to the results using ozone as the only oxidant are too small to declare one run to be 'better' than the other (MNB: 1.3 ozone, 0.9 bromine, −0.8 OH, −0.3 H_2O_2) (correlation 0.52 ozone, 0.54 bromine, 0.54 OH, 0.49 H_2O_2).

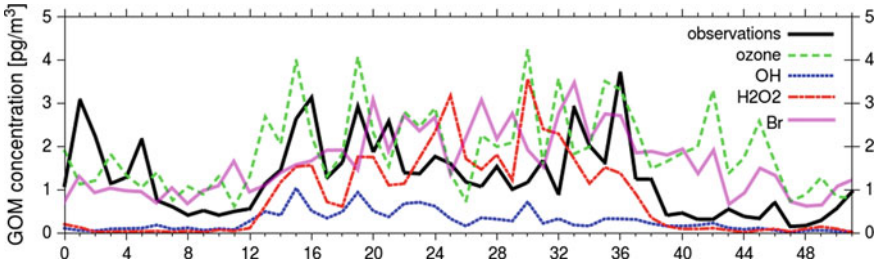

Fig. 83.1 Observed (*solid black line*) and modelled GOM concentration at Waldhof for 2009. Data is based on a COSMO-CMAQ run using different oxidants

83.4 Vertical Profiles

Before looking at GOM concentrations in higher altitudes we investigated whether the models are able to reproduce the vertical distribution of elemental gaseous mercury. For this we used new observations from the GMOS project. This includes speciated ground based measurements at Waldhof, Germany, speciated measurements in the PBL and lower free troposphere from the ETMEP-2 air craft campaing and TGM and GEM measurements in the upper free troposphere and lower stratosphere from the CARIBIC project (Weigelt et al. 2015). The GEM observations from ETMEP-2 is based on two TEKRAN units and a Lumex instrument. In Fig. 83.2 is can be seen that results from both model setups (COSMO-CMAQ and

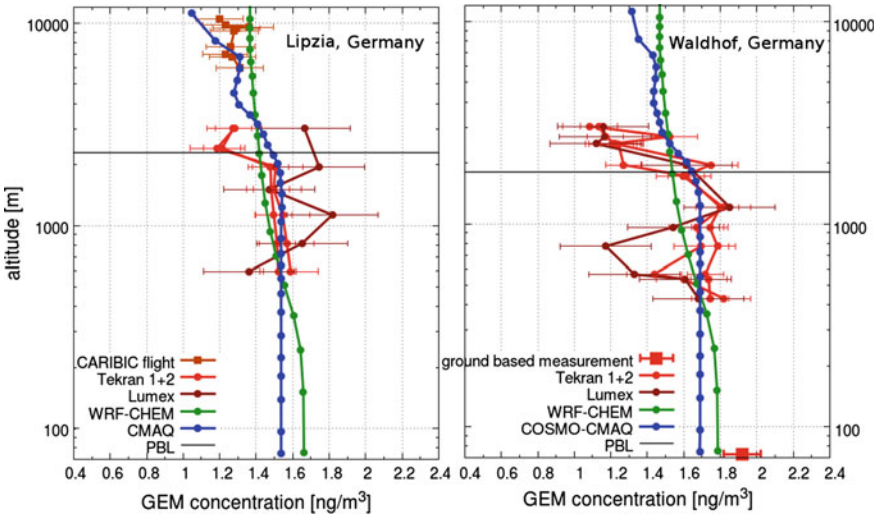

Fig. 83.2 Vertical profiles of GEM at Lipzia (*left*) and Waldhof (*right*). Data is for 1 hour in the afternoon of the 23rd (*left*) and 24rd (*right*) of August 2013

WRF-CHEM) lie mostly within the uncertainty range of the observations. Differences between the models are within 10 %. Considering that we compare the observations to a single hourly model value the agreement between model and measurement is intriguing. Only the WRF-CHEM setup is unable to reproduce the elevated GEM concentrations at the ground level. However, both models agree with the concentrations inside the PBL and exhibit a decrease in the free troposphere.

Given the good results for the vertical distribution of GEM we analysed the modelled concentrations for GOM using the different oxidation reactions. Inside the PBL we found only little difference in GOM for-mation. However, in the lower free troposphere the bromine reaction resulted in much higher concentrations compared to Ozone and OH (Fig. 83.3). The observations include only a single GOM sample for Lipzia and Waldhof. However, in Waldhof the sample was mostly taken inside the free troposphere, while in Lipzia the sample was mostly taken inside the PBL. Generally, the longer the aircraft was inside the free troposphere, the higher GOM concentrations were observed (Weigelt et al. 2015). The assumption of an increased concentration of GOM in the lower free troposphere is also backed by recent observations in the U. S. Brooks et al. (2014) and other groups found increased GOM concentrations in altitudes between 2 and 5 km.

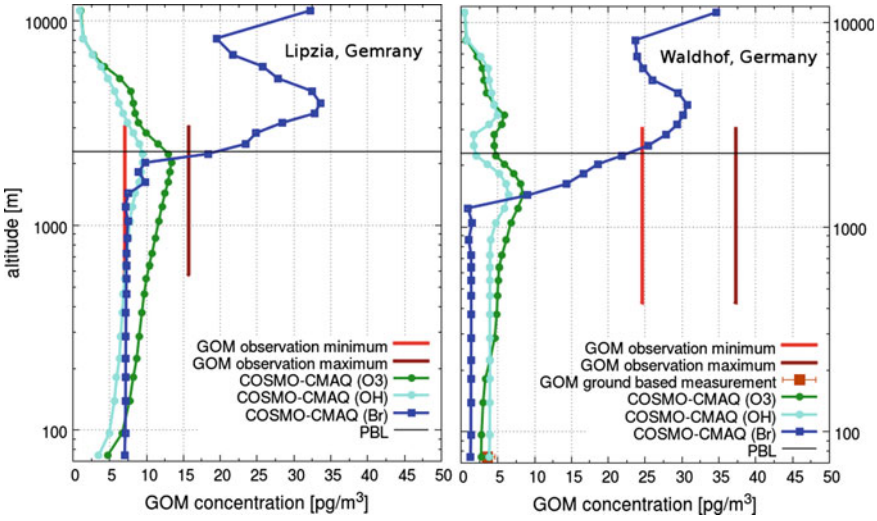

Fig. 83.3 GOM observations compared to COSMO-CMAQ model results using different oxidation reactions for GEM at Lipzia (*left*) and Waldhof (*right*). Data is for 1 hour in the afternoon of the 23rd (*left*) and 24rd (*right*) of August 2013. The elevated measurements from the ETMEP-2 campaign are single denuder samples for the whole vertical profiles and their uncertainty

83.5 Conclusion

Recent measurements of the vertical distribution of gaseous oxidized mercury (GOM) in the troposphere have shown pronounced GOM peaks of up to several hundred pg/m^3 in the free troposhpere (in an altitude between between 2 and 5 km). Higher values have been observed for summer than for winter. In a model sensitivity analysis using different oxidants for the formation of GOM on a regional domain in the mid latitudes we found that only bromine related reactions led to the observed peak of GOM above the PBL. In contrast, a comparison with ground based observations gave good results for both ozone and bromine reactions. The implication of this work is, that we need more observations of speciated mercury in the free troposhere in order to further constraint the atmospheric oxidation chemistry.

References

Bieser J, Matthias V, Travnikov O, Hedgecock MI, Gencarelli C, De Simone F, Weigelt A, Zhu J (2014) Impact of mercury chemistry on regional concentration and deposition patterns. In: Gyring S-E, Batchvarova E (eds) Air pollution modeling and its application, vol XXIII, pp 189–195

Brooks S, Ren X, Cohen M, Luke WT, Kelley P, Artz R, Hynes A, Landing W, Martos B (2014) Airborne vertical profiling of mercury speciation near Tullahoma, TN, USA. Atmosphere 5:557–574. doi:10.3390/atmos5030557

Weigelt A, Ebinghaus R, Pirrone N, Ammoscate I, Bieser J, Bödewadt J, Esposito G, Slemr F, van Velthoven PFJ, Zahn A, Ziereis H (2015) Tropospheric mercury vertical profiles between 500 and 10,000 m in central Europe. Atmos Chem Phys 15(20):28217–28247. doi:10.5194/acpd-15-28217-2015

Chapter 84
On the Spatial Support of Time Series of Monitoring Data for Model Evaluation

Efisio Solazzo and Stefano Galmarini

Abstract We use time series of hourly records of ozone for a whole year (2006) collected by the European AirBase network to analyse the area of representativeness of monitoring stations and find, for similar class of stations (urban, suburban, rural), large heterogeneity and high sensitivity to the density of the network and to the noise of the signal. This suggests the mere station classification to be not a suitable method to help select the pool of stations used in model evaluation. Therefore a novel, more robust technique is developed consisting in studying the spatial properties of the associativity of the spectral component of the ozone time series, in an attempt to determine the level of homogeneity.

84.1 Introduction

This study investigates the use and limitations of monitoring data of relevance for the correct assessment of air quality modelling systems, with focus on the spatial representativeness and the homogeneity of signals. The aim is to provide modellers a methodology for selecting homogeneous spatially distributed signal which also carries information about its spatial support. We introduce a method for the estimation of the area of representativeness of monitoring receptors and the limitations it imposes on its use for model evaluation. We then propose a novel methodology consisting in studying the associativity of the spectral decomposition of the pollutants time series rather than the raw data. The criterion beyond such choice consists in assuming that components pertaining to different scales may show different levels of associativity and still be usable selectively to evaluate their counterpart in model data. Should that be the case only the components of similar associativity should be compared with the modelled counterpart.

E. Solazzo (✉) · S. Galmarini
European Commission, Joint Research Centre, Institute for Environment and Sustainability, Air and Climate Unit, Ispra, Italy
e-mail: efisio.solazzo@jrc.ec.europa.eu

D.G. Steyn and N. Chaumerliac (eds.), *Air Pollution Modeling and its Application XXIV*, Springer Proceedings in Complexity,
DOI 10.1007/978-3-319-24478-5_84

84.2 The Area of Representativeness

We initially estimate the distance at which the influence of the signal of each receptor is felt by the other receptors of the AirBase network. For this we apply variogram analysis complemented with a fitting procedure (Solazzo et al. 2013). Results show that the range (the distance after which the memory of the signal of the receptor can be considered lost) is approximately the same for all three categories of stations (urban, suburban, rural), thus not informative for selecting stations to be used to evaluate regional scale air quality models (Fig. 84.1). Refer to Solazzo and Galmarini (2015) for details.

84.3 Stations Associativity and Implications for Model Evaluation

Hourly time series of ozone concentrations have been first decomposed using an iterative moving average approach known as Kolmogorov-Zurbenko (kz) low-pass filter. The components of interest for the analysis are the intra-day (ID) component (periods less than 12 h), the diurnal (DU) component (periods of half-day to ~2.5 days), the synoptic (SY) component (between ~2.5 and ~21 days), the long-term (LT) component (between ~21 and ~90 days) and the seasonal (SE) component (base line containing periods longer than 90 days). Hierarchical clustering was applied to the spectral components of the hourly-ozone monitored time series in Europe. By examining the clusters of receptors produced at different

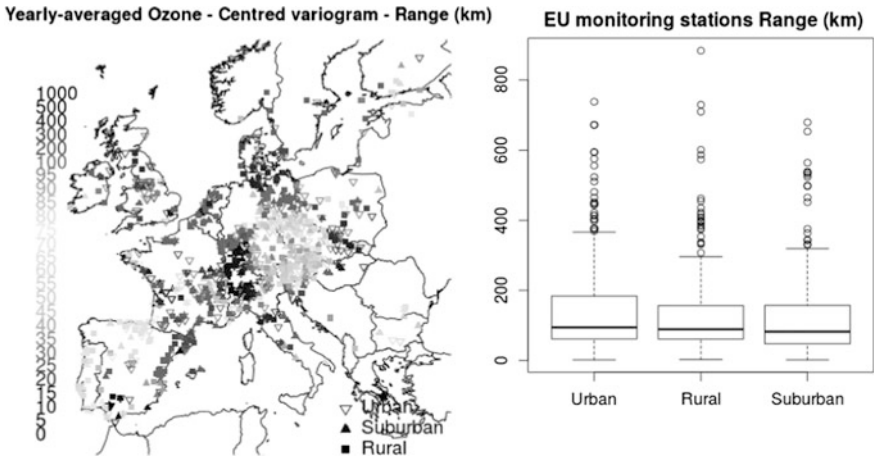

Fig. 84.1 Range (*left*) calculated using the point-centred variogram method at the AirBase monitoring sites. Percentile distribution (*right*) of the range (up to 1000 km and nugget < 50 ppb^2) by area-type. *Tick black line* is the median

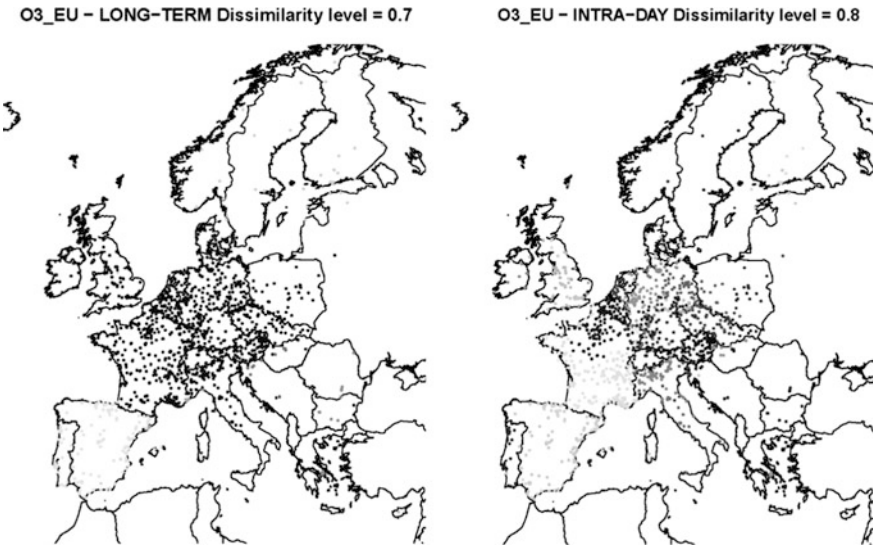

Fig. 84.2 Spatial associativity for time series components of ozone

level of similarity we find the spatial associativity of Fig. 84.2. Grouping of seasonal component confirms a strong correlation between all stations, up to a level of correlation of 0.75. Below the value of 0.25 some heterogeneity appears. When moving to examine the LT component at $d_0 = 0.7$ a strong spatial structure is detected (Fig. 84.2a). The result is a net trans-boundary grouping, most notably between Spain and France, and between the Scandinavian countries and the rest of the continent. The signal recorded at these stations has a higher correlation with stations of the same countries (even if far apart) than with stations across the border (although sited within their immediate vicinity). The SY component at $d_0 = 0.4$ (similarity of 0.6) and the ID component (Fig. 84.2b) confirms the same marked country-wise grouping, starting from high level of dissimilarity (~ 0.85), suggesting this latter component to be removed prior to carry out a model evaluation study. When repeating the analysis using model results from AQMEII, the detected cross-border associativity patterns are not captured by the modeling systems, supporting the argument that lack of harmonization among countries and networks can originate noise that deteriorates the information of the monitoring data for use in model evaluation and development.

When the portions of the signal that are not representative are removed from both measured and modelled data and the remaining components compared, the models performance improve. In fact the mean square error between the fifteen regional models participating to AQMEII and the hourly ozone concentration, over all the AirBase receptors is reduced on average of over 2.5 % (ranging from 1.1 to 6.2 %, with the ensemble mean improved by 2 %) when the ID component is removed from both the modelled and the observed time-series, for the all year.

Similar range of improvement for the mean squared error is achieved when considering the maximum daily concentration. When the analysis is restricted to the summer months (June–August) the noise suppression results in improved accuracy of 5 % on average (ranging from 1.4 to 9.6 %, with the ensemble mean improved by 4.3 %).

84.4 Conclusions

Analysis of spatial representativeness has been carried out on the AirBase stations and by using gridded model outputs as proxy of concentration. While the categorization of stations contained in the meta-data is not a viable indicator of the spatial extension of the area of influence of a receptor, we find that variogram methods in conjunction to spatially uniform proxy fields might provide a valid alternative. These methods, however, have a large degree of dependence on the quality of the field and on the fitting procedure itself and are probably better suited for isolated receptors. On the other hand, the method of searching for spatial grouping of stations based on signal frequency, with the aim of identifying homogeneous regions to facilitate model evaluation, has revealed to be more robust, allowing i) to capture the 'portion' of desired signal detected by each stations, even those located in heavily polluted urban areas, and ii) to discard the unwanted part. This feature is of high significance in a context of dynamic and diagnostic model evaluation (full details are provided in Solazzo and Galmarini, 2015). More specifically we find:

- Only the spectral components with high signal-to-noise ratio (SE, DU) exhibit grouping properties across the European continent as a whole, showing regions where the signal of these components is homogeneous. Using only the stations of these homogeneous regions will facilitate the model evaluation activity and interpretation of the results. The identification of these regions also indicates a novel strategy for sensitivity analysis and process-evaluation of models. For instance, clustering of the DU components can reveal which stations are most sensitive to the ozone diurnal cycle and use only those to diagnose models capability to reproduce it.
- The other components (LT, SY, ID) have surprisingly shown country-sensitive grouping properties: the signal is more strongly associated among stations sited in the same country but hundreds of kilometres apart than among stations sited on either side of the country border and only a few kilometres apart. This behaviour belongs to all European countries. Trans-boundary effects of fast fluctuating components cannot be captured by the modelling systems and should be removed prior of any model-to-data comparison.
- By filtering-out the ID component, the model accuracy (in terms of mean square error) improves significantly by up to 5 % on average over fifteen modelling systems for the months of June–August and on average of 2.5 % for the whole year and for the daily maximum concentration.

Question and Answer

Questioner: P. Makar

Question: Is there any way to distinguish between low correlations due to instrumental error versus due to stations representativeness?

Answer: In case of a dense network, the signal recorded by a faulty station is likely to be spotted more easily than in the case of isolate stations. In fact, if the correlation among a close group of stations (cluster) is uniform and only for one of them the correlation is lower, then that station requires closer inspection and the error would be diagnosed. On the other hand, if the station is isolated or close to a highly localized emission source the faulty signal would be harder to detect.

Questioner: J. Bieser

Question: How large is, on average, the fraction of the error that cannot be reduced on regional domains due to the effect being on a sub-grid scale?

Answer: We have found that the intra-day (ID) portion of the signal (for ozone concentration) recorded by the stations is weakly representative and models with grid spacing exceeding $\sim$10–15 km might show an increase of the mean square error of $\sim$5 % due to the limited representativeness of the stations for the ID share of the signal. The error is indeed due to sub-grid processes that cannot be picked up by the model.

References

Solazzo E et al (2013) Report of 2013 WG2/SG1 activity on spatial representativity. European Commission EUR 26539 EN—Joint Research Centre, Institute for the Environment and Sustainability, Luxembourg, 22 p. doi:10.2788/17619

Solazzo E, Galmarini S (2015) Comparing apples with apples: Using spatially distributed time series of monitoring data for model evaluation. Atmos Environ 112:234–245

Chapter 85
Validation of the WRF-CMAQ Two-Way Model with Aircraft Data and High Resolution MODIS Data in the CA 2008 Wildfire Case

David C. Wong, Chenxia Cai, Jonathan Pleim, Rohit Mathur and Mark S. Murphy

Abstract A new WRF-CMAQ two-way coupled model was developed to provide a pathway for chemical feedbacks from the air quality model to the meteorological model. The essence of this interaction is focused on the direct radiative effects of scattering and absorbing aerosols in the troposphere that in turn affect radiation calculations in the meteorological model, WRF. We tested this two-way coupled model with a high aerosol loading episode resulting from a wildfire outbreak in California in June 2008. We evaluate various aspects of the model with traditional statistical approaches, a comparison with radiation measurements, and AOD measurements from high resolution (500 m) MODIS data.

85.1 Introduction

Traditionally, the Community Multiscale Air Quality (CMAQ) model is driven by the Weather Research and Forecast (WRF) model, forming a one way data interaction pathway without chemical feedbacks to the meteorology. Recently, we coupled the WRF and CMAQ models to create a two-way coupled modeling system to facilitate feedbacks between chemistry and meteorology through the use of memory resident buffer data files (Wong et al. 2012). Simulated aerosol composition and size distributions are used to estimate the optical properties of aerosols

D.C. Wong (✉) · J. Pleim · R. Mathur · M.S. Murphy
Atmospheric Modeling and Analysis Division, National Exposure Research Laboratory, US Environmental Protection Agency, 109 T.W. Alexander Drive, Research Triangle Park, NC 27711, USA
e-mail: wong.david-c@epa.gov

C. Cai
California Air Resources Board, Sacramento, CA, USA

D.G. Steyn and N. Chaumerliac (eds.), *Air Pollution Modeling and its Application XXIV*, Springer Proceedings in Complexity,
DOI 10.1007/978-3-319-24478-5_85

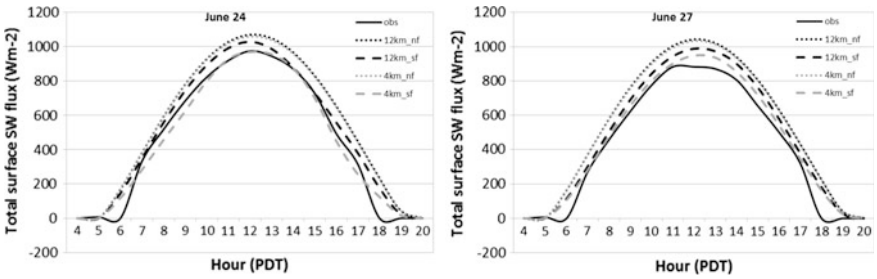

Fig. 85.1 Total surface short wave radiation comparison between measurements at Hanford, CA (*black*), and with (*dash line*) and without (*dotted line*) direct aerosol feedback

which are then used in the radiation calculations in WRF. Thus, direct radiative effects of scattering and absorbing aerosols in the troposphere estimated from the spatially and temporally varying simulated aerosol distributions are fed back to the WRF radiation calculations, resulting in "two-way" coupling between the atmospheric dynamical and chemical modeling components.

85.2 Experiment Domain and Model Setup

To examine the effectiveness of the coupled system to capture aerosol radiative feedback effects, we conducted a simulation with 12 and 4 km grid resolutions of a wildfire event in California (Fig. 85.1) for the period of 10 June–30 June 2008 where the first 10 days are used as spin-up period and are not considered in the analysis. Widespread wildfires resulted in significant particulate matter (PM) pollution during mid-to-late June 2008 in California and surrounding states. The two-way coupled model was based on WRF 3.4 and CMAQ 5.0.1.

85.3 Modelling Results

The wildfires occurred between 6/20 and 6/30 primarily in the northern part of the state. Table 85.1 shows basic statistical performance of the modeled ozone, PM2.5, radiation and temperature compared with CARB (California Air Resources Board) observation data in that time period and with stations located in the northern part (latitude ≥ 38) of the state.

In terms of ozone, with or without aerosol feedback as well as running with higher resolution does not make any major difference. PM25 shows similar behavior for most metrics but the 4 km simulation does show higher correlation with observations than the 12 km simulation. However, total short wave surface radiation shows a very positive result. When including aerosol feedbacks, the reduction of the average in the

Table 85.1 Model statistical performance (12 km *top* and 4 km *bottom*) comparing runs with no aerosol feedback (nf) and runs with direct aerosol feedback (sf)

	O3 (ppb)		PM25 (ug/m^3)		Rad (W/m^2)		Temp (K)	
	nf	sf	nf	sf	nf	sf	nf	sf
MB	5.816	4.043	6.827	3.300	27.827	−33.582	−5.459	−5.797
ME	14.823	14.440	32.637	33.407	170.832	148.856	6.840	7.031
RMSE	19.818	19.241	53.014	53.638	217.920	200.217	8.768	8.892
Mean	49.989	48.216	53.992	50.465	542.830	481.421	292.523	292.184
Obs mean	44.173	44.173	47.165	47.165	515.002	515.002	297.978	297.978
R	0.699	0.697	0.410	0.400	0.778	0.801	0.529	0.535
	O3 (ppb)		pm25 (ug/m^3)		Rad (W/m^2)		Temp (K)	
	nf	sf	nf	sf	nf	sf	nf	sf
MB	7.524	5.550	0.431	−4.857	75.090	−0.522	−1.449	−1.978
ME	15.215	14.625	29.103	28.633	145.616	112.554	3.341	3.431
RMSE	20.224	19.555	48.101	45.198	184.261	148.856	4.871	4.900
Mean	51.697	49.724	47.597	42.308	581.934	506.320	296.355	295.827
Obs mean	44.173	44.173	47.165	47.165	506.844	506.844	297.801	297.801
R	0.697	0.694	0.455	0.477	0.869	0.888	0.777	0.793

4 km case is 25 % higher than in the 12 km case: 75 W/m^2 versus 60 W/m^2, respectively. Mean error (ME) and root mean square error (RMSE) reduces significantly in both 12 and 4 km cases. Furthermore, the 4 km simulation does provide substantial improvement over the 12 km case. Surface temperature is directly associated with surface radiation which reflects in correlation, however, ME and RMSE both increase slightly when feedback is enabled.

Figure 85.1 confirms the excellent radiation performance when including direct aerosol feedback. The overestimation of radiation is reduced significantly and with 4 km resolution, the reduction is even stronger and the model closely matches observations.

Trinidad Head, CA is located on the northern part of the coast and was not significantly affected by the wild fires for most of the episode, as suggested by the low AOD values shown in Fig. 85.2. However, during the early hours of 6/27 (Julian day 179), observed AOD increases rapidly while the model values remain much lower (left panel). Later in the day the model values were more reflective of the observed data, though generally lower with the exception of a 2-h window. The 4 km model run generally estimated greater AOD values, particularly during hours 17 and 18 (GMT) (179.7, 179.75).

We also compared high resolution (500 m) MODIS AOD with our model results as shown in Fig. 85.3. The general AOD pattern from the model matches with the MODIS data but the magnitude from the model is much lower than observed. Note that much of the black area in the MODIS plot is way over scale with peak AOD values up to 41. In addition, the 4 km case does have three distinct black spots (circled in Fig. 85.3) that do not show in the 12 km case.

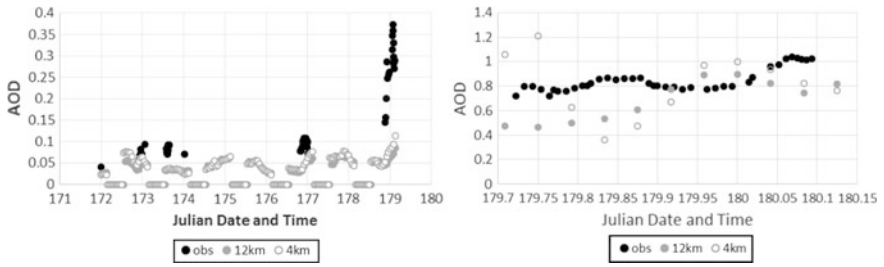

Fig. 85.2 AOD comparison of measurements obtained at Trinidad Head, CA (AERONET site)

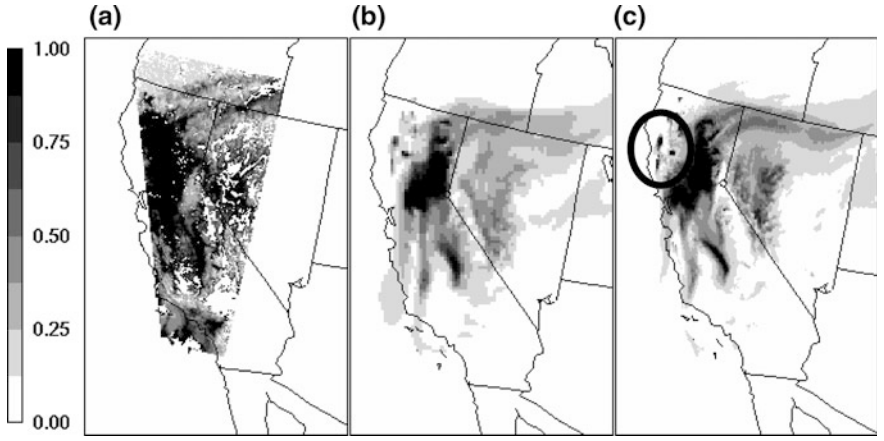

Fig. 85.3 Comparison of high resolution MODIS data with model results (6/24 12 pm)

85.4 Conclusions

The newly developed WRF-CMAQ two-way coupled modeling system was tested during a wildfire scenario which represents a high aerosol loading case. A 12 km resolution run was accompanied with a 4 km run to better capture steep elevation gradients in the study area. The main purpose for coupling interaction is to include the direct radiative effects of scattering and absorbing aerosols in the troposphere which, in turn, affect radiation calculations in the meteorological model, WRF. With feedback, the model was able to reduce the total short wave surface radiation dramatically. With higher resolution, the effect was enhanced.

In terms of air quality, we have examined the impact of this two-way coupled model on ozone and PM_{25}. When the amount of solar radiation that reaches the ground was reduced due to presence of aerosol in the atmosphere, it reduced the PBL height. This will increase the concentration of certain pollutants such as PM25. In fact, our results show slight improvement when feedback is on. However, with ozone, the two-way model does not show any difference in performance. The

production and consumption of ozone is far more complex than PM25. Understanding and assessing the impact of aerosol direct radiative effects on ozone life cycle requires further research.

Acknowledgments and Disclaimer The 500 m high resolution MODIS data was obtained from Mr. Steve Reid of Sonomatech. The United States Environmental Protection Agency through its Office of Research and Development funded and managed the research described here. It has been subjected to the Agency's administrative review and approved for publication. Although it has been reviewed by EPA and approved for publication, it does not necessarily reflect their policies or views.

Reference

Wong DC, Pleim J, Mathur R, Binkowski F, Otte T, Gilliam R, Pouliot G, Xiu A, Young JO, Kang D (2012) WRF-CMAQ two-way coupled system with aerosol feedback: software development and preliminary results. Geosci Model Dev 5:299–312

Chapter 86
Metamodels for Ozone: Comparison of Three Estimation Techniques

P. Steven Porter, S.T. Rao, Christian Hogrefe, Edith Gégo and Rohit Mathur

Abstract A metamodel for ozone is a mathematical relationship between the inputs and outputs of an air quality modeling experiment, permitting calculation of outputs for scenarios of interest without having to run the model again. In this study we compare three metamodel estimation techniques applied to an 18 year long CMAQ simulation covering the Northeastern US (NEUS). The estimation methods considered here include projection onto latent structures, stochastic kriging and a combination of principal components and stochastic kriging.

86.1 Introduction

Metamodels are used to estimate the response of pollutant concentrations to changes in emission or meteorology. Scenarios of interest addressed here include discerning the impact of meteorological versus emission forcing, the ozone response to mobile versus other anthropogenic source emissions, and changes over time in ozone response to emission changes.

Although this article has been reviewed by the EPA and approved for publication, it does not necessarily reflect EPA's policies or views.

This work was made possible by Coordinating Research Council contract A-89.

P.S. Porter (✉) · E. Gégo
Porter-Gego, Idaho Falls, ID, USA
e-mail: psp@srv.net

S.T. Rao
North Carolina State University, Raleigh, NC 27695, USA

C. Hogrefe · R. Mathur
AMAD/NERL, U.S.E.P.A., Research Triangle Park, Durham, NC, USA

D.G. Steyn and N. Chaumerliac (eds.), *Air Pollution Modeling and its Application XXIV*, Springer Proceedings in Complexity,
DOI 10.1007/978-3-319-24478-5_86

86.2 Methods

86.2.1 Photochemical Modeling

Model	: MM5v3.7.2 CMAQv4.5.1, CB4, aero3, years 1988–2005
Emissions	: NEI1990, 1996–2001, OTC2002, OTC2009 (SMOKE)
Domain	: Northeastern U.S., 36/12 km
Boundary conditions	: ECHAM5-MOZART
Primary Output	: hourly ozone
Output Manipulation	: monthly mean of 8 h daily maximum at each 12 km model grid (details in Hogrefe et al. 2009)

86.2.2 Statistical Methods

CMAQ-simulated 8 h daily maximum ozone values were modeled as a function of monthly mean emission and meteorological variables at each photochemical model grid point. VOC and NOx emissions were divided amongst area, point, mobile, and biogenic sources. Meteorological variables included planetary boundary layer height, temperature, surface solar radiation, water vapor mixing ratio and wind speed.

Projection onto latent vectors (PLS) is a regression of the principal components (PCs) of the predictor variables (emissions and meteorology) onto the predictands (ozone) (Wold et al. 2001). Typically a few predictor PCs are able to explain most of the variability of the predictands, thereby reducing the dimension of a regression problem. For the PLS metamodel, the gridded collection of emissions and meteorology (8 emission sources, 5 meteorological variables × 6175 model grids) was reduced to 8 PCs. The PCs form an orthogonal basis, while the PLS model itself is linear.

Stochastic kriging (SK) is a geostatistical method developed for metamodeling. Emissions and meteorology play the role that location coordinates play in geostatistical estimation (Ankenman et al. 2010). An interpolated estimate looks like:

$$\hat{\boldsymbol{Y}} = \boldsymbol{\mu} + \boldsymbol{B}_1\boldsymbol{Y}_1 + \boldsymbol{B}_2\boldsymbol{Y}_2 + \boldsymbol{B}_3\boldsymbol{Y}_3 + \boldsymbol{B}_4\boldsymbol{Y}_4 + \boldsymbol{B}_5\boldsymbol{Y}_5 \ldots + \boldsymbol{B}_n\boldsymbol{Y}_n + \boldsymbol{\varepsilon}_i \qquad (86.1)$$

The Y_i are neighbors of an ozone value of interest ($\hat{Y}$) in the sense that they are close to $\hat{Y}$ in terms of emissions and meteorology. The B_i are constants derived from the correlation between ozone values as a function of their distance apart (in terms of emissions and meteorology). Although SK is a linear method, it has a nonlinear response to changes in emissions and meteorology.

A third method (PCSK) uses SK to estimate ozone from the principal components of the predictors. PCSK has a nonlinear response to changes in emissions and meteorology, as well as an orthogonal basis for the predictors.

86.3 Results and Discussion

The ozone response of the PLS model to one standard deviation change in the emission and meteorology is linear while the responses of the SK model are non-linear (Fig. 86.1). (The ozone response of PCSK is the same as SK.) The root-mean squared error for PLS, SK and PCSK derived from leave-one-out cross validation are similar for all three methods (Fig. 86.2, domain-wide median values

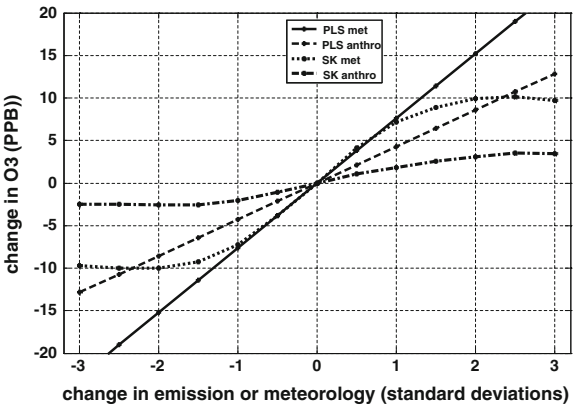

Fig. 86.1 Metamodel response to change: PLS and meteorology (-), PLS and anthropogenic emissions (–), SK and meteorology (…), SK and anthropogenic emissions (.-)

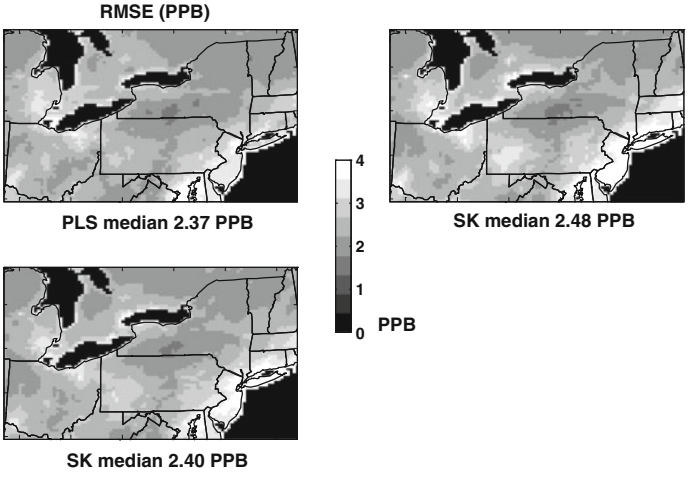

Fig. 86.2 Cross-validation RMSE of PLS (*upper left*), SK (*upper right*) and PCSK (*lower left*)

displayed under each panel). The RMSE of PLS estimates are slightly (and significantly) smaller than those of SK and PCSK.

Ozone responses to fixed (at 2005 values) and variable meteorology/biogenic emissions are shown in Fig. 86.3. The solid line (constant meteorology) reflects the downward trend in emissions during the time span of the model experiment, while the dashed line includes additional variability due to meteorology. By fixing anthropogenic emissions (at their 2005 levels), one could also determine which years had meteorology conducive to ozone formation. For this simulation, the years 1999 and 2000 had the most and least ozone conducive meteorology, respectively (not shown).

Metamodels were also compared with respect to their ability to attribute changes in ozone between 1988 and 2005 to meteorology, anthropogenic emissions, and mobile source NOx alone (Table 86.1). CMAQ estimated domain-wide changes in monthly mean ozone were −15.1 ppb. The change in ozone attributable to total anthropogenic emissions ranged from −5.5 to −8.4. When anthropogenic NOx is fixed at 2005 levels, SK, PLS and PCSK attribute −4.6, −5.4 and −5.5 ppb of ozone change to VOC reductions, respectively. Ozone change attributed by SK to NOx is much smaller (−0.9 ppb) than those found using PLS and PCSK (−3.3 and −4.5 ppb, respectively). SK also attributed less change to mobile NOx sources than did PLS and PCSK.

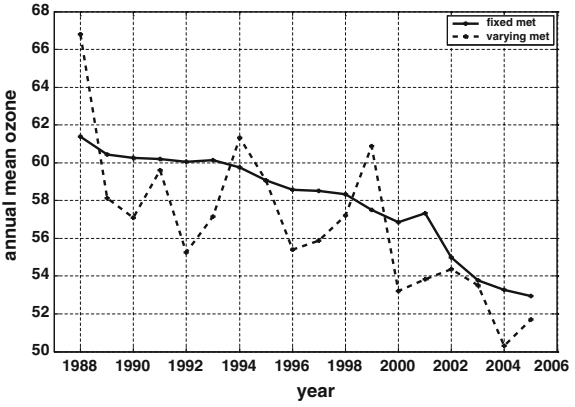

Fig. 86.3 Ozone versus year for constant 2005 (-) and variable meteorology (- -)

Table 86.1 Ozone change 1988–2005 (ppb)

Method:	CMAQ change	All	Meta model attribution to anthropogenic emissions		
			VOCs	NOx	Mobile NOx
SK	−15.1	−5.5	−4.6	−0.9	−0.8
PLS	−15.1	−8.4	−5.4	−3.3	−2.1
PCSK	−15.1	−8.4	−5.5	−4.5	−2.5

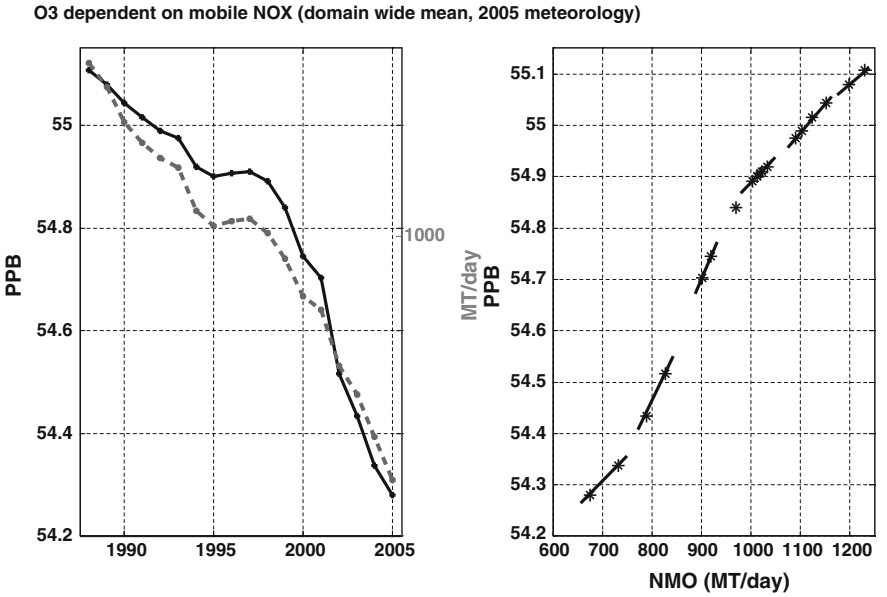

Fig. 86.4 *Left panel* Ozone versus year with constant meteorology and emissions other than mobile source NOx (-) and mobile source emissions (–). *Right panel* ozone versus NOx mobile source emissions

The ozone response to changes in mobile NOx emissions was estimated using PCSK with all emissions except mobile NOx fixed at 2005 levels, and meteorology also fixed at 2005 values (Fig. 86.4). The left panel of Fig. 86.4 compares ozone dependent only on mobile NOx (solid line) with mobile NOx emissions (dashed line). The right panel of Fig. 86.4 shows mobile NOx-dependent ozone versus mobile NOx emissions. This panel indicates that the ozone response decreases as emissions are reduced (smaller slope at lower emission values).

86.4 Summary

Of the three metamodels, PLS has a linear ozone response to changes in emissions and meteorology, while SK and PCSK have nonlinear responses. The predictors for PLS and PCSK form an orthogonal basis, while the correlation among SK predictors is kept unchanged (the performance of SK may be affected by correlated predictor variables.) The ozone change attributed to emissions by PLS and PCSK is greater than that attributed by SK. In addition, the three metamodels show different magnitudes of response to NOx, yet within each metamodel mobile NOx response

is significant relative to anthropogenic NOx response. The results also reveal that mean ozone concentrations simulated by CMAQ are responsive to changes in meteorology as well as changes in emissions.

References

Ankenman B, Nelson BL, Staum J (2010) Stochastic kriging for simulation metamodeling. Oper Res 58(2):371–382

Hogrefe C, Lynn B, Goldberg R, Rosenzweig C, Zalewsky E, Hao W, Doraiswamy P, Civerolo K, Ku J, Sistla G, Kinney P (2009) A combined model-observation approach to estimate historic gridded fields of PM2.5 mass and species concentrations. Atmos Environ 43:2561–2570

Wold S, Sjostrom M, Eriksson L (2001) PLS–regression: a basic tool of chemometrics. Chemometr Intell Lab Syst 58:109–130

Chapter 87
Disparate $PM_{2.5}$ Metrics from Measurement and Modelling: Implications for Assessing $PM_{2.5}$ Regulatory Compliance

John Paul Sutton

Abstract A study has been done to investigate the difference in the modelled bound water component of $PM_{2.5}$ air mass concentration when modelled to correspond to different measurement methods. The study found that the June average $PM_{2.5}$ air mass concentration along a transect through southern England for a 2020 emissions scenario differed by 89 % when modelled corresponding to the two different measurement methods. It is, therefore, clear from this study that careful consideration needs to be taken to ensure that the modelled $PM_{2.5}$ air mass concentration corresponds to the appropriate measurement method.

Particulate matter (PM) is the term used to describe condensed phase (solid or liquid) particles suspended in the atmosphere. $PM_{2.5}$ is the mass concentration of particulate matter with diameter less than 2.5 μm. The objective of current $PM_{2.5}$ legislation in Europe is to reduce the long-term exposure of the population to $PM_{2.5}$. The anticipated reduction in $PM_{2.5}$ air concentration over the next decade is likely to be only a few % per year. So measurement and modelling of these reductions needs to be as accurate as possible. At present the measurement and modelling of $PM_{2.5}$ remains challenging (AQEG 2012). In particular, different measurement methods can produce significantly different $PM_{2.5}$ air mass concentrations depending on the partial or total loss of semi-volatile particle components during the measurement process, and because variable amounts of water can remain bound to the particles. The approach used for regulatory purposes to address this issue has been to standardise a reference measurement method. The 2008 Ambient Air Quality Directive specifies a standard manual gravimetric measurement method for $PM_{2.5}$ as the reference method. In particular, it specifies that $PM_{2.5}$ samples are weighed at a temperature of 20 °C and a relative humidity of 50 %. As the different measurement methods can produce

J.P. Sutton (✉)
RWE Generation UK, Windmill Hill Business Park, Whitehill Way, Swindon SN5 6PB, UK
e-mail: john.sutton@rwe.com

D.G. Steyn and N. Chaumerliac (eds.), *Air Pollution Modeling and its Application XXIV*, Springer Proceedings in Complexity,
DOI 10.1007/978-3-319-24478-5_87

significantly different $PM_{2.5}$ air mass concentrations, it is clearly important that the modelling of the mass concentrations matches as closely as possible the measurement method used to assess regulatory compliance.

To assess the importance of the above, a study was done using CMAQ v4.7. The official version of the CMAQ air quality model outputs the bound water component of $PM_{2.5}$ corresponding to ambient temperature and relative humidity. In this study the capability of the CMAQ model has been extended to output the bound water component of $PM_{2.5}$ under conditions corresponding to the gravimetric method. This allowed the difference in bound water component of $PM_{2.5}$ air mass concentration when modelled corresponding to the gravimetric method compared to that predicted for ambient atmospheric conditions, to be investigated. The scenario modelled by CMAQ was for a 2020 emissions scenario and used 2003 meteorological data produced by the WRF model. The $PM_{2.5}$ air mass concentration was output for each hour during the month of June on a 5 km grid covering the whole of the UK. The June average $PM_{2.5}$ air mass concentration was calculated along the transect shown in Fig. 87.1. This transect goes from the west coast of England to the East coast, passing through central London. The darker grid squares in Fig. 87.1 correspond to urban areas. Figure 87.2 compares the June average $PM_{2.5}$ air mass concentration along the transect modelled corresponding to "Gravimetric" and "Ambient" conditions. The portion of the transect corresponding to the London urban area has been shaded in Fig. 87.2. The figure shows the fraction of the $PM_{2.5}$ air mass concentration which is bound water. It is clear from the figure that the amount of bound water differed considerably when modelled to correspond to the two different measurement methods. As bound water is a large fraction of the $PM_{2.5}$

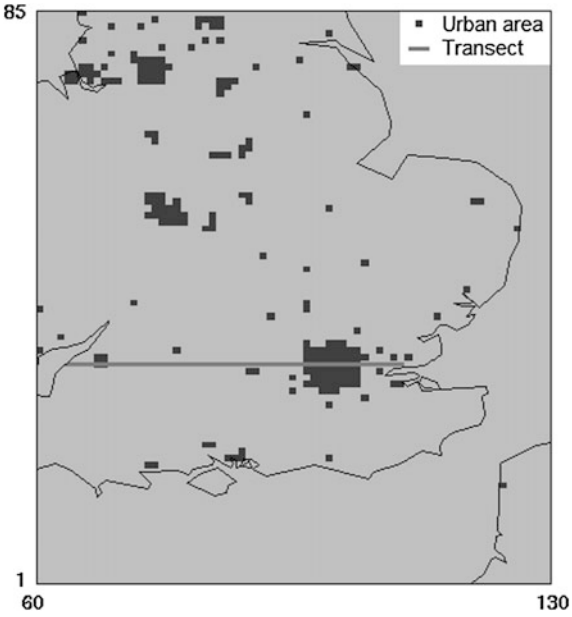

Fig. 87.1 Map of UK showing the transect through central London from the west coast to the east coast of England used for this study

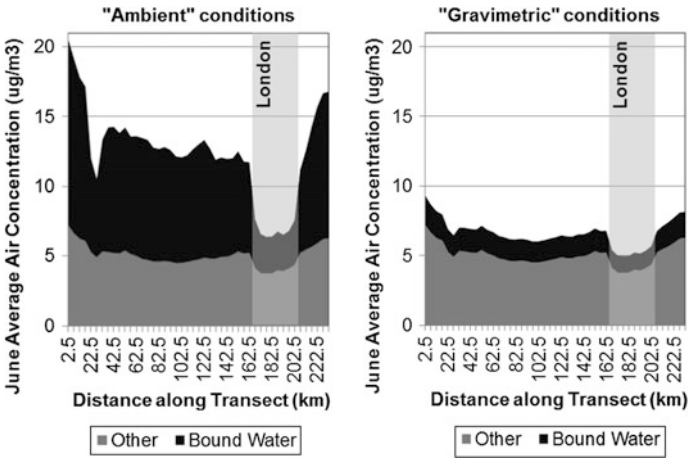

Fig. 87.2 Comparison of the June average $PM_{2.5}$ air mass concentration along the transect modelled, corresponding to "Ambient" and "Gravimetric" conditions. The portion of the transect corresponding to the London urban area has been shaded. The *plots* shows the fraction of the $PM_{2.5}$ air mass concentration which is bound water

air mass concentration, this difference in the amount of modelled bound water results in a large difference in the $PM_{2.5}$ air mass concentration when modelling was done to correspond to the two different measurement methods. The June average $PM_{2.5}$ air mass concentration along the transect was found to be 89 % higher when modelled corresponding to ambient atmospheric conditions than when modelled corresponding to the gravimetric method. It can also be seen in the figure that the amount of modelled bound water differs significantly inside and outside the London urban area for the "Ambient" conditions plot. This is because the ambient temperature and relative humidity differed significantly inside and outside the London urban area for the modelled scenario. This highlights the risk in comparing modelled $PM_{2.5}$ air mass concentration between urban and rural regions, when the modelling does not sufficiently match the appropriate measurement method. There will be similar risks in analysing trends in modelled $PM_{2.5}$ air mass concentration over time.

The results obtained by this study using CMAQ for the fraction of bound water in $PM_{2.5}$ when modelled corresponding to the gravimetric method, are supported by the results described in Tsyro (2005). The Tsyro study compared the chemical composition of $PM_{2.5}$ modelled by EMEP with gravimetric measurements. EMEP modelled the bound water component of $PM_{2.5}$ corresponding to gravimetric conditions. The Tsyro study found that the modelled bound water component of $PM_{2.5}$ would account for a significant fraction of the unaccounted measured $PM_{2.5}$ mass. The fraction of bound water in $PM_{2.5}$ modelled corresponding to gravimetric conditions is of similar magnitude for the CMAQ and EMEP studies.

87.1 Implications

- When modelling $PM_{2.5}$ air mass concentration to assess regulatory compliance or model performance, careful consideration needs to be taken to ensure that the modelled $PM_{2.5}$ air mass concentration corresponds to the appropriate measurement method.
- For modelling studies relating to $PM_{2.5}$ regulatory compliance in Europe, the appropriate measurement method is the gravimetric measurement method.
- There are significant risks in interpreting spatial and temporal variation of modelled $PM_{2.5}$ air mass concentration, when modelling does not match the appropriate measurement method.
- Additional functionality is being developed for CMAQ to output $PM_{2.5}$ bound water suitable for applications relating to $PM_{2.5}$ regulatory compliance in Europe (Roselle 2015).

Acknowledgments This work was funded jointly by RWE and E.ON. The CMAQ modelling used in this study was based on modelling work supported by the Joint Environmental Programme, which is jointly funded by RWE npower, E.ON UK, Drax Power Ltd, Scottish & Southern Energy, EDF Energy, GDF Suez, Eggborough Ltd, Scottish Power and Centrica.

References

AQEG (2012) Fine Particulate Matter ($PM_{2.5}$) in the United Kingdom, air quality expert group. Report prepared by the air quality expert group for the department for environment, food and rural affairs, Scottish executive, Welsh assembly government and department of the environment in Northern Ireland, PB13837, December 2012

Roselle S (2015) Personal communication with Shawn Roselle, Branch Chief for US Environmental Protection Agency, February 2005

Tsyro SG (2005) To what extent can aerosol water explain the discrepancy between model calculated and gravimetric PM10 and $PM_{2.5}$?. Atmos Chem Phys 5:515–532. SRef-ID: 1680-7324/acp/2005-5-515, February 2005

Chapter 88
Evaluation of Simulated Particulate Matter Spread in 2010 Russian Wildfire Case Using Air Quality Monitoring Data

Ketlin Reis, Velle Toll, Riinu Ots, Marko Kaasik, Joana Soares, Mikhail Sofiev, Marje Prank and Aarne Männik

Abstract This study is focused on a wild-land fire episode in 2010, August 7–9, when the plume of severe wildfires in European part of Russia reached Estonia and southern Finland, thus giving a chance to evaluate the modelling results against a relatively dense network of air quality monitoring stations. The chemistry-transport model SILAM, driven by the ECMWF meteo fields, was run within the European domain of AQMEII2 model validaton exercise with a 0.2-degree grid resolution, applying the AQMEII2 chemical and aerosol boundary conditions. The modelling results were compared with measured three-hourly average concentrations of $PM_{2.5}$ in Estonia and Finland. The observed peak values in most of stations reached 60–80 μg/m^3 (narrow peaks in the easternmost stations: up to 106 μg/m^3 in Estonia and 220 μg/m^3 in Finland, whereas SILAM predicted up to 75 μg/m^3). Remarkably enhanced particulate matter concentrations were found in all 7 continental (rural and urban) monitoring stations of Estonia, reproduced by the model within 10 % of the peak values in 5 stations. The general shape of the peak was reproduced by SILAM within 3–6 h of a time error. The model runs suggest that the wildfires were not solely responsible for enhanced concentrations: the continental aerosols constituted about a half of the total mass. The westernmost maritime station in Estonia was left almost untouched by the plume. Remarkable direct effect of the aerosols on boundary-layer meteorological conditions, PBL height, near-surface wind and temperature was found during this episode when the aerosol direct radiative effect was considered in numerical weather prediction model HARMONIE.

K. Reis (✉) · V. Toll · R. Ots · M. Kaasik · A. Männik
Institute of Physics, University of Tartu, Tartu, Estonia
e-mail: ketlin.reis@ut.ee

J. Soares · M. Sofiev · M. Prank
Finnish Meteorological Institute, Helsinki, Finland

D.G. Steyn and N. Chaumerliac (eds.), *Air Pollution Modeling and its Application XXIV*, Springer Proceedings in Complexity,
DOI 10.1007/978-3-319-24478-5_88

88.1 Introduction

Wildfires are important sources of aerosols and aerosols affect the distribution of heat and moisture in the atmosphere through their feedback mechanisms. Considering aerosol influence in numerical weather prediction can improve the accuracy of the numerical forecast. The further aim of this study is online coupled modelling based on System for Integrated modeLling of Atmospheric coMposition (SILAM) and Hirlam Aladin Research for Mesoscale Operational Numerical Weather Prediction in Euromed (HARMONIE) model. Therefore validation of input data from SILAM is necessary. This study is focused on a wild-land fire episode in 2010, August 7–9, when the plume of severe wildfire smoke in the European part of Russia reached Estonia and southern Finland, thus giving a unique chance to evaluate the modelling results against a relatively dense network of air quality monitoring stations.

88.2 Methods

The dispersion of total aerosol and all aerosol components separately was simulated with chemistry-transport model SILAM (http://silam.fmi.fi/). SILAM output was compared with measured three-hourly average concentrations of $PM_{2.5}$ (PM10 if $PM_{2.5}$ was not measured) in Estonia and Finland. There were nine monitoring stations in Estonia and seven monitoring stations in Finland (Fig. 88.1).

The SILAM model version 5.2, driven by the European Centre for Medium-Range Weather Forecasts (ECMWF) meteo fields, was run within the European domain of AQMEII2 model validaton exercise with a 0.2-degree grid resolution, applying also the AQMEII2 chemical and aerosol boundary fields. Anthropogenic emissions originated from Monitoring Atmospheric Composition and Climate (MACC) inventory, IS4FIRESv1 (Sofiev et al. 2009) wildfire emissions were used.

HARMONIE model is used for the meteorological simulation with aerosol feedback (direct radiative effect) included using external aeorosol optical depth (AOD) from SILAM as input. In the HARMONIE model ECMWF radiation parameterizations are used (Seity et al. 2011). Two-stream shortwave radiation scheme (Fouquart and Bonnel 1980) with six spectral bands is utilised. For calculating the aerosol direct radiative effect, AOD on model levels changing in time and constant single scattering albedo and asymmetry parameter for each spectral interval is used.

88.3 Results and Discussion

In Estonia the observed $PM_{2.5}$ peak value reached 80 $\mu g/m^3$ (narrow peak up to 106 $\mu g/m^3$ in the easternmost station), whereas SILAM predicted total aerosol up to 75 $\mu g/m^3$. In Finland the concentration of measured $PM_{2.5}$ amounted to 220 $\mu g/m^3$,

Fig. 88.1 $PM_{2.5}$ monitoring stations in Estonia and Finland chosen for this study

while computations made with SILAM predicted concentrations up to 70 μg/m^3. Remarkably enhanced particulate matter concentrations were found in 12 monitoring stations out of 16, reproduced by the model within 10 % of the peak values in 6 stations (Fig. 88.2).

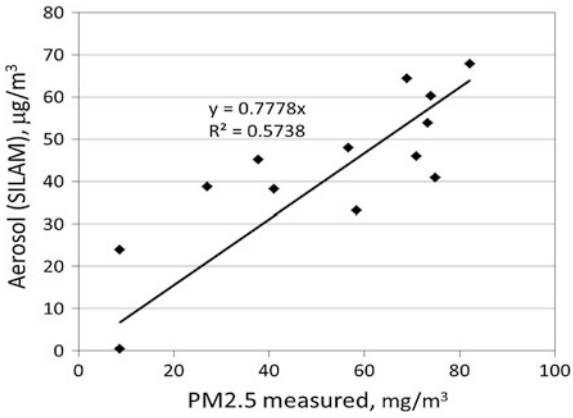

Fig. 88.2 Concentration modelled *versus* measured aerosol at 12:00 UTC, August 8, 2010 in monitoring stations of Estonia and Southern Finland

SILAM tends to predict too large extent of the smoke plume to west, but underestimates in the east, where $PM_{2.5}$ concentrations are highest. The plume did not reach the westernmost sites Vilsandi and Turku as SILAM predicted. In other stations the general shape of the peak—the concentration rise in August 7th and sharp decrease at night of 9th—was reproduced by SILAM within 3–6 h of a time error. SILAM is giving two high peaks, whereas measurement shows only a minor one in August 7 (Fig. 88.3).

The model runs suggest that the wildfires were not solely responsible for enhanced concentrations: the continental aerosols—ground dust and secondary

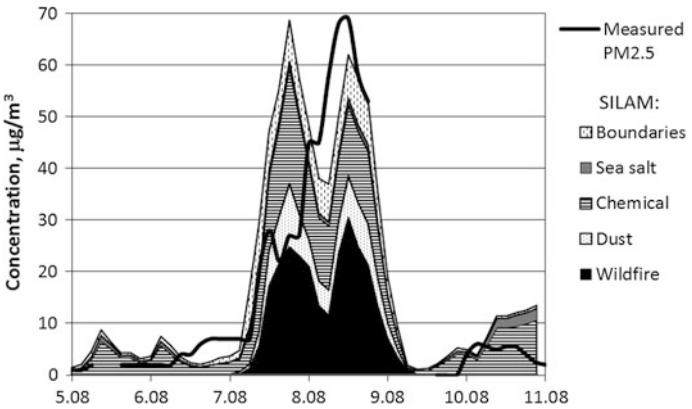

Fig. 88.3 Composition of SILAM total aerosol during August 5 to 11, 2010, in Lahemaa monitoring station (missing data points in measurements were caused by power outages)

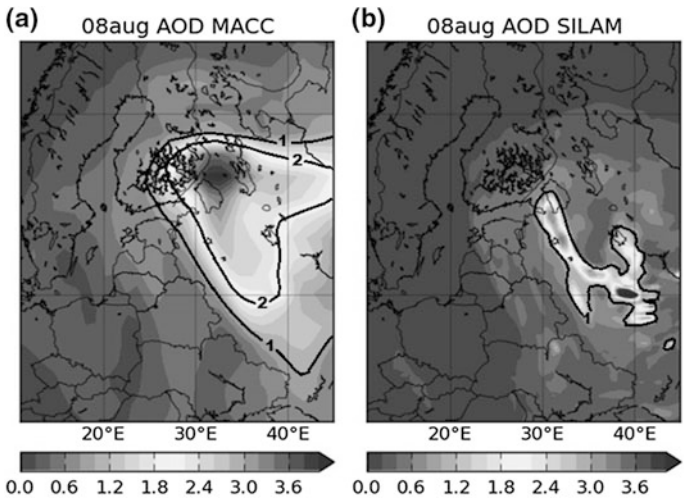

Fig. 88.4 AOD from MACC IFS re-analysis (**a**) and SILAM forecast (**b**), at 12 UTC August 8, 2010

inorganic aerosol—constituted about a half of the total mass. The rest of it was mostly anthropogenic and continental aerosol, including desert dust (Fig. 88.3).

Comparison of predicted and re-analysed AOD during the peak of event is shown in Fig. 88.4. The plume predicted by SILAM has highest values in smaller area that does not reach Estonia and Finland. However, the analysis show rather high AOD at eastern border of both countries.

Remarkable direct effect of the aerosols on boundary-layer meteorological conditions, PBL height, near-surface wind and temperature was found during this episode when the aerosol direct radiative effect was considered in numerical weather prediction model HARMONIE.

Acknowledgements This study was funded by Estonian Research Council research project IUT20-11 and ETF grant 8795. The in-situ particulate matter monitoring data is provided by Estonian Environmental Research Centre and http://www.ilmanlaatu.fi/.

References

Fouquart Y, Bonnel B (1980) Computations of solar heating of the earth's atmosphere- a new parameterization. Beiträge zur Physik der Atmosphäre 53:35–62b

Seity Y, Brousseau P, Malardel S, Hello G, Béénard P, Bouttier F, Lac C, Masson V (2011) The AROME-France convective-scale operational model. Mon Weather Rev 139(3):976–991

Sofiev M, Vankevich R, Lotjonen M, Prank M, Petukhov V, Ermakova T, Koskinen J, Kukkonen J (2009) An operational system for the assimilation of the satellite information on wild-land fires for the needs of air quality modelling and forecasting. Atmos Chem Phys 9 (18):6833–6847

Chapter 89
De praeceptis ferendis: Air Quality Multi-model Ensembles

Ioannis Kioutsioukis and Stefano Galmarini

Abstract Ensembles of air quality models have been shown to outperform single models in many cases. Starting from the theoretical evidence behind this empirical ascertainment, we present the conditions granting an ensemble superior to any single model. As those conditions are not systematically met, we also investigate two additional ensemble estimators for which a sound mathematical framework exists. In view of producing a single improved forecast out of the ensemble, the three candidate ensemble estimators, namely the unconditional ensemble mean, the weighted ensemble mean and the mean of the sub-ensemble with the right trade-off between accuracy and diversity, are evaluated against data generated in the context of AQMEII (Air Quality Model Evaluation International Initiative). The pitfalls of training such ensembles are investigated. Overall, following a proper training procedure, the sophisticated ensemble averaging techniques were shown to have higher skill compared to solely ensemble averaging forecasts.

89.1 Introduction

The forecast error of the unconditional ensemble mean (mme) outperforms the error of each individual ensemble member only if the assumption that the models are independent and identically distributed (i.i.d.) around the true state is satisfied. Given that this assumption is rarely met in practice, in this study we explore the benefits of ensemble forecasting in the form of conditional averaging through either a weighting scheme that keeps all members or a reduced ensemble that makes use

I. Kioutsioukis (✉) · S. Galmarini
European Commission, Joint Research Centre, Institute for Environment and Sustainability, Air and Climate Unit, 21027 Ispra, Italy
e-mail: kioutio@upatras.gr

I. Kioutsioukis
Laboratory of Atmospheric Physics, Physics Department, University of Patras, 26500 Rio, Greece

D.G. Steyn and N. Chaumerliac (eds.), *Air Pollution Modeling and its Application XXIV*, Springer Proceedings in Complexity,
DOI 10.1007/978-3-319-24478-5_89

of only an *effective number of models* (M_{EFF}). All time-series utilised originate from the unprecedented database built within the Air Quality Modelling Evaluation International Initiative (AQMEII). Both approaches result in the optimum distribution of the models in the respective workspace.

89.2 Methodology

Under the assumed condition that the models are all unbiased (bias has been removed from the models through a statistical post-processing procedure), there exist analytical formulas for the weights derived from single or multi-point optimization. For the one-dimensional case, the optimal weights have the general form:

$$\bar{\boldsymbol{w}} = \frac{\boldsymbol{K}^{-1}\boldsymbol{l}}{\left(\boldsymbol{K}^{-1}\boldsymbol{l}, \boldsymbol{l}\right)}$$

where $\boldsymbol{K}$ is the error covariance matrix and $\boldsymbol{l}$ the unitary vector. The weights are neither strictly positive nor bounded, implying the existence of a potential risk that may arise from improper training.

Analytical decomposition of the ensemble error in the form of bias-variance-covariance (bvc) or accuracy-diversity (ad) provides pathways for member selection that satisfy certain conditions. The bvc decomposition has the form:

$$MSE(\bar{f}) = \overline{bias^2} + \frac{1}{M}\overline{varE} + \left(1 - \frac{1}{M}\right)\overline{covE}$$

where M is the number of models and the letter E denotes error matrix. As the number of models in the ensemble increases, the error converges to the covariance term. Models with negatively correlated errors within the ensemble could lower the value of this term. The ad decomposition has the form:

$$MSE(\bar{f}) = E\left(\frac{1}{M}\sum_{i=1}^{M}(f_i - \mu)^2 - \frac{1}{M}\sum_{i=1}^{M}(f_i - \bar{f})^2\right)$$

where μ, f_i and *fbar* are the observations, models and ensemble mean respectively.

Here, the minimization of the ensemble error requires the right trade-off between the accuracy (first term) and the diversity (second term).

The persistence of the weights and the selected members via the error decompositions is prerequisite for safe predictions with the conditional ensemble average.

89.3 Results

The error of the ensemble mean is superior to the mean of the individual model errors but is not necessarily better than the skill of the "locally" best model (Kioutsioukis and Galmarini, 2014). The conditions leading to an ensemble superior to the best single model depend on the skill difference among members and the amount of redundancy in the ensemble. Figure 89.1a shows that those conditions are met at roughly half of the examined stations for the case of ground level O_3 (JJA).

A 2-month training period was found necessary for the stabilization of the optimal weights. On the other hand, even smaller training length was adequate for robust estimates for the members of the optimal cluster with respect to their accuracy and diversity. The implementation of the acquired weights/clusters into a validation dataset has shown that using the optimal weights (cluster), the improvement across all stations over the mme was up to 35 % (25 %) for the RMSE and around 85 % (57 %) for the median hit rate.

The decomposition of the skill as a function of the effective number of models (M_{EFF}) demonstrated that for ozone, the three products were converging with increasing M_{EFF} (Fig. 89.1b). Those cases were generally occurring for intermediate concentration ranges, that all models are somehow tuned to replicate. On the other end, as M_{EFF} was decreasing and the ensemble was departing from behaving as an i.i.d. sample, the error gain from mmeS (optimal cluster mme) or mmeW (optimal weighted mme) over mme was gradually increasing. The extreme records were generally found in the asymmetric range of the ensemble.

The presented methodological framework can be easily implemented in ensemble air quality modelling studies. For example, it could be implemented in the

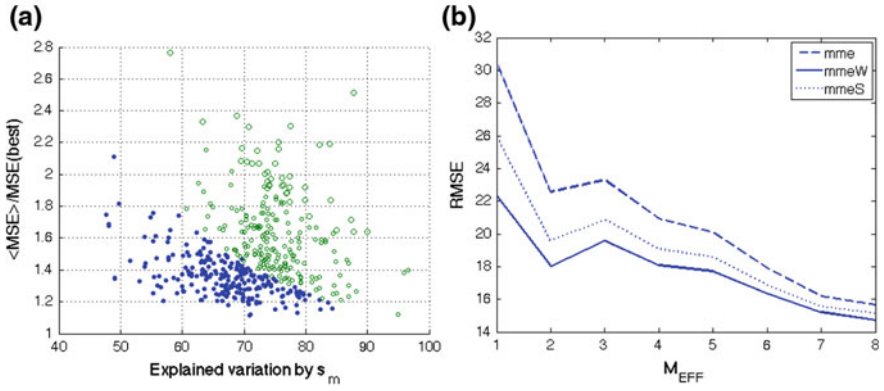

Fig. 89.1 **a** The indicator RMSE (mme)/RMSE (best single model) as a function of redundancy (explained variation by the maximum eigenvalue s_m) and model skill difference (<MSE>/MSE (best), evaluated at all observation sites. *Filled markers* indicate indicator values lower than 1. **b** Forecast Skill of mme, mmeS and mmeW from the 451 stations for the test dataset as a function of M_{EFF}

POSEIDON project to improve the quality and the validity of the numerical simulations that investigate the impact on air quality of major emitters such as harbours.

Acknowledgments This work was partially supported from the EU-Poseidon project.

Reference

Kioutsioukis I, Galmarini S (2014) De praeceptis ferendis: good practice in multi-model ensembles. Atm Chem Phys (and the references therein) 14:11791–11815

Chapter 90
Influence of WRF Parameterization on Coupled Air Quality Modeling Systems

Goran Gašparac, Amela Jeričević and Branko Grisogono

Abstract This study presents the continuation and exploration of the research by application of regional and high resolution air quality (AQ) models. Separate 'offline' (WRF—CAMx) and 'online' (WRF Chem) coupling modeling systems were used to evaluate the contribution of the local anthropogenic sources over the Republic of Croatia. Within the research with the NWP WRF model, various tests were made with the implementation of the new, improved mixing length scale in MYJ PBL scheme. Default and modified setup of the NWP WRF model was tested on different ABL stability conditions and coupled with AQ models. Experiments with different AQ models also encompassed different time periods with relatively high concentrations in rural and urban areas. Using complex atmospheric chemistry models it was possible to analyze the main processes contributing to the relatively high concentration on regional and local scale and to compare the performance of two different coupling modeling systems.

90.1 Introduction

During November 2011, persistent stable meteorological conditions led to relatively high PM_{10} concentrations over Pannonian basin. The particular situation was characterized as an interruption by strong NE bora flow that initiated the resuspension of crustal elements into the air. On 10th of November at the beginning of the analysed period, moderately strong north-easterly wind ~ 10 m/s started to blow over Hungary and Croatia and the onset of bora wind with wind gusts up to

G. Gašparac (✉)
Geophysical and Ecological Modeling Ltd., Zagreb, Croatia
e-mail: ggasparac@gekom.hr

A. Jeričević
Croatian Civil Aviation Agency, Zagreb, Croatia

B. Grisogono
Department of Geophysics, Faculty of Science, University of Zagreb, Zagreb, Croatia

D.G. Steyn and N. Chaumerliac (eds.), *Air Pollution Modeling and its Application XXIV*, Springer Proceedings in Complexity,
DOI 10.1007/978-3-319-24478-5_90

22 m/s on the northern Adriatic coast. The bora wind reached maximum on 12th of November on the Adriatic while inland, the north-easterly wind weakened and calm light winds prevailed in high pressure field that dominated until 16th of November. To encompass periods with measured pick values the further analysis were performed on the period from 10th to 20th of November.

90.2 Modelling Approach

Using monitored air quality and meteorological data, backward air mass trajectories and the results of NWP WRF model, PM_{10} contributions were investigated at urban and rural stations in Croatia, Hungary and Serbia. Regional EMEP model was used for simulation of long range, trans-boundary transport of PM_{10} concentrations and the composition of particulate matter. Within the research with the NWP WRF model, various tests were made with implementation of the new, improved mixing length (ML) in MYJ PBL scheme which is uniformly valid in neutral and static stable airflows. ML scale is defined as a physical quantity describing the size of the most relevant eddies in a modeled turbulent flow. It is a theoretical and immeasurable quantity and its parameterization is considered as a major weakness of turbulent models (Grisogono et al. 2011, Mellor and Yamada 1982). A new 'z-less' ML scale parameterization proposed in Grisogono (2010) and previously tested with the MIUU model (Grisogono and Belušić 2008) was implemented in the WRF NWP and WRF-Chem model in order to test its influence in both 'online' and 'offline' coupled modeling systems.

90.3 Results and Discussion

First analyses were performed with EMEP model to determine areas with problematic air quality situations. From Fig. 90.1a, b it can be seen that the highest concentrations on domain originate from Milano and were transported to the western part of Croatia. The EMEP model showed also increased concentrations over Pannonian basin mainly due to trans-boundary effect. Preliminary simulations with WRF Chem model, Fig. 90.1c, d showed similar positions of the maximum concentrations of the PM_{10}. Both models estimated same magnitude of PM_{10} concentrations, but due to higher horizontal resolution, WRF Chem provided more details, especially in the vicinity of larger urban areas. In comparison with WRF Chem model, EMEP showed generally higher concentrations over whole domain which can be due to better emission definition in EMEP model. Previous research with the NWP WRF (not shown here) showed that WRF with modified ML is able to reproduce stable ABL conditions (SABL) and persistent low wind speed. In sensitivity analysis with ML scale in WRF Chem model, the results showed overall higher PM_{10} concentrations in a case with new ML Fig. 90.1e, f, except in areas

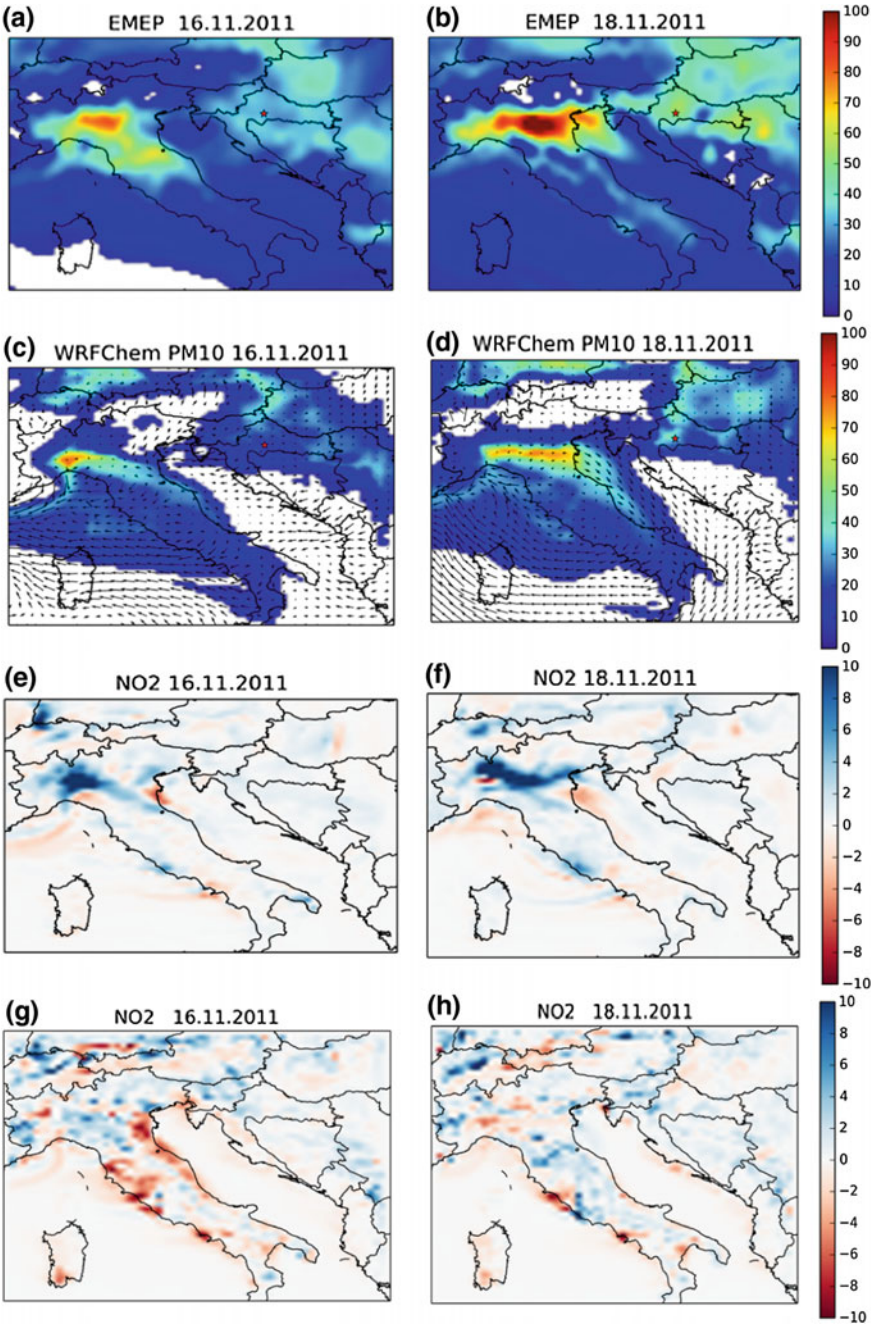

Fig. 90.1 Daily averaged PM_{10} concentrations in $\mu g/m^3$ from EMEP model for 16th (**a**), and 18th Nov 2011 (**b**). Daily averaged PM_{10} concentrations in $\mu g/m^3$ from WRF Chem model for 16th (**c**), and 18th Nov 2011 (**d**). Differences in daily averaged NO_2 concentrations in $\mu g/m^3$ between default and modified WRF Chem for 16th (**e**), and 18th Nov 2011 (**f**). Differences in daily averaged NO_2 concentrations in $\mu g/m^3$ between default and modified WRF—CAMx for 16th (**g**), and 18th Nov 2011 (**h**). *Red dot* is the location of the city of Sisak

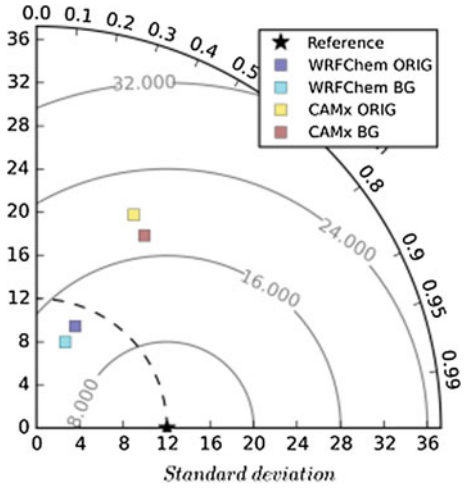

Fig. 90.2 Taylor diagram for the city of Sisak presenting comparison of 'offline' and 'online' coupled modeling systems, with and without new ML scale

with higher emissions (Milano area) where were also the largest discrepancies. The first preliminary simulations of 'offline' coupled modeling system WRF—CAMx with new ML scale, showed very different influence in comparison with WRF Chem model—Fig. 90.1g, h. The discrepancies were scattered on whole domain mainly located above continental parts and were not in correlation with locations of emission sources contrary to WRF Chem model. The comparison of NO_2 modeled concentrations against measurements from the urban station Sisak (Fig. 90.2) showed better correlation in case with new ML for 'offline' simulations contrary to the 'online' simulations where there was no significant difference.

90.4 Conclusions

Various numerical models (EMEP, WRF Chem and WRF—CAMx) were applied over SE part of Europe in order to evaluate the contribution of local anthropogenic sources over the Croatia. Regional EMEP model showed increased PM_{10} concentrations in Pannonian basin mainly due to trans-boundary effect triggered with meteorological conditions. First preliminary results of the WRF Chem model showed generally lower concentrations over domain but similar positions as the EMEP model of the highest PM_{10} concentrations. Within the research with the NWP WRF model, various tests were made with new ML implemented in MYJ PBL in both 'offline' and 'online' coupled modeling systems. Both preliminary results of WRF Chem and WRF—CAMx showed overall higher concentrations with new ML scale. The largest discrepancies were located in the areas with higher emissions in simulations with WRF Chem model; contrary to WRF-CAMx simulations where discrepancies did not showed any correlation with locations of emission sources. In comparison against measurements, the new ML scale in

WRF-CAMx coupled modeling system tends to improve modeling performance, but in WRF Chem did not gave any significant difference. Future work will encompass evaluation of applied models with new ML on other monitoring stations in Pannonian basin. It will include more detailed emission inventory and model intercomparison with other air quality and meteorological parameters in order to establish appropriate modeling approach of the air quality modeling over the Croatia.

References

Grisogono B (2010) Generalizing 'z-less' mixing length for stable boundary layers. Q J R Meteorol Soc 136:213–221

Grisogono B, Belušić D (2008) Improving mixing length-scale for stable boundary layers. Q J R Meteorol Soc 134:215–219

Grisogono B, Milovac J, Telišman Prtenjak M, Bašić T (2011) An airflow over the Dinaric Alps simulated with a modified mixing-length formulation in WRF model. In: 31st international conference on Alpine meteorology, Aviemore, Scotland

Mellor LG, Yamada T (1982) Development of a turbulence closure model for geophysical fluid problems. Rev Geophys Space Phys 20:851–875

Chapter 91
High-Resolution Air Quality Forecasts with MOCAGE Chemistry Transport Model

Mathieu Joly, Béatrice Josse, Matthieu Plu, Joaquim Arteta, Jonathan Guth and Frédérik Meleux

Abstract MOCAGE is the 3D global off-line chemistry transport model (CTM) run at Météo-France since 2005 for air quality operational forecasts. Three nested domains are used, with decreasing resolutions (globe, Europe, and France), and 47 vertical levels (from the surface to 5 hPa). For the global and the European domain, input meteorological forcing fields are Météo-France ARPEGE forecasts. For France, and for the first day of forecast, MOCAGE uses the operational outputs of Météo-France non-hydrostatic AROME model. This high-resolution (2.5 km) meteorological model is supposed to better represent urban processes (e.g., the urban heat island), which are of strong interest for air quality applications. The purpose of this study is to test the increase of resolution of the CTM MOCAGE over France from 0.1° to 0.025° (i.e. the native resolution of the input meteorological fields).

Poster presentation.

Key topic: Model assessment and verification.

M. Joly (✉) · B. Josse · M. Plu · J. Arteta · J. Guth
Météo-France CNRM-GAME, Toulouse, France
e-mail: mathieu.joly@meteo.fr

B. Josse
e-mail: beatrice.josse@meteo.fr

M. Plu
e-mail: matthieu.plu@meteo.fr

J. Arteta
e-mail: joaquim.arteta@meteo.fr

J. Guth
e-mail: jonathan.guth@meteo.fr

F. Meleux
INERIS, Paris, France
e-mail: frederik.meleux@ineris.fr

D.G. Steyn and N. Chaumerliac (eds.), *Air Pollution Modeling and its Application XXIV*, Springer Proceedings in Complexity,
DOI 10.1007/978-3-319-24478-5_91

91.1 Description of the High-Resolution Configuration

At the resolution 2.5 km, the convection is solved by the forcing meteorological model AROME, which is non-hydrostatic. In the CTM MOCAGE, the convection parameterization used at low resolution (≥10 km) has therefore to be turned off.

Because the convection parameterization has been switched off, the CTM does not produce its own convective precipitation and cloudiness anymore. Hopefully, those missing fields can be output—and in a more realistic way—by the meteorological model. A comparison made at the resolution 10 km showed that 3d precipitation fluxes from the meteorological model do not improve much the forecasts, whereas more realistic 3d cloudiness fields lead to a great improvement of the ozone forecasts.

The dynamical time-step of the CTM has been reduced from 60 to 15 min, and the frequency of the forcing fields has been increased from 3-hourly to hourly. Surprisingly, hourly forecasts do not improve the ozone forecast (whatever the season), and the increase of the dynamical time-step leads to a slight increase in ozone surface concentrations.

91.2 First Results at High-Resolution

The model has been run for the daily forecasts of three summer months (JAS 2013) and one winter month (January 2014).

Because the emissions inventory has been kept identical (resolution 8 km), the increase in the resolution of the CTM has globally a weak impact on the performances of air quality forecasts at the surface.

However, at high resolution, the vertical velocity at the surface increases, especially by night, due to a better representation of the relief. In some cases, especially in winter, this leads to a strong ozone positive bias (ozone seems to be trapped in the lower levels). For NO_2 and PM_{10} this change in vertical velocity has no significant impact.

91.3 Conclusions and Further Work

This study demonstrates the technical feasibily (and numercial stability!) of a high-resolution configuration of the chemistry transport model MOCAGE used at Météo-France for operational air quality forecasts.

Further works will include:

- the use of a 1 km inventory (regridded at our 2.5 km resolution),
- various improvements already available at lower-resolution (e.g., secondary inorganic aerosols),
- tuning of the model time-steps,
- and a work on the transport and turbulence schemes to solve the problem of ozone bias in winter.

Part VIII
Data Assimilation and Air Quality Forecasting

Chapter 92
Saharan Dust as a Causal Factor of Significant Cloud Cover Along the Saharan Air Layer in the Atlantic Ocean

Pavel Kishcha, Arlindo M. da Silva, Boris Starobinets and Pinhas Alpert

Abstract The tropical Atlantic is frequently affected by Saharan dust intrusions. Based on MODIS cloud fraction (CF) data during the 10 year study period, we found that these dust intrusions contribute to significant cloud cover along the Saharan Air Layer (SAL). Below the temperature inversion at the SAL's base, the presence of large amounts of settling dust particles, together with marine aerosols, produces meteorological conditions suitable for the formation of shallow stratocumulus clouds. The significant cloud fraction along the SAL together with clouds over the Atlantic Inter-tropical Convergence Zone contributes to the 20 % hemispheric CF asymmetry between the tropical North and South Atlantic. This leads to the imbalance in strong solar radiation, which reaches the sea surface between the tropical North and South Atlantic, and, consequently, affects climate formation in the tropical Atlantic. Therefore, despite the fact that, over the global ocean, there is no noticeable hemispheric asymmetry in cloud fraction, over the significant area such as the tropical Atlantic the hemispheric asymmetry in CF takes place. Saharan dust is also the major contributor to hemispheric aerosol asymmetry over the tropical Atlantic. The NASA GEOS-5 model with aerosol data assimilation was used to extend the MERRA reanalysis with five atmospheric aerosol species (desert dust, sulfates, organic carbon, black carbon, and sea-salt). The obtained 10 year (2002–2012) MERRA-driven aerosol reanalysis dataset (aka MERRAero) showed that, over the tropical Atlantic, dust and carbonaceous aerosols were

P. Kishcha (✉) · B. Starobinets · P. Alpert
Department of Geosciences, Tel-Aviv University, Tel-Aviv, Israel
e-mail: pavel@cyclone.tau.ac.il

A.M. da Silva
Global Modeling and Assimilation Office, NASA/GSFC, Greenbelt, MD, USA

D.G. Steyn and N. Chaumerliac (eds.), *Air Pollution Modeling and its Application XXIV*, Springer Proceedings in Complexity,
DOI 10.1007/978-3-319-24478-5_92

distributed asymmetrically relative to the equator, while other aerosol species were distributed more symmetrically.

92.1 Introduction

The NASA GEOS-5 modeled aerosol data set (aka MERRAero) was used in the current study in order to estimate the contribution of different aerosol species to hemispheric aerosol asymmetry over the tropical Atlantic Ocean. GEOS-5 includes a module representing atmospheric aerosols (Colarco et al. 2010). This aerosol module is based on a version of the Goddard Chemistry, Aerosol, Radiation, and Transport (GOCART) model (Chin et al. 2002). GOCART treats the sources, sinks, and chemistry of desert dust; sulfate; sea salt; black carbon and organic carbon aerosols. Both dust and sea salt have wind-speed dependent emission functions, while sulfate and carbonaceous species have emissions principally from fossil fuel combustion, biomass burning, and bio-fuel consumption, with additional biogenic sources of organic carbon. An important feature of GEOS-5 is including aerosol data assimilation using aerosol optical thickness (AOT) retrieved from MODIS instruments on board the NASA Terra and Aqua satellites. Our main point is that, over the tropical Atlantic, not only is Saharan dust responsible for the pronounced hemispheric aerosol asymmetry, but it also contributes to significant cloud cover along the Saharan Air Layer (Kishcha et al. 2014, 2015). Over the tropical Atlantic in July, along the Saharan Air Layer, MODIS cloud fraction (CF) data showed cloud cover up to 0.8–0.9. This cloud fraction along the SAL together with clouds over the Atlantic Inter-tropical Convergence Zone contributes to the hemispheric CF asymmetry between the tropical North and South Atlantic. This leads to the imbalance in strong solar radiation, which reaches the sea surface between the tropical North and South Atlantic, and, consequently, affects climate formation in the tropical Atlantic.

92.2 Method

As discussed by Kishcha et al. (2014, 2015), meridional distribution of modeled total AOT and AOT of various aerosol species, zonal averaged over the tropical Atlantic (30^{o}N–30^{o}S), was used to estimate the contribution of various aerosol species to hemispheric aerosol asymmetry over the tropical Atlantic. For the purpose of comparing meridional distribution of cloud fraction with that of AOT during the same 10-year period (July 2002–June 2012), Collection 5.1 of MODIS-Terra L3 monthly daytime cloud fraction (CF) data, with horizontal resolution $1^{o} \times 1^{o}$ was used. Furthermore, to analyze meridional rainfall distribution, the Tropical Rainfall Measuring Mission (TRMM) monthly $0.25° \times 0.25°$ Rainfall Data Product (3B43 Version 7) was used.

92.3 Results and Discussion

The obtained results are described in detail by Kishcha et al. (2014, 2015). With respect to different oceans, only over the Atlantic Ocean did MERRAero demonstrate that desert dust dominated all other aerosol species and was responsible for hemispheric aerosol asymmetry there. MERRAero showed that, over the tropical Atlantic, dust and carbonaceous aerosols were distributed asymmetrically relative to the equator, while other aerosol species were distributed more symmetrically (Kishcha et al. 2014, 2015).

MERRAero showed that there are strong seasonal variations of hemispheric aerosol asymmetry. Hemispheric aerosol asymmetry is most pronounced during the season from March to July, when large amounts of Saharan dust are transported across the Atlantic (Fig. 92.1a). Saharan dust dominates other aerosol species over the tropical North Atlantic (Fig. 92.1a). Dust AOT, averaged separately over the tropical North Atlantic, is one order of magnitude higher than dust AOT averaged over the tropical South Atlantic (Kishcha et al. 2014, 2015). Therefore, dust is the major contributor to hemispheric aerosol asymmetry over the tropical Atlantic, based on GEOS-5 modeling. In September and October, when the dust contribution to total AOT decreases, we have a completely different picture: there is no noticeable hemispheric asymmetry in total AOT between the tropical North and

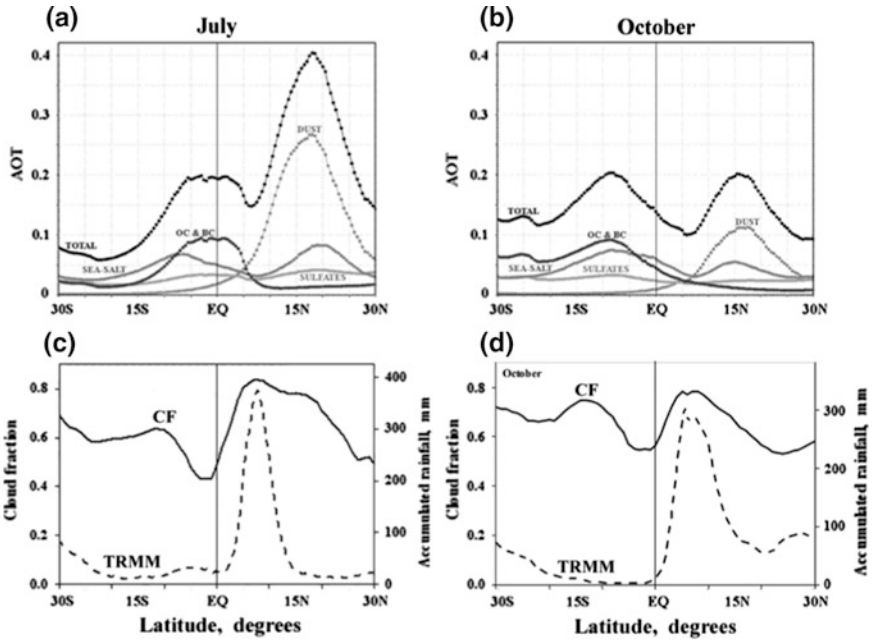

Fig. 92.1 Comparisons between meridional distribution of AOT/CF/TRMM rainfall during (**a** and **c**) the season of pronounced hemispheric aerosol asymmetry and (**b** and **d**) during the season with no noticeable hemispheric aerosol asymmetry

South Atlantic Oceans (Fig. 92.1b). This is because the contribution of carbonaceous aerosols to total AOT in the South Atlantic is approximately equal to the contribution of dust to total AOT in the tropical North Atlantic (Fig. 92.1b).

With respect to meridional distribution of cloud fraction, Fig. 92.1c illustrate that, during the season of pronounced hemispheric aerosol asymmetry, there is hemispheric asymmetry in CF. During the season with no noticeable aerosol asymmetry, there is no noticeable hemispheric asymmetry in CF (Fig. 92.1d). Therefore, over the tropical Atlantic, hemispheric asymmetry in aerosols is accompanied by hemispheric asymmetry in cloud cover (Kishcha et al. 2015), in contrast to the situation over the global ocean (Kishcha et al. 2009).

In each month of the year, the main CF maximum coincides with the Inter-Tropical Convergence Zone (ITCZ), which is characterized by intensive rainfall (Fig. 92.1c, d). In the summer months (when pronounced hemispheric dust asymmetry was observed), MODIS CF data showed significant CF (up to 0.8) to the north from the main CF maximum, over the latitudes of transatlantic dust transport within the Saharan Air Layer (SAL) (Fig. 92.1c). The GEOS-5 model data showed that the significant CF to the north of the Atlantic ITCZ could be associated with the maximum in dust AOT over the latitudes of the Saharan Air Layer (SAL), between approximately 12°N and 24°N in the North Atlantic (Fig. 92.1a, c). The significant cloud fraction along SAL, together with clouds over the Atlantic ITCZ, contributes to hemispheric asymmetry in CF over the tropical Atlantic. In July, CF averaged separately over the tropical North Atlantic is 20 % higher than that averaged over the tropical South Atlantic. This leads to the imbalance in strong solar radiation reaching the sea surface between the tropical North and South Atlantic and affects climate formation in the tropical Atlantic.

Kishcha et al. (2015) showed that the ocean area of SAL with Saharan dust transported across the Atlantic is covered by significant cloudiness up to 0.8–0.9. The area of SAL with significant CF is characterized by limited precipitation. This indicates that clouds along the SAL are not developed enough. The temperature inversion below the SAL base prevents deep cloud formation; this explains limited precipitation in these zones. On the other hand, meteorological conditions below the temperature inversion at the SAL base include significant atmospheric humidity and the presence of large amounts of settling dust particles together with marine aerosols. As known, aerosol species often combine to form mixed particles, with properties different from those of their components (Andreae et al. 2009). Mineral dust particles are known to be not very efficient cloud condensation nuclei (CCN), unless they are coated with soluble materials (Andreae et al. 2009). Using airplane measurements, Levin et al. (2005) showed that dust transport over the sea could lead to sea-salt coating on dust particles. Coating settling dust particles with sea-salt could modify them into efficient CCN. Being below the temperature inversion and acting as efficient CCN, Saharan dust particles coated with sea-salt contribute to the formation of shallow stratocumulus clouds. This physical mechanism, based on the influence of Saharan dust on stratocumulus clouds below the temperature inversion, could explain the observed significant cloud cover (CF up to 0.8–0.9) along the Saharan Air Layer (Kishcha et al. 2015).

Kishcha et al. (2015) analyzed possible relationships between properties of clouds in the area of SAL and those of Saharan dust, using MODIS L3 gridded monthly data ($1^o \times 1^o$) of the effective radius of cloud droplets for liquid water clouds. They found that the effective radius of cloud droplets increases with distance from the Sahara. This can be explained by the decrease in CCN numbers associated with the decreasing numbers of settling Saharan dust particles with distance from the Sahara, in accordance with the observed decrease in dust AOT. This relationship supports the above-mentioned physical mechanism of cloud formation below the SAL's base.

References

Andreae MO, Hegg DA, Baltensperger U (2009) Sources and nature of atmospheric aerosols. In: Levin Z, Cotton W (eds) Aerosol pollution impact on precipitation. Springer, Dordrecht, pp 45–90

Chin M, Ginoux P, Kinne S, Torres O, Holben B, Duncan BN, Martin RV, Logan J, Higurashi A, Nakajima T (2002) Tropospheric aerosol optical thickness from the GOCART model and comparisons with satellite and sun photometer measurements. J Atmos Phys 59:461–483

Colarco P, da Silva A, Chin M, Diehl T (2010) Online simulations of global aerosol distributions in the NASA GEOS-4 model and comparisons to satellite and ground-based aerosol optical depth. J Geophys Res 115:D14207. doi:10.1029/2009JD012820

Kishcha P, Starobinets B, Kalashnikova O, Long CN, Alpert P (2009) Variations in meridional aerosol distribution and solar diming. J Geophys Res 114:D00D14. doi:10.1029/2008JD010975

Kishcha P, da Silva A, Starobinets B, Long CN, Kalashnikova O, Alpert P (2014) Meridional distribution of aerosol optical thickness over the tropical Atlantic Ocean. Atmos Chem Phys Discuss 14:23309–23339. doi:10.5194/acpd-14-23309-2014

Kishcha P, da Silva A, Starobinets B, Long CN, Kalashnikova O, Alpert P (2015) Saharan dust as a causal factor of hemispheric asymmetry in aerosols and cloud cover over the tropical Atlantic Ocean. Int J Remote Sens. 36:3423-3445. doi: 10.1080/01431161.2015.1060646

Levin Z, Teller A, Ganor E, Yin Y (2005) On the interactions of mineral dust, sea-salt particles, and clouds: a measurement and modeling study from the Mediterranean Israeli dust experiment campaign. J Geophys Res 110:D20202. doi:10.1029/2005JD005810

Chapter 93
Source-Impact Forecasting for Dynamic Air Quality Management: Application to Prescribed Burn Management

M. Talat Odman, Aditya A. Pophale, Rushabh D. Sakhpara, Yongtao Hu, Armistead G. Russell and Michael E. Chang

Abstract The newly developed weather-based prescribed burn forecasting capability presents new opportunities for dynamic air quality management. Forecasting of burn emissions has been incorporated into the HiRes-2 Air Quality Forecasting System. Forecasts are being produced daily for air quality and the impacts of power plant, traffic and prescribed burn emissions. The ultimate goal is to integrate these air quality forecasts into the burn permitting operations.

93.1 Introduction

Air quality forecasts provide useful information for avoiding exposure to high pollution levels. However, forecasting a pollution episode is not sufficient for circumventing it. Additional information is needed about the contribution of various emission sources to the imminent episode. If it were known which sources will be responsible and by how much, a quick response plan could be implemented for avoidance of the episode or its mitigation. This is a dynamic air quality management paradigm where the sources targeted for control and the level of controls are episode-specific. Prescribed burning (PB) is one source that is more prone to dynamic management than others. This type of biomass burning is practiced to maintain a healthy forest ecosystem and reduce the wildfire risk. Unlike power plants or on-road vehicles that cannot be curtailed without significant economic, social and political consequences, prescribed burns can be deferred to another day.

M. Talat Odman (✉) · A.A. Pophale · R.D. Sakhpara · Y. Hu · A.G. Russell
School of Civil and Environmental Engineering, Georgia Institute of Technology, Atlanta, GA 30332-0512, USA
e-mail: odman@gatech.edu

M.E. Chang
Brook Byers Institute for Sustainable Systems, Georgia Institute of Technology, Atlanta, GA 30332-0595, USA

D.G. Steyn and N. Chaumerliac (eds.), *Air Pollution Modeling and its Application XXIV*, Springer Proceedings in Complexity,
DOI 10.1007/978-3-319-24478-5_93

We have expanded our air quality forecasting system, HiRes (Hu et al. 2010), to forecast the impacts of various emission sources. Using the sensitivities calculated by DDM-3D (Napelenok et al. 2008) the impacts of each source category to the forecasted ozone and $PM_{2.5}$ concentrations are calculated. For dynamic management purposes the impacts of power plant, on-road vehicle and PB emissions are forecasted. Since DDM-3D uses the local slope of the response curve to calculate the sensitivity of pollutant concentrations to emissions, an accurate estimation of baseline emissions is necessary for reliable forecasting of their impacts. Power plant and traffic emissions typically exhibit relatively small day-to-day variations around annual or seasonal averages. Of course, there are some exceptions to this such as peaking of power plant emissions due to excessive electricity demand during heat waves. PB emissions, on the other hand, exhibit drastic day-to-day changes more often. While the burning activity increases in winter and spring for ecological reasons, it is subject to large weather-related fluctuations due to technical reasons. For example, no burns are attempted on rainy days. These fluctuations in PB emissions necessitate forecasting of burn conditions based on weather.

93.2 HiRes-2 Forecasting System

The HiRes system has been in operation since 2006 for air quality forecasting in Georgia, USA. In addition to the incorporation of the new impact forecasting capability, HiRes went through a major upgrade, recently. Now, the system uses the most recent versions of the meteorology and air quality models, namely WRF3.6 and CMAQ5.0.2. Further, the sensitivities to power plant and on-road vehicle emissions provided by the DDM-3D feature of CMAQ are used in an inverse modeling context to continuously "correct" those emissions for a better match between model predictions and near real-time observations. Ground level $PM_{2.5}$ measurements and NASA MODIS retrievals of AOD are used to drive the corrections. Finally, the higher resolution coverage has been extended to other states in the Southeastern USA.

To forecast prescribed burns a classification tree was built using the fire meteorology and burn permit data in Georgia for the years 2010–2013. If more than 40 hectares per day were permitted for treatment by PB in any county ($\sim$160 counties in Georgia), we defined that day as a "burn day" for that county. The tree classifies the days using 20 meteorological parameters observed at the nearest fire-weather station ($\sim$20 stations in Georgia) as predictor variables. Some parameters, such as the season, the state of the weather, rainfall amount in the last 24 h and wind direction, have stronger correlations with the burns than others. The tree is built by splitting a branch based on parameter values, until all the branches lead to either a "burn" or "no-burn" outcome.

When a burn day is forecasted for a given county, the average daily burn area is distributed to the lands of institutional and large commercial burners according to their burning patterns and randomly to other forested areas to represent the fraction

Table 93.1 Results of the evaluation of the fire forecasting model

Metric	Value
Accuracy	0.85
Precision	0.32
Recall	0.34
F1 score	0.33

of small burners. The fuel loads, in mass per unit area of the burn plots, are obtained from the Fuel Characteristic Classification System (FCCS) maps.[1] Then, using the forecasted fuel moistures and other meteorological parameters relevant to the burn, the fuel consumption amounts are calculated using the CONSUME model.[2] Next, fire emissions are estimated using the emission factors (EFs) defined as mass of pollutant emitted per unit mass of fuel consumed. The EFs used here are based on field measurements at various locations in the Southeastern USA. Finally, the plume rise is calculated as described in Garcia-Menendez et al. (2014) and the emissions are distributed to the CMAQ layers.

93.3 Preliminary Results

To validate the use of the classification tree approach for burn forecasting, we split the data into two sets: randomly selected 60 % of the data were used as a training dataset to build the tree model and the remaining 40 % was used as a testing dataset to evaluate the model. Four metrics were used in the evaluation: (1) Accuracy or the overall correctness of the model, (2) Precision or the accuracy in predicting burn days, (3) Recall or the number of accurate burn days over the number of burn days, and F1 score, which is the harmonic mean of precision and recall. The values of these metrics listed in Table 93.1 indicate a fairly accurate forecast.

The new system has been operational since January 1, 2015. The results for ozone, $PM_{2.5}$ and the source impact forecasts are published daily at our website.[3] Figure 93.1 shows the $PM_{2.5}$ and impact forecasts for February 14, 2015. Exceedance of the 35 μg m^{-3} daily average $PM_{2.5}$ standard is expected for the purple colored grid cells in the upper left panel. A comparison of different source impacts revealed that PB impacts shown in the lower left panel would be responsible for this exceedance. With this information, the amount of area permitted to be burned can be restricted to avoid the forecasted exceedance.

[1] http://www.fs.fed.us/pnw/fera/fccs/maps.shtml.

[2] http://www.fs.fed.us/pnw/fera/research/smoke/consume/index.shtml.

[3] https://forecast.ce.gatech.edu.

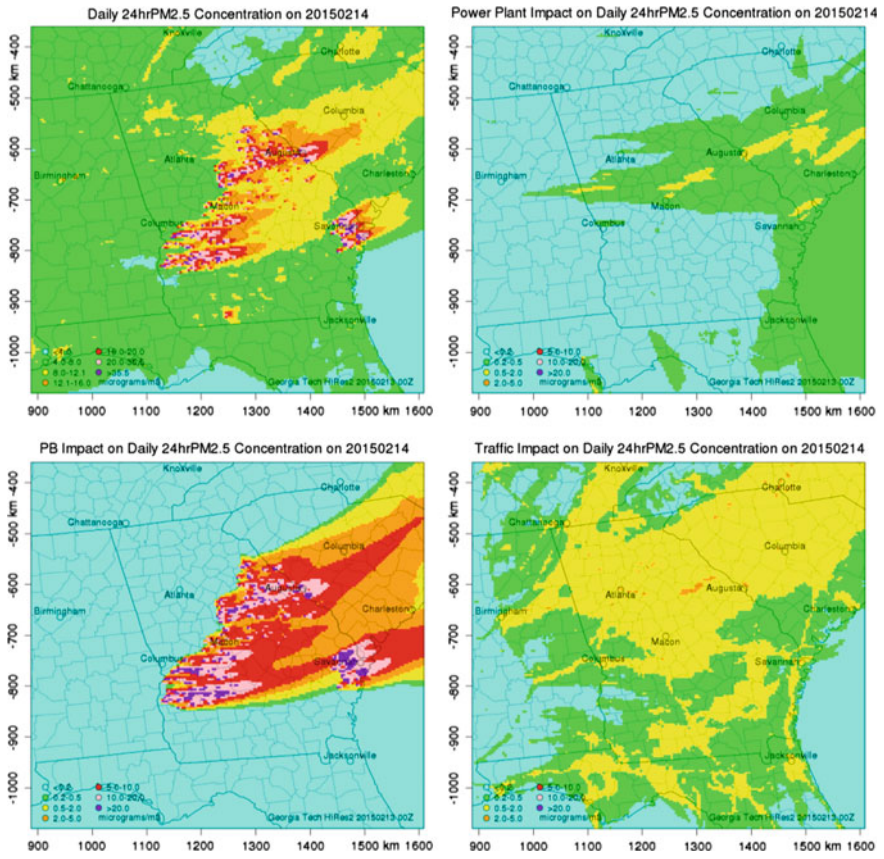

Fig. 93.1 Forecasted 24-h average $PM_{2.5}$ concentrations, in μg m^{-3} (*upper left*), and contributions by power plant (*upper right*), prescribed burn (*lower left*), and traffic (*lower right*) emissions in Georgia USA on February 14, 2015

93.4 Conclusions

The new version of the HiRes air quality forecasting system incorporates new elements targeted for dynamic air quality management. Forecasts of the impacts of power plants, traffic and prescribed burn emissions can be used for averting air pollution episodes. Burns are particularly amenable to dynamic management.

Acknowledgments This research was supported by US EPA's Science to Achieve Results Program (RD83521701). The statements made here do not represent the official views of US EPA.

Questioner: Paul Makar

Question: Are there any observations to suggest that the smoke plumes are affecting the PBL height downwind? If so, how might this affect your forecasts?

Answer: This is a very important issue as the interaction between the plume and the boundary layer is quite complex. Gases and particles in a smoke plume may significantly change the optical properties of the atmospheric layer occupied by the plume. Through radiation, this may affect the boundary layer height downwind as well as the mixing of the smoke plume. To my knowledge, there are no observations to verify these hypotheses. However, there is modeling evidence that cannot be ignored. For example, using a two-way coupled meteorology and air quality modeling system, WRF-CMAQ, Wong et al. (2012) have shown that when particulate matter concentrations reach significant levels due to wildfires, direct radiative effects, primarily scattering and absorption of incoming radiation, result in a reduction of short-wave radiation reaching the surface, causing a reduction in surface temperatures as well as a reduction in PBL heights downwind. Whether prescribed burns, which are of lower intensity compared to wildfires, can create such effects is yet to be demonstrated. In our present forecasting system, the meteorology is not coupled to air quality; only air quality is coupled to meteorology. In other words, the meteorological model does not know the presence of smoke plumes. Therefore, no changes in PBL height occur due to prescribed burns. Our plans for the future include upgrading to a two-way coupled modeling system such as WRF-CMAQ. Once we do that, we would be in a much better position to answer your question.

References

Garcia-Menendez F, Hu Y, Odman MT (2014) Simulating smoke transport from wildland fires with a regional-scale air quality model: sensitivity to spatiotemporal allocation of fire emissions. Sci Total Environ 493(0):544–553

Hu YT, Chang ME, Russell AG, Odman MT (2010) Using synoptic classification to evaluate an operational air quality forecasting system in Atlanta. Atmos Pollut Res 1(4):280–287

Napelenok SL, Cohan DS, Odman MT, Tonse S (2008) Extension and evaluation of sensitivity analysis capabilities in a photochemical model. Environ Model Softw 23(8):994–999

Wong DC, Pleim J, Mathur R, Binkowski F, Otte T, Gilliam R, Pouliot G, Xiu A, Young JO, Kang D (2012) WRF-CMAQ two-way coupled system with aerosol feedback: software development and preliminary results. Geosci Model Dev 5(2):299–312

Chapter 94
Observing System Simulation Experiments (OSSEs) for Air Quality Applications

R. Timmermans, W. Lahoz, J.-L. Attié, V.-H. Peuch, D. Edwards, H. Eskes and P. Builtjes

Abstract In the past few years a growing amount of space observations focusing on atmospheric composition has become available and this trend will continue with the launch of new satellites (ESA-Sentinels, NASA-TEMPO and JAXA air quality and climate mission) in the near future. To justify the production and launch of these expensive instruments, there is a need for determining the added value of future satellite instruments and their optimal design in an objective way. One methodology that can do so is the OSSE (Observing System Simulation Experiment). Although extensively used in the meteorological community, it's use in the field of air quality and climate is still limited and a common approach is desirable. Based on existing studies and experience in the meteorological community we have identified requirements for each of the OSSE elements for

R. Timmermans (✉) · P. Builtjes
Department of Climate, Air and Sustainability, TNO, Princetonlaan 6, 3584 CB Utrecht, The Netherlands
e-mail: renske.timmermans@tno.nl

W. Lahoz
Norwegian Institute for Air Research (NILU), Instituttveien 18, 2027 Kjeller, Norway

J.-L. Attié
University of Toulouse, LA UMR 5560 and
CNRM-GAME, URA1357, CNRS—Météo-France, Toulouse, France

V.-H. Peuch
ECMWF, Shinfield Park, Reading, Berkshire RG2 9AX, UK

D. Edwards
National Center for Atmospheric Research (NCAR), P.O. Box 3000, Boulder CO 80307-3000, USA

H. Eskes
Royal Netherlands Meteorological Institute (KNMI), P.O. Box 201, 3730 AE De Bilt, The Netherlands

P. Builtjes
Free University Berlin (FUB), Carl-Heinrich-Becker-Weg 6-10, 12165 Berlin, Germany

D.G. Steyn and N. Chaumerliac (eds.), *Air Pollution Modeling and its Application XXIV*, Springer Proceedings in Complexity,
DOI 10.1007/978-3-319-24478-5_94

performing a realistic OSSE. Using illustrative examples from existing air quality OSSEs we will present the methodology and the requirements for the application of OSSEs to satellite observations of atmospheric composition.

94.1 Introduction

In the past few years a growing amount of space observations focusing on atmospheric composition has become available and this trend will continue with the launch of new satellites (ESA-Sentinels, NASA-TEMPO and JAXA air quality and climate mission) (Lahoz 2010; Chance et al. 2013; Akimoto et al. 2008) in the near future. To justify the production and launch of these expensive instruments, there is a need for determining the added value of future satellite instruments and their optimal design in an objective way. One methodology that can do so is the OSSE (Observing System Simulation Experiment). Although extensively used in the meteorological community, it's use in the field of air quality and climate is still limited and a common approach is desirable.

The OSSE technique was first used for air quality applications in 2009. Timmermans et al. (2009) showed the added value of aerosol optical depth observations from a proposed instrument on analyses and forecasts of particulate matter (PM), and Edwards et al. (2009) investigated the impact of CO observations from a geostationary satellite in the lowermost troposphere. Since then several research teams have developed OSSEs for investigating the value of future satellite observations of ozone, NO_2, CO, CO_2 and aerosols (i.e., particulate matter) (e.g. Claeyman et al. 2011; Yumimoto 2013; Zoogman et al. 2014). These studies show that OSSEs are a powerful tool for determining the value of future observations and for defining requirements for specific instruments. However, a common approach is desired to make sure the OSSEs provide useful and realistic results.

In this study we shortly describe the OSSE methodology and using illustrative examples from existing air quality OSSEs we will present the requirements for the application of OSSEs to satellite observations of atmospheric composition.

94.2 The OSSE Method

OSSEs are experiments used to determine the potential impact of future observing systems in an existing monitoring or forecasting system. Figure 94.1 shows a schematic of the OSSE method. Observations from the future observing system are simulated through a nature run (NR), which is intended to simulate the true state of the atmosphere, and an observation simulator, which takes into account the instrument description, observing strategy, retrieval algorithm, error characteristics and presence of clouds. The simulated observations are subsequently assimilated

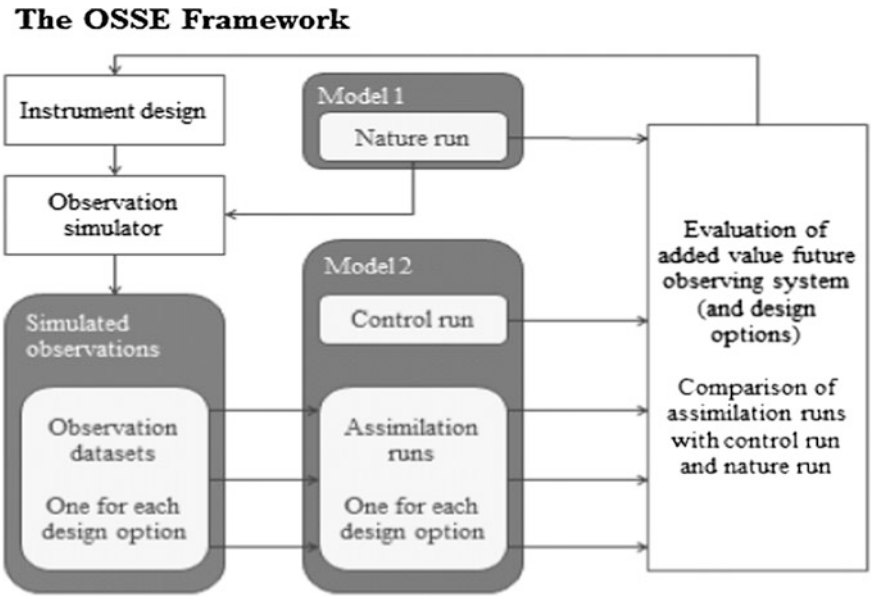

Fig. 94.1 Schematic of OSSE framework

into another model and the impact of the observations is evaluated through comparison with a control run (CR) and the NR.

Figure 94.2 shows an illustrative example of a recent OSSE. In this OSSE the value of two different small instrument designs (A and B) observing NO_2 on the

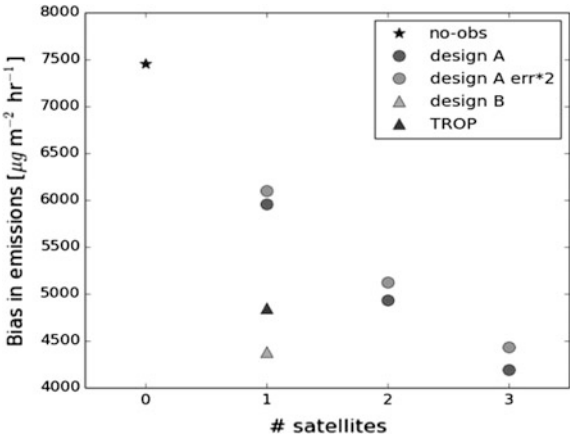

Fig. 94.2 Relative bias in NO_2 emission estimates for a region with persistent bias as function of the number of instruments assimilated in the model, three small instruments of design A are required to achieve a similar impact as a regular sized instrument (TROP) or a single design B instrument

emission estimates of NOx is evaluated compared to the value of a regular sized instrument (TROP). It nicely shows the potential of the OSSE method in identifying optimal instrument design for a specified application.

94.3 OSSE Requirements

Based on existing studies and experience in the meteorological community we have identified requirements for each of the OSSE elements for performing a realistic OSSE. These requirements are the following: (1) a realistic nature run to simulate the true state of the atmosphere; (2) an observation simulator including full instrument description, full radiative transfer models or scene-dependent averaging kernels, cloud information, product retrieval scheme, and realistic error and error correlation estimates; (3) a well-established data assimilation model different from the nature run model; (4) model independent results; (5) a calibration run; and (6) a dedicated quantitative evaluation focusing on the driving science questions, and including statistical significance of the results. More details can be found in the recently published paper Timmermans et al. (2015).

Question and Answer

Questioner: F. Lenartz

Question: Do you transform your data to make them Gaussian? If yes what is the impact of the distribution?

Answer: We do not transform the data itself to a Gaussian distribution but we do add noise with a Gaussian distribution to simulate instrument and other random errors.

References

Akimoto H, Kasai Y, Kita K (eds) (2008) Planning a geostationary atmospheric observation satellite, National Institute of Information and Communications Technology

Chance K, Liu X, Suleiman RM, Flittner DE, Al-Saadi J, Janz SJ (2013) Tropospheric emissions: monitoring of pollution (TEMPO). In: Proceedings of SPIE 8866, earth observing systems XVIII, doi:10.1117/12.2024479

Claeyman M, Attié J-L, Peuch V-H, El Amraoui L, Lahoz WA, Josse B, Joly M, Barré J, Ricaud P, Massart S, Piacentini A, von Clarmann T, Höpfner M, Orphal J, Flaud J-M, Edwards DP (2011) A thermal infrared instrument on board a geostationary platform for CO and O_3 measurements in the lowermost troposphere: observing system simulation experiments (OSSE). Atmos Meas Tech 4:1637–1661. doi:10.5194/amt-4-1637-2011

Edwards DP, Arellano AF Jr, Deeter MN (2009) A satellite observation system simulation experiment for carbon monoxide in the lowermost troposphere. J Geophys Res 114:D14304. doi:10.1029/2008JD011375

Lahoz WA (2010) Data assimilation, making sense of observations. In: Lahoz W, Khattatov B, Ménard R (eds) (2010) Springer

Timmermans RMA, Segers AJ, Builtjes PJH, Vautard R, Siddans R, Elbern H, Tjemkes SAT, Schaap M (2009) The added value of a proposed satellite imager for ground level particulate matter analyses and forecasts. IEEE-JSTARS (J Sel Top Appl Earth Obs Remote Sens), pp 271–283. doi: 10.1109/JSTARS.2009.2034613

Timmermans RMA, Lahoz WA, Attié J-L, Peuch V-H, Curier RL, Edwards DP, Eskes HJ, Builtjes PJH (2015) Observing system simulation experiments for air quality. Atmos Environ. doi:10.1016/j.atmosenv.2015.05.032

Yumimoto K (2013) Impacts of geostationary satellite measurements on CO forecasting: an observing system simulation experiment with GEOS-Chem/LETKF data assimilation system. Atmos Environ 74:123–133. doi:10.1016/j.atmosenv.2013.03.032

Zoogman P, Jacob DJ, Chance K, Worden HM, Edwards DP, Zhang L (2014) Improved monitoring of surface ozone by joint assimilation of geostationary satellite observations of ozone and CO. Atmos Env 84:254–261. doi:10.1016/j.atmosenv.2013.11.048

Chapter 95
Estimation of Anthropogenic CO_2 Emission from Ozone Monitoring Instrument Tropospheric NO_2 Columns Using Chemistry Transport Modelling Over North Western Europe

R.L. Curier, R. Kranenburg, M. Jozwicka, R. Timmermans and H. Denier van der Gon

Abstract This pilot study focusing on Rotterdam and Paris investigates innovative means to use earth observation data as additional constraints to estimate anthropogenic city-scale CO_2 fluxes. NO_2 tropospheric column from OMI is used as a proxy. The LOTOS-EUROS chemistry transport model equipped with a source apportionment module was used to track and label the origin of NO_2 at OMI overpass. Next, this information is combined with source specific reported anthropogenic NO_2/CO_2 ratio to derive co-emitted CO_2 per source sector. In this paper, preliminary results are presented and the added value of the use of remote sensing data and regional air quality models to infer information on anthropogenic emissions is discussed.

95.1 Introduction

Despite the Kyoto Protocol, global CO_2 emissions are continuously growing at a pace of 2–3 % per year, reaching a level in 2013 that is 60 % above emissions in 1990. The current European legislation aims at an emission reduction target of 20–30 % by the year 2020 compared to 1990 (the "20-20-20" targets introduced in the EU 2020 climate and energy package). Countries report their annual CO_2 emissions based on (energy) statistics which include fossil fuel consumptions and fuel types by activity. However, statistics may be incomplete, uncertain or less reliable in some parts of the world. High resolution anthropogenic CO_2 fluxes cannot yet be detected by earth observation, however this information is available for NO_2.

R.L. Curier (✉) · R. Kranenburg · M. Jozwicka · R. Timmermans · H.D. van der Gon
Department of Climate, Air and Sustainability, TNO, Utrecht, The Netherlands
e-mail: lyana.curier@tno.nl

D.G. Steyn and N. Chaumerliac (eds.), *Air Pollution Modeling and its Application XXIV*, Springer Proceedings in Complexity,
DOI 10.1007/978-3-319-24478-5_95

Combustion processes in the transport, industry, and energy sectors are important sources for both CO_2 and NOx which are co-emitted in source and technology-specific ratios. We investigate the use of satellite observations and chemistry transport modelling equipped with a source apportionment module (Kranenburg et al. 2012) to invert anthropogenic CO_2 emissions from the Ozone Monitoring Instrument (OMI, Levelt et al. 2006) NO_2 observations. Ultimately, this pilot could contribute to a routinely monitoring of anthropogenic CO_2 emissions at a regional to global scale.

95.2 Methodology

The LOTOS-EUROS chemistry transport modelling of NO_2 by source sector was combined with satellite observations to track and label the origin of NO_2 in the OMI NO_2 columns. Next, this information is used to derive co-emitted CO_2 by source sector. The anthropogenic CO_2 contribution to the total CO_2 emission is low and the validation of this exercise remains quite difficult. Therefore, we combine, on one hand, the contribution of each source sector to the NO_2 OMI VCD is retrieved by means of LOTOS-EUROS (Schaap et al. 2008) and its source apportionment module which tracks the contribution of specified sources through the whole simulation. This means that for all oxidized nitrogen components at every time step and each grid cell the origin is tracked through each process. Here, the emissions were categorized per source sector and hour of emission to account for the short life time of NOx in the atmosphere and the large temporal variability in emission strengths for the different source sectors. In this study, a LOTOS-EUROS run was performed for 2011 over Europe using TNO MACC-II emission (Kuenen et al. 2011) and TNO bottom-up CO_2 emission inventories and we follow power generation, industrial combustion, road transport, other transports, agriculture, and "other" which are the remaining sectors. And on the other hand, the analysis of an high resolution emission dataset over the Rotterdam Rijnmond area highlighted that the NOx/CO_2 anthropogenic emission ratio for each source sector can be represented by a single mean value. This mean value is then used to extract the equivalent antoropogenic CO_2 concentrations from the OMI NO_2 observations.

95.3 Preliminary Results

This section succintly presents preliminary results of this pilot study. First, the OMI NO_2 column sensitivity to source sector is evaluated then the anthropogenic CO_2 extracted from OMI NO_2 observations.

1. **Assessment of OMI NO_2 column sensitivity to source sector contribution**. Figure 95.1 presents the modeled contribution per source sector and hour of

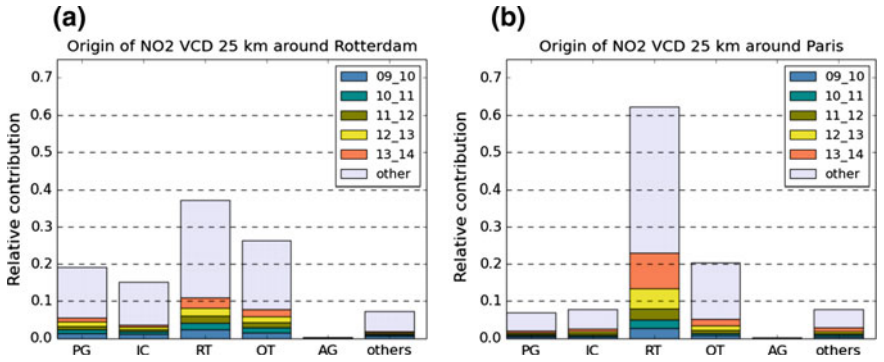

Fig. 95.1 Contribution of various source sectors as function of the time of emission to the total anthropogenic NOx emission at OMI overpass for Paris (*left*) and Rotterdam(*right*). *PG* Power Generation, *IC* Industrial Combustion, *RT* Road Transport, *OT* Other Transports, *A* Agriculture, *O* Other sectors

emission over the Paris (left) and Rotterdam (right) regions at OMI overpass time (i.e. 1.30 pm local time). It can be seen that at overpass time 90 % of the NO_2 concentrations observed by OMI can be attributed to combustion processes occurring in road transport, other transport, power plants and industry. However, the contribution is more or less evenly distributed over these source sectors while in Paris the signal is mainly dominated by contribution from road transport (over 60 %). At both locations, about 30 % of the modeled OMI signal results from NOx emissions in the three hours prior to OMI overpass.

2. **Anthropogenic CO_2 concentration per source sector**. Figure 95.2 is a boxplot representation of the anthropogenic CO_2 concentration in a 25 km radius around Paris and Rotterdam for the main source sectors for the year 2011 at OMI overpass. At first glance, it can be seen that the total anthropogenic CO_2

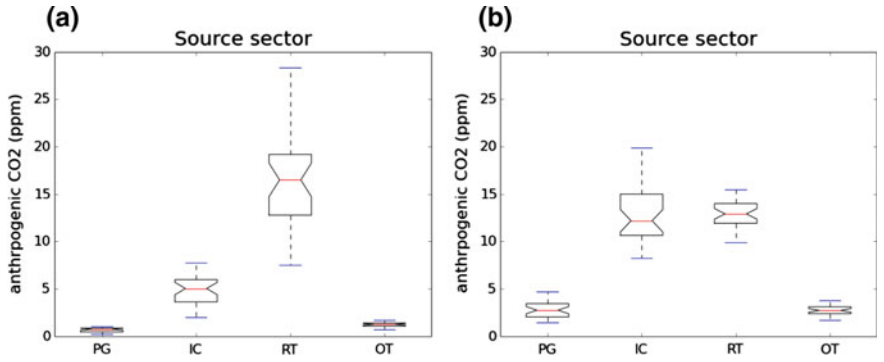

Fig. 95.2 Statistic representation of the anthropogenic CO_2 concentration over Paris and Rotterdam for the main source sectors. *PG* Power Generation, *IC* Industrial Combustion, *RT* Road Transport, *OT* Other Transports

concentrations retrieved are in agreement with the literature estimates (i.e. 6 % of ambient CO_2 is of anthropogenic origin.) These boxplots allow us to have a visual assessment of the anthropogenic CO_2 concentrations around Paris and Rotterdam. We observe that when it comes to power generation and other transport there is almost no dispersion for both Paris and Rotterdam. While, in the case of Paris, the boxplot and whisker highlight large dispersion for CO_2 concentrations from the road transport sector with a skewness toward the lower values. Around Rotterdam, it appears that the major source of CO_2 at OMI overpass are road transport and industrial combustion.

95.4 Outlook

This study is a first attempt to estimate the anthropogenic contribution to the ambient CO_2 in Paris and Rotterdam. The study of anthropogenic emission by analyzing observations of co-emitted species is not new (Brioud et al. 2013). However, here we create a more detailed product by relating the CO_2 to NOx which are co-emitted in source and technology-specific ratios. This method presents two main innovative aspects: 1. Exploitation of OMI observations and ground observations to characterize the anthropogenic CO_2 emission across Europe. 2. Exploitation of a chemistry transport model which can discriminate between source sectors contribution and reported emisison to characterize the NOx/CO_2 ratio across Europe. The source apportionement study suggest that observations of boundary layer NO_2 contain significant information to enable the estimate of anthropogenic CO_2 emissions. This study initially focuses for application across Europe as proof of principle Hence, it would be beneficial to perform re-evaluation of state-of-the-art knowledge and to identify opportunities for other domains of interest, in a possibly less data rich environment. Given the demand for city CO_2 budgets by large cities in growing economies where no good bottom-up estimate is available, satellite based estimates may provide a very useful starting point for mitigation.

References

Brioude J, Angevine WM, Ahmadov R, Kim SW, Evan S, McKeen SA, Hsie EY, Frost GJ, Neuman JA, Pollack IB, Peischl J, Ryerson TB, Holloway J, Brown SS, Nowak JB, Roberts JM, Wofsy SC, Santoni GW, Oda T, Trainer M (2013) Top-down estimate of surface flux in the los angeles basin using a mesoscale inverse modeling technique: assessing anthropogenic emissions of co, no_x and co_2 and their impacts. Atmos Chem Phys 13: 3661–3677

Kranenburg R, Hendriks C, Schaap M, Segers A (2012) Source apportionment using lotos-euros: module description and evaluation. Geosci Model Dev Discuss 5:3957–3991

Kuenen J, van der Gon HD, Visschedijk A, van der Brugh H, van Gijlswijk R (2011) MACC European emission inventory for the years 2003–2007. Technical report TNO-060-UT-2011-00588, TNO, Utrecht, The Netherlands

Levelt PF, Van Den Oord GHJ, Dobber M, Eskes H, Van Weele M, Veefkind P, Van Oss R, Aben I, Jongma RT, Landgraf J, De Vries J, Visser H (2006) Tropomi and tropi: Uv/vis/nir/swir instruments. In: Proceedings of SPIE. The International Society for Optical Engineering

Schaap M, Timmermans RMA, Roemer M, Boersen GAC, Builtjes PJH, Sauter FJ, Velders GJM, Beck JP (2008) The Lotos-Euros model: description, validation and latest developments. Int J Environ Pollut 32:270–290

Chapter 96
Update on NOAA's Operational Air Quality Predictions

Ivanka Stajner, Pius Lee, Jeffery McQueen, Roland Draxler, Phil Dickerson and Sikchya Upadhayay

Abstract NOAA provides operational predictions of ozone and wildfire smoke for the United States (U.S.) and predictions of airborne dust over the contiguous 48 states. Predictions are produced beyond midnight of the following day at 12 km spatial and hourly temporal resolution and are available at http://airquality.weather.gov/. Ozone predictions and testing of fine particulate matter ($PM_{2.5}$) predictions combine the NOAA National Centers for Environmental Prediction (NCEP) operational North American Mesoscale (NAM) weather predictions with inventory based emission estimates from the EPA and chemical processes within the Community Multiscale Air Quality (CMAQ) model. Predictions of smoke and dust from dust storms use the Hybrid Single Particle Lagrangian Integrated Trajectory (HYSPLIT) model. Verification of ozone and developmental aerosol predictions relies on AIRNow compilation of observations from surface monitors. Verification of smoke and dust predictions uses satellite retrievals of smoke and dust.

Ozone prediction accuracy is maintained in recent years, while pollution sources are changing, through updates in emission source estimates and updates in the model configuration. Emissions for operational ozone predictions were updated using EPA projections of mobile sources for 2012. Trends in NO_x from satellite and ground observations show a good agreement with emission updates over large U.S. cities. Updated CMAQ model with CB05 mechanism and AERO4 aerosol module was implemented for operational ozone prediction in January 2015. Updates include monthly varying lateral boundary conditions, modified dry deposition, constraints on minimum planetary boundary height, and changes to the lifetime of organic nitrate. Testing of $PM_{2.5}$ predictions from the same system modulates soil emissions by snow and ice cover, and includes emissions of windblown dust and particles emitted from forest fires. Further development of $PM_{2.5}$ predictions will

I. Stajner (✉) · P. Lee · J. McQueen · R. Draxler · S. Upadhayay
National Oceanic and Atmospheric Administration (NOAA), Washington, USA
e-mail: ivanka.stajner@noaa.gov

P. Dickerson
Environmental Protection Agency (EPA), Washington, USA

S. Upadhayay
Syneren Technologies Corporation, Arlington, USA

D.G. Steyn and N. Chaumerliac (eds.), *Air Pollution Modeling and its Application XXIV*, Springer Proceedings in Complexity,
DOI 10.1007/978-3-319-24478-5_96

explore bias correction approaches. Longer-term plans include comprehensive linkages between NAQFC predictions for the U.S. and global atmospheric composition predictions, as resources allow.

96.1 Introduction

The National Air Quality Forecasting Capability (NAQFC) has been providing operational air quality predictions for the United States (U.S.) since 2004 over expanding domains (Stajner et al. 2012). Current operational NAQFC predictions include: predictions of ozone and wildfire smoke nationwide and predictions of airborne dust from dust storms over the contiguous 48 states. These predictions are produced beyond midnight of the following day at 12 km resolution and hourly time intervals. They are distributed as maps and numerical values of predicted pollutant concentrations at http://airquality.weather.gov/.

96.2 Updates to Air Quality Predictions

NAQFC ozone predictions combine the National Oceanic and Atmospheric Administration (NOAA) National Centers for Environmental Prediction (NCEP) operational North American Mesoscale (NAM) weather predictions with inventory based emissions estimates from the U.S. Environmental Protection Agency (EPA) and chemical processes within the Community Multiscale Air Quality (CMAQ) model. Routine verification of ozone predictions relies on AIRNow compilation of observations from surface monitors. The ozone prediction system has evolved from that described by Otte et al. (2005) to use the latest operational weather model, updated emissions data, and an updated chemical mechanism (CB05).

Gaseous and particulate emissions from anthropogenic area, mobile and point sources as well as natural biogenic, sea-salt, wildfire smoke and dust emissions are used as inputs for NAQFC ozone predictions and developmental testing of fine particulate matter ($PM_{2.5}$) predictions. The EPA 2005 National Emission Inventory version 1 (NEI05v1) is used for U.S. sources, the 1999 Mexico National Emissions Inventories for Mexico, and the 2006 Environment Canada (EC) Emission Inventories for Canada. Emission data sources and processing methods for NAQFC ozone predictions have been updated since June 1, 2012. Four major updates for the emission estimates include: (1) an update of on-road emissions using a projection from 2005 to 2012; (2) an update of off-road area source emissions with a projection from 2005 to 2012; (3) a yearly update for point source emissions using measurements and energy projection for sulfur dioxide (SO_2) and nitrogen oxides (NO_x); and (4) an update of all Canadian emissions using the 2006 EC emission

inventory. A comparison of changes in NO_x emissions used by (NAQFC), and those observed by U.S. EPA's ground-based Air Quality System network, and NASA's Ozone Monitoring Instrument over large U.S cities from 2005 to 2012 all show decreases in over that period, albeit smaller for emissions used by NAQFC than for observed data (Tong et al. 2015). Performance of ozone and NO_2 predictions improved following 2012 emissions update (Pan et al. 2014).

A version of Carbon Bond Mechanism (CB05) in CMAQ was in experimental testing for several years and became operational for ozone predictions on January 29th, 2015. Rate constants were updated and reactions that characterize conditions ranging from urban to remote troposphere and AER04 configuration for aerosol chemistry were added. Changes most relevant for ozone prediction include reactions that recycle NO_x and radical reactions resulting in faster removal of organic nitrate. High ozone bias in the CB05-based system, which manifested itself most strongly in the southeastern U.S. during summertime (Chai et al. 2013), was reduced concurrently with reduction in NO_2 bias (Fig. 96.1a), with 2012 emissions update and the following 2011 model updates. The aerodynamic resistance term in the dry deposition velocity calculation was modified based on Monin-Obukhov

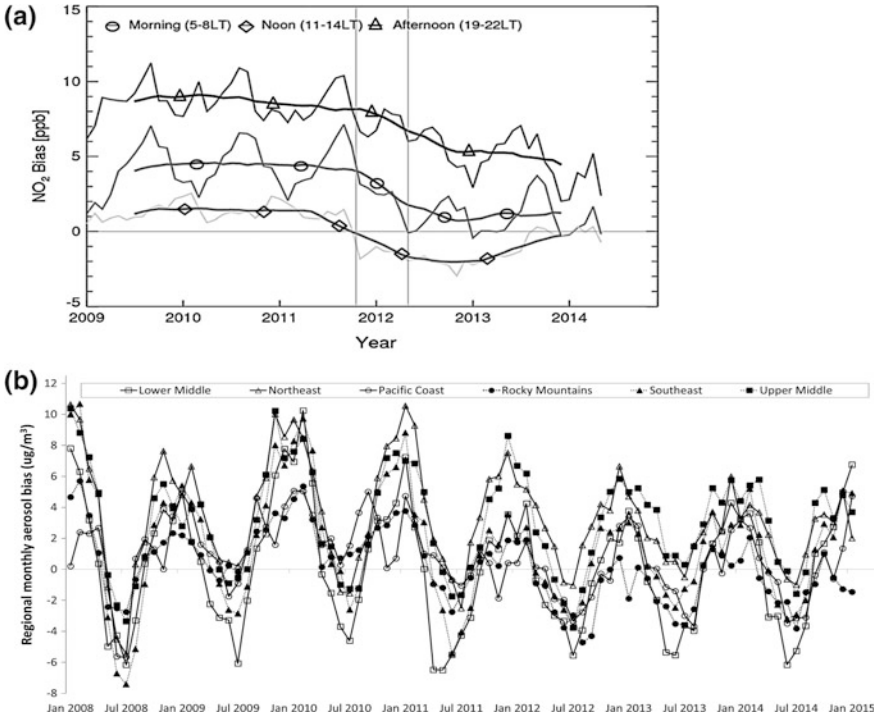

Fig. 96.1 **a** NO_2 bias by time of the day in the experimental ozone model (Kim et al. 2014). Vertical lines indicate time of model update in 2011 and emission update in 2012. **b** Average monthly bias by U.S. region for developmental $PM_{2.5}$ predictions

similarity theory (based on CMAQ version 4.7). Satellite derived canopy height and density were included. Tree canopy height was scaled to roughness length in computation of dry deposition velocities. A minimum PBL height of 50 m avoids total suppression of vertical diffusive mixing (Huang et al. 2012). Monthly-varying lateral boundary conditions for 36 gaseous and aerosol species from the GEOS-Chem global chemical model simulation for year 2006 are included below 7 km altitude (Tang et al. 2008; Bey et al. 2001).

Developmental testing of $PM_{2.5}$ predictions was improved by including particulate emissions from wildfires, dust from dust storms, and suppression of soil emissions when terrain is covered by ice or snow. Testing of $PM_{2.5}$ predictions shows seasonal biases (Fig. 96.1b, Stajner et al. 2012). The unspeciated $PM_{2.5}$ category, which includes soil aerosols contributed to the high bias in wintertime. Low bias for secondary organic aerosols (SOA) in the summer may be reduced by incorporating a more recent CMAQ version with parameterized SOA processes. An algorithm for post-processing of $PM_{2.5}$ predictions to remove bias using AirNow $PM_{2.5}$ observations by Djalalova et al. (2015) is being tested for use in real-time $PM_{2.5}$ predictions. Linkage of NAQFC predictions with the global aerosol model predictions through lateral boundary conditions to account for aerosol transport from external sources is being tested.

Predictions of wildfire smoke and dust from dust storms using HYSPLIT model had only minor scientific updates recently, except for a switch to an automated detection of fires in Canada, Mexico and Central America that provides inputs for smoke emissions since September 30th, 2014.

Questions and Answers

Questioner: Christian Hogrefe
Question: Could you please elaborate on how you implemented the snow-cover based adjustment of primary $PM_{2.5}$ emissions in winter? Which emission sectors are adjusted?

Answer: Snow cover of more than 25 % suppresses dust emissions represented by PMFINE (fine mode non-speciated particles) and PMC (coarse mode non-speciated particles) emissions. These emission species are allocated into A25 J and ASOIL in the CMAQ model. The suppression of emissions is applied to all sectors that emit fugitive dust. The major sector is anthropogenic fugitive dust emissions (afdust), which includes five source categories: paved road, unpaved road dust, quarrying/mining, agricultural operations and construction (*Daniel Tong, personal communication*).

Questioner: Paul Makar
Question: Have you looked at the spatial distribution of the $PM_{2.5}$ bias correction and what sort of issues with $PM_{2.5}$ does it identify?

Answer: Testing and evaluation of $PM_{2.5}$ bias correction is ongoing. Preliminary results indicate domain-wide a reduction in both bias and root-mean-square error and an increase in correlation with observations as a function of the forecast hour. Evaluations of the spatial distribution of the bias correction and of day-to-day variability of bias corrected predictions are ongoing.

References

Bey I, Jacob DJ, Yantosca RM et al (2001) Global modeling of tropospheric chemistry with assimilated meteorology: model description and evaluation. J Geophys Res 106(D19):23073–23095

Chai T, Kim HC, Lee P et al (2013) Evaluation of the United States National Air Quality Forecast Capability experimental real-time predictions in 2010 using Air Quality System ozone and NO2 measurements. Geosci Model Dev 6(5):1831–1850

Djalalova I, Delle Monache L, Wilczak J (2015) PM2.5 analog forecast and Kalman filter postprocessing for the Community Multiscale Air Quality (CMAQ) model. Atmos Environ. doi:10.1016/j.atmosenv.2015.02.021

Huang J, McQueen J, Tang Y et al (2012) Improving air quality forecasting over Lakes and surrounding regions. Presented at 92nd AMS annual meeting, New Orleans, 26 Jan 2012

Kim HC, Lee P, Pan L et al (2014) Comprehensive comparisons of NAQFC surface and column NO2 with satellites, surface, and field campaign measurements during 2009–2014. Presented at 2014 CMAS conference on October 29, 2014

Otte TL, Pouliot G, Pleim JE et al (2005) Linking the Eta Model with the Community Multiscale Air Quality (CMAQ) modeling system to build a national air quality forecasting system. Weather Forecast 20:367–384

Pan L, Tong D, Lee P et al (2014) Assessment of NOx and Ozone forecasting performance in the US NAQFC before and after the 2012 major emissions updates. Atmos Environ 95:610–619

Stajner I, Davidson P, Byun D et al (2012) National air quality forecast capability: expanding coverage to include particulate matter. In: Steyn DG, Castelli ST (eds) NATO/ITM air pollution modeling and its application XXI. Springer, Netherlands, pp 379–384. doi:10.1007/978-94-007-1359-8_64

Tang Y, Lee P, Tsidulko M et al (2008) The impact of lateral boundary conditions on CMAQ predictions over the continental US: a sensitivity study compared to ozonesonde data. Environ Fluid Mech 9:43–58. doi:10.1007/s10652-008-9092-5

Tong DQ, Lamsal L, Pan L et al (2015) Long-term NOx trends over large cities in the United States during the 2008 Recession: intercomparison of satellite retrievals, ground observations, and emission inventories. Atmos Environ. doi:10.1016/j.atmosenv.2015.01.035

Chapter 97
Observing System Simulation Experiments (OSSEs) Using a Regional Air Quality Application for Evaluation

Pius Lee, Robert Atlas, Gregory Carmichael, Youhua Tang, Brad Pierce, Arastoo Pour Biazar, Li Pan, Hyuncheol Kim, Daniel Tong and Weiwei Chen

Abstract Satellite-based and high-altitude airborne remotely sensed air quality data complement land-based and routinely commercial-flight and other measurement-campaign acquired remotely sensed and in situ observations. It is important to optimize the combination and placement of these wide ranges of measurements and data acquisition options for cost-effectiveness. Under this initiative we attempt to quantify the gain by a regional state-of-the-science chemical data assimilation and chemical transport modeling system when incremental sets of observation are acquired into the system. This study represents a first step in a series

P. Lee (✉) · Y. Tang · L. Pan · H. Kim · D. Tong · W. Chen
Air Resources Laboratory (ARL), NOAA, College Park, MD, USA
e-mail: pius.lee@noaa.gov

R. Atlas
Atlantic Oceanographic and Meteorological Laboratory, NOAA, Miami, FL, USA

G. Carmichael
Department of Chemical and Biochemical Engineering, University of Iowa, Iowa City, IA, USA

Y. Tang · L. Pan · H. Kim · D. Tong
Cooperative Institutes for Satellite and Climate, University of Maryland, College Park, MD, USA

B. Pierce
National Environmental Satellite and Information Service (NESDIS), Madison, WI, USA

A.P. Biazar
Department of Atmospheric Science, University Alabama, Huntsville, AL, USA

D. Tong
Center for Spatial Information Science and Systems, George Mason University, Fairfax, VA, USA

W. Chen
Northeast Institute of Geography and Agroecology, Chinese Academy of Sciences, Changchun, China

D.G. Steyn and N. Chaumerliac (eds.), *Air Pollution Modeling and its Application XXIV*, Springer Proceedings in Complexity,
DOI 10.1007/978-3-319-24478-5_97

of steps to ingest such proposed incremental additions of observation. The efficacy of such proposals is quantified systematically by Observation Simulation System Experiments (OSSEs). We compared two end-to-end regional air quality forecasting simulations using: (a) the Weather Forecasting and Research (WRF) regional application initialized by the U.S. national Weather Service (NWS) Global Forecasting System (GFS) coupled with the U.S. Environmental Protection Agency Community Multi-scale Air Quality (CMAQ) chemical model (Byun and Schere 2006), and (b) the same as above but with a new GFS enhanced by assimilating a fictitious addition of Atmospheric Infrared Sounder (AIRS) retrieved radiances at 13 km spatial resolution at nadir from a proposed geostationary satellite positioned over 75°W staring over the U.S. Both sensitivity runs were performed in 12 km horizontal grid resolution and with daily initialization for 12 days between July 29 and August 9 2005. Noticeable forecast skill improvement in surface concentration for O_3 and particulate matter smaller than 2.5 μm in diameter ($PM_{2.5}$) was achieved.

97.1 Introduction

Observing System Simulation Experiments (OSSEs) are an important tool for evaluating the potential impact of proposed new observing systems, as well as for evaluating trade-offs in observing system design, and in developing and in assessing improved methodology for assimilating new observations. Between NOAA and its partners, application of OSSEs determined correctly the quantitative potential for several proposed satellite observing systems to improve weather analysis and prediction prior to their launch, evaluated trade-offs in orbits, coverage and accuracy for space-based winds LIDARS, and were used in the development of a methodology that led to the first beneficial impacts of satellite surface winds on numerical weather prediction (Atlas 1997).

In this study we attempted to apply OSSEs to air quality (AQ) modeling. In this attempt we did not propose an instrument for chemical constituent detection or measurement targeting the chemical composition of the lower troposphere—though its efficacy is likely the greatest as alluded in an extraneous study mentioned in Sect. 97.4. Nonetheless, in this work we used an additional set of meteorological observations to benefit AQ modeling indirectly. Space-based and high-altitude airborne meteorological measurements offer an effective way to supplement the conventional observations. The trend in observation acquisition system is to rely more on remote sensing from high altitude or space due to the data demand for finer resolution in space and time, large number of constituents, and large geographical coverages. The inventory-type "bottom-up" approach using book-keeping surveys is prohibitively costly. This situation is obviously more applicable to AQ scenarios as emission and land-use changes can happen rather quicker than decadal scales. NOAA launched a multiple line office Quantitative Observing System Assessment Program (QOSAP) to estimate the returns of investment in various proposed change

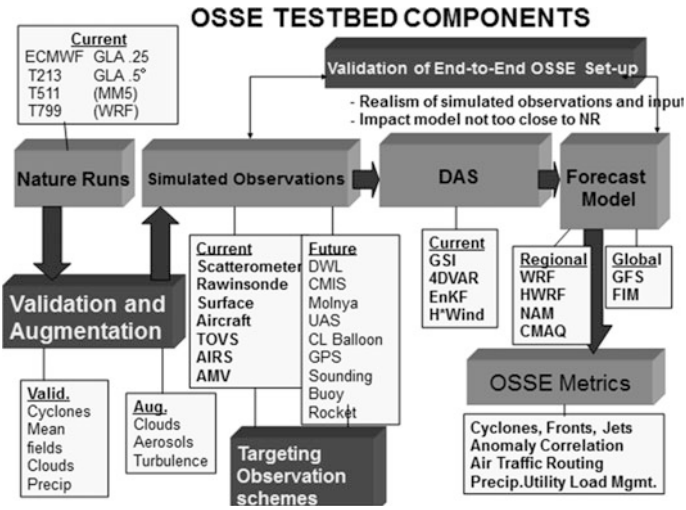

Fig. 97.1 QOSAP with CMAQ as a forecast model

or addition to the weather observation systems which NOAA is using or may begin to use. This study represents an air quality component of QOSAP. Figure 97.1 shows one configuration of the series of OSSEs that maybe involved in the QOSAP. It depicts nature runs accompanied by verifiable targeted fields where robust observation is or will be augmented for availability. It shows observations that straddle both present and future. The right column boxes encapsulate the impact quantification in various measures and in terms of benefits in its down-stream applications (Fig. 97.1).

It is note that CMAQ is placed under the category for regional forecasting models (Fig. 97.1). This study demonstrates an OSSE air quality (AQ) application. It involves CMAQ to be benefited through data assimilation to ingest wind vector and moisture data by a fictitious future geostationary satellite to be situated over North America. The outcome of this OSSE will be the quantification of the efficacy of such proposed observations helping to capture the AQ phenomenon more correctly in terms of metrics customarily used in AQ sciences.

97.2 Air Quality Forecasting as an OSSE Evaluator

Had there been an AIRS instrument from space with a constant stare over Conterminous U.S. (CONUS), the continuity and sheer volume of the data would have been valuable for constraining wind, latent and sensible heat fluxes in meteorological simulations. Its large swath of observation strengthens fidelity for global meteorological models. We chose to place this futuristic satellite equipped with AIRS retrieved radiances with 2378 channels spanning 3.7–15.4 μm in wavelengths

at 13 km spatial resolution at nadir from a proposed geostationary satellite positioned over 75°W (dubbed GOES_G13). We compared two end-to-end regional air quality (AQ) forecasting simulations using: (a) the WRF regional application initialized by the U.S. NWS GFS coupled with the CMAQ chemical transport model; and (b) the same as (a) but with GOES_G13 data feeding GFS. CMAQ simulations are in 12 km grid spacing with daily initialization for 12 days between July 29 and August 9 2005.

97.3 Configuration of the Evaluator

The air quality forecasting down-stream user of the OSSE described by the sensitivity cases in Sect. 97.2 is comprised of an off-line coupled WRF and CMAQ modeling system. Tables 97.1 and 97.2 show the parameterization packages selected for WRF and CMAQ, respectively.

97.4 Results and Summary

Observing System Simulation Experiments (OSSEs) is increasingly recognized as a powerful tool to quantify the benefits of reconstructing or forecasting the state of the atmosphere with measurable accuracy improvement metrics when new observation systems are proposed. In Sects. 97.2 and 97.3 we performed such quantification for proposing to add a hyperspectral AIRS instrument onboard a geostationary satellite over 75°W with nadir resolution at 13 km staring over CONUS. The data catapulted NWS GFS to reduce the RMSE for its 500 hPa geopotential height significantly within 95 % confidence levels as shown in Fig. 97.2. This benefit is funneled 3 tiers downstream to CMAQ, a NWS regional air quality forecasting model: (1) GFS provides initialization and boundary condition for WRF regional simulation,

Table 97.1 WRF physics selections

WRF-ARW	North America in 12 km horizontal grid spacing
Map projection and grid staggering	Lambert conformal & Arakawa C staggering
Vertical coordinate	42 σ-p unevenly spaced levels
Advection	RK3 (Skamarock and Weisman 2009)
Short and long wave radiation	RRTMG (Lacono et al. 2008)
PBL Physics	Mellor-Yamada-Janjic level 2.5 closure
Surface layer scheme	Monin-Obukhov Similarity with viscous sub-layer
Land surface model	NCEP NOAH (Ek et al. 2003)
Cloud microphysics	Thompson et al. (2008)
Cloud convective mixing	Betts-Miller-Janic mass adjustment

Table 97.2 CMAQ physics and chemistry selections

CMAQ4.7.1	Emission as the national forecast (Pan et al. 2014)
Map projection and grid staggering	Lambert conformal conic and Arakawa C grid staggering
Vertical coordinate	42 σ-p unevenly spaced levels
Gas chemistry	CB05 with 156 reactions
Aerosol chemistry	Aero5 with updated evaporation enthalpy values
Anthropogenic emission	US EPA 2005NEI as base year. Mobile sources projection used ground monitor measured trends. Area and non-road sources used US EPA CSPR, point sources uses 2004 CEM data
	WRAP oil and gas data
Biogenic	BEIS-3.14
Lateral chem boundary condition	RAQM (Pierce et al. 2003)

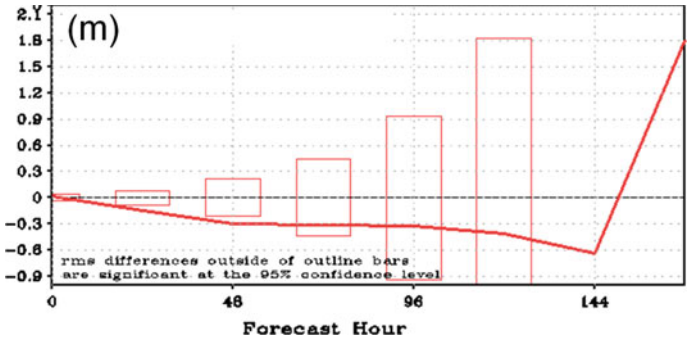

Fig. 97.2 Difference in RMSE between the GFS performances in terms of the predicted 500 hPa geopotential heights between Case (a) base, and (b) with GOES_G13 data. When the difference falls outside the boxes it indicates it is within 95 % confidence

(2) WRF provides meteorological fields to CMAQ, and (3) CMAQ predicts surface level pollutant concentrations. It is anticipated that CMAQ may not see a large impact due to the dumping and averaging intrinsic in the parameterization and numeric iterations in these multiple tiered modeling and data assimilation systems. Figures 97.3 and 97.4 show a overlaid comparison of time series for observed and predicted surface O_3 concentration at hourly intervals over Northeast and Southeastern US, respectively, during the first week of August 2005 between a basic run without the fictitious AIRS instrument and a sensitivity run accounting data from the instrument. There is only numerically a second significant figure impact for all metrics such as for RMSE. However, we also performed studies to ingest air quality related satellite data to quantify RMSE reduction in CMAQ's predicted field such as particulate matter smaller than 2.5 μm in diameter ($PM_{2.5}$). Had one ingested NASA Terra and Aqua Moderate Resolution Imaging Spectrometer aerosol optical depth

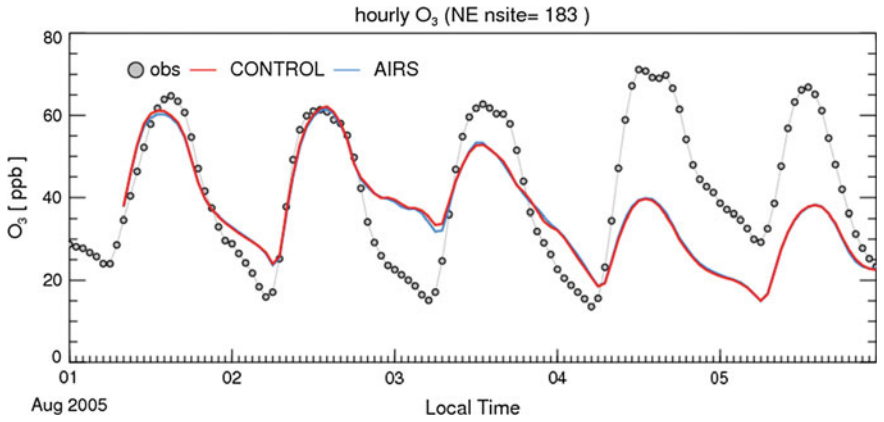

Fig. 97.3 Overlays of predicted surface O3: Case a (*red line*), Case b with GOES_G13 data (*blue line*), and obs by US EPA (*open circle*)

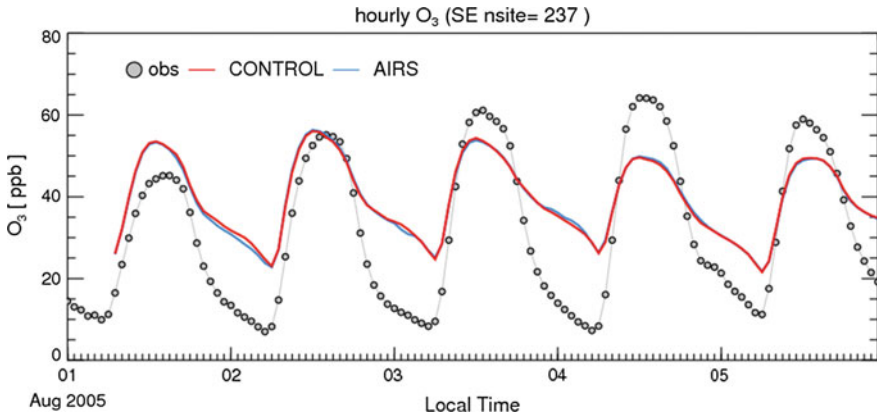

Fig. 97.4 Overlays of predicted surface O3: Case a (*red line*), Case b with GOES_G13 data (*blue line*), and obs by US EPA (*open circle*)

and US EPA surface monitor $PM_{2.5}$. One can gain as much as 500 % reduction in RMSE for prediction for $PM_{2.5}$ (Table 97.3) over a similar season over Eastern US. Therefore it is concluded that OSSEs is indispensable for air quality related observation systems.

Table 97.3 CMAQ's $PM_{2.5}$ prediction in Eastern US in July 2011: (a) no data assimilation (b) data assimilation with satellite AOD

PM2.5 24 h avg	Obs. mean	Mean bias	RMSE	Corr. Coef.
Case (a)	19.8	−0.67	24.18	0.49
Case (b)	19.8	1.15	5.79	0.53

References

Atlas R (1997) Atmospheric observation and experiments to assess their usefulness in data assimilation. J Meteorol Soc Jpn 75:111–130

Byun D, Schere KL (2006) Review of the governing equations, computational algorithms, and other components of the models-3 community Multiscale Air Quality (CMAQ) modeling system. Appl Mech Rev 59:51–77

Ek MB, Mitchell KE, Lin Y, Rogers E, Grunmann P, Koren V, Gayno G, Tarpley JD (2003) Implementation of Noah land surface model advances in the National Centers for Environmental Prediction operational mesoscale Eta model. J Geophys Res 108:8851. doi:10.1029/2002JD003296

Lacono MJ, Delamere JS, Mlawer EJ, Shephard MW, Clough SA, Collins WD (2008) Radiative forcing by long-lived greenhouse gases: Calculations with the AER Radiative transfer models. J Geophys Res 113, D13103 doi:10.1029/2008JD009944

Pan L, Tong DQ, Lee P, Kim H, Chai T (2014) Assessment of NOx and O_3 forecasting performances in the U.S. National Air Quality Forecasting Capability before and after the 2012 major emissions updates. Atmos Environ 95:610–619. doi:10.1016/j.atmosenv.2014.06.020

Skamarock WC, Weisman ML (2009) The impact of positive-de nite moisture transport on NWP precipitation forecasts. Mon Wea Rev 137:488–494

Pierce RB, Al-Saadi JA, Schaack T, Lenzen A, Zapotocny T, Johnson D, Kittaka C, Buker M, Hitchman MH, Tripoli G, Fairlie TD, Olson JR, Natarajan M, Crawford J, Fishman J, Avery MA, Browell EV, Creilson J, Kondo Y, Sandholm ST (2003) Regional Air Quality Modeling System (RAQMS) predictions of the tropospheric ozone budget over east Asia. J Geophys Res 108(D21):8825. doi:10.1029/2002JD003176

Thompson G, Field PR, Rasmussen RM, Hall WD (2008) Explicit Forecasts of winter precipitation using an improved bulk microphysics scheme. Part II: Implementation of a new snow parameterization. Mon Wea Rev 136:5095–5115

Chapter 98
Inverse Modelling of Volcanic SO_2 Emissions Using the 4D-Var Method

Julius Vira and Mikhail Sofiev

Abstract This study compares two approaches for data assimilation in forecasting volcanic plumes of sulphuric dioxide released in the eruption of Grimsvötn in 2011. The first data assimilation approach is source term inversion, where the data are used for estimating an effective source term. In the second approach, the assimilation proceeds in cycles, and the observations are used for updating the initial condition. In both cases, the SO2 retrievals by the OMI instrument are assimilated. The results indicate that the source term inversion is more effective at constraining the three-dimensional structure of the plume. However, as the transport distance increases, updating the initial condition provides a better fit to the column observations.

98.1 Introduction

Quantitative predictions of volcanic plumes are often difficult to obtain due to lack of accurate information of the atmospheric emissions during the eruption (Zehner 2012). While estimates of the total volcanic ash release can sometimes be derived using the observed plume heights, the available parameterisations (e.g. Mastin et al. 2009) are uncertain and must be supplemented with an estimate of the particle size distribution.

The difficulties due to uncertain source term can be mitigated by introducing observations into the simulation. One approach for this is the source term inversion (Eckhardt et al. 2008), where an effective source term is obtained by minimising the discrepancy between the observed and simulated concentrations. A second option is

J. Vira (✉) · M. Sofiev
Finnish Meteorological Institute, Erik Palménin aukio 1, 00560 Helsinki, Finland
e-mail: julius.vira@fmi.fi

D.G. Steyn and N. Chaumerliac (eds.), *Air Pollution Modeling and its Application XXIV*, Springer Proceedings in Complexity,
DOI 10.1007/978-3-319-24478-5_98

to use the observations to determine an initial condition for the subsequent forecast. This can be achieved (Flemming and Inness 2013) by using the methods of data assimilation developed for numerical weather prediction.

98.2 Observations and Model Setup

The observations used in this study are provided by the SO2 product (Yang et al. 2007) of the Ozone Monitoring Instrument (OMI). Based on recommendations of the data provider, the STL (lower stratosphere) version was chosen.

The atmospheric dispersion of SO2 is simulated by the SILAM chemistry-transport model (Sofiev et al. 2015). In addition to 3D advection and diffusion, the model includes removal of SO2 by wet and dry deposition. The gas-phase oxidation by the hydroxyl (OH) radical is included as a first-order process with a prescribed OH concentration.

The impact of data assimilation or source term inversion is studied in a hindcast experiment covering the time from 22 May until 27 May, 2011. In order to evaluate the effect of forecast lead time, the time covered by observations is varied. First, the assimilation is performed using the data for first 24 h. Then, the coverage of observations is extended in increments of 24 h until the end of the hindcast period. The period is thus covered by multiple simulations, each based on a different set of observations. The setup is presented schematically in Fig. 98.1.

For updating the model initial conditions, the observations are assimilated in sequential windows of 24 h. The source term inversions are based on 24, 48 and 72 h; increasing the observation coverage beyond 72 h did not change the results significantly.

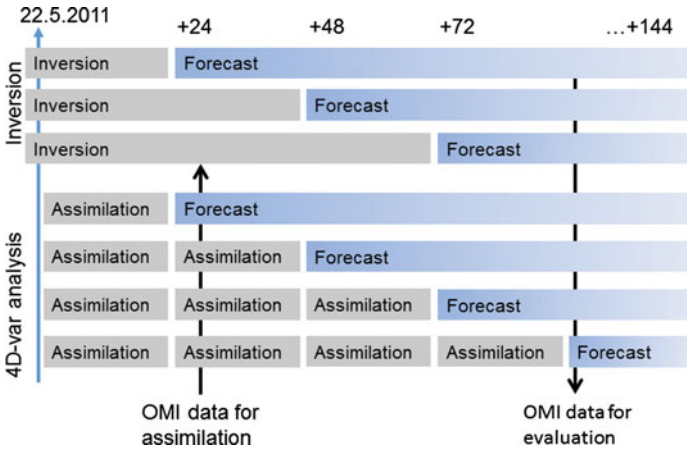

Fig. 98.1 Schematic diagram of the hindcast experiment for the Grimsvötn eruption

98.3 Results and Discussion

An example of the observed and simulated SO2 column densities is shown in Fig. 98.2. The forecasts with 24 and 48 h lead times (upper panels) show fair agreement with the observations (represented by the analysis field, lower-left panel), although the both predictions suffer from excessive horizontal dispersion. The simulation based on source term inversion (lower-right panel) appears less smeared, but the concentration is underestimated considerably and the extent of the plume is not fully captured.

Figure 98.3 aims to quantify the differences in forecast skill, measured by the spatial correlation coefficient. The correlation between the analysis and the OMI observations is between 0.85 and 0.95, but for most days, the correlation decreases quickly in the forecast window. The correlation coefficient for simulations based on the source term inversion remains between about 0.4 and 0.8, but shows only small variation due to forecast length.

The results from the inversion with 48 h of observations are nearly identical to those with 72 h of observations, and only slightly better than those based on just 24 h of observations. This indicates that the inversion becomes insensitive to the additional observations as the transport distance increases. Nevertheless, the inverse simulations were more skillful than those with the 4D-Var initialization for forecast lengths of 48 h or longer.

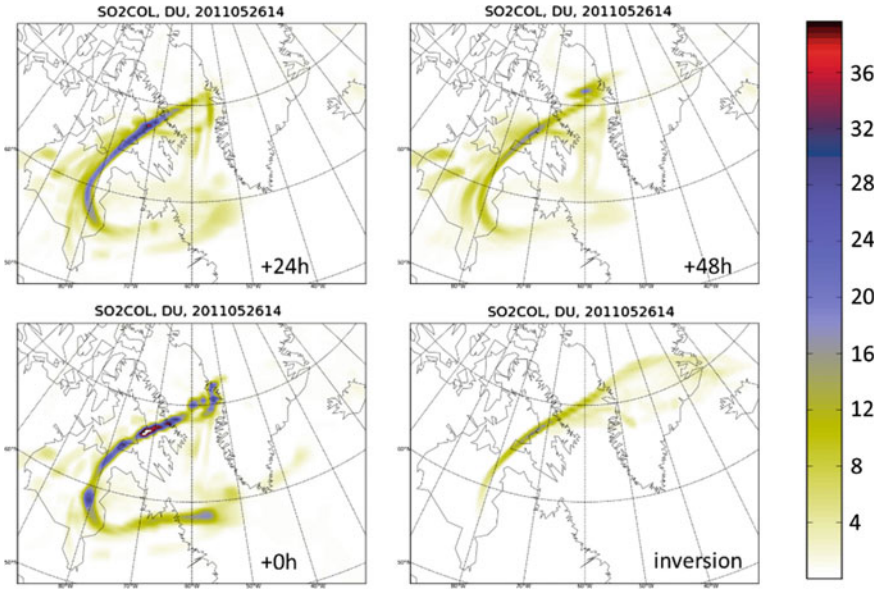

Fig. 98.2 The SO2 column density (DU) for May 26, 2011, 15 UTC in forecasts based on data assimilation with 24 and 48 h times (*top panels*). The analysis field is shown in lower *left panel*. The forecast field based on source term inversion is shown in lower *right panel*

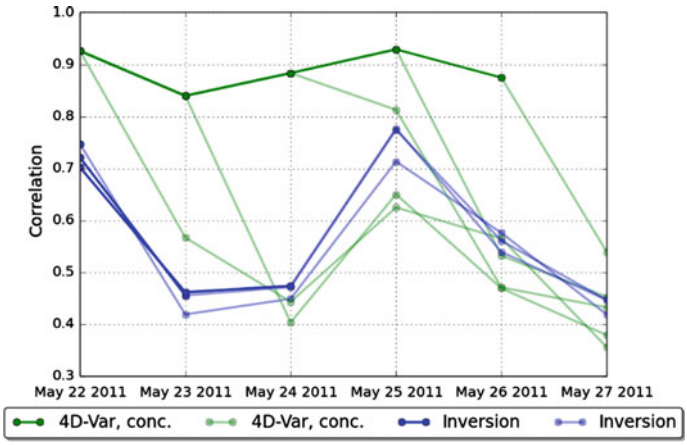

Fig. 98.3 Correlation coefficient between OMI observations and model using source term inversion (*blue lines*) and initialization (*green lines*). The dark lines correspond to values within the assimilation window. Each bright line corresponds to a forecast with a different initial time

The lateral spreading observed for the 4D-Var initialization based forecasts (Fig. 98.2) is caused by vertical variation of the winds. Since the pattern is not present in the SO2 observations, this strongly suggests that the assimilation scheme was unable to localise the plume vertically.

In conclusion, emission inversion and data assimilation are both feasible approaches for improving predictions of volcanic tracers. Using data assimilation to initialize the forecasts has the advantage of updating the predictions continuously to match the observations. However, compared to the assimilation scheme used here, the emission inversion was able to better capture the three-dimensional features of the plume.

Acknowledgments This work has been funded by ESA projects VAST and SMASH. The authors thank NASA for provision of the OMI SO2 data.

Questions and answers

Questioner: Ivanka Stajner
Question: How is dependence of OMI SO2 retrieved amount on assumed plume height accounted for in you method? Quick drop in forecast skill within 24 h implicates that plume height may be displaced in the model. Have you used any ground measurements for verification of plume height or emitted amounts for this retrospective case study?

Answer: The dependence of SO2 retrievals on plume height could be considered using a vertically varying weighting function. In the current study this was not

done, because the sensitivity information is not provided with the SO2 product. Based on radar observations, Petersen et al. (2012, Earth System Science Data) reported eruption plume heights between 10–15 km, which is consistent with the results of the source term inversion. However, the injection heights of ash and SO2 have been found (Moxnes et al. 2014, JGR) to differ strongly in the Grimsvötn eruption.

Questioner: Amir Hakami
Question: What is the advantage of using a variational framework when the source is only extended over a grid cell and few layers?

Answer: For short eruptions, like the Grimsvötn (2011), the variational method indeed has no particular advantage. However, for longer episodes, such as the 2010 Eyjafjallajökull eruption, the dimension of parameter vector can be thousands, which makes the variational solution much cheaper than evaluating source-receptor matrix explicitly.

References

Eckhardt S, Prata AJ, Seibert P, Stebel K, Stohl A (2008) Estimation of the vertical profile of sulfur dioxide injection into the atmosphere by a volcanic eruption using satellite column measurements and inverse transport modeling. Atmos Chem Phys 8:3881–3897. doi:10.5194/acpd-8-3761-2008

Flemming J, Inness A (2013) Volcanic sulfur dioxide plume forecasts based on UV-satellite retrievals for the 2011 Grímsvötn and the 2010 Eyjafjallajökull eruption. J Geophys Res Atmos 118:10172–10189. doi:10.1002/jgrd.50753

Mastin LG, Guffanti M, Servranckx R, Webley P, Barsotti S, Dean K, Durant A, Ewert JW, Neri A, Rose WI (2009) A multidisciplinary effort to assign realistic source parameters to models of volcanic ash-cloud transport and dispersion during eruptions. J Volcanol Geotherm Res 186:10–21. doi:10.1016/j.jvolgeores.2009.01.008

Moxnes ED, Kristiansen NI, Stohl A, Clarisse L, Durant A, Weber K, Vogel A (2014) Separation of ash and sulfur dioxide during the 2011 Grimsvötn eruption. J Geophys Res 119:7477–7501. doi:10.1002/2013JD021129

Petersen GN, Bjornsson H, Arason P, von Löwis S (2012) Two weather radar time series of the altitude of the volcanic plume during the May 2011 eruption of Grímsvötn, Iceland. Earth Syst Sci Data 4:121–127. doi:10.5194/essdd-5-281-2012

Sofiev M, Vira J, Kouznetsov R, Prank M, Soares J, Genikhovich E (2015) Construction of an Eulerian atmospheric dispersion model based on the advection algorithm of M. Galperin: dynamic cores. Geosci Model Dev Discuss 8:2905–2947. doi:10.5194/gmdd-8-2905-2015

Yang K, Krotkov NA, Krueger AJ, Carn SA, Bhartia PK, Levelt PF (2007) Retrieval of large volcanic SO 2 columns from the Aura Ozone Monitoring Instrument: Comparison and limitations. J Geophys Re. 112:D24S43. doi:10.1029/2007JD008825

Zehner C (ed) (2012) Monitoring volcanic ash from space. ESA-EUMETSAT workshop on the 14 April to 23 May 2010 eruption at the Eyjafjöll volcano, South Iceland (ESA/ESRIN, 26–27 May 2010). ESA Publication STM-280

Chapter 99
Improving Air Quality Forecasts Using High Resolution Pollutant Climatologies and Surface Observations

Lucy Sarah Neal, Marie Tilbee and Paul Agnew

Abstract An existing bias correction technique has been extended to intelligently incorporate urban centre and roadside observations by using high (1 km) resolution pollution climatologies. The results show that this can give important improvements in forecast skill, particularly during rush hours where a clear distinction between urban and rural areas becomes more apparent.

99.1 Introduction

To examine links between air quality and health impacts, studies often require pollutant data at the scale of individual urban districts. This paper describes a new bias correction technique which has been developed to use high resolution pollutant climatology datasets for the UK to improve lower spatial resolution air quality model data. The air quality model employed in this work is the UK Met Office's air quality forecast model AQUM (Savage et al. 2013), which runs at 12 km resolution over a domain covering the UK and Western Europe. A bias correction method, SPPO (Statistical Post-Processing of Observations), has been developed for this model to use recent pollutant observations to adjust the forecast (Neal et al. 2014). The current operational forecast system makes use of remote, rural, suburban and urban background observation sites only. However this method has now been further developed in order to also use urban centre and roadside sites to provide detailed hourly forecasts at a potential 1 km scale.

L.S. Neal (✉) · M. Tilbee · P. Agnew
Met Office, FitzRoy Road, Exeter EX1 3PB, UK
e-mail: lucy.neal@metoffice.gov.uk

D.G. Steyn and N. Chaumerliac (eds.), *Air Pollution Modeling and its Application XXIV*, Springer Proceedings in Complexity,
DOI 10.1007/978-3-319-24478-5_99

99.2 Methodology

The current bias correction method, SPPO, calculates a residual difference between observations and model forecast values at all remote, rural, urban background and suburban measurement sites. The observations are taken from the AURN (Automatic Urban and Rural Network, http://uk-air.defra.gov.uk/networks/network-info?view=aurn). Kriging is then used to map these residuals to a single spatial field which can be combined with the model forecast field for each output time.

This current method does not make use of the many extra observations that are available at urban centre and roadside sites. If this method were used without special adaptations, a rural area which only has roadside monitoring sites nearby would be affected by the model bias at the roadside sites, resulting in an inaccurate prediction. For some pollutants, such as NO_2 which for AQUM has a known positive bias at rural sites but a negative bias at urban sites (Savage et al. 2013), this is particularly important. This paper therefore describes a new extension to the SPPO method to allow sensible use of these extra urban centre and roadside observations.

Annual average background concentration maps are available for the UK at 1 km resolution (Defra 2014) for NO_2, O_3, SO_2, PM2.5 and PM10. By comparing values from these maps at AURN sites to annual average observed concentrations, threshold values were determined to distinguish between rural, urban background and urban centre regions on the 1 km maps. All points on these maps can then be expressed as a linear combination of the three different region types. For O_3 the background maps are given in units of number of days on which the daily max 8-hr concentration is greater than 120 μgm^{-3}. This does not allow for distinction between urban and rural areas so for O_3 the NO_2 background map is used instead.

The extended SPPO method still calculates residual differences between observations and model forecasts, including all the original sites but now also using urban centre and roadside. Unlike the original method, a spatial field of residuals is instead produced separately for remote and rural sites, urban background and suburban sites, and urban centre and roadside sites to produce three separate fields of residuals. These fields are then combined using the linear combinations determined from the 1 km maps described above. The resulting merged residual field is then added to the model forecast field.

99.3 Results

The impact of this new method has been tested by running the original regional scale SPPO and the new extended version on raw operational AQUM forecast data over approximately 7 months, from 20th March 2013 to 13th October 2013, which incorporates several periods of elevated concentrations for different pollutants.

Table 99.1 NO_2 and O_3 statistics for 20th March–13th October 2013 for the original SPPO method and the extended SPPO scheme across all sites and split into separate types

	All sites		Remote & rural sites		Urban background & suburban sites		Roadside & urban centre sites	
NO_2	Original	Extended	Original	Extended	Original	Extended	Original	Extended
No. of sites	104	104	14	14	47	47	43	43
Correlation	0.43	0.51	0.60	0.60	0.58	0.62	0.39	0.44
Bias (μgm^{-3})	−7.03	−4.27	1.84	0.92	−1.02	1.29	−15.89	−11.56
RMSE (μgm^{-3})	19.39	18.06	8.27	7.77	12.08	12.48	26.56	24.11
O_3	Original	Extended	Original	Extended	Original	Extended	Original	Extended
No. of sites	77	77	22	22	39	39	16	16
Correlation	0.71	0.72	0.72	0.72	0.71	0.71	0.68	0.69
Bias (μgm^{-3})	2.16	0.17	−1.02	−0.41	1.39	−0.45	8.35	2.43
RMSE (μgm^{-3})	18.49	17.98	17.00	16.78	18.34	18.46	20.73	18.48

Results below concentrate on NO_2 and O_3, but similar results have also been found for PM10, PM2.5 and SO_2.

Statistics for NO_2 and O_3 are given in Table 99.1. There is a noticeable improvement in the bias for both these species across all sites, but also improvements if specific site types are considered. For example the positive NO_2 bias for rural sites has decreased, while the negative bias at urban centre sites has become less negative. Other statistics such as correlation and RMSE have improved similarly.

This change in bias is shown graphically in Fig. 99.1 which shows the diurnal variation of the bias. In the raw model output the bias changes drastically during the course of the day with the model performing particularly poorly around the rush hours. Although the original SPPO method goes some way towards rectifying these problems, the new extended method gives further improvement still, producing more uniform, smaller biases.

Example contour plots are given in Fig. 99.2 for a single time during rush hour, illustrating the extra detail given by using the extended SPPO scheme. There is a clear distinction between urban and rural areas, with major roads being resolved.

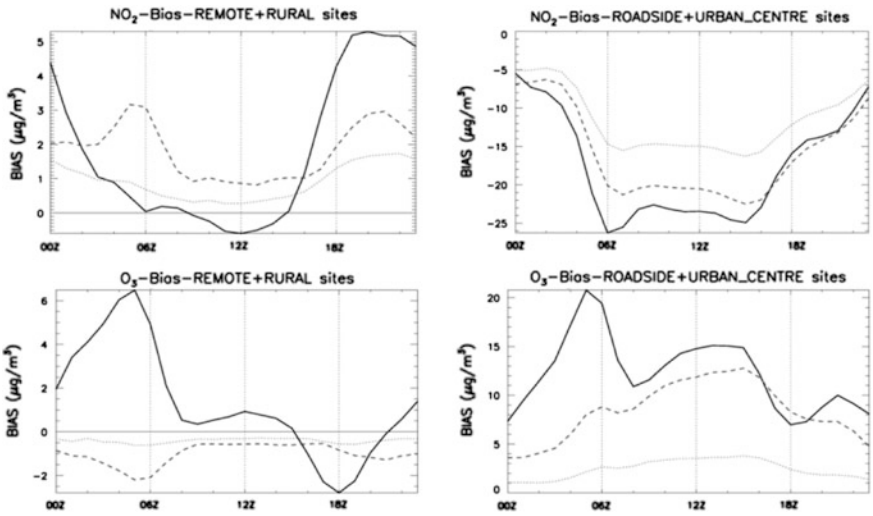

Fig. 99.1 NO_2 (*top*) and O_3 (*bottom*) diurnal variation in bias for 20th March–13th October 2013, for remote and rural sites, compared to roadside and urban centre sites. Raw AQUM data is shown in black (*solid line*), the original SPPO is given in *dark grey* (*dashed line*) and the extended SPPO scheme is plotted in *light grey* (*dotted line*)

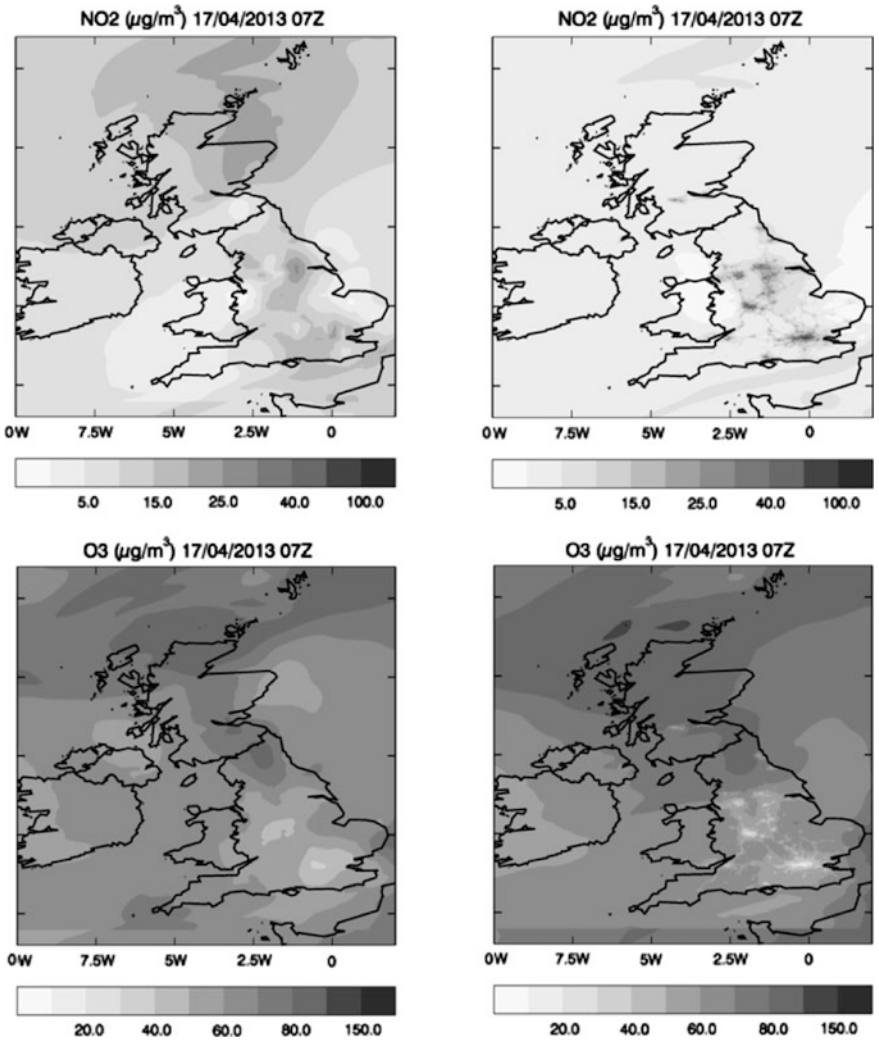

Fig. 99.2 Contour plots for 17th April 2013 at 07Z for NO_2 (*top*) and O_3 (*bottom*) comparing output from the original SPPO on the *left* and the extended SPPO scheme on the *right*

99.4 Conclusions

The careful inclusion of urban centre and roadside observations has been shown to give significant improvements in regional air quality forecasts. The extended SPPO scheme is of most benefit for distinguishing between urban and rural areas, consequently leading to an improved diurnal cycle in pollutant concentrations. The new scheme therefore improves the applicability of regional forecasts to urban areas.

The ability to provide air quality data at 1 km resolution, but only requiring the computational expense of a 12 km regional chemistry model, is important for health impact work as it allows direct comparison of postcode level health data with air quality model output across the entire country.

99.5 Questions and Answers

Questioner: D.G. Steyn.

Question: Since your "correction" is achieved by an adjustment based on climatology, does this not mean you will have difficulty capturing extreme values?

Answer: The climatology is only used to distinguish between rural/urban/roadside regions. We should in theory capture more extremes—for example at urban and roadside areas where the extended bias correction scheme may increase the NO_2 concentrations and not be dampened down by the rural NO_2 biases of the opposite sign.

Questioner: B. Carissimo

Question: You apply the procedure for NO_2 and O_3. In Paris we have numerous NO_2 mean street measurements but only a few O_3 city centre measurements. Do you have enough O_3 mean street measurements compared to NO_2?

Answer: We have 16 urban centre and roadside sites for O_3 (although 43 for NO_2). The way the extended system works, it does not require O_3 sites in every city as the residual from any urban centre/roadside sites are Kriged across the entire domain to cover all other cities. The system may not work as well when applied to a single city with only a few measurement sites, but there are enough O_3 sites for our domain. As the O_3 and NO_2 corrections are treated independently of each other, it does not matter that there are many more NO_2 measurements than for O_3.

References

Defra (2014) Air pollution concentration maps: A user guide for local authorities. http://laqm.defra.gov.uk/documents/Background-maps-user-guide-v1.0.pdf. Accessed 5 Feb 2015

Neal LS, Agnew P, Moseley S, Ordóñez C, Savage NH, Tilbee M (2014) Application of a statistical post-processing technique to a gridded, operational, air quality forecast. Atmos Environ 98:385–393. ISSN 1352-2310. http://dx.doi.org/10.1016/j.atmosenv.2014.09.004

Savage NH, Agnew P, Davis LS, Ordóñez C, Thorpe R, Johnson CE, O'Connor FM, Dalvi M (2013) Air quality modelling using the Met Office Unified Model (AQUM OS24-26): model description and initial evaluation. Geosci Model Dev 6:353–372. doi:10.5194/gmd-6-353-2013

Chapter 100
Application and Evaluation of MODIS LAI, FPAR, and Albedo Products in the WRF/CMAQ System

Limei Ran, Jonathan Pleim, Robert Gilliam, Christian Hogrefe, Frank Binkowski and Larry Band

Abstract MODIS vegetation and albedo products provide a more realistic representation of surface conditions for input to the WRF/CMAQ modeling system. However, the initial evaluation of ingesting MODIS data into the system showed mixed results, with increased bias and error for 2-m temperature and reduced bias and error for 2-m mixing ratio. Recently, the WRF/CMAQ land surface and boundary layer processes have been updated. In this study, MODIS vegetation and albedo data are input to the updated WRF/CMAQ meteorology and air quality simulations for 2006 over a North American (NA) 12-km domain. The evaluation of the simulation results shows that the updated WRF/CMAQ system improves 2-m temperature estimates over the pre-update base modeling system estimates. The MODIS vegetation input produces a realistic spring green-up that progresses through time from the south to north. Overall, MODIS input reduces 2-m mixing ratio bias during the growing season. The NA west shows larger positive O_3 bias during the growing season because of reduced gas phase deposition resulting from lower O_3 deposition velocities driven by reduced vegetation cover. The O_3 bias increase associated with the realistic vegetation representation indicates that further improvement may be needed in the WRF/CMAQ system.

100.1 Introduction

Leaf area index (LAI), vegetation fraction (VF), and surface albedo are important parameters controlling latent heat flux and deposition of various atmospheric gases and particles in meteorology and air quality modeling systems such as WRF/CMAQ.

L. Ran (✉) · F. Binkowski · L. Band
Institute for the Environment, University of North Carolina at Chapel Hill, Chapel Hill NC 27599, USA
e-mail: lran@unc.edu

J. Pleim · R. Gilliam · C. Hogrefe
Atmospheric Modeling and Analysis Division, U.S. EPA, Research Triangle Park, NC 27711, USA

D.G. Steyn and N. Chaumerliac (eds.), *Air Pollution Modeling and its Application XXIV*, Springer Proceedings in Complexity,
DOI 10.1007/978-3-319-24478-5_100

WRF/CMAQ is composed of the National Center for Atmospheric Research (NCAR) Weather Research and Forecast (WRF) model and the United States (US) Environmental Protection Agency (EPA) Community Multiscale Air Quality (CMAQ) model (Pleim and Ran 2011). These WRF/CMAQ parameters are currently specified in the land surface model (LSM) look-up tables by land use category with some simple seasonal adjustments, or are derived from monthly averaged satellite vegetation parameters. Table-prescribed surface representations clearly limit the ability of WRF/CMAQ to capture seasonal landscape changes (e.g. phenology and albedo) and disturbances (e.g. fires, storm damages) in annual retrospective simulations.

LSM performance has improved with the availability of many global satellite products such as LAI and FPAR (fraction of absorbed photosynthetically active radiation, used as VF surrogate) at temporal scales ranging from daily to annual, and surface albedo and emissivity derived from Moderate Resolution Imaging Spectroradiometer (MODIS) satellite data. Ran et al. (2015) assimilated MODIS-derived LAI, FPAR and albedo into the WRF/CMAQ simulations with the Pleim-Xiu (PX) LSM, thereby providing more up-to-date, accurate, and detailed landscape information. They demonstrated that MODIS spatial and temporal vegetation representation is much more realistic in the arid western U.S. than PX LSM look-up table values. In addition, MODIS albedo, excluding snow covered areas, describes heterogeneous surfaces better than the albedo calculated in the current PX LSM WRF. However, their 30 day summer WRF/CMAQ simulations with MODIS input show mixed results, with overall greater error and bias in temperature, but reduced error and bias in moisture. The PX LSM intentionally exaggerates LAI and VF for the US arid west so that its soil moisture-nudging scheme is more effective in simulating surface temperature and mixing ratio. MODIS vegetation values over the western US indicate the presence of less vegetation along with warmer and drier surface conditions. Estimated O_3 production increases in response to warmer temperatures, while less O_3 is removed as the result of lower dry deposition velocities driven by smaller LAI and VF values, even with deeper planetary boundary layer (PBL) depths. The increased temperature and O_3 errors associated with the more realistic representation of vegetation from MODIS suggest that improvements may still be needed in the WRF/CMAQ surface physics.

Since the study by Ran et al. (2015), the WRF/CMAQ modeling system has updates in the soil-vegetation and PBL processes (Pleim et al. 2015). The goal of this research is to apply year-long MODIS LAI, FPAR, and albedo to the updated WRF/CMAQ system for 2006 meteorology and air quality simulations over the North America 12 km domain. The simulated meteorology and air quality results are evaluated against measurement data to demonstrate benefits of using satellite LAI, FPAR and albedo data with seasonality in the air quality modeling system.

100.2 Data and Method

The 2006 gap-filled and smoothed MODIS LAI and FPAR data (MOD15A2GFS) at 1 km resolution (Gao et al. 2008) from the US North American Carbon Program (NACP) and MODIS bidirectional reflectance distribution function (BRDF) albedo products (MCD43A1 and MCD43A2) at 500 m resolution (Schaaf et al. 2002) are obtained and processed for the modeling domain grids. Black-sky, white-sky, and blue-sky albedos for non-snow covered areas are computed in the PX LSM with the changing solar zenith angle using simple polynomial equations with MODIS BRDF/albedo parameters. WRF version 3.4 and CMAQ version 5.0.2 are used for this study. The modified WRF/CMAQ for MODIS input is further updated for changed soil-vegetation and PBL processes as described by Pleim et al. (2015). The offline CMAQ simulations for this research use the same emissions, boundary/initial conditions, and configuration described in the study by Hogrefe et al. (2014) for the second phase of the Air Quality Model Evaluation International Initiative (AQMEII) study. Detailed information on WRF and CMAQ model physics selections are provided Ran et al. (2015).

The WRF simulations are conducted for 2006, starting from the last week of 2005 for spin-up on the 12-km domain. The CMAQ simulations are conducted for April, August and October, starting seven days before the start of each month for spin-up. The 12-km domain contains 299 by 459 grid cells and 34 vertical levels extending from the surface to the 50-hPA level over the conterminous US, southern Canada, and northern Mexico. The simulations use the land use data from 2006 30-meter National Land Cover Database (NLCD) for the US and MODIS land cover data at 500 m resolution for the areas outside the US. Two WRF scenarios: (1) Base case with standard WRF and (2) MODIS case with modified WRF for MODIS LAI, FPAR and albedo inputs, and two CMAQ simulation scenarios (1) Base case with WRF Base case meteorology and (2) MODIS case with WRF MODIS case meteorology are used for this study.

100.3 Results and Analysis

The meteorology simulation with MODIS input from the updated WRF clearly shows improvements over pre-update estimates of 2-m temperature, with mean absolute error 1.460 K and bias 0.168 K in comparison with the Meteorological Assimilation Data Ingest System (MADIS) observation data from the US National Oceanic and Atmospheric Administration (NOAA) over the August 10 to September 9 period. For the same period, the pre-updated WRF simulation with MODIS input has mean absolute error 1.584 K and bias 0.607 K. Unlike the previous study by Ran et al. (2015), the updated WRF model, ingesting realistic MODIS vegetation data does not result in greater error and bias in 2-m temperature. 2-m temperature (T), mixing ratio (Q), and 10-m wind speed (WS) for the base and

MODIS case WRF simulations are evaluated domain-wide based on monthly average mean bias (MB) and mean absolute error (MAE) statistics computed from the model and MADIS observation data for seasonality impact assessment. The monthly average MB and MAE for 2-m Q for 2006 annual simulation is displayed in Fig. 100.1. The base and MODIS case WRF simulations have similar monthly average MAE for 2-m Q. However, the MODIS case WRF simulation shows significant reduction of monthly average MB from April to September. MODIS input clearly helps reduce 2-m Q bias during the growing season, from the Spring green-up to the early Fall brown-down. Both monthly average MB and MAE show little difference for 2-m T and 10-m WS between the base and MODIS case WRF simulations. Since vegetation directly influences surface fluxes, modeled latent heat (LE) fluxes from the base and MODIS cases are compared with the FLUXNET measurements at the Tonzi Ranch site in California (Fig. 100.2). While both the base case (solid line) and the MODIS case (dot) are too high in comparison with the site measurements (diamond line) the LE estimated from the MODIS case is closer to observations for the period.

The change in estimated surface O_3 attributable to the use of MODIS inputs stands out most among the chemical species modeled in CMAQ, because the O_3 dry deposition flux has a strong stomatal pathway in vegetated areas. The west has higher ambient O_3 concentrations during the growing season because of lower LAI (less vegetation) and VF estimates from MODIS input that result in lower O_3 deposition velocity and less O_3 removal. The updated WRF/CMAQ has reduced O_3 bias in comparison with the pre-updated WRF/CMAQ (Pleim et al. 2015) in spite of the still positive bias for 8 h-max O_3 in the CMAQ runs with MODIS input in the southwestern US.

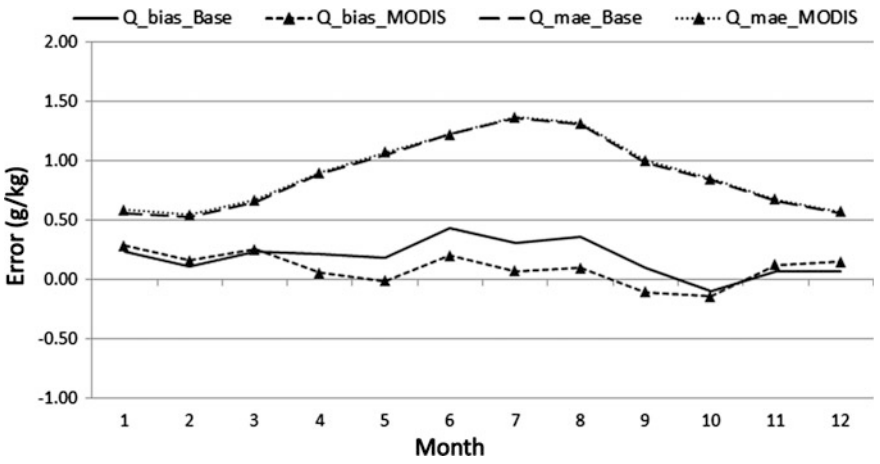

Fig. 100.1 2006 Monthly average mean bias (MB) and mean absolute error (MAE) for 2-m mixing ratio (Q)

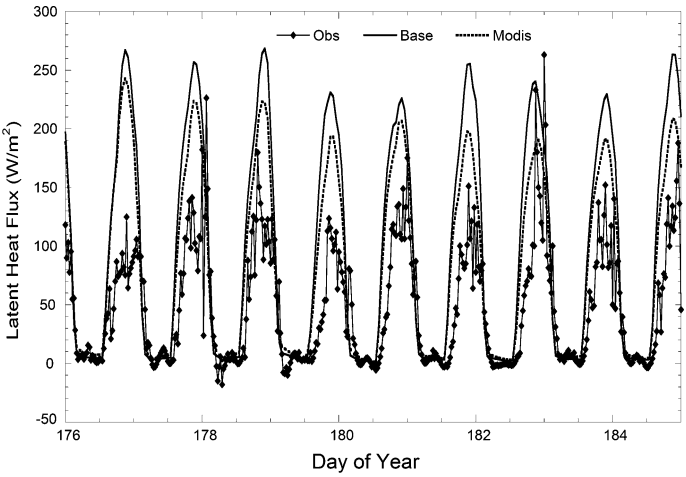

Fig. 100.2 Diurnal latent heat flux (LE) from the base and MODIS cases compared with FLUXNET, June 25 to July 04, 2006 at the Tonzi Ranch site in California, U.S

100.4 Conclusions and Ongoing Work

MODIS LAI, FPAR, and albedo data add realism to WRF/CMAQ, with much better spatial and seasonal vegetation and surface representation. MODIS vegetation and albedo input reduce 2-m Q bias during the growing season. Areas with small values of VF such as the Western US show higher surface ozone concentrations due to lower O_3 deposition. The MODIS input still produces positive 8 h-max O_3 bias, but the negative 8 h-max O_3 bias at the high end of the observation range is slightly reduced. Overall, the MODIS input in the updated WRF system improves the meteorology simulation. However, the larger simulated ozone bias suggests that further improvements are needed in WRF/CMAQ, particularly with regards to dry deposition processes associated with sparse vegetation. Further improvement of the WRF/CMAQ model is ongoing, with the implementation and evaluation of a photosynthesis-based vegetation model in PX LSM WRF/CMAQ with MODIS inputs.

Acknowledgments and Disclaimer Although this work has been has been reviewed by EPA and approved for publication, it does not necessarily reflect their policies or views.

Question and Answer

Questioner: D.G. Steyn.

Question: In many of your maps, you present variables (O3 & MLD) with strong diurnal variation at a fixed time (2000 UTC). Surely, it would be better to present these quantities at the same local time.

Answer: For the large scale modeling over the conterminous US domain which crosses four time zones, it is often questionable to select just one UTC time across the domain for displaying surface fluxes and deposition. Often, surface fluxes show big changes around peak temperature time which varies seasonally from around 2–3 pm LT in mid-winter to about 4–5 pm LT in mid-summer. Yes, it could be better to show the quantities at the same local summer time. We evaluated O_3 and surface fluxes changes over different hours. It appears that O_3 shows big difference around 20Z which corresponds to 1 and 2 pm for the Pacific and Mountain Daylight summer time zones. Thus, we selected 20Z to display the whole domain flux and O_3 differences because most vegetation change from the use of MODIS input is in the US western drylands.

References

Gao F, Morisette J, Wolfe R, Ederer G, Pedelty J, Masuoka E, Myneni R, Tan B, Nightingale J (2008) An algorithm to produce temporally and spatially continuous MODIS-LAI time series. IEEE Geosci Remote Sens Lett 5(1):60–64

Hogrefe C, Pouliot G, Wong D, Torian A, Roselle S, Pleim J, Mathur R (2014) Annual application and evaluation of the online coupled WRF–CMAQ system over North America under AQMEII phase 2. Atmos Environ (in press)

Pleim JE, Ran L (2011) Surface flux modeling for air quality applications. Atmosphere 2(3):271–302

Pleim J, Gilliam AR, Appel W, Ran L (2015) Recent advances in modeling of the atmospheric boundary layer and land surface in the coupled WRF-CMAQ model. In: 34th International technical meeting on air pollution modelling and its application, Montpellier, France, 4–8 May 2015

Ran L, Gilliam R, Binkowski FS, Xiu A, Pleim J, Band L (2015) Sensitivity of the WRF/CMAQ modeling system to MODIS LAI, FPAR, and albedo. J Geophys Res Atmos (accepted)

Schaaf CB, Gao F, Strahler AH, Lucht W, Li X, Tsang T, Strugnell NC, Zhang X, Jin Y, Muller JP, Lewis P, Barnsley M, Hobson P, Disney M, Roberts G, Dunderdale M, Doll C, d'Entremont R, Hu B, Liang S, Privette JL (2002) First operational BRDF, albedo and nadir reflectance products from MODIS. Remote Sens Environ 83:135–148

Chapter 101
Application of a Land Cover Indicator to Characterize Spatial Representativeness of Air Quality Monitoring Stations Over Italy

Antonio Piersanti, Luisella Ciancarella, Giuseppe Cremona, Gaia Righini and Lina Vitali

Abstract In order to achieve a cost-effective control of air quality in one region and to evaluate effects on population of long term exposure to air pollution, the assessment of spatial representativeness of air quality monitoring stations is of fundamental relevance. In this work, the area of representativeness has been assessed by means of a synthetic indicator describing the dependency of concentration on land cover distribution. The rationale is that, the more variable is the indicator in the surroundings of the station, the less representative are the concentrations measured at the air quality station in the surroundings. Pollutants under investigation were PM2.5 and O_3 and the CORINE land cover map of 2006 was used with ad hoc modifications. The variability of the indicator was explored within circular buffers around the sites, with increasing radii resulting below the established threshold of 20 % for almost all cases. Results showed that the methodology allows an useful and quick assessment of spatial representativeness of a monitoring site, without the need of dedicated measurement campaigns.

101.1 Introduction

Spatial representativeness of air quality monitoring stations is related to the variability of pollutants concentrations around the monitoring site (Spangl et al. 2007) and plays a key role in monitoring networks design and optimization, for maximizing spatial coverage, avoiding redundant stations and assessing people's exposure to air pollution. Monitoring and modelling are the two practical ways to obtain concentrations data covering the surroundings of the site, both requiring

A. Piersanti (✉) · L. Ciancarella · G. Cremona · G. Righini · L. Vitali
Laboratory for Atmospheric Pollution, ENEA—Bologna Research Center,
Via Martiri di Monte Sole 4, 40129 Bologna, Italy
e-mail: antonio.piersanti@enea.it

D.G. Steyn and N. Chaumerliac (eds.), *Air Pollution Modeling and its Application XXIV*, Springer Proceedings in Complexity,
DOI 10.1007/978-3-319-24478-5_101

important resources for settling experimental campaigns on many points, or for a complete model set-up with the proper spatial scale and resolution (Santiago et al. 2013; Martin et al. 2014). Therefore, measured and modelled concentrations are rarely available for an actual and quick assessment of spatial representativeness of existing or planned monitoring stations. In order to overcome these limitations, in this work we used surrogate data for concentrations, i.e. land cover around monitoring stations, relying on a causal relationship with concentrations: indeed, land cover patterns are representative of actual locations of emissions, and emissions are the main cause of concentrations. Once assessed the robustness of the empirical relationship between land cover and concentrations, the method allows to use freely available datasets of land cover with large spatial coverage, for a low cost and first-look assessment of spatial representativeness of monitoring sites. More in detail, the applied approach is based on the calculation of a synthetic, pollutant-dependent, land cover indicator and on the analysis of its variability in the neighbourhood of the selected monitoring site. The methodology, developed by Janssen et al. (2012) and first applied in Belgium, has been here tested in a very different territorial context, for the assessment of spatial representativeness of the Italian network of special purpose air quality monitoring stations, currently underway.

101.2 Materials and Methods

The synthetic pollutant-dependent land cover indicator (β) is defined in Janssen et al. (2012) by the formulation of Fig. 101.1 where, assuming a reference area around the monitoring site, n_{CLi} is the fraction of the area corresponding to CLi class of land cover and a_i is a weight coefficient, determining the influence of CLi class as a potential determinant of pollutant concentration.

The CORINE land cover map of 2006 for Italy was collected and then tailored to our study by an aggregation of the original 44 classes (CORINE 3rd level) into 11 CLi classes including the integration of the road network class, using more detailed layers with national coverage.

The indicator was applied to assess the spatial representativeness of a selection of background monitoring stations in Italy, both rural and urban. Pollutants under investigation were PM2.5 and O_3: the indicator was optimized for each pollutant by means of a statistical procedure applied on an independent calibration dataset (time series of concentration measurements in Italy and land cover around measurement sites). In particular, the a_i weight coefficients were calculated by means of a

$$\beta = \log\left[1 + \left(\frac{\sum_i a_i \cdot n_{CLi}}{\sum_i n_{CLi}}\right)\right]$$

Fig. 101.1 Definition of the land cover indicator as formulated by Janssen et al. (2012)

statistical optimization of the function $C(\beta) = n\beta^2 + m\beta + q$, where the dependency of the concentration C on the land cover indicator is explicated. The optimization was carried out by a multivariable regression on measured concentration values obtained from the national database of air quality measurements, using 2007 annual averages. Since the optimization relies on measured concentrations, a_i are pollutant-dependent. After the calibration, each station under investigation assumed a value of the indicator, calculated in a circular buffer with 2 km radius centered at the station.

The variability of the indicator was then explored, using several circular buffers of land cover around the sites with increasing radii (5, 7.5, 10 km): Fig. 101.2 shows an example of land cover buffering around the Ripatransone (Central Italy, Marche region) rural background monitoring station applied to PM2.5. The spatial representativeness of the station has been quantitatively assessed comparing the value of the indicator resulted from each buffer with the one calculated in the 2 km buffer: a difference of less or more than 20 % indicates whether or not the station measurement represents the concentration value inside the buffer. In this analysis a threshold value of 20 % was set according to literature (Martin et al. 2014) and since it is compatible with the quality objectives for most monitoring data included in the Air Quality Directive (15 and 25 %, depending on the measured pollutant). The land cover indicator resulted below the established threshold of 20 % for almost all cases.

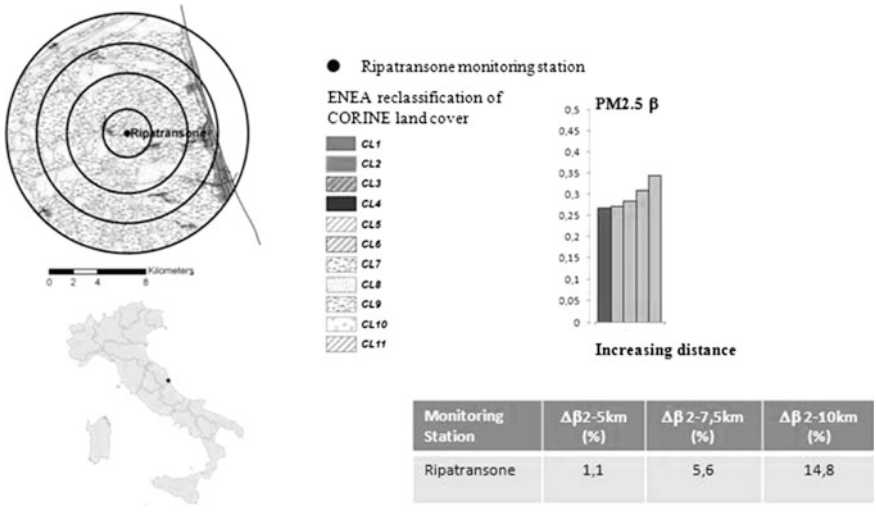

Monitoring Station	Δβ2-5km (%)	Δβ2-7,5km (%)	Δβ2-10km (%)
Ripatransone	1,1	5,6	14,8

Fig. 101.2 Land cover buffering around Ripatransone rural background station at increasing radii (2, 5, 7.5, 10 km) and the indicator calculation about PM2.5

101.3 Conclusions

The methodology applied in this work to detect spatial representativeness of monitoring stations is based on the use of land cover data as a proxy variable of concentration to determine spatial variations of the polluting factor in analysis, at increasing distance from the selected site. The rationale relies on a simplified description of atmospheric pollution processes where an empirical relationship is assumed between physical objective factors influencing air pollution and concentrations recorded by air quality monitoring stations. This assumption is widely used in air quality assessment, in particular when insufficient data on emissions and meteorology and/or limited resources prevent from a detailed representation of pollution processes. The empirical relationship has a simplified formulation, therefore the quality of results strongly depends on the selected dataset of measured concentrations, used in the calibration stage. Indeed, this method is robust when annual time series of measured concentrations are available from a consolidated and spatially uniform monitoring network, allowing a good calibration of the applied indicator. Results showed that the methodology allows an useful and quick assessment of spatial representativeness of a monitoring site, without the need of dedicated measurement campaigns. Moreover, the use of a high-resolution land cover database allows detailed assessment of spatial representativeness, very useful for urban and suburban monitoring sites.

Acknowledgments This work is part of the Cooperation Agreement for the starting up the Italian National Network of Special Purpose Monitoring Station, funded by the Italian Ministry for Environment, Territory and Sea.

References

Janssen S, Dumont G, Fierens F, Deutsch F, Maiheu B, Celis D, Trimpeneers E, Mensink C (2012) Land use to characterize spatial representativeness of air quality monitoring stations and its relevance for model validation. Atmos Environ 59:492–500

Martin F, Fileni L, Palomino I, Vivanco MG, Garrido JL (2014) Analysis of the spatial representativeness of rural background monitoring stations in Spain. Atmos Pollut Res 5(4):779–788

Santiago JL, Martín F, Martilli A (2013) A computational fluid dynamic modelling approach to assess the representativeness of urban monitoring stations. Sci Total Environ 454–455:61–72

Spangl W, Schneider J, Moosmann L, Nagl C (2007) Representativeness and classification of air quality monitoring stations—Final Report. Umweltbundesamt report, Vienna

Chapter 102
Dynamic Data Fusion Approach for Air Quality Assessment

Lucia Paci, Giovanni Bonafè and Carlo Trivisano

Abstract Data fusion procedures are developed to fill the gap between monitoring networks and CTMs. However, they often do not account for temporal dynamics, leading to potential inaccurate air quality assessment and forecasting. We propose a statistical data fusion strategy for combing the CTM output with monitoring data in order to improve air quality assessment and forecasting in the Emilia-Romagna region, Italy. We employ a dynamic linear model to accommodate dependence across time and obtain air pollution assessment and forecasting for the current and next two days. Finally, air pollution forecast maps are provided at high spatial resolution using universal kriging and exploiting the CTM output. We apply our strategy to particulate matter (PM_{10}) concentrations during winter 2013.

102.1 Introduction

The Po Valley in Northern Italy is a semi-closed basin surrounded by complex orography. Since Po Valley is a densely populated and heavily industrialized area, air pollution is a major issue. Due to the urban sprawl, air quality networks alone cannot cover properly the whole region for detailed epidemiological analyses. On the other hand, chemistry-transport models (CTMs) often have systematic biases.

Data fusion systems are supposed to fill the gap between monitoring networks and CTMs. However, they often do not account for temporal dynamics, leading to potential inaccurate assessment of some features, such as the persistence which can

L. Paci (✉) · C. Trivisano
University of Bologna, Via delle Belle Arti, 41, Bologna, Italy
e-mail: lucia.paci2@unibo.it

C. Trivisano
e-mail: carlo.trivisano@unibo.it

G. Bonafè
Regional Agency for Environmental Protection in the Emilia-Romagna,
Viale Silvani 6, Bologna, Italy
e-mail: gbonafe@arpa.emr.it

D.G. Steyn and N. Chaumerliac (eds.), *Air Pollution Modeling and its Application XXIV*, Springer Proceedings in Complexity,
DOI 10.1007/978-3-319-24478-5_102

play a key role for short-term health effects. Also, temporal dynamics plays an important role in providing accurate air quality forecasting.

We propose a statistical data assimilation strategy for fusing the CTM output with monitoring data in order to improve air quality assessment and forecasting in the Po Valley. We employ dynamic linear modeling to accommodate dependence across time and obtain air quality forecasting for the current and next 2 days. High-resolution maps are provided using universal kriging and exploiting the CTM output available for future days. Bias-correction of site-specific forecasts is quite common as well as fusing CTMs' simulations with observed data for assessment purposes is a widespread practice. However, blending these two steps in air quality assessment and forecasting is challenging.

Our strategy is applied to particulate matter (PM_{10}) concentrations over the Emilia-Romgna region in the Po Valley during winter 2013.

102.2 Data

NINFA is an operational model suite used at Arpa (the regional EPA of Emilia-Romagna) for air quality assessment and forecast purposes, and to support policymakers, by evaluating the impact of emissions reduction scenarios. The core of NINFA (Stortini et al. 2007) is the chemistry-transport model CHIMERE (Menut et al. 2013), run daily over a domain covering Northern Italy with a resolution of 5 km. Boundary conditions are provided by Prev'Air (CHIMERE-Europe). Emission data are provided by regional, national and continental inventories. Meteorological input is provided by the non-hydrostatic model COSMO-I7 (COSMO-Italy). On daily basis, NINFA produces air pollution estimates for the previous day (analysis) and the predictions for the current and next 2 days (forecasting).

The air quality monitoring network of Emilia-Romagna region includes 47 stations, of which 42 measuring particulate matter PM_{10}. Observations (mg/m^3) collected from 30 background stations are used in this study.

102.3 Dynamic Data Fusion Modeling

A two-stage data assimilation strategy is proposed. At the first stage, we employ a dynamic linear model to combine observed PM_{10} with the CTM output and provide air quality assessment and forecasting at monitoring locations. Secondly, universal kriging procedure is applied to produce high-resolution PM_{10} forecast maps for the current and next 2 days.

The dynamic linear model, developed as a result of the popularity of Kalman filtering methods, provides a dynamical state-space system that evolves from a pair of state and observation equations; see Durbin and Koopman (2001) for a

comprehensive overview. The Kalman filter has been used recently as bias-correction technique for improving air quality forecasts of ground-based ozone and particulate matter (Kang et al. 2008; Borrego et al. 2011).

Let Y_t be the PM_{10} concentration observed at day t for a given monitoring site. Let Z_t denote the PM_{10} concentration simulated by the CTM at time t for a given grid cell and interpolated to the corresponding site. Hence, for each monitoring site, we assume a dynamic regression model with time-varying coefficients given by:

$$Y_t = \beta_{0,t} + \beta_{1,t} Z_t + \varepsilon_t \tag{102.1}$$

where ε_t is a white noise error term with mean zero and variance τ^2. The temporal evolution is described in a latent space via the state equations:

$$\beta_{0,t} = \beta_{0,t-1} + \eta_{0,t} \qquad \beta_{1,t} = \beta_{1,t-1} + \eta_{1,t} \tag{102.2}$$

where $\eta_{0,t}$ and $\eta_{1,t}$ are two independent white noise sequences with mean zero and variance σ_0^2 and σ_1^2, respectively.

State-space model (102.1)–(102.2) (hereafter SSM) enables us to retrospectively study the behavior of the system (smoothing) and predict future observations (forecasting) based on a part of the observation sequence. Estimation and forecasting are solved by computing the conditional distributions of the quantities of interest, given the available information. The analysis is performed using KFAS R-package.

Finally, smoothing and forecasting stages are followed by a spatial interpolation step, in order to produce high-resolution forecast maps for the current and next 2 days of PM_{10} pollution. We employ the universal Kriging (Cressie 1993) to obtain such forecast maps using the predictions simulated by the CTM for future days.

102.4 Results

Figure 102.1 presents an illustration of the impact of the application of the SSM relative to both the observations and the NINFA output. The figure shows the time series of average PM_{10} observations (black dots), NINFA output (continued line) and SSM forecast (dashed line) for the current day during the period from October 2013 to March 2014. We note that SSM forecasts are closer to the observations, revealing the improvement of our strategy over the raw NINFA output.

Figure 102.2 shows the PM_{10} forecast maps obtained from NINFA (top panels) and SSM (bottom panels) for the current and next 2 days. SSM keeps the main features of the PM_{10} fields, as simulated by NINFA, with higher concentrations in the plain and lower levels in the Apennines. However, the gradient between mountain and plain is smoother. Moreover, SSM adds an interesting and realistic small-scale

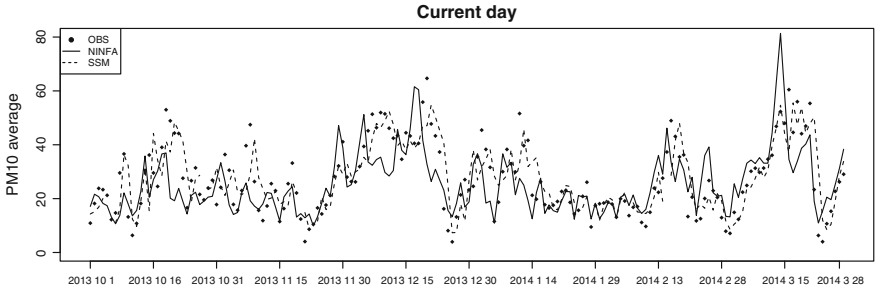

Fig. 102.1 Mean regional PM_{10} concentrations (mg/m^3) (*black dots*), Chemistry-Transport Model NINFA output (*continued line*) and SSM forecasts (*dashed line*) for the current day during the period from October 2013 to March 2014

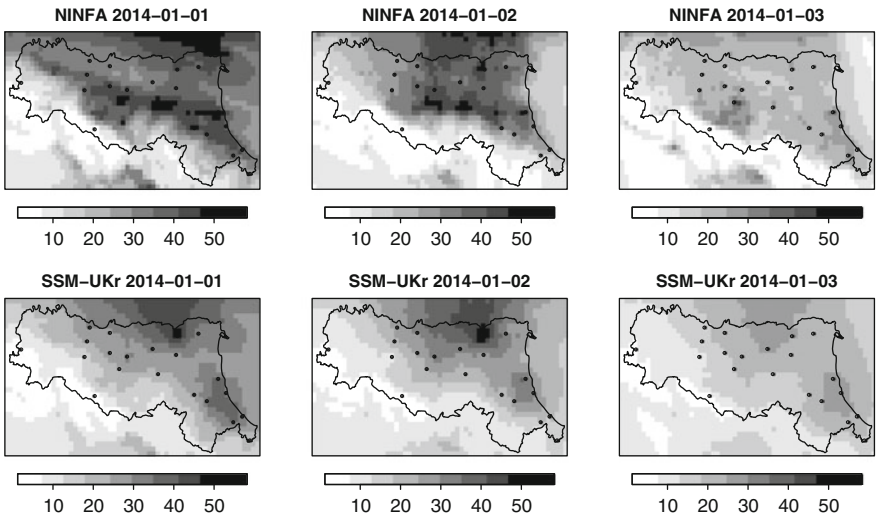

Fig. 102.2 PM_{10} forecast maps; NINFA output (*top panels*) and SSM predictions (*bottom panels*) for the current and next 2 days. *Dots* represent monitoring stations

feature: concentrations in the area of Bologna are lower on January 1st and 2nd, probably because of the breeze flowing from the small valleys close to the city.

The proposed method shows promising results. More extensive evaluation is still ongoing. Our strategy provides the decision-maker with the opportunity to plan short-term actions to reduce pollution, taking into account not only the air quality forecast, but also its confidence interval.

Acknowledgments This research was carried out as part of the "Supersito" Project, which was supported and financed by Emilia-Romagna Region and Regional Agency for Prevention and Environment. The first and third author were also supported by FIRB 2012 grant (project no. RBFR12URQJ) provided by the Italian Ministry of Education, Universities and Research.

References

Borrego C, Monteiro A, Pay M, Ribeiro I, Miranda A, Basart S, Baldasano J (2011) How bias-correction can improve air quality forecasts over portugal. Atmos Environ 45:6629–6641

Cressie N (1993) Statistics for spatial data. Wiley, New York

Durbin J, Koopman S (2001) Time series analysis by state space methods. Oxford University Press, Oxford

Kang D, Mathur R, Rao ST, Yu S (2008) Bias adjustment techniques for improving ozone air quality forecasts. J Geophys Res 113(D23308). doi:10.1029/2008JD010151

Menut L, Bessagnet B, Khvorostyanov D, Beekmann M, Blond N, Colette A, Coll I, Curci G, Foret G et al (2013) CHIMERE 2013: a model for regional atmospheric composition modelling. Geosci Model Dev 6:981–1028

Stortini M, Deserti M, Bonaf`e G, Minguzzi E (2007) Long-term simulation and validation of ozone and aerosol in the Po Valley. In: Borrego C, Renner E (eds) Developments in environmental sciences, vol 6, pp 768–770. Elsevier

Chapter 103
The Performance and Issues of a Regional Chemical Transport Model During Discover-AQ 2014 Aircraft Measurements Over Colorado

Youhua Tang, Li Pan, Pius Lee, Daniel Tong, Hyun-Cheol Kim, Jun Wang and Sarah Lu

Abstract The National Oceanic and Atmospheric Administration (NOAA) National Centers for Environmental Prediction operates the U.S. Air Quality Forecasting Capability (NAQFC) which uses primarily the U.S Environmental Protection Agency's Community Multi-Scale Air Quality (CMAQ) model. NAQFC focuses on surface ozone and $PM_{2.5}$ (particle matter with diameter <2.5 μm), which impacts human-health. Near surface ozone mainly comes from photochemical reactions of NO_x and volatile organic compounds (VOCs). Its sources in upper layers could come from either long-range transport or stratospheric ozone. Most $PM_{2.5}$ comes from near-surface primary emissions or secondary generation from photochemical reactions. During the summer 2014 NASA Discover-AQ-Colorado program, the NOAA Air Resources Laboratory (ARL) provided a real-time forecast in support of aircraft measurements with 12 km CONUS (Contiguous United States) and 4 km nested domains. Here we compare the model results with the aircraft data to investigate our predictions.

Y. Tang (✉) · L. Pan · P. Lee · D. Tong · H.-C. Kim
NOAA Air Resources Laboratory, 5830 University Research Court, College Park, MD 20740, USA
e-mail: youhua.tang@noaa.gov

Y. Tang · L. Pan · D. Tong · H.-C. Kim
Cooperative Institute for Climate and Satellites, University of Maryland, College Park, MD 20740, USA

D. Tong
Center for Spatial Information Science and Systems, George Mason University, Fairfax, VA 22030, USA

J. Wang
NOAA/NCEP/EMC, 5830 University Research Court, College Park, MD 20740, USA

S. Lu
Atmospheric Sciences Research Center, State University of New York, Albany, NY 12203, USA

D.G. Steyn and N. Chaumerliac (eds.), *Air Pollution Modeling and its Application XXIV*, Springer Proceedings in Complexity,
DOI 10.1007/978-3-319-24478-5_103

103.1 Model Settings

In this study, the Weather Research and Forecasting Advance Research WRF (WRF-ARW) regional meteorological model (version 3.4.1) was used to drive CMAQ version 5.0.2. The physical/chemical schemes are listed in Tables 103.1 and 103.2 for WRF and CMAQ, respectively. The WRF-ARW was driven by the NCEP Global Forecasting System (GFS) real-time forecast. During the forecast period, we ran two domains: 12 km CONUS and 4 km nested domain over Colorado with the NEI (National Emission Inventory) 2005, projected to the year 2014 (Pan et al. 2014; Tong et al. 2015), and static lateral boundary condition (LBC) (monthly averaged profiles extracted from the GEOS-Chem (Bey et al. 2001)). Both the meteorological and air-quality models have 42 vertical layers up to 50 hPa. In our

Table 103.1 WRF-ARW dynamic and physical options used in this study

	Schemes	Remarks and reference
Advection	Runge-Kutta 3 advection scheme	Wicker and Skamarock (2002)
Shortwave radiation	Dudhia	Dudhia (1989)
Longwave radiation	RRTM	Mlawer et al. (1997)
PBL turbulent mixing	Yonsei University Scheme	Hong et al. (2006)
Cloud micro physics	WRF single-moment, 6-class scheme	Hong and Lim (2006)
Surface layer heat/momentum exchange	MM5 similarity scheme	Zhang and Anthes (1982)
Land surface exchange	Unified Noah land surface model	Tewari et al. (2004)

Table 103.2 CMAQ dynamic, physical, and chemical options used in this study

	Parameterization scheme	Remarks and reference
Advection	Piece-wise parabolic method	Mathur et al. (2005)
PBL turbulent mixing	Asymmetric Convective model2	Pleim (2007)
Cloud convection mixing	Asymmetric Convective model	Mathur et al. (2005)
Surface layer heat/momentum exchange	Monin-Obukhov similarity theory	Monin and Obukhov (1954)
Gas phase chemistry	Carbon Bond mechanism version 5 with Toluene and Chloride chemistry (cb05tucl)	Sarwar et al. (2011)
Photolytic attenuation by clouds	WRF clear sky flux and cloud fraction	Mathur et al. (2005)
Aerosol size distribution	Tri-modal log-normal distribution	Binkowski and Shankar (1995)
Aerosol chemistry	Module Aero5 of CMAQ4.7.1	Binkowski and Shankar (1995)
Dry deposition	M3Dry	Mathur et al. (2005)

post run, the emission changed to NEI-2011, and NGAC (NEMS (NOAA Environmental Modeling System) GFS Aerosol Component) dust and ozone LBC were used for the 12 km CONUS domain. NGAC's O_3 or GFS-O_3 was treated as a 3-D prognostic variable (Moorthi and Iredell 1998) after being initialized daily with Solar Backscatter Ultra Violet-2 (SBUV-2) satellite data.

103.2 Results and Discussions

103.2.1 The Impact of GFS-O_3 LBC

The NASA Discover-AQ 2014 had its first scientific flight on July 17, 2014. Figure 103.1 shows the predicted ozone from two 12 km models compared to P-3B aircraft observations. One noticeable difference between the models is that the 12 km forecast run (12 km_NEI05) with static LBC tends to over-predict ozone when the altitude >4500 m for the flight segments before 17:40UTC and 19:20–21:30UTC. The 12 km post run (12 km_NEI11_NGAC) does a better job for those segments but over-predicts low-altitude (<3 km) ozone for the flight segment of 17:10–19:20UTC. This flight comparison gives an example showing that NGAC's dynamic GFS-O_3 LBC can help the model's upper-layer performance.

Figure 103.2 shows the modeled O_3 versus the observation for all the 13 P-3B flights. The forecast run with static LBC did not show O_3 variance above 3 km, and had poor correlation with the observation. With GFS-O_3 LBC, the post run shows a noticeable improvement in the correlation. For the altitude below 2 km, the post run slightly improved the correlation coefficent, but had slightly poorer correlation

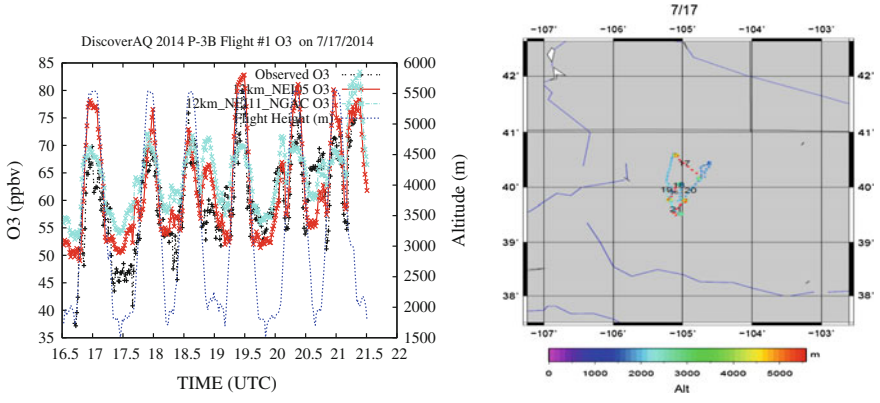

Fig. 103.1 12 km model predicted O_3 compared with P-3B aircraft measurement on 07/17/2014. The *right panel* shows the flight path over Colorado

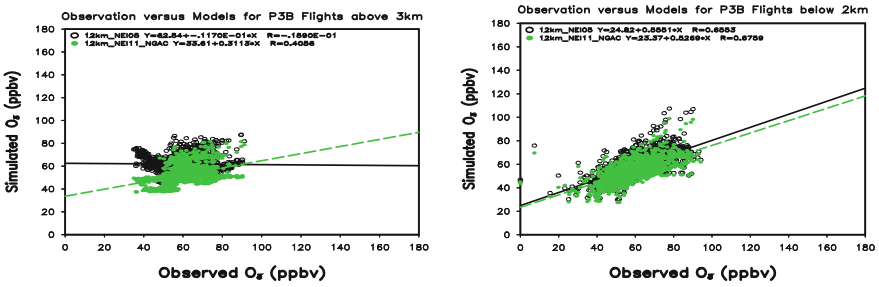

Fig. 103.2 Two 12 km model predicted O_3 compared with all P-3B aircraft measurements above 3 km and below 2 km

slope. Overall the impact of LBC changes for the lower layers were not strong, indicating that the emission change effect was not significant.

103.2.2 The Impact of NEI-2011 Emission Inventory

In order to assess the impact of the model's emission change (NEI05 versus NEI11), Fig. 103.3 shows the NO_y comparison for the P3-B flight segments below 2 km. Both emission inventories yielded very similar performance. Although their overall correlation slopes are 0.45 and 0.42, the model actually had NO_y over-prediction when observing $NO_y < 25$ ppbV. So this result suggests that we might have over-estimated NO_x emission, except over certain emission peculiar locations and types which were not covered by the NO_x emission inventories.

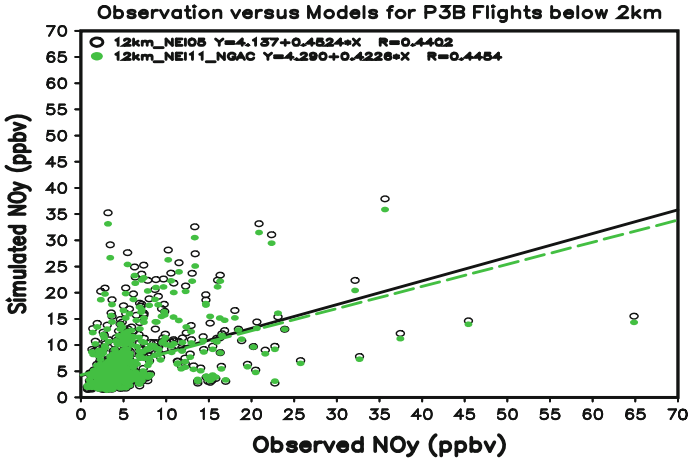

Fig. 103.3 Two 12 km model predicted NO_y compared with all P-3B aircraft measurements below 2 km

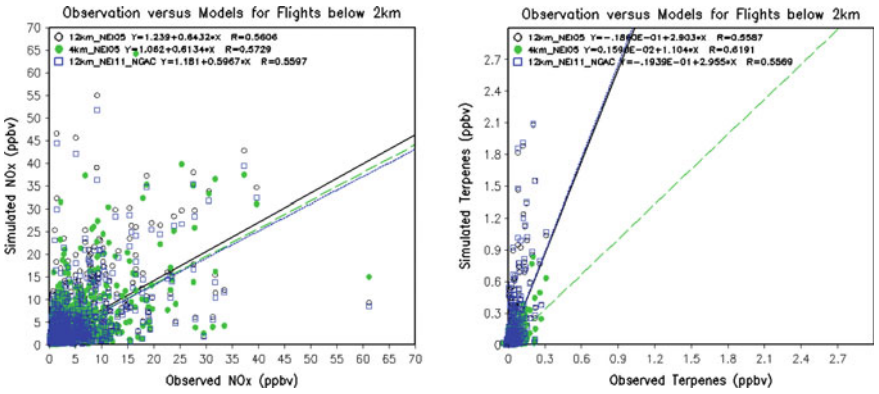

Fig. 103.4 Model simulated NO_x and Terpenes compared with all P-3B aircraft measurements below 2 km

103.2.3 Model Resolution Issue

For most cases in the upper layers, the 4 km run was not superior to the 12 km run. Its major advantage was for short-lived emitted species, such as NO_x and Terpenes. Figure 103.4 shows the 3 model comparisons for NOx and Terpenes below 2 km. For NO_x, the 4 km run showed slightly better improvement over the two 12 km runs in term of correlation coefficient. Its terpene prediction was much better than the two 12 km results. This result implies that the high-resolution land-use was helpful for the CMAQ's BEIS biogenic scheme. It also shows that the NEI2011 emission inventory for NO_x was barely changed, which was consistent with the NO_y correlation results in Fig. 103.3.

103.3 Summary

In this study, we evaluated our 12 and 4 km CMAQ runs with 2014 Discover-AQ P-3B aircraft data. The difference between two emission inventories was relatively small over the Colorado region. The 4 km run shows slightly better results for short-lived emitted species, e.g. NOx and terpenes. The static LBC failed to capture the O_3 variation in the upper layers, e.g. above 3 km, and the GFS-O_3 LBC improved the upper-layer O_3 prediction. For the layers below 2 km, the impact of LBC change was not strong during this period over the Colorado region. The model results for NO_x and NO_y were not as good as those for O_3 in the lower layers, and still needed improvement. The model tended to over-predict NO_y when $NO_y < 25$ppbv, and we need to investigate further whether this over-prediction was due to overestimated emission or under-predicted chemical/physical loss of NO_y.

References

Bey I, Jacob DJ, Yantosca RM, Logan JA, Field B, Fiore AM, Li Q, Liu H, Mickley LJ, Schultz M (2001) Global modeling of tropospheric chemistry with assimilated meteorology: model description and evaluation. J Geophys Res 106:23073–23096

Binkowski FS, Shankar U (1995) The regional particulate model 1. Model description and preliminary results. J Geophys Res 100(D12):26109–26191

Dudhia J (1989) Numerical study of convection observed during the winter monsoon experiment using a mesoscale two–dimensional model. J Atmos Sci 46:3077–3107

Hong S-Y, Noh Y, Dudhia J (2006) A new vertical diffusion package with an explicit treatment of entrainment processes. Mon Weather Rev 134:2318–2341

Hong S-Y, and Lim J-OJ (2006) The WRF single-moment 6-class microphysics scheme (WSM6). Asia-Pacific J Atmos Sci 42(2):129–151

Mathur R, Pleim J, Schere K, Pouliot G, Young J, Otte T (2005) The community Multiscale Air Quality (CMAQ) model: model configuration and enhancements for 2006 air quality forecasting. In: Air quality forecaster focus group meeting. Washington D.C., U.S.A, 16 Sept 2005

Mlawer EJ, Taubman SJ, Brown PD, Lacano MJ, Clough SA (1997) Radiative transfer for inhomogeneous atmospheres: RRTM, a validated correlated-k model for the longwave. J Geophys Res: Atmos (1984–2012) 102.D14:16663–16682

Monin AS, Obukhov AMF (1954). Basic laws of turbulent mixing in the surface layer of the atmosphere. Contrib. Geophys. Inst. Acad. Sci. USSR 151:163–187

Moorthi S, Iredell M (1998). Prognostic ozone: changes to the 1998 NCEP operational MRF model analysis/forecast system: the use of TOVS level 1-b radiances and increased vertical diffusion

Pan L, Tong DQ, Lee P, Kim H, Chai T (2014) Assessment of NO_x and O_3 forecasting performances in the U.S. National Air Quality Forecasting Capability before and after the 2012 major emissions updates. Atmos Environ 95:610–619

Pleim JE (2007). A combined local and nonlocal closure model for the atmospheric boundary layer. Part I: Model description and testing. J Appl Meteorol Climatol 46(9):1383–1395

Sarwar G et al (2011) Impact of a new condensed toluene mechanism on air quality model predictions in the US. Geosci Model Dev 4:183–193. doi:10.5194/gmd-4-183-2011

Tong DQ, Lamsal L, Pan L, Ding C, Kim H, Lee P, Chai T, Pickering KE, Stajner I (2015) Long-term NO_x trends over large cities in the United States during the Great Recession: Comparison of satellite retrievals, ground observations, and emission inventories. Atmos Environ 107:70–84

Tewari M et al (2004) Implementation and verification of the unified NOAH land surface model in the WRF model. In: 20th conference on weather analysis and forecasting/16th conference on numerical weather prediction, pp 11–15

Wicker LJ, Skamarock WC (2002) Time-splitting methods for elastic models using forward time schemes. Mon Weather Rev 130:2088–2097

Zhang D-L, Anthes RA (1982) A high–resolution model of the planetary boundary layer: sensitivity tests and comparisons with SESAME–79 data. J Appl Meteor 21:1594–1609